ANTI-CANCER DRUG-INDUCED CARDIOTOXICITY

EDITED BY: Susan Currie, Margaret Rose Cunningham, Michael Cross and Helen Louise Maddock

PUBLISHED IN: Frontiers in Cardiovascular Medicine

frontiers Research Topics

ISSN 1664-8714
ISBN 978-2-83250-210-5
DOI 10.3389/978-2-83250-210-5

About Frontiers

Frontiers is more than just an open-access publisher of scholarly articles: it is a pioneering approach to the world of academia, radically improving the way scholarly research is managed. The grand vision of Frontiers is a world where all people have an equal opportunity to seek, share and generate knowledge. Frontiers provides immediate and permanent online open access to all its publications, but this alone is not enough to realize our grand goals.

Frontiers Journal Series

The Frontiers Journal Series is a multi-tier and interdisciplinary set of open-access, online journals, promising a paradigm shift from the current review, selection and dissemination processes in academic publishing. All Frontiers journals are driven by researchers for researchers; therefore, they constitute a service to the scholarly community. At the same time, the Frontiers Journal Series operates on a revolutionary invention, the tiered publishing system, initially addressing specific communities of scholars, and gradually climbing up to broader public understanding, thus serving the interests of the lay society, too.

Dedication to Quality

Each Frontiers article is a landmark of the highest quality, thanks to genuinely collaborative interactions between authors and review editors, who include some of the world's best academicians. Research must be certified by peers before entering a stream of knowledge that may eventually reach the public - and shape society; therefore, Frontiers only applies the most rigorous and unbiased reviews.
Frontiers revolutionizes research publishing by freely delivering the most outstanding research, evaluated with no bias from both the academic and social point of view. By applying the most advanced information technologies, Frontiers is catapulting scholarly publishing into a new generation.

What are Frontiers Research Topics?

Frontiers Research Topics are very popular trademarks of the Frontiers Journals Series: they are collections of at least ten articles, all centered on a particular subject. With their unique mix of varied contributions from Original Research to Review Articles, Frontiers Research Topics unify the most influential researchers, the latest key findings and historical advances in a hot research area! Find out more on how to host your own Frontiers Research Topic or contribute to one as an author by contacting the Frontiers Editorial Office: frontiersin.org/about/contact

ANTI-CANCER DRUG-INDUCED CARDIOTOXICITY

Topic Editors:
Susan Currie, University of Strathclyde, United Kingdom
Margaret Rose Cunningham, University of Strathclyde, United Kingdom
Michael Cross, University of Liverpool, United Kingdom
Helen Louise Maddock, Coventry University, United Kingdom

Citation: Currie, S., Cunningham, M. R., Cross, M., Maddock, H. L., eds. (2022). Anti-Cancer Drug-Induced Cardiotoxicity. Lausanne: Frontiers Media SA. doi: 10.3389/978-2-83250-210-5

Table of Contents

frontiers in Cardiovascular Medicine

ORIGINAL RESEARCH
published: 30 October 2020
doi: 10.3389/fcvm.2020.594685

Red Blood Cell Distribution Width Is a Predictive Factor of Anthracycline-Induced Cardiotoxicity

Daiki Yaegashi, Masayoshi Oikawa, Tetsuro Yokokawa, Tomofumi Misaka, Atsushi Kobayashi, Takashi Kaneshiro, Akiomi Yoshihisa, Kazuhiko Nakazato, Takafumi Ishida and Yasuchika Takeishi*

Department of Cardiovascular Medicine, Fukushima Medical University, Fukushima, Japan

Background: Red blood cell distribution width (RDW) is associated with prognosis in widespread cardiovascular fields, but little is known about relationship with the onset of cancer therapeutics-related cardiac dysfunction (CTRCD).

Objectives: The purpose of this study was to assess whether RDW could predict the onset of CTRCD by anthracycline.

Methods: Consequential 202 cancer patients planed for anthracycline treatment were enrolled and followed up for 12 months. The patients were divided into 2 groups based on the median value of baseline RDW before chemotherapy [low RDW group, $n = 98$, 13.0 [12.6–13.2]; high RDW group, $n = 104$, 14.9 [13.9–17.0]]. Cardiac function was assessed serially by echocardiography at baseline (before chemotherapy), as well as at 3, 6, and 12 months after chemotherapy with anthracycline.

Results: Baseline left ventricular end systolic volume index and ejection fraction (EF) were similar between two groups. After chemotherapy, EF decreased at 3- and 6-month in the high RDW group [baseline, 64.5% [61.9–68.9%]; 3-month, 62.6% [60.4–66.9%]; 6-month, 63.9% [60.0–67.9%]; 12-month, 64.7% [60.8–67.0%], $P = 0.04$], but no change was observed in low RDW group. The occurrence of CTRCD was higher in high RDW group than in low RDW group (11.5 vs. 2.0%, $P = 0.008$). When we set the cut-off value of RDW at 13.8, sensitivity and specificity to predict CTRCD were 84.6 and 62.0%, respectively. Multivariable logistic regression analysis revealed that baseline RDW value was an independent predictor of the development of CTRCD [odds ratio 1.390, 95% CI [1.09–1.78], $P = 0.008$]. The value of net reclassification index (NRI) and integrated discrimination improvement (IDI) for detecting CTRCD reached statistical significance when baseline RDW value was added to the regression model including known risk factors such as cumulative anthracycline dose, EF, albumin, and the presence of hypertension; 0.9252 (95%CI 0.4103–1.4402, $P < 0.001$) for NRI and 0.1125 (95%CI 0.0078–0.2171, $P = 0.035$) for IDI.

Conclusions: Baseline RDW is a novel parameter to predict anthracycline-induced CTRCD.

Keywords: cardio-oncology, anthracycline, red blood cell distribution width, cancer therapeutics-related cardiac dysfunction, heart failure 2

OPEN ACCESS

Edited by:
Susan Currie, University of Strathclyde, United Kingdom

Reviewed by:
Alessandra Cuomo, Federico II University Hospital, Italy
George Lazaros, Hippokration General Hospital, Greece

****Correspondence:***
Masayoshi Oikawa
moikawa@fmu.ac.jp

Specialty section:
This article was submitted to Cardio-Oncology, a section of the journal Frontiers in Cardiovascular Medicine

Received: *14 August 2020*
Accepted: *06 October 2020*
Published: *30 October 2020*

Citation:
Yaegashi D, Oikawa M, Yokokawa T, Misaka T, Kobayashi A, Kaneshiro T, Yoshihisa A, Nakazato K, Ishida T and Takeishi Y (2020) Red Blood Cell Distribution Width Is a Predictive Factor of Anthracycline-Induced Cardiotoxicity. Front. Cardiovasc. Med. 7:594685. doi: 10.3389/fcvm.2020.594685

INTRODUCTION

Anthracycline-containing chemotherapy is highly effective and widely used in cancer treatments. However, anthracycline-induced cardiotoxicity is associated with a poor prognosis in cancer survivors, and the frequency of onset depends on risk factors including cumulative dose of anthracycline, elderly or pediatric population, concomitant or previous radiation therapy, pre-existing cardiovascular diseases, and concomitant use of human epidermal growth factor receptor 2 (HER2) inhibitors (1). Several hypotheses have been proposed for the mechanisms of anthracycline-induced cardiotoxicity, such as oxidative stress, iron accumulation in myocardial cells, mitochondrial dysfunction, and topoisomerase 2β dysfunction (2–5). Most anthracycline-induced cardiotoxicity occurs within the first year of chemotherapy, and early detection and treatment may recover cardiac function (6). Therefore, assessment of cardiac function should be performed to detect early phase of cardiotoxicity, and accurate predictors are required to identify patients predisposed to anthracycline-induced cardiotoxicity.

Red blood cell distribution width (RDW) is a simple and rapid measurement of the heterogeneity of erythrocyte volume. Growing body of evidence suggests that high RDW is strongly associated with poor prognosis in widespread cardiovascular diseases such as acute coronary syndrome, heart failure, and pulmonary hypertension (7–9). However, the association between anthracycline-induced cardiotoxicity and RDW have not been rigorously examined. The purpose of the present study was to assess whether baseline RDW could predict the onset of cancer therapeutics-related cardiac dysfunction (CTRCD) by anthracycline-containing chemotherapy.

METHODS

Study Subjects and Protocol

We enrolled 234 consecutive cancer patients, planned for initial anthracycline-containing chemotherapy at Fukushima Medical University hospital from February 2017 to September 2019 (**Figure 1**). Patients were excluded if they were died or transferred to other hospitals within 12 months follow-up period ($n = 32$). Remaining 202 patients were divided into 2 groups based on the median value of RDW (13.6) before chemotherapy: low RDW group, $n = 98$, 13.0 [12.6–13.2] and high RDW group, $n = 104$, 14.9 [13.9–17.0].

Hypertension was defined as a history of use of antihypertensive drug or systolic blood pressure of ≥140 mmHg, and/or diastolic blood pressure ≥90 mmHg. Diabetes was defined as a recent use of insulin treatment or hypoglycemic drug, or hemoglobin A1c ≥6.5%. Dyslipidemia was defined as a history of use of cholesterol-lowering drugs, or triglyceride was ≥150 mg/dl, low density lipoprotein cholesterol was ≥140 mg/dl, and/or high-density lipoprotein cholesterol was ≤40 mg/dl. Cumulative dose of anthracycline was expressed as a doxorubicin equivalent (1). HER 2 inhibitor included trastuzumab and pertuzumab. Radiation therapy was defined as irradiation to the mediastinum. Transthoracic echocardiography and blood sampling test were performed at baseline, as well as at 3, 6, and 12 months after administration of anthracyclines. All procedures used in this research were approved by the Ethical Committee of Fukushima Medical University Hospital.

Echocardiography

Transthoracic echocardiography was performed by a trained sonographer, and images were checked by another trained sonographer and an echo-cardiologist. We measured cardiac function using EPIQ 7G (Philips Healthtech, Best, Netherland). EF was calculated using the modified Simpson's method according to the guideline from the American Society of Echocardiography and the European Association of Cardiovascular Imaging (10). The left ventricular (LV) mass was calculated using the following formula:

$$\begin{aligned}&\textbf{Left ventricular (LV) mass}\\&=\textbf{0.8}\times\left[\textbf{1.04}\times\left\{\left(\textbf{LV diastolic diameter}+\textbf{interventricular septum wall thicness}+\textbf{LV posterior wall thicness}\right)^{\textbf{3}}-\left(\textbf{LV diastolic diameter}\right)^{\textbf{3}}\right\}\right]+\textbf{0.6g}\,[10].\end{aligned}$$

CTRCD was defined as a decrease in EF more than 10% points, to a value < 53% (11). LV diastolic dimension index, LV systolic dimension index, LV end-diastolic volume index, LV end-systolic volume index, and left atrial volume index (LAVI) were measured using B-mode ultrasound.

Blood Sampling

Blood sampling was performed in a stable condition after an overnight fast. High sensitivity cardiac troponin I (TnI) was measured using an assay based on Luminescent Oxygen Channeling Immunoassay technology, and run on a Dimension EXL integrated chemistry system (Siemens Healthcare Diagnostics, Deerfield, IL, USA). B-type natriuretic peptide (BNP) levels were measured using a specific immunoradiometric assay (Shionoria BNP kit, Shionogi, Osaka, Japan). RDW was measured using a DxH800 (Beckman Coulter, Inc., Fullerton, CA, USA).

Statistical Analysis

All statistical analyzes were performed using SPSS version 26 (IBM, Armonk, New York, USA) or R software packages version 3.6.3 (R core team 2020, Vienna, Austria). We used the Shapiro-Wilk test to discriminate which variables were normally or not normally distributed. Normally distributed variables were shown as mean ± standard deviation. Non-normally distributed variables were indicated by median with interquartile range. Category variables were shown in numbers and percentage. Student's *t*-test was used for variables following a normal distribution, the Mann-Whitney *U*-test was used for variables of the non-normal distribution, and the χ-square test was used for categorical variables. The time course of EF (baseline, 3-, 6-, and 12-month after the administration of anthracyclines) was evaluated using the Friedman test.

Logistic regression analysis was performed to identify variables relating to the occurrence of CTRCD. We selected variables as follows: age, sex, hypertension, dyslipidemia, diabetes mellitus, current or past smoker, cumulative anthracycline dose,

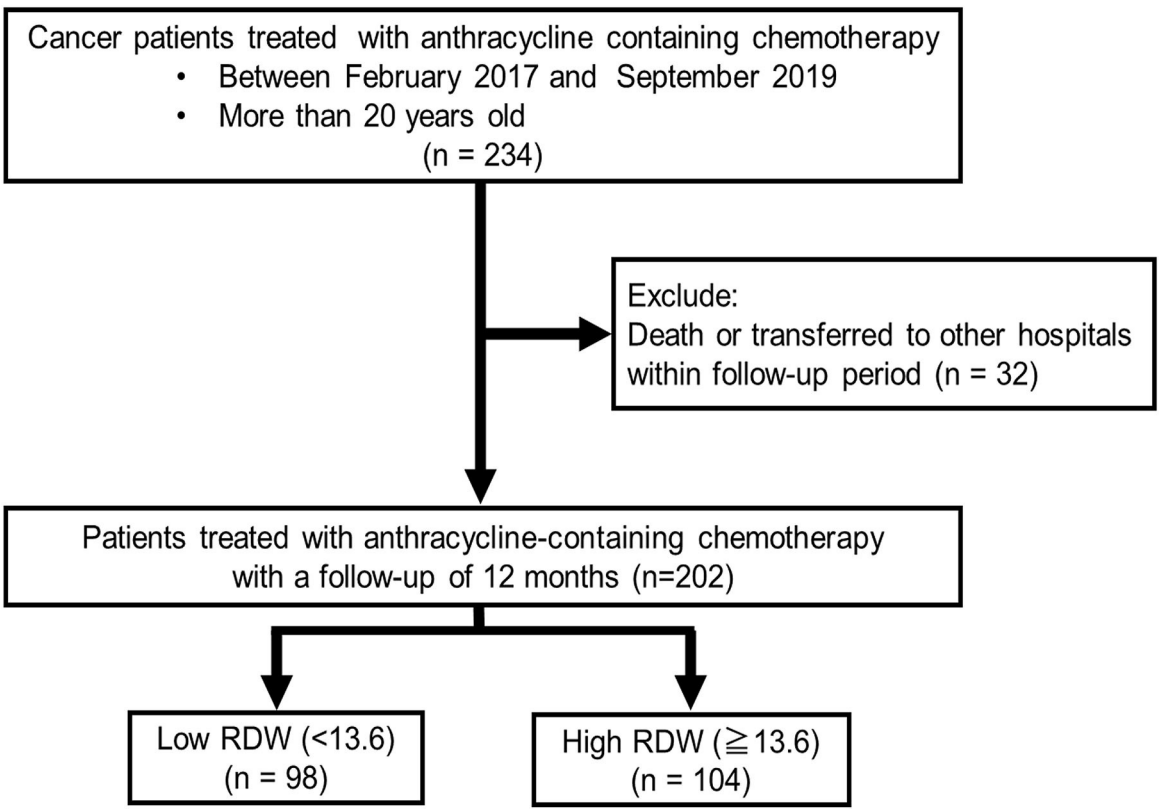

FIGURE 1 | Patient cohort selection.

use of HER2 inhibitor, BNP, albumin, LV mass index, LV end-diastolic volume index, LV end-systolic volume index, EF, LAVI, and RDW. Akaike Information Criteria was used for selecting variables for multivariate analysis. Receiver operator characteristic curve (ROC) analysis was performed to determine the optimal cut-off value of RDW for predicting the occurrence of CTRCD. The improvement by adding RDW to discrimination and net reclassification of risks was assessed by the estimation of both integrated discrimination improvement (IDI) and net reclassification improvement (NRI). The *P*-value of 0.05 or less was defined as significant.

RESULTS

Table 1 showed patient characteristics at the baseline of chemotherapy. The median value of RDW of all patients before chemotherapy was 13.6, and patients were divided into 2 groups based on the median value. Of 202 patients, 104 patients were grouped as high RDW group (13.6 and above), and 98 patients were grouped as low RDW group (< 13.6). There were no statistical differences in age, sex, coronary risk factors, cumulative anthracycline dose, the usage of HER2 inhibitor, and radiation therapy between the two groups. High RDW group included lower rate of breast cancer (60.2 vs. 43.2%, $P = 0.016$). Laboratory data showed that hemoglobin and mean corpuscular volume were lower in high RDW group, but BNP and TnI levels at baseline were similar between the two groups. The usage of angiotensin-converting enzyme (ACE) inhibitors, angiotensin II receptor blockers (ARB), β-blockers were similar between the two groups. Echocardiographic data demonstrated that LVEDVI, LVMI, and EF at baseline were similar between the two groups. Laboratory data showed similar liver and renal function.

Time-dependent changes in EF are displayed in **Figure 2**. EF decreased at 3- and 6-month after chemotherapy in high RDW group [baseline, 64.5% [61.9–68.9%]; 3-month, 62.6% [60.4–66.9%]; 6-month, 63.9% [60.0–67.9%]; 12-month, 64.7% [60.8–67.0%], $P = 0.04$, **Figure 2B**], but no change was observed in low RDW group (**Figure 2A**). The occurrence of CTRCD during the 12-month follow-up period was higher in high RDW group than in low RDW group [$n = 12$ [11.5%] vs. $n = 2$ [2.0%] $P = 0.008$]. When we set the cut-off value of RDW at 13.8 from the ROC analysis, sensitivity, specificity, and area under the curve to predict CTRCD were 84.6, 62.0, and 0.769%, respectively, as shown in **Figure 3**. Multivariable logistic regression analysis revealed that RDW at baseline was an independent predictor of the development of CTRCD [odds ratio 1.390, 95% CI [1.09–1.78], $P = 0.008$; **Table 2**].

To assess the importance of adding RDW more precisely, NRI, and IDI were calculated using the variables with or without RDW. The value of NRI and IDI for detecting CTRCD reached

TABLE 1 | Baseline clinical characteristics of patients with high or low RDW.

	Low RDW ($n = 98$)	High RDW ($n = 104$)	*P*-value
Age, years	58.0 (47.5–66.0)	54.0 (45.0–65.0)	0.396
Female, n (%)	81 (82.6)	81 (77.8)	0.395
Body mass index, kg/m²	22.9 ± 3.7	23.7 ± 4.5	0.161
Cardiovascular risk factor			
Hypertension, n (%)	21 (21.4)	26 (25.0)	0.426
Dyslipidemia, n (%)	34 (34.6)	23 (22.1)	0.101
Diabetes mellitus, n (%)	10 (10.2)	12 (11.5)	0.669
Current or past smokers, n (%)	33 (33.6)	36 (34.6)	0.849
Family history of CAD, n (%)	9 (9.1)	14 (13.4)	0.270
CKD (eGFR<60 ml/min/1.73 m²), n (%)	15 (15.3)	15 (14.4)	0.858
Pre-treatment cardiovascular medications			
Aspirin, n (%)	2 (2.0)	3 (2.8)	0.528
Statin, n (%)	9 (9.1)	10 (9.6)	0.916
β-blocker, n (%)	1 (1.0)	2 (1.9)	0.522
ACE inhibitor and/or ARB, n (%)	18 (18.3)	12 (11.5)	0.173
Anti-cancer treatment			
Cumulative anthracycline dose, mg/m²	200 (180–240)	180 (150–250)	0.203
HER2 inhibitor, n (%)	15 (15.3)	10 (9.6)	0.220
Radiation therapy, n (%)	7 (7.1)	6 (5.7)	0.774
Oncological disease			
Breast cancer, n (%)	59 (60.2)	45 (43.2)	0.016
Hematological tumor, n (%)	20 (20.4)	33 (31.7)	0.068
Gynecologic tumor, n (%)	10 (10.2)	14 (13.4)	0.475
Osteosarcoma, n (%)	8 (8.1)	9 (8.6)	0.900
Other solid tumor, n (%)	1 (1.0)	3 (2.8)	0.333
Laboratory data			
BNP, pg/ml	11.2 (6.6–19.8)	12.4 (5.9–22.7)	0.665
Troponin I, ng/ml	0.017 (0.017–0.017)	0.017 (0.017–0.017)	0.776
Total protein, g/dl	7.10 (6.8–7.5)	7.0 (6.7–7.4)	0.187
Albumin, g/dl	4.2 (3.9–4.5)	4.0 (3.8–4.3)	0.003
AST, U/L	18 (15–21)	19 (15–24)	0.788
ALT, U/L	15 (12–21)	14 (10–25)	0.560
LDH, U/L	181 (153–215)	197 (165–244)	0.060
BUN, mg/dl	13.0 (10.7–15.0)	13.0 (10.0–15.0)	0.509
Creatinine, mg/dl	0.65 (0.57–0.76)	0.66 (0.57–0.78)	0.588
eGFR, ml/min/1.73 m²	77.0 (63.7–89.2)	72.0 (65.0–89.0)	0.705
Total cholesterol, mg/dl	201.9 ± 36.9	191.5 ± 42.6	0.099
Triglyceride, mg/dl	106 (68.2–166.7)	107.5 (79.7–227.5)	0.979
High density lipoprotein cholesterol, mg/dl	54.9 ± 15.0	53.1 ± 15.5	0.458
Low density lipoprotein cholesterol, mg/dl	120.7 ± 30.9	113.2 ± 36.4	0.157
Hemoglobin A1c, %	5.6 (5.4–5.8)	5.7 (5.5–6.1)	0.185
C-reactive protein, mg/dl	0.11 (0.04–0.38)	0.16 (0.07–0.70)	0.024
Uric acid, mg/dl	4.3 (3.4–5.3)	4.7 (3.6–5.3)	0.876
D dimer, μg/ml	0.5 (0.5–0.925)	0.9 (0.5–2.3)	<0.001
White blood cell, μl	5,550 (4,450–6,800)	5,500 (4,200–7,200)	0.958
Hemoglobin, g/dl	13.1 (12.4–13.8)	11.8 (10.5–13.2)	<0.001
MCV, fl	93.0 ± 4.2	89.2 ± 8.9	<0.001
PLT, × 10^3/μl	252.5 ± 72.8	246.6 ± 96.1	0.624
RDW	13.0 (12.6–13.2)	14.9 (13.9–17.0)	<0.001
Echocardiographic data			
LVDdI, mm/m²	26.6 (24.5–29.2)	26.3 (24.5–28.5)	0.604
LVDsI, mm/m²	16.2 ± 2.4	16.4 ± 2.8	0.680
LVMI, g/m²	67.8 (58.7–82.1)	71.3 (61.8–84.9)	0.076
LVEDVI, ml/m²	47.0 ± 13.6	46.6 ± 18.6	0.844
LVESVI, ml/m²	16.1 (13.4–20.9)	16.2 (12.4–20.1)	0.668
EF, %	64.1 ± 4.9	65.1 ± 5.2	0.181
LAVI, ml/m²	22.8 (17.1–28.4)	22.9 (17.3–31.5)	0.333
E/A	0.97 (0.75–0.20)	1.01 (0.76–1.19)	0.710
Mitral regurgitation (mild and above) n, (%)	20 (20.2)	17 (16.5)	0.793
Aortic regurgitation (mild and above) n, (%)	7 (7.1)	8 (7.8)	0.850
Aortic stenosis (mild and above) n, (%)	0	2 (1.9)	0.259
TR-PG, mmHg	19.3 (16.2–22.3)	19.0 (15.0–23.0)	0.463
RVD, mm	27.2 ± 6.3	28.7 ± 5.6	0.098

Values are indicated by mean ± SD, median with interquartile range or n (%). Monoclonal antibodies include HER2 inhibitor. Radiation therapy includes only irradiation to the mediastinum. Hemato-oncologic disease include Hodgkin disease, Non-Hodgkin disease, acute myeloid leukemia, acute lymphocytic leukemia, and chronic lymphocytic leukemia. Gynecologic tumor include uterine cancer or sarcoma and ovarian cancer. Other solid tumors include thymoma, soft tissue tumor, teratoma.

ACE, angiotensin-converting enzyme; ARB, angiotensin II receptor blocker; BNP, B-type natriuretic peptide; CAD, coronary artery disease; CKD, chronic kidney disease; eGFR, estimated glomerular filtration rate; GLS, global longitudinal strain; HER2, human epidermal growth factor receptor 2; LAVI, left atrial volume index; LV, left ventricular; LVDdI, LV diastolic dimension index; LVDsI, LV systolic dimension index; LVEDVI, LV end-diastolic volume index; EF, ejection fraction; LVESVI, LV end-systolic volume index; LVMI, LV mass index; MCV, mean corpuscular volume; RVD, right ventricular dimension; TR-PG, tricuspid pressure gradient.

statistical significance when baseline RDW value was added to the model including cumulative dose of anthracycline, EF, albumin and hypertension; 0.9252 (95%CI 0.4103–1.4402, $P < 0.001$) for NRI and 0.1125 (95%CI 0.0078–0.2171, $P = 0.035$) for IDI.

DISCUSSION

In the present study, we revealed the clinical features of RDW in patients treated with anthracycline. First, EF was temporary decreased in high RDW patients. Second, the occurrence of anthracycline-induced CTRCD was significantly higher in high RDW patients. Third, high RDW at baseline was an independent predictor of the development of CTRCD.

Oxidative stress, iron accumulation in myocardial cells, mitochondrial dysfunction, and topoisomerase 2β dysfunction

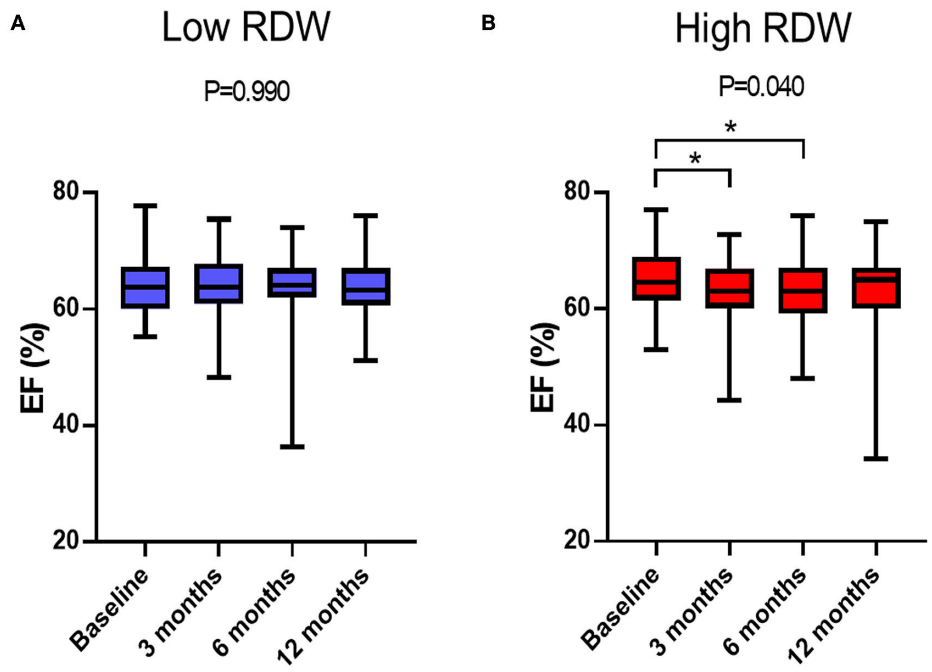

FIGURE 2 | Time-dependent changes in EF after anthracycline treatment. **(A)** Changes in EF in low RDW group. **(B)** Changes in EF in high RDW group. *$P < 0.05$.

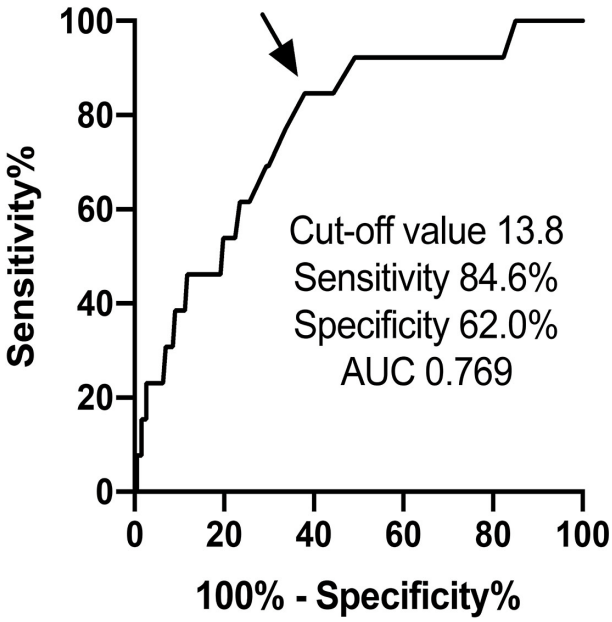

FIGURE 3 | ROC curve analysis of RDW predicting the occurrence of CTRCD by anthracycline.

have been proposed as major mechanisms of anthracycline-induced cardiotoxicity (2–5). The excess production of free radicals by the quinone group from aglycons of anthracycline induces oxidation of protein, nucleic acid, and lipid, leading to cellular damage (4). It has been reported that elevation of RDW is also associated with oxidative stress as well as aging, inflammation, malnutrition, and renal dysfunction (12, 13). Among those factors, oxidative stress induces bone marrow dysfunction, leading to abnormal heme synthesis, and hemoglobin production that increased in RDW. In the present study, the patients with high RDW at baseline demonstrated time-dependent decrease in EF and higher occurrence of CTRCD. These findings raise the possibility that the patients with high RDW already had been exposed to increased oxidative stress before chemotherapy, and were more vulnerable to additional oxidative stress by anthracycline, resulting in the development of CTRCD.

Although underlying mechanisms of interaction between RDW and CTRCD remains to be elucidated, to the best of our knowledge, this is the first report to demonstrate the association between RDW and CTRCD.

The utility of RDW has been reported in not only cardiovascular disease, but also cancer prognosis. High RDW are associated with unfavorable survival in many types of cancers including breast cancer (14), hematological tumor (15), gynecological cancer (16, 17), and osteosarcoma (18). Although there is no clear explanation of the relationship between RDW and cancer prognosis, RDW can be a promising biomarker for assessment of the risk of CTRCD and cancer prognosis. Cardinale et al. (6) reported that 78% patients with anthracycline-induced cardiotoxicity showed a full or partial recovery with heart failure therapy. In this cohort, one patient presented < 40% of ejection fraction at 6-month follow-up. He was administered β-blockers and ACE inhibitors soon after the onset of CTRCD. Then, his

TABLE 2 | Parameters associated with the occurrence of CTRCD.

	Univariable		Multivariable*	
	Odds Ratio (95% CI)	***P*-value**	**Odds Ratio (95% CI)**	***P*-value**
Age, per 1-year increase	0.986 (0.950–1.023)	0.455		
Female	0.898 (0.239–0.384)	0.874		
Hypertension	0.511 (0.110–2.371)	0.391	0.264 (0.03–1.78)	0.171
Dyslipidemia	0.186 (0.024–1.446)	0.110		
Diabetes mellitus	0.586 (0.073–4.711)	0.615		
Current or past smoker	0.299 (0.065–1.374)	0.121		
Cumulative anthracycline dose, mg/m² per 1.0 increase	1.010 (1.004–1.016)	0.001	1.010 (1.00–1.02)	<0.001
HER2 inhibitor	0.526 (0.066–4.201)	0.544		
Radiation therapy	1.077 (0.130–8.941)	0.945		
BNP, pg/ml per 1.0 increase	1.000 (0.976–1.025)	0.998		
Albumin, per 1.0 increase	0.469 (0.171–1.286)	0.141	0.367 (0.09–1.35)	0.131
LVMI, g/m² per 1.0 increase	0.998 (0.970–1.027)	0.876		
LVEDVI, ml/m² per 1.0 increase	0.994 (0.959–1.024)	0.574		
LVESVI, ml/m² per 1.0 increase	1.072 (0.970–1.178)	0.149		
EF, per 1.0 increase	0.926 (0.826–1.038)	0.186	0.868 (0.75–1.01)	0.058
LAVI, ml/m² per 1.0 increase	0.999 (0.967–1.031)	0.824		
RDW, per 1.0 increase	1.378 (1.126–1.687)	0.002	1.390 (1.09–1.78)	0.008

**adjusted for hypertension, cumulative anthracycline dose, albumin, ejection fraction, and RDW categorical variables.*
CI, Confidence interval; CTRCD, cancer therapeutics-related myocardial disorder; RDW, red blood cell distribution width.

ejection fraction recovered to over 50% at 12-month follow-up. We speculate that early initiation of cardioprotective therapy induced a recovery of cardiac function. Thus, early detection and treatments of CTRCD are essential to minimize cardiac damage induced by anthracyclines. TnI and BNP are widely used surrogate biomarkers to detect CTRCD, but the elevation occurs after starting anthracycline chemotherapy (19). Compared to them, RDW can predict the development of CTRCD before chemotherapy. By assessing RDW before chemotherapy, precise follow-up management can be scheduled, and indication of prophylaxis treatment can be discussed. To date, several clinical studies have demonstrated that angiotensin-converting enzyme and beta-adrenergic receptor blockers prevent cardiac dysfunction after anthracycline chemotherapy (20). According to previous reports of anti-oxidative effects of carvedilol and ACE inhibitor (21), the efficacy of prophylaxis may be expected to the patients with high RDW.

In the present study, the calculation of NRI, and IDI demonstrated the significance of RDW for the prediction of CTRCD. The utility of RDW should be considered when managing cancer patients treated with anthracycline-containing chemotherapy.

LIMITATION

This study was performed using a relatively small number of patients and short follow-up period by a single center. Longer follow-up and larger population data were needed to confirm the importance of RDW to the development of CTRCD and cardiovascular prognosis. According to 2016 ESC position paper (1), 3 dimensional-based LVEF have advantages to assess cardiac function compared to Simpson's method, and global longitudinal strain reveals subtle changes in left ventricular function, and thus detects myocardial damage in the early stage before reduces in left ventricular ejection fraction (22). Further studies using 3 dimentional echocardiography and global longitudinal strain are desirable in the future.

CONCLUSION

Baseline RDW identifies high risk patients with anthracycline-induced CTRCD.

DATA AVAILABILITY STATEMENT

The raw data supporting the conclusions of this article will be made available by the authors, without undue reservation.

ETHICS STATEMENT

The studies involving human participants were reviewed and approved by Ethical Committee of Fukushima Medical University Hospital. The patients/participants provided their written informed consent to participate in this study.

AUTHOR CONTRIBUTIONS

MO conceived of the presented idea. MO and DY developed the theory and performed the computations. TY, TM, AK, TK, AY, and KN verified the analytical methods. YT and TI supervised the findings of this work. All authors discussed the results and contributed to the final manuscript.

FUNDING

This work was supported by JSPS KAKENHI (Grant Number JP20K08493).

ACKNOWLEDGMENTS

The authors thank for Ms. H. Kobayashi for data management.

REFERENCES

1. Zamorano JL, Lancellotti P, Munoz DR, Aboyans V, Asteggiano R, Galderisi M, et al. 2016 ESC Position Paper on cancer treatments and cardiovascular toxicity developed under the auspices of the ESC Committee for Practice Guidelines: The Task Force for cancer treatments and cardiovascular toxicity of the European Society of Cardiology (ESC). *Eur Heart J.* (2016) 37:2768–801. doi: 10.1093/eurheartj/ehw211
2. Horenstein MS, Vander Heide RS, L'Ecuyer TJ. Molecular basis of anthracycline-induced cardiotoxicity and its prevention. *Mol Genet Metab.* (2000) 71:436–44. doi: 10.1006/mgme.2000.3043
3. Link G, Tirosh R, Pinson A, Hershko C. Role of iron in the potentiation of anthracycline cardiotoxicity: identification of heart cell mitochondria as a major site of iron-anthracycline interaction. *J Lab Clin Med.* (1996) 127:272–8. doi: 10.1016/S0022-2143(96)90095-5
4. Ichikawa Y, Ghanefar M, Bayeva M, Wu R, Khechaduri A, Naga Prasad SV, et al. Cardiotoxicity of doxorubicin is mediated through mitochondrial iron accumulation. *J Clin Invest.* (2014) 124:617–30. doi: 10.1172/JCI72931
5. Zhang S, Liu X, Bawa-Khalfe T, Lu LS, Lyu YL, Liu LF, et al. Identification of the molecular basis of doxorubicin-induced cardiotoxicity. *Nat Med.* (2012) 18:1639–42. doi: 10.1038/nm.2919
6. Cardinale D, Colombo A, Bacchiani G, Tedeschi I, Meroni CA, Veglia F, et al. Early detection of anthracycline cardiotoxicity and improvement with heart failure therapy. *Circulation.* (2015) 131:1981–8. doi: 10.1161/CIRCULATIONAHA.114.013777
7. Abrahan LL, Ramos JDA, Cunanan EL, Tiongson MDA, Punzalan FER. Red cell distribution width and mortality in patients with acute coronary syndrome: a meta-analysis on prognosis. *Cardiol Res.* (2018) 9:144–52. doi: 10.14740/cr732w
8. Felker GM, Allen LA, Pocock SJ, Shaw LK, McMurray JJ, Pfeffer MA, et al. Red cell distribution width as a novel prognostic marker in heart failure: data from the CHARM Program and the Duke Databank. *J Am Coll Cardiol.* (2007) 50:40–7. doi: 10.1016/j.jacc.2007.02.067
9. Hampole CV, Mehrotra AK, Thenappan T, Gomberg-Maitland M, Shah SJ. Usefulness of red cell distribution width as a prognostic marker in pulmonary hypertension. *Am J Cardiol.* (2009) 104:868–72. doi: 10.1016/j.amjcard.2009.05.016
10. Lang RM, Badano LP, Mor-Avi V, Afilalo J, Armstrong A, Ernande L, et al. Recommendations for cardiac chamber quantification by echocardiography in adults: an update from the American society of echocardiography and the European association of cardiovascular imaging. *J Am Soc Echocardiogr.* (2015) 28:1–39.e14. doi: 10.1016/j.echo.2014.10.003
11. Plana JC, Gaiderisi M, Barac A, Ewer MS, Bonnie Ky, Scherrer-Crosbie M, et al. Expert consensus for multimodality imaging evaluation of adult patients during and after cancer therapy: a report from the American society of echocardiography and the European association of cardiovascular imaging. *J Am Soc Echocardiogr.* (2014) 27:911–39. doi: 10.1016/j.echo.2014.07.012
12. salvagno gl, sanchis-gomar f, picanza A, Lippi G. Red blood cell distribution width: a simple parameter with multiple clinical applications. *Crit Rev Clin Lab Sci.* (2015) 52:86–105. doi: 10.3109/10408363.2014.992064
13. Lippi G, Cervellin G, Sanchis-Gomar F. Red blood cell distribution width and cardiovascular disorders. Does it really matter which comes first, the chicken or the egg? *Int J Cardiol.* (2016) 206:129–30. doi: 10.1016/j.ijcard.2016.01.122
14. Yao D, Wang Z, Cai H, Li Y, Li B. Relationship between red cell distribution width and prognosis in patients with breast cancer after operation: a retrospective cohort study. *Biosci Rep.* (2019) 39:BSR20190740. doi: 10.1042/BSR20190740
15. Podhorecka M, Halicka D, Szymczyk A, Macheta A, Chocholska S, Hus M, et al. Assessment of red blood cell distribution width as a prognostic marker in chronic lymphocytic leukemia. *Oncotarget.* (2016) 7:32846–53. doi: 10.18632/oncotarget.9055
16. Li Z, Hong N, Robertson M, Wang C, Jiang G. Preoperative red cell distribution width and neutrophil-to-lymphocyte ratio predict survival in patients with epithelial ovarian cancer. *Sci Rep.* (2017) 7:43001. doi: 10.1038/srep43001
17. Kemal Y, Demirag G, Baş B, Önem S, Teker F, Yücel I. The value of red blood cell distribution width in endometrial cancer. *Clin Chem Lab Med.* (2015) 53:823–7. doi: 10.1515/cclm-2014-0699
18. Zheng J, Yuan X, Guo W. Relationship between red cell distribution width and prognosis of patients with osteosarcoma. *Biosci Rep*. (2019) 39:BSR20192590. doi: 10.1042/BSR20192590
19. Oikawa M, Yoshihisa A, Yokokawa T, Misaka T, Yaegashi D, Miyata M, et al. Cardiac troponin I predicts elevated B-type natriuretic peptide in patients treated with anthracycline-containing chemotherapy. *Oncology.* (2020) 98:653–60. doi: 10.1159/000507585
20. Blanter JB, Frishman WH. The preventive role of angiotensin converting enzyme inhibitors/angiotensin-ii receptor blockers and β-adrenergic blockers in anthracycline- and trastuzumab-induced cardiotoxicity. *Cardiol Rev.* (2019) 27:256–59. doi: 10.1097/CRD.0000000000000252
21. Chin BS, Langford NJ, Nuttall SL, Gibbs CR, Blann AD, Lip GY. Anti-oxidative properties of beta-blockers and angiotensin-converting enzyme inhibitors in congestive heart failure. *Eur J Heart Fail.* (2003) 5:171–4. doi: 10.1016/S1388-9842(02)00251-9
22. Berliner D, Beutel G, Bauersachs J. Echocardiography and biomarkers for the diagnosis of cardiotoxicity. *Herz.* (2020). doi: 10.1007/s00059-020-04957-5. [Epub ahead of print].

Conflict of Interest: The authors declare that the research was conducted in the absence of any commercial or financial relationships that could be construed as a potential conflict of interest.

frontiers in Cardiovascular Medicine

ORIGINAL RESEARCH
published: 01 February 2021
doi: 10.3389/fcvm.2020.630480

Sunitinib and Imatinib Display Differential Cardiotoxicity in Adult Rat Cardiac Fibroblasts That Involves a Role for Calcium/Calmodulin Dependent Protein Kinase II

*Calum J. McMullen, Susan Chalmers, Rachel Wood, Margaret R. Cunningham and Susan Currie**

Strathclyde Institute of Pharmacy and Biomedical Sciences, University of Strathclyde, Glasgow, United Kingdom

OPEN ACCESS

Edited by:
Carlo Gabriele Tocchetti, University of Naples Federico II, Italy

Reviewed by:
Edoardo Bertero, University Hospital Würzburg, Germany
Claudia Penna, University of Turin, Italy
Edoardo Lazzarini, University of Zurich, Switzerland

***Correspondence:**
Susan Currie
susan.currie@strath.ac.uk

Specialty section:
This article was submitted to Cardio-Oncology, a section of the journal Frontiers in Cardiovascular Medicine

Received: *17 November 2020*
Accepted: *29 December 2020*
Published: *01 February 2021*

Citation:
McMullen CJ, Chalmers S, Wood R, Cunningham MR and Currie S (2021) Sunitinib and Imatinib Display Differential Cardiotoxicity in Adult Rat Cardiac Fibroblasts That Involves a Role for Calcium/Calmodulin Dependent Protein Kinase II. Front. Cardiovasc. Med. 7:630480. doi: 10.3389/fcvm.2020.630480

Background: Tyrosine kinase inhibitors (TKIs) have dramatically improved cancer treatment but are known to cause cardiotoxicity. The pathophysiological consequences of TKI therapy are likely to manifest across different cell types of the heart, yet there is little understanding of the differential adverse cellular effects. Cardiac fibroblasts (CFs) play a pivotal role in the repair and remodeling of the heart following insult or injury, yet their involvement in anti-cancer drug induced cardiotoxicity has been largely overlooked. Here, we examine the direct effects of sunitinib malate and imatinib mesylate on adult rat CF viability, Ca^{2+} handling and mitochondrial function that may contribute to TKI-induced cardiotoxicity. In particular, we investigate whether Ca^{2+}/calmodulin dependent protein kinase II (CaMKII), may be a mediator of TKI-induced effects.

Methods: CF viability in response to chronic treatment with both drugs was assessed using MTT assays and flow cytometry analysis. Calcium mobilization was assessed in CFs loaded with Fluo4-AM and CaMKII activation *via* oxidation was measured *via* quantitative immunoblotting. Effects of both drugs on mitochondrial function was determined by live mitochondrial imaging using MitoSOX red.

Results: Treatment of CFs with sunitinib (0.1–10 μM) resulted in concentration-dependent alterations in CF phenotype, with progressively significant cell loss at higher concentrations. Flow cytometry analysis and MTT assays revealed increased cell apoptosis and necrosis with increasing concentrations of sunitinib. In contrast, equivalent concentrations of imatinib resulted in no significant change in cell viability. Both sunitinib and imatinib pre-treatment increased Angiotensin II-induced intracellular Ca^{2+} mobilization, with only sunitinib resulting in a significant effect and also causing increased CaMKII activation *via* oxidation. Live cell mitochondrial imaging using MitoSOX red revealed that both sunitinib and imatinib increased mitochondrial superoxide production in a concentration-dependent manner. This effect in response to both drugs was suppressed in the presence of the CaMKII inhibitor KN-93.

Conclusions: Sunitinib and imatinib showed differential effects on CFs, with sunitinib causing marked changes in cell viability at concentrations where imatinib had no

effect. Sunitinib caused a significant increase in Angiotensin II-induced intracellular Ca^{2+} mobilization and both TKIs caused increased mitochondrial superoxide production. Targeted CaMKII inhibition reversed the TKI-induced mitochondrial damage. These findings highlight a new role for CaMKII in TKI-induced cardiotoxicity, particularly at the level of the mitochondria, and confirm differential off-target toxicity in CFs, consistent with the differential selectivity of sunitinib and imatinib.

Keywords: sunitinib, cardiac fibroblast, CaMKII, cardiotoxicity, imatinib

INTRODUCTION

Cardiotoxicity is a recognized adverse effect of many clinically important drugs and has led to the withdrawal of a number of agents after their introduction to the market (1). Anti-cancer drugs are prevalent among the drug categories that exhibit cardiotoxicity and this can seriously impact upon cancer patient survival. In the long term, patients receiving anti-cancer drugs may be at a greater risk of death from cardiovascular disease than cancer (2). Conventional approaches for assessing cardiotoxic effects are similar to the indices used for assessing heart disease, including measurement of cardiac troponin and natriuretic peptides (3, 4). These markers usually only show significant changes after damage to the heart has occurred. Consequently, there is a real need to identify early onset biomarkers and signaling pathways that are switched on soon after initiating anti-cancer therapy and that correlate with adverse effects on the heart. This will be essential for the development of safer anti-cancer drugs in the future.

A prominent and well-recognized feature of anti-cancer drug-induced cardiotoxicity in cardiac myocytes (CMs) is the accumulation of damaging reactive oxygen species (ROS). Functional effects of ROS accumulation include CM hypertrophy, impaired contraction, apoptosis and autophagy, all of which are key features of cardiotoxicity (5). Importantly though, drug-induced cardiotoxicity does not only affect the contractile cells of the heart. Evidence is emerging that anti-cancer drugs can also have off-target damaging effects on other cells of the cardiovascular system including cardiac fibroblasts (CFs), endothelial cells (ECs), vascular smooth muscle cells (VSMCs), immune cells and cardiac progenitor cells (6). In a healthy heart there is considerable functional interaction between different cell types, particularly between the CMs and CFs. The latter cell type not only secrete chemical mediators that can influence cardiac contractility, but also provide components of extracellular matrix that ensure structural stability (7). In cardiovascular disease, CFs play a pivotal role in cardiac remodeling and in the accompanying contractile dysfunction by exhibiting hyper-proliferation and producing excess collagen. The resulting fibrosis is a key contributor to cardiac dysfunction (8). Recent studies have suggested that anti-cancer therapies can mirror the effects observed in CFs from diseased hearts, including increased oxidative stress and ROS accumulation similar to that seen in CMs but resulting in cardiac fibrosis and potential diastolic dysfunction (9–11).

Among the more novel anti-cancer agents to emerge in recent years are those that prevent cancer cell proliferation and angiogenesis *via* "selective" targeted tyrosine kinase and vascular endothelial growth factor receptor (VEGFR) inhibition. Unfortunately, these targeted therapies cause cardiotoxicity *via* both on-target (blocking VEGFR in cardiac cells) and off-target (non-VEGFR) effects (12). Understanding the cellular mechanisms that underpin these cardiotoxic effects will be crucial in improving the safety profile of tyrosine kinase inhibitors (TKIs), especially since these drugs are currently the standard treatment for several types of malignancy. The extent of TKI-induced cardiotoxicity may vary considerably across different members of the TKI drug group. Understanding the fundamental reasons for these differences is essential for tailoring future safer treatments. It is possible that different cardiotoxic responses may reflect an individual drug's capacity for on-target vs. off-target effects (13).

Two well-known TKIs that are currently in clinical use are imatinib and sunitinib. Imatinib mesylate is used for the treatment of chronic myeloid leukemia, gastrointestinal stromal tumors and hypereosinophilic syndrome. Imatinib works by targeting the ABL ATP binding site, stabilizing the inactive form of ABL, preventing tyrosine autophosphorylation and therefore kinase phosphorylation of substrates in cancerous cells, ultimately inducing apoptosis (14). There have been various reports of cardiotoxicity associated with imatinib. At a cellular level the cardiotoxic response has been suggested to include apoptosis as well as necrosis of CMs and this is as a result of mitochondrial dysfunction, ATP depletion and cytochrome C release (15). However, there is speculation over whether the concentrations of imatinib that exert the toxic effects reported on cardiac cells are clinically relevant (16). Despite evidence for cardiotoxicity, overall adverse effects on the heart following imatinib treatment appear relatively uncommon, ranging from 0.5 to 1.7% (17, 18). Sunitinib malate (SUTENT®) on the other hand has been reported to exert a wide range of cardiotoxic effects. Reports of hypertension and congestive heart failure in patients receiving sunitinib therapy ranges from 17 to 43% and 3 to 18% (19) respectively. Sunitinib is commonly used to treat renal cancers and has shown considerable benefit in patients with metastatic renal carcinoma (20). Sunitinib has been suggested to have a number of off-target effects that can adversely affect the heart. Examples of off-target effects include inhibition of AMP-activated protein kinase (21) and activation of calcium/calmodulin dependent protein kinase (CaMKII) (22), both of which, if chronically affected, can result in cardiac dysfunction.

Previous work by our group has highlighted that CaMKII activation occurs in guinea pig hearts following chronic

administration of clinically relevant concentrations of either imatinib or sunitinib (22). Increased cardiac CaMKIIδ expression and CaMKII activity were shown to occur in the absence of any overt cardiac dysfunction. We suggested that these changes could reflect early adaptations by the heart to these TKIs which could precede the onset of contractile dysfunction. As such, we suggested that CaMKII might be a useful early onset marker for TKI-induced cardiotoxicity. Our original work comprised *in vivo* assessment of cardiac function following acute and chronic TKI treatment. CaMKII was assessed in whole cardiac homogenate preparations from TKI-treated hearts. Crucially, there was no investigation of specific cellular responses to either imatinib or sunitinib, evidence that we need to inform us upon more tailored clinical treatments going forward. In order to characterize the cardiotoxic effects of imatinib and sunitinib in more detail, the current study has, for the first time, compared the effects of both TKIs on adult rat CFs across a range of clinically relevant concentrations. Cell phenotype and viability have been assessed along with effects on mitochondrial superoxide production. Here we present novel evidence for distinct differences in the cellular responses to both drugs in CFs. Importantly, we also identify a common role for CaMKII in both imatinib and sunitinib-mediated mitochondrial superoxide production.

METHODS

Cardiac Fibroblast Isolation

All procedures were performed under sterile conditions and conformed to local ethical review committee guidelines as well as to the Guide for the Care and Use of Laboratory Animals published by the US National Institutes of Health (NIH Publication No. 85-23, revised 1996) and Directive 2010/63/EU of the European Parliament. CFs were isolated from male Sprague-Dawley rats weighing between 250 and 350 g. Rats were sacrificed *via* cervical dislocation and ventricular CFs isolated under sterile conditions *via* the bulk collagenase digestion method described previously (23). Briefly, isolated hearts were washed in Ca^{2+} free Krebs solution (120 mM NaCl, 5.4 mM KCl, 0.52 mM NaH_2PO_4, 20 mM HEPES, 11.1 mM glucose, 3.5 mM $MgCl_2$, 20 mM taurine, 10 mM creatine) supplemented with 1 mM EGTA, 1% (v/v) penicillin/streptomycin; pH 7.4. The aorta and atria were then excised before the remaining ventricular tissue was finely chopped in a digestion buffer containing 0.8 mg/ml collagenase type 1 (Worthington Chemical, UK) and 0.3 mg/ml protease XIV (Sigma-Aldrich) prepared in Ca^{2+} free Krebs solution. The isolated CFs were resuspended in CF growth medium [DMEM supplemented with 20% (v/v) FBS, 2% (v/v) penicillin/ streptomycin and 1% (v/v) L-glutamine] before being plated in a T75 culture flask and incubated (37°C, 5% CO_2). The CF growth media was replenished after 4–5 h of incubation to remove non-adherent cells. The media was replenished 24 h post-isolation to remove any remaining cell debris. Subsequent media changes conducted at 48 h intervals thereafter as per the standard cell culture protocol until 70–80% confluent.

Drug Treatment

CFs were grown to ∼75% confluence in CF growth medium (outlined above) and were treated with sunitinib malate and imatinib mesylate at the indicated concentrations for 18 h in the same CF growth medium containing 20% serum (outlined above). Stock concentrations of drugs were diluted in DMEM supplemented with 2% (v/v) penicillin/streptomycin and 1% (v/v) L-glutamine prior to addition. Working concentrations were based on clinically relevant concentrations previously published (22, 24). Where appropriate, 5 μM KN-93 was added for 2 h pre-treatment prior to the addition of drug for 18 h.

Imaging of Cells

Cell phenotype and growth was monitored using a Nikon Eclipse (TE300) inverted microscope (Nikon, Tokyo, Japan) and a Leica EC3 digital camera affixed to a Leica DM IL LED inverted microscope at 10× magnification (Leica Biosystems, Wetzlar, Germany).

Immunofluorescence

CFs, human umbilical vein endothelial cells (HUVECs), colonic smooth muscle cells (SMCs) and myofibroblasts (MFs) were seeded in 12-well plates containing 13 mm glass coverslips at a density of 1.5×10^4 cells/ml and cultured until 40–60% confluent. MFs were obtained following passage of CFs to p4 or p5 and were initially identified visually based on dramatic change in cell phenotype where MFs were significantly larger and rounder. Cells were fixed in 3.6% (v/v) formaldehyde in phosphate buffered saline (PBS) for 10 min at room temperature before being permeabilised with 0.25% Triton X-100 in PBS for 10 min at room temperature. Cells were then blocked in 1% (w/v) BSA in PBS for 30 min before incubation with primary antibody diluted in 1% (w/v) BSA in PBS overnight at room temperature [vimentin 1:400; Sigma-Aldrich (V5255)], von Willebrand factor [vWF; 1:100; Abcam (ab6994)] and smooth muscle cell actin [SMCa; 1:200; Abcam (ab7817)]. Following overnight incubation, coverslips were washed three times with PBS before being blocked in 1% (w/v) BSA in PBS for 15 min at room temperature. Coverslips were then incubated (covered) with the corresponding Alexa Fluor™ 488 secondary antibody {1:100; Thermo Fisher, Renfrew, UK [Mouse (A-11001); Rabbit (A-11008)]} in 1% (w/v) BSA in PBS for 1 h at room temperature. Following further washes in PBS, samples were stained with DAPI (1:2,000) for 5 min before being mounted onto glass coverslips with Mowiol® and stored at 4°C until imaged. Samples were imaged using the EVOS™ FL Auto Imaging System (Thermo Fisher) at 20× magnification.

MTT Assays for Cell Death Determination

CFs were seeded in a 96-well plate at a density of 2.5×10^4 cells/well and cultured in growth medium for 24 h prior to drug treatment. Treated samples were incubated with 3-(4,5-dimethylthiazol-2-yl)-2, 5-diphenyltetrazolium bromide MTT (10 μg/ml) prepared in fresh growth medium for 2 h (37°C, 5% CO_2). In living cells, mitochondrial dehydrogenases convert MTT to purple MTT formazan crystals. The purple formazan crystals were resuspended in DMSO and cell viability assessed *via* optical density at a wavelength of 570 nm. Data was expressed as a percentage of control untreated cells.

Flow Cytometry (FC) Analysis

CFs were seeded in a 12-well plate at a density of 5×10^4 cells/well and cultured in growth medium until 70% confluent and then treated as per the *in vitro* drug treatment protocol. CFs were also treated with H_2O_2 for 18 h to provide single stain controls (600 μM H_2O_2 annexin V (AnV) control and 1.5 mM H_2O_2 propidium iodide (PI) control). Once treated, the media from each well was collected into individual FACS tubes. Samples were then dissociated using TrypLE™ Express (37°C) and collected into their respective FACS tubes alongside the previously collected media. Wells were then washed with PBS and added to the corresponding FACS tube to ensure all cells were recovered before being centrifuged at 1,000 g for 5 min. The samples were washed with PBS and 100 μl of AnV binding buffer (BD Biosciences, UK) added to each FACS tube. AnV (BD Biosciences, UK) (5 μl) was then added to all FACS tubes except the control (unstained) and the PI single stain (1.5 mM H_2O_2 treated) samples. The samples were then covered with aluminum foil to omit light and incubated for 15 min at room temperature. Following incubation, 400 μl of 1:500 PI [Thermo Fisher (P3566)] in AnV binding buffer was added to all FACS tubes except the control (unstained) and annexin V single stain (600μM H_2O_2 treated) samples. 400μl of AnV binding buffer was added to the control (unstained) and AnV single stain (750μM H_2O_2 treated) samples. The samples were then analyzed using the BD FACSCanto flow cytometer (BD Biosciences, California, USA) and FlowJo v9 (FlowJo LLC, Oregon, USA).

Western Blotting

For assessing Total-CaMKIIδ and Phos-CaMKII expression, CFs were lysed in 150 μl of LDS sample buffer [25% (v/v) 4× Nu PAGE LDS Sample Buffer (Thermo) and 75 mM DTT] and denatured at 100°C for 5 min. For assessing Ox-CaMKII expression, CFs were lysed in the absence of the reducing agent DTT. Protein lysates were loaded onto 4–20% Mini-PROTEAN TGX Precast Protein Gels and subjected to electrophoresis at 120 V for 110 min in running buffer (3.5 mM SDS, 192 mM glycine, and 25 mM tris base) using a Mini-PROTEAN Tetra chamber (Bio-Rad Laboratories Ltd., UK) at room temperature. Proteins were then transferred to nitrocellulose membranes (0.45 μm pore, GE Healthcare, UK) in transfer buffer [192 mM glycine, 25 mM tris base, 20% (v/v) methanol] using a MiniTrans-Blot Electrophoretic Transfer Cell (Bio-Rad Laboratories Ltd., UK) at a constant current of 280 mA for 110 min at room temperature. Membranes were then blocked in 5% (w/v) BSA in TBS-T [20 mM Tris base, 150 mM NaCl, adjusted to pH = 7.4, and 0.1% (v/v) Tween 20] for 120 min at room temperature. The membranes were then incubated with the appropriate primary antibody in 0.5% (w/v) BSA in TBS-T (0.1%) overnight at 4°C {Ox-CaMKII [1:5,000; Insight biotechnology Limited (GTX36254)]; Phos-CaMKII [1:5,000; Badrilla (A010-50)]; CaMKIIδ [1:5,000; Eurogentec (custom made)]; GAPDH [1;100,000; Abcam (ab8245)]}. Membranes were then washed in TBS-T (0.1% Tween) followed by incubation in the corresponding secondary antibody (1,5,000; Jackson ImmunoResearch, Cambridge, UK [Mouse (715-035-150); Rabbit (111-035-144)] in 0.5% (w/v) BSA in TBS-T (0.1% Tween) for 90 min at room temperature. This was followed by a further wash in TBS-T (0.1% Tween) before being developed *via* enhanced chemiluminescence and exposure onto X-ray film. For re-probing purposes, membranes were stripped in Tris-based buffer (31 mM Tris base, 35 mM SDS containing 0.7%, pH = 6.7). X-ray film was then scanned on a HP Deskjet 2540 printer scanner and densitometry was carried out using Image J software (25). Blotting data was normalized as indicated in the relevant figure legends and samples processed as percentage of control untreated signal.

Intracellular Calcium Release

Cells were seeded into black sided, clear bottomed 96-well plate at a density of 2.5×10^4 cells/well and cultured for 24 h before treatment with sunitinib and imatinib as described previously. Culture medium was aspirated and the cells washed twice with HBSS (136.9 mM NaCl, 5.4 mM KCl, 1.3 mM $CaCl_2$, 0.4 mM $MgSO_4 \cdot 7H_2O$, 0.5 mM $MgCl_2.6H_2O$, 0.3 mM $Na_2HPO_4.2H_2O$, 0.4 mM KH_2PO_4, 5.6 mM glucose, 4.2 mM $NaHCO_3$). Cells were then incubated with 2 μM Fluo4-AM Ca^{2+} indicator dye in Fluo4 buffer [1 mM MgCl, 1.5 mM CaCl, 0.3 mM probenecid, and 0.1% (w/v) BSA in HBSS] for 2 h (37°C, 5% CO_2). Cells were then washed twice with Fluo4 buffer before adding 80 μl of Fluo4 buffer to each well. A compound plate was prepared using the ligands of interest, diluted to 3× the final concentration in Fluo4 buffer. The plate reader transfers 40 μl of compound to each well, diluting the compound 1:3 to reach a 1× desired final concentration for each sample. Fluorescence excitation was then measured using a Flexstation 3 microplate reader (Molecular Devices, Wokingham, UK) at Ex:494/Em:525 nm and SoftMax® Pro software, version 5.4.3.

MitoSOX Live Cell Imaging

MitoSOX fluorescence was recorded on a Nikon TiE inverted epifluorescence microscope with 40× 1.3 NA oil immersion objective, illuminated with 515 nm excitation light (Pe4000 multi-LED; CoolLED, Andover, UK) and emitted light >550 nm selected by dichroic mirror and captured on an ORCA Flash 4.0 CMOS camera (Hamamatsu, Welwyn Garden City, UK). Cell imaging chambers were placed inside a stage-top incubator (H301; OKO labs, Naples, Italy) and maintained at 37°C throughout the imaging process. CFs were seeded into the 8-well chambers at a density of 2.5×10^4 cells/well, cultured in CF growth medium for 24 h and then treated as per the *in vitro* drug treatment protocol. Antimycin A (10 μM) was used as a positive control. The treated samples were then washed with HBSS before being incubated with 3 μM MitoSOX Red for 5 min at room temperature in the absence of light. CFs were recorded for 5 min using WinFluor V4 0.8 live cell imaging software. Signals were normalized by selecting 10 cells from each sample and measuring fluorescence intensity for each cell. A blinded process was used for cell selection. Fluorescence intensity was then measured using ImageJ software (25).

Statistics

Data are presented as mean values ± S.E.M of n observations, where n represents the number of samples. Comparisons

were assessed by one-way ANOVA with *post-hoc* Dunnett's-test using GraphPad Prism (version 7.0a). *P*-values <0.05 were considered significant.

RESULTS

Sunitinib Treatment Alters Cardiac Fibroblast Phenotype

The phenotype of healthy CFs was first established *via* immunohistochemistry and brightfield imaging. Immunohistological staining showed a strong positive stain for vimentin in untreated isolated CFs, consistent with healthy, undifferentiated CFs. To exclude the possibility of contamination with SMCs or ECs, CFs were also stained for smooth muscle cell alpha actin (SMCa) (a marker of smooth muscle cell phenotype) and von Willebrand Factor (vWF) (a marker of endothelial cell phenotype). Staining was compared across CFs, myofibroblasts (MFs), SMCs and ECs. Although a positive stain for both SMCa and vWF was obtained in CFs, staining was significantly less than that obtained in the positive controls for SMCs and of a very different pattern than that seen in the positive controls for HUVECs. Staining was also less than that obtained in the phenotypically transformed MFs (**Figure 1A**).

In order to assess the effects of imatinib and sunitinib on CF phenotype, cells were treated with increasing concentrations of drug (1–10 μM) for 18 h and then subjected to brightfield imaging (**Figure 1B**). Sunitinib-induced changes in CF phenotype were evident at 1 μM sunitinib and became more apparent as concentrations increased. Sunitinib-treated CFs appeared larger and more transparent, with the formation of vacuole-like structures evident in the main cell body. Obvious cell loss was apparent at 10 μM sunitinib. The observed changes in CF phenotype were associated with subtle changes in cell marker expression determined *via* quantitative immunoblotting, although these changes were not statistically significant (data not shown). Imatinib treatment did not have any discernible effect on CF phenotype until much higher concentrations.

Sunitinib Treatment Causes Cardiac Fibroblast Cell Death

To determine whether the changes in phenotype correlated with reduced cell viability, MTT assays and FACS analysis were performed. MTT assays revealed that sunitinib, but not imatinib, reduced CF viability (**Figure 2**). CF viability was significantly reduced at 3 and 10μM sunitinib, consistent with the cell loss observed in brightfield imaging.

Further analysis *via* FACS confirmed these findings. Sunitinib treatment caused a reduction in the number of healthy cells (**Figure 3B**) with a concomitant increase in the number of early and late apoptotic cells at 3 and 10 μM treatments, as well as

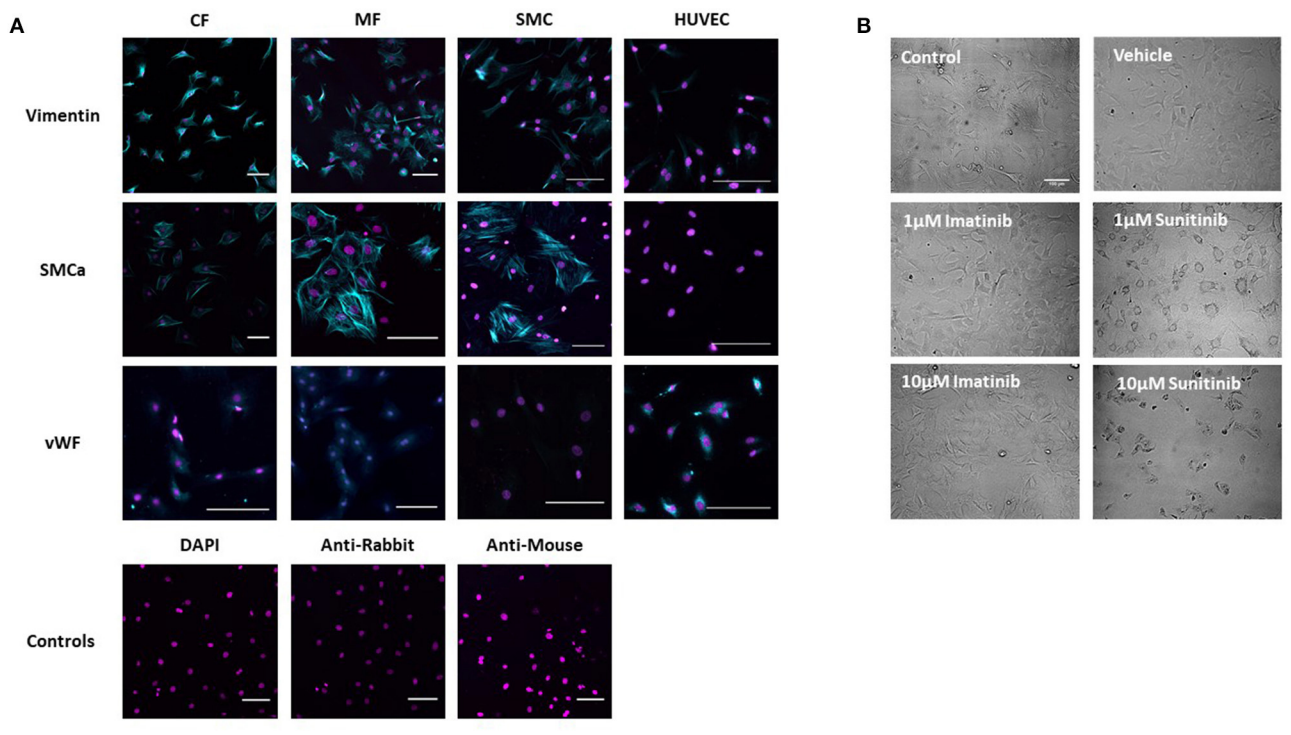

FIGURE 1 | Assessment of Cardiac Fibroblast phenotype. **(A)** CF phenotype was confirmed *via* immunohistochemistry by staining for vimentin, smooth muscle cell alpha actin (SMCa) and von Willebrand Factor (vWF). Staining was compared between CFs and myofibroblasts (MF). Smooth muscle cells (SMC) and human umbilical vein endothelial cells (HUVECs) were used as positive controls. Cells treated with DAPI alone and secondary antibodies alone were used as negative controls. **(B)** Brightfield images showing CF treated with sunitinib and imatinib (0.1–10 μM) for 18 h in the presence of serum. Scale bar 100 μm. Images are from one experiment, representative of two others.

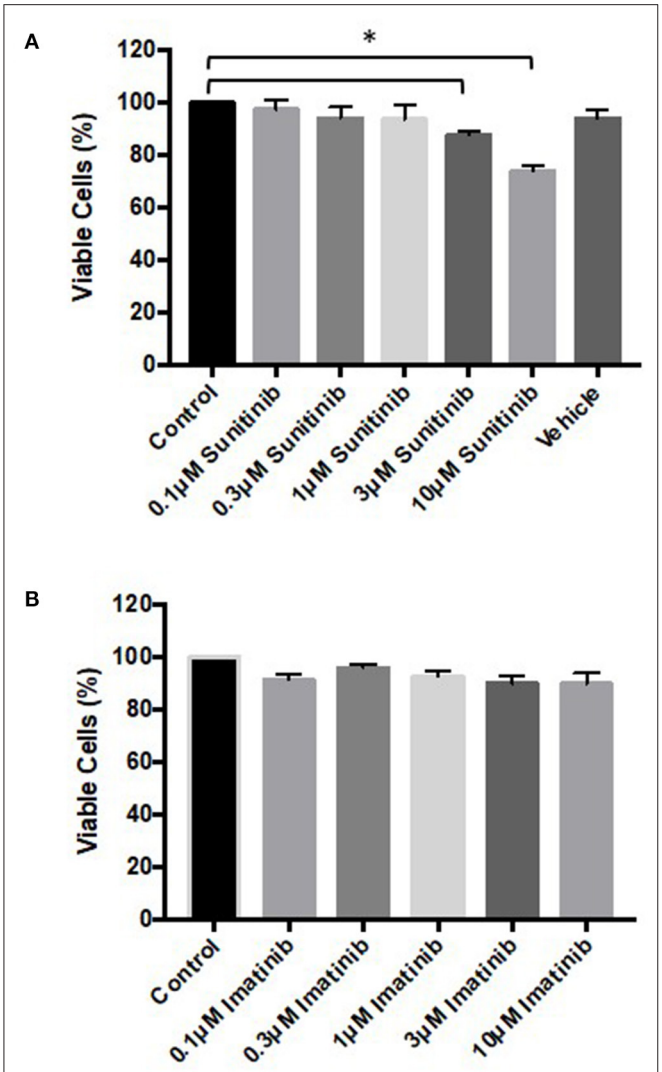

FIGURE 2 | Sunitinib treatment reduces cardiac fibroblast viability. Cells were treated with sunitinib or imatinib (0.1–10 μM) in the presence of serum for 18 h. Cell proliferation was assessed *via* MTT assays. **(A)** Sunitinib treated CF **(B)** imatinib treated CF. Results are expressed as mean ± S.E.M and are normalized to control ($n = 3$, $^*p < 0.05$).

an increase in necrotic cells at 3μM reaching significance for necrosis at 10 μM sunitinib (**Figure 3B**). Imatinib treatment had no significant effect on CF viability (**Figure 4**).

TKI Treatment Increases Angiotensin II-Induced Ca^{2+} Mobilization in Cardiac Fibroblasts

Altered Ca^{2+} handling is known to be associated with cell injury and death. Given the effects of TKI treatment, particularly sunitinib, on CF phenotype and viability (**Figures 1**–**4**), the possibility that either drug may affect Ca^{2+} mobilization in CFs was investigated. The effects of TKI pre-treatment on agonist-induced Ca^{2+} mobilization were examined. We have previously used Angiotensin II (AngII) to induce intracellular Ca^{2+} release in CFs (26) so this was applied to CFs in the current study to elicit responses.

AngII was first applied to CFs across a range of concentrations (0.01–10 μM) to determine a suitable concentration that would elicit a sub-maximal Ca^{2+} release in CFs (**Figures 5A,B**). Ang II at 0.3 μM elicited a rapid release of Ca^{2+} with a peak of ∼80% of maximum. Using this sub-maximal concentration ensured that any subsequent effects of TKI pre-treatment (stimulatory or inhibitory) could be determined. CFs were pre-treated with a range of concentrations of either sunitinib (0.001–1 μM) or imatinib (0.01–1 μM) for 18 h and were then subjected to stimulation with 0.3 μM Ang II to induce Ca^{2+} release. Responses were compared with AngII responses in untreated cells. Cells treated with sunitinib only did not evoke intracellular calcium release (**Figures 5C,F**). Sunitinib pre-treatment resulted in a dose-dependent increase in AngII-evoked Ca^{2+} release (**Figure 5C**) with significance observed at 1 μM sunitinib (**Figures 5D,F**). Imatinib pre-treatment, even at higher concentrations, did not result in any significant effect on AngII-evoked Ca^{2+}release (**Figures 5E,F**).

Sunitinib Treatment Increases Oxidized CaMKII Expression in Cardiac Fibroblasts

The effects of TKI treatment on agonist-induced intracellular Ca^{2+} mobilization, combined with the effects on cell viability, raised the possibility that TKIs may affect Ca^{2+} dependent processes within CFs and, in particular Ca^{2+}-dependent protein activation. Previous work has shown that the Ca^{2+} dependent protein kinase, CaMKII, is activated and expression levels of the delta isoform (CaMKIIδ) are significantly increased in guinea pig cardiac homogenates following *in vivo* infusion of sunitinib and imatinib (22). We therefore examined the effects of chronic (18 h) treatment of CFs with both TKIs (at 1 and 10 μM) on CaMKIIδ expression and CaMKII activation (*via* either phosphorylation or oxidation). TKI treatment of CFs did not alter CaMKIIδ expression (**Figure 6A**) nor was phosphorylation of CaMKII affected. Interestingly though, sunitinib treatment did increase CaMKII activation *via* oxidation at 1 μM sunitinib. There was a subsequent decrease in oxidation at 10 μM sunitinib likely due to cell death as indicated by the lower signal for GAPDH (**Figures 6C,D**). Imatinib treatment had no discernible effect on CaMKII expression or activation.

TKI Treatment Increases Mitochondrial Superoxide Production That Is Reversed With CaMKII Inhibition

Since sunitinib can cause activation of CaMKII *via* oxidation in CFs, we next explored whether TKI treatment may result in elevated levels of reactive oxygen species (ROS) in these cells. Furthermore, we were intrigued to explore the possibility that any TKI-mediated increase in ROS may be *via* CaMKII-mediated effects at the level of the mitochondria. To investigate the possible role of mitochondrial ROS in mediating the cardiotoxic mechanism of TKIs, the mitochondrial superoxide indicator, MitoSOX Red, was used to determine changes in mitochondrial superoxide production.

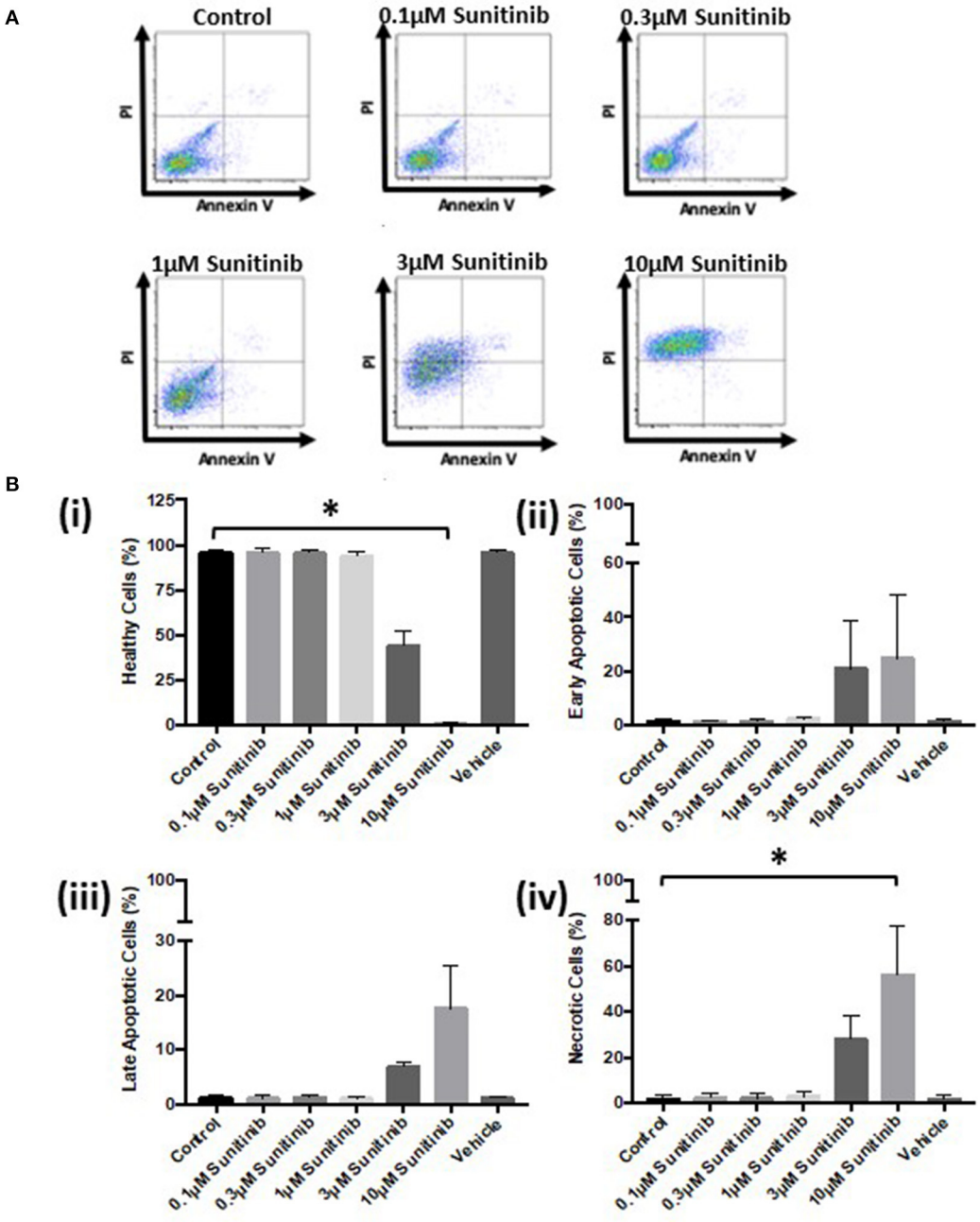

FIGURE 3 | Sunitinib treatment causes increased necrosis in cardiac fibroblasts. Cells were treated with sunitinib (0.1–10 μM) in the presence of serum for 18 h. Cell viability was determined by PI and AnV staining. **(A)** Representative flow cytometry dot plots with double Annexin V-APC/PI staining for cells treated with sunitinib. **(B)** Histograms detailing the percentage of **(i)** healthy **(ii)** early apoptotic **(iii)** late apoptotic and **(iv)** necrotic cells following sunitinib treatment. Results are expressed as mean ± S.E.M ($n = 3$, $^*p < 0.05$).

Live cell imaging revealed that both sunitinib and imatinib significantly increased mitochondrial superoxide production in CFs. This is evident at all concentrations tested and the fold-changes observed following TKI treatment were markedly higher than that observed with the mitochondrial complex III inhibitor Antimycin A, which was used as a positive control for increased superoxide production (**Figures 7A(i),(ii)**). Sunitinib resulted in considerably higher fluorescence than imatinib (**Figures 7B(i)** vs. **7C(i)**), again suggesting the increased potency and cardiotoxic potential of sunitinib when compared with imatinib. Interestingly, when CFs were pre-treated with the CaMKII inhibitor KN-93, sunitinib-mediated superoxide production was significantly reduced (**Figure 8A**). Moreover, in cells treated with 10 μM imatinib,

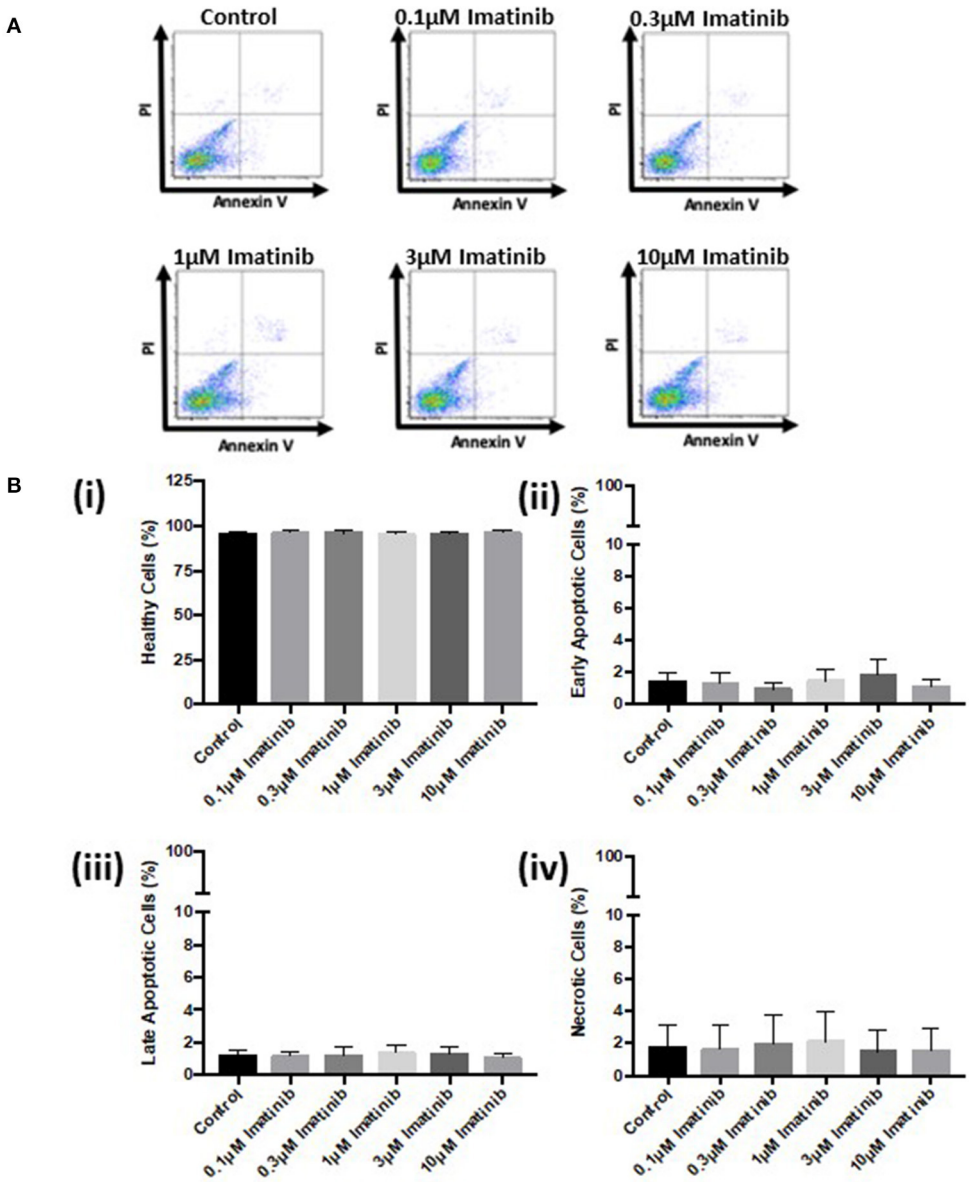

FIGURE 4 | Imatinib treatment does not cause apoptosis or necrosis in cardiac fibroblasts. Cells were treated with imatinib (0.1–10 μM) in the presence of serum for 18 h. Cell viability was then determined by PI and AnV staining. **(A)** Representative flow cytometry dot plots with double Annexin V-APC/PI staining for cells treated with sunitinib. **(B)** Histograms detailing the percentage of **(i)** healthy **(ii)** early apoptotic **(iii)** late apoptotic and **(iv)** necrotic cells following imatinib treatment. Results are expressed as mean ± S.E.M ($n = 3$).

KN-93 pre-treatment completely abolished imatinib-induced mitochondrial superoxide production (**Figure 8B**).

DISCUSSION

In the current study we have evaluated the effects of sunitinib and imatinib on both phenotype and function of adult rat CFs to gain insight into possible mechanisms underlying the cardiotoxic profiles of both drugs in the non-contractile fibroblasts of the heart. Effects on cell phenotype, viability, intracellular Ca^{2+} release and mitochondrial superoxide production were assessed and, for the first time, a potential role for CaMKII activation *via* oxidation as an underlying mechanism of action of sunitinib in CFs was highlighted. Interestingly, but unsurprisingly, sunitinib and imatinib exerted differential effects on CFs and this may provide an indication of the broader cardiotoxic potential of each drug.

Initial characterization of CFs was performed using immunocytochemistry and this revealed distinct vimentin staining of CFs with low levels of SMCa and altered distribution of vWF confirming results from previous studies (27, 28). Importantly, the distinction between CFs and MFs was

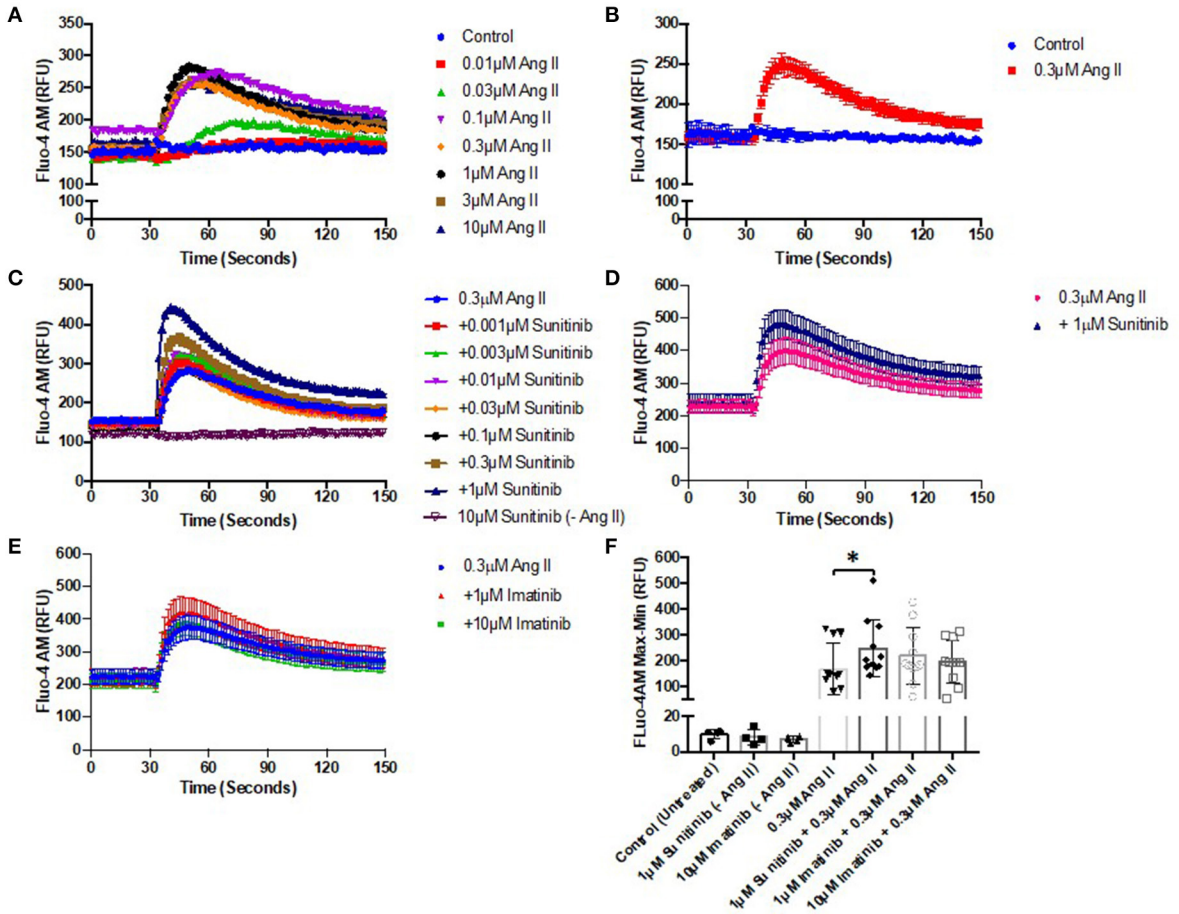

FIGURE 5 | Sunitinib increases Angiotensin II—induced Ca^{2+} mobilization in cardiac fibroblasts. **(A)** Effect of increased AngII concentrations (0.01–10 μM) on intracellular Ca^{2+} mobilization **(B)** Representative trace of Ca^{2+} mobilization in response to 0.3 μM AngII stimulation **(C)** Effects of increasing concentrations of sunitinib (0.001–1 μM) on AngII induced Ca^{2+} mobilization. Sunitinib in the absence of Ang II is also shown. Results shown are mean data from one experiment, representative of five other experiments. **(D)** Comparison of maximal (1 μM) sunitinib Ang II-induced Ca^{2+} mobilization vs. control. **(E)** Effects of increasing concentrations of imatinib (1–10 μM) on AngII induced Ca^{2+} mobilization. **(F)** Effects of TKI-treatment on peak agonist-induced Ca^{2+} mobilization. Calcium mobilization was determined by measuring fluorescence at Ex:494/Em:525 nm. Results are expressed as mean ± S.E.M of 6 biological replicates, $^*p < 0.05$.

highlighted with a clear difference in phenotype and SMCa staining across the two (**Figure 1A**). Treatment of CFs with sunitinib and imatinib at relatively low concentrations (1–10 μM) and in the presence of serum enabled a realistic assessment of the potential for these drugs to affect CF phenotype and performance in the clinical setting. Previous investigations have often used much higher concentrations of drugs which may not be clinically relevant (29) and very few studies have assessed the effects on CFs (11). Sunitinib induced clear alterations in cell phenotype and viability at concentrations as low as 1 μM whereas imatinib effects were less pronounced and phenotypic changes only started to become evident at a 10-fold higher concentration. This pattern was maintained when the effects of both drugs on cell viability were studied in more detail. Using MTT assays and FACS analysis, a sunitinib-induced reduction in viability was observed at 3 and 10 μM with significant levels of necrosis occurring at 10 μM (**Figures 2**, **3**). There were no significant effects of imatinib at any of the concentrations tested (**Figures 2**, **4**). These observations fit with the differences observed in cardiotoxicity reported for these drugs in the clinic (29–31). Differences in % viability were detected across MTT and flow cytometry and this reflects the differences in sensitivity between both assays. Importantly, imatinib did not induce any measurable change in viability assessed via either assay.

Previous work by our group has highlighted that acute and chronic treatment of guinea pigs with sunitinib and imatinib can alter the expression and/or activity of CaMKII measured in ventricular cardiac homogenates (22). CaMKII is well-established as a pivotal molecule in cardiac physiology regulating cellular processes such as excitation-contraction coupling, cellular mechanics and energetics (32, 33). CaMKII is also recognized as an important mediator of pathological signaling and remodeling in disease (34, 35). As well as a recognized role in cardiomyocyte physiology and pathophysiology, a role for CaMKII in CF dysfunction has also been highlighted (27). The

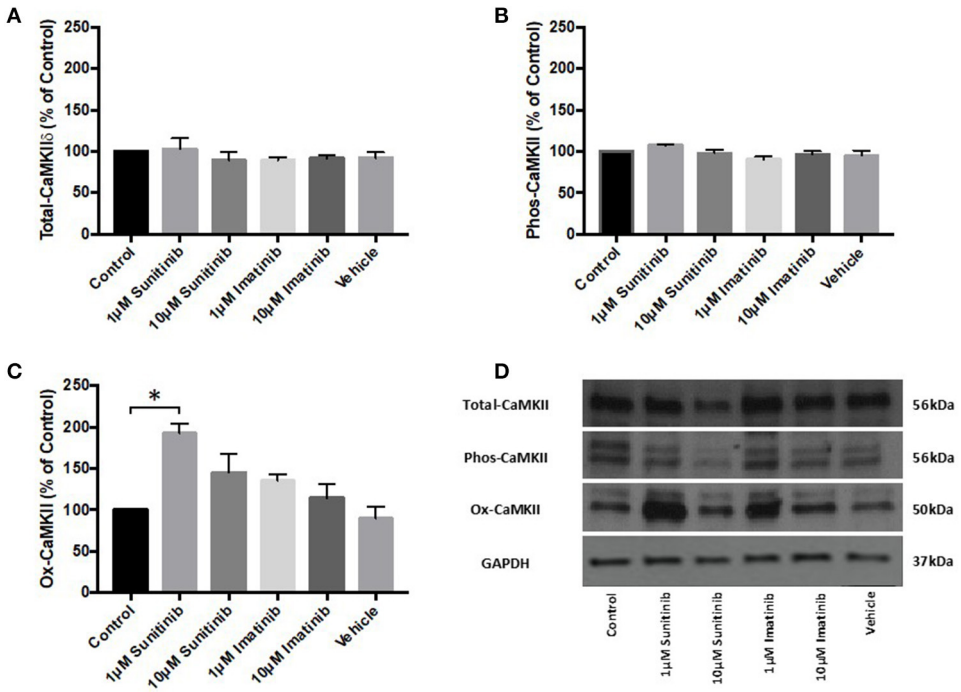

FIGURE 6 | Sunitinib treatment increases ox-CaMKII expression in cardiac fibroblasts. Following the indicated treatments with either sunitinib or imatinib, CaMKIIδ expression or CaMKII activation *via* phosphorylation or oxidation was determined *via* quantitative immunoblotting **(A)** CaMKIIδ expression, normalized to GAPDH **(B)** Phos-CaMKII expression, normalized to CaMKIIδ **(C)** Ox-CaMKII expression, normalized to CaMKIIδ **(D)** Representative immunoblot showing CaMKIIδ expression and CaMKII activation following TKI treatment. Results are expressed as mean ratios protein: GAPDH ± S.E.M and are normalized to control ($n = 3$, $^*p < 0.05$).

possibility that sunitinib and/or imatinib might alter CaMKII activity in CFs has not previously been explored but this could be a central factor contributing to the underlying mechanism of cardiotoxicity. In particular, given the contribution that CFs have to extracellular matrix deposition and to cardiac myocyte function, detrimental effects on CF viability by TKIs could impact directly upon cardiac contractility leading in particular to impaired diastolic function. Interestingly, sunitinib was able to increase AngII-mediated intracellular Ca^{2+} release and this trend was evident at all concentrations of sunitinib tested (0.001–1 μM), becoming significant at 1 μM. Lower concentrations were used in these experiments to closely mirror plasma concentrations that are seen in patients (24, 36) and to investigate whether intracellular signaling (in the form of Ca^{2+} release) may be more sensitive to drug-induced effects than those effects observed phenotypically and functionally. Although imatinib appeared to increase intracellular Ca^{2+}, this effect was not significant even up to 10 μM imatinib. This raises the potential that sunitinib (and possibly imatinib) may have for exacerbating Ca^{2+}-activated responses. The contribution that excess Ca^{2+} release has toward apoptosis and necrosis is well-documented (37, 38). Sustained CaMKII activation is a central feature of these pathological processes and the enzyme is initially activated in response to increased intracellular [Ca^{2+}]. CaMKII can also be activated by post-translational modifications downstream of Ca^{2+}/calmodulin binding. This can include autophosphorylation, oxidation, *S*-nitrosylation and *O*-GlcNAcylation. All of these modifications can occur during sustained and pathological activation (39). Here, for the first time, we have investigated the ability of both sunitinib and imatinib to induce either phosphorylation or oxidation of CaMKII. As well as the possibility that both drugs may activate CaMKII *via* elevations in intracellular Ca^{2+}, data shown here suggest that sunitinib can also cause oxidation of CaMKII in CFs (**Figure 6**). Oxidation of CaMKII is able to alter the Ca^{2+} sensitivity of the enzyme enabling activation at low intracellular [Ca^{2+}] and sustaining activity in the absence of Ca^{2+}/calmodulin (40, 41) and this may be a means by which the cardiotoxic effects of CaMKII are harnessed by certain anti-cancer drugs. This mode of activation of CaMKII may be a distinguishing feature in differences in mechanism of action between the two TKIs although this would require further investigation. Interestingly, CaMKII has been linked to activation of a regulated form of necrosis, termed necroptosis (33). Necroptosis can be triggered *via* activation of receptor-interacting protein (RIP3) which has CaMKII as a substrate, and it has been shown that disruption of either RIP3 or CaMKII can significantly reduce cell death (42). Here we have shown that sunitinib can induce necrosis (we have not assessed necroptosis) and can activate CaMKII. It is possible that the two processes are linked in the mechanism of action of sunitinib-induced cardiotoxicity in CFs.

Since increased oxidation of CaMKII was evident following sunitinib treatment, we investigated whether either sunitinib

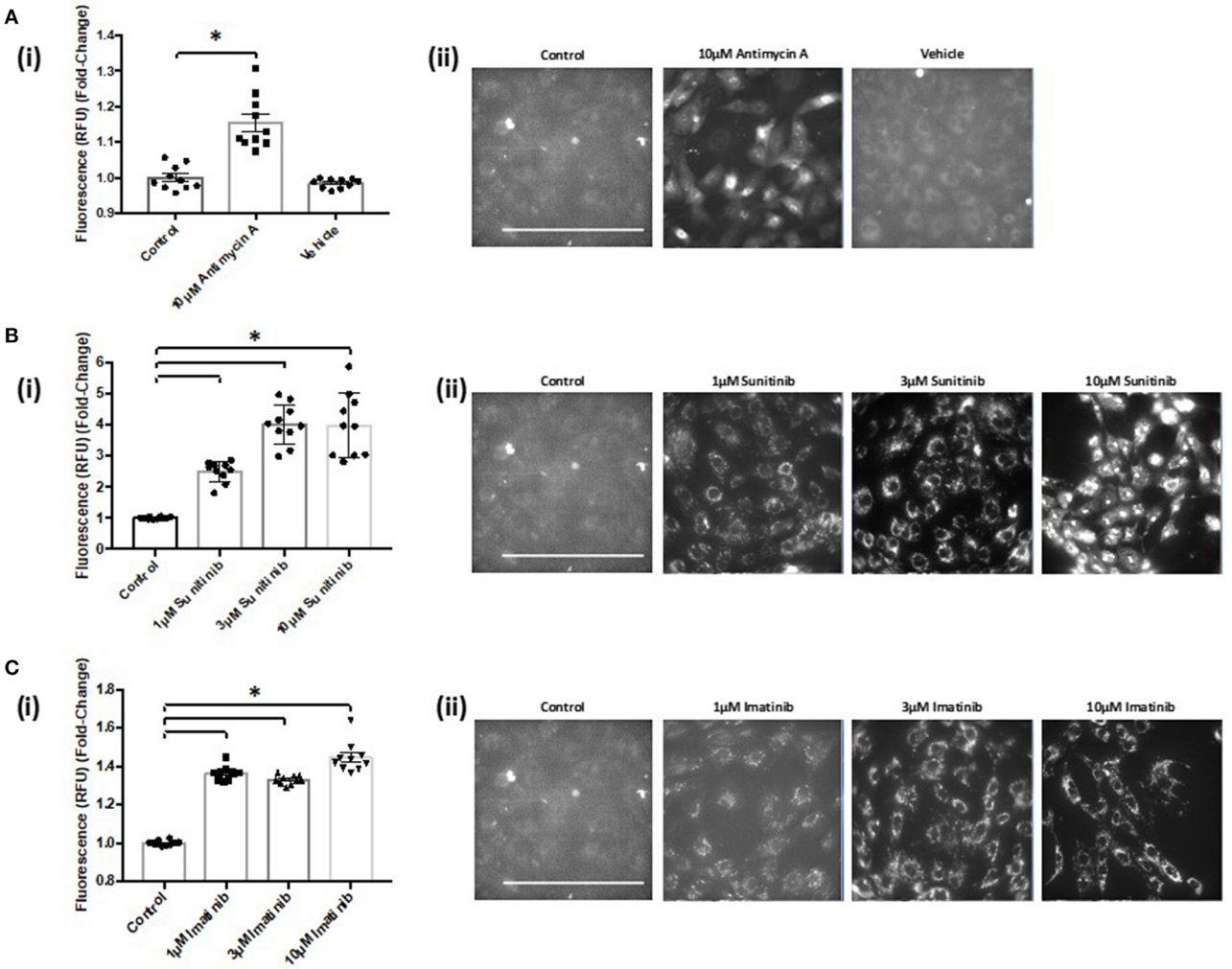

FIGURE 7 | Sunitinib and imatinib treatments both cause increased mitochondrial superoxide production in cardiac fibroblasts. **(Ai)** Histogram showing superoxide production assessed via fluorescence intensity in antimycin A and vehicle treated CFs **(Aii)** Representative images of MitoSOX Red analysis of antimycin A and vehicle treated samples. **(Bi)** Superoxide production assessed via fluorescence intensity in sunitinib treated CFs **(Bii)** Representative images of MitoSOX Red analysis of sunitinib treated samples. **(Ci)** Superoxide production assessed via fluorescence intensity in imatinib treated CFs **(Cii)** Representative images of MitoSOX Red analysis of imatinib treated samples. Scale bar 100 μm. Results shown are mean data from one experiment ($n = 10$), representative of two other experiments (*$p < 0.05$).

or imatinib treatment could result in increased levels of mitochondrial superoxide. Although the role of ROS in cardiac pathophysiology remains unclear, ROS have been implicated in a variety of processes that affect cardiac function, both contractile and non-contractile processes (43, 44). While ROS have been implicated in the pathogenesis of anthracycline induced cardiotoxicity, there is less evidence of the effects of ROS in TKI-induced cardiotoxicity, particularly relating to effects on non-contractile cells of the heart. Importantly, current evidence suggests that anti-oxidant therapy does not offer cardioprotection against anthracycline-induced cardiotoxicity (5). Therefore, a better understanding of how ROS production may be mediated by anti-cancer agents and relate to cardiotoxic effects is required. Here we have shown that both sunitinib and imatinib can induce significant increases in mitochondrial superoxide in CFs following 18 h treatment and this occurs across all concentrations tested (1–10 μM) (**Figure 7**). Interestingly, when we pre-treat CFs with a CaMKII inhibitor (KN-93) and repeat TKI treatment at the highest concentrations of TKI tested (10 μM), the effects of both sunitinib and imatinib on mitochondrial superoxide production are abrogated (**Figure 8**). It is likely that KN-93 will inhibit global CaMKII in the CF and this may explain why we see an effect on imatinib induced superoxide production in the absence of any quantifiable CaMKII activation in this study. These results highlight that interventions interfering with CaMKII targeting to the mitochondria or with CaMKII oxidation are worthy of further study. Methionine sulfoxide reductase A (MsrA)

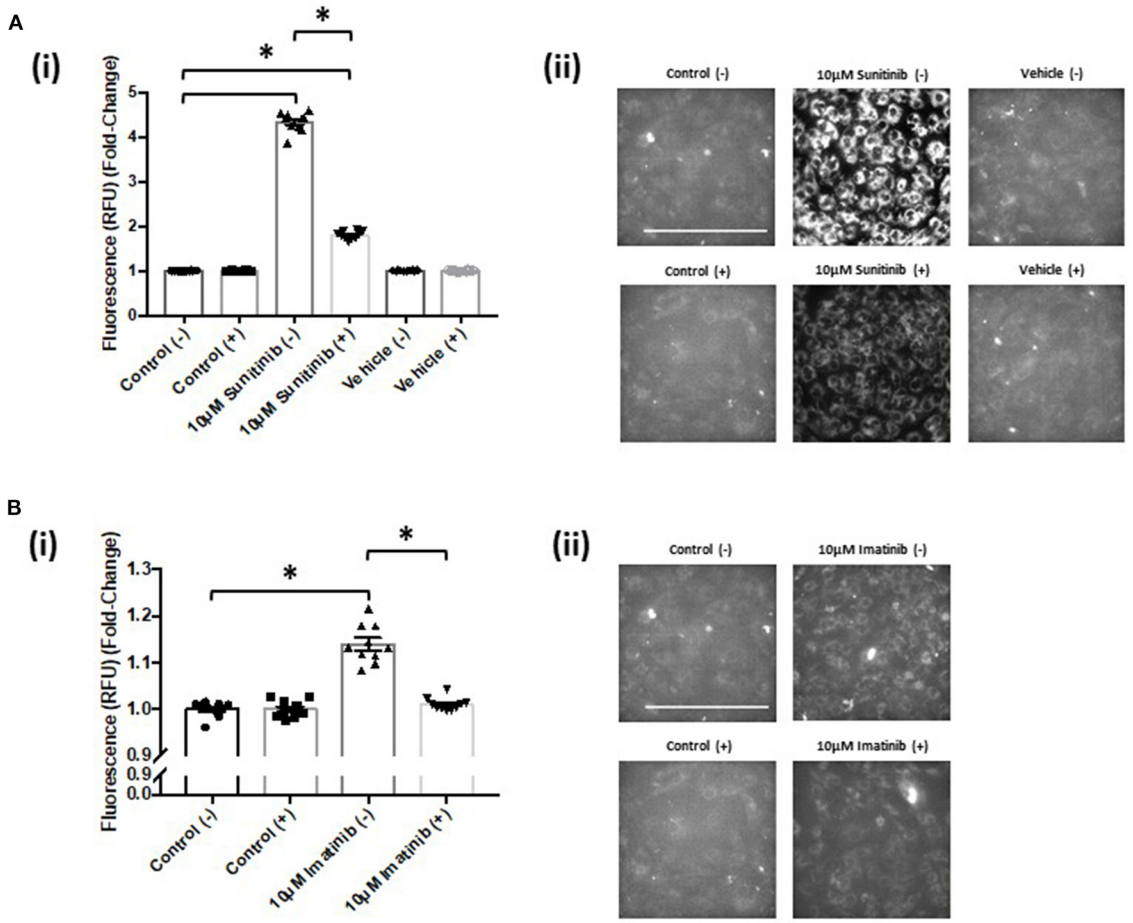

FIGURE 8 | KN-93 reduces mitochondrial superoxide production in both sunitinib and imatinib treated cardiac fibroblasts. **(Ai)** Superoxide production assessed *via* fluorescence intensity in sunitinib treated CF in the presence (+) or absence (–) of 5 μM KN-93. **(Aii)** Representative images of MitoSOX Red analysis of sunitinib treated samples in the presence (+) or absence (–) of KN-93. **(Bi)** Superoxide production assessed *via* fluorescence intensity in imatinib treated CF in the presence (+) or absence (–) of KN-93. **(Bii)** Representative images of MitoSOX Red analysis of imatinib treated samples in the presence (+) or absence (–) of KN-93. Scale bar 100 μm. Results shown are mean data and images from one experiment where the same control (–) presented previously for non-KN 93 treatment has been used as a reference comparison for control (+) ($n = 10$). Imatinib and sunitinib treatments from the same experiment have been presented separately for clarity and are representative of two other experiments (*$p < 0.05$).

can reduce oxidized CaMKII and could be a promising target to limit TKI-induced oxidative stress (40). It is possible that sunitinib-induced effects on CaMKII oxidation and superoxide production are not mutually exclusive and one may exacerbate the other driving toxicity (**Figure 9**). These mitochondrial events are already known to be a central feature of myocardial disease (45).

Recent work using transgenic mice and computational modeling has shown that myocardial infarction surgery causes significant elevation of mitochondrial CaMKII along with left ventricular dilatation. Pathological remodeling is reversed in mice with genetic mitochondrial CaMKII inhibition (46). The significance of mitochondrial targeted CaMKII activation and inhibition in the switch between normal function and pathological consequences is striking and is pertinent to the results presented in the current study.

CONCLUSION

For the first time we have demonstrated differential cardiotoxic effects in adult CFs in response to sunitinib and imatinib at low, clinically relevant concentrations of each drug. We have shown that sunitinib is capable of mediating an increase in agonist-induced $[Ca^{2+}]_i$ and can activate CaMKII *via* oxidation. Both drugs lead to significant elevation of mitochondrial superoxide production and this is reversed in the presence of CaMKII inhibition. The implications of these results suggest that TKI-mediated cardiotoxicity could be reduced or reversed *via* targeted CaMKII inhibition. Development of CaMKII inhibitors to target heart disease is already ongoing. The use of more targeted CaMKII inhibitors in the treatment of anti-cancer drug cardiotoxicity could be an additional niche area for the pharmaceutical industry and fundamentally, could

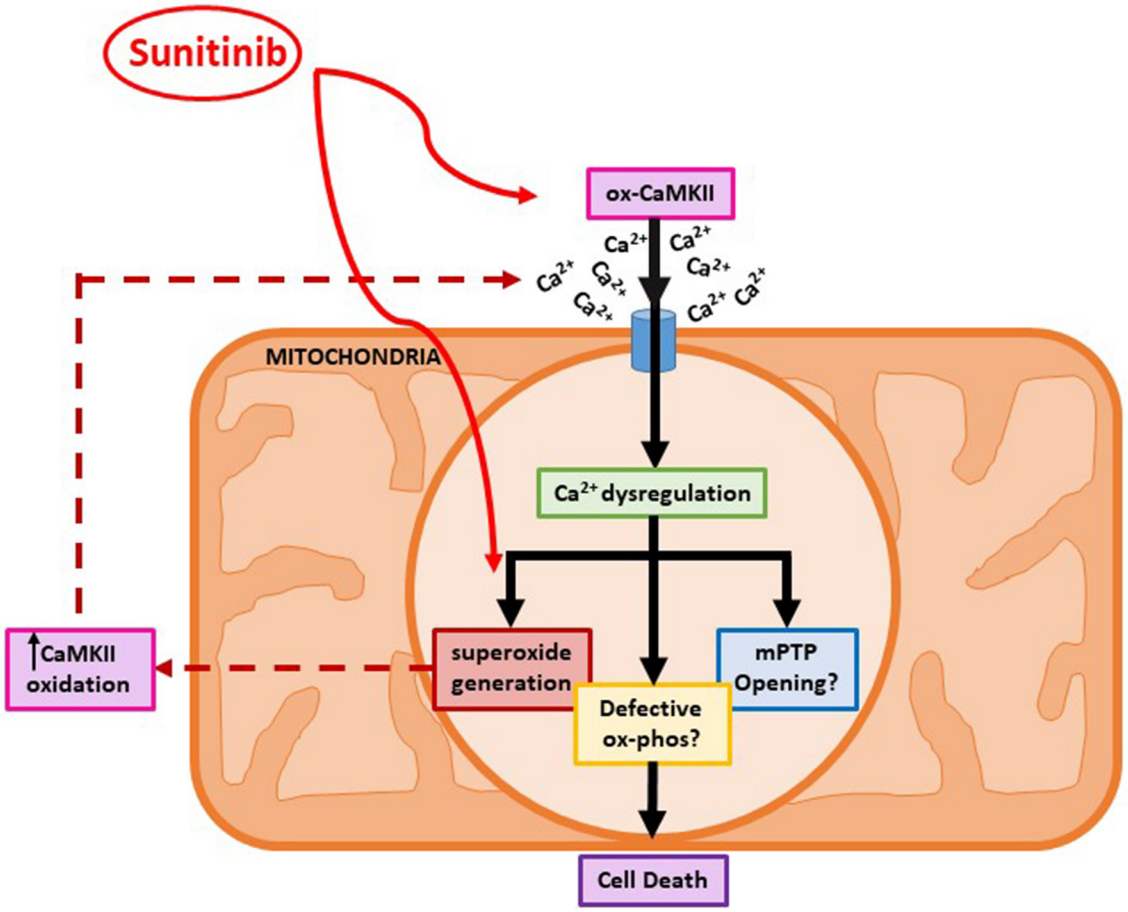

FIGURE 9 | A proposed mechanism for sunitinib-induced mitochondrial dysfunction in adult cardiac fibroblasts. Schematic showing proposed sunitinib-induced events at the level of the mitochondria in CFs. Sunitinib treatment may exert direct effects on mitochondrial superoxide production that can then result in CaMKII oxidation. Sunitinib-induced increases in CaMKII oxidation and activation can then go on to cause elevated superoxide production so a positive feedback loop may exist exacerbating the cardiotoxic effects. The combination of elevated CaMKII oxidation and increased superoxide production ultimately causes toxicity at the level of the mitochondria and can contribute to CF cell death.

represent a new and important therapeutic approach in the field of cardio-oncology.

DATA AVAILABILITY STATEMENT

The raw data supporting the conclusions of this article will be made available by the authors, without undue reservation.

AUTHOR CONTRIBUTIONS

SCu and MC worked on the conception and organization of the research project. Experimental work was conducted predominantly by CM. Data analysis was conducted by CM, SCh, RW, and MC. SCu and CM wrote the first draft of the manuscript. MC and SCh reviewed the manuscript. All authors read and approved the final version of the manuscript.

FUNDING

This work was supported by a Princess Royal Scholarship (Tenovus Scotland) to CM (S170866).

ACKNOWLEDGMENTS

We would like to thank Dr. Augusto Montezano and Dr. Livia De Lucca Canargo, University of Glasgow, for the gift of primary smooth muscle cells for our study. We would also like to thank Graeme Mackenzie and Margaret MacDonald for their technical assistance with this work. Thanks also to Brian Leiper, Carol Whitehouse, Lee Wheeler, and Peter Conte for their assistance with the animal husbandry.

REFERENCES

1. Curigliano G, Cardinale D, Dent S, Criscitiello C, Aseyev O, Lenihan D, et al. Cardiotoxicity of anti-cancer treatments: epidemiology, detection and management. *CA Cancer J Clin*. (2016) 66:309–25. doi: 10.3322/caac.21341
2. Carver JR, Shapiro CL, Ng A, Jacobs L, Schwartz C, Virgo KS, et al. American society of clinical oncology clinical evidence review on the ongoing care of adult cancer survivors: cardiac and pulmonary late effects. *J Clin Oncol*. (2007) 25:3991–4008. doi: 10.1200/JCO.2007.10.9777
3. Henri C, Heinonen T, Tardif JC. The role of biomarkers in decreasing risk of cardiac toxicity after cancer therapy. *Biomarkers Cancer*. (2016) 8:39–45. doi: 10.4137/BIC.S31798
4. Kilickap S, Barista I, Akgul E. cTnT can be a useful marker for early detection of anthracycline cardiotoxicity. *Ann Oncol*. (2005) 16:798–804. doi: 10.1093/annonc/mdi152
5. Angsutararux P, Luanpitpong S, Issaragrisil S. Chemotherapy-induced cardiotoxicity: overview of the roles of oxidative stress. *Oxid Med Cell Longev*. (2015) 2015:795602. doi: 10.1155/2015/795602
6. Gambardella J, Trimarco B, Iaccarino G, Sorriento D. Cardiac nonmyocyte cell functions and crosstalks in response to cardiotoxic drugs. *Oxid Med Cell Longev*. (2017) 2017:1089359. doi: 10.1155/2017/1089359
7. Camelliti P, Borg TK, Kohl P. Structural and functional characterisation of cardiac fibroblast. *Cardiovasc Res*. (2005) 65:40–51. doi: 10.1016/j.cardiores.2004.08.020
8. Porter KE, Turner NA. Cardiac fibroblasts: at the heart of myocardial remodelling. *Pharmacol Therap*. (2009) 123:255–78. doi: 10.1016/j.pharmthera.2009.05.002
9. Narikawa M, Umemura M, Tanaka R, Hikichi M, Nagasako A, Fujita T, et al. Doxorubicin induces trans-differentiation and MMP1 expression in cardiac fibroblasts *via* cell death-independent pathways. *PLoS ONE*. (2019) 14:e0221940. doi: 10.1371/journal.pone.0221940
10. CJ McMullen, C McCluskey, SJ Kim, Laovitthayanggoon S, MacDonald M, Safar M, et al. Anti-cancer tyrosine kinase inhibitors increase oxidative stress in primary cardiac fibroblasts. *Heart J*. (2018) 104:4.SCF22. doi: 10.1136/heartjnl-2018-SCF.22
11. Burke MJ, Walmsley R, Munsey TS, Smith AJ. Receptor tyrosine kinase inhibitors cause dysfunction in adult rat cardiac fibroblasts *in vitro*. *Toxicol In Vitro*. (2019) 58:178–86. doi: 10.1016/j.tiv.2019.03.026
12. Chen MH, Kerkela R, Force T. Mechanisms of cardiac dysfunction associated with tyrosine kinase inhibitor cancer therapies. *Circulation*. (2008) 118:84–95. doi: 10.1161/CIRCULATIONAHA.108.776831
13. Cheng H, Force T. Why do kinase inhibitors cause cardiotoxicity and what can be done about it? *Circ Res*. (2010) 106:21–34. doi: 10.1016/j.pcad.2010.06.006
14. Beininger M, Buchdunger E, Druker BJ. The development of imatinib as a therapeutic agent for chronic myeloid leukaemia. *Blood*. (2005) 105:2640–53. doi: 10.1182/blood-2004-08-3097
15. Kerkela R, Grazette L, Yacobi R, Illiescu C, Patten R, Beahm C. et al. Cardiotoxicity of the cancer therapeutic agent imatinib mesylate. *Nat Med*. (2006) 12:908–16. doi: 10.1038/nm1446
16. Wenyue Hu, Lu S, McAlpine I, Jamieson JD, Lee DU, Marroquin L, et al. Mechanistic investigation of imatinib-induced cardiac toxicity and the involvement of c-Abl kinase. *Toxicol Sci*. (2012) 129:188–99. doi: 10.1093/toxsci/kfs192
17. Atallah E, Durand JB, Kantarjian H, Cortes J. Congestive heart failure is a rare event in patients receiving imatinib therapy. *Blood*. (2007) 110:1233–7. doi: 10.1182/blood-2007-01-070144
18. Hatfield A, Owen S, Pilot PR. In reply to cardiotoxicity of the cancer therapeutic agent imatinib mesylate. *Nat Med*. (2007) 13:15–6. doi: 10.1038/nm0107-13a
19. Chen Z, Ai D. Cardiotoxicity associated with targeted anti-cancer therapies. *Mol Clin Oncol*. (2016) 4:675–81. doi: 10.3892/mco.2016.800
20. Rock EP, Goodman V, Jiang JX, Mahjoob K, Verbois SL, Morse D, et al.. Food and drug administration drug approval summary: Sunitinib malate for the treatment of gastrointestinal stromal tumor and advanced renal cell carcinoma. *Oncologist*. (2007) 12:107–13. doi: 10.1634/theoncologist.12-1-107
21. Kerkela R, Woulfe KC, Durand JB, Vagnozzi R, Kramer D, Chu TF, et al. Sunitinib-induced cardiotoxicity is mediated by off-target inhibition of AMP-activated protein kinase. *Clin Transl Sci*. (2009) 2:15–25. doi: 10.1111/j.1752-8062.2008.00090.x
22. Mooney L, Skinner M, Coker SJ, Currie S. Effects of acute and chronic sunitinib treatment on cardiac function and calcium/calmodulin dependent protein kinase II. *Br J Pharmacol*. (2015) 172:4342–54. doi: 10.1111/bph.13213
23. Lawan A, Al-Harthi S, Cadalbert L, McCluskey AG, Grant A, Boyd M, et al. Genetic deletion of the DUSP-4 gene reveals an essential non-redundant role for MKP-2 in cell survival. *J Biol Chem*. (2011) 286:12933–43. doi: 10.1074/jbc.M110.181370
24. Kitagawa D, Yokota K, Gouda M, Narumi Y, Ohmoto H, Nishiwaki E, et al. Activity-based kinase profiling of approved tyrosine kinase inhibitors. *Genes Cells*. (2013) 18:110–22. doi: 10.1111/gtc.12022
25. Schneider CA, Rasband WS, Eliceiri KW. NIH Image to ImageJ: 25 years of image analysis. *Nat Methods*. (2012) 9:671–5. doi: 10.1038/nmeth.2089
26. Currie S, Martin TP, Salleh H, McCluskey C, Bushell TJ. IP3R contribution to ventricular cardiac fibroblast function in healthy and hypertrophied mouse hearts. *FASEB J*. (2016) 30:S1–1178.2.
27. Martin TP, Lawan A, Robinson E, Grieve DJ, Plevin RJ, Paul A, et al. Adult cardiac fibroblast proliferation is modulated by calcium/calmodulin dependent protein kinase II in normal and hypertrophied hearts. *Pflugers Arch*. (2014) 466:319–30. doi: 10.1007/s00424-013-1326-9
28. Martin TP, McCluskey C, Cunningham MR, Beattie J, Paul A, Currie S. Calcium/calmodulin dependent protein kinase II delta interacts with IKKβ and modulates NFκB signalling in mouse heart. *Cell Signall*. (2018) 51:166–75. doi: 10.1016/j.cellsig.2018.07.008
29. Will Y, Dykens JA, Nadanaciva S, Hirakawa B, Jamieson J, Marroquin LD. et al. Effect of the multitargeted tyrosine kinase inhibitors imatinib, dasatinib, sunitinib and sorafenib on mitochondrial function in isolated rat heart mitochondria and H9c2 cells. *Toxicol Sci*. (2008) 106:153–61. doi: 10.1093/toxsci/kfn157
30. Wolf A, Couttet P, Dong M, Grenet O, Heron M, Junker U, et al. Imatinib does not induce cardiotoxicity at clinically relevant concentrations in preclinical studies. *Leuk Res*. (2010) 34:1180–8. doi: 10.1016/j.leukres.2010.01.004
31. Mellor HR, Bell AR, Valentin JP, Roberts RRA. Cardiotoxicity associated with targeting kinase pathways in cancer. *Toxicol Sci*. (2011) 120:14–32. doi: 10.1093/toxsci/kfq378
32. Bers DM. Calcium cycling and signalling in cardiac myocytes. *Ann Rev Physiol*. (2008) 70:23–49. doi: 10.1146/annurev.physiol.70.113006.100455
33. Beckendorf J, van den Hoogenhof MMG, Backs J. Physiological and unappreciated roles of CaMKII in the heart. *Bas Res Cardiol*. (2018) 113:29–41. doi: 10.1007/s00395-018-0688-8
34. Anderson ME, Brown JH, Bers DM. CaMKII in myocardial hypertrophy and heart failure. *J Mol Cell Cardiol*. (2011) 51:468–73. doi: 10.1016/j.yjmcc.2011.01.012
35. Backs J, Backs T, Neef S, Kreusser MM, Lehmann LH, Patrick DM, et al. The delta isoform of CaM kinase II is required for pathological cardiac hypertrophy and remodelling after pressure overload. *Proc Natl Acad Sci USA*. (2009) 106:2342–7. doi: 10.1073/pnas.0813013106
36. Lankheet NA, Knapen LM, Schellens JH, Beijnen JH, Steeghs N, Huitema AD. Plasma concentrations of tyrosine kinase inhibitors imatinib, erlotinib and suntinib in routine clinical outpatient cancer care. *Ther Drug Monit*. (2014) 36:326–34. doi: 10.1097/FTD.0000000000000004
37. Li GY, Fan B, Zheng YC. Calcium overload is a critical step in programmed necrosis of ARPE-19 cells induced by high concentrations of H2O2. *Biomed Envtl Sci*. (2010) 23:371–7. doi: 10.1016/S0895-3988(10)60078-5
38. Pinton P, Giorgi C, Siviero R, Zecchini E, Rizzuto R. Calcium and apoptosis. ER-mitochondrial calcium transfer in the control of apoptosis. *Oncogene*. (2008) 27:6407–18. doi: 10.1038/onc.2008.308
39. Mollova MY, Katus HA, Backs J. Regulation of CaMKII signalling in cardiovascular disease. *Front Pharmacol*. (2015) 6:178. doi: 10.3389/fphar.2015.00178
40. Erickson JR, Joiner MA, Guan X, Kutschke W, Yang J, Oddis CV, et al. A dynamic pathway for calcium-independent activation of CaMKII by methionine oxidation. *Cell*. (2008) 133:462–74. doi: 10.1016/j.cell.2008.02.048

41. Palomeque J, Rueda OV, Sapia L, Valverde CA, Salas M, Petroff MV. Angiotensin II induced oxidative stress resets the Ca2+ dependence of CaMKII and promotes a death pathway conserved across different species. *Circ Res*. (2009) 105:1204–12. doi: 10.1161/CIRCRESAHA.109.204172
42. Zhang T, Zhang Y, Cui M, Jin L, Wang Y, Lv F, et al. CaMKII is a RIP3 substrate mediating ischemia and oxidative stress-induced myocardial necroptosis. *Nat Med*. (2016) 22:175–82. doi: 10.1038/nm.4017
43. Giordano FJ. Oxygen, oxidative stress, hypoxia and heart failure. *J Clin Inv*. (2015) 115:500–8 doi: 10.1172/JCI200524408
44. Mercurio V, Cuomo A, Dessalvi CC, Deidda M, Di Lisi D, Novo G et al. Redox imbalances in ageing and metabolic alterations: implications in cancer and cardiac diseases. An overview from the working group of cardiotoxicity and cardioprotection of the Italian society of cardiology (SIC). *Antioxidants*. (2020) 9:641. doi: 10.3390/antiox9070641
45. Luo M, Anderson ME. Mechanisms of altered Ca^{2+} handling in heart failure. *Circ Res*. 113:690–708. doi: 10.1161/CIRCRESAHA.113.301651
46. Luczak ED, Wu Y, Granger JM, Joiner MA, Wilson NR, Gupta A. Mitochondrial CaMKII causes adverse metabolic reprogramming and dilated cardiomyopathy. *Nat Commun*. (2020) 11:4416. doi: 10.1038/s41467-020-18165-6

Conflict of Interest: The authors declare that the research was conducted in the absence of any commercial or financial relationships that could be construed as a potential conflict of interest.

frontiers in Cardiovascular Medicine

MINI REVIEW
published: 03 February 2021
doi: 10.3389/fcvm.2021.619650

Immune Checkpoint Inhibitors: Cardiotoxicity in Pre-clinical Models and Clinical Studies

Shirley Xu[1,2], *Umesh C. Sharma*[2], *Cheyanna Tuttle*[1] *and Saraswati Pokharel*[1]*

[1] Division of Thoracic Pathology and Oncology, Department of Pathology, Roswell Park Comprehensive Cancer Center, Buffalo, NY, United States, [2] Department of Medicine, Jacob's School of Medicine and Biomedical Sciences, University at Buffalo, Buffalo, NY, United States

Since the approval of the first immune checkpoint inhibitor (ICI) 9 years ago, ICI-therapy have revolutionized cancer treatment. Lately, antibodies blocking the interaction of programmed cell death protein (PD-1) and ligand (PD-L1) are gaining momentum as a cancer treatment, with multiple agents and cancer types being recently approved for treatment by the US Food and Drug Administration (FDA). Unfortunately, immunotherapy often leads to a wide range of immune related adverse events (IRAEs), including several severe cardiac effects and most notably myocarditis. While increased attention has been drawn to these side effects, including publication of multiple clinical observational data, the underlying mechanisms are unknown. In the event of IRAEs, the most widely utilized clinical solution is administration of high dose corticosteroids and in severe cases, discontinuation of these ICIs. This is detrimental as these therapies are often the last line of treatment options for many types of advanced cancer. In this review, we have systematically described the pathophysiology of the PD-1/PD-L1 axis (including a historical perspective) and cardiac effects in pre-clinical models, clinical trials, autoimmune mechanisms, and immunotherapy in combination with other cancer treatments. We have also reviewed the current challenges in the diagnosis of cardiac events and future directions in the field. In conclusion, this review will delve into this expanding field of cancer immunotherapy and the emerging adverse effects that should be quickly detected and prevented.

Keywords: cardio-oncology, immunotherapy, PD-1—PDL-1 axis, immune check inhibitor (ICI), immune related adverse effects

OPEN ACCESS

Edited by:
Margaret Rose Cunningham, University of Strathclyde, United Kingdom

Reviewed by:
Nicola Maurea, Istituto Nazionale Tumori Fondazione G. Pascale (IRCCS), Italy
Ian Paterson, University of Alberta, Canada

***Correspondence:**
Saraswati Pokharel
saraswati.pokharel@roswellpark.org

Specialty section:
This article was submitted to Cardio-Oncology, a section of the journal Frontiers in Cardiovascular Medicine

Received: *20 October 2020*
Accepted: *06 January 2021*
Published: *03 February 2021*

Citation:
Xu S, Sharma UC, Tuttle C and Pokharel S (2021) Immune Checkpoint Inhibitors: Cardiotoxicity in Pre-clinical Models and Clinical Studies. Front. Cardiovasc. Med. 8:619650. doi: 10.3389/fcvm.2021.619650

INTRODUCTION

Immunotherapy is an emerging avenue for targeting cancer, particularly for difficult to treat cancers, like melanoma and non-small cell lung cancer (1). As a target for one type of ICI, some tumor cells express PD-L1 on their surface to evade detection by T-cells, which have the corresponding receptor PD-1 (**Figure 1A**). Monoclonal antibodies designed against PD-1 and PD-L1 are used to block that interaction, allowing for T-cell activation, ultimately leading to tumor cell death (**Figure 1B**). However, PD-L1 is also expressed by other, non-immune cells to maintain self-tolerance (**Figure 1A**) (2). There have been a wide range of different IRAEs, which are often reversible and associated with treatment response in most patients. More severe forms of IRAEs have been recorded, mostly with combined ICI medications. These IRAEs have led to

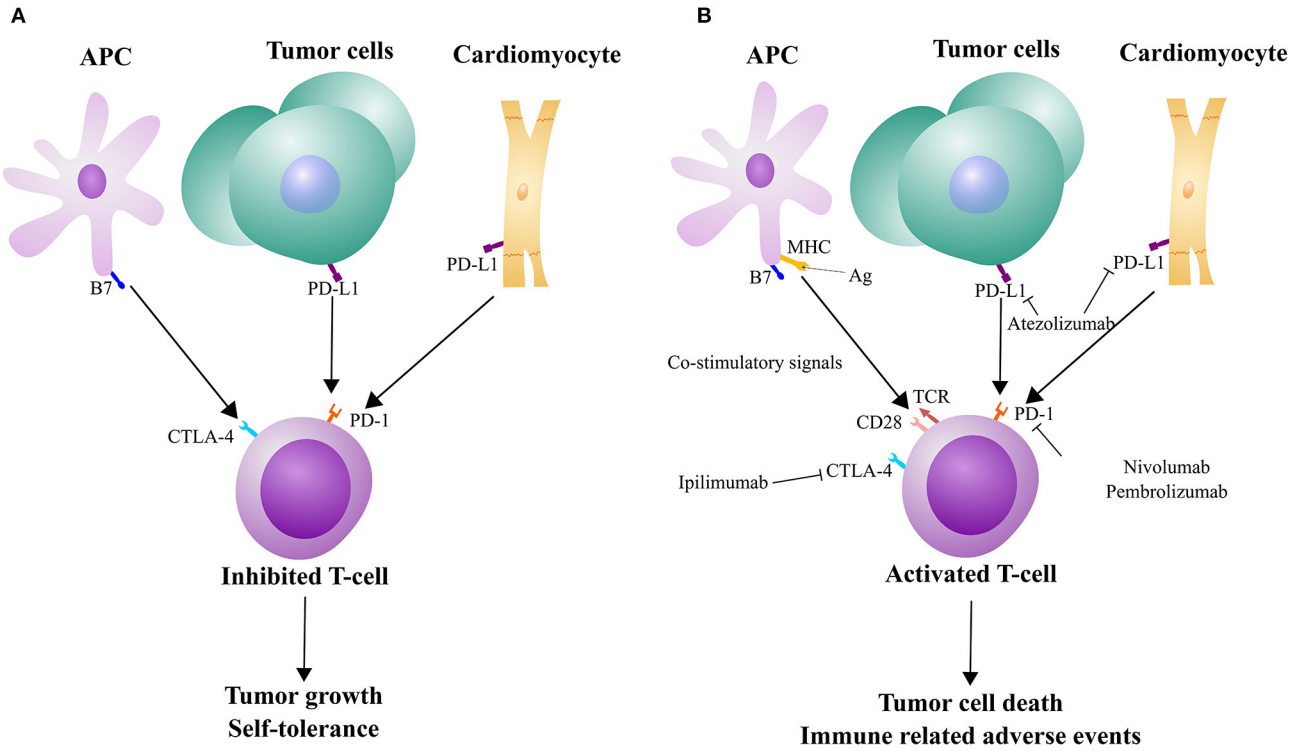

FIGURE 1 | Mechanisms of tumor evasion, immunotherapy, and cardiac autoimmunity in relation to immune checkpoints. **(A)** T-cells can receive inhibitory signals from CTLA-4 and PD-1/PD-L1 that tumor cells can also take advantage of. However, the pathways are also used to maintain self-tolerance. **(B)** T-cell activation can occur with co-stimulation from MHC/TCR and B7/CD28 interactions and immune checkpoint inhibitors. While these T-cells can be used to kill tumor cells, this therapy may come at the expense of immune-related adverse events, such as against cardiac cells.

the discontinuation of therapy in nearly 40% patients (2). Skin and gastrointestinal reactions are common but one of the most severe side effects is myocarditis. While the rate of early onset myocarditis in clinical trials was rare (<1% incidence at the time of FDA approval), the frequency increased with combination immunotherapy (2–4). There have also been reports of several other cardiotoxic effects, including pericarditis and myocardial infarction (4). Drobni et al. (5) reported a three-fold increased risk of atherosclerotic cardiovascular events with ICI use. While steroids are commonly used in the management of IRAEs, immunosuppressive agents are indicated for severe or steroid-refractory cases. Still, based on the severity of symptoms, IRAEs can lead to delay or discontinuation of ICI therapy (6). As these ICIs are being increasingly utilized in cancer patients, the rate of myocarditis has also increased (7).

Despite the rise of ICI-induced myocardial diseases, there is a gap in knowledge related to the pathological mechanisms. Several pre-clinical studies have attempted to model the clinical findings but produced discrepant results. Although PD-1 knockout mice display different cardiomyopathies (8, 9), cardiac inflammation has been difficult to model in animals with only PD-1/PD-L1 antibodies. In this review, we will cover the basic pathophysiology of PD-1/PD-L1 blockade, pre-clinical models, early clinical trials, recent combination therapy protocols, and proposed autoimmune mechanisms for these pathologies. Finally, we will conclude with current challenges diagnosing these cardiac events.

Basic Pathophysiology of PD-1/PD-L1 Axis

The PD-1 receptor was discovered in a screen of genes associated with apoptosis and found to be inducible on T- and B-cells (10, 11). In a knockout mouse, the animals developed autoimmune effects that varied in organs and mouse strains (12). Nishimura et al. predicted that PD-1 suppresses the immune system for self-tolerance. The ligand PD-L1 was found by Dong et al. (13) to negatively regulate T-cells. However, the ligand was not elucidated to interact with the PD-1 receptor until later by Freeman et al. (14) Along with the other ligand PD-L2 (15), these groups found PD-L1 displayed on antigen presenting cells (APC) and tumor cells (16, 17).

Functionally, tumor cells can evade immune detection by displaying PD-L1 on the surface of their cells via "innate" and "adaptive" responses (18). Ongoing studies are also investigating PD-L1 expression as a predictor of ICI efficacy or future tumor relapse. Innate, constitutive expression differs from adaptive, downstream effects of inflammatory cytokines. While some cancer cell lines, such as melanoma, often do not constitutively produce PD-L1 *in vivo*, expression is stimulated significantly by interferon-γ (IFN-γ) and with interleukin-1α (IL-1α) and IL-27 (19). These cytokines influence expression via distinct signaling

pathways that may work synergistically and allow for tumor resistance to immunotherapy treatments.

By blocking this PD-1/PD-L1 interaction through ICIs, immune cells (such as cytotoxic T-cells) are allowed to attack tumor cells. In that regard, immune cell infiltration in the tumor microenvironment may affect the efficacy of immunotherapy (20). Some tumors have little to no immune infiltration, which may be due to lack of immune cell trafficking to the site (21). PD-L1 is often upregulated in tumors in response to inflammation in an attempt to neutralize the immune cell response. As a result, the infiltrating immune cells exhibit a phenotype of decreased function, including expression of negative regulators like PD-1, where T-cells are present but have reduced cytotoxic function (21). Overall, there are many interactions between the tumor and immune cells that either enhance or hinder ICI therapy.

The PD-1/PD-L1 axis has progressed rapidly from its discovery to cancer treatment. By employing the immune system against tumor cells, this innovative therapy can be utilized for a number of cancer types. However, IRAEs and autoimmune events were observed even early on in pre-clinical experiments.

Early Pre-clinical and Clinical Studies

Subsequent work on the PD-1 receptor found that knockout had varying effects based on the background of the mice. Interestingly, PD-1 knockout in C57BL/6 mice displayed a normal phenotype (22). However, in a BALB/c knockout, Nishimura et al. (12) observed dilated cardiomyopathy, reduced cardiac function, and antibody deposition on cardiomyocytes. Further images from Okazaki et al. (8) showed mouse serum cross-reactivity against rat tissue cardiac troponin I (cTnI). Administration of cTnI antibodies to wild-type mice also led to decreased ejection fraction (EF) and increased calcium current *in vitro*.

In the more autoimmune susceptible MRL mouse strain, PD-1 knockout led to fatal myocarditis and the formation of autoantibodies against cardiac myosin (9). The MRL mouse phenotype simulates disease in the same tissues as humans with lupus, except the mice lack overt heart disease, increasing the importance of this finding (23). This could explain why ICI therapy is poorly tolerated by patients with pre-existing autoimmune diseases (3). However, patients with these conditions are excluded from clinical trials and the benefits vs. risks should be considered with an individual's disease progression (24). With the MRL mice, Wang et al. (9) proposed that mouse fatalities were due to congestive heart failure as a result of heart dilation. They also found T-cells in the heart and PD-L1 expressed on cardiomyocytes.

In contrast, Grabie et al. (25) found that endothelial PD-L1 expression was upregulated in their induced model of $CD8^+$ T-cell-mediated myocarditis. Blockade of PD-L1 led to increased cardiac inflammation and circulating cTnI. PD-L1 has been found in non-immune cells and the expression in either cardiomyocytes or endothelial cells supports self-tolerance and the progression of cardiotoxic IRAEs.

Yet due to strain variability in mice, the low rate of myocarditis, and lack of diagnostic modalities in both animals and patients, it is difficult to induce and detect these adverse cardiac effects in pre-clinical models. Additionally, humans and mice are exposed to different antigens, limiting the ability to model IRAEs. In response, an option is to lower immune self-tolerance in mice through genetic modifications (26).

In clinical trials, the occurrence of myocarditis in clinical trials was rare but may be underestimated from lack of routine diagnostic imaging and cardiac monitoring. In an early analysis of ICI-induced myocarditis, 46% of patients also experienced a major adverse cardiac event (MACE), including cardiac arrest or death. Many cases had abnormal electrocardiogram, increased levels of cardiac troponin, and reduced left ventricular EF below 50% (27). Clinical biopsies and autopsies have confirmed cases of immunotherapy-related myocarditis and observed T-cells (27) and macrophages infiltrated in the heart (3). Similarly, in a mouse model, PD-1 blockade significantly increased cytotoxic T-cells in the myocardium (28). In another mouse study, PD-1 antibodies influenced macrophage infiltration and subsequent M1 polarization (29). However, translational discrepancies between mouse models and the clinical presentation of IRAEs hinder mechanistic research and possible therapeutic options. Finally, in this review, we will investigate the adverse effects of multimodality treatment and autoimmune mechanisms.

Autoimmune Side Effects in Combination With Radiation Therapy

Radiation and immunotherapy have been separately utilized to treat cancer, but both have limiting side effects on several organs, including the heart. As with other cancer treatments, immunotherapy with radiotherapy is being investigated as a more efficacious treatment option than monotherapy. Although the combination of radiation and immunotherapy is not currently common in practice, it may become more prevalent as ICIs gain more use as front-line treatment options. Some researchers have studied the cardiac side effects of immunotherapy in subsets of patients who underwent prior radiation exposure. While the disease response to ICI was found to be better in irradiated patients, ICI-related pulmonary toxicity was significantly higher in this cohort. The cardiotoxic potential of such combination therapy warrants further studies (30).

Animal and clinical studies show synergistic efficacy of combination therapy with radiation and ICIs (28, 30, 31). Researchers have also observed an abscopal effect where the treatment is potent against even non-irradiated tumor cells (30, 31). Other data supported that ablative radiation has anti-tumor effects dependent on cytotoxic T-cells (32). While this combination therapy may enhance anti-tumor effects (31), it comes at the risk of cumulative cardiotoxicity. Combined with radiation, PD-1 blockade appears to exacerbate radiation-initiated cardiac inflammation (28). Cumulative cardiotoxicity and inflammation have been observed in mouse models with thoracic irradiation and PD-1 blockade (33). However, radiation targeted to the lungs and PD-1 antibody did not cause mortality, suggesting cardiac inflammation as the primary mediator (28). Radiation-induced heart disease has been characterized with fibrosis and acute production of inflammatory cytokines (34) and can be compounded with ICI-induced cardiac dysfunction.

The presence of PD-L1 on non-immune cells is associated with self-tolerance from immune cells (2). Previous work has shown that PD-L1 can be induced *in vitro* on cardiomyocytes (35) and endothelial cells (36) with the addition of IFN-γ, although untreated cardiomyocytes did not have detectable levels of PD-L1 while endothelial cells had constitutive expression. In the study investigating cardiomyocytes, Seko et al. proposed IFN-γ may be produced by infiltrating immune cells in viral myocarditis. Radiotherapy itself may cause cardiac inflammation, including immune cell infiltration. In their model of viral myocarditis, PD-1 blockade increased myocardial inflammation and IFN-γ expression (35).

Autoimmune Side Effects With Combination Immunotherapy

The FDA first approved Ipilimumab in 2011 (anti-cytotoxic T-lymphocyte associated protein-4 or CTLA-4). Since accepting Pembrolizumab and Nivolumab in 2014 (anti-PD-1) and Atezolizumab in 2016 (anti-PD-L1), these ICIs have seen expanded use in more cancer types (37–40). The agency also approved a combination immunotherapy with Ipilimumab and Nivolumab in 2015 (41). This specific combination of ICIs has been shown to be more efficacious than monotherapy in several clinical trials for melanoma, non-small cell lung cancer, and colorectal cancer (42–45). While the use of multiple immunotherapy agents has gained traction, it often comes at the expense of additional toxicity. In an analysis on Vigibase of ICI case reports from global WHO data, Wei et al. (46) reported that combination blockade against CTLA-4 and PD-1/PD-L1 had an increased rate of myocarditis than monotherapy alone (1.22% vs. 0.54%).

Combination therapy appeared to induce IFN-γ and tumor necrotic factor (TNF-α) production in mouse cardiac tissue (28). Furthermore, older treatments with CTLA-4 blockade had higher rates of IRAEs and the combination of PD-1 and CTLA-4 inhibition led to increased myocarditis cases (27). In contrast to the PD-1/PD-L1 axis, CTLA-4 is expressed on activated T-cells and leads to downstream deregulation of T-cell function. Du et al. (47) proposed that anti-CTLA-4 therapy and IRAEs have distinct mechanisms of action and showed that within the tumor microenvironment, CTLA-4 blockade locally decreases Tregs and allows other T-cells to elicit their effects. In contrast, IRAEs may be caused by activation and expansion of autoreactive T-cells in lymphoid organs. CTLA-4 knockout causes severe myocarditis, inflammation of numerous organs, and early death (48). Additionally, CTLA-4 and PD-1 utilize distinct mechanisms of the Akt pathway, which can function for synergistic tumor regulation and IRAEs (49).

Du et al. (47) were able to differentiate the mechanisms of CTLA-4 immunotherapy and adverse effects by administering Ipilimumab in a humanized *CTLA4* knock-in mouse. When this model included PD-1 antibody, severe IRAEs were observed, including inflammation of many organs. The researchers observed dilated cardiomyopathy, myocarditis, and elevated serum cTnI. The combination treatment amplified the severity of autoimmune reaction with more autoreactive T-cells and Tregs.

Recently, Wei et al. (46) created a mouse model with heterozygous CTLA-4 loss and PD-1 knockout to model clinical myocarditis, which displayed cardiac electrical abnormalities, myocardial inflammation, and increased mortality. Interestingly, they used Abatacept (a recombinant CTLA-4 and IgG fusion protein) to rescue the inflammation and prevent mortality in mice. However, the clinical utility of this approach will warrant further studies, especially considering its unknown effects on tumor growth.

Combination therapy against both PD-1 and PD-L1 can also have negative consequences. Liu et al. (50) observed fulminant cardiotoxicity from sequential PD-1 and PD-L1 blockade in a patient with lung adenocarcinoma. A similar treatment protocol in mice showed an increased anti-tumor effect but at the expense of myocardial injury and lesions. Other studies have observed increased expression of PD-L1 in injured cardiomyocytes in attempts to attenuate T-cell infiltration following inflammation (3, 51). In response, Liu et al. proposed that concurrent or subsequent blockade of PD-L1 after injury may exacerbate inflammation and lead to fulminant myocarditis.

Mechanisms of Autoimmunity and Potential Autoantigens

Previously, patients with prior autoimmune diseases were not included in immunotherapy clinical trials. Retrospective studies have shown that there is a similar or slightly higher rate of IRAEs with these patients, although the effects are often manageable without the need to end ICI treatment (52–54). Current ongoing clinical trials (NCT03816345) will aid in elucidating the safety of immunotherapy (specifically Nivolumab) with a larger sample size and patients with a spectrum of autoimmune diseases.

In a mouse model, experimental autoimmune myocarditis (EAM) was induced by injecting a fragment of cardiac myosin to induce inflammation (55). Tsuruoka et al. observed more severe adverse effects with subsequent PD-1 blockade, including increased immune cell infiltration and expression of interleukins, collagen, and PD-L1. However, cardiac function was not significantly changed. In contrast, concurrent PD-1 antibody administration appeared to decrease $CD4^+$ cell counts and there were no changes in the expression of previously observed genes. As the authors concluded, this data may support that prior autoimmune deficiencies can affect the presence of subsequent IRAEs.

At present, there are also different proposed mechanisms as to whether T-cell reactivity to antigens or autoantibody formation play a role in IRAEs (24). While the presence of immune cell infiltration, most often T-cells, is confirmation of myocarditis, previous animal and clinical data also support the role of autoantibodies. Another hypothesis is a "shared" antigen between cardiomyocytes and tumor cells that stimulates the T-cell infiltration of the myocardium (56). In addition, autoreactive T-cells (some sensitive to cardiac antigens) may be unintentionally released into the periphery from maturation in the thymus (57).

Elevated cardiac troponin levels in serum are a common biomarker for myocardial injury and cardiac troponin T (cTnT)

was previously found to be elevated in a majority of ICI-induced myocarditis cases (27). Interestingly, autoantibodies against cTnT were observed in a patient with fatal Pembrolizumab-mediated myocarditis (58). Two further patient samples of ICI-mediated myocarditis displayed deposition of IgG in foci and the presence of autoimmune-related Th17 cells (59). In one of those patients, there was also an increased expression of autoimmunity-associated genes and serum presence of an immunogenic cTnI peptide and IgG against that sequence. However, not all cases of ICI-mediated myocarditis have observed similar IgG deposition. Bockstahler et al. proposed a potential mechanism where self-tolerance is abrogated by PD-1/PD-L1 blockade. Subsequent tissue damage releases self-antigens, such as cardiac troponin or myosin from cardiomyocytes. The authors hypothesized that antigen presentation by dendritic cells and inflammatory cytokines can lead to increased self-reactive $CD4^+$ T-cells. These cells can then differentiate to Th17 effector cells, thereby decreasing Tregs and supporting the formation of autoantibodies.

Based on observations of IgG deposition against cTnI and cardiomyocytes in previous mouse models, Bockstahler et al. (59) injected mice with immunogenic cTnI peptide to create a model of EAM. Similar to patient samples, there were leukocyte infiltration and fibrosis in the myocardium. While autoimmune mechanisms involving self-antigens and antibodies are being investigated, modified mouse models are being developed to resemble patient presentation. In addition, new multimodality treatment protocols are utilized in clinical settings and simulated in animals with often synergistic positive and negative effects.

DISCUSSION

At present, ICI-related myocarditis is difficult to detect in patients, even with serial testing of cardiac troponin levels. cTnT was previously found to be elevated in a majority of ICI-induced myocarditis cases (27). However, in a study of ICI-treated non-small cell lung cancer cases, most patients with detectable cTnI concentration could be linked to a pre-existing heart disease. One patient had no previously diagnosed heart disease and was hypothesized to have benign, Nivolumab-induced myocarditis (60). In their conclusion, Sarocchi et al. supported the use of cardiac troponin testing with an emphasis on baseline conditions and pre-existing disease.

In contrast, many cases do not display decreased LVEF but a recent study observed decreased global longitudinal strain (GLS), with or without preserved EF, that correlated with MACE (61). While endomyocardial biopsies are definitive (but invasive) confirmations of myocarditis, cardiac magnetic resonance imaging (MRI) and strain analysis (calculated from MRI) could also be used to detect abnormalities (62). As ICIs are gaining more utility in a number of cancer types, there will be a growth in the patient population being treated and therefore the cases of myocarditis. It will be necessary to increase screening procedures and research into the pathophysiology of such adverse side effects. Sensitive cardiac troponin tests can detect initial, subtle changes in the heart but abnormalities should be further investigated with diagnostic imaging, as shown in **Table 1** (63). Echocardiogram can detect regional wall motion abnormalities or decreased systolic function; however, these abnormalities are detected only in a subset of patients (27). Cardiac MRI is superior to echocardiography, allowing tissue characterization of myocardial edema, inflammation, and fibrosis. Because ICI-related myocarditis could lead to the discontinuation of immunotherapy, tissue diagnosis from an endomyocardial biopsy is still recommended whenever feasible (64).

TABLE 1 | Diagnostic considerations for ICI-induced myocarditis and cardiotoxic events.

1. Assessment of risk factors	Prior cardiovascular events and risk factors for atherosclerotic coronary artery disease
2. Biomarker analysis	• Baseline and serial cardiac troponin I • B-type natriuretic peptide
3. Diagnostic testing and imaging	• Electrocardiogram for abnormal PR, QRS and QTc intervals, and evidence of atrial and ventricular arrhythmias • Echocardiogram to assess cardiac function and myocardial wall motion • Cardiac MRI for increased T2-signal intensity, and abnormal early and late gadolinium signal intensity in contrast-enhanced MRI • Tagged cine MRI for strain analysis
4. Endomyocardial biopsy	• Tissue edema • Lymphocyte and macrophage infiltration

Another obstacle to characterizing these adverse side effects is the lack of robust animal models. PD-1 knockout mice have shown variable phenotypes but some of the seminal work on the PD-1/PD-L1 axis observed a range of autoimmune and cardiac defects. Currently, multimodality treatment options have gained traction for cancer therapy but may also have synergistic, negative side effects. While these side effects are being investigated in clinical trials, radiation and combination immunotherapy protocols could also be utilized in animal models. Based on the clinical experience, a combination immunotherapy treatment could better exhibit ICI-induced myocarditis in an animal model. There is also the utility of genetic models, including recent advancements by Wei et al. (46) to create a CTLA-4 and PD-1 genetically altered mouse model which showed myocarditis in a similar pattern as seen in patients. Overall, the diagnosis, pathology, and treatment of IRAEs is complex and requires more research as immunotherapy matures into a more common cancer treatment option.

AUTHOR CONTRIBUTIONS

SX took the lead in writing the review while CT contributed sections of the Early Pre-clinical and Clinical Studies. UCS

conceived the review subject and outline while both UCS and SP provided feedback and additional references. UCS also aided the creation of **Table 1** and clinical considerations. UCS and SP provided feedback and additional references. All authors contributed to the article and approved the submitted version.

FUNDING

UCS was supported by Mentored Career Development Award from the NIH/NHLBI K08HL131987. SP was supported by NIH R21 HL154028.

REFERENCES

1. Farkona S, Diamandis EP, Blasutig IM. Cancer immunotherapy: the beginning of the end of cancer? *BMC Med*. (2016) 14:73. doi: 10.1186/s12916-016-0623-5
2. Varricchi G, Galdiero MR, Marone G, Criscuolo G, Triassi M, Bonaduce D, et al. Cardiotoxicity of immune checkpoint inhibitors. *ESMO Open*. (2017) 2:e000247-e. doi: 10.1136/esmoopen-2017-000247
3. Johnson DB, Balko JM, Compton ML, Chalkias S, Gorham J, Xu Y, et al. Fulminant myocarditis with combination immune checkpoint blockade. *New Engl J Med*. (2016) 375:1749–55. doi: 10.1056/NEJMoa1609214
4. Lyon AR, Yousaf N, Battisti NML, Moslehi J, Larkin J. Immune checkpoint inhibitors and cardiovascular toxicity. *Lancet Oncol*. (2018) 19:e447–58. doi: 10.1016/S1470-2045(18)30457-1
5. Drobni Zsofia D, Alvi Raza M, Taron J, Zafar A, Murphy Sean P, Rambarat Paula K, et al. Association between immune checkpoint inhibitors with cardiovascular events and atherosclerotic plaque. *Circulation*. (2020) 142:2299–311. doi: 10.1161/CIRCULATIONAHA.120.049981
6. Escudier M, Cautela J, Malissen N, Ancedy Y, Orabona M, Pinto J, et al. Clinical features, management, and outcomes of immune checkpoint inhibitor-related cardiotoxicity. *Circulation*. (2017) 136:2085–7. doi: 10.1161/CIRCULATIONAHA.117.030571
7. Moslehi JJ, Salem J-E, Sosman JA, Lebrun-Vignes B, Johnson DB. Increased reporting of fatal immune checkpoint inhibitor-associated myocarditis. *Lancet*. (2018) 391:933. doi: 10.1016/S0140-6736(18)30533-6
8. Okazaki T, Tanaka Y, Nishio R, Mitsuiye T, Mizoguchi A, Wang J, et al. Autoantibodies against cardiac troponin I are responsible for dilated cardiomyopathy in PD-1-deficient mice. *Nat Med*. (2003) 9:1477. doi: 10.1038/nm955
9. Wang J, Okazaki I-M, Yoshida T, Chikuma S, Kato Y, Nakaki F, et al. PD-1 deficiency results in the development of fatal myocarditis in MRL mice. *Int Immunol*. (2010) 22:443–52. doi: 10.1093/intimm/dxq026
10. Ishida Y, Agata Y, Shibahara K, Honjo T. Induced expression of PD-1, a novel member of the immunoglobulin gene superfamily, upon programmed cell death. *EMBO J*. (1992) 11:3887–95. doi: 10.1002/j.1460-2075.1992.tb05481.x
11. Agata Y, Kawasaki A, Nishimura H, Ishida Y, Tsubat T, Yagita H, et al. Expression of the PD-1 antigen on the surface of stimulated mouse T and B lymphocytes. *Int Immunol*. (1996) 8:765–72. doi: 10.1093/intimm/8.5.765
12. Nishimura H, Nose M, Hiai H, Minato N, Honjo T. Development of lupus-like autoimmune diseases by disruption of the PD-1 gene encoding an ITIM motif-carrying immunoreceptor. *Immunity*. (1999) 11:141–51. doi: 10.1016/S1074-7613(00)80089-8
13. Dong H, Zhu G, Tamada K, Chen L. B7-H1, a third member of the B7 family, co-stimulates T-cell proliferation and interleukin-10 secretion. *Nat Med*. (1999) 5:1365–9. doi: 10.1038/70932
14. Freeman GJ, Long AJ, Iwai Y, Bourque K, Chernova T, Nishimura H, et al. Engagement of the PD-1 immunoinhibitory receptor by a novel B7 family member leads to negative regulation of lymphocyte activation. *J Exp Med*. (2000) 192:1027–34. doi: 10.1084/jem.192.7.1027
15. Latchman Y, Wood CR, Chernova T, Chaudhary D, Borde M, Chernova I, et al. PD-L2 is a second ligand for PD-1 and inhibits T cell activation. *Nat Immunol*. (2001) 2:261–8. doi: 10.1038/85330
16. Dong H, Strome SE, Salomao DR, Tamura H, Hirano F, Flies DB, et al. Tumor-associated B7-H1 promotes T-cell apoptosis: a potential mechanism of immune evasion. *Nat Med*. (2002) 8:793–800. doi: 10.1038/nm730
17. Iwai Y, Ishida M, Tanaka Y, Okazaki T, Honjo T, Minato N. Involvement of PD-L1 on tumor cells in the escape from host immune system and tumor immunotherapy by PD-L1 blockade. *Proc Natl Acad Sci USA*. (2002) 99:12293–7. doi: 10.1073/pnas.192461099
18. Pardoll DM. The blockade of immune checkpoints in cancer immunotherapy. *Nat Rev Cancer*. (2012) 12:252–64. doi: 10.1038/nrc3239
19. Chen S, Crabill GA, Pritchard TS, McMiller TL, Wei P, Pardoll DM, et al. Mechanisms regulating PD-L1 expression on tumor and immune cells. *J Immunother Cancer*. (2019) 7:305. doi: 10.1186/s40425-019-0770-2
20. Herbst RS, Soria J-C, Kowanetz M, Fine GD, Hamid O, Gordon MS, et al. Predictive correlates of response to the anti-PD-L1 antibody MPDL3280A in cancer patients. *Nature*. (2014) 515:563–7. doi: 10.1038/nature14011
21. Liu D, Jenkins RW, Sullivan RJ. Mechanisms of resistance to immune checkpoint blockade. *Am J Clin Dermatol*. (2019) 20:41–54. doi: 10.1007/s40257-018-0389-y
22. Keir ME, Freeman GJ, Sharpe AH. PD-1 regulates self-reactive $CD8^+$ T cell responses to antigen in lymph nodes and tissues. *J Immunol*. (2007) 179:5064. doi: 10.4049/jimmunol.179.8.5064
23. Lucas JA, Menke J, Rabacal WA, Schoen FJ, Sharpe AH, Kelley VR. Programmed death ligand 1 regulates a critical checkpoint for autoimmune myocarditis and pneumonitis in MRL mice. *J Immunol*. (2008) 181:2513–21. doi: 10.4049/jimmunol.181.4.2513
24. Postow MA, Sidlow R, Hellmann MD. Immune-related adverse events associated with immune checkpoint blockade. *N Engl J Med*. (2018) 378:158–68. doi: 10.1056/NEJMra1703481
25. Grabie N, Gotsman I, DaCosta R, Pang H, Stavrakis G, Butte Manish J, et al. Endothelial programmed death-1 ligand 1 (PD-L1) regulates $CD8^+$ T-cell-mediated injury in the heart. *Circulation*. (2007) 116:2062–71. doi: 10.1161/CIRCULATIONAHA.107.709360
26. Liu J, Blake SJ, Harjunpää H, Fairfax KA, Yong MCR, Allen S, et al. Assessing immune-related adverse events of efficacious combination immunotherapies in preclinical models of cancer. *Cancer Res*. (2016) 76:5288–301. doi: 10.1158/0008-5472.CAN-16-0194
27. Mahmood SS, Fradley MG, Cohen JV, Nohria A, Reynolds KL, Heinzerling LM, et al. Myocarditis in patients treated with immune checkpoint inhibitors. *J Am Coll Cardiol*. (2018) 71:1755–64. doi: 10.1016/j.jacc.2018.02.037
28. Du S, Zhou L, Alexander GS, Park K, Yang L, Wang N, et al. PD-1 Modulates radiation-induced cardiac toxicity through cytotoxic T lymphocytes. *J Thorac Oncol*. (2018) 13:510–20. doi: 10.1016/j.jtho.2017.12.002
29. Xia W, Zou C, Chen H, Xie C, Hou M. Immune checkpoint inhibitor induces cardiac injury through polarizing macrophages via modulating microRNA-34a/Kruppel-like factor 4 signaling. *Cell Death Dis*. (2020) 11:575. doi: 10.1038/s41419-020-02778-2
30. Shaverdian N, Lisberg AE, Bornazyan K, Veruttipong D, Goldman JW, Formenti SC, et al. Previous radiotherapy and the clinical activity and toxicity of pembrolizumab in the treatment of non-small-cell lung cancer: a secondary analysis of the KEYNOTE-001 phase 1 trial. *Lancet Oncol*. (2017) 18:895–903. doi: 10.1016/S1470-2045(17)30380-7
31. Twyman-Saint Victor C, Rech AJ, Maity A, Rengan R, Pauken KE, Stelekati E, et al. Radiation and dual checkpoint blockade activate non-redundant immune mechanisms in cancer. *Nature*. (2015) 520:373–7. doi: 10.1038/nature14292
32. Lee Y, Auh SL, Wang Y, Burnette B, Wang Y, Meng Y, et al. Therapeutic effects of ablative radiation on local tumor require $CD8^+$ T cells: changing strategies for cancer treatment. *Blood*. (2009) 114:589–95. doi: 10.1182/blood-2009-02-206870
33. Myers CJ, Lu B. Decreased survival after combining thoracic irradiation and an anti-PD-1 antibody correlated with increased T-cell infiltration into cardiac and lung tissues. *Int J Radiat Oncol Biol Phys*. (2017) 99:1129–36. doi: 10.1016/j.ijrobp.2017.06.2452

34. Taunk NK, Haffty BG, Kostis JB, Goyal S. Radiation-induced heart disease: pathologic abnormalities and putative mechanisms. *Front Oncol*. (2015) 5:39. doi: 10.3389/fonc.2015.00039
35. Seko Y, Yagita H, Okumura K, Azuma M, Nagai R. Roles of programmed death-1 (PD-1)/PD-1 ligands pathway in the development of murine acute myocarditis caused by coxsackievirus B3. *Cardiovasc Res*. (2007) 75:158–67. doi: 10.1016/j.cardiores.2007.03.012
36. Eppihimer MJ, Gunn J, Freeman GJ, Greenfield EA, Chernova T, Erickson J, et al. Expression and regulation of the PD-L1 immunoinhibitory molecule on microvascular endothelial cells. *Microcirculation*. (2002) 9:133–45. doi: 10.1080/713774061
37. Yervoy (ipilimumab) Drug Approval Package Food and Drug Administration website (2011) Available online at: https://www.accessdata.fda.gov/drugsatfda_docs/nda/2011/125377Orig1s000TOC.cfm (accessed September 8, 2020).
38. Keytruda (pembrolizumab) Drug Approval Package Food and Drug Administration Website (2014). Available online at: https://www.accessdata.fda.gov/drugsatfda_docs/nda/2014/125514Orig1s000TOC.cfm (accessed September 8, 2020).
39. Opdivo (nivolumab) Drug Approval Package Food and Drug Administration Website (2014). Available online at: https://www.accessdata.fda.gov/drugsatfda_docs/nda/2014/125554Orig1s000TOC.cfm (accessed September 8, 2020).
40. Tecentriq (Atezolizumab) Drug Approval Package Food and Drug Administration Website (2016). Available online at: https://www.accessdata.fda.gov/drugsatfda_docs/nda/2016/761041Orig1_toc.cfm (accessed September 30, 2020).
41. Mullard A. FDA approves first immunotherapy combo. *Nat Rev Drug Discov*. (2015) 14:739. doi: 10.1038/nrd4779
42. Postow MA, Chesney J, Pavlick AC, Robert C, Grossmann K, McDermott D, et al. Nivolumab and Ipilimumab versus Ipilimumab in Untreated Melanoma. *New Engl J Med*. (2015) 372:2006–17. doi: 10.1056/NEJMoa1414428
43. Larkin J, Chiarion-Sileni V, Gonzalez R, Grob JJ, Cowey CL, Lao CD, et al. Combined nivolumab and ipilimumab or monotherapy in untreated melanoma. *N Engl J Med*. (2015) 373:23–34. doi: 10.1056/NEJMoa1504030
44. Hellmann MD, Rizvi NA, Goldman JW, Gettinger SN, Borghaei H, Brahmer JR, et al. Nivolumab plus ipilimumab as first-line treatment for advanced non-small-cell lung cancer (CheckMate 012): results of an open-label, phase 1, multicohort study. *Lancet Oncol*. (2017) 18:31–41. doi: 10.1016/S1470-2045(16)30624-6
45. Overman MJ, Lonardi S, Wong KYM, Lenz H-J, Gelsomino F, Aglietta M, et al. Durable clinical benefit with nivolumab plus ipilimumab in DNA mismatch repair-deficient/microsatellite instability-high metastatic colorectal cancer. *J Clin Oncol*. (2018) 36:773–9. doi: 10.1200/JCO.2017.76.9901
46. Wei SC, Meijers WC, Axelrod ML, Anang N-AAS, Screever EM, Wescott EC, et al. A genetic mouse model recapitulates immune checkpoint inhibitor-associated myocarditis and supports a mechanism-based therapeutic intervention. *Cancer Discov*. (2020) 2020:CD-20-0856. doi: 10.1158/2159-8290.CD-20-0856
47. Du X, Liu M, Su J, Zhang P, Tang F, Ye P, et al. Uncoupling therapeutic from immunotherapy-related adverse effects for safer and effective anti-CTLA-4 antibodies in CTLA4 humanized mice. *Cell Res*. (2018) 28:433–47. doi: 10.1038/s41422-018-0012-z
48. Waterhouse P, Penninger JM, Timms E, Wakeham A, Shahinian A, Lee KP, et al. Lymphoproliferative disorders with early lethality in mice deficient in Ctla-4. *Science*. (1995) 270:985–8. doi: 10.1126/science.270.5238.985
49. Parry RV, Chemnitz JM, Frauwirth KA, Lanfranco AR, Braunstein I, Kobayashi SV, et al. CTLA-4 and PD-1 receptors inhibit T-cell activation by distinct mechanisms. *Mol Cell Biol*. (2005) 25:9543–53. doi: 10.1128/MCB.25.21.9543-9553.2005
50. Liu S-Y, Huang W-C, Yeh H-I, Ko C-C, Shieh H-R, Hung C-L, et al. Sequential blockade of PD-1 and PD-L1 causes fulminant cardiotoxicity-from case report to mouse model validation. *Cancers*. (2019) 11:580. doi: 10.3390/cancers11040580
51. Baban B, Liu JY, Qin X, Weintraub NL, Mozaffari MS. Upregulation of programmed death-1 and its ligand in cardiac injury models: interaction with GADD153. *PLoS ONE*. (2015) 10:e0124059. doi: 10.1371/journal.pone.0124059
52. Menzies AM, Johnson DB, Ramanujam S, Atkinson VG, Wong ANM, Park JJ, et al. Anti-PD-1 therapy in patients with advanced melanoma and preexisting autoimmune disorders or major toxicity with ipilimumab. *Ann Oncol*. (2017) 28:368–76. doi: 10.1093/annonc/mdw443
53. Leonardi GC, Gainor JF, Altan M, Kravets S, Dahlberg SE, Gedmintas L, et al. Safety of programmed death-1 pathway inhibitors among patients with non-small-cell lung cancer and preexisting autoimmune disorders. *J Clin Oncol*. (2018) 36:1905–12. doi: 10.1200/JCO.2017.77.0305
54. Tison A, Quéré G, Misery L, Funck-Brentano E, Danlos FX, Routier E, et al. Safety and efficacy of immune checkpoint inhibitors in patients with cancer and preexisting autoimmune disease: a nationwide, multicenter cohort study. *Arthritis Rheumatol*. (2019) 71:2100–11. doi: 10.1002/art.41068
55. Tsuruoka K, Wakabayashi S, Morihara H, Matsunaga N, Fujisaka Y, Goto I, et al. Exacerbation of autoimmune myocarditis by an immune checkpoint inhibitor is dependent on its time of administration in mice. *Int J Cardiol*. (2020) 313:67–75. doi: 10.1016/j.ijcard.2020.04.033
56. Zhou Y-W, Zhu Y-J, Wang M-N, Xie Y, Chen C-Y, Zhang T, et al. Immune checkpoint inhibitor-associated cardiotoxicity: current understanding on its mechanism, diagnosis and management. *Front Pharmacol*. (2019) 10:1350. doi: 10.3389/fphar.2019.01350
57. Tajiri K, Ieda M. Cardiac complications in immune checkpoint inhibition therapy. *Front Cardiovasc Med*. (2019) 6:3. doi: 10.3389/fcvm.2019.00003
58. Martinez-Calle N, Rodriguez-Otero P, Villar S, Mejías L, Melero I, Prosper F, et al. Anti-PD1 associated fulminant myocarditis after a single pembrolizumab dose: the role of occult pre-existing autoimmunity. *Haematologica*. (2018) 103:e318-21. doi: 10.3324/haematol.2017.185777
59. Bockstahler M, Fischer A, Goetzke CC, Neumaier HL, Sauter M, Kespohl M, et al. Heart-specific immune responses in an animal model of autoimmune-related myocarditis mitigated by an immunoproteasome inhibitor and genetic ablation. *Circulation*. (2020) 141:1885–902. doi: 10.1161/CIRCULATIONAHA.119.043171
60. Sarocchi M, Grossi F, Arboscello E, Bellodi A, Genova C, Dal Bello MG, et al. Serial troponin for early detection of nivolumab cardiotoxicity in advanced non-small cell lung cancer patients. *Oncologist*. (2018) 23:936–42. doi: 10.1634/theoncologist.2017-0452
61. Awadalla M, Mahmood SS, Groarke JD, Hassan MZO, Nohria A, Rokicki A, et al. Global longitudinal strain and cardiac events in patients with immune checkpoint inhibitor-related myocarditis. *J Am Coll Cardiol*. (2020) 75:467–78. doi: 10.1016/j.jacc.2019.11.049
62. Karthikeyan B, Sonkawade SD, Pokharel S, Preda M, Schweser F, Zivadinov R, et al. Tagged cine magnetic resonance imaging to quantify regional mechanical changes after acute myocardial infarction. *Magn Reson Imaging*. (2020) 66:208–18. doi: 10.1016/j.mri.2019.09.010
63. Palaskas N, Lopez-Mattei J, Durand Jean B, Iliescu C, Deswal A. Immune checkpoint inhibitor myocarditis: pathophysiological characteristics, diagnosis, and treatment. *J Am Heart Assoc*. (2020) 9:e013757.
64. Hu J-R, Florido R, Lipson EJ, Naidoo J, Ardehali R, Tocchetti CG, et al. Cardiovascular toxicities associated with immune checkpoint inhibitors. *Cardiovasc Res*. (2019) 115:854–68. doi: 10.1093/cvr/cvz026

Conflict of Interest: The authors declare that the research was conducted in the absence of any commercial or financial relationships that could be construed as a potential conflict of interest.

frontiers in Cardiovascular Medicine

ORIGINAL RESEARCH
published: 23 February 2021
doi: 10.3389/fcvm.2021.587149

The Effects of Repeat-Dose Doxorubicin on Cardiovascular Functional Endpoints and Biomarkers in the Telemetry-Equipped Cynomolgus Monkey

Michael J. Engwall[1]*, *Nancy Everds*[2], *James R. Turk*[1] and *Hugo M. Vargas*[1]

[1] Translational Safety and Bioanalytical Sciences, Amgen Inc., Thousand Oaks, CA, United States, [2] Non-clinical Sciences, Seattle Genetics, Inc., Seattle, WA, United States

OPEN ACCESS

Edited by:
Susan Currie,
University of Strathclyde,
United Kingdom

Reviewed by:
Matt Skinner,
Vivonics Preclinical Limited,
United Kingdom
Derek Leishman,
Eli Lilly, United States

***Correspondence:**
Michael J. Engwall
mengwall@amgen.com

Specialty section:
This article was submitted to Cardio-Oncology, a section of the journal Frontiers in Cardiovascular Medicine

Received: 24 July 2020
Accepted: 18 January 2021
Published: 23 February 2021

Citation:
Engwall MJ, Everds N, Turk JR and Vargas HM (2021) The Effects of Repeat-Dose Doxorubicin on Cardiovascular Functional Endpoints and Biomarkers in the Telemetry-Equipped Cynomolgus Monkey.
Front. Cardiovasc. Med. 8:587149.
doi: 10.3389/fcvm.2021.587149

Purpose: Doxorubicin-related heart failure has been recognized as a serious complication of cancer chemotherapy. This paper describes a cardiovascular safety pharmacology study with chronic dosing of doxorubicin in a non-human primate model designed to characterize the onset and magnitude of left ventricular dysfunction (LVD) using invasive and non-invasive methods.

Methods: Cynomolgus monkeys ($N = 12$) were given repeated intravenous injections of doxorubicin over 135 days (19 weeks) with dosing holidays when there was evidence of significantly decreased hematopoiesis; a separate group ($N = 12$) received vehicle. Arterial and left ventricular pressure telemetry and cardiac imaging by echocardiography allowed regular hemodynamic assessments and determination of LVD. Blood samples were collected for hematology, clinical chemistry, and assessment of cardiac troponin (cTnI) and N-terminal pro b-type natriuretic peptide (NT-proBNP). Myocardial histopathology was a terminal endpoint.

Results: There was variable sensitivity to the onset of treatment effects, for example 25% of doxorubicin-treated animals exhibited LVD (e.g., decreases in ejection fraction) following 50–63 days (cumulative dose: 8–9 mg/kg) on study. All animals deteriorated into heart failure with additional dosing 135 days (total cumulative dose: 11–17 mg/kg). Reductions in arterial pressure and cardiac contractility, as well as QTc interval prolongation, was evident following doxorubicin-treatment. Both cTnI and NT-proBNP were inconsistently higher at the end of the study in animals with LVD. Measurements collected from control animals were consistent and stable over the same time frame. Minimal to mild, multifocal, vacuolar degeneration of cardiomyocytes was observed in 7 of 12 animals receiving doxorubicin and 0 of 12 animals receiving vehicle.

Conclusions: This repeat-dose study of doxorubicin treatment in the cynomolgus monkey demonstrated a clinically relevant pattern of progressive heart failure. Importantly, the study revealed how both telemetry and non-invasive echocardiography measurements could track the gradual onset of LVD.

Keywords: doxorubicin, macaca fascicularis, heart failure, QTc interval prolongation, echocardiography, telemetry, troponin

INTRODUCTION

Doxorubicin (Adriamycin) has been a common treatment for cancer since its introduction in the 1960s. It is well-known that treatment is associated with cardiotoxicity which can progress to congestive heart failure (CHF) (1). This concern limits the use of doxorubicin in human patients. An early paper stated the core concerning issue: "*The morbidity and mortality rates related to anthracycline-induced cardiotoxicity will continue to increase because of several factors: significant cardiac injury, which occurs even with low-dose therapy and commonly occurs with therapeutic doses; the use of monitoring techniques that are often insensitive to subclinical cardiac damage; lack of effective cardio protection; and late-onset ventricular impairment occurring in asymptomatic patients years after uncomplicated anthracycline treatment*" (2). These concerns persist to this day.

The mechanism underlying the cardiovascular toxicity may be related to the generation of reactive oxygen species (ROS) but it is well-appreciated that the toxicity is multifactorial and includes effects stemming from mitochondrial impairment and disruptions of myocyte calcium handling (3–5). The toxicity is also strongly linked to the generation of secondary metabolites, which can vary among the anthracyclines (6). More recently, there has been a growing concern with delayed-onset degradation of cardiac function (8). While the damage to the heart is thought to be immediate, a patient's compensatory mechanisms may delay the onset of clinically detectable changes for years (7). With lifetime doxorubicin doses of 400–450 mg/m^2, a heart failure incidence of 5% (10% in older patients) can be expected (8). Additionally, the combination of doxorubicin with other cancer therapies (e.g., trastuzumab) augments the risk of cardiotoxicity (9).

While clinical diagnostic tests are poor predictors of long-term prognosis, they are used to diagnose and document the extent of functional changes as cardiac injury progresses. ECG changes such as QTc prolongation emerge during development of sequelae to treatment (10). Likewise, measurements of cardiac function derived from echocardiography such as ejection fraction and fractional shortening as well as indices of diastolic function are decreased in the patients who develop heart disease following treatment with doxorubicin (11). Recent papers from a consortium of pharmaceutical companies highlighted the utility of measurements of left ventricular endpoints (e.g., dP/dt_{max}, an index of cardiac contractility) as a biomarker of cardiac function (12, 13).

The clinical manifestation of doxorubicin-related cardiotoxicity has been modeled in several; preclinical species such as rats, mice, rabbits, and dogs (14–18). The dosages and dosing intervals used varied considerably across the studies. With regard to higher species like the non-human primate,

TABLE 1A | Doxorubicin dosing schedule indicating dosing levels on specific dosing days, dosing holidays, and indication of when animals were euthanized due to deteriorating cardiovascular function.

NHP#	Doxorubicin dose (mg/kg IV) and treatment day																		
	1	8	15	22	29	36	43	50	57	63	70	78	86	92	99	106	113	120	127	135
104928	2	2	2			1		1		1	1	1	1	1	1	1	1			
104929	2	2	2			1		1		1		1		1		1		1		
104930	2	2	2			1		1		1	1	1	1	1	1	1	1			
104931	2	2	2			1		1		1	1	1	1	1	1	1	1			
104932	2	2	2			1		1		1	1	1								
104933	2	2	2			1		1		1	1	1	1	1	1	1	1	1		
104934	2	2	2			1		1		1	1	1	1		1					
104935	2	2	2			1		1		1	1	1	1	1	1	1	1	1		
104936	2	2	2			1		1		1	1	1	1	1						
104937	2	2	2			1		1		1	1	1	1	1	1	1	1			
104938	2	2	2			1		1		1	1	1	1	1						
104939	2	2	2			1		1		1	1	1	1	1						

Gray box: dosing holiday; black box: unscheduled sacrifice. The study concluded on day 135.
There were no unscheduled sacrifices in the control group.

TABLE 1B | Plasma levels of doxorubicin (dox) at 8 and 24 h after intravenous dosing.

	Day 1		Day 36		Day 78		Day 113	
	8 h	24 h	8 h	24 h	8 h	24 h	8 h	24 h
Dox (ng/ml)	31.6 ± 5.7	15.8 ± 3.5	16.5 ± 4.2	8.0 ± 1.6	19.0 ± 5.5	9.1 ± 2.7	16.4 ± 3.5	6.3 ± 1.3

All values are means ± SD (N = 12; except day 113 was N = 6).

TABLE 2 | Cumulative dose estimation for each animal treated with doxorubicin.

NHP#	Total dose[a] mg/kg	Mean dosing phase weight[b] (kg)	Total dose[c] (mg)	Dose/body surface area[d] (mg/m^2)
104928	16	5.4	86	192
104929	13	4.6	53	156
104930	16	4.9	79	192
104931	16	4.5	72	192
104932	11	5.3	58	132
104933	17	4.5	77	204
104934	13	4.9	63	156
104935	17	5.4	92	204
104936	13	4.7	61	156
104937	16	5.9	94	192
104938	13	8.9	116	156
104939	13	8.8	114	156
Average (SD)	14.5 ± 2.0	5.6 ± 1.6	81 ± 20	174 ± 24

[a] *Total dose is a sum of each dose (mg/kg) administered to an individual animal during the dosing phase.*
[b] *Mean body weight was calculated for all body weight intervals in the dosing phase for each individual animal.*
[c] *Estimated total cumulative dose is the total dose (mg/kg) administered multiplied by the mean body weight (kg) for each individual animal.*
[d] *The dose per body surface area was determined by multiplying the total dose (mg/kg) administered to individual monkeys by a species-specific mass constant, k_m. For monkeys, the k_m was 12 kg/m^2 (24).*
Cumulative dose levels were dependent on number of doses given which was limited by tolerability.

three evaluations of doxorubicin were conducted. One early study used cynomolgus monkeys treated with doxorubicin (1 mg/kg monthly) for 26 months (19). Although clinical signs of congestive heart failure were observed in the majority (8/10) of animals, no quantitative measurements of cardiac function were collected. In a second study (reported in abstract form), a different doxorubicin dose regimen (2 mg/kg/week for 3 weeks followed by 1 mg/kg/2 weeks until evidence of cardiac dysfunction occurred) was used in cynomolgus monkeys, although the magnitude of echocardiography changes was not stated (20). Lastly, Takayama et al. (21) demonstrated that doxorubicin (1 mg/kg/every 4 weeks for 114 months) administration caused myocardial structural changes related to heart failure, but no functional measurements were collected from those animals.

Given the important role and value of non-human primate in cardiovascular safety assessments for new therapeutics (22), and the lack of nonclinical information on the sensitivity of non-human primate to doxorubicin-induced cardiovascular toxicity, we characterized the effect of this clinically relevant anticancer therapeutic in the cynomolgus monkey to better understand the translational value of this animal model. In this study, serial measures of cardiac function were examined in cynomolgus monkeys given repeated doses of Dox. Assessments included telemetry collection of electrocardiograms, hemodynamics, circulating levels of cTnI and echocardiography. The study used a dose regimen based on prior literature that was intended to produce progressive decreases in left ventricular systolic function while endeavoring to avoid non-cardiovascular toxicities (e.g., leukopenia) also associated with doxorubicin treatment.

METHODS

The effects of doxorubicin treatment on measures of cardiac function were characterized in cynomolgus monkeys over an observation period of up to 135 days. The study was performed at Covance Laboratories, Inc. (Madison, WI).

Animal Care and Treatment

Male cynomolgus monkeys (*Macaca fascicularis*) of Chinese origin obtained from Covance Research Products, Inc. (2–12 years old; 3–12 kg), were housed in stainless steel cages. Animals selected for this study were based on age (planned retirement from the colony) and expiring telemetry battery life. Care and use of animals was as specified by United States Department of Agriculture Animal Welfare Act (9 CFR, Parts 1, 2, and 3) and as described in the Guide for the Care and Use of Laboratory Animals (23). Animals were individually or socially housed indoors in species-specific housing at an Association

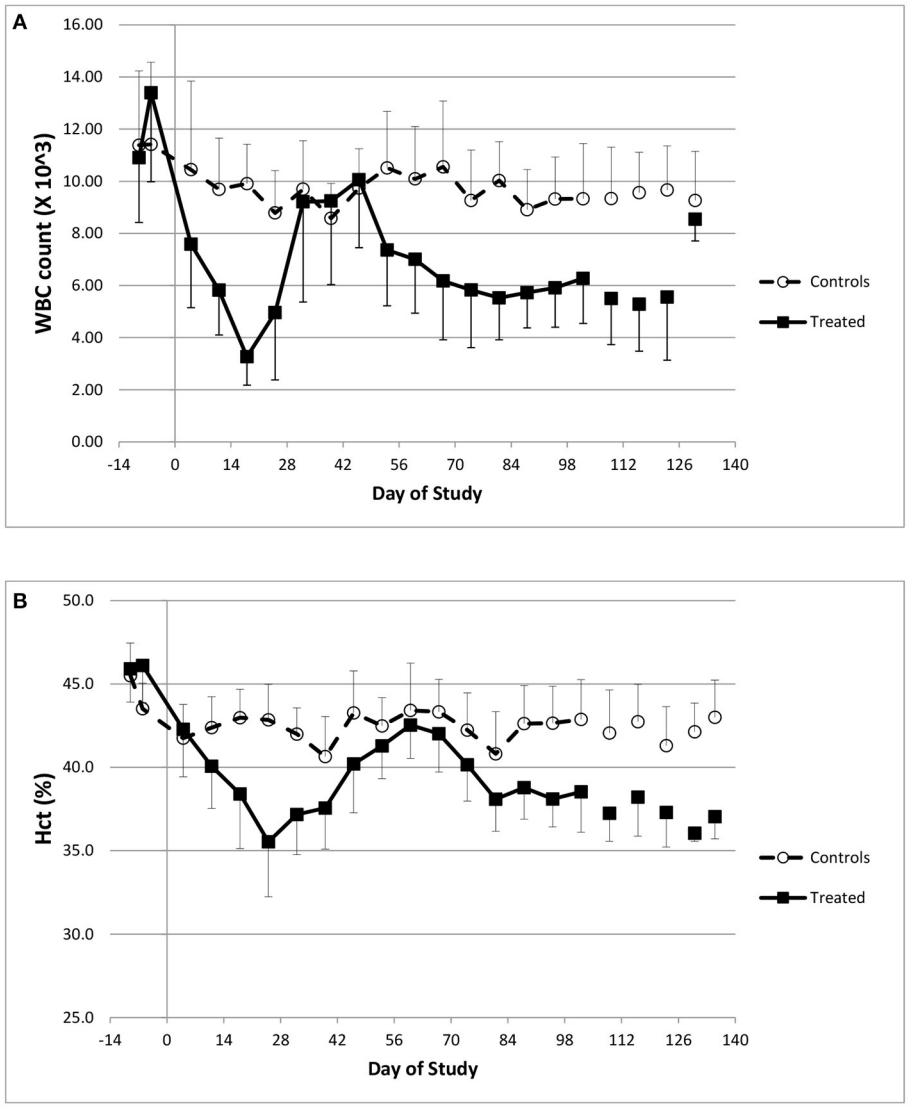

FIGURE 1 | Hematology changes. Changes in white blood cell counts **(A)** and Hematocrit **(B)** over the course of the study.

for Assessment and Accreditation of Laboratory Animal Care-accredited facility. All research protocols were approved by the Covance Institutional Animal Care and Use Committee (IACUC) prior to dose administration. Certified Primate Diet (#5048, PMI, Richmond, IN) was provided daily in amounts appropriate for the age and size of the animals. Animals had *ad libitum* access to water (automatic watering system or bottle), were maintained in standard housing conditions (12:12 h light:dark cycle; 20° −26°C; 30–70% humidity) and had enrichment opportunities, e.g., food treats, fresh fruit, toys, and social interaction. A veterinary medical treatment plan was developed (pre-study) to provide supportive care based on clinical observations, clinical pathology data, hemodynamic findings, and/or echocardiography findings, including the management of pain and suffering (euthanasia). Palliative and prophylactic procedures were based upon consensus agreement between the study director and attending laboratory animal veterinarian. Terminal procedures included scheduled (day 135; last day of study) or unscheduled (due to morbidity or poor health) euthanasia by deep anesthesia by ketamine/sodium pentobarbital injection and exsanguination. Final blood samples (vena cava) were collected on all animals (when possible) and a complete macroscopic examination was performed at necropsy. Heart tissues (right and left ventricular free walls and ventricular septum) were collected, processed and embedded in paraffin for evaluation by light microscopy.

Animals had been previously instrumented ∼1.5 years before the start of the study with telemetry units from Data Science International (DSI). Either D70-PCT (13 animals) or D70-PCTP (11 animals) units were used for collection of electrocardiograms

TABLE 3 | Summary of echocardiographic and telemetry measurements following doxorubicin treatment in cynomolgus monkey.

		Day of study					
Parameter	**Treatment**	**0**	**15-18**	**36-39**	**56-63**	**91-92**	**Final**
Ejection fraction	Vehicle	0.82 ± 0.08	0.79 ± 0.04	0.82 ± 0.05	0.80 ± 0.06	0.82 ± 0.05	0.80 ± 0.06
	Doxorubicin	0.84 ± 0.07	0.80 ± 0.05	0.79 ± 0.10	0.76 ± 0.06	0.67 ± 0.16*	0.48 ± 0.12
Fractional shortening	Vehicle	0.42 ± 0.08	0.38 ± 0.04	0.41 ± 0.05	0.39 ± 0.06	0.40 ± 0.06	0.39 ± 0.06
	Doxorubicin	0.43 ± 0.07	0.39 ± 0.05	0.39 ± 0.09	0.35 ± 0.05*	0.30 ± 0.11*	0.18 ± 0.06
LVDs (cm)	Vehicle	1.04 ± 0.19	1.09 ± 0.14	1.08 ± 0.13	1.14 ± 0.17	1.11 ± 0.19	1.15 ± 0.18
	Doxorubicin	0.98 ± 0.20	1.10 ± 0.19	1.13 ± 0.21	1.20 ± 0.20	1.39 ± 0.37	1.64 ± 0.25
LV contractility (dP/dtmax)	Vehicle	2,309 ± 477	2,859 ± 872	2,815 ± 816	3,304 ± 1,019	2,866 ± 955	2,746 ± 693
	Doxorubicin	2,710 ± 894	2,368 ± 702	2,531 ± 745	2,706 ± 923	2,088 ± 417	1,812 ± 360
QTc (msec)	Vehicle	276 ± 27	277 ± 29	276 ± 25	269 ± 25	267 ± 28	271 ± 25
	Doxorubicin	299 ± 26	324 ± 25*	321 ± 26*	313 ± 27*	331 ± 32*	350 ± 49
Heart rate (bpm)	Vehicle	106 ± 11	120 ± 23	116 ± 19	114 ± 19	115 ± 21	111 ± 19
	Doxorubicin	112 ± 17	113 ± 17	121 ± 17	115 ± 20	133 ± 25	138 ± 28
Mean BP (mm Hg)	Vehicle	70 ± 12	76 ± 13	76 ± 14	76 ± 13	73 ± 13	75 ± 15
	Doxorubicin	76 ± 13	77 ± 15	77 ± 16	75 ± 17	69 ± 18*	66 ± 20

All values are means ± SD (N = 12). Final = last available measurement prior to scheduled or unscheduled sacrifice.
**Statistically different from vehicle treated animals ($p < 0.05$). As Final was on different days for different animals, no statistical assessment is denoted.*

(ECG), body temperature, blood pressure, and left ventricular pressure (LVP) measurements. All animals had been used previously in multiple cardiovascular pharmacology studies but had not been administered any test article for at least 2 weeks prior to study start. The animals used in this study were scheduled for termination due to the duration of their instrumentation.

Doxorubicin Dose Regimen

Male animals were randomly divided into vehicle ($N = 12$, average: 6.37 kg) and doxorubicin-treatment ($N = 12$, average: 5.74 kg) groups. The vehicle group contained seven PCT-implanted monkeys (arterial pressure and ECG) and five PCTP-implanted monkeys (arterial and left ventricular pressures and ECG). The doxorubicin group contained six PCT-implanted monkeys and six PCTP-implanted monkeys. Animals were administered weekly intravenous administrations (1 mL/kg) of either sterile saline or 2 (or 1) mg/kg doxorubicin followed by a 2 mL/kg sterile saline flush. Animals administered doxorubicin were given a temporary dosing holiday when neutrophil counts were <1,000/μL. Dosing holidays were also put in place when there was echocardiographic evidence of systolic heart failure (Fractional Shortening ≤ 18%) (**Table 1**).

Telemetry

Data Sciences International (DSI) Dataquest® OpenART® telemetry equipment was used to generate and acquire the data input. This system transferred the data to a PONEMAH Physiology Platform analysis system. The arterial pressure and body temperature raw signal were digitized at a sampling rate of 250 Hz; the left ventricular pressure (LVP) and ECG were digitized at a sampling rate of 500 Hz. Pre-treatment baseline measurements of ECG and blood pressure measurements were collected for a 24-h period ∼1 week prior to dosing (study day −6). To avoid procedure related disruption of the cardiovascular data, on-study telemetry data was collected continuously with a logging rate of 60 s from ∼46 to 67 h post-treatment (∼21 h). Cardiovascular data were monitored on a weekly basis for the remainder of the study (denoted as days 1, 8, 16, 22, 29, 36, 43, 50, 57, 63, 70, 78, 92, 99, 106,113, 120, and 127). Telemetry units failed during the study for 3 animals (I04923 (vehicle) I04937 and I04932 (doxorubicin) on days 30, 37, and 72, respectively. During dosing holidays, data was collected at times approximating those used for dosing days. Telemetric data were reduced into 1-h time bins for analysis. The QT interval was corrected for heart rate (RR interval) using an individual animal correction formula [QTc = QT + [IACF * (750-RR)], where RR is denoted in msec]. The IACF was derived from a plot of the QT vs. RR interval values collected in at baseline for each animal.

Echocardiography

All echocardiography measurements were done with ketamine anesthesia. Principal measurements included left ventricular internal dimensions during diastole and systole, interventricular septal thickness, and left ventricular free wall during diastole from the M-mode. The aortic dimension (diastole) and left atrial dimension (diastole) were measured using a two-dimension image. The primary endpoints used for assessing cardiac function were fractional shortening and ejection fraction and were calculated using the left ventricular measurements. Two baseline measurements (days −4 and −1) of echocardiographic parameters were collected prior to the start of dosing. Echocardiographic endpoints were collected on an approximately biweekly basis for the remainder of the study (days 18, 25, 39, 56, 67, 77, 91, 105, 116, and 127).

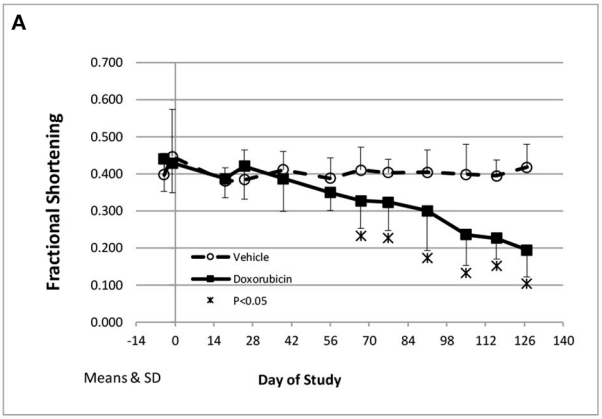

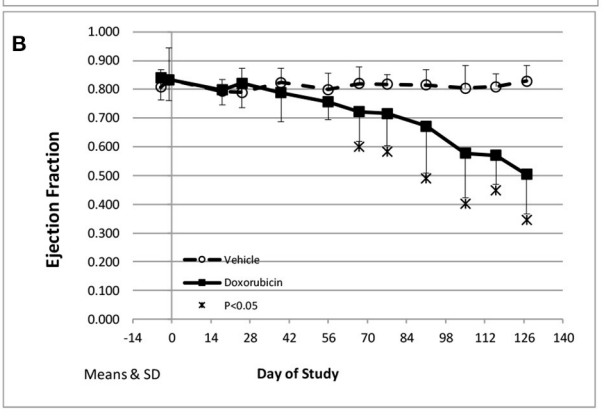

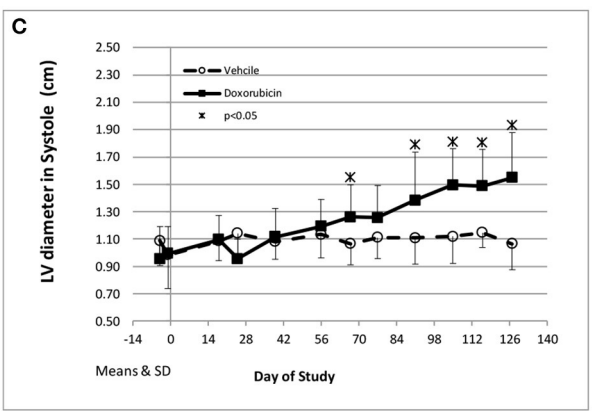

FIGURE 2 | Echocardiography endpoints. Changes in fractional shortening **(A)**, ejection fraction **(B)**, and left ventricular systolic diameter **(C)** over the course of the study. *Statistically different from vehicle treatment.

Blood Sample Analysis

Blood was collected for hematology and clinical chemistry parameters, cardiac biomarkers of acute myocyte damage (cTnI) and heart failure (NT-proBNP), and doxorubicin exposure. Generally, blood was collected from all animals (unanesthetized; femoral vein) twice during the pre-study acclimation period and then at weekly intervals during the treatment phase starting on day 2. Plasma samples were prepared and analyzed in accord to protocol for each endpoint. On four study days, additional blood samples were acquired to measure plasma doxorubicin levels after the initial 2 mg/kg dose (day 1; 8 and 24 h) and following 1 mg/kg (days 36, 78, and 113; 8 and 24 h). The following instruments/methods were used for clinical pathology analysis: hematology: Advia 2120 or 120; coagulation: Stago (Parsippany, NJ); clinical chemistry: Roche Analytics Modular Chemistry Analyzer (Indianapolis, IN); NT-proBNP: ALPCO (human kit BI-20852W) ELISA (Salem, NH); cTnI: Immulite, BeckmanCoulter, Brea, CA.

Statistical Analysis

Telemetry data were divided into analysis blocks based on photoperiod (light and dark cycles). Circadian changes in heart rate and blood pressure are readily observed in non-human primates and reflect changes in autonomic tone. Data collected by telemetry were analyzed for dosing phase data only. The variance-covariance structure used in the analysis was the one providing the smallest Akaike Information Criterion out of the two: Compound Symmetry and Heterogeneous Compound Symmetry. Because the days were not equally spaced throughout the study period, the Autoregressive (1) and Heterogeneous Autoregressive (1) variance-covariance structures were not investigated. For each analysis block separately, a repeated-measures ANOVA (*Baseline* + *Treatment* + *Day* + *Treatment x Day*) was conducted. *Baseline* was the average for each animal from the pre-dose (Study Day −7) data collection period. If the main effect, *Treatment*, was significant and the *Treatment x Day* interaction was not significant, the data were averaged and analyzed across all the days; if the *Treatment x Day* interaction was significant, the data were analyzed at each day separately. A significance level of 0.05 was used for all testing. Echocardiography data was analyzed separately using a simple two-tailed t-test at for each collection and assuming unequal variance.

RESULTS

Doxorubicin Treatment, Tolerability, and Overt Clinical Signs

Over the 135 experimental days, NHP received weekly injections of doxorubicin to induce heart failure, and the control group was given vehicle in the same manner. All doxorubicin-treated animals required dosing holidays (of various durations) due to treatment-related reductions in white blood cell counts (e.g., no treatment on days 22, 29, 43, 57, etc.; **Table 1A**), an indication of drug-induced bone marrow toxicity. Following three consecutive doses of 2 mg/kg, the dose was lowered to 1 mg/kg for the remainder of the study to minimize bone marrow effects and other clinical effects associated with doxorubicin. This dose modification improved tolerability and all 12 doxorubicin-treated animals survived through study day 100. Plasma levels of doxorubicin were proportionally lower following the dose reduction to 1 mg/kg (**Table 1B**). The cumulative doxorubicin dose per animal ranged from 11 to 17 mg/kg, or 132–204 mg/m^2 when expressed per body surface area (**Table 2**). Following day 100, 10 animals underwent unscheduled euthanasia ($N = 1$ on days 103, 105,107, 109, 114; $N = 2$

TABLE 4A | Relationship between contractile function, cardiac biomarkers, QTc interval and myocyte injury in NHP treated chronically with doxorubicin.

NHP#	Dox (mg/kg)	Telemetry unit type	Functional effect or endpoint impacted*					
			dP/dT Max	EF	QTc interval	cTnI	NT-pro-BNP	Cardiac injury
104928	16	BP + LVP						Minimal (U)
104929	13	BP + LVP						(S)
104930	16	BP + LVP						Mild (U)
104931	16	BP + LVP						Minimal (S)
104932	11	BP + LVP						Mild (U)
104933	17	BP + LVP						(U)
104934	13	BP	ND					(U)
104935	17	BP	ND					(U)
104936	13	BP	ND					Mild (U)
104937	16	BP	ND		ND			Mild (U)
104938	13	BP	ND					(U)
104939	13	BP	ND					Minimal (U)

**Cardiac contractility (dP/dtmax derived from LVP): >10% reduction = red; <10% = green. Ejection fraction (EF): >10% reduction = red; <10% = green. QTc interval: >10% prolongation = red; <10% prolongation = green. Troponin (cTnI): ≥2 samples with signal (>0.05 ng/ml) = red; 1/0 samples with signal = green. Natriuretic peptide (NT-pro-BNP): ≥2 samples with signal (>0.05 ng/ml) = red; no signal = green. Cardiac injury: presence of vacuolation = red; no vacuolation = green.*
S, Scheduled sacrifice; U, Unscheduled sacrifice.
ND, not determined due to lack of LVP instrumentation or ECG failure.

TABLE 4B | Relationship between contractile function, cardiac biomarkers, QTc interval and myocyte injury in NHP treated chronically with Vehicle.

NHP#	Dose (mg/kg)	Telemetry unit type	Functional effect or endpoint impacted*					
			dP/dT Max	EF	QTc interval	cTnI	NT-pro-BNP	Cardiac injury
104916	0	BP + LVP						(S)
104917	0	BP + LVP						(S)
104918	0	BP + LVP						(S)
104919	0	BP + LVP						(S)
104920	0	BP + LVP						(S)
104921	0	BP	ND					(S)
104922	0	BP	ND					(S)
104923	0	BP	ND		ND			(S)
104924	0	BP	ND					(S)
104925	0	BP	ND					(S)
104926	0	BP	ND					(S)
104927	0	BP	ND					(S)

**Cardiac contractility (dP/dtmax derived from LVP): >10% reduction = red; no effect (<10%) = green. Ejection fraction (EF): >10% reduction = red; no effect (<10%) = green. QTc interval: >10% prolongation = red; no effect (<10% prolongation) = green. Troponin (cTnI): ≥2 samples with signal (>0.05 ng/ml) = red; 1/0 samples with signal = green. Natriuretic peptide (NT-pro-BNP): ≥2 samples with signal (>0.05 ng/ml) = red; no signal = green; excluded as signal was observed at baseline (pre-dose phase) = gray. Cardiac injury: presence of vacuolation = red; no vacuolation = green.*
S, Scheduled sacrifice; U, Unscheduled sacrifice.
ND, not determined due to lack of LVP instrumentation or ECG failure.
No histopathological evidence of cardiac injury was seen in any of the vehicle treated animals and all were sacrificed as scheduled.

on day 123; $N = 3$ on day 130) for moribund condition (4/10) and/or compromised heart function (10/10) (**Table 1**). All doxorubicin-treated monkeys euthanized at an unscheduled or scheduled interval demonstrated systolic heart failure (e.g., reduced fractional shortening, ejection fraction, and increased left ventricular systolic dimensions).

Multiple clinical observations were noted for doxorubicin-treated monkeys compared with controls throughout the dosing phase. These included: dry and discolored skin (10/12), low food consumption (12/12), red/orange discolored urine (10/12), vomitus (6/12), and non-formed/liquid/discolored feces (3/12). The overall incidence of effects was relatively low given the number of animals and duration of the study. The observations of dry and/or discolored skin correlated to increased incidence of scabs, broken skin, and sores. In the second half of the study (days 61–135), observations of declining animal health and moribund status included hunched posture, squinted eyes, pale skin, hypoactivity, decreased reactivity to stimuli, labored

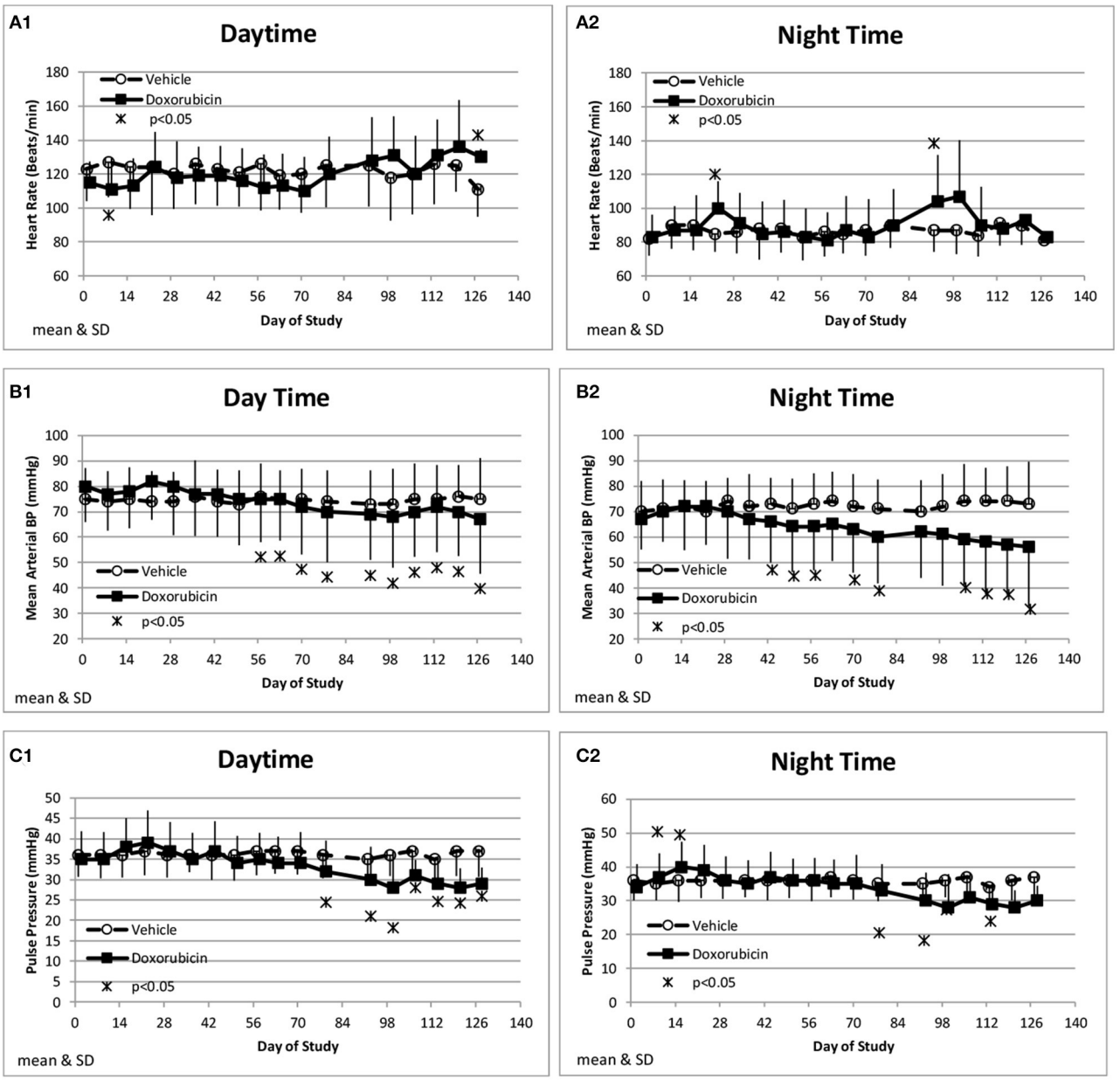

FIGURE 3 | Hemodynamic changes. Changes in heart rate **(A)**, Mean Blood Pressure **(B)**, and Pulse pressure **(C)** averaged over the day (1) and night (2) time frames over the course of the study.

respirations, recumbent posture, coughing, and feeling cold to touch.

Hematology data indicated that doxorubicin caused profound reductions in white blood cell counts (**Figure 1A**), in particular neutrophil levels. At baseline (pre-dose), the normal neutrophil count ranged from 5.1–7.5 $\times$ $10^3/\mu L$, but after three consecutive doses of 2 mg/kg, doxorubicin lowered the average count to 670 $\times$ $10^3/\mu L$ (study day 18); the onset of neutropenia triggered the temporary suspension of treatment. In addition, doxorubicin caused minimal to mild reductions in red cell mass (i.e., red blood cell count, hemoglobin concentration), and hematocrit (**Figure 1B**) during the dosing phase. These hematological effects were attributed to bone marrow dysfunction, were reversible and recovered to near normal levels following the dosing holiday period.

Onset of Heart Failure: Echocardiography Endpoints

The key cardiovascular effects of doxorubicin are shown in **Table 3** and **Figures 2A–C**. At baseline, all echocardiographic parameters (FS%, EF%, and left ventricular systolic diameter) were not significantly different. However, the final collected

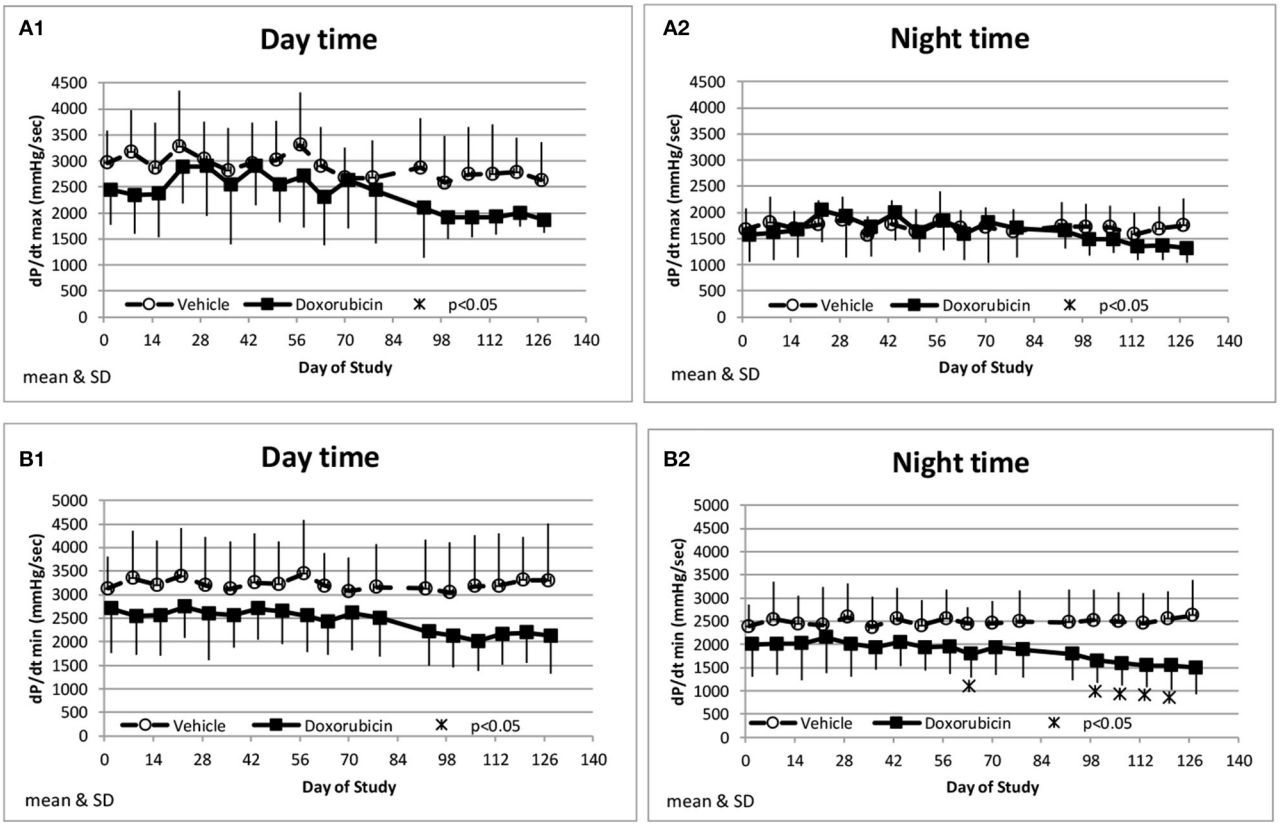

FIGURE 4 | Measurements of indices of cardiac contractility. Changes in dP/dtmax during the day and night cycle times **(A1,A2)**, and dP/dtmin **(B1,B2)** averaged over the day and night time frames over the course of the study.

measurements from each animal indicated heart failure as all indices were significantly different in the doxorubicin-treated animals compared to baseline value or compared to vehicle. The earliest echocardiographic alteration associated with doxorubicin was decreased left ventricular systolic function (FS% and EF%), followed by an increase in the left ventricular systolic dimension (**Figures 2A–C**). Systolic dysfunction was noted in two doxorubicin-treated monkeys as early as days 39–56 but was clearly evident in 3/12 monkeys by day 67. Between study days 67 and 127, all doxorubicin-treated monkeys exhibited systolic failure [reduced fractional shortening (**Figure 2A**), ejection fraction (**Figure 2B**) and increased left ventricular systolic diameter (**Figure 2C**)]. Over the last four assessment intervals (Study Days 91, 105, 116, and 127), mean fractional shortening progressively decreased by 26–54%, and mean ejection fraction progressively decreased by 18–39% in doxorubicin-treated monkeys compared with time-matched controls.

Onset of Heart Failure: Telemetry Endpoints

Along with the decrease in cardiac contractility, doxorubicin progressively lowered mean arterial pressure (**Table 4**). Mean arterial pressure was significantly lower in the light and dark cycles from Study Days 43 through 127 by 7–17 mmHg (−10 to −23%) (**Figures 3B1,B2**). Arterial pulse pressure (the difference between systolic and diastolic pressure) was significantly lower by 4–9 mmHg (−11 to −24%) in doxorubicin-treated monkeys beginning around Study Days 78–92 through the end of the dosing phase (**Figures 3C1,C2**), indicating a decrease in arterial stiffness. Doxorubicin had no effect on left ventricular end diastolic pressure (data not shown). Beginning on Study Day 92 through the end of the dosing phase, dP/dtmin values were lower in the dark cycle by 881–1,125 mmHg/s (−35 to −43%) in doxorubicin-treated animals compared with controls, with statistical significance noted at most time points; a similar pattern and magnitude was evident in the light cycle but did not reach statistical significance (**Figure 4**, **Table 4**). The dP/dtmax values trended lower in doxorubicin-treated monkeys by 665–824 mmHg/s (−26 to −30%) in the light cycle from Study Days 92 through 127; a similar pattern was evident in the dark cycle beginning on Study Day 99 but with a smaller magnitude.

Doxorubicin treatment had no effect on sinoatrial (PR interval) or ventricular (QRS interval) conduction times (data not shown), but significantly and progressively cause delayed ventricular repolarization (QTc intervals) that was observed during the day and night data collection time frames (**Figures 5A,B**). The QTc interval was significantly (>10 ms) prolonged from baseline in doxorubicin-treated monkeys after

study day 50. During the dark cycle, the QTc interval was prolonged by 41–104 ms (14–37%; days 50–127). During the light cycle, the QTc interval was prolonged by 38–74 ms (14–27%; days 70–127). Heart rate was mildly higher after day 90 by 11–19 bpm (9–17%) (**Table 4**, **Figures 3A1**,**A2**, **5A–D**).

Cardiac Biomarkers

Troponin (cTnI) levels were increased slightly above baseline values in 8/12 animals administered doxorubicin at one or more intervals. Most of the increases occurred after day 60 of the dosing phase (**Figures 6A,B**). In the control group, cTnI levels were consistently low (< 0.05 ng/mL) with only a single excursion above 0.2 ng/mL (day 35). Based on qualitative assessment, the surgical insertion and sustained presence of a transmural left ventricular pressure catheter had no impact on cTnI levels.

Two vehicle treated animals had elevated NT-proBNP over the course of the study (including pre-dose) with no other indication of heart failure (e.g., normal EF%) and that data was therefore excluded. NT-proBNP was increased (>1 ng/mL) in several treated animals (8/12) over the course of the study while only one of the remaining ten vehicle treated animal exceeded 1 ng/mL (**Figures 7A,B**). There was no evidence of any impact of the instrumentation on the NT-proBNP levels.

Like cTnI, NT-Pro-BNP levels where elevated in some doxorubicin-treated animals after day 60, a time frame that coincided with onset of heart failure. Plots of final biomarker levels vs. EF% and FS% was created to examine the relationship of cardiac biomarkers level with the degree of heart failure, but no clear correlation was observed (**Figures 8A,B**).

Myocardial Histopathology

Minimal (three of 12 animals) to mild (four of 12 animals), multifocal, vacuolar degeneration of cardiomyocytes was observed in seven of 12 animals receiving doxorubicin and zero of 12 animals receiving vehicle (**Tables 4A**, **4B**, **Figure 9**). Cytoplasmic vacuolation of cardiomyocytes was observed more often in animals that were euthanized in a moribund condition compared with those that survived to scheduled termination. Light microscopic evidence of cytoplasmic vacuolation of cardiomyocytes was consistently associated with elevation of cTnI (six of seven NHP with cardiac injury), however, elevation of cTnI was not uniformly associated with cardiac injury (**Table 4B**: see NHP #104933 and 104935).

DISCUSSION AND CONCLUSIONS

This study successfully documented the time course of LVD following chronic treatment with doxorubicin, which clearly indicates that heart failure can be recapitulated in the cynomolgus monkey. Left ventricular contractile function was assessed with both direct measurement of left ventricular pressure and echocardiography, and telemetry measurements were used to monitor hemodynamics and cardiac conduction and repolarization over the course of the study. Cardiac biomarkers were also tracked to monitor cardiac damage (cTnI) and ventricular wall stress (NT-proBNP). Finally, cardiac tissues

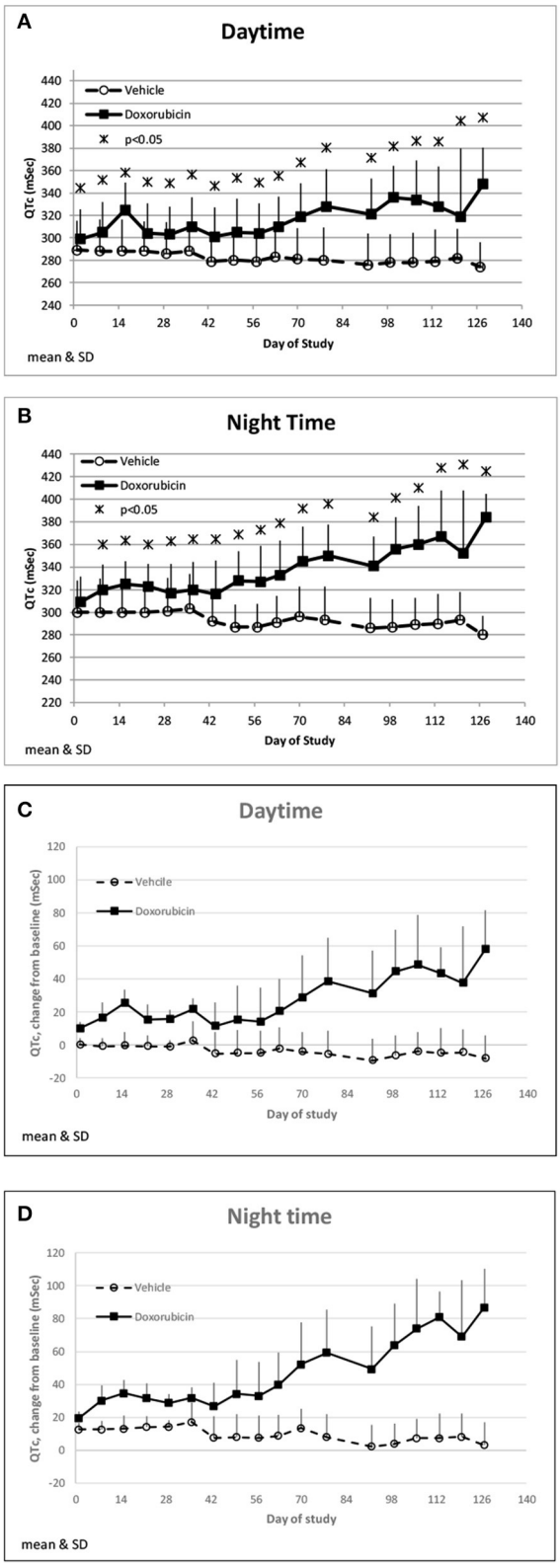

FIGURE 5 | QTc changes. Changes in QTc averaged over the day **(A)** and night **(B)** time frames over the course of the study. Changes in QTc from baseline averaged over the day **(C)** and night **(D)** time frames over the course of the study.

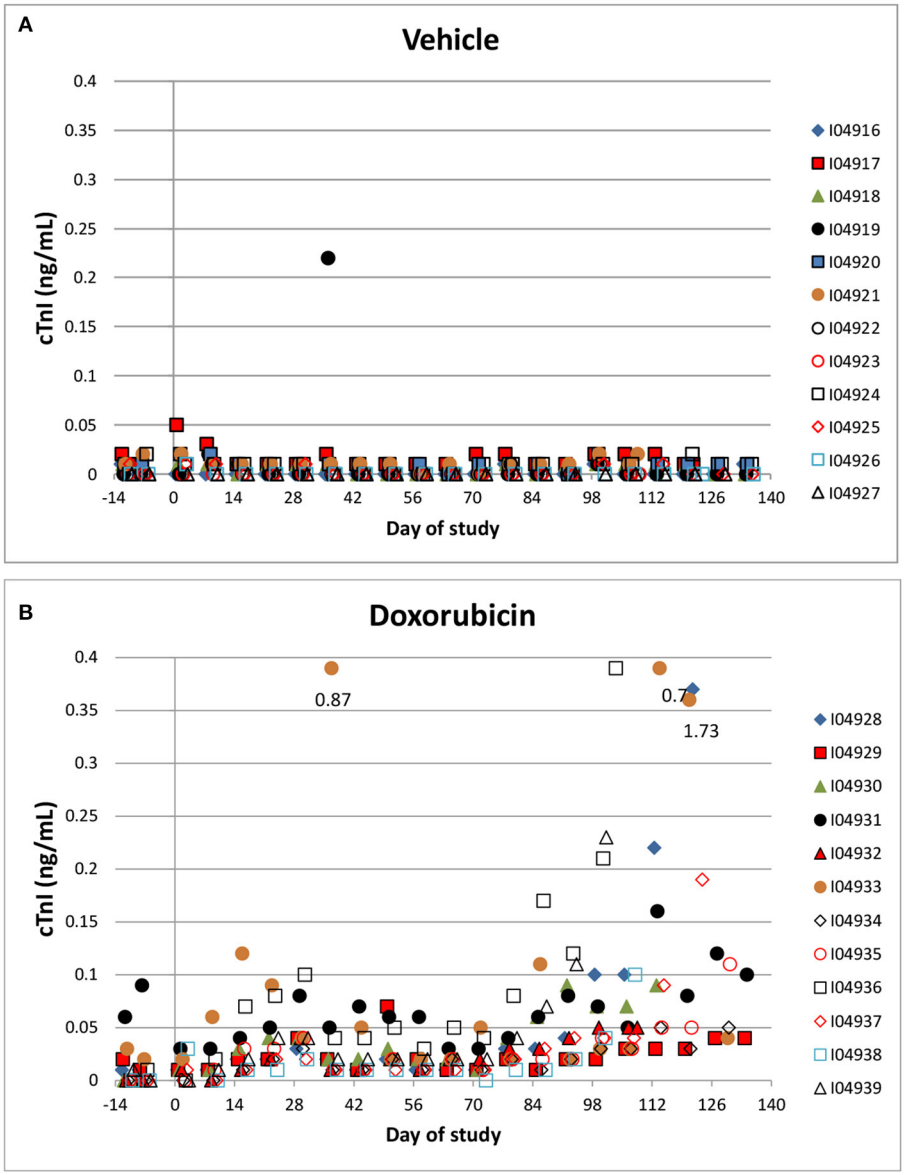

FIGURE 6 | Cardiac Troponin. Changes in individual animal cTnI in control **(A)** a treated **(B)** animals over the course of the study. Filled markers denote animals equipped with LVP catheters.

were examined to determine the incidence of histopathological changes. The integrated use of these cardiovascular endpoints highlight their utility and value in detecting drug-induced LVD and heart failure in this species and validates their use for cardiovascular safety assessment.

Echocardiography is a common clinical method used to measure doxorubicin-related cardiotoxicity, which has a slow onset time in human (25–27). the current study confirms that long-term treatment with doxorubicin caused cardiac dysfunction in all treated animals, and myocyte degeneration (confirmed by histopathology) was observed in a portion of cynomolgus monkeys, as in humans (28). The progressive nature of doxorubicin-induced heart failure with reduced ejection fraction (and fractional shortening) in monkeys (EF: 20–25%) is consistent with clinical phenotype and delayed onset observed in patients (25–27, 29).

In our study, reductions in ejection fraction and fractional shortening were also reflected by trends toward decreases in left ventricular dP/dt_{max} (decreased inotropy) and dP/dt_{min} (decreased lusitropy) (**Figure 4**). LVP telemetry is an invasive method but it is a sensitive technique for the continual measurement of cardiac contractility in free-moving unanesthetized animals (12). Thus, it avoids the confounding influence of anesthetic sedation and/or restraint that is required

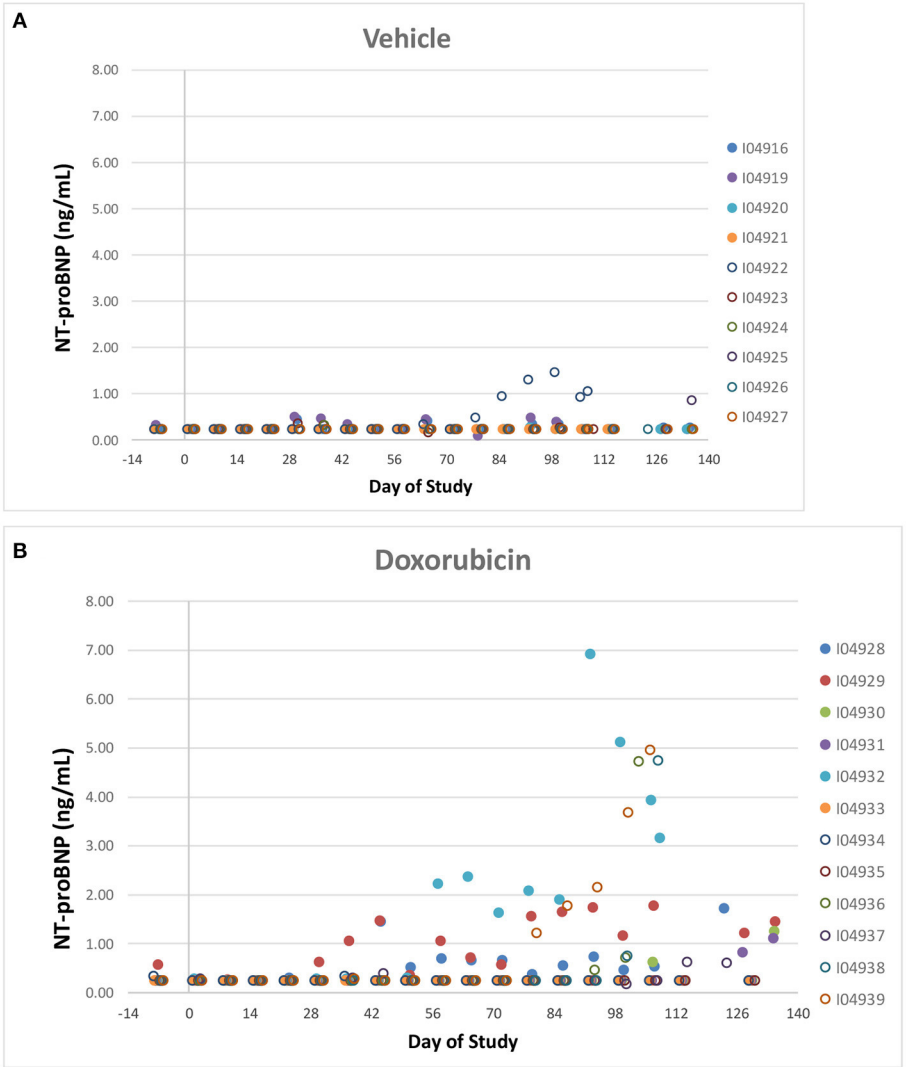

FIGURE 7 | NT-proBNP. Individual animal NT-proBNP measurements in control **(A)** a treated **(B)** animals over the course of the study. Filled markers denote animals equipped with LVP catheters.

to perform echocardiography in monkeys. The lack of functional or biomarker differences between the animals instrumented for blood pressure only vs. blood and ventricular pressure instrumentation suggests that a transmural ventricular catheter did not impact the negative inotropic response to doxorubicin. Doxorubicin has been shown to decrease left ventricular contractility in other species (dogs) both acutely (17) and after chronic treatment (30). The changes in cardiac function were accompanied by enlargement of left ventricular systolic diameter. The increase in left ventricular diameter during systole in this study is consistent with the observed decrease in ejection fraction and fractional shortening. Interestingly, the left ventricular diastolic diameter did not markedly increase in the same time frame, and therefore the decrease in function was not accompanied by signs of cardiac hypertrophy as has been reported with other models (7, 31).

Troponin release (cTnI) is a marker of cardiac myocyte damage and is useful clinically for diagnosing cardiac damage resulting from myocardial infarction. Previous studies in rats (14, 32) and dogs (33) have demonstrated doxorubicin-related cTnI increases. However, in this study, while individual animals had sporadic increases in cTnI, there were no consistent changes. The incidence and magnitude of increases in cTnI was greater toward the end of the study, concurrent with changes indicating decreased cardiac function. It is possible that the gradual onset of the compromise in cardiac function did not cause sufficient ongoing myocyte damage to result in sustained increases in cTnI. The limits of detection for the assay used in this study have been superseded by newer high- and ultra-high sensitivity assays and it is possible that more consistent treatment-related small changes in cTnI could be detected by those assays (32, 34).

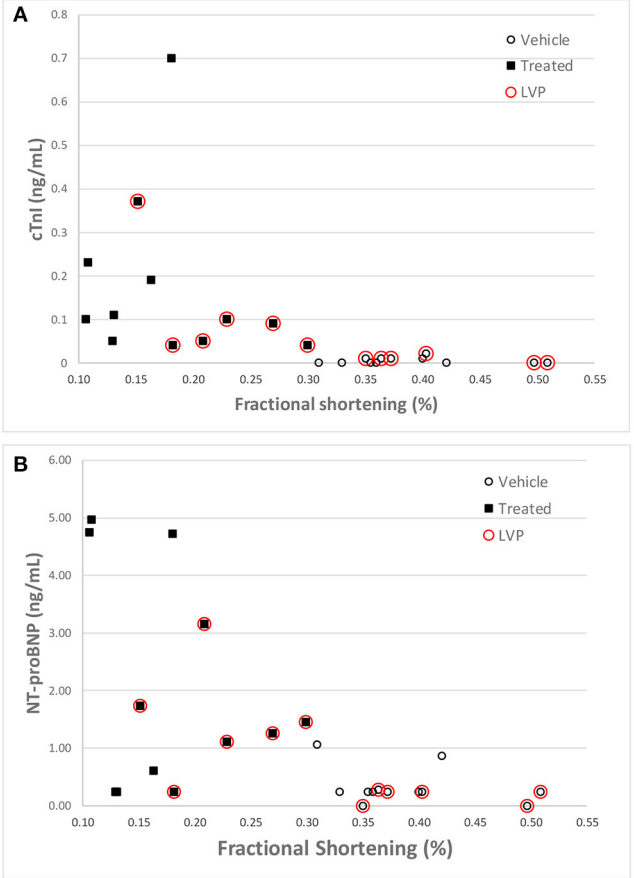

FIGURE 8 | Correlation of cTnI **(A)** and NT-proBNP **(B)** levels with Fractional Shortening measurements at the final echocardiography measurement for each animal. Red circles denote animals equipped with LVP catheters.

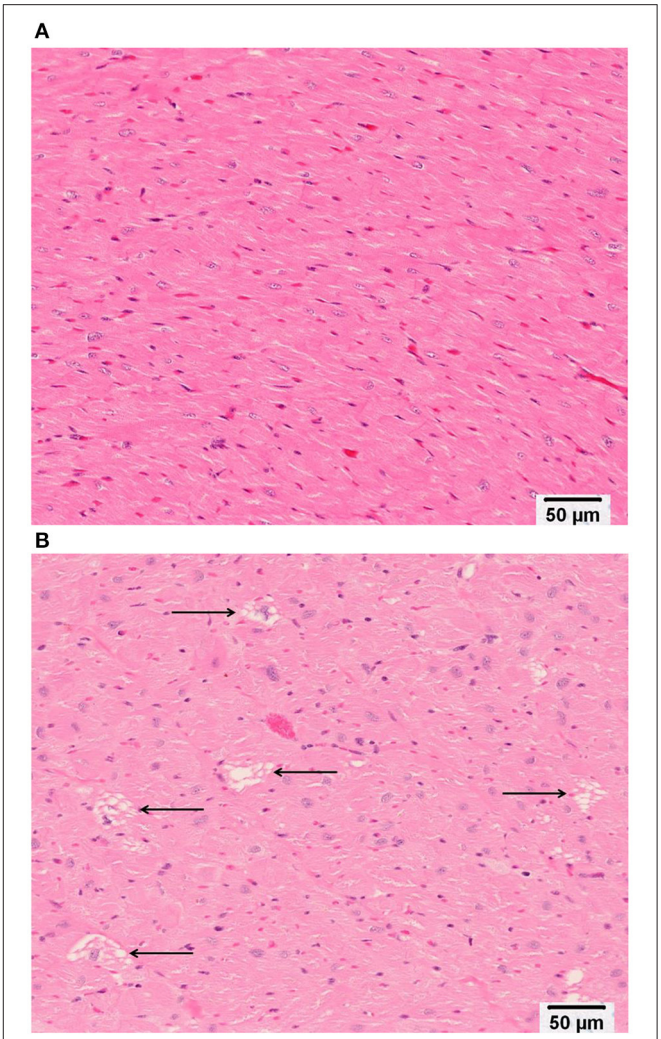

FIGURE 9 | Representative photomicrographs of heart tissue from **(A)** a Vehicle treated animal with normal myocardium; and **(B)** Doxorubicin treated animals with multifocal, cytoplasmic vacuolar degeneration of cardiomyocytes (arrows). Bar equals 50 microns.

Naturetic peptides (BNP and NT-proBNP) are considered to be the "gold standard" for diagnosis of heart failure in the clinic (35, 36) with NT-proBNP preferred by some due to a longer persistence in the blood. NT-proBNP has been used clinically to predict cardiac damage associated with anthracycline treatment (37). In this study, two control animals had consistently elevated NT-proBNP levels for much of the study (however levels were reduced at the end of the study). As these animals had normal left ventricular function over this time frame, the underlying reason for this elevation is unknown and has been excluded. Both cTnI and NT-proBNP were occasionally but not consistently higher at the end of the study in animals with LVD. The reason for the lack of good correlation is not known. NT-proBNP has rarely been measured in the NHP though increases have been reported in animals treated with an immune checkpoint inhibitor (38). The observed progressive increase in QTc in the treated animals is likely due to structural changes in the myocardium (minimal to mild degeneration of cardiomyocytes) of affected animals. Similar changes have been observed in human clinical studies with doxorubicin and other cancer therapeutics. However, treatment-related QTc increases have been observed with no concomitant changes in ejection fraction (10, 39). The underlying mechanisms for the QTc change, which are specifically not related to direct or indirect hERG channel blockade (40) are unclear, but likely reflect electric remodeling and loss of repolarization reserve secondary to doxorubicin-induced heart failure.

Blood pressure decreased slightly, and heart rates tended to increase in treated animals after week 43. Although the mechanism of these changes is not clear, they may be related to the changes in sympathetic tone concurrent with the decline in cardiac function.

Other studies have demonstrated that doxorubicin can cause detrimental effects to mitochondria and the sarcoplasmic reticulum (41). This histopathological analysis in this study was limited to light microscopy, where there was only minimal to mild vacuolation of cardiomyocytes (seven of 12 treated animals). Overall, based on the study results, dramatic cardiovascular

functional changes seen in the doxorubicin-treated animals were not accompanied by severe histopathological changes.

The original dose selected, 2 mg/kg/week, caused bone marrow toxicity that resulted in progressively decreased neutrophil counts. A dosing holiday for all the animals allowed the neutrophil counts to recover. The subsequent 1 mg/kg every other week dosing regimen spared neutrophil counts but was insufficient to degrade cardiac function. An increase in dose to 1 mg/kg/week resulted in generally progressive decreases in ejection fraction and fractional shortening. There was also evidence of variable response to treatment in that some animals required additional dosing holidays (due to decreased neutrophil counts) while others tolerated the weekly dosing schedule until study termination.

This study demonstrated the ability to detect progressive changes in cardiac function related to heart failure using telemetry and echocardiography in the cynomolgus monkey administered clinically relevant levels of the anthracycline oncology agent doxorubicin. This study demonstrated the utility and sensitivity of serial echocardiography to detect decreases in cardiac function. These echocardiographic changes were generally accompanied in more than half of the doxorubicin treated animals by changes in clinical biomarkers such as cTnI and NT-proBNP concentrations and occasional histopathological lesions. This type of adaptive study design, where doses were modified based on monitored clinical pathology endpoints is potentially more relevant for study of the impact of interventions designed to ameliorate toxicity related to anthracycline treatment which has been advocated by others (42). This required flexibility illustrates the difficulty of modeling the clinical liability of late or delayed decreases in cardiac function with a standard preclinical study design. The cardiac liability is only replicated with a dosing paradigm that avoids overt toxicity while maintaining a high enough dose to produce cardiac toxicity. The serial measurements of cardiac function presented here provided a unique documentation of the progressive decreases in cardiac function during heart failure in the NHP after repeated administration of doxorubicin.

DATA AVAILABILITY STATEMENT

The raw data supporting the conclusions of this article will be made available by the authors, without undue reservation.

ETHICS STATEMENT

All research protocols were approved by the Testing Facility Institutional Animal Care and Use Committees (IACUC) prior to dose administration.

AUTHOR CONTRIBUTIONS

All authors listed have made a substantial, direct and intellectual contribution to the work, and approved it for publication.

FUNDING

The authors declare that this study received funding from Amgen Inc. The funder was not involved in the study design, collection, analysis, interpretation of data, the writing of this article or the decision to submit it for publication.

ACKNOWLEDGMENTS

We thank Dr. Jaqueline Walisser who directed the study a Covance Laboratories, Dr. Meg Sleeper who provided the echocardiography measurements and Ms. Irene Soto for project management.

REFERENCES

1. Bristow MR, Billingham ME, Mason JW, Daniels JR. Clinical spectrum of anthracycline antibiotic cardiotoxicity. *Cancer Treat Rep.* (1978) 62:873–9.
2. Shan K, Lincoff AM, Young JB. Anthracyline-Induced Cardiotoxicity. *Ann Intern Med.* (1996) 125:47–58. doi: 10.7326/0003-4819-125-1-199607010-00008
3. Zang S, Liu X, Bawa-Khalfe T, Lu L, Yi LL, Liu LF, et al. Identification of the molecular basis of doxorubicin-induced cardiotoxicity. *Nat Med.* (2012) 18:1639–45. doi: 10.1038/nm.2919
4. Montaigne D, Hurt C, Neviere R. Mitochondria death/survival signaling pathways in cardiotoxicity induced by anthracyclines and anticancer-targeted therapies. *Biochem Res Int.* (2012) 2012:951539. doi: 10.1155/2012/951539
5. Takahashi SS, Denvir MA, Harder L, Miller DJ, Cobbe SM, Kawakami, M, et al. Effects of in vitro and in vivo exposure to doxorubicin (adriamycin) on caffeine-induced Ca2+ release from sarcoplasmic reticulum and contractile protein function in 'chemically-skinned'rabbit ventricular trabeculae. *Jap J Pharm.* (1998) 76:405–13. doi: 10.1254/jjp.76.405
6. Minotti G, Menna P, Salvatorelli E, Cairo G, Gianni L. Anthracyclines: molecular advances and pharmacologic developments in antitumor activity and cardiotoxicity. *Pharmacol Rev.* (2004) 56:185–229. doi: 10.1124/pr.56.2.6
7. Ewer MS, Lippman SM. Type II chemotherapy-related cardiac dysfunction: time to recognize a new entity. *J Clin Oncol.* (2005) 23:2900–2. doi: 10.1200/JCO.2005.05.827
8. Eschenhagen T, Force T, Ewer MS, De Keulenaer GW, Suter TM, Anker SD, et al. Cardiovascular side effects of cancer therapies: a position statement from the heart failure association of the european society of cardiology. *Eur J Heart Fail.* (2011) 13:1–10. doi: 10.1093/eurjhf/hfq213
9. Sparano JA. Doxorubicin/Taxane combinations: cardiac toxicity and pharmacokinetics. *Semin Oncol.* (1999) 26:14–9.
10. Nousiainen T, Vanninen E, Rantala A, Jantunen E, Hartikainen J. QT dispersion and late potentials during doxorubicin therapy for non-Hodgkin's lymphoma. *J Intern Med.* (1999) 245:359–64. doi: 10.1046/j.1365-2796.1999.00480.x
11. Lee BH, Goodenday LS, Muswick GJ, Yasnoff WA, Leighton RF, Skell RT, et al. Alterations in left ventricular diastolic function with doxorubicin therapy. *J Am Coll Cardiol.* (1987) 9:184–8. doi: 10.1016/S0735-1097(87)80099-2
12. Guth BD, Chiang AY, Doyle J, Engwall MJ, Guillon JM, Hoffmann P, et al. The evaluation of drug-induced changes in cardiac inotropy in dogs: Results from a HESI-sponsored consortium. *J Pharmacol Toxicol Methods.* (2015) 75:70–90. doi: 10.1016/j.vascn.2015.02.002

13. Pugsley MK, Guth B, Chiang A, Doyle J, Engwall M, Guillon JM, et al. A HESI consortium update on cardiac contractility endpoints. *J Pharmacol Toxicol Methods.* (2016) 100:390–1. doi: 10.1016/j.vascn.2016.02.180
14. Cove-Smith L, Woodhouse N, Hargreaves A, Kirk J, Smith S, Price SA, et al. An integrated characterization of serological, pathological, and functional events in doxorubicin-induced cardiotoxicity. *Toxicol Sci.* (2014) 140:3–15. doi: 10.1093/toxsci/kfu057
15. Migrino RQ, Aggarwal D, Konorev E, Brahmbhatt T, Bright M, Kalyanaraman B, et al. Early detection of doxorubicin cardiomyopathy using two-dimensional strain echocardiography. *Ultrasound Med Biol.* (2008) 34:208–14. doi: 10.1016/j.ultrasmedbio.2007.07.018
16. Hanai K, Takabe K, Manabe S, Nakano M, Kohda A, Matsuo M. Evaluation of cardiac function by echocardiography in dogs treated with doxorubicin. *J Toxicol Sci.* (1996) 21:1–10. doi: 10.2131/jts.21.1
17. Ditchey RV, LeWinter MM, Higgins CB. Acute effects of doxorubicin (adriamycin) on left ventricular function in dogs. *Int J Cardiol.* (1984) 6:341–50. doi: 10.1016/0167-5273(84)90194-3
18. Manno RA, Grassetti A, Oberto G, Nyska A, Ramot Y. The minipig as a new model for the evaluation of doxorubicin-induced chronic toxicity. *J Appl Toxicol.* (2016) 36:1060–72. doi: 10.1002/jat.3266
19. Sieber SM, Correa P, Young DM, Dalgard DW, Adamson RH. Cardiotoxic and possible leukemogenic effects of adriamycin in nonhuman primates. *Pharmacology.* (1980) 20:9–14. doi: 10.1159/000137337
20. Malik M, Allison DE, Dybdal N, Lum BL. Trastuzumab (recombinant humanized monoclonal anti-HER2) clearance is not altered in a non-clinical model of doxorubicin-induced cardiotoxicity. *Proc Am Assoc Cancer Res.* (2004) 45 (Suppl):1245.
21. Takayama S, Thorgeirsson UP, Adamson RH. Chemical carcinogenesis studies in nonhuman primates. *Proc Japan Acad Series B.* (2008) 84:176–88. doi: 10.2183/pjab.84.176
22. Heyen J, Vargas H. The use of nonhuman primates in cardiovascular safety assessment. In: Bluemel J. Korte S, Schenck E, & Weinbauer G, editors. *The Nonhuman Primate in Nonclinical Drug Development and Safety Assessment*. San Francisco, CA: Academic Press (2015) 551–78. doi: 10.1016/B978-0-12-417144-2.00029-9
23. Clark JD, Gebhart GF, Janet CG, Keeling ME, Kohn DF. The 1996 guide for the care and use of laboratory animals. *ILAR J.* (1997) 38:41–48.
24. Food and Drug Administration. *Guidance for Industry: Estimating the Maximum Safe Starting Dose in Initial Clinical Trials for Therapeutics in Adult Healthy Volunteers*. Beltsville, MD: Center for Drug Evaluation and Research (CDER) (2005) 1245.
25. Parisi AF, Moynihan PF, Folland ED. Echocardiographic evaluation of left ventricular function. *Med Clin North Am.* (1980) 64:61–81. doi: 10.1016/S0025-7125(16)31625-X
26. Steinherz LJ, Steinherz PG, Tan CT, Heller G, Murphy ML. Cardiac toxicity 4 to 20 years after completing anthracycline therapy. *JAMA.* (1991) 266:1672–7. doi: 10.1001/jama.1991.03470120074036
27. Lipshultz SE, Lipsitz SR, Sallan SE, Dalton VM, Mone SM, Gelber RD, et al. Chronic progressive cardiac dysfunction years after doxorubicin therapy for childhood acute lymphoblastic leukemia. *J Clin Oncol.* (2005) 23:2629–36. doi: 10.1200/JCO.2005.12.121
28. Isner JM, Ferrans VJ, Cohen SR, Witkind BG, Virmani R, Gottdiener JS et al. Clinical and morphologic cardiac findings after anthracycline chemotherapy: analysis of 64 patients studied at necropsy. *Am. J. Card.* (1983) 51:1167–1174.
29. Geisberg CA, Sawyer DB. Mechanisms of anthracycline cardiotoxicity and strategies to decrease cardiac damage. *Curr Hypertens Rep.* (2010) 12:404–10. doi: 10.1007/s11906-010-0146-y
30. Astra LI, Hammond R, Tarakji K, Stephenson LW. Doxorubicin-Induced Canine CHF. *J Card Surg.* (2003) 18:301–6. doi: 10.1046/j.1540-8191.2003.02032.x
31. Toyoda Y, Okada M, Kashem MA. A canine model of dilated cardiomyopathy induced by repetitive intracoronary doxorubicin administration. *J Thorac Cardiovasc Surg.* (1998) 115:1367–73. doi: 10.1016/S0022-5223(98)70221-1
32. Reagan WJ, York M, Berridge B, Schultze E, Walker D, Pettit S. Comparison of cardiac troponin I and T, including the evaluation of an ultrasensitive assay, as indicators of doxorubicin-induced cardiotoxicity. *Toxicol Pathol.* (2013) 41:1146–58. doi: 10.1177/0192623313482056
33. Burgener IA, Kovacevic A, Mauldin GN, Lombard CW. Cardiac troponins as indicators of acute myocardial damage in dogs. *J Vet Internal Med.* (2006) 20:277–83. doi: 10.1111/j.1939-1676.2006.tb02857.x
34. Herman EH, Knapton A, Rosen E, Thompson K, Rosenzweig B, Estis J, et al. A multifaceted evaluation of imatinib-induced cardiotoxicity in the rat. *Toxicolic Pathol.*(2011) 39:1091–106 doi: 10.1177/0192623311419524
35. Maisel AS, Choudhary R. Biomarkers in acute heart failure—state of the art. *Nat Rev Cardiol.* (2012) 9:478–90. doi: 10.1038/nrcardio.2012.60
36. Latini R, Masson S. NT-PROBNP: a guide to improve the management of patients with heart failure. *EJIFCC.* (2013) 24:78–84.
37. Romano S, Fratini S, Ricevuto E, Procaccini V, Stifano G, et al. Serial measurements of NT-proBNP are predictive of not-high-dose anthracycline cardiotoxicity in breast cancer patients. *Br J Cancer.* (2011) 105:1663. doi: 10.1038/bjc.2011.439
38. Ji C, Roy MD, Golas J, Vitsky A, Ram S, Kumpf SW, et al. Myocarditis in cynomolgus monkeys following treatment with immune checkpoint inhibitors. *Clin Cancer Res.* (2019) 25:4735–48. doi: 10.1158/1078-0432.CCR-18-4083
39. Curigliano G, Mayer EL, Burstein HJ, Winer EP, Goldhirsch A. Cardiac toxicity from systemic cancer therapy: a comprehensive review. *Prog Cardiovasc Dis.* (2010) 53:94–104. doi: 10.1016/j.pcad.2010.05.006
40. Vargas HM, Bass AS, Koerner J, Matis-Mitchell S, Pugsley MK, Skinner M, et al. Evaluation of drug-induced QT interval prolongation in animal human studies: a literature review of concordance. *Br J Pharmacol.* (2015) 172:4002–11. doi: 10.1111/bph.13207
41. Zhou S, Starkov A, Froberg MK, Leino RL, Wallace KB. Cumulative and irreversible cardiac mitochondrial dysfunction induced by doxorubicin. *Cancer Res.* (2001) 61:771–7.
42. Gianni L, Herman EH, Lipshultz SE, Minotti G, Sarvazyan N, Sawyer DB. Anthracycline cardiotoxicity: from bench to bedside. *J Clin Oncol.* (2008) 26:3777–84. doi: 10.1200/JCO.2007.14.9401

Conflict of Interest: All authors were employed by Amgen, Inc. NE is employed by Seattle Genetics.

The authors declare that the research was conducted in the absence of any commercial or financial relationships that could be construed as a potential conflict of interest.

frontiers in Cardiovascular Medicine

CASE REPORT
published: 19 March 2021
doi: 10.3389/fcvm.2021.655808

Case Report: QT Prolongation and Abortive Sudden Death Observed in an 85-Year-Old Female Patient With Advanced Lung Cancer Treated With Tyrosine Kinase Inhibitor Osimertinib

Moë Kondo[1], *Megumi Kisanuki*[1], *Yosuke Kokawa*[1], *Seiichiro Gohara*[1], *Osamu Kawano*[1], *Shuntaro Kagiyama*[1], *Toru Maruyama*[2]*, *Keita Odashiro*[1] *and Yoshihiko Maehara*[1]

[1] *Division of Cardiology, Department of Internal Medicine, Kyushu Central Hospital, Fukuoka, Japan,* [2] *Department of Hematology, Oncology and Cardiovascular Medicine, Kyushu University Hospital, Fukuoka, Japan*

OPEN ACCESS

Edited by:
Margaret Rose Cunningham, University of Strathclyde, United Kingdom

Reviewed by:
Gavin Oudit, University of Alberta, Canada
Martino Deidda, University of Cagliari, Italy

***Correspondence:**
Toru Maruyama
maruyama@artsci.kyushu-u.ac.jp

Specialty section:
This article was submitted to Cardio-Oncology, a section of the journal Frontiers in Cardiovascular Medicine

Received: *19 January 2021*
Accepted: *22 February 2021*
Published: *19 March 2021*

Citation:
Kondo M, Kisanuki M, Kokawa Y, Gohara S, Kawano O, Kagiyama S, Maruyama T, Odashiro K and Maehara Y (2021) Case Report: QT Prolongation and Abortive Sudden Death Observed in an 85-Year-Old Female Patient With Advanced Lung Cancer Treated With Tyrosine Kinase Inhibitor Osimertinib. Front. Cardiovasc. Med. 8:655808. doi: 10.3389/fcvm.2021.655808

Cardiac arrest occurred in an 85-year-old female administered osimertinib for advanced lung cancer expressing epidermal growth factor receptor (EGFR) mutations. Electrocardiogram (ECG) recorded at recurrence of spontaneous circulation showed sinus rhythm associated with mild QT prolongation (QTc = 455 ms) to which silent myocardial ischemia and coadministration of itraconazole and herbal drug causing hypokalemia (2.1 mEq/L) may have contributed. Discontinuation of osimertinib, itraconazole and herbal drug, potassium supplementation and percutaneous coronary intervention alleviated QT prolongation (QTc = 432 ms). Osimertinib is the third-generation tyrosine kinase inhibitor lengthening QT interval, and careful monitoring of ECG, serum potassium and drugs coadministered during chemotherapy including osimertinib are highly required.

Keywords: cancer, herbal drug, osimertinib, QT prolongation, cardiooncology

INTRODUCTION

Cardiovascular complications of anticancer drugs are the main interest within the field of cardiooncology (1). Osimertinib, a third-generation tyrosine kinase inhibitor (TKI), is a first-line therapy for patients with cancer expressing epidermal growth factor receptor (EGFR) mutations. This anticancer drug has adverse effects including cardiotoxicity such as coronary tonus elevation and QT prolongation in electrocardiogram (ECG), because vascular and cardiac potassium channels are regulated largely by EGFR tyrosine kinase (2). However, osimertinib-induced QT prolongation leading to the possible development of Torsades de Pointes (TdP) has received less attention (3). We herein describe a case of 85-year-old female patient with EGFR driver mutant lung cancer treated with osimertinib, which lengthened QT interval causing abortive sudden cardiac death (SCD).

CASE DESCRIPTION

An 85-year-old female was conveyed by ambulance to the emergency room of our hospital due to cardiac arrest. She had lost her consciousness at 15:15 after she visited the outpatient clinic of another hospital for the treatment with advanced lung cancer (adenocarcinoma: cT2aN1M1b, Stage IVB). Bystander resuscitation was started immediately after the cardiac arrest, and emergency call was requested at 15:18. Ambulance crews confirmed cardiac arrest at 15:28, and she restored spontaneous circulation at 15:34 after the first discharge of public automated external defibrillator (AED). When she admitted to our hospital by ambulance at 15:40, her body temperature was 36.2°C, consciousness level in Glasgow Coma Scale was E1V1M1, and reflex to light was prompt. Blood pressure was 154–103 mmHg, pulse was regular, and its rate was 81 bpm. No abnormal physical findings were found. She had been started administration of oral osimertinib (40 mg once daily) as a first-line therapy of lung cancer after confirming EGFR mutation (T790M), oral itraconazole (200 mg once daily) for prevention of opportunistic fungal infection and crude herbal anticancer drug used in Chinese traditional medicine (TJ-48). She had no complaint of chest oppression or syncope nor family history of unexpected or abortive SCD in her relatives.

Laboratory examination on admission included serum chemistry showing total protein 5.8 g/dL, albumin 3.2 g/dL, CK 215 IU/L (CK-MB 19 IU/L), CRP 0.3 mg/dL, BNP 348.5 pg/mL, troponin T (TnT) 0.01 ng/mL, Na 139 mEq/L, Ca 9.2 mEq/L, and K 2.1 mEq/L. Hematology indicated mild anemia (hemoglobin of 10.3 g/dl) associated with white blood cell and platelet counts of 8,500/μL and 25.1 × 10^4/μL, respectively. ECG showed sinus rhythm, left axis deviation, flat or inverted T waves observed in II, III, aV_F, V_{5-6}, and QT prolongation (grade I), i.e., QT interval corrected by heart rate ($QTc = QT/RR^{0.5}$) was 455 ms (**Figure 1A**). Chest X-ray showed cardiomegaly and chest computed tomography demonstrated bilateral pleural effusion (**Figures 2A**,**B**). Ejection fraction was 64% on echocardiogram. Chemotherapeutic regimen including osimertinib, oral itraconazole and herbal medicine (TJ-48) were discontinued, and supplementation of potassium was started. Considering possible ischemic T wave changes (**Figure 1A**), coronary angiogram was performed. Stenotic lesion (99%) was found in the right coronary artery (segment 1) and collateral circulation supplied from left anterior descending artery was observed (**Figures 3A**,**B**). Percutaneous coronary intervention (PCI) was completed successfully by stent implantation at the culprit lesion (**Figures 3C**,**D**). QTc interval after the successful PCI and restoration of hypokalemia (K of 4.0 mEq/L) was 432 ms (**Figure 1B**), and she discharged on foot 33 days after admission without any neurological sequelae of cardiac arrest. Administration of osimertinib (40 mg once daily) was resumed in the hospital where she had been started chemotherapy under the monitoring of ECG and serum potassium concentration while coadministration of itraconazole and herbal drug was interrupted.

DISCUSSION

Osimertinib is an oral, third-generation TKI as an emerging therapeutic modality in various cancers with EGFR T790M mutation (2). One of the obstacles for wide use of this promising anticancer agent is QT prolongation. QT interval is lengthened as a result of ventricular potassium current reduction and late sodium current augmentation (4). Bian et al. (5) reported a first case of 85-year-old male patient with advanced non-small cell lung cancer associated with TdP induced by oral osimertinib (80 mg once daily) and concomitant intravenous moxifloxacin, a broad-spectrum fluoroquinolone antibiotics known to lengthen the QT interval (QTc of 484 ms). Hypokalemia (2.94 mEq/L), impaired left ventricular ejection fraction (41%) and coadministration of moxifloxacin were concluded to underlie the development of TdP. They lost this case and hence cautioned cardio-oncologists to identify cancer patients at high risk of QT prolongation leading to the development of TdP (5). Cancer development and apoptosis is governed by driver mutation of signal transduction process mediated by several growth factor receptor including EGFR which is linked to many potassium channels, i.e., Kv1.3 (6), Kv10.1 (7), Kv4.3 (8), and Kir2.3 (9) are modulated by EGFR kinase via phosphorylation of tyrosine in their specific residues. These potassium channels regulate vascular tonus and QT interval in ECG. Therefore, EGFR-TKI shows variable cardiotoxicity including vascular constriction and QT prolongation. Although the serum concentration of osimertinib was not monitored, and genetic testing of hereditary long QT syndrome was not performed in this case, careful ECG monitoring is essential for cancer patients under the chemotherapy including osimertinib (10).

QT interval is regulated strictly by many factors including basic heart rate, electrolytes, body temperature, sex hormones, and so on. Therefore, key factor of QT prolongation in this case is not determined easily. This case is an 85-year-old female patient, and old woman *per se* is a risk factor of QT prolongation (1). Oral itraconazole, a representative antifungal agent, is known to elevate the serum concentration of osimertinib due to competitive metabolism mediated by cytochrome P450 3A4 (CYP3A4). Chronic myocardial ischemia requiring PCI and hypokalemia (2.1 mEq/L) caused partly by Chinese herbal drug may have also contributed to the QT prolongation. Osimertinib causes coronary tonus elevation induced by vascular constriction mediated by inhibition of vascular EGFR (10), which may have aggravated silent myocardial ischemia in this case. Chinese traditional medicine of TJ-48 is used widely in Japan under the adjuvant anticancer therapeutic strategy as in this case. This herbal medicine is reported to enhance the efficacy of chemotherapy and to attenuate the adverse effects and complications of anticancer treatment (11). However, long-term use of Chinese herbal medicines is sometimes associated with hypokalemia caused by pseudoaldosteronism that is evoked by licorice contained in many herbal medicines. Although the incidence of hypokalemia induced by the administration of TJ-48 is not reported, such incidence by other Chinese medicine

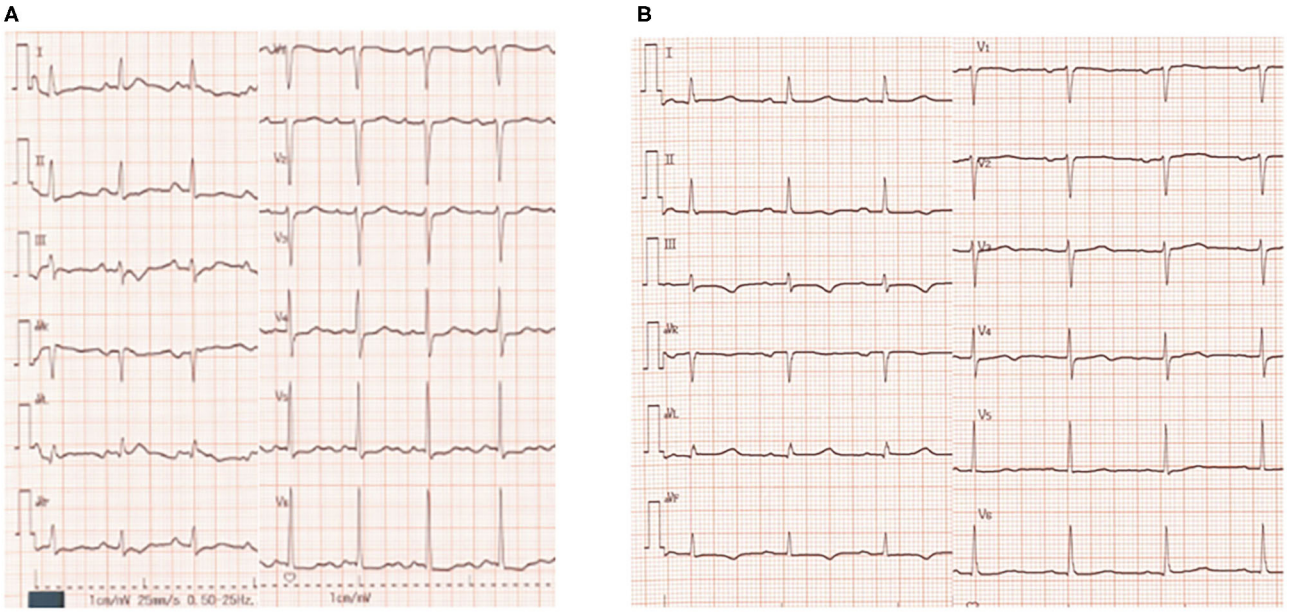

FIGURE 1 | Twelve-lead electrocardiogram (ECG) on admission **(A)** and before discharge **(B)**. QTc interval was 455 ms **(A)** and 432 ms **(B)**, respectively. Herat rate correction of QT interval was performed by Bazett's formula.

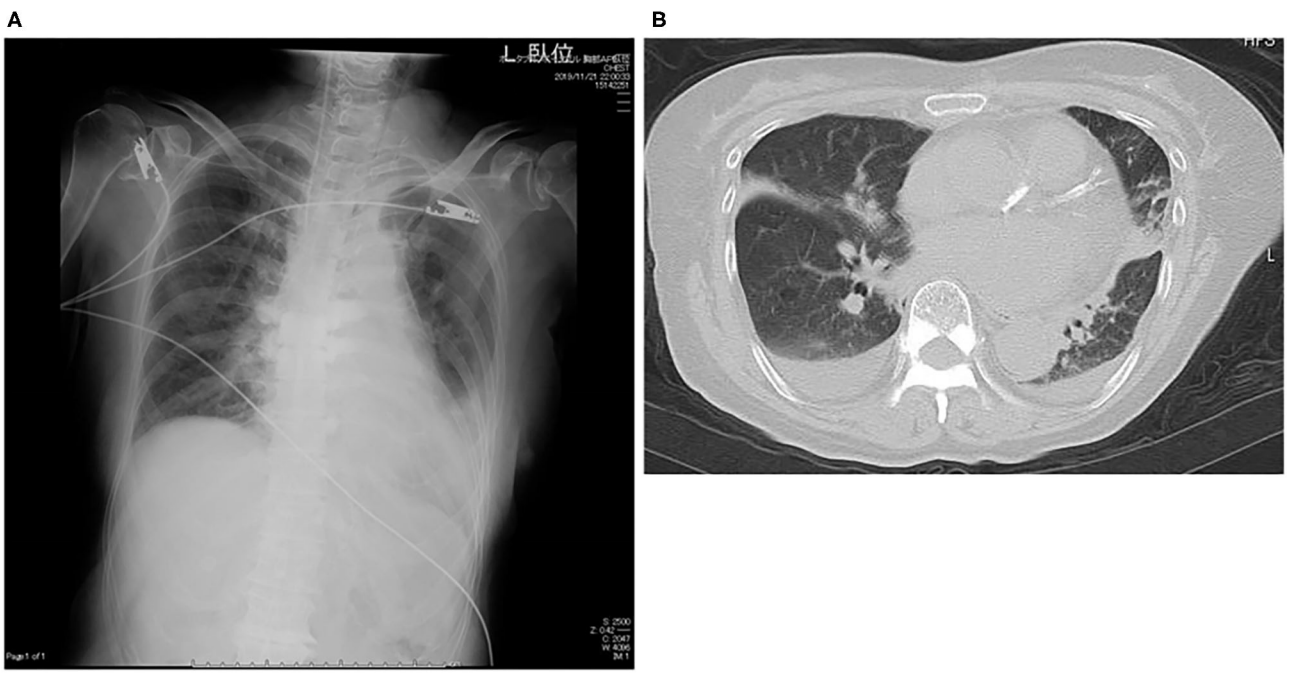

FIGURE 2 | Chest X-ray on admission **(A)** and chest computed tomography during hospitalization **(B)**.

ranges from 6.6% (TJ-54) to 33% (TJ-9 and TJ-68) according to the Japanese Adverse Drug Report Database (12).

Considering the serum chemistry (normal CK-MB isozyme and negative TnT test) and echocardiographic left ventricular wall motion, cardiac arrest caused by acute coronary syndrome was unlikely. Silent myocardial ischemia is associated with QT prolongation caused by electrical instability and sympathovagal imbalance (13), and QT prolongation *per se* is responsible for SCD whatever the causes to prolong QT intervals are (14). Well-developed collateral circulation may have made coronary artery

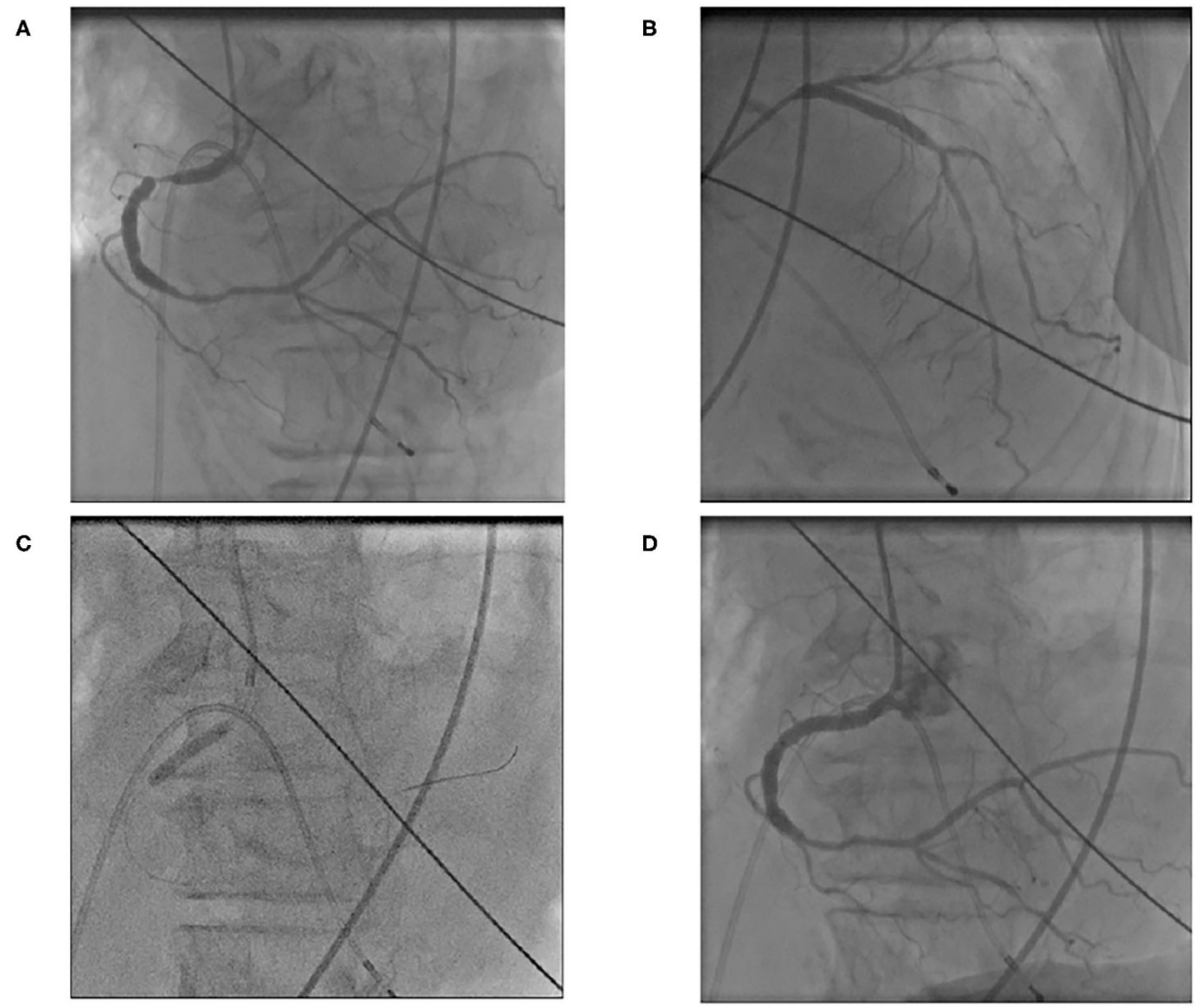

FIGURE 3 | Right coronary angiogram showed severe (99%) stenotic lesion in segment 1 **(A)**. Collateral circulation from left anterior descending artery was visualized **(B)**. Stent implantation was performed **(C)** and right coronary angioplasty was completed **(D)**.

disease silent in this case (**Figures 3A**,**B**). This case description includes limitations, i.e., ECG was not retrieved from AED, serum TnT was assayed only once, and serum concentration of osimertinib was not assayed. In spite of these limitations, cardiac arrest in this case was supposed to be due to possible development of TdP based on several predisposing factors lengthening QT interval. Because defibrillation by means of public AED restored her spontaneous circulation, and recurrence of cardiac arrest was prevented after normalization of QT interval by elective PCI, discontinuation of causative drugs and potassium supplementation. Although QT prolongation in this case was grade I, this interval was measured at rest and supine position. QT interval dynamicity is accentuated by daily physical activity (15), and the relation between sudden increase in QT interval and the development of TdP is open to debate. This case taught us the necessity of collaboration between oncologists and cardiologists in the earlier clinical course of cancer patients.

CONCLUSIONS

We have described an 85-year-old female patient with EGFR-mutant advanced lung cancer treated with standard regimen of osimertinib, which underlay in part grade I QT prolongation causing abortive SCD. Reversible factors promoting QT prolongation were removed after admission and this patient was discharged safely. Although osimertinib-induced QT prolongation is mild to moderate (grade I or II) and not frequent (3–10%) in AURA study and FLAURA trial to verify the safety and efficacy of osimertinib (16, 17), TdP may be induced by standard dose of osimertinib, when multiple risk factors to lengthen QT interval are incidentally overlapped. Careful ECG monitoring and appropriate management of risk factors lengthening QT interval such as interacting drugs, electrolyte imbalance and cardiac ischemia during chemotherapy including osimertinib are highly required.

DATA AVAILABILITY STATEMENT

The raw data supporting the conclusions of this article will be made available by the authors, without undue reservation.

ETHICS STATEMENT

Written informed consent was obtained from the individual(s) for the publication of any potentially identifiable images or data included in this article.

AUTHOR CONTRIBUTIONS

This case report article was carried out in collaboration between all coauthors. MKo was taking main care of this case. MKi had an equal contribution to this case report. YK was supervising MKo and MKi. SG was performing PCI in this case. OK was investigating the novelty and the rarity of this case. SK was exploring the literature relating to this case. TM performed writing of the main part of this manuscript. KO had the initial concept of this manuscript preparation and provided this manuscript with deep insight. YM supervised collaboration of the cardiology team. All authors read and approved the final manuscript.

ACKNOWLEDGMENTS

We thank ward staffs of Kyushu Central Hospital for clinical assistance.

REFERENCES

1. Sadasivan C, Zhabyeyev P, Labib D, White JA, Paterson DI, Oudit GY. Cardiovascular toxicity of PI3Kα inhibitors. *Clin Sci.* (2020) 134:2595–622. doi: 10.1042/CS20200302
2. Schiefer M, Hendriks LEL, Dinh T, Lalji U, Dingemans AC. Current perspective: osimertinib-induced QT prolongation: new drugs with new side-effects need careful patient monitoring. *Eur J Cancer.* (2018) 91:92–8. doi: 10.1016/j.ejca.2017.12.011
3. Porta-Sánchez A, Gilbert C, Spears D, Amir E, Chan J, Nanthakumar K, et al. Incidence, diagnosis, and management of QT prolongation induced by cancer therapies. A systematic review. *J Am Heart Assoc.* (2017) 6:e007724. doi: 10.1161/JAHA.117.007724
4. Zhabyeyev P, McLean B, Chen X, Vanhaesebroeck B, Oudit GY. Inhibition of PI3Kinase-α is pro-arrhythmic and associated with enhanced late Na^+ current, contractility, and Ca^{2+} release in murine hearts. *J Mol Cell Cardiol.* (2019) 132:98–109. doi: 10.1016/j.yjmcc.2019.05.008
5. Bian S, Tang X, Lei W. A case of torsades de pointes induced by the third-generation EGRF-TKI, osimertinib combined with moxifloxacin. *BMC Pulm Med.* (2020) 20:181. doi: 10.1186/s12890-020-01217-4
6. Teisseyre A, Palko-Labuz A, Sroda-Pomianek K, Michalak K. Voltage-gated potassium channel Kv1.3 as a target in therapy of cancer. *Front Oncol.* (2019) 9:933. doi: 10.3389/fonc.2019.00933
7. Wu W, Dong MQ, Wu XG, Sun HY, Tse HF, Lau CP, et al. Human ether-à-go-go gene potassium channels are regulated by EGFR tyrosine kinase. *Biochim Biophys Acta.* (2012) 1823:282–9. doi: 10.1016/j.bbamcr.2011.10.010
8. Zhang YH, Wu W, Sun HY, Deng XL, Cheng LC, Li X, et al. Modulation of human cardiac transient outward potassium current by EGFR tyrosine kinase and Src-family kinases. *Cardiovasc Res.* (2012) 93:424–33. doi: 10.1093/cvr/cvr347
9. Zhang DY, Zhang YH, Sun HY, Lau CP, Li GR. Epidermal growth factor receptor tyrosine kinase regulates the human inward rectifier potassium K(IR)2.3 channel, stably expressed in HEK 293 cells. *Br J Pharmacol.* (2011) 164:1469–78. doi: 10.1111/j.1476-5381.2011.01424.x
10. Chaar M, Kamta J, Ait-Oudhia S. Mechanisms, monitoring, and management of tyrosine kinase inhibitors-associated cardiovascular toxicities. *Onco Targets Ther.* (2018) 11:6227–37. doi: 10.2147/OTT.S170138
11. Wang Z, Qi F, Cui Y, Zhao L, Sun X, Tang W, et al. An update on Chinese herbal medicines as adjuvant treatment of anticancer therapeutics. *Biosci Trends.* (2018) 12:220–39. doi: 10.5582/bst.2018.01144
12. Ishida T, Kawada K, Morisawa S, Jobu K, Morita Y, Miyamura M. Risk factors for pseudoaldosteronism with Yokusankan use: analysis using the Japanese Adverse Drug Report (JADER) database. *Biol Pharm Bull.* (2020) 43:1570–6. doi: 10.1248/bpb.b20-00424
13. Tomassoni G, Pisanó E, Gardner L, Krucoff MW, Natale A. QT prolongation and dispersion in myocardial ischemia and infarction. *J Electrocardiol.* (1998) 30(Suppl.):187–90. doi: 10.1016/s0022-0736(98)80073-3
14. O'Neal WT, Singleton MJ, Roberts JD, Tereshchenko LG, Sotoodehnia N, Chen LY, et al. Association between QT interval components and sudden cardiac death: the ARIC study. *Circ Arrhythm Electrophysiol.* (2017) 10:e005485. doi: 10.1161/CIRCEP.117.005485
15. Nakaji G, Fujihara M, Fukata M, Yasuda S, Odashiro K, Maruyama T, et al. Open-loop, clockwise QT-RR hysteresis immediately before the onset of torsades de pointes in type 2 long QT syndrome. *J Electrocardiol.* (2010) 43:261–3. doi: 10.1016/j.jelectrocard.2009.12.005
16. Yang JCH, Ahn MJ, Kim DW, Ramalingam SS, Sequist LV, Su WC, et al. Osimertinib in pretreated T790M-positive advanced non-small-cell lung cancer: AURA study phase II extension component. *J Clin Oncol.* (2017) 35:1288–96. doi: 10.1200/JCO.2016.70.3223
17. Soria JC, Ohe Y, Vansteenkiste J, Reungwetwattana T, Chewaskulyong B, Lee KH, et al. Osimertinib in untreated EGFR mutated advanced non-small-cell lung cancer. *N Engl J Med.* (2018) 378:113–25. doi: 10.1056/NEJMoa1713137

Conflict of Interest: The authors declare that the research was conducted in the absence of any commercial or financial relationships that could be construed as a potential conflict of interest.

frontiers in Cardiovascular Medicine

ORIGINAL RESEARCH
published: 01 April 2021
doi: 10.3389/fcvm.2021.605993

Exercise Training Preserves Myocardial Strain and Improves Exercise Tolerance in Doxorubicin-Induced Cardiotoxicity

Igor L. Gomes-Santos[1†], Camila P. Jordão[1], Clevia S. Passos[1], Patricia C. Brum[2], Edilamar M. Oliveira[2], Roger Chammas[3], Anamaria A. Camargo[4] and Carlos E. Negrão[1,2]*

[1] Faculdade de Medicina, Heart Institute (InCor), Hospital das Clínicas, Universidade de São Paulo, São Paulo, Brazil, [2] School of Physical Education and Sport, Universidade de São Paulo, São Paulo, Brazil, [3] Faculdade de Medicina, Cancer Institute of the State of São Paulo (ICESP), Hospital das Clínicas, Universidade de São Paulo, São Paulo, Brazil, [4] Centro de Oncologia Molecular, Hospital Sírio-Libanês, São Paulo, Brazil

OPEN ACCESS

Edited by:
Jun-ichi Abe, University of Texas MD Anderson Cancer Center, United States

Reviewed by:
Martino Deidda, University of Cagliari, Italy
Christian Cadeddu Dessalvi, University of Cagliari, Italy

***Correspondence:**
Igor L. Gomes-Santos
igomesdossantos@mgh.harvard.edu

†Present address:
Igor L. Gomes-Santos, Department of Radiation Oncology, Massachusetts General Hospital and Harvard Medical School, Boston, MA, United States

Specialty section:
This article was submitted to Cardio-Oncology, a section of the journal Frontiers in Cardiovascular Medicine

Received: *14 September 2020*
Accepted: *01 March 2021*
Published: *01 April 2021*

Citation:
Gomes-Santos IL, Jordão CP, Passos CS, Brum PC, Oliveira EM, Chammas R, Camargo AA and Negrão CE (2021) Exercise Training Preserves Myocardial Strain and Improves Exercise Tolerance in Doxorubicin-Induced Cardiotoxicity. Front. Cardiovasc. Med. 8:605993. doi: 10.3389/fcvm.2021.605993

Doxorubicin causes cardiotoxicity and exercise intolerance. Pre-conditioning exercise training seems to prevent doxorubicin-induced cardiac damage. However, the effectiveness of the cardioprotective effects of exercise training concomitantly with doxorubicin treatment remains largely unknown. To determine whether low-to-moderate intensity aerobic exercise training during doxorubicin treatment would prevent cardiotoxicity and exercise intolerance, we performed exercise training concomitantly with chronic doxorubicin treatment in mice. Ventricular structure and function were accessed by echocardiography, exercise tolerance by maximal exercise test, and cardiac biology by histological and molecular techniques. Doxorubicin-induced cardiotoxicity, evidenced by impaired ventricular function, cardiac atrophy, and fibrosis. Exercise training did not preserve left ventricular ejection fraction or reduced fibrosis. However, exercise training preserved myocardial circumferential strain alleviated cardiac atrophy and restored cardiomyocyte cross-sectional area. On the other hand, exercise training exacerbated doxorubicin-induced body wasting without affecting survival. Finally, exercise training blunted doxorubicin-induced exercise intolerance. Exercise training performed during doxorubicin-based chemotherapy can be a valuable approach to attenuate cardiotoxicity.

Keywords: exercise, cardiac function, speckle tracking, doxorubicin, cardiotoxicity, fatigue

INTRODUCTION

Doxorubicin (Doxo) is an antineoplastic agent widely used to treat various cancer types over the last decades. Its clinical applications, however, are hampered by several adverse side effects. It affects healthy organs and systems as well (1), by inducing cardiotoxicity (2) and contributing to tiredness and exercise intolerance, also reported as cancer-related fatigue (3, 4).

Previous studies demonstrated that Doxo-induced cardiotoxicity is a dose-dependent phenomenon, defining safety ranges for Doxo in preventing heart failure (HF) (5–7). However, Doxo treatment remains prevalently associated with ventricular dysfunction, characterized by a reduction of left ventricular (LV) ejection fraction (EF) > 10% from baseline or displaying

LVEF < 50% (5, 7). Although clinically overt cardiotoxicity occurs in ∼6% of cancer patients, at least one in seven patients will present subclinical cardiotoxicity, and 1 out of 10 will experience an adverse cardiovascular event (8). This borderline impairment of ventricular function may not reach the minimum guideline-levels for starting a pharmacological intervention during cancer treatment, but it might account for the high incidence of cardiovascular morbidity and mortality observed in previously treated patients, even several years after defeating cancer (9, 10). Hence, finding strategies to prevent Doxo-related adverse effects are highly desirable.

Exercise training (ExTr) has been suggested as a non-pharmacological approach against Doxo-induced cancer-related fatigue and cardiotoxicity (1, 11–15). Several studies have consistently demonstrated a protective role of ExTr when performed before chemotherapy in preclinical models. However, it remains unknown whether ExTr performed *concomitantly* with Doxo-based treatment prevents cardiotoxicity (15). Considering the adherence to ExTr programs in cancer patients declines as the dose of ExTr intensity increases (16), we tested the hypothesis that a low-to-moderate intensity aerobic ExTr program during Doxo treatment would prevent cardiotoxicity and exercise intolerance.

METHODS

Animal Care and Experimental Protocol

All animals care and procedures were conducted following the National Council for the Control of Animal Experimentation (CONCEA) and approved by the Institutional Scientific Committee of the Heart Institute (InCor-HCFMUSP) and the Ethics Committee on Animal Use (CEUA) of the University of São Paulo Medical School (FMUSP). Eight-week-old male C57BL/6J mice were enrolled in the study. Mice were evaluated for exercise capacity and LV structure and function and then assigned into three groups: Control (no exercise, saline-treated, $n = 12$), Doxo (no exercise, treated with doxorubicin, $n = 20$) and Doxo + ExTr (exercise-trained, treated with doxorubicin, $n = 20$). They were kept in a temperature-controlled room with a 12:12-h light-dark cycle and free access to a standard diet and water. The animals were euthanized by cervical dislocation under deep anesthesia. The heart was dissected to separate right ventricle (RV), left ventricle (LF), and septum, allowing the assessment of RV hypertrophy using Fulton's index (RV/LV + S). Heart and Lungs were weighted for determination of absolute (wet tissue, in mg) or relative (normalized by tibia length, mm) mass. Heart samples (LV) were then snap-frozen in liquid nitrogen and stored at −80°C for biochemical and histological analysis.

Echocardiography

The LV evaluations were performed using a preclinical ultrasound system (Vevo 2100 Imaging System, Visual Sonics, Canada), and mice were sedated with 5% isoflurane and kept under anesthesia by continuous administration of 1–1.5% of isoflurane with 1 L/min 100% O_2 to maintain light sedation throughout the procedure. Transthoracic echocardiography was performed using a 40-MHz transducer positioned on the mice shaved chest with contact gel, and images were stored on cine loops at the time of the study using a digital Two-dimensional B mode with short-axis views at the level of the papillary muscle. LV dimensions were measured in the B-mode, in the 2-dimensional parasternal long-axis view. All the analyses were conducted according to the American Society of Echocardiography guidelines (17). Strain analysis was based on speckle tracking technique (18), which uses acoustic backscatter on 2D grayscale ultrasound images (two-dimensional cinematic images) as tissue marker, allowing the quantification of myocardial deformation along the longitudinal, radial, and circumferential axes, according to myocardial fiber orientation. The parasternal long-axis view provided a longitudinal and radial strain and strain rate. Circumferential and radial strain and strain rates were obtained from the parasternal short-axis view. Both long- and short-axis views are divided automatically into six segments for speckle tracking throughout the cardiac cycle and their average provided global (longitudinal, circumferential, and radial) parameters.

Determination of Exercise Capacity and Prescription of Exercise Training

Maximal running capacity tests were performed at baseline and at the end of the experimental protocol on a mouse running treadmill, providing parameters of exercise tolerance (running time, in s and running performance, in J) and proper exercise prescription, as described previously (19). The ExTr program consisted of a continuous, low-to-moderate aerobic ExTr (∼40–50% of maximal exercise capacity at 0% grade, 40 min per session, 4 days per week for 5 weeks).

Doxorubicin Treatment

Doxorubicin was obtained from the Cancer Institute, University of São Paulo Medical School (ICESP-HCFMUSP) pharmacy. Doxo was administered once a week via intraperitoneal injections of 5 mg/kg for 5 weeks (20). Saline groups received 0.9% saline injection on the same volume of Doxo-treated groups (0.1 mL). Mice were not subjected to ExTr on the day of Doxo or saline injections, neither for the following 2 days.

Western Blot

Protein expression levels were analyzed by immunoblotting. Frozen samples from LV were homogenized in Tris-HCl buffer (100 mM Tris-HCl, 50 nM NaCl, 1% Triton, pH 7.4) and protease/phosphatase inhibition cocktail (1:100, Sigma-Aldrich, USA). After centrifugation (10,000 × g, 4°C, 10 min), we recovered the supernatant and added a loading buffer (Laemmli 1:1, Sigma-Aldrich, USA). Samples (30 μg) were then transferred to SDS-PAGE in 10% acrylamide gels and submitted electrophoresis and then electrically transferred to a nitrocellulose membrane (BioRad Biosciences, USA). The membranes were incubated in a blocking solution (5% BSA, 10 mM Tris-HCl, pH 7.6, 150 mM NaCl, e 0.1% Tween 20) for 3 h in room temperature, then overnight in 4°C with primary antibodies. The primary antibodies binding was detected using secondary antibodies with peroxidase

activity, reaction detected by chemiluminescence (Amersham Biosciences, USA), and visualized by autoradiography. Mouse monoclonal anti-GATA4 (Santa Cruz sc-25310, 1:500), rabbit polyclonal anti-SOD1[Cu-Zn] (Abcam ab16831, 1:2,000), rabbit polyclonal anti-SOD2[Mn] (Abcam ab13533, 1:5,000) and mouse monoclonal anti-SOD3[EC] (Abcam ab80946, 1:1,000) total expression levels were normalized by a housekeep gene (mouse monoclonal anti-ß-actin, Santa Cruz sc-47778), and rabbit monoclonal anti-phospho-ERK1/2 [Thr202/Tyr 204] (Cell Signaling #4377, 1:1,000) as ratio to total rabbit monoclonal anti-ERK1/2 (Cell Signaling #4695, 1:1,000). We also analyzed GATA4 in the cytosolic and nuclear fractions. The cytosolic and nuclear fractions were obtained by an extraction kit (NER-PER, ThermoFisher Scientific, EUA). We used Image-J (National Institute of Health, USA) software to quantify immunoblots density.

Histological Analysis

Cross-sectional rings of the mid-left ventricles were frozen in nitrogen-cooled isopentane. Then, samples were serially sliced into 10-μm cross-sections from the proximal to the distal region using a cryostat (Micron HM505E, Zeiss, Germany). The fiber cross-sectional area (CSA) was evaluated in transverse cardiomyocytes, stained with Griffonia simplicifolia lectin (1 h at room temperature), and imaged at 40x magnification. CSA of adjacent cardiomyocytes from at least three slides per mice, $n = 2$ mice per group were pooled, averaging ∼300 cardiomyocytes per group. Collagen deposition was quantified in cardiac sections stained with Picrossirius Red, and imaged under 40x objective. The images were thresholded, and the interstitial collagen fractional area was averaged from at least five fields per slide, $n = 5$ mice per group, and expressed as a percentage. Images were acquired using a Leica Quantimet 520 (Cambridge Instruments, UK), and analyzed with Image J (National Institute of Health, USA).

Statistical Analysis

Results are expressed as Mean ± SEM. Statistical analyses were performed using GraphPad Prism software. Kaplan-Meier plots were generated and a log-rank test performed to compare exercise time tolerance curves. Endpoints were compared by one-way ANOVA with Tuckey's multiple comparison tests or Student *t*-test to detect group differences. We used linear regression for correlative analysis. In all cases, we considered as significant a $P \leq 0.05$.

RESULTS

Doxo-Induced LVEF Reduction Is Not Prevented by ExTr

We first conducted a maximal exercise capacity test to properly prescribe ExTr, as well as echocardiography to set

TABLE 1 | Physical characteristics, ventricular morphology and function, and effort tolerance at baseline.

	Co	Doxo	Doxo + ExTr	*P*-value
Bodyweight, g	23.6 ± 0.43	23.3 ± 0.46	23.1 ± 0.2	0.66
HR, bpm	437 ± 24	387 ± 26	365 ± 31	0.93
Left ventricular morphology				
LVEDD, mm	3.61 ± 0.09	3.60 ± 0.08	3.58 ± 0.11	0.49
LVESD, mm	2.44 ± 0.14	2.54 ± 0.15	2.43 ± 0.22	0.89
IVS, mm	0.77 ± 0.01	0.76 ± 0.03	0.79 ± 0.02	0.63
LVPW, mm	0.69 ± 0.03	0.64 ± 0.02	0.69 ± 0.02	0.32
Systolic function				
LVEF, %	60.1 ± 4.92	56.0 ± 5.29	59.6 ± 7.05	0.61
LVFS, %	32.4 ± 3.29	29.5 ± 3.55	32.8 ± 4.82	0.49
LVEDV, μL	55.3 ± 3.61	54.9 ± 3.03	54.4 ± 3.63	0.81
LVESV, μL	22.3 ± 3.27	24.4 ± 3.38	23.3 ± 4.83	0.58
CO, mL/min	14.6 ± 1.80	11.4 ± 1.05	11.4 ± 1.72	0.17
SV, μL	33.0 ± 3.25	30.4 ± 2.96	31.1 ± 3.26	0.85
Diastolic function				
Mitral E velocity, mm/s	478 ± 57.9	574 ± 46.5	481 ± 59.9	0.99
Mitral A velocity, mm/s	200 ± 36.8	269 ± 39.1	201 ± 20.4	0.49
Mitral E/A ratio	2.78 ± 0.44	2.31 ± 0.32	2.20 ± 0.20	0.47
Exercise tolerance				
Running distance, m	665 ± 41.3	603 ± 52.3	621 ± 27.5	0.66
Running performance, J	154 ± 11.6	140 ± 11.8	143 ± 6.14	0.98

n = 8–11 Control, n = 8–9 Doxo, n = 7–9 Doxo + ExTr. One-Way ANOVA.

CO, cardiac output; HR, heart rate; IVS, interventricular septal wall thickness; LVEDD, left ventricular end-diastolic diameter; LVEDV, left ventricular end-diastolic volume; LVESV, left ventricular end-systolic volume; LVEF, left ventricular ejection fraction; LVESD, left ventricular end-systolic diameter; LVPW, left ventricular posterior wall thickness; LVSF, left ventricular stroke fraction; SV, stroke volume.

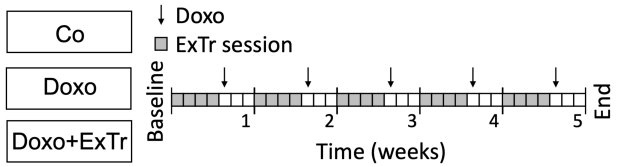

FIGURE 1 | Experimental design. Doxorubicin was administered weekly (5 mg/kg i.p. for 5-wk), concomitantly with low-to-moderate intensity aerobic exercise training (40–50% maximal exercise capacity for 40 min, 4 days per week), or follow-up. Co, control ($n = 12$); Doxo, doxorubicin ($n = 20$); Doxo + ExTr, doxorubicin + exercise training ($n = 20$); ExTr, exercise training.

baseline cardiac parameters (displayed in **Table 1**). We then applied a Doxo treatment previously established (**Figure 1**) (20), exposing mice to an accumulated dose of 25 mg/kg. Echocardiography confirmed Doxo-induced cardiotoxicity, characterized by reduced cardiac output (CO) and LVEF (**Table 2** and **Figures 2A,B**). LVEF reduced 26% with Doxo alone, and 22% under Doxo + ExTr in comparison to Control (**Figure 2B**). Under conventional echocardiography, ExTr was not able to prevent Doxo-induced LV dysfunction expressed by CO and LVEF (**Figures 2A,B**), LV fractional shortening (FS), and stroke volume (SV) (**Table 2**).

The Myocardial Circumferential Strain Is Preserved With ExTr

Speckle tracking analysis indicated that Doxo significantly affected the circumferential SAX strain (**Figure 2C**) and strain rate (SR) (**Figure 2E**). Those are quantifications of how much the myocardium has deformed in every cycle and at what velocity, respectively. They represent the vector of strain and SR of six regional segments (**Figures 2D,F**, schematic localization of each segment in **Figure 2G**). Cardiac strain analysis showed that ExTr prevented the deleterious effects of Doxo in the SAX circumferential strain and SR (**Figure 2**). ExTr brought the posterior wall (PW), inferior free wall (IFW), and posterior septum (PS) toward normal ranges, therefore normalizing global parameters of circumferential strain and SR in SAX (**Figures 2C–G**). This suggests a benefic effect of ExTr on regional myocardial contractility.

ExTr Prevents Doxo-Induced Cardiopulmonary Atrophy

Pathological analysis indicated Doxo induced atrophy of cardiac and pulmonary tissue (**Table 2** and **Figure 3**). Cardiac mass (**Figure 3A**), left ventricle (**Figure 3B**), and lung (**Figure 3C**) relative mass were reduced with Doxo, as well as Fulton's index (**Figure 3D**). ExTr partially alleviated Doxo effects on these parameters. Histological analysis showed Doxo reduces the cross-sectional area of cardiomyocytes (**Figure 3E**), further confirming cardiac atrophy. Importantly, ExTr sustained a normal cardiomyocyte area. Doxo also induced a ∼3-fold increase in myocardial fibrosis that was not prevented by ExTr (**Figure 3F**). Cardiac levels of the GATA4, a transcription factor that is associated with compensatory response to cardiac injury in the adult heart (21), was significantly reduced under Doxo treatment. ExTr did not restore GATA4 expression, but it attenuated Doxo effects (**Figure 4A**). As the activity of GATA4 is mainly coordinated by its translocation and nuclear activation, we determined the protein expression levels specifically in the nucleus and in the cytosol. Despite a visual trend toward the reduction of nuclear translocation by Doxo and restoration by ExTr, no statistical significance was observed in the differential expression of GATA4 (**Figure 4B**). ExTr trend to increase phosphorylated-to-total ERK ratio to Doxo group (**Figure 4C**). No differences were found in the protein expression levels of the different isoforms of superoxide dismutase (SOD) enzymes (**Figures 4E–H**).

ExTr Exacerbates Doxo-Induced Body Wasting

Doxo induced body wasting, and ExTr exacerbated it (**Figure 5A**). However, ExTr did not affect survival under doxo treatment (**Figure 5B**). One explanation is ExTr might have increased caloric expenditure, as we did not observe changes in food intake among groups (data not shown). This is also supported by the fact that ExTr partially preserved brown adipose tissue (BAT) (**Figure 5C**), but not white (WAT) fat depots mass (**Figure 5D**), reduced under Doxo treatment. No changes were observed in skeletal muscle mass (**Figure 5E**).

ExTr Blunts Effort Intolerance Induced by Doxo Treatment

We quantified running capacity (**Figure 6**), as it predicts maximal oxygen uptake and cardiopulmonary performance (22). We observed a strong trend toward the reduction of running distance under Doxo treatment, in comparison to baseline levels (**Figure 6A**). Running performance (a more sensitive method that takes bodyweight in consideration) showed an almost 40% decline induced by Doxo in comparison to the Co group (**Figure 6B**). ExTr was able to increase the distance covered from baseline in 37%, completely preventing Doxo-induced impaired running performance (**Figures 6A,B**, respectively). Comparing Doxo-treated groups alone, all mice subjected to ExTr sustained exercise for significantly longer periods than Doxo-treated only (**Figure 6C**). Interestingly, we found a significant negative correlation between running performance and SAX circumferential strain rate (**Figure 6D**).

DISCUSSION

Anthracycline-based chemotherapies are widely used to treat oncologic patients, but it is associated with strong adverse effects, as cardiotoxicity and cancer-related fatigue. As standard care improved, patients are now more likely to survive cancer (23). Hence, strategies to alleviate treatment side effects, prevent the development of co-morbidities, and enhance the quality of life are needed.

Although the role of ExTr to prevent Doxo-induced cardiac dysfunction has been consistently demonstrated in preclinical models, the vast majority of these studies started weeks or

TABLE 2 | Physical characteristics, ventricular morphology, and function after 5 weeks of saline or doxorubicin treatment.

	Co	Doxo	Doxo + ExTr	*P*-value
Bodyweight, g	25.3 ± 0.71	21.3 ± 0.61*	19.2 ± 0.43*	< 0.001
HR, bpm	414 ± 13	416 ± 30	389 ± 26	0.65
Wet cardiac mass, mg	102.1 ± 2.63	75.2 ± 2.48*	81.1 ± 4.75*	< 0.001
Wet LV, mg	81.7 ± 2.19	62.0 ± 2.31*	65.9 ± 3.64*	< 0.001
Wet lung, mg	209.1 ± 9.17	157.3 ± 12.6*	170.8 ± 12.4*	0.007
Left ventricular morphology				
LVEDD, mm	3.81 ± 0.16	3.59 ± 0.13	3.51 ± 0.12	0.33
LVESD, mm	2.57 ± 0.14	2.83 ± 0.14	2.74 ± 0.13	0.44
IVS, mm	0.82 ± 0.04	0.71 ± 0.03	0.73 ± 0.03	0.16
LVPW, mm	0.71 ± 0.03	0.67 ± 0.03	0.67 ± 0.02	0.59
Systolic function				
LVFS, %	32.8 ± 1.66	21.3 ± 1.93*	22.3 ± 1.72*	< 0.001
LVEDV, μL	63.9 ± 6.00	54.7 ± 4.64	52.2 ± 4.32	0.25
LVESV, μL	25.2 ± 3.35	31.2 ± 3.60	29.0 ± 3.56	0.48
SV, μL	38.7 ± 3.22	23.5 ± 2.05*	23.2 ± 1.52*	< 0.001
Diastolic function				
Mitral E velocity, mm/s	431 ± 32.5	433 ± 41.1	390 ± 38.6	0.66
Mitral A velocity, mm/s	227 ± 23.6	201 ± 65.9	208 ± 31.5	0.89
Mitral E/A ratio	2.01 ± 1.85	3.35 ± 1.12	2.16 ± 0.39	0.27
Speckle-tracking				
LAX Longitudinal strain, %	−11.8 ± 1.57	−17.9 ± 2.50	−15.5 ± 2.13	0.75
LAX Longitudinal SR, 1/s	−5.1 ± 1.04	−6.67 ± 1.14	−7.46 ± 0.89	0.18
LAX Radial strain, %	19.4 ± 3.13	30.8 ± 4.83(0.09)	30.2 ± 2.64(0.09)	0.04*
LAX Radial SR, 1/s	6.57 ± 1.45	8.87 ± 1.25	9.01 ± 0.74	0.28
SAX Radial strain, %	32.6 ± 2.96	25.9 ± 3.52	26.3 ± 2.97	0.23
SAX Radial SR, 1/s	8.58 ± 0.97	7.82 ± 0.50	8.36 ± 0.72	0.84

*n = 7–12 Control, n = 6–9 Doxo, n = 6–11 Doxo+ExTr. *P ≤ 0.05 vs. Control by One-Way ANOVA and Tukey's multiple comparisons test.*
CO, cardiac output; HR, heart rate; IVS, interventricular septal wall thickness; LAX, long axis view; LVEDD, left ventricular end-diastolic diameter; LVEDV, left ventricular end-diastolic volume; LVESV, left ventricular end-systolic volume; LVEF, left ventricular ejection fraction; LVESD, left ventricular end-systolic diameter; LVPW, left ventricular posterior wall thickness; LVSF, left ventricular stroke fraction; SAX, short axis view; SR, strain rate; SV, stroke volume; TL, tibia length.

even months before either an acute (bolus administration of an accumulated dose of Doxo) or chronic treatment (fractioned dose along time) [find an overview in (24)]. This approach may be relevant to investigate potential mechanisms, but it might not reflect the pathophysiological events observed in the clinical practice. That because a cytotoxic chemotherapy treatment usually starts as soon as possible after diagnosis, limiting the available window for ExTr pre-conditioning.

Some authors analyzed ExTr concomitantly with Doxo, by applying short-term protocols. However, a short treatment period does not allow enough time to the deterioration of systolic function, as expected with chronic Doxo administration (25). Other accessed ventricular function after a wash-out period (12, 20). However, this approach is more likely to favor recovery (26) and, hence, does not necessarily reflect Doxo-induced cardiotoxicity during cancer treatment. The same problem occurs to studies modeling rehabilitation, with ExTr beginning once the cardiomyopathy is established (11), rather than recapitulating a cancer survivorship context. We designed this study to model an ExTr program that started *concomitantly* with chronic cytotoxic treatment with Doxo-based chemotherapy. The synergistic effect of ExTr on the anti-tumoral activity of Doxo has been previously demonstrated (25, 27). Moreover, tumors *per se* can induce ventricular dysfunction (28–30). Therefore, we decided to study non-tumor bearing mice.

The pathophysiology of Doxo-induced cardiotoxicity is complex, and several distinct mechanisms have been established [see (5) for concise review]. On the other hand, chronic and late effects are seemingly related to transcriptional activity abnormalities (20), and the transcription factor GATA4 has been mechanistically implicated (2, 31). In postnatal hearts, GATA4 is essential for cardiomyocyte survival after injury or stress (21). Hence, by inhibiting GATA4, Doxo blunts the cardiac capacity of responding to injury, triggering apoptosis, and autophagy, therefore leading to cardiac atrophy. So far, there is no commercially available pharmacological treatment targeting GATA4. However, studies from our group and others (32, 33) demonstrated that ExTr modulates GATA4, potentially indicating a mechanism for ExTr-induced cardioprotection to Doxo.

ExTr imposes a higher cardiac workload, inducing angiogenesis and hypertrophy of cardiomyocytes, and GATA4 triggers this physiological process (21, 32, 33).

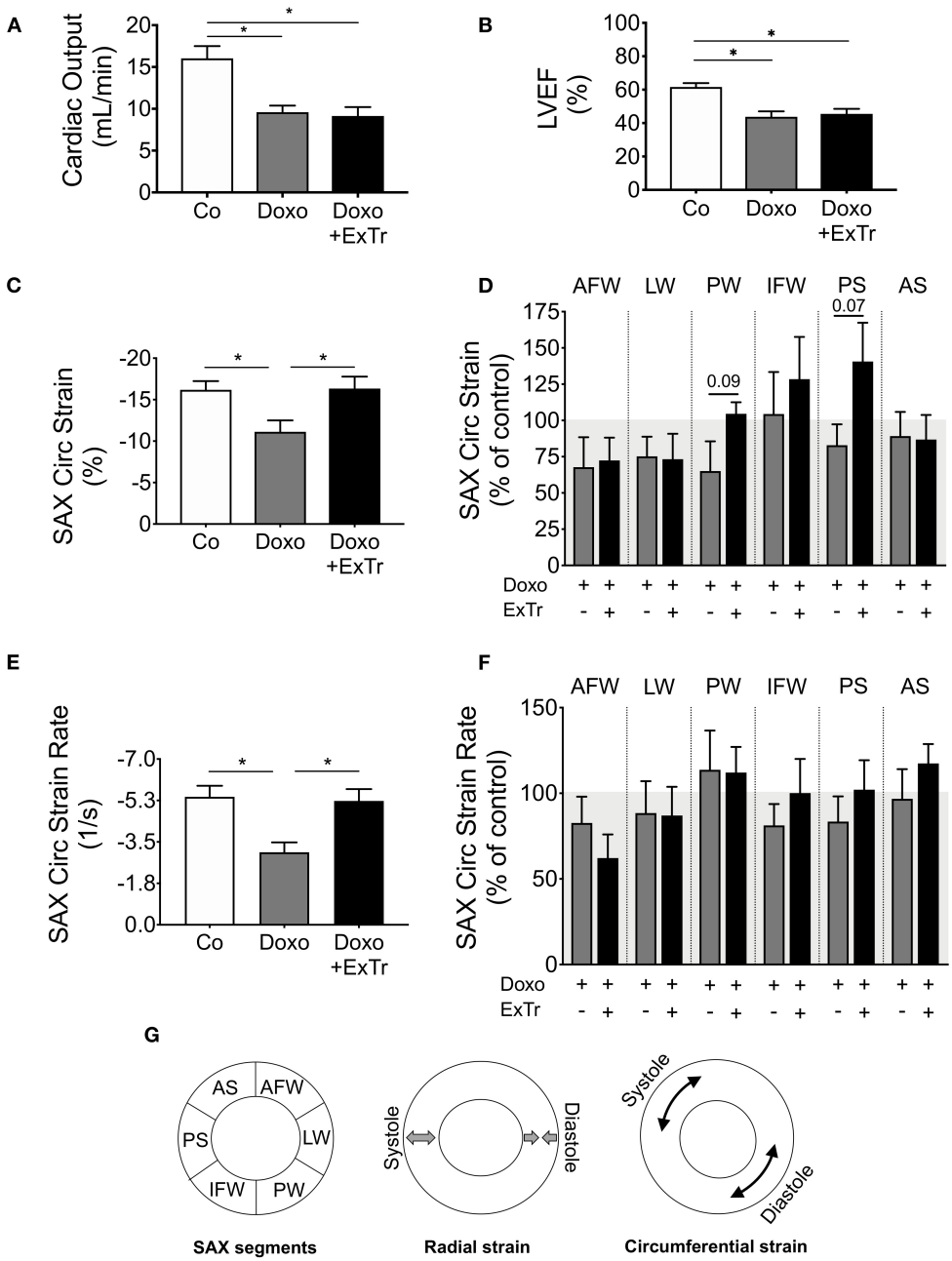

FIGURE 2 | Exercise training alleviates Doxo-induced cardiac dysfunction. Doxo impairs CO **(A)** and LVEF **(B)**. However, speckle tracking showed ExTr preserved SAX cardiac contractility, both in the Circ strain **(C,D)** and strain rate **(E,F)**, expressed as a final vector from strain **(B)** and strain rate **(D)** of different cardiac segments **(D,F)**. AFW, anterior free wall; AS, anterior septum; CO, cardiac output; Circ, circumferential; IFW, inferior free wall; LW, lateral wall; LVEF, left ventricular ejection fraction; PS, posterior septum; PW, posterior wall; SAX, short axis). Conceptual analysis of speckle tracking on **(G)**. $n = 6$–11 per group. Group abbreviations as in **Figure 1**. $^*P \leq 0.05$.

However, overexpression of GATA4 is also associated with decompensated cardiac hypertrophy, as it occurs in neuroendocrine overactivation-induced HF (33). On the other hand, in diabetes-induced cardiac atrophy, a similar phenotype observed in response to Doxo, GATA4 activity is reduced (32). Importantly, ExTr brings the activity of GATA4 back to normal physiological ranges in both situations. Hence, one would expect that, if ExTr prevents Doxo-induced cardiotoxicity, it would be by sustaining the transcriptional activity of GATA4 (24). In our study, ExTr alleviated but was not able to restore the expression levels of GATA4 (**Figures 4A,B,D**). This might explain why ExTr did not prevent Doxo-induced reduction of

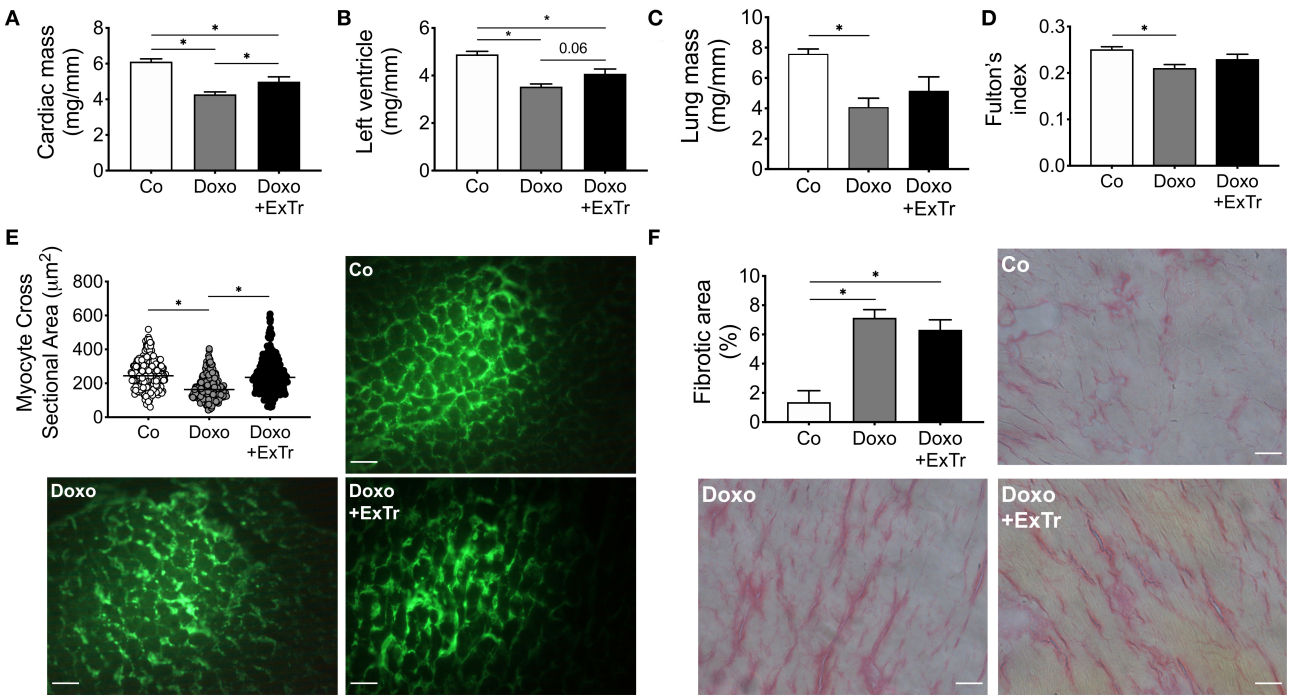

FIGURE 3 | ExTr alleviates Doxo-induced cardiopulmonary atrophy. Doxo induces cardiac **(A)**, left ventricle **(B)**, and lung **(C)** mass atrophy (normalized by tibia length and expressed in mg/mm), which is alleviated by ExTr. Fulton's index (RV/LV + S) reduces with Doxo and is partially preserved by ExTr **(D)**. ExTr prevents cardiomyocyte atrophy induced by Doxo **(E)**. Doxo increases cardiac collagen deposition that is not prevented by ExTr **(F)**. Group abbreviations as in **Figure 1**. N = 8–11 **(A–D)**, >500 cardiomyocytes pooled from n = 2–3 **(E)** and n = 5 **(F)** per group. $^*P \leq 0.05$.

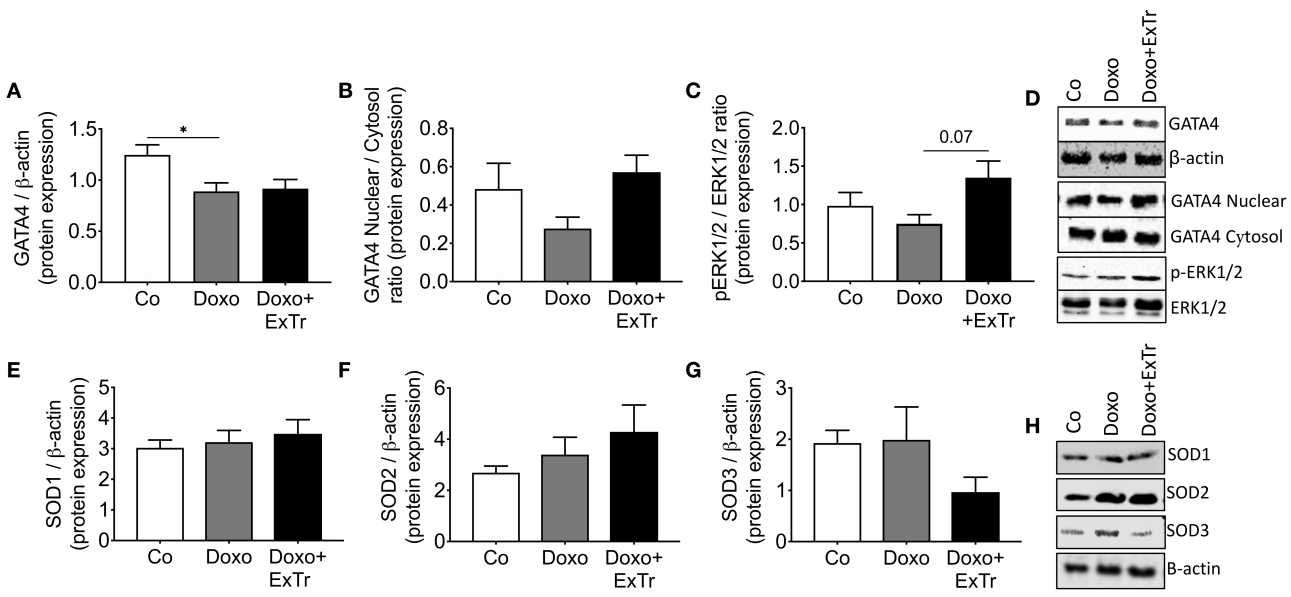

FIGURE 4 | Molecular markers of Doxo-induced cardiotoxicity. Cardiac protein expression of GATA4 analyzed by densitometry and normalized against β-actin **(A)** and its nuclear/cytosol ratio **(B)**; the ratio of pERK-to-total-ERK **(C)** and representative blots **(D)**; protein levels of the antioxidant enzyme superoxide dismutase isoforms 1 **(E)**, 2 **(F)**, or 3 **(G)** and its representative blots **(H)**. GATA4, GATA binding protein 4; ERK, extracellular signal-regulated kinases; pERK, phosphorylated ERK; SOD, superoxide dismutase. Group abbreviations as in **Figure 1**. n = 5–8 per group. $^*P \leq 0.05$.

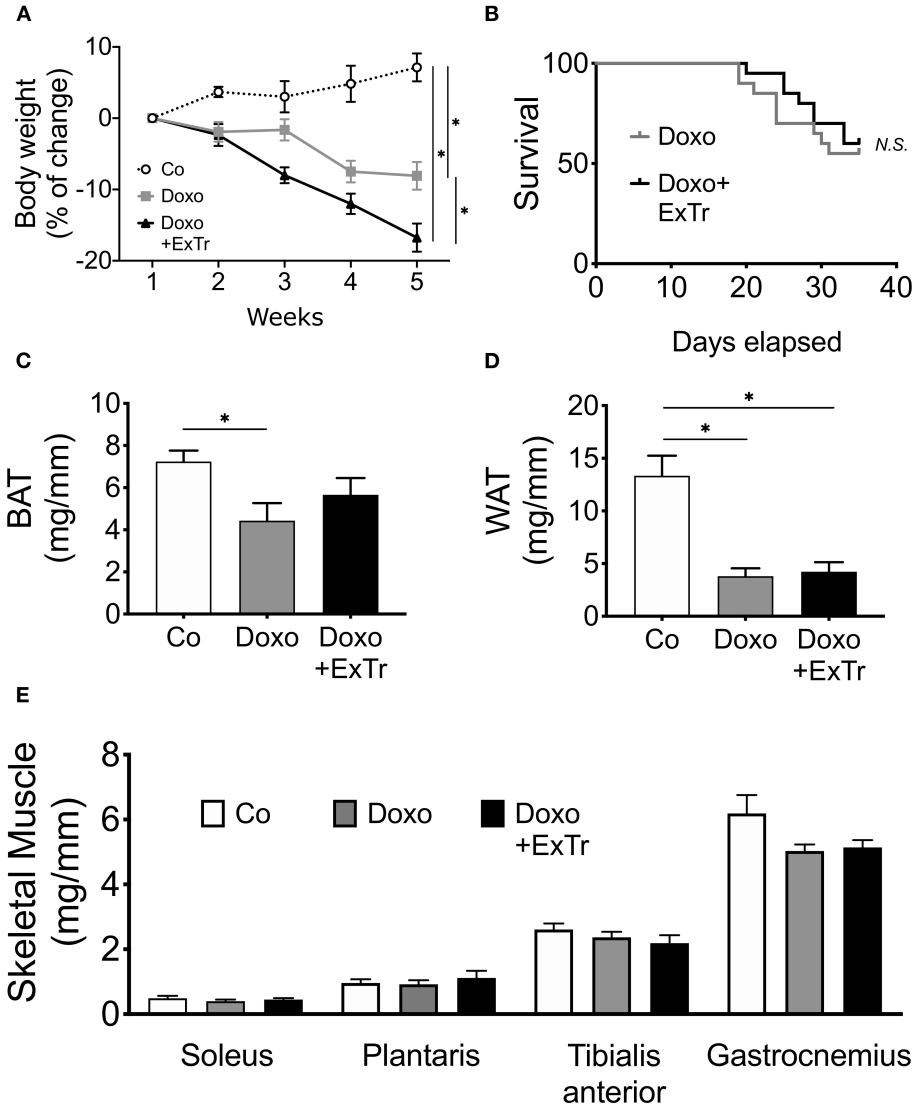

FIGURE 5 | ExTr exacerbates Doxo-induced body wasting. Doxo induces body wasting, which is exacerbated by ExTr **(A)**, although without negatively affecting survival **(B)**. Doxo affects fat depots mass, reducing both BAT **(C)** and WAT **(D)** adipose tissue. ExTr attenuates BAT mass wasting, but not WAT. No changes were found in skeletal muscle mass **(E)**. BAT, brown adipose tissue; WAT, white adipose tissue. Group abbreviations as in **Figure 1**. $n = 12$–20 per group **(A,B)** or $n = 8$–10 **(C–E)**. $^*P \leq 0.05$.

LVEF (**Figure 2B**). We cannot exclude the possibility that ExTr favors the regain of ventricular function over time, perhaps even rescuing GATA4 activity. The main explanation for the attenuated GATA4 response to ExTr relies on DNA machinery to function. Doxo is a non-selective inhibitor of topoisomerase (20, 34), an essential enzyme for cell replication and DNA promoting activity. Once topoisomerase is inhibited, it impairs the binding of a transcription factor to the promoter region (34), leading to cardiotoxicity (20). It is likely that, in an "acute" phase [i.e., right after the treatment termination (35)], Doxo still inhibits GATA4 transcriptional activity, preventing ExTr to exert a major early-phase protective effect.

A great deal of studies implicated the increased oxidative stress (ROS) in Doxo-induced cardiotoxicity (36). ExTr is known to reduce cardiac ROS in cardiovascular diseases (13). Here, we assessed the protein levels of SOD as surrogate markers of anti-oxidative capacity, as these are the main enzymes to convert superoxide radicals into hydrogen peroxide and oxygen. As in previous reports, Doxo did not change the expression of SOD in the heart (12). However, in our study, ExTr alone was not able to enhance SOD activity as well. We did not directly measure cardiac ROS generation. Hence we cannot rule out the possibility that ExTr alleviates ROS, which could also explain the modest ExTr effect on myocardial contractility.

Doxo provoked myocardial strain and strain rate abnormalities, analyzed by the speckle tracking technique (37–40). This technique has demonstrated superiority to detect cardiac abnormalities—especially subclinical—over the

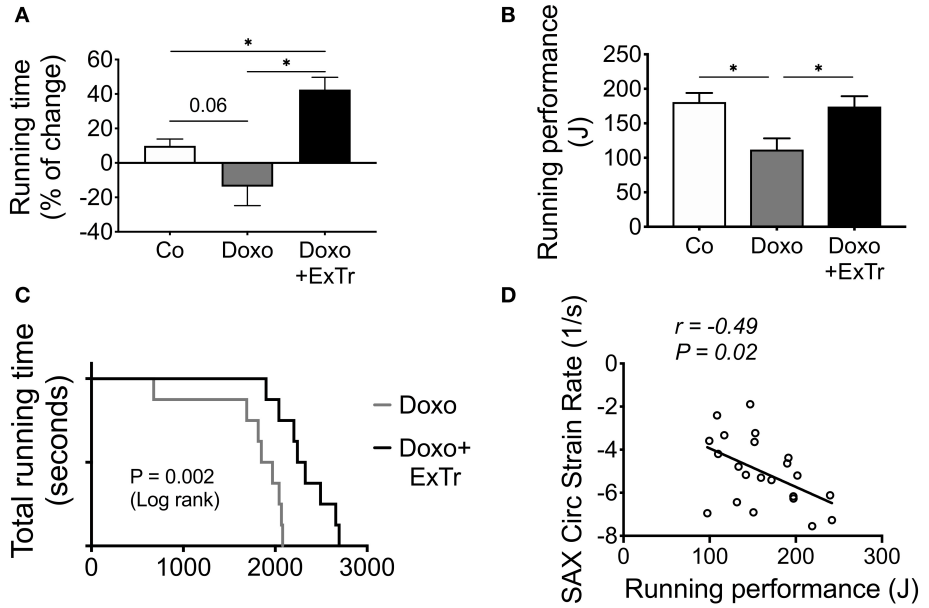

FIGURE 6 | ExTr blunts Doxo-induced effort intolerance. Effort tolerance, determined maximal running capacity, shows Doxo total running time from Baseline trend to impair **(A)**, and running performance **(B)** and total running time **(C)** were reduced. Interestingly, the better the cardiac contractility (strain rate), the higher is exercise capacity **(D)** among Doxo-treated groups. J, joule; SAX, short axis. Group abbreviations as in **Figure 1**. $n = 10–12$ per group. $^*P \leq 0.05$.

conventional echocardiography, as myocardial strain reduction is frequent in cancer patients and precedes LVEF reduction that cannot be anticipated by other parameters (37). In our study, we observed a significant impairment of circumferential strain and strain rate in the SAX, which was abrogated by ExTr. We further analyzed each of the six segments that compose the final strain vector (**Figures 2C–F**). As can be observed, ExTr trends toward bringing reduced myocardial strain under Doxo back to normal ranges. Surprisingly, Doxo did not change LV longitudinal strain or radial strain. Longitudinal strain has been used for the early detection of LV impairment in a variety of cardiac diseases. Moreover, longitudinal strain changes are prognostic of cardiotoxicity in patients (41). One possibility is that longitudinal, radial, and circumferential strains change at a different rate (42). By measuring only at one-time point, we might have missed eventual changes in some parameters. Besides, endocardial fibers are mainly longitudinaly oriented, while mid-wall are more circumferential oriented (43). Thus, orientation and local geometry might respond differently to exercise-induced hemodynamic stress. Stewart and collaborators demonstrated that acute exercise transiently reduces longitudinal strain globally (44). In contrast, this intervention only causes reduction in the apical portion of the circumferential strain. ExTr induces physiological modification of cardiac geometry toward cavity expansion in response to repeated bouts of transient hemodynamic overload (45, 46). In our study, we did not find significant changes in cavity size or fibrotic depots. These findings suggest that the LV morphology is differently affected by ExTr under Doxo administration. Circumferential strain in the short axis is more sensitive in identifying LV remodeling (47), which seems to explain why circumferential strain was more sensitive than other strain parameters in our study. Finally, one should consider differences among species. Circumferential strain seems to represent more similar LV contractility patterns in mice and humans (48), which enhances the translational findings of our study. Notably, the circumferential strain is pointed out as more relevant to the cardio-oncology population, by its superior sensitivity to detect patients under higher risk of developing Doxo-induced cardiotoxicity (38). Certainly, regional changes along time and in response to different stimuli is an interesting topic for further studies.

The myocardial strain has also been demonstrated to precede recovery in other cardiovascular diseases. Investigating mice after myocardial infarction, speckle tracking analysis detected that improvements in cardiac strain occurred before regaining of LVEF functionality (38). In our model, we observed both a reduction of myocardial strain and LVEF under Doxo influence. ExTr normalized this parameter. Whether myocardial strain normalization by ExTr indicates a future full recovery of Dox-induced LVEF dysfunction remains to be determined.

Exercise prompts physiological stress to the cardiovascular system and, by doing so, provide an informative assessment of cardiovascular function (38). McKillop and coworkers, more than three decades ago, demonstrated that, by adding exercise response to a prediction model based on LVEF, the sensitivity nearly doubled, reaching 100% chance to detect Doxo-induced cardiotoxicity compared to resting LVEF alone (49). Others also suggested the inclusion of exercise tests as an important tool, especially to avoid underestimation of subclinical dysfunction (49, 50) or to distinguish from pre-existent coronary artery disease (51). Indeed, ongoing clinical trials are investigating whether exercise intolerance and cancer fatigue can predict

cardiotoxicity and cardiovascular events in the next decade (NCT02791581, ClinicalTrials.gov). Here, we showed that ExTr improved exercise capacity, preventing Doxo-induced exercise intolerance and, hence, counteracting cancer-related fatigue. Interestingly, a significant correlation between myocardial contractility and exercise capacity was observed (**Figure 6D**). Of note, exercise capacity is a predictor of survivorship across different types of cancer, some of them traditionally treated with Doxo (52–54). Hence, our study suggests that ExTr improves cardiovascular fitness and counteract Doxo-induced cardiotoxicity.

Study Limitations

We studied male mice as it has been reported a protective role of the female sex in Doxo-induced cardiotoxicity (53). Hence, the implications of the present study may offer limited insights for the female population. The fact that we narrowed down our molecular analysis to specific, previously selected pathways, may have limited the strength of our mechanistic conclusions. Also, we studied low-to-moderate intensity aerobic exercise. However, it is possible that higher exercise dose would elicit superior effects (15, 55).

CONCLUSION

Our findings suggest that low-to-moderate intensity aerobic ExTr program performed concomitantly with Doxo treatment does not prevent Doxo-induced LVEF reduction but attenuates cardiac atrophy, preserves myocardial strain, and enhances exercise tolerance. Therefore, ExTr can be a valuable approach to alleviate Doxo-induced cardiotoxicity.

DATA AVAILABILITY STATEMENT

The raw data supporting the conclusions of this article will be made available by the authors, without undue reservation.

ETHICS STATEMENT

The animal study was reviewed and approved by Ethics Committee on Animal Use (CEUA) of the University of São Paulo Medical School (FMUSP).

AUTHOR CONTRIBUTIONS

IG-S, CN, RC, and AC: designed experiments. IG-S, CJ, and CP: performed experiments. IG-S and CJ: analyzed data. PB, EO, RC, AC, and CN: provided laboratory space, reagents, and technical support. IG-S and CN: wrote the manuscript. IG-S, CJ, CP, PB, EO, RC, AC, and CN: edited the manuscript. CN: supervised the study. All authors: contributed to the article and approved the submitted version.

FUNDING

The study supported by Fundação de Amparo à Pesquisa do Estado de São Paulo (FAPESP) (#2015/22814-5). IG-S received scholarship from FAPESP (#2014/13690-8 and #2016/21320-1), same as and CSP (#2015/19076-2), in cooperation agreement with Coordenação de Aperfeiçoamento de Pessoal de Nível Superior (CAPES). PB, EO, and CN were supported by Conselho Nacional de Desenvolvimento Científico e Tecnológico (CNPq) (#306261/2016-2, #313479/2017-8, and #303573/2015-5). The funders had no role in the study design, data collection and analysis.

ACKNOWLEDGMENTS

We appreciate experimental support from Joao Lucas Penteado Gomes and Tassia S. Rodrigues Costa, as well as fruitful discussions with Marcelo Vailati Negrão and other laboratory members.

REFERENCES

1. Smuder AJ. Exercise stimulates beneficial adaptations to diminish doxorubicin-induced cellular toxicity. *Am J Physiol Regul Integr Comp Physiol.* (2019) 317:R662–72. doi: 10.1152/ajpregu.00161.2019
2. Kobayashi S, Volden P, Timm D, Mao K, Xu X, Liang Q. Transcription factor GATA4 inhibits doxorubicin-induced autophagy and cardiomyocyte death. *J Biol Chem.* (2010) 285:793–804. doi: 10.1074/jbc.M109.070037
3. Eyob T, Ng T, Chan R, Chan A. Impact of chemotherapy on cancer-related fatigue and cytokines in 1312 patients: a systematic review of quantitative studies. *Curr Opin Support Palliat Care.* (2016) 10:165–79. doi: 10.1097/SPC.0000000000000205
4. Bower JE. Cancer-related fatigue–mechanisms, risk factors, and treatments. *Nat Rev Clin Oncol.* (2014) 11:597–609. doi: 10.1038/nrclinonc.2014.127
5. Vejpongsa P, Yeh ET. Prevention of anthracycline-induced cardiotoxicity: challenges and opportunities. *J Am Coll Cardiol.* (2014) 64:938–45. doi: 10.1016/j.jacc.2014.06.1167
6. Von Hoff DD, Layard MW, Basa P, Davis HL Jr, Von Hoff AL, et al. Risk factors for doxorubicin-induced congestive heart failure. *Ann Intern Med.* (1979) 91:710–7. doi: 10.7326/0003-4819-91-5-710
7. Ewer MS, Ewer SM. Cardiotoxicity of anticancer treatments: what the cardiologist needs to know. *Nat Rev Cardiol.* (2010) 7:564–75. doi: 10.1038/nrcardio.2010.121
8. Lotrionte M, Biondi-Zoccai G, Abbate A, Lanzetta G, D'Ascenzo F, Malavasi V, et al. Review and meta-analysis of incidence and clinical predictors of anthracycline cardiotoxicity. *Am J Cardiol.* (2013) 112:1980–4. doi: 10.1016/j.amjcard.2013.08.026
9. Moser EC, Noordijk EM, van Leeuwen FE, le Cessie S, Baars JW, Thomas J, et al. Long-term risk of cardiovascular disease after treatment for aggressive non-Hodgkin lymphoma. *Blood.* (2006) 107:2912–9. doi: 10.1182/blood-2005-08-3392
10. Park NJ, Chang Y, Bender C, Conley Y, Chlebowski RT, van Londen GJ, et al. Cardiovascular disease and mortality after breast cancer in postmenopausal women: results from the Women's Health Initiative. *PLoS ONE.* (2017) 12:e0184174. doi: 10.1371/journal.pone.0184174
11. Lee Y, Kwon I, Jang Y, Cosio-Lima L, Barrington P. Endurance exercise attenuates doxorubicin-induced cardiotoxicity. *Med Sci Sports Exerc.* (2019). 52:25–36. doi: 10.1249/MSS.0000000000002094
12. Dolinsky VW, Rogan KJ, Sung MM, Zordoky BN, Haykowsky MJ, Young ME, et al. Both aerobic exercise and resveratrol supplementation attenuate

doxorubicin-induced cardiac injury in mice. *Am J Physiol Endocrinol Metab.* (2013) 305:E243–53. doi: 10.1152/ajpendo.00044.2013
13. Marques-Aleixo I, Santos-Alves E, Torrella JR, Oliveira PJ, Magalhaes J, Ascensao A. Exercise and doxorubicin treatment modulate cardiac mitochondrial quality control signaling. *Cardiovasc Toxicol.* (2018) 18:43–55. doi: 10.1007/s12012-017-9412-4
14. Gilchrist SC, Barac A, Ades PA, Alfano CM, Franklin BA, Jones LW, et al. Cardio-oncology rehabilitation to manage cardiovascular outcomes in cancer patients and survivors: a scientific statement from the American Heart Association. *Circulation.* (2019) 139:e997–1012. doi: 10.1161/CIR.0000000000000679
15. Scott JM, Nilsen TS, Gupta D, Jones LW. Exercise therapy and cardiovascular toxicity in cancer. *Circulation.* (2018) 137:1176–91. doi: 10.1161/CIRCULATIONAHA.117.024671
16. Huang HP, Wen FH, Tsai JC, Lin YC, Shun SC, Chang HK, et al. Adherence to prescribed exercise time and intensity declines as the exercise program proceeds: findings from women under treatment for breast cancer. *Support Care Cancer.* (2015) 23:2061–71. doi: 10.1007/s00520-014-2567-7
17. Lang RM, Bierig M, Devereux RB, Flachskampf FA, Foster E, Pellikka PA, et al. G. Chamber Quantification Writing, G. American Society of Echocardiography's, C. Standards, and E. European Association of, Recommendations for chamber quantification: a report from the American Society of Echocardiography's Guidelines and Standards Committee and the Chamber Quantification Writing Group, developed in conjunction with the European Association of Echocardiography, a branch of the European Society of Cardiology. *J Am Soc Echocardiogr.* (2005) 18:1440–63. doi: 10.1016/j.echo.2005.10.005
18. Bauer M, Cheng S, Jain M, Ngoy S, Theodoropoulos C, Trujillo A, et al. Echocardiographic speckle-tracking based strain imaging for rapid cardiovascular phenotyping in mice. *Circ Res.* (2011) 108:908–16. doi: 10.1161/CIRCRESAHA.110.239574
19. Gomes-Santos IL, Fernandes T, Couto GK, Ferreira-Filho JC, Salemi VM, Fernandes FB, et al. Effects of exercise training on circulating and skeletal muscle renin-angiotensin system in chronic heart failure rats. *PLoS ONE.* (2014) 9:e98012. doi: 10.1371/journal.pone.0098012
20. Zhang S, Liu X, Bawa-Khalfe T, Lu LS, Lyu YL, Liu LF, et al. Identification of the molecular basis of doxorubicin-induced cardiotoxicity. *Nat Med.* (2012) 18:1639–42. doi: 10.1038/nm.2919
21. Heineke J, Auger-Messier M, Xu J, Oka T, Sargent MA, York A, et al. Cardiomyocyte GATA4 functions as a stress-responsive regulator of angiogenesis in the murine heart. *J Clin Invest.* (2007) 117:3198–210. doi: 10.1172/JCI32573
22. Petrosino JM, Heiss VJ, Maurya SK, Kalyanasundaram A, Periasamy M, LaFountain RA, et al. Graded maximal exercise testing to assess mouse cardio-metabolic phenotypes. *PLoS ONE.* (2016) 11:e0148010. doi: 10.1371/journal.pone.0148010
23. Shapiro CL. Cancer survivorship. *N Engl J Med.* (2018) 379:2438–50. doi: 10.1056/NEJMra1712502
24. Scott JM, Khakoo A, Mackey JR, Haykowsky MJ, Douglas PS, Jones LW. Modulation of anthracycline-induced cardiotoxicity by aerobic exercise in breast cancer: current evidence and underlying mechanisms. *Circulation.* (2011) 124:642–50. doi: 10.1161/CIRCULATIONAHA.111.021774
25. Sturgeon K, Schadler K, Muthukumaran G, Ding D, Bajulaiye A, Thomas NJ, et al. Concomitant low-dose doxorubicin treatment and exercise. *Am J Physiol Regul Integr Comp Physiol.* (2014) 307:R685–92. doi: 10.1152/ajpregu.00082.2014
26. Zhu W, Shou W, Payne RM, Caldwell R, Field LJ. A mouse model for juvenile doxorubicin-induced cardiac dysfunction. *Pediatr Res.* (2008) 64:488–94. doi: 10.1203/PDR.0b013e318184d732
27. Schadler KL, Thomas NJ, Galie PA, Bhang DH, Roby KC, Addai P, et al. Tumor vessel normalization after aerobic exercise enhances chemotherapeutic efficacy. *Oncotarget.* (2016) 7:65429–440. doi: 10.18632/oncotarget.11748
28. Springer J, Tschirner A, Haghikia A, von Haehling S, Lal H, Grzesiak A, et al. Prevention of liver cancer cachexia-induced cardiac wasting and heart failure. *Eur Heart J.* (2014) 35:932–41. doi: 10.1093/eurheartj/eht302
29. Cramer L, Hildebrandt B, Kung T, Wichmann K, Springer J, Doehner W, et al. Cardiovascular function and predictors of exercise capacity in patients with colorectal cancer. *J Am Coll Cardiol.* (2014) 64:1310–9. doi: 10.1016/j.jacc.2014.07.948
30. da Costa TSR, Urias U, Negrao MV, Jordao CP, Passos CS, Gomes-Santos IL, et al. Breast cancer promotes cardiac dysfunction through deregulation of cardiomyocyte Ca(2+)-handling protein expression that is not reversed by exercise training. *J Am Heart Assoc.* (2021) 10:e018076. doi: 10.1161/JAHA.120.018076
31. Kim Y, Ma AG, Kitta K, Fitch SN, Ikeda T, Ihara Y, et al. Anthracycline-induced suppression of GATA-4 transcription factor: implication in the regulation of cardiac myocyte apoptosis. *Mol Pharmacol.* (2003) 63:368–77. doi: 10.1124/mol.63.2.368
32. Broderick TL, Parrott CR, Wang D, Jankowski M, Gutkowska J. Expression of cardiac GATA4 and downstream genes after exercise training in the db/db mouse. *Pathophysiology.* (2012) 19:193–203. doi: 10.1016/j.pathophys.2012.06.001
33. Oliveira RS, Ferreira JC, Gomes ER, Paixao NA, Rolim NP, Medeiros A, et al. Cardiac anti-remodelling effect of aerobic training is associated with a reduction in the calcineurin/NFAT signalling pathway in heart failure mice. *J Physiol.* (2009) 587:3899–910. doi: 10.1113/jphysiol.2009.173948
34. Collins I, Weber A, Levens D. Transcriptional consequences of topoisomerase inhibition. *Mol Cell Biol.* (2001) 21:8437–51. doi: 10.1128/MCB.21.24.8437-8451.2001
35. Albini A, Pennesi G, Donatelli F, Cammarota R, De Flora S, Noonan DM. Cardiotoxicity of anticancer drugs: the need for cardio-oncology and cardio-oncological prevention. *J Natl Cancer Inst.* (2010) 102:14–25. doi: 10.1093/jnci/djp440
36. Xu MF, Tang PL, Qian ZM, Ashraf M. Effects by doxorubicin on the myocardium are mediated by oxygen free radicals. *Life Sci.* (2001) 68:889–901. doi: 10.1016/S0024-3205(00)00990-5
37. Laufer-Perl M, Derakhshesh M, Milwidsky A, Mor L, Ravid D, Amrami N, et al. Usefulness of global longitudinal strain for early identification of subclinical left ventricular dysfunction in patients with active cancer. *Am J Cardiol.* (2018) 122:1784–9. doi: 10.1016/j.amjcard.2018.08.019
38. Narayan HK, French B, Khan AM, Plappert T, Hyman D, Bajulaiye A, et al. Noninvasive measures of ventricular-arterial coupling and circumferential strain predict cancer therapeutics-related cardiac dysfunction. *JACC Cardiovasc Imaging.* (2016) 9:1131–41. doi: 10.1016/j.jcmg.2015.11.024
39. Khouri MG, Hornsby WE, Risum N, Velazquez EJ, Thomas S, Lane A, et al. Utility of 3-dimensional echocardiography, global longitudinal strain, and exercise stress echocardiography to detect cardiac dysfunction in breast cancer patients treated with doxorubicin-containing adjuvant therapy. *Breast Cancer Res Treat.* (2014) 143:531–9. doi: 10.1007/s10549-013-2818-1
40. Rea D, Coppola C, Barbieri A, Monti MG, Misso G, Palma G, et al. Strain analysis in the assessment of a mouse model of cardiotoxicity due to chemotherapy: sample for preclinical research. *In Vivo.* (2016) 30:279–90.
41. Cheung YF, Hong WJ, Chan GC, Wong SJ, Ha SY. Left ventricular myocardial deformation and mechanical dyssynchrony in children with normal ventricular shortening fraction after anthracycline therapy. *Heart.* (2010) 96:1137–41. doi: 10.1136/hrt.2010.194118
42. Hoffman M, Kyriazis ID, Lucchese AM, de Lucia C, Piedepalumbo M, Bauer M, et al. Myocardial strain and cardiac output are preferable measurements for cardiac dysfunction and can predict mortality in septic mice. *J Am Heart Assoc.* (2019) 8:e012260. doi: 10.1161/JAHA.119.012260
43. Stevens C, Hunter PJ. Sarcomere length changes in a 3D mathematical model of the pig ventricles. *Prog Biophys Mol Biol.* (2003) 82:229–41. doi: 10.1016/S0079-6107(03)00023-3
44. Stewart GM, Chan J, Yamada A, Kavanagh JJ, Haseler LJ, Shiino K, et al. Impact of high-intensity endurance exercise on regional left and right ventricular myocardial mechanics. *Eur Heart J Cardiovasc Imaging.* (2017) 18:688–96. doi: 10.1093/ehjci/jew128
45. Carneiro-Junior MA, Primola-Gomes TN, Quintao-Junior JF, Drummond LR, Lavorato VN, Drummond FR, et al. Regional effects of low-intensity endurance training on structural and mechanical properties of rat ventricular myocytes. *J Appl Physiol 1985.* (2013) 115:107–15. doi: 10.1152/japplphysiol.00041.2013
46. Azevedo LF, Perlingeiro PS, Hachul DT, Gomes-Santos IL, Brum PC, Allison TG, et al. Sport modality affects bradycardia level and its mechanisms

of control in professional athletes. *Int J Sports Med.* (2014) 35:954–9. doi: 10.1055/s-0033-1364024
47. Hung CL, Verma A, Uno H, Shin SH, Bourgoun M, Hassanein AH, et al. Longitudinal and circumferential strain rate, left ventricular remodeling, and prognosis after myocardial infarction. *J Am Coll Cardiol.* (2010) 56:1812–22. doi: 10.1016/j.jacc.2010.06.044
48. Kusunose K, Penn MS, Zhang Y, Cheng Y, Thomas JD, Marwick TH, et al. How similar are the mice to men? Between-species comparison of left ventricular mechanics using strain imaging. *PLoS ONE.* (2012) 7:e40061. doi: 10.1371/journal.pone.0040061
49. McKillop JH, Bristow MR, Goris ML, Billingham ME, Bockemuehl K. Sensitivity and specificity of radionuclide ejection fractions in doxorubicin cardiotoxicity. *Am Heart J.* (1983) 106:1048–56. doi: 10.1016/0002-8703(83)90651-8
50. Hauser M, Gibson BS, Wilson N. Diagnosis of anthracycline-induced late cardiomyopathy by exercise-spiroergometry and stress-echocardiography. *Eur J Pediatr.* (2001) 160:607–10. doi: 10.1007/s004310100830
51. Bae JH, Schwaiger M, Mandelkern M, Lin A, Schelbert HR. Doxorubicin cardiotoxicity: response of left ventricular ejection fraction to exercise and incidence of regional wall motion abnormalities. *Int J Card Imaging.* (1988) 3:193–201. doi: 10.1007/BF01797717
52. Jones LW, Courneya KS, Mackey JR, Muss HB, Pituskin EN, Scott JM, et al. Cardiopulmonary function and age-related decline across the breast cancer survivorship continuum. *J Clin Oncol.* (2012) 30:2530–7. doi: 10.1200/JCO.2011.39.9014
53. Moulin M, Piquereau J, Mateo P, Fortin D, Rucker-Martin C, Gressette M, et al. Sexual dimorphism of doxorubicin-mediated cardiotoxicity: potential role of energy metabolism remodeling. *Circ Heart Fail.* (2015) 8:98–108. doi: 10.1161/CIRCHEARTFAILURE.114.001180
54. Vainshelboim B, Lima RM, Edvardsen E, Myers J. Cardiorespiratory fitness, incidence and mortality of lung cancer in men: a prospective cohort study. *J Sci Med Sport.* (2019) 22:403–7. doi: 10.1016/j.jsams.2018.10.002
55. Montero D, Lundby C. Refuting the myth of non-response to exercise training: 'non-responders' do respond to higher dose of training. *J Physiol.* (2017) 595:3377–87. doi: 10.1113/JP273480

Conflict of Interest: The authors declare that the research was conducted in the absence of any commercial or financial relationships that could be construed as a potential conflict of interest.

frontiers in Cardiovascular Medicine

BRIEF RESEARCH REPORT
published: 06 April 2021
doi: 10.3389/fcvm.2021.653648

Cardiac Energetics Before, During, and After Anthracycline-Based Chemotherapy in Breast Cancer Patients Using ^{31}P Magnetic Resonance Spectroscopy: A Pilot Study

Gillian Macnaught[1,2], Olga Oikonomidou[3,4], Christopher T. Rodgers[5], William Clarke[6], Annette Cooper[1], Heather McVicars[3,4], Larry Hayward[3,4], Saeed Mirsadraee[7], Scott Semple[1,2†] and Martin A. Denvir[2†]*

[1] Edinburgh Imaging Facility, Queen's Medical Research Institute, University of Edinburgh, Edinburgh, United Kingdom, [2] Centre for Cardiovascular Sciences, Queen's Medical Research Institute, University of Edinburgh, Edinburgh, United Kingdom, [3] Edinburgh Cancer Research Centre, University of Edinburgh, Edinburgh, United Kingdom, [4] Edinburgh Cancer Centre, Western General Hospital, Edinburgh, United Kingdom, [5] Department of Clinical Neurosciences, Wolfson Brain Imaging Centre, University of Cambridge, Cambridge, United Kingdom, [6] Division of Cardiovascular Medicine, Radcliffe Department of Medicine, University of Oxford Centre for Clinical Magnetic Resonance Research (OCMR), Level 0, John Radcliffe Hospital, Oxford, United Kingdom, [7] Department of Cardiology, Royal Brompton Hospital, London, United Kingdom

OPEN ACCESS

Edited by:
Margaret Rose Cunningham, University of Strathclyde, United Kingdom

Reviewed by:
Ian Paterson, University of Alberta, Canada
Kenneth Mangion, University of Glasgow, United Kingdom

***Correspondence:**
Scott Semple
scott.semple@ed.ac.uk

†These authors share last authorship

Specialty section:
This article was submitted to Cardio-Oncology, a section of the journal Frontiers in Cardiovascular Medicine

Received: *14 January 2021*
Accepted: *12 March 2021*
Published: *06 April 2021*

Citation:
Macnaught G, Oikonomidou O, Rodgers CT, Clarke W, Cooper A, McVicars H, Hayward L, Mirsadraee S, Semple S and Denvir MA (2021) Cardiac Energetics Before, During, and After Anthracycline-Based Chemotherapy in Breast Cancer Patients Using ^{31}P Magnetic Resonance Spectroscopy: A Pilot Study. Front. Cardiovasc. Med. 8:653648. doi: 10.3389/fcvm.2021.653648

Purpose: To explore the utility of phosphorus magnetic resonance spectroscopy (^{31}P MRS) in identifying anthracycline-induced cardiac toxicity in patients with breast cancer.

Methods: Twenty patients with newly diagnosed breast cancer receiving anthracycline-based chemotherapy had cardiac magnetic resonance assessment of left ventricular ejection fraction (LVEF) and ^{31}P MRS to determine myocardial Phosphocreatine/Adenosine Triphosphate Ratio (PCr/ATP) at three time points: pre-, mid-, and end-chemotherapy. Plasma high sensitivity cardiac troponin-I (cTn-I) tests and electrocardiograms were also performed at these same time points.

Results: Phosphocreatine/Adenosine Triphosphate did not change significantly between pre- and mid-chemo (2.16 ± 0.46 vs. 2.00 ± 0.56, $p = 0.80$) and pre- and end-chemo (2.16 ± 0.46 vs. 2.17 ± 0.86, $p = 0.99$). Mean LVEF reduced significantly by 5.1% between pre- and end-chemo (61.4 ± 4.4 vs. 56.3 ± 8.1 %, $p = 0.02$). Change in PCr/ATP ratios from pre- to end-chemo correlated inversely with changes in LVEF over the same period ($r = -0.65$, $p = 0.006$). Plasma cTn-I increased progressively during chemotherapy from pre- to mid-chemo (1.35 ± 0.81 to 4.40 ± 2.64 ng/L; $p = 0.01$) and from mid- to end-chemo (4.40 ± 2.64 to 18.33 ± 13.23 ng/L; $p = 0.001$).

Conclusions: In this small cohort pilot study, we did not observe a clear change in mean PCr/ATP values during chemotherapy despite evidence of increased plasma cardiac biomarkers and reduced LVEF. Future similar studies should be adequately powered to take account of patient drop-out and variable changes in PCr/ATP and could include T1 and T2 mapping.

Keywords: chemotherapy, breast cancer, cardiac energetics, troponin, ejection fraction

INTRODUCTION

Anthracyclines are widely used in the treatment of breast cancer and are well-recognized to carry increased risk of cardiotoxicity (1–3). This can occur as an early, acute manifestation, or many years after treatment as late onset cardiomyopathy (4, 5). It is increasingly apparent that there may be a chronic subclinical phase associated with low grade cardiac injury with no apparent clinical impact on the contractile function of the heart (6). This period may remain latent for many years with the patient remaining asymptomatic and with apparently normal cardiac function. Identification of early and subtle cardiac dysfunction during this period could provide a window of opportunity for therapeutic intervention if those at risk or those experiencing this low-grade decline could be accurately identified. Recent studies have suggested that it might be possible to detect subclinical cardiac dysfunction using echocardiographic strain measurements of the left ventricle and that such changes might predict future risk of developing cardiac dysfunction (7, 8). Other studies have suggested that plasma levels of cardiac troponin could also provide a useful marker of early and ongoing cardiac injury following anthracycline treatment (9, 10).

Left Ventricular Ejection Fraction (LVEF), assessed by a variety of imaging methods, is recognized as insensitive for the detection of early anthracycline-induced cardiomyopathy (11). The widely used values for a clinically relevant decline in ejection fraction associated with clinical symptoms of heart failure, or an asymptomatic decrease in LVEF of 10% to <55% (10, 12) represent a relatively late manifestation of cardiac toxicity. In some cases, by the time a reduction in LVEF occurs the patient may have irreversible cardiac damage. As cancer survival rates increase there is a clear need not only to identify early markers of anthracycline myocardial toxicity but also to explore new techniques that could potentially identify baseline characteristics, pre-chemotherapy, that might predict the likelihood of developing subsequent cardiotoxicity. An accurate method of identifying, and possibly even predicting, early cardiac toxicity could aid oncologists in optimizing chemotherapy treatment whilst limiting the short and long-term cardiotoxic effects of these agents.

This study explores the potential utility of phosphorus magnetic resonance spectroscopy (^{31}P-MRS) acquired using a clinical 3T MR system to identify early anthracycline-induced cardiac toxicity and baseline predisposition to cardiac injury. This technique measures the phosphocreatine/adenosine triphosphate concentration ratio (PCr/ATP), which reflects cardiac cellular energetics. The normal range of PCr/ATP is approximately 1.8–2.2, whereas decreased PCr/ATP is associated with a drop in available energy reserve in the heart, associated with many forms of heart failure (13, 14).

Conventional cardiac investigations of electrocardiogram and ultra-high sensitivity plasma cardiac troponin-I (cTn-I) have also been applied. To our knowledge PCr/ATP has not previously been used sequentially to assess cardiac injury in breast cancer patients before, during, and after chemotherapy.

METHODS

Ethics Statement

This study was approved by the South East Scotland Research Ethics Committee (14/SS/1041) and all participants gave full written informed consent.

Study Population and Recruitment

Twenty female breast cancer patients with no prior exposure to anthracyclines scheduled to receive anthracycline-based chemotherapy either in the adjuvant or the neoadjuvant setting were recruited from the Breast clinic at the South East Scotland Cancer Center over a period of 18 months. The combination chemotherapy regimens were either six cycles of adjuvant FEC-80 [Fluorouracil, Epirubicin (80 mg/m^3), cyclophosphamide], or three cycles of FEC [Fluorouracil, Epirubicin (100 mg/m^3), cyclophosphamide] followed by three cycles of Docetaxel (FEC-T). Four patients had a history of hypertension: two treated with ramipril and two with bendroflumethiazide (**Table 1**). None of the patients had coronary heart disease, diabetes, hypercholesterolemia, or heart failure at baseline.

The mean time between each scan was 7 weeks (range 6–12 weeks) and was designed flexibly to allow for the oncology team to defer or postpone the next chemo-treatment for clinical reasons including chemotherapy-related side effects including nausea, fatigue, and general malaise.

Thirteen healthy volunteers (48.8 ± 11.2 years, range 31–60) with no background medical conditions and on no medications underwent a single MRI imaging protocol and a single ^{31}P MRS as described for patients. Phosphocreatine/Adenosine Triphosphate Ratios and left ventricular ejection fraction were calculated for each volunteer. Scanning was repeated for three of these normal subjects to assess repeatability of measurements. The maximum difference between repeated PCr/ATP measurements and repeated LVEF measurements for volunteers defined the cut-off above which a real change could be assumed to occur in patients between pre- to mid-chemotherapy, mid- to end-chemotherapy, and pre- to end-chemotherapy. Volunteers did not undergo ECG or plasma troponin measurements and did not undergo sequential repeat MR scans.

High Sensitivity Cardiac Troponin-I (cTn-I) Measurements

Blood samples were taken immediately prior to the first and fourth chemotherapy cycles and within 2 weeks of completion of the sixth chemotherapy cycle. Plasma Cardiac Tn-I was measured using a high sensitivity assay (ARCHITECT *STAT* Troponin I assay; Abbott Laboratories). This assay has a limit of detection of 1.2 ng/L, with a coefficient of variation of 23% at the limit of detection (1.2 ng/L) and <10% at 6 ng/L (15). The upper reference limit, determined by the manufacturer as the 99th centile of samples from 4,590 healthy individuals, is 16 ng/L in women (15). As part of clinical follow-up, cTn-I was also measured within 3 months of completion of chemotherapy in patients where values increased above the normal range (0–16 ng/l) at any time point during chemotherapy.

TABLE 1 | Patient population clinical characteristics and treatment regimens.

Patient	Age range (years)	Smoking history	BMI	Menopausal status	Hyper-tension	Chemo-therapy	Trastuzumab	Cancer side	Radiotherapy
1	60–70	No	28	Post	No	FEC-T	No	R	Yes
2	60–70	No	31	Post	No	FEC	No	R	Yes
3	40–50	No	24	Pre	No	FEC-T	No	R	No
4	50–60	No	31	Post	No	FEC80	No	L	Yes
5	40–50	Yes	28	Pre	No	FEC-T	No	R	Yes
6	50–60	No	38	Post	No	FEC-T	No	L	Yes
7	30–40	No	24	Pre	No	FEC-T	No	L	No
8	50–60	Yes	32	Post	No	FEC-T	No	L	Yes
9	60–70	No	26	Post	Yes*	FEC80	No	R	Yes
10	50–60	No	25	Pre	No	FEC-T	No	R	Yes
11	30–40	No	28	Pre	No	FEC80	No	L	Yes
12	50–60	No	30	Pre	No	FEC-T	No	R	Yes
13	50–60	Yes	24	Post	No	FEC-T	Yes	L	Yes
14	40–50	No	36	Pre	No	FEC-T	No	R	Yes
15	50–60	No	35	Post	Yes*	FEC-T	No	L	Yes
16	40–50	No	23	Pre	Yes**	FEC80	No	R	Yes
17	50–60	No	27	Post	Yes**	FEC80	No	L	Yes
18	40–50	No	26	Pre	No	FEC-T	Yes	L+R	Yes
19	30–40	Yes	30	Pre	No	FEC-T	No	L	Yes
20	50–60	No	32	Pre	No	FEC-T	No	L	Yes

Cardiac history of any of angina, hypertension, previous myocardial infarction, heart failure. Chemotherapy regimen: FEC80—six cycles of Fluorouracil, Epirubicin (80 mg/m^3), cyclophosphamide. FEC-T—three cycles of Fluorouracil, Epirubicin, (100 mg/m^3), cyclophosphamide followed by three cycles of docetaxel.

**Hypertension treated with ramipril.*

***Hypertension treated with Bendroflumethiazide.*

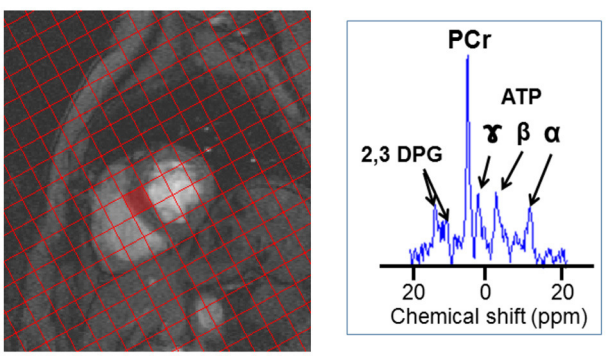

FIGURE 1 | ^{31}P-MRS spectrum acquisition. An example of the voxel positioning for ^{31}P-MRS acquisition spectrum, the spectrum acquired at the mid-septum, denoted by the red square, is analyzed. An example of a ^{31}P MR spectrum is also shown (B) with resonances corresponding to phosphocreatine (PCr), γ, β, and α adenosine triphosphate (ATP), and 2,3-diphosphoglycerate (2,3 DPG) labeled.

Cardiac Magnetic Resonance Imaging (CMRI)

Participants attended the Edinburgh Imaging QMRI facility at three time points: pre-, mid-, and end-chemotherapy. Mid-chemotherapy was defined as between cycles 3 and 4 and end-chemotherapy was within 27 ± 19 days of completing cycle 6. On each occasion participants were positioned head first supine in a 3T Verio MR scanner (Siemens Healthineers, Erlangen, Germany) between anterior and posterior parts of an 8-element cardiac ^{31}P receive array coil (Rapid Biomedical, Rimpar, Germany).

Phosphorus Magnetic Resonance Spectroscopy

The ^{31}P MRS protocol used for this study has been described in detail elsewhere (16). In brief the total MR protocol acquisition time including positioning, set-up and acquisition of cine MR imaging to calculate ejection fraction and MRS was 60 min. ^{31}P MR spectra were acquired over 30 min using a 3D UTE-CSI pulse sequence (TR/TE = 1,000/∼0.6 ms, FOV = 350 × 350 × 350 mm^3, 22 × 22 × 10 CSI matrix). A flip angle (α) of 30° was applied to the mid-septum of the myocardium. Voxels were carefully planned so that one full voxel was aligned with the mid-septum. **Figure 1** shows an example of the planning of the voxel positioning. While spectra are acquired from each voxel, that acquired from the mid-septum voxel (denoted by the red square in **Figure 1**) is the spectrum used for analysis. The ^{31}P MRS acquisition was not ECG gated.

Analysis of the ^{31}P spectra was carried out using a custom Matlab implementation of AMARES (17) and was analyzed by two independent observers blinded to the time-point of analysis. This analysis quantifies the amount of phosphocreatine (PCr) and adenosine triphosphate (ATP) present in the cardiac spectrum as a concentration ratio

("PCr/ATP"). The PCr/ATP ratio was corrected for saturation effects and blood contamination. Phosphocreatine/Adenosine Triphosphate Ratios were calculated for each of the three time-points.

Left Ventricular Ejection Fraction

A series of Cardiac Magnetic Resonance (CMR) cine images were acquired from base to apex in the short axis plane using the system's integrated body coil (TrueFISP sequence: TR/TE = 85.8/1.45 ms, $\alpha = 50^{\circ}$, FOV = 400 × 338 mm^2, matrix = 256 × 205, Grappa acceleration factor = 3, slice thickness = 8 mm). Two independent operators subsequently calculated the LVEF from these images using QMass® software (Medis, Leiden, The Netherlands). This was carried out for images acquired at each time point.

We used the definition of the Cardiac Review and Evaluation Committee (CREC) supervising Trastuzumab trials which defined cardiotoxicity as a decrease in LVEF of 5 points to <55% *with* accompanying signs or symptoms of heart failure, or a decline of 10 points to <55% *without* heart failure signs or symptoms (10, 12).

Electrocardiograms

A 12-lead ECG was acquired at each of the three time points immediately prior to each MRI scan. These were reported by a Cardiologist and any abnormalities grouped by ST segment change, left ventricular hypertrophy and changes in the QT interval.

Statistical Analysis

All statistical analysis was carried out using Minitab 17 Statistical Software (Minitab 17 Statistical Software (2010), State College, PA: Minitab, Inc.). Data were analyzed using paired Student's *t*-tests or one-way ANOVA as appropriate. Associations between various parameters were assessed using Pearson's Coefficient. Significance was accepted at $p \leq 0.05$.

The mean PCr/ATP ratio for age-matched female healthy controls was 1.75 ± 0.59 (range 1.11–2.18, $n = 13$). In three healthy volunteers with repeat measurements of PCr/ATP the difference in values between scans were 0.58, 0.53, and 0.20. This was consistent with other published work suggesting that a change in PCr/ATP of 0.5, with 95% confidence, could be detected with a sample size of nine patients using a similar protocol as that used in patients with heart failure (18). However, since we could not accurately predict the change in PCr/ATP associated with the anthracycline regimes used in our patients we recognized that, taking drop-out into account, we might not be adequately powered to detect a smaller change in PCr/ATP even with the proposed 20 patients agreed with our ethical review board.

RESULTS

Patient Characteristics

All participants were women with median age 51 (range 31–67 years) and median body mass index 28 (range 23–36). Six patients (30%) received FEC80, fourteen (70%) received FEC-T chemotherapy, and eighteen (90%) received radiotherapy. Two patients treated with the FEC-T received Trastuzumab from the mid-chemo time point. Ten patients had left sided tumors and one had left and right sided tumors. Nine participants were post-menopausal.

All participants attended their pre-chemotherapy MRI scan while five were unable to attend the mid-chemotherapy scan due to inter-current illness and one was unable to attend the final end-chemotherapy MRI scan.

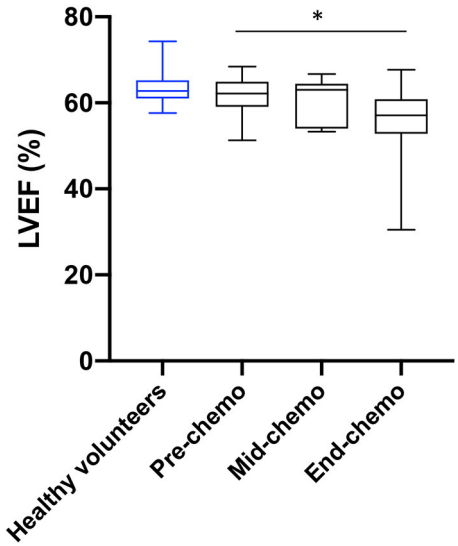

FIGURE 2 | Left ventricular ejection fraction in healthy volunteers and in breast cancer patients during chemotherapy. Healthy volunteer left ventricular ejection fraction (LVEF, blue, $n = 13$) and sequential LVEF in patients (black) pre- ($n = 20$), mid- ($n = 15$), and end-chemotherapy ($n = 19$) acquired by cardiac magnetic resonance (CMR) imaging [box and whiskers plot, values are mean ± SD, and 95% confidence intervals, $^*P = 0.02$ for change from pre-to end chemo in patients (paired *t*-test)].

Cardiac Magnetic Resonance Imaging (CMR)

The mean LVEF for healthy volunteers was 63.6 ± 4.5% with range 57.6–74.3%. Differences in repeated measurements of LVEF for three volunteers were 0.5, 0.6, and −0.5%, indicating a very high degree of repeatability.

Left ventricular ejection fraction was calculated for all 20 participants prior to chemotherapy, 15 at mid-chemotherapy, and 19 at end-chemotherapy.

The mean (± standard deviation) LVEF at pre-, mid-, and end-chemotherapy was 61.6 ± 4.4, 60.5 ± 5.2, and 56.3 ± 8.1% respectively (**Figure 2**). There was a significant decrease in LVEF between pre- and end-chemotherapy ($p = 0.02$). There was no significant difference in LVEF between patients receiving FEC80 ($n = 5$) and those receiving FEC-T ($n = 12$) at mid (57.7 ± 5.6 vs. 61.9 ± 4.7%, respectively, $p = 0.14$) or end-chemo time-points (55.9 ± 3.9 vs. 56.5 ± 9.6%, respectively, $p = 0.94$). Left ventricular mass did not change significantly between pre-chemo and end-chemo (83.2 ± 11.9 vs. 82.0 ± 10.7g; $p = 0.78$).

In total, six patients experienced a significant decrease in LVEF according to agreed criteria (10). Three symptomatic patients (with breathlessness) experienced a 5% decrease in LVEF from pre- to mid-chemo. Two of these patients had no further change in LVEF from mid- to end-chemo and one had a significant increase. Three additional patients experienced a decrease of 10% in LVEF from mid- to end-chemo. One patient, receiving FEC-T, became symptomatic during treatment with associated ankle swelling and breathlessness associated with a 30% fall in LVEF between pre- and end-chemo to 30.5%. This patient responded rapidly to low dose diuretics and fluid restriction and was assessed by the cardiology team with full recovery of cardiac function within 2 weeks.

Cardiac Energetics Assessed by ^{31}P-MRS

^{31}P MR spectra were successfully acquired for 19 breast cancer patients pre-chemotherapy, 11 at mid-chemotherapy, and 17 end-chemotherapy. Missing scans were due to inter-current illness or technical issues for one participant at the pre-chemotherapy scan, four mid-chemotherapy, and two end-chemotherapy. An example patient ^{31}P spectrum is shown in **Figure 1**. There was no significant difference in the mean PCr/ATP ratio between healthy controls and patients at the pre-chemo time point (1.94 ± 0.42 vs. 2.16 ± 0.46, respectively, $p = 0.11$).

For the patient cohort there was no significant difference in mean sequential values for PCr/ATP ratio comparing pre-, mid-, and end-chemotherapy time-points. However, there was a significant negative correlation between the change in PCr/ATP from pre- to mid-chemotherapy and the subsequent change in PCr/ATP from mid- to end chemotherapy ($r = -0.68$, $p = 0.04$). The mean change in the PCr/ATP ratio at mid- and at end-chemotherapy relative to the mean baseline value is plotted in **Figure 3**.

Plasma High Sensitivity Cardiac Troponin-I

Plasma cardiac cTn-I-I levels (ng/L) were low-normal (<5 ng/L) in all patients at baseline prior to starting chemotherapy and increased progressively by mid-chemo with a further rise at the time of the last chemo cycle (**Figure 4**). The threshold cTn-I level for identifying acute coronary syndrome (ACS) in women in our center is 16 ng/L and is based on the 99th upper centile of the normal range for a large sample of patients (15). In our study, while all participants showed a small but significant rise in mean cTn-I value between baseline and mid-chemo (1.35 ± 0.81 to 4.40 ± 2.64 ng/L, $p = 0.0001$) none of these values exceeded the ACS threshold (16 ng/L). By end-chemo there was a further significant increase in mean plasma cTn-I (4.40 ± 2.64 to 14.84 ± 8.73 ng/L, $p = 0.0001$) with six cTn-I values above the ACS threshold. These six patients, and a further three patients with borderline normal cTnI levels at end-chemo, were invited back 2–3 months after end of chemotherapy for longer term follow-up with repeat blood cTn-I. In all cases cTn-I had returned to normal level (mean ± SD, 1.55 ± 0.88 ng/L).

The specific type of chemotherapy regime had no impact on cTn-I levels. At mid-chemotherapy cTn-I was not significantly higher in patients receiving FEC-T compared to FEC80 (5.0 ± 2.9 vs. 3.0 ± 0.89 ng/L, respectively, $p = 0.12$) or at end-chemo in patients receiving FEC80 compared to those receiving FEC-T (18.3 ± 12.0 vs. 13.2 ± 6.7 ng/L, respectively, $p = 0.24$). As expected, the side of the cancer had no impact on cTn-I levels at any of the time points studied (end-chemo: left 15.1 ± 8.1 vs. right 15.5 ± 10.1, $p = 0.92$).

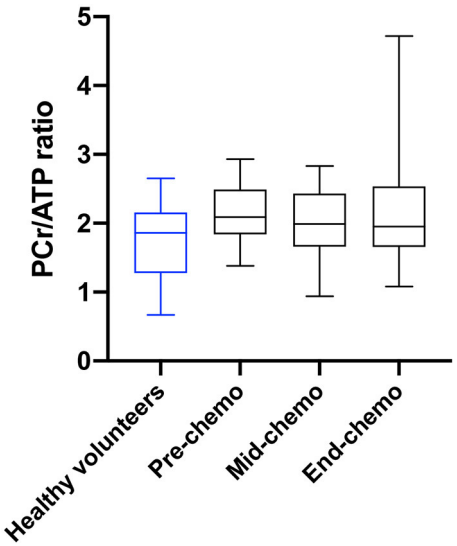

FIGURE 3 | PCr/ATP ratio in healthy volunteers and in breast cancer patients during chemotherapy. Myocardial PCr/ATP ratio (box and whiskers plot) in healthy volunteers (blue) and in breast cancer patients (black) pre, mid, and at end of chemotherapy [$p = 0.80$ for pre-chemo vs. mid-chemo and $p = 0.99$ for pre to end chemo (one-way ANOVA with Tukey multiple comparison test)].

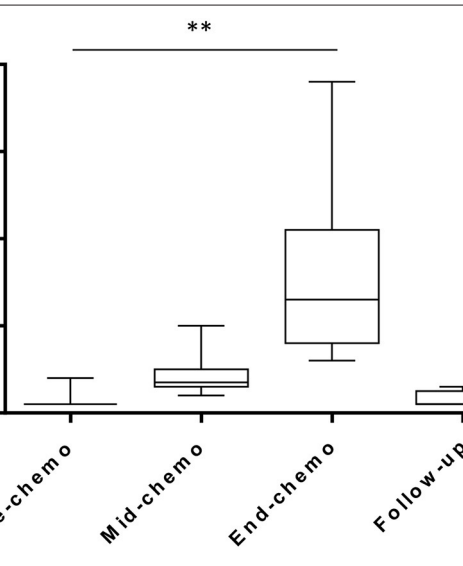

FIGURE 4 | Plasma cardiac troponin levels during chemotherapy in breast cancer patients. High sensitivity cardiac troponin-I levels pre-, mid-, and end-chemotherapy [box and whiskers plot, **indicates $P < 0.001$ for change from pre-chemo (paired *t*-test)] and at 2–3 months follow-up in patients with values above the normal range at end-chemo ($n = 9$).

Electrocardiograms (ECG)

There were no significant changes in PR interval or QRS duration during chemotherapy. There was a small but significant increase in the corrected QT interval (QTc) from 422 ± 15 to 438 ± 13 ms ($p = 0.0001$) with most of this increase occurring between baseline and mid-chemo. Overall, no patient showed an increase of QTc of >60 ms or a QTc above 500 ms.

Exploratory Analysis of Possible Association Between LVEF, PCr/ATP, QT Interval, and Cardiac Troponin-*I*

A significant negative correlation was found between the change in PCr/ATP ratio and the change in LVEF from pre-chemo to end-chemo ($r = -0.65$, $p = 0.006$, **Supplementary Figure**). A significant negative correlation was also found between the change in PCr/ATP ratio from pre- to end-chemotherapy and the change in LVEF from mid- to end-chemotherapy ($r = -0.77$, $p = 0.002$). There was no apparent association between cTn-I and LVEF or PCr/ATP any of the time points. There was also no association found between changes in the corrected QT interval in the electrocardiogram and changes in cTn-I or changes in the QT interval and changes in LVEF. There was no apparent effect of trastuzumab treatment on cTn-I levels.

In total, six patients displayed cTn-I values above the normal range at the end-chemo timepoint. When examining each of these patients on an individual basis, no clear relationship was observed between cTn-I and baseline clinical data, including pre-existing hypertension or smoking history, LVEF or PCr/ATP ratio.

DISCUSSION

This study has explored the applicability of PCr/ATP ratio, measured using ^{31}P MRS, to detect early anthracyclines-induced cardiac injury in a pilot cohort. The widely accepted cellular mechanism underlying anthracycline-induced cardiac toxicity is based on generation of reactive oxygen species (ROS) resulting from mitochondrial damage associated with elevated intracellular iron (19). Such damage to mitochondria is likely to cause early perturbations in high energy phosphates within cardiomyocytes and hence is the rationale for assessing ^{31}P-MRS in this clinical setting. In addition, cardiotoxicity associated with breast cancer treatment is categorized as either type I, associated with irreversible cardiomyocyte death, or type II due to reversible cardiomyocyte dysfunction (9). Impaired cardiac energetics could represent a possible underlying mechanism for type II toxicity.

We compared PCr/ATP ratio with other markers of cardiotoxicity including high sensitivity plasma cardiac Tn-I, ECG parameters, and cardiac magnetic resonance imaging assessment of LVEF. While these conventional factors suggested a progressive cardiotoxic effect of chemotherapy there was no clear signal in the PCr/ATP ratio data. The possible reasons for this are discussed.

Cardioprotection during chemotherapy has been demonstrated using ACE inhibitors (20), statins (21), angiotensin receptor antagonists (22), but not metoprolol (22). Dexrazoxane has been shown to reduce cardiac troponin release during anthracycline based chemotherapy (23). Only two patients in our study received ACE inhibitors for management of high blood pressure and hence background drug therapy is unlikely to have impacted our findings. Allopurinol (24) and metformin (25) have also been shown to affect cardiac energetics and these possibly merit further study using ^{31}P-MRS to assess their mechanism of action during chemotherapy.

Patient specific factors such as age and physical fitness are also known to affect PCr/ATP ratio. Jakovljevic et al. (26) found that PCr/ATP ratio was significantly reduced in older compared to younger women. They also found that older women who are physically active maintained high PCr/ATP ratios similar to younger sedentary women. Genetic factors are also known to play a part in susceptibility to cardiotoxicity in response to chemotherapy (27). Therefore, physical activity, pre-treatment levels of physical fitness, and genetics could provide intrinsic protection during chemotherapy, potentially impacting on the effects of chemotherapy on PCr/ATP.

While we observed a significant decrease in LVEF between pre and end chemotherapy by approximately 5% we also observed a negative association between changes in PCr/ATP ratio and LVEF between pre- and end-chemotherapy. This finding is not consistent with studies in dilated cardiomyopathy (unrelated to anthracyclines) where low PCr/ATP ratios were associated with reduced LVEF (28, 29) and while this was a pilot study, we had predicted a fall in PCr/ATP ratios in line with or perhaps preceding a fall in LVEF. The reasons for this are not clear. There is possibly a more complex relationship between energetics and LVEF in the setting of anthracycline chemotherapy compared to other forms of cardiomyopathy or the relatively modest reduction in mean LVEF of 5% was not sufficient to reveal a measurable change in PCr/ATP ratio during the course of the chemotherapy regimen. A further reason for the lack of clear change in PCr/ATP ratio is the possibility of a type 2 statistical error. Since the number of patients clinically well enough to have a ^{31}P-MRS scan at mid-chemo time point fell from 20 to 11, this small number was at the predicted limit to allow us to detect a significant change in PCr/ATP ratio. Furthermore, this mid-chemo time point was important in that all 20 patients had been receiving anthracyclines over the previous 6 weeks in the run up to this mid-point scan. Thereafter, most patients (14) switched to docetaxel for the last three chemo-cycles thus diminishing our chances of detecting an effect on the final scan. It is therefore possible that cardiac energetics recovered in the 14 patients treated with Docetaxel for the final three chemo cycles. In addition, the relatively low cumulative dose of anthracyclines used may have limited cardiotoxicity.

Overall, the fall in LVEF, increase in QT interval on ECG and the rise in cardiac troponin together suggest that there was some degree of cardiac toxicity in our cohort. The very slight fall in PCr/ATP ratio at mid-chemo, while non-significant, is therefore highly intriguing and merits further study addressing the issues highlighted in our pilot. Furthermore, the sensitivity of ^{31}P-MRS scans could be significantly improved by using higher magnetic field strengths (7T) (30, 31).

CONCLUSIONS

This study investigated ^{31}P MRS in assessing cardiac energetics of breast cancer patients undergoing chemotherapy in a pilot cohort. Our findings have highlighted the challenges of serial cardiac imaging studies during complex chemotherapy regimens and outlined a pathway by which this technique could be further explored to establish its potential for detection of cardiac energetics during chemotherapy. Future studies should take account of a potentially high level of patient drop-out, background factors that could influence cardiac PCr/ATP ratio, such as age, physical fitness, and regular medications, and should seek to improve sensitivity using 7T MRI. Future studies could include assessment of Trastuzumab on ^{31}P MR myocardial imaging and changes in T1 and T2 mapping.

DATA AVAILABILITY STATEMENT

The original contributions presented in the study are included in the article/**Supplementary Material**, further inquiries can be directed to the corresponding author/s.

ETHICS STATEMENT

The studies involving human participants were reviewed and approved by Lothian Research Ethics Committee. The patients/participants provided their written informed consent to participate in this study.

AUTHOR CONTRIBUTIONS

GM, SS, OO, and MD conceived and designed the study and wrote the ethics application. OO, HM, and LH recruited patients, collated clinical data, and collected bloods for troponin. GM, SS, CR, AC, WC, and SM performed and reported the scans. MD, OO, GM, and SS wrote the manuscript. All authors contributed to the article and approved the submitted version.

FUNDING

This study was funded by the Edinburgh and Lothians Health Foundation and The Margaret Lee Breast Cancer Fund. Funding for the 31P array used in this study was provided by the British Heart Foundation Centre of Research Excellence award. CR is funded by a Sir Henry Dale Fellowship from the Welcome Trust and Royal Society (098436/Z/12/Z).

SUPPLEMENTARY MATERIAL

The Supplementary Material for this article can be found online at: https://www.frontiersin.org/articles/10.3389/fcvm.2021.653648/full#supplementary-material

Supplementary Figure | Associations between the change in PCr/ATP ratio and change in LVEF during chemotherapy.

REFERENCES

1. Bristow MR, Mason JW, Billingham ME, Daniels JR. Doxorubicin cardiomyopathy: evaluation by phonocardiography, endomyocardial biopsy, and cardiac catheterization. *Ann Intern Med.* (1978) 88:168–75. doi: 10.7326/0003-4819-88-2-168
2. Friedman MA, Bozdech MJ, Billingham ME, Rider AK. Doxorubicin cardiotoxicity. Serial endomyocardial biopsies and systolic time intervals. *JAMA.* (1978) 240:1603–6. doi: 10.1001/jama.1978.03290150049023
3. Praga C, Beretta G, Vigo PL, Lenaz GR, Pollini C, Bonadonna G, et al. Adriamycin cardiotoxicity: a survey of 1273 patients. *Cancer Treat Rep.* (1979) 63:827–34.
4. Steinherz LJ, Steinherz PG, Tan CT, Heller G, Murphy ML. Cardiac toxicity 4 to 20 years after completing anthracycline therapy. *JAMA.* (1991) 266:1672–7. doi: 10.1001/jama.1991.03470120074036
5. Pein F, Sakiroglu O, Dahan M, Lebidois J, Merlet P, Shamsaldin A, et al. Cardiac abnormalities 15 years and more after adriamycin therapy in 229 childhood survivors of a solid tumour at the Institut Gustave Roussy. *Br J Cancer.* (2004) 91:37–44. doi: 10.1038/sj.bjc.6601904
6. Cardinale D, Colombo A, Bacchiani G, Tedeschi I, Meroni CA, Veglia F, et al. Early detection of anthracycline cardiotoxicity and improvement with heart failure therapy. *Circulation.* (2015) 131:1981–8. doi: 10.1161/CIRCULATIONAHA.114.013777
7. Florescu M, Magda LS, Enescu OA, Jinga D, Vinereanu D. Early detection of epirubicin-induced cardiotoxicity in patients with breast cancer. *J Am Soc Echocardiogr.* (2014) 27:83–92. doi: 10.1016/j.echo.2013.10.008
8. Charbonnel C, Convers-Domart R, Rigaudeau S, Taksin AL, Baron N, Lambert J, et al. Assessment of global longitudinal strain at low-dose anthracycline-based chemotherapy, for the prediction of subsequent cardiotoxicity. *Eur Heart J Cardiovasc Imaging.* (2017) 18:392–401. doi: 10.1093/ehjci/jew223
9. Mokuyasu S, Suzuki Y, Kawahara E, Seto T, Tokuda Y. High-sensitivity cardiac troponin I detection for 2 types of drug-induced cardiotoxicity in patients with breast cancer. *Breast Cancer.* (2015) 22:563–9. doi: 10.1007/s12282-014-0520-8
10. Seidman A, Hudis C, Pierri MK, Shak S, Paton V, Ashby M, et al. Cardiac dysfunction in the trastuzumab clinical trials experience. *J Clin Oncol.* (2002) 20:1215–21. doi: 10.1200/JCO.2002.20.5.1215
11. Cardinale D, Sandri MT, Martinoni A, Tricca A, Civelli M, Lamantia G, et al. Left ventricular dysfunction predicted by early troponin I release after high-dose chemotherapy. *J Am Coll Cardiol.* (2000) 36:517–22. doi: 10.1016/S0735-1097(00)00748-8
12. Thavendiranathan P, Wintersperger BJ, Flamm SD, Marwick TH. Cardiac MRI in the Assessment of cardiac injury and toxicity from cancer chemotherapy. A systematic review. *Circ Cardiovasc Imaging.* (2013) 6:1080–91. doi: 10.1161/CIRCIMAGING.113.000899
13. Ventura-Clapier R, Garnier A, Veksler V, Joubert F. Bioenergetics of the failing heart. *Biochim Biophys Acta.* (2011) 1813:1360–72. doi: 10.1016/j.bbamcr.2010.09.006
14. Hudsmith LE, Neubauer S. Magnetic resonance spectroscopy in myocardial disease. *JACC.* (2009) 2:87–96. doi: 10.1016/j.jcmg.2008.08.005
15. Shah AS, Anand A, Sandoval Y, Lee KK, Smith SW, Adamson PD et al. High-sensitivity cardiac troponin I at presentation in patients with suspected acute coronary syndrome: a cohort study. *Lancet.* (2015) 386:2481–8. doi: 10.1016/S0140-6736(15)00391-8
16. Rodgers CT, Robson MD. Coil combination for receive array spectroscopy: are data-driven methods superior to methods using computed field maps? *Magn. Reson. Med.* (2016) 75:473–87. doi: 10.1002/mrm.25618
17. Purvis L, Clarke W, Biasiolli L, Robson M, Rodgers C. Linewidth constraints in Matlab AMARES using per-metabolite T_2 and per-voxel ΔBo. In: *Proceedings of the 22nd Annual Meeting of ISMRM.* Milan (2014) Abstract 2885.

18. Tyler DJ, Emmanuel Y, Cochlin LE, Hudsmith LE, Holloway CJ, Neubauer S, et al. Reproducibility of 31P cardiac magnetic resonance spectroscopy at 3 T. *NMR Biomed*. (2009) 22:405–13. doi: 10.1002/nbm.1350
19. Ichikawa Y, Ghanefar M, Bayeva M, Wu R, Khechaduri A, Naga Prasad SV, et al. Cardiotoxicity of doxorubicin is mediated through mitochondrial iron accumulation. *J Clin Invest.* (2014) 124:617–30. doi: 10.1172/JCI72931
20. Cardinale D, Colombo A, Sandri MT, Lamantia G, Colombo N, Civelli M, et al. Prevention of high-dose chemotherapy–induced cardiotoxicity in high-risk patients by angiotensin-converting enzyme inhibition. *Circulation.* (2006) 114:2474–81. doi: 10.1161/CIRCULATIONAHA.106.635144
21. Acar Z, Kale A, Turgut M, Demircan S, Durna K, Demir S, et al. Efficiency of atorvastatin in the protection of anthracycline-induced cardiomyopathy. *J. Am. Coll. Cardiol*. (2011) 58:988–9. doi: 10.1016/j.jacc.2011.05.025
22. Gulati G, Heck SL, Ree AH, Hoffmann P, Schulz-Menger J, Fagerland MW, et al. Prevention of cardiac dysfunction during adjuvant breast cancer therapy (PRADA): a 2× 2 factorial, randomized, placebo-controlled, double-blind clinical trial of candesartan and metoprolol. *Eur. Heart J*. (2016) 37:1671–80. doi: 10.1093/eurheartj/ehw022
23. Lipshultz SE, Rifai N, Dalton VM, Levy DE, Silverman LB, Lipsitz SR, et al. The effect of dexrazoxane on myocardial injury in doxorubicin-treated children with acute lymphoblastic leukemia. *N Engl J Med.* (2004) 35:145–53. doi: 10.1056/NEJMoa035153
24. Hirsch GA, Bottomley PA, Gerstenblith G, Weiss R. Allopurinol acutely increases ATP energy delivery in failing human hearts. *J Am Coll Cardiol.* (2012) 59:802–8. doi: 10.1016/j.jacc.2011.10.895
25. Kobashiwaga LC, Xu YC, Padbury JF, Tseng YT, Yano N. Metformin protects cardiac myocytes from doxorubicin induced cytotoxicity through an AMP-activated protein kinase dependent signalling pathway: an *in vitro* study. *PLoS ONE* 9:e104888. doi: 10.1371/journal.pone.0104888
26. Jakovljevic DG, Papakonstantinou L, Blamire AM, MacGowan GA, Taylor R, Hollingsworth KG, et al. Effect of physical activity on age-related changes in cardiac function and performance in women. *Circ. Cardiovasc. Imaging.* (2015) 8:e002086. doi: 10.1161/CIRCIMAGING.114.002086
27. Linschoten M, Teske AJ, Cramer MJ, van der Wall E, Asselbergs FW. Chemotherapy-related cardiac dysfunction: a systematic review of genetic variants modulating individual risk. *Circ. Genom. Precis. Med.* (2018) 11:e001753. doi: 10.1161/CIRCGEN.117.001753
28. Bottomley PA, Panjrath GS, Lai S, Hirsch GA, Wu K, Najjar SS, et al. Metabolic rates of ATP transfer through creatine kinase (CK Flux) predict clinical heart failure events and death. *Sci Transl Med.* (2013) 5:215re3. doi: 10.1126/scitranslmed.3007328
29. Neubauer S, Horn M, Cramer M, Harre K, Newell JB, Peters W, et al. Myocardial phosphocreatine-to-ATP ratio is a predictor of mortality in patients with dilated cardiomyopathy. *Circulation.* (1997) 96:2190–6. doi: 10.1161/01.CIR.96.7.2190
30. Rodgers CT, Clarke WT, Snyder C, Vaughan JT, Neubauer S, Robson MD. Human cardiac 31P magnetic resonance spectroscopy at 7 Tesla. *Magn. Reson. Med*. (2014) 72:304–15. doi: 10.1002/mrm.24922
31. Stoll VM, Clarke WT, Levelt E, Liu A, Myerson SG, Robson MD, et al. Dilated cardiomyopathy: phosphorus 31 MR spectroscopy at 7 T. *Radiology.* (2016) 281:409–17. doi: 10.1148/radiol.2016152629

Conflict of Interest: The authors declare that the research was conducted in the absence of any commercial or financial relationships that could be construed as a potential conflict of interest.

frontiers in Cardiovascular Medicine

MINI REVIEW
published: 23 April 2021
doi: 10.3389/fcvm.2021.634291

Anti-cancer Therapy Leads to Increased Cardiovascular Susceptibility to COVID-19

*Caroline Lozahic, Helen Maddock and Hardip Sandhu**

Faculty Research Centre for Sport, Exercise and Life Sciences, Faculty of Health and Life Sciences, Coventry University, Coventry, United Kingdom

Anti-cancer treatment regimens can lead to both acute- and long-term myocardial injury due to off-target effects. Besides, cancer patients and survivors are severely immunocompromised due to the harsh effect of anti-cancer therapy targeting the bone marrow cells. Cancer patients and survivors can therefore be potentially extremely clinically vulnerable and at risk from infectious diseases. The recent global outbreak of the novel coronavirus severe acute respiratory syndrome coronavirus 2 (SARS-CoV-2) and its infection called coronavirus disease 2019 (COVID-19) has rapidly become a worldwide health emergency, and on March 11, 2020, COVID-19 was declared a global pandemic by the World Health Organization (WHO). A high fatality rate has been reported in COVID-19 patients suffering from underlying cardiovascular diseases. This highlights the critical and crucial aspect of monitoring cancer patients and survivors for potential cardiovascular complications during this unprecedented health crisis involving the progressive worldwide spread of COVID-19. COVID-19 is primarily a respiratory disease; however, COVID-19 has shown cardiac injury symptoms similar to the cardiotoxicity associated with anti-cancer therapy, including arrhythmia, myocardial injury and infarction, and heart failure. Due to the significant prevalence of micro- and macro-emboli and damaged vessels, clinicians worldwide have begun to consider whether COVID-19 may in fact be as much a vascular disease as a respiratory disease. However, the underlying mechanisms and pathways facilitating the COVID-19-induced cardiac injury in cancer and non-cancer patients remain unclear. Investigations into whether COVID-19 cardiac injury and anti-cancer drug-induced cardiac injury in cancer patients and survivors might synergistically increase the cardiovascular complications and comorbidity risk through a "two-hit" model are needed. Identification of cardiac injury mechanisms and pathways associated with COVID-19 development overlapping with anti-cancer therapy could help clinicians to allow a more optimized prognosis and treatment of cancer survivors suffering from COVID-19. The following review will focus on summarizing the harmful cardiovascular risk of COVID-19 in cancer patients and survivors treated with an anti-cancer drug. This review will improve the knowledge of COVID-19 impact in the field of cardio-oncology and potentially improve the outcome of patients.

Keywords: SARS-CoV-2, COVID-19, ACE2, cytokine storm, anti-cancer drug-induced cardiac injury

OPEN ACCESS

Edited by:
Carlo Gabriele Tocchetti, University of Naples Federico II, Italy

Reviewed by:
Claudia Penna, University of Turin, Italy
Kerstin Timm, University of Oxford, United Kingdom

****Correspondence:***
Hardip Sandhu
hardip.sandhu@coventry.ac.uk

Specialty section:
This article was submitted to Cardio-Oncology, a section of the journal Frontiers in Cardiovascular Medicine

Received: *27 November 2020*
Accepted: *09 March 2021*
Published: *23 April 2021*

Citation:
Lozahic C, Maddock H and Sandhu H (2021) Anti-cancer Therapy Leads to Increased Cardiovascular Susceptibility to COVID-19. Front. Cardiovasc. Med. 8:634291. doi: 10.3389/fcvm.2021.634291

INTRODUCTION

For the past 40 years, the cancer survival rate has increased considerably due to the improvement in cancer diagnosis and treatment (1, 2). Unfortunately, anti-cancer drug therapy of cancer patients can lead to serious cardiac injury adverse effects, such as hypertension, arrhythmia, stroke, and heart failure (3). These harmful anti-cancer drug-mediated cardiac injury adverse effects are difficult to diagnose and prevent and can appear years after the anti-cancer treatment is completed. Regrettably, long-term anti-cancer drug-mediated cardiac injury can lead to increased mortality of cancer survivors (4). Anti-cancer therapy is very harsh and can adversely affect the bone marrow cells, which can lead to a severe immune deficiency in cancer patients and survivors (5). In particular, a delay of the adaptive response with antibodies is observed in cancer patients and survivors, and this can lead to an increase in the susceptibility to develop severe infections caused by common viruses like influenza (6, 7).

A novel coronavirus named SARS-CoV-2 causing COVID-19 appeared in Wuhan, China, toward the end of 2019. Within a few months, SARS-CoV-2 spread all over the world and was declared as a global pandemic by WHO on the March 11, 2020. Initial studies showed that COVID-19 mainly targeted and damage the respiratory system (8–11); however, recent studies have reported that COVID-19 can also induce cardiovascular complications, such as dysrhythmias, venous thromboembolic events, myocarditis, myocardial injury, acute myocardial infarction, and heart failure (12).

The myocardial injury associated with COVID-19 could harm cancer survivors, who are already at high risk of suffering from an anti-cancer therapy-induced cardiac injury (13). The possible relation and overlap between the myocardial injury mechanism of COVID-19 and the anti-cancer therapy-induced cardiac injury is a major cause of concern in the clinic. In this review, we will identify cardiac injury mechanisms and pathways during COVID-19 development and the possible comorbidity risk through a "two-hit" model cancer patients and survivors are facing.

ANTI-CANCER THERAPY AND CARDIAC INJURY

Anti-cancer Drugs Associated With Cardiac Injury

While the anti-cancer therapy options available to cancer patients have improved over the past decades, a rise in cardiac adverse effects as a result of anti-cancer therapy has emerged as a considerable cause for concern in cancer survivors. Various types of chemotherapeutic anti-cancer drugs can induce cardiac injury (14). Some of the most potent cardiotoxic anti-cancer drugs belong to the anthracycline group, such as doxorubicin (3). Anthracyclines can induce cardiac injury through different intracellular mechanisms including oxidative stress (15), mitochondrial dysfunction, reactive oxygen species production (16), apoptosis (17), and myofibril damage (18). Other chemotherapy drugs responsible for cardiac complications include taxoids, antimetabolites, immune checkpoint inhibitors (ICIs), alkylating agents, and tyrosine kinase inhibitors (19, 20). The antimetabolite 5-fluorouracil can interfere with the nucleic acid function (21), and 5-fluorouracil treatment can induce arrhythmia, silent myocardial ischemia, and congestive heart failure in cancer patients (3). Therapy with ICIs has been associated with atherosclerosis, venous thromboembolism, vasculitis, Takotsubo syndrome, myocarditis, and hypertension (22–24). The alkylating agent cyclophosphamide has both cardiotoxic and immunosuppressive adverse effects (25), and cyclophosphamide treatment can lead to arrhythmia, cardiac tamponade, and congestive heart failure (3, 26). The tyrosine kinase inhibitor sunitinib inhibits ribosomal S6 kinase activity to induce cellular apoptosis (27), and sunitinib therapy can induce cardiomyocyte death and hypertrophy, which can lead to hypertension or, in the severe case, to congestive heart failure (27).

Assessment of Cardiac Injury

Anti-cancer therapy-induced cardiac injury can be assessed by imaging techniques and various circulating myocardial injury biomarkers. Doppler echocardiography and echocardiographic left ventricular ejection fraction (LVEF) are non-invasive techniques used in the clinic to detect myocardial injury (28). Cardiac injury can also be monitored through assessment of relevant circulating biomarkers levels, such as cardiac troponin I (cTnI) and B-type natriuretic peptide (BNP) (29). Cardiac damages lead to an increase in cTnI, while the rise of left ventricle wall stress leads to increased BNP levels (29). The "gold standard" in the clinic to determine the onset and stage of cardiac injury is a combination of LVEF assessment and determining the circulating levels of cTnI and BNP.

Anti-cancer Therapy Can Lead to Immunocompromised Status in Cancer Patients

Cancer patients treated with anti-cancer drugs are at an increased risk of developing infections and have fatal outcomes as a result of immunodeficiency, due to the harsh effect of anti-cancer therapy on the bone marrow cells (30). Cancer survivors tend to have more frequently influenza infections and acute respiratory infections than the general population (31). Moreover, childhood cancer survivors are more likely to develop acute respiratory disease after influenza infection due to their weak immunity (7). Further to this, pre-existing cardiovascular diseases can

Abbreviations: ACE, angiotensin-converting enzyme; ACE2, angiotensin-converting enzyme 2; Ang(1–7), angiotensin 1–7; Ang II, angiotensin II; ARDS, acute respiratory distress syndrome; BNP, B-type natriuretic peptide; COVID-19, coronavirus disease 2019; cTnI, cardiac troponin I; ER, endoplasmic reticulum; ERIG, endoplasmic reticulum–Golgi intermediate compartment; ICI(s), immune checkpoint inhibitor(s); ICU, intensive care unit; LVEF, left ventricular ejection fraction; NF-κβ, nuclear factor kappa-light-chain-enhancer; RAS, renin angiotensin system; RIG-I, retinoic acid-inducible gene-I; ROS, reactive oxygen species; SARS-CoV-2, severe acute respiratory syndrome coronavirus 2; TLR, Toll-like receptors; TMPRSS2, type 2 transmembrane serine protease; cTnI, cardiac troponin I; cTnT, cardiac troponin T; WHO, World Health Organization.

aggravate in high-risk cancer survivors (32). The infection-related complications observed in cancer survivors highlight that they are at high risk from the new COVID-19 pandemic.

NOVEL GLOBAL PANDEMIC COVID-19

SARS-CoV-2 Transmission

The novel zoonotic RNA virus SARS-CoV-2 leading to COVID-19 is from a large family of enveloped single-stranded zoonotic RNA viruses (9). WHO has reported over 113 million COVID-19 cases and over 2.5 million COVID-19-related deaths worldwide (by March 1, 2021). SARS-CoV-2 is transmitted human-to-human by indirect or direct contact through mucus membranes (i.e., mouth, eyes, or nose). Transmission is primarily mediated through airborne microparticles encapsulating the SARS-CoV-2 viral inoculum being inhaled in the nasal cavity, followed by aspiration of the SARS-CoV-2 microparticles into the lung, where SARS-CoV-2 then triggers the viral infection (33).

COVID-19 Symptoms

SARS-CoV-2 infection can induce systematic and respiratory disorders (34). The most common symptoms of COVID-19 are high fever, consistent dry cough, and loss of smell and taste sense (10). Several COVID-19 patients showed symptoms of viral pneumonia, such as sore throat, fatigue, and myalgia (11). The most serious cases of SARS-CoV-2 infections have fatal outcomes. The period from the onset of symptoms to death ranges from 6 to 41 days, depending on the vulnerability of the patient (35).

COVID-19 was first considered as a respiratory disease, due to the acute respiratory distress syndrome (ARDS). Indeed, in critical COVID-19 cases, patients suffer from dyspnoea, RNAaemia (i.e., detection of SARS-CoV-2 RNA in blood serum), and hypoxemia, and ground-glass opacities have been observed in sub-pleural regions of both of their lungs (36, 37). However, recent studies have shown that COVID-19 can cause inflammation-associated complications in other systems, such as the cardiovascular, cerebral, and gastrointestinal systems (10).

COVID-19 Risk Factors

The key prognostic risk factors in patients with COVID-19 include obesity, metabolic syndrome, diabetes mellitus, hyperglycaemia, coagulopathy, cigarette smoking, previous cardiovascular diseases, hypertension, previous cardiotoxic anticancer therapies, and active cancer. Furthermore, in cancer patients infected with COVID-19, the additional risk factors include various active anti-cancer treatments, such as chemotherapy, radiotherapy, and bone marrow or stem cell transplants (24). The most consistent predictors of poor outcomes of COVID-19 are age and gender (**Figure 1**). A higher incidence of fatalities is observed in the elderly COVID-19 patients compared to younger patients. The exact mechanisms involved are yet to be discovered; however, the increased prevalence of frailty and cardiovascular disease in the elderly population is thought to be due to pre-existing endothelial dysfunction and loss of endogenous cardioprotective mechanisms (38). Gender also plays an important factor in the clinical outcome following the contraction of COVID-19. Regardless of their age, women are less susceptible to severe infection outcomes, and fewer women are dying of COVID-19-related complications than age-matched males. The gender-associated difference in COVID-19 outcome is thought to be linked to two key mediators of viral attachment to cell membranes, namely, the angiotensin-converting enzyme (ACE) 2 receptor (ACE2) for the spike protein of coronaviruses, and the type 2 transmembrane serine protease (TMPRSS2), which cleaves the spike protein and thereby facilitates the attachment and fusion of the virus to cell membranes (39, 40). In particular, the ACE and ACE2 expression levels and the resulting ACE/ACE2 activity ratio are important factors for COVID-19 infection outcome. ACE has pro-inflammatory and pro-oxidant effects, whereas ACE2 has anti-inflammatory and antioxidant effects (41, 42). The ACE/ACE2 activity ratio has shown to be lower in serum samples of females compared to male serum samples, and the lower ACE/ACE2 activity ratio could be one of the factors that protect female COVID-19 patients from developing severe complications (42). In older COVID-19 patients, the worse outcome has been attributed to the presence of lower ACE2 levels compared to younger patients and thus the subsequent upregulation of pro-inflammatory pathways through angiotensin II (43).

COVID-19 Mechanism of Action

SARS-CoV-2 Transmission and Replication

SARS-CoV-2 is transmitted through the surface mucus membranes in the host human cells, where the viral surface spike protein binds to the cellular entry receptor ACE2 facilitating viral entry into host cells (44). The cellular serine protease TMPRSS2 cleaves the SARS-CoV-2 spike protein, thus allowing the attachment and fusion of SARS-CoV-2 virus to the host cell membrane and release of viral RNA in the host cell cytosol (40). The viral RNA is translated in the endoplasmic reticulum by the Golgi complex to produce more virions contained in double membrane vesicles, which are released in the extracellular matrix by exocytosis (45, 46) (**Figure 2**).

ACE2 Receptors Involved in Cardiac Function

ACE2 is highly expressed in lung, heart, and kidneys, and is a key negative regulator of the renin angiotensin system (RAS) through angiotensin II expression adjustments (47). SARS-CoV-2 downregulates ACE2 expression by binding to ACE2 receptors (47). In a murine model, the decrease in ACE2 promoted an increase of angiotensin II level in alveolar cells, which causes an increase of pulmonary vascular permeability leading to pulmonary oedema and lung dysfunction (48). Another study demonstrated that the loss of ACE2 promoted the upregulation of hypoxia-inducible gene (i.e., BNIP3 and PAI-1) expression in a murine model (49). All in all, the increase of vascular permeability, hypoxia, and hyper-inflammation caused by COVID-19 leads to ARDS, which is characterized by pulmonary oedema (50).

The ACE2 receptors are also expressed in vascular endothelium cells (51) and are key regulators of cardiovascular homeostasis (52). Knockout of the ACE2 gene expression in

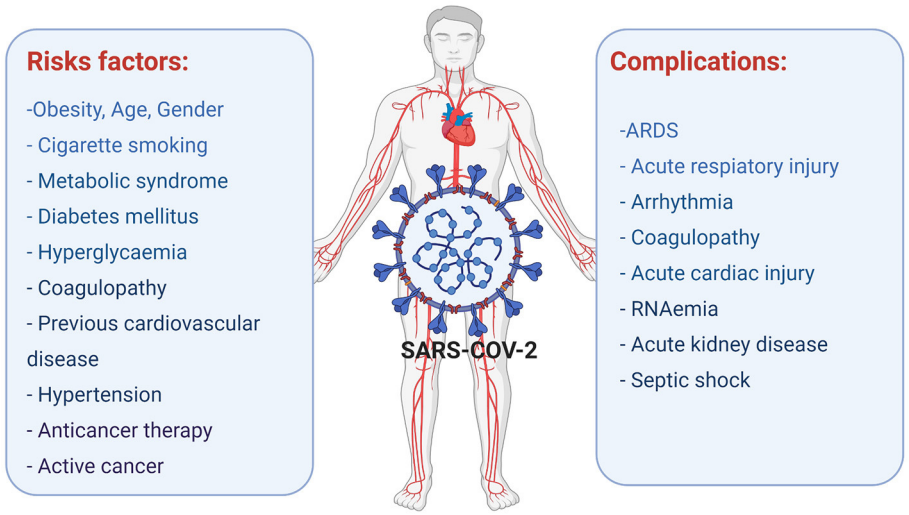

FIGURE 1 | Overview of the COVID-19 risk factors and complications observed in COVID-19 patients leading to cardiac injury (figure created with Biorender.com).

murine hearts leads to an increase in angiotensin II levels and severe diminution of cardiac contractility when compared to wild-type mice, thus indicating that ACE2 receptors are essential regulators of cardiac function and ACE2 loss induces myocardial injury (49).

SARS-CoV-2 Triggered Immune Response

A viral infection is followed by the innate and adaptive responses of the immune system. In the innate response, the viral RNA is considered as a pathogen-associated molecular pattern and is detected by the pattern recognition receptors. Viral RNA is detected by the Toll-like receptors (TLR) in the endosomes, and retinoic acid-inducible gene-I (RIG-I)-like receptors detect the viral RNA in the cytoplasm (53). This innate response is followed by the adaptive immune response by T-cells, which play a key role in viral infection by regulating the balance between the risk of autoimmunity and overactive inflammation. $CD4^+$ T-cells promote the production of antibodies specific to the virus by activating T-dependent B-cells. In addition, T-helper cells produce pro-inflammatory cytokines via the nuclear factor kappa-light-chain-enhancer (NF-κβ) signaling pathway and regulatory T-cells maintain the homeostasis of the immune system. Finally, the cytotoxic $CD8^+$ T-cells exterminate the infected cells through antigen recognition (53–55) (**Figure 3**).

In patients with COVID-19, several studies have highlighted the increase of neutrophils, leukocytes, and lymphopenia. The neutrophil–lymphocyte ratio is a marker of systemic inflammation due to an infection and is increased during COVID-19 (55). In a cohort study including 452 patients in Wuhan, China, an increase of interleukins IL-2, IL-6, IL-8, IL-10, and NF-κβ was observed in COVID-19-infected patients (55). IL-6 levels are increased during infection and IL-6 is a significant modulator of the cytokine storm. Moreover, there is a significant increase in the IL-6 levels in severe cases of COVID-19, when compared to mild COVID-19 cases (55, 56). A correlation between the severity of COVID-19 and the increase of pro-inflammatory cytokines have been observed in COVID-19 patients (57). COVID-19 damages specific tissue, which can aggravate the cytokine production, leading to the development of a cytokine storm, characterized by an excessive production of pro-inflammatory cytokines and the recruitment of macrophages and granulocytes. The cytokine storm can lead to more damage in lung tissue, ARDS (58), and myocardial injury (59).

COVID-19 and Cardiac Injury

Cardiac complications in patients infected by SARS-CoV-2 have been reported, particularly in severe COVID-19 cases (60, 61). Thrombotic complications, such as microvascular thrombosis, venous thromboembolic disease, and stroke, have been identified in severe COVID-19 cases (62). The mechanism of action is thought to be SARS-CoV-2 invading ACE2 receptors expressed on the surface of endothelial cells (63). The subsequent endothelial inflammation process in COVID-19 patients induces a dysfunction of the endothelial homeostasis, and this can lead to severe and life-threatening (micro)thrombotic complications, such as pulmonary embolism, deep vein thrombosis, and stroke (64, 65). Further to this, ACE2 receptors are highly expressed in the heart and can lead to ACE2-dependent myocardial infarction (66). COVID-19 has also been shown to cause cardiac injury by directly targeting the cardiac cells (67, 68).

In a cohort of 416 COVID-19 patients, cardiac injury was determined by the assessment of serum cardiac markers levels, including high-sensitivity troponin I, and by measurement of abnormalities in electrocardiography readings. All cardiac injury trials in these COVID-19 patients were similar to those observed during myocardial ischemia. This cohort study showed a very

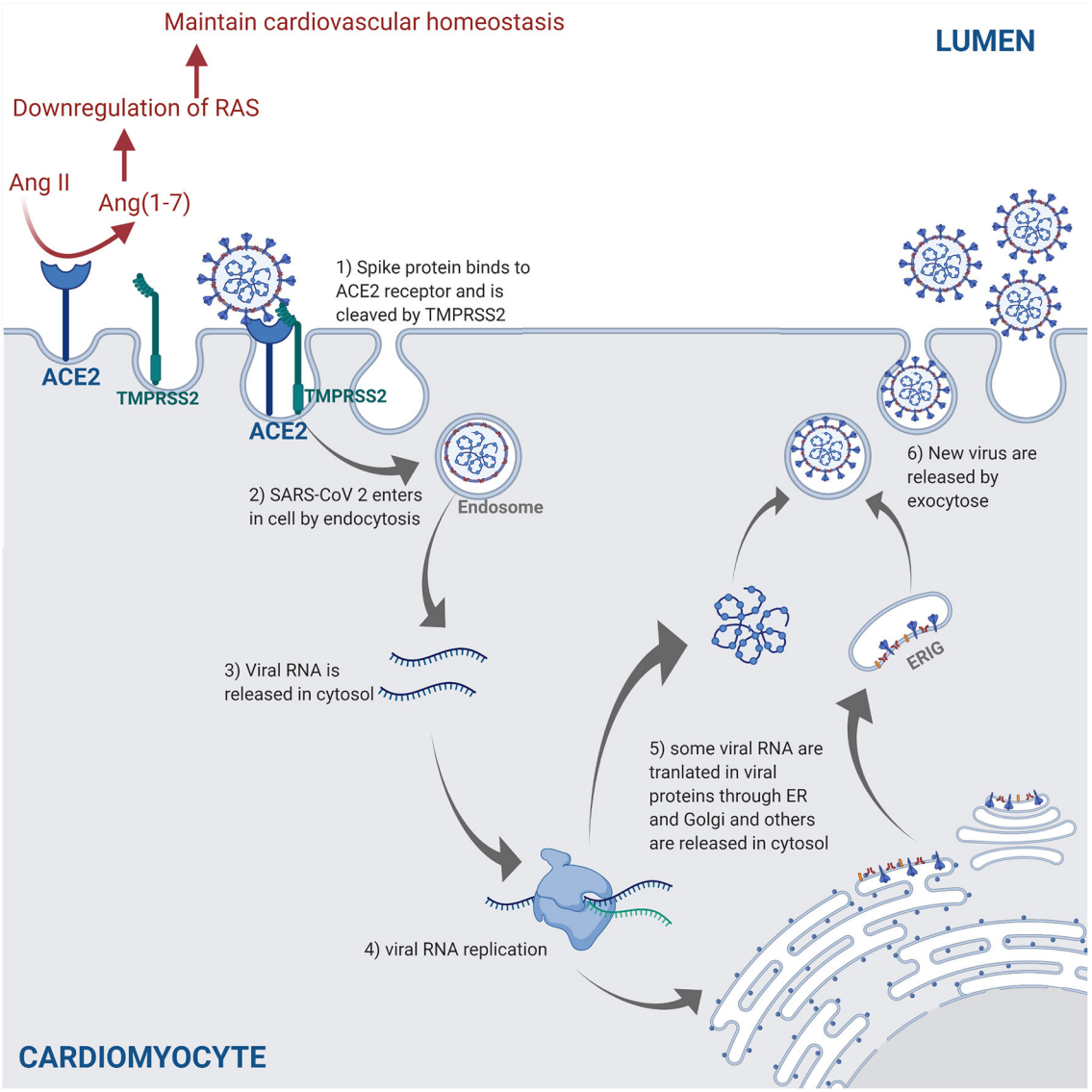

FIGURE 2 | The SARS-CoV-2 pathway in the host cells. The spike protein of the virus binds to the cellular receptor angiotensin-converting enzyme 2 (ACE2) and is cleaved by the type 2 transmembrane serine protease (TMPRSS2). This allows entry into the host cell by endocytosis. Following the entry of SARS-CoV-2, viral RNA is released into the cytoplasm and replicated. Viral RNA is translated by the endoplasmic reticulum (ER) by Golgi complex and form the endoplasmic reticulum–Golgi intermediate compartment (ERIG). Viral RNA enters into ERIG by budding to form novel virions. These virions are released from the infected cells by exocytosis. The ACE2 receptor is a negative regulator of the renin angiotensin system (RAS) and converts angiotensin II (Ang II) into angiotensin 1–7 [Ang(1–7)]. The downregulation of the RAS allows to maintain the cardiovascular homeostasis (figure created with Biorender.com).

high mortality rate of 51% among COVID-19 patients with cardiac injury complications. The study compared biomarkers levels and radiographic findings in 82 COVID-19 patients with cardiac injury with 334 COVID-19 patients without cardiac injury. According to their comparison, COVID-19 patients with cardiac injury had a significantly higher mortality risk than COVID-19 patients without cardiac injury (67). In another cohort study, 7.2% of the 138 hospitalized COVID-19 patients developed an acute cardiac injury after being infected by SARS-CoV-2, and these patients represented 22.2% of the COVID-19 patients admitted to the intensive care unit (ICU). The results of this study suggest that the manifestation of acute cardiac injury correlates to an imparted outcome in COVID-19 patients (69).

The cardiac injury mechanisms of action involved during COVID-19 infection remain unclear; however, it could be due to altered expression of ACE2 receptors and involvement of the cytokine storm (70, 71). Additionally, the myocardial injury could be caused by cardiac stress induced by hypoxia from ARDS (72). In two independent single-patient clinical case reports

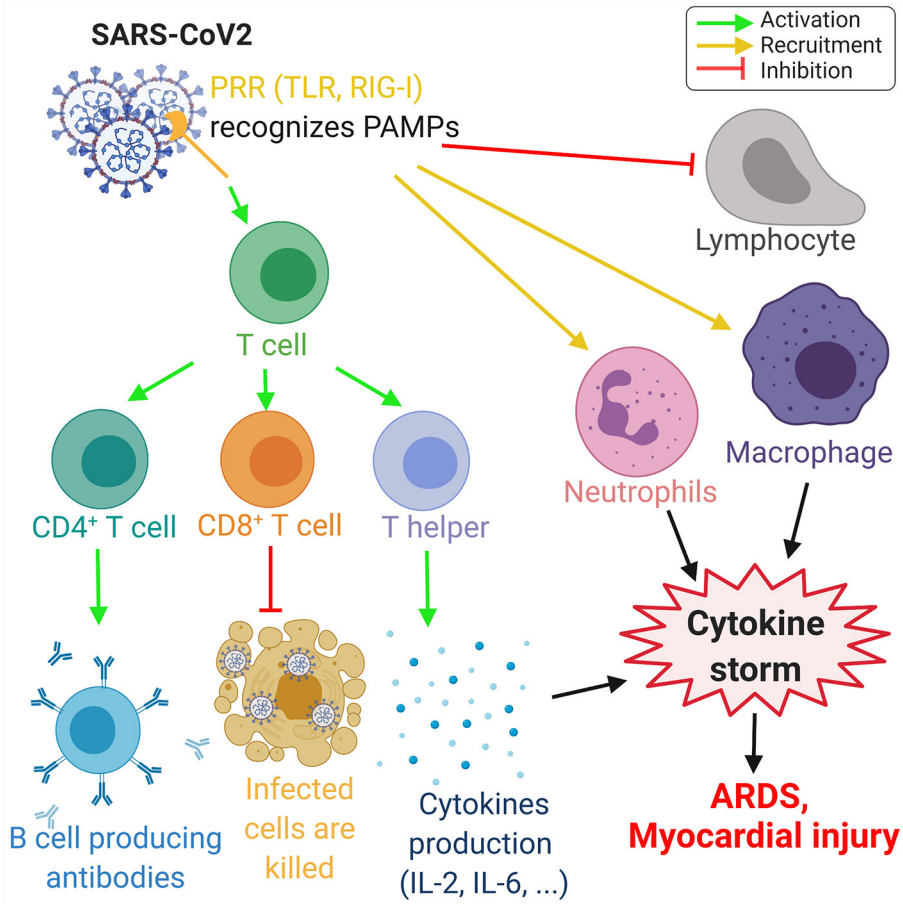

FIGURE 3 | Overview of the immune response to COVID-19. The proteins on SARS-CoV-2 membrane are recognized as pathogen-associated molecular pattern by the pattern recognition receptors (PRRs), such as Toll-like receptors (TLR) and retinoic acid-inducible gene-I (RIG-I)-like receptors. This recognition leads to the activation of T-cells, which differentiate in $CD4^+$ T-cells, $CD8^+$ T-cells, and T-helper cells that induce, respectively, the production of antibodies by B-cells, the deaths of infected cells, and the cytokine production, such as interleukins IL-2 and IL-6. Moreover, SARS-CoV-2 invasion leads to the recruitment of neutrophils and macrophage and induce a lymphopenia. The increase of neutrophils and macrophages associated with the cytokine production leads to a hyperinflammation called the cytokine storm. This cytokine storm leads to acute respiratory distress syndrome (ARDS) and myocardial damage. Green arrows refer to activating effects, orange arrows refer to recruitment effects, and the red lines refer to inhibiting effects (figure created with Biorender.com).

from China, the individual patients infected by SARS-CoV-2 were hospitalized and were suffering from both pneumonia and cardiac symptoms. The COVID-19 patients had elevated troponin T level, abnormal echocardiography, decreased LVEF, and elevated IL-6 levels, which could indicate a possible ongoing cytokine storm. The prognosis of clinicians was that the patients were suffering from fulminant myocarditis induced by SARS-CoV-2 (73, 74). Other studies have suggested that myocarditis represents 7% of deaths due to COVID-19 complications (75). However, most of these reports are based on assumptions and are not based on confirmed myocarditis diagnoses (76).

Studies have shown that COVID-19 patients suffering from severe complications are affected by arrhythmia (69, 77). Indeed, viral infections like COVID-19 are associated with myocardial inflammation, which can lead to cardiac arrhythmia (70). Other studies have observed an increase of D-dimer levels and fibrin degradation products in COVID-19 patients, and these features are known as indicators of disseminated intravascular coagulation and pulmonary embolism (70, 78). A report based on 106 pulmonary CT angiograms from COVID-19 patients showed that 30% of the patients had acute pulmonary with high D-dimer threshold and argued that this could be due to an increase in the blood coagulation level following the cytokine storm (79).

COVID-19 AND CANCER PATIENTS AND SURVIVORS

Increased COVID-19 Complications and Comorbidity in Cancer Patients and Survivors

Cancer patients have an estimated two-fold increased risk of contracting SARS-CoV-2 compared to the general population

(80). In a cohort study of 1,590 Chinese patients suffering from COVID-19, it was noted that 1.13% of them were cancer patients/survivors, which is higher than the overall 0.29% cancer incidence in China. Among the 18 cancer survivors, 4 of them had completed chemotherapy or surgery the past month, 12 were cancer survivors in routine follow-up, and 2 did not report their cancer history. This study showed that COVID-19 patients with recently completed anti-cancer therapy were those experiencing the most severe COVID-19 complications, and some of these patients died before the onset of COVID-19 treatment. Therefore, recent completion of anti-cancer therapy seems to be an important risk factor for developing severe complications during COVID-19 infection (81).

In another study from Wuhan, China, 28 cancer patients with COVID-19 were monitored closely for complications: 54% of them developed severe complication, 21% were admitted to ICU, 38% were considered to be in a life-threatening condition, and 28% died as a result of their complication. The cancer survivors started with developing the most common symptoms of COVID-19 consisting of a high fever and a consistent cough; however, the COVID-19 complications escalated quickly and they also developed anamia and hypoproteinaemia, leading to a reduction of immunocompetence and increasing the risk of developing respiratory complications. The last two symptoms, anamia and hypoproteinaemia, are not common in COVID-19 patients without any anti-cancer therapy history. COVID-19 patients with a previous anti-cancer therapy history seem to develop dyspnoea at an earlier stage compared to COVID-19 patients without previous cancer history. This study strongly indicates that cancer patients and survivors might have a higher risk of developing viral infection with severe complications due to their immunocompromised status (82). Please refer to **Table 1** for an overview of comorbidities and complications observed in COVID-19 patients suffering from cardiac injury identified in the studies included in this review.

Anti-cancer Drug-Induced Cardiovascular Injury Might Increase COVID-19 Complication Risks

Certain anti-cancer drugs can cause severe cardiotoxicity through increased fibrosis, oxidative stress, apoptosis, and necrosis in myocardial cells, thus increasing the risk of cardiomyopathies and heart failure. The anti-cancer drug-induced cardiotoxicity could exacerbate COVID-19-mediated cardiac injury and dysfunction. These drugs include anthracyclines (83, 84), tyrosine kinase inhibitors (85, 86), proteasome inhibitors (87), human epidermal growth factor receptor 2 blocking antibodies (88), and ICIs (89). The intracellular mechanisms involved during anthracycline-induced injury in cardiomyocytes include (a) binding to nuclear and mitochondrial DNA and interfering with replication, (b) inhibiting the TOPO II enzyme leading to the damaged DNA during the cell replication process, (c) disturbing the Ca^{2+} influx into the cell, (d) disruption of Ca^{2+} homeostasis in the mitochondria leading to an increase in reactive oxygen species (ROS) production and oxidative stress, (e) contractile dysfunction due to decreased expression of the Ca^{2+} pump SERCA2a in the sarcoplasmic reticulum, and (f) preventing the release of iron from ferritin and facilitating the reduction of anthracycline–Fe^{3+} complexes leading to ROS production. ROS production, DNA damage, and contractile dysfunction can all lead to cellular apoptosis (3). **Figure 4** describes the molecular mechanisms involved during anthracycline treatment-induced injury in cardiomyocytes and link them to the SARS-CoV-2 infection pathway.

A clinical study assessed the outcome of underlying cardiovascular complications in 138 hospitalized COVID-19 patients in Wuhan, China, with underlying cardiac comorbidities: 58% patients were suffering from hypertension, 22% patients had diabetes, and 25% already had a cardiovascular disease (69). Similar findings were published in another report, where 416 hospitalized COVID-19 patients were suffering from co-existing cardiovascular diseases: 60% patient had hypertension, 24% patients suffered from diabetes, 29% patient had coronary heart disease, while 15% patients had suffered chronic heart failure (67). According to the National Health Commission of the People's Republic of China, 35% of COVID-19 patients had hypertension and 17% suffered from coronary heart disease prior to their COVID-19 development (69). These studies indicate that patients with myocardial injury due to underlying cardiovascular diseases are more likely at risk to develop severe complications as a result of SARS-CoV-2 infection (67, 69, 71). Further to this, anti-cancer drugs can trigger late-term cardiovascular adverse effects, such as hypertension, cardiac dysfunction, thromboembolic events, and ischemia heart disease, and these cardiovascular complications are considered high risk factors of developing severe complications during COVID-19 infection in cancer survivors (90).

Cancer patients have a high risk of venous thromboembolism, particularly cancer patients treated with pro-inflammatory drugs and radiotherapy (91, 92). Therapy with anti-cancer drugs has also been associated with venous thromboembolism, which potentially could exacerbate the COVID-19-induced intravascular coagulative damages. These anti-cancer drugs lined with venous thromboembolism adverse effects include anti-VEGF therapies, tyrosine-kinase inhibitors, platinum-based drugs, proteasome inhibitors, hormonal therapy, and immunomodulators (93). Cancer patients initiating or continuing ICI therapy are facing a dilemma during the COVID-19 pandemic. A potential COVID-19 infection is characterized by mild to severe inflammation of the lungs and other organs. Both the ICI-induced immune-related adverse events and the COVID-19-caused inflammation include unrestrained immune and cytokine activation; therefore, ICI therapy could impact the course of COVID-19 and worsen the outcome (94). Cancer patients treated with ICIs are at increased risk of developing myocarditis, and recently, there have been increasing reports that COVID-19 is also associated with the development of myocarditis, with inflammatory

TABLE 1 | Comorbidities and complications in COVID-19 patients suffering from cardiac injury identified in the studies included in this review.

References	COVID-19 patients (ICU admission %)	Male (%)	Age (median)	Comorbidities and cancer type (if specified)	COVID-19 complications
Huang et al. (10)	41 (32% ICU)	73.00%	49	Diabetes (20%), Hypertension (15%), Cardiovascular diseases (15%), Chronic obstructive pulmonary disease (2%), Malignancy (2%), Chronic liver disease (2%).	ARDS (29%), RNAaemia (15%), Acute cardiac injury (12%), Secondary infection (10%), Acute kidney injury (7%), Shock (7%).
Qin et al. (55)	452	52.00%	58	Hypertension (29.5%), Tuberculosis (19.7%), Diabetes (16.4%), Cardiovascular disease (5.9%), Malignant tumor (3.1%), Chronic obstructive pulmonary disease (2.6%), Cerebrovascular disease (2.4%), Chronic kidney disease (2.2%), Chronic liver disease (1.3%).	–
Wichemann et al. (62)	12 (all dead)	75.00%	73	Coronary heart disease (50%), Arterial hypertension (25%), Chronic obstructive pulmonary disease (25%), Obesity (25%), Diabetes (25%), Bronchial asthma (25%), Nicotine abuse (16.7%), Atrial fibrillation (16.7%), Chronic kidney disease (16.7%), Parkinson disease (16.7%), Peripheral artery disease (8.3%), Granulomatous pneumopathy (8.3%), Dementia (8.3%), Epilepsy (8.3%), Trisomy 21 (8.3%), Non–small cell lung cancer (8.3%), Ulcerative colitis (8.3%).	Deep venous thrombosis (58%), pulmonary embolism (33%).
Shi et al. (67)	416	49.30%	64	Hypertension (30.5%), Diabetes (14.4%), Coronary heart disease (10.6%), Cerebrovascular disease (5.3%), Chronic heart failure (4.1%), Chronic renal failure (3.4%), Chronic obstructive pulmonary disease (2.9%), Cancer (2.2%), Hepatitis B infection (1.0%).	ARDS (23.3%), Electrolyte disturbance (7.2%), Hypoproteinemia (6.5%), Anamia (3.1%), Coagulation disorders (2.9%), Acute kidney injury (1.9%).
Han et al. (68)	273 (5.5% ICU)	35.53%	58.95	–	–
Wang et al. (69)	138 (26% ICU)	54.30%	56	Hypertension (31.2%), Cardiovascular disease (14.5%), Diabetes (10.1%), Malignancy (7.2%), Cerebrovascular disease (5.1%), COPD (2.9%), Chronic kidney disease (2.9%), Chronic liver disease (2.9%), HIV infection (1.4%).	ARDS (19.6%), Arrhythmia (16.7%), Shock (8.7%), Acute cardiac injury (7.2%), Acute kidney injury (3.6%).
Zeng et al. (73)	1	100.00%	63	Allergic cough for 5 years. Previous smoking history. Decrease of the cardiac function.	Severe pneumonia, ARDS, fulminant myocarditis, multiple organ dysfunction syndrome.
Hu et al. (74)	1	100.00%	37	Markers of myocardial injury elevated.	Fulminant myocarditis with cardiogenic shock and pulmonary infection.
Liu et al. (77)	137	44.50%	57	Chronic diseases (17.5%), Diabetes (10.2%), Hypertension (9.5%), Cardiovascular disease (7.3%), Chronic obstructive pulmonary disease (1.5%), Malignancy (1.5%). 84% of patients have elevated C-reactive protein levels.	–
Liang et al. (81)	1,600	Cancer patients: 61.10% Non-cancer patients: 57.20%	Cancer patients: 63.1 Non-cancer patients: 48.7	Chronic obstructive pulmonary disease, Diabetes, Hypertension, Coronary heart disease, Cerebrovascular disease, Viral hepatitis type B, Malignant tumor, Chronic kidney disease, and Immunodeficiency. Cancer types: 17 patients with solid cancers including lung cancer and breast cancer), and 1 patient with lymphoma.	–
Zhang et al. (82)	28 (21.4% ICU)	60.70%	65	Diabetes (14.3%), Chronic cardiovascular and cerebrovascular disease (including hypertension and coronary heart disease) (14.3%), Chronic liver disease (including chronic hepatitis B and cirrhosis) (7.1%). Chronic pulmonary disease (including chronic obstructive pulmonary disease and asthma) (3.6%). 82% of patients have elevated C-reactive protein levels. Cancer types: Lung (25%), esophagus (14.3%), Breast (10.7%), Laryngocarcinoma (7.1%), Liver (7.1%), Prostatic (7.1%), Cervical (3.6%), Gastric (3.6%), Colon (3.6%), Rectum (3.6%), Nasopharynx (3.6%), Endometrial (3.6%), Ovarian (3.6%), and Carcinoma of testis (3.6%).	ARDS (28.6%), Pulmonary embolism suspected (7.1%), Acute myocardial infarction (3.6%), Septic shock (3.6%).

ARDS, acute respiratory distress syndrome.

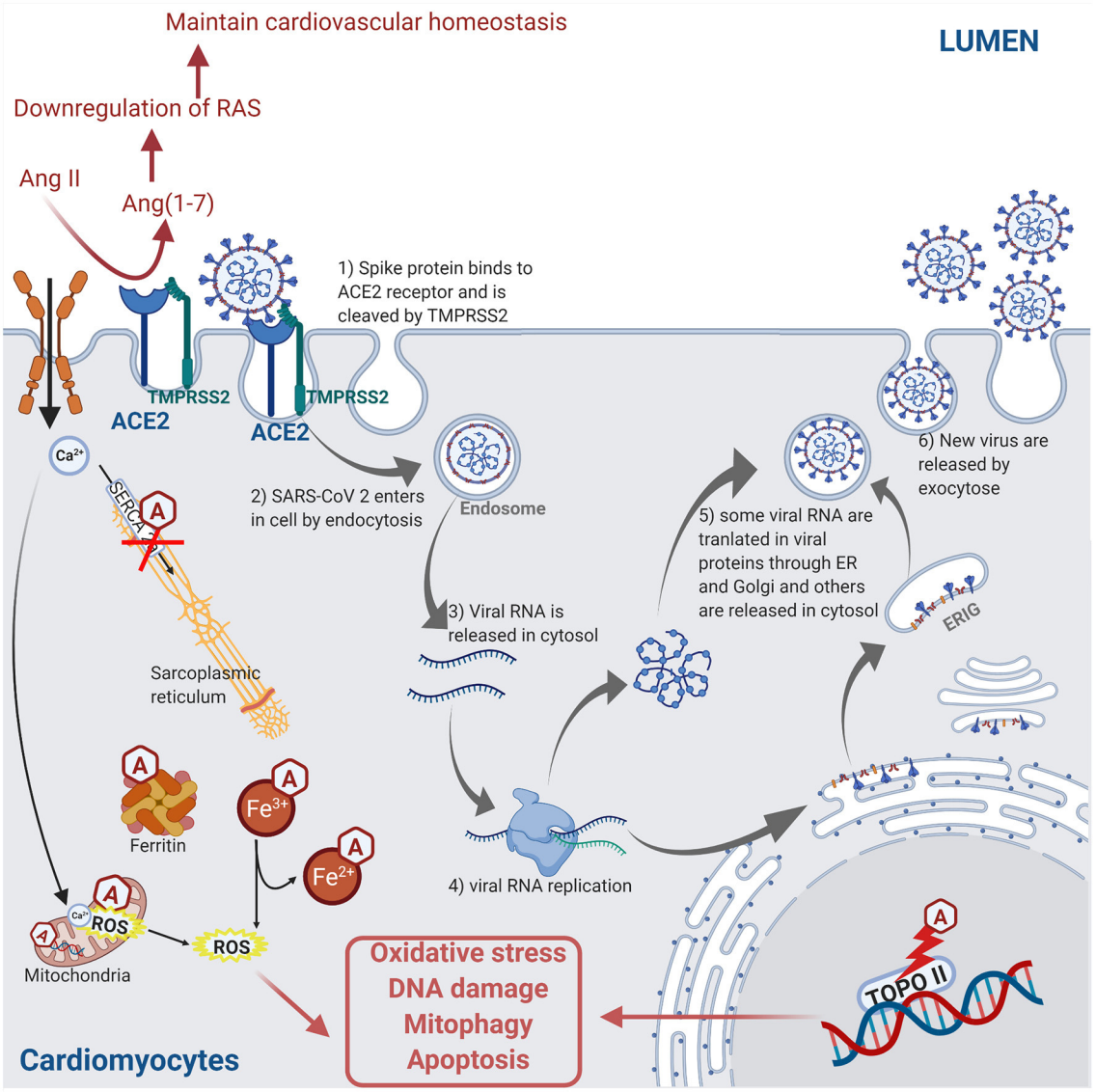

FIGURE 4 | Molecular mechanisms involved during anthracycline (Hexagonal box with "A") treatment and SARS-CoV-2 infection in cardiomyocyte leading to injury. Anthracycline can bind to nuclear and mitochondrial DNA and interfere with the cell replication process. The TOPO II enzyme can be inhibited by anthracycline, leading to the damaged DNA during cell replication. Anthracycline can also disturb the Ca^{2+} influx into the cell. The disruption of Ca^{2+} homeostasis by anthracycline in the mitochondria leads to an increase of reactive oxygen species (ROS) production and oxidative stress. Moreover, the expression of the Ca^{2+} pump SERCA2a in the sarcoplasmic reticulum is decreased by anthracycline, which induces contractile dysfunction. Anthracycline can also prevent the release of iron from ferritin and facilitate the reduction of anthracycline–Fe^{3+} complexes leading to ROS production. Combined, these anthracycline mechanisms lead to increased ROS production, DNA damage, and contractile dysfunction, which leads to cellular apoptosis. Please refer to **Figure 2** legend for a detailed description of the SARS-CoV-2 pathway (figure created with Biorender.com).

cellular infiltrate similar to that seen in ICI-induced myocarditis (95, 96).

Comorbidity Could Follow a "Two-Hit" Model

Cancer survivors can unfortunately suffer from subclinical myocardial injury due to adverse effect from their anti-cancer therapy (97). A study showed that 65% of cancer survivors treated with anthracycline ended with subclinical cardiac injury (98). Patients treated with anthracycline may suffer from subclinical left ventricle dysfunction, which can possibly lead to clinical cardiomyopathy (99). The cardiac reserve can be defined as "the increase in cardiac function from rest to peak exercise." In cancer survivors, anthracycline treatment reduces the cardiac reserve, and this parameter can be used as a marker of subclinical cardiac myocardial injury (90). Several reports have concluded that the risk of developing cardiac dysfunction increases over

the years after completion of anthracycline cancer treatment, and in the most severe adverse effect cases, heart failure is observed (100–103).

The subclinical cardiac dysfunction post-anti-cancer treatment could potentially serve as a risk factor for COVID-19-induced cardiac injury. Indeed, myocardial injury caused by COVID-19 infection can worsen the outcome consequences in patients with reduced cardiac reserve, leading to the development of severe cardiac complications in these patients. The cardiovascular complications from COVID-19 infection could provoke an acceleration of the myocardial injury resulting from anti-cancer treatment in a "two-hit" manner, as both COVID-19 infection and anti-cancer therapy can lead to myocardial injury (13). As mentioned previously, SARS-CoV-2 downregulates ACE2 expression by binding to ACE2 receptors (47), and ACE2 receptors are essential regulators of cardiac function (49). Therefore, in cancer patients and survivors that have undertaken anti-cancer therapy, a COVID-19 infection increases the potential for cardiac dysfunction due to the SARS-CoV-2-induced downregulation of ACE2 receptor expression. Further to this, the level of the cytokine storm modulator interleukin IL-6 has shown to be increased in more severe cases of COVID-19 compared to mild cases (55, 56). Interleukin IL-6 is produced by tumor cells, and an elevated level of IL-6 has been reported in various cancer types, such as lung cancer (104), renal cell carcinoma (105), and ovarian cancer (106). As a result of this, the elevated levels of IL-6 observed in cancer patients and survivors can exacerbate the effect of a potential COVID-19-mediated cytokine storm in infected patients also through IL-6, which can lead to increased injury in both lung (58) and myocardial tissue (59). On a positive note, a Review by Vivarelli et al. based on preliminary case studies with limited number of patients has hypothesized that cancer patients treated with anti-PD-1 or anti-PD-L1 antibody ICI therapy might potentially benefit from a boosted anti-viral immune response in addition to the T-cell cytotoxic response against cancer (107).

However, more studies are needed to get a better understanding of intracellular cardiac injury mechanisms due to COVID-19 infection and to unravel if these intracellular mechanisms overlap with the anti-cancer drug-induced cardiac injury pathways and mechanisms.

CONCLUSION

COVID-19 is a new challenge for cancer patients and survivors treated with cardiotoxic anti-cancer drugs. Cancer patients and survivors are immunocompromised and are therefore more susceptible to develop severe complications resulting from COVID-19 infection. In addition to targeting the respiratory system and causing havoc in the lungs, COVID-19 can induce cardiovascular complications and myocardial injury. Understanding the pathways that lead to cardiac complications during the COVID-19 infection can lead to the development of more targeted and tailored therapy options in at-risk groups, such as cancer patients and survivors, and thus improve the outcome of vulnerable patient groups.

AUTHOR CONTRIBUTIONS

All authors contributed to the concept, planning, and writing of this mini-review, and approved the manuscript prior to submission.

FUNDING

CL was on a DTA3-funded PhD scholarship for unrelated work and HS was her director of studies. HS and HM were funded for their research by Coventry University for unrelated work.

ACKNOWLEDGMENTS

The authors would like to thank Jayini Thakore for her generous support with proofreading the manuscript.

REFERENCES

1. O'Dowd A. Long term cancer survival rates double in England and Wales in past 40 years. *BMJ.* (2010) 341:c3750. doi: 10.1136/bmj.c3750
2. Siegel R, DeSantis C, Virgo K, Stein K, Mariotto A, Smith T, et al. Cancer treatment and survivorship statistics, 2012. *CA Cancer J Clin.* (2012) 62:220–41. doi: 10.3322/caac.21149
3. Sandhu H, Maddock H. Molecular basis of cancer-therapy-induced cardiotoxicity: introducing microRNA biomarkers for early assessment of subclinical myocardial injury. *Clin Sci.* (2014) 126:377–400. doi: 10.1042/CS20120620
4. Volkova M, Russell R. Anthracycline cardiotoxicity: prevalence, pathogenesis and treatment. *Current Cardiol Rev.* (2011) 7:214–20. doi: 10.2174/157340311799960645
5. Rebe C, Ghiringhelli F. Cytotoxic effects of chemotherapy on cancer and immune cells: how can it be modulated to generate novel therapeutic strategies? *Future Oncol.* (2015) 11:2645–54. doi: 10.2217/fon.15.198
6. Tichelli A, Socie G. Considerations for adult cancer survivors. *Hematol Am Soc Hematol Educ Prog.* (2005) 2005:516–22. doi: 10.1182/asheducation-2005.1.516
7. Heo J, Chun M, Oh YT, Noh OK, Kim L. Influenza among breast cancer survivors in south korea: a nationwide population-based study. *In Vivo.* (2017) 31:967–72. doi: 10.21873/invivo.11155
8. Gattinoni L, Coppola S, Cressoni M, Busana M, Rossi S, Chiumello D. COVID-19 does not lead to a "typical" acute respiratory distress syndrome. *Am J Respir Crit Care Med.* (2020) 201:1299–300. doi: 10.1164/rccm.202003-0817LE
9. Lai CC, Shih TP, Ko WC, Tang HJ, Hsueh PR. Severe acute respiratory syndrome coronavirus 2 (SARS-CoV-2) and coronavirus disease-2019 (COVID-19): the epidemic and the challenges. *Int J Antimicrob Agents.* (2020) 55:105924. doi: 10.1016/j.ijantimicag.2020.105924
10. Huang C, Wang Y, Li X, Ren L, Zhao J, Hu Y, et al. Clinical features of patients infected with 2019 novel coronavirus in Wuhan, China. *Lancet.* (2020) 395:497–506. doi: 10.1016/S0140-6736(20)30183-5
11. Verity R, Okell LC, Dorigatti I, Winskill P, Whittaker C, Imai N, et al. Estimates of the severity of coronavirus disease 2019: a model-based analysis. *Lancet Infect Dis.* (2020) 20:669–77. doi: 10.1016/S1473-3099(20)30243-7
12. Long B, Brady WJ, Koyfman A, Gottlieb M. Cardiovascular complications in COVID-19. *Am J Emerg Med.* (2020) 38:1504–7. doi: 10.1016/j.ajem.2020.04.048

13. Zordoky B. Cardiovascular vulnerability to COVID-19 in cancer survivors. *Preprints.* (2020). doi: 10.20944/preprints202004.0128.v1
14. Suter TM, Ewer MS. Cancer drugs and the heart: importance and management. *Eur Heart J.* (2013) 34:1102–11. doi: 10.1093/eurheartj/ehs181
15. Minotti G, Menna P, Salvatorelli E, Cairo G, Gianni L. Anthracyclines: molecular advances and pharmacologic developments in antitumor activity and cardiotoxicity. *Pharmacol Rev.* (2004) 56:185–229. doi: 10.1124/pr.56.2.6
16. Gille L, Nohl H. Analyses of the molecular mechanism of adriamycin-induced cardiotoxicity. *Free Radic Biol Med.* (1997) 23:775–82. doi: 10.1016/S0891-5849(97)00025-7
17. Kaufmann SH, Earnshaw WC. Induction of apoptosis by cancer chemotherapy. *Exp Cell Res.* (2000) 256:42–9. doi: 10.1006/excr.2000.4838
18. Ito H, Miller SC, Billingham ME, Akimoto H, Torti SV, Wade R, et al. Doxorubicin selectively inhibits muscle gene expression in cardiac muscle cells in vivo and in vitro. *Proc Natl Acad Sci USA.* (1990) 87:4275–9. doi: 10.1073/pnas.87.11.4275
19. Raschi E, Vasina V, Ursino MG, Boriani G, Martoni A, De Ponti F. Anticancer drugs and cardiotoxicity: insights and perspectives in the era of targeted therapy. *Pharmacol Ther.* (2010) 125:196–218. doi: 10.1016/j.pharmthera.2009.10.002
20. Friedman CF, Proverbs-Singh TA, Postow MA. Treatment of the immune-related adverse effects of immune checkpoint inhibitors: a review. *JAMA Oncol.* (2016) 2:1346–53. doi: 10.1001/jamaoncol.2016.1051
21. Longley DB, Harkin DP, Johnston PG. 5-fluorouracil: mechanisms of action and clinical strategies. *Nat Rev Cancer.* (2003) 3:330–8. doi: 10.1038/nrc1074
22. Varricchi G, Galdiero MR, Tocchetti CG. Cardiac toxicity of immune checkpoint inhibitors: cardio-oncology meets immunology. *Circulation.* (2017) 136:1989–92. doi: 10.1161/CIRCULATIONAHA.117.029626
23. Zhou YW, Zhu YJ, Wang MN, Xie Y, Chen CY, Zhang T, et al. Immune checkpoint inhibitor-associated cardiotoxicity: current understanding on its mechanism, diagnosis and management. *Front Pharmacol.* (2019) 10:1350. doi: 10.3389/fphar.2019.01350
24. Quagliariello V, Bonelli A, Caronna A, Conforti G, Iovine M, Carbone A, et al. SARS-CoV-2 infection and cardioncology: from cardiometabolic risk factors to outcomes in cancer patients. *Cancers.* (2020) 12:3316. doi: 10.3390/cancers12113316
25. Mullins GM, Anderson PN, Santos GW. High dose cyclophosphamide therapy in solid tumors: therapeutic, toxic, and immunosuppressive effects. *Cancer.* (1975) 36:1950–8. doi: 10.1002/cncr.2820360904
26. Goldberg MA, Antin JH, Guinan EC, Rappeport JM. Cyclophosphamide cardiotoxicity: an analysis of dosing as a risk factor. *Blood.* (1986) 68:1114–8. doi: 10.1182/blood.V68.5.1114.1114
27. Chu TF, Rupnick MA, Kerkela R, Dallabrida SM, Zurakowski D, Nguyen L, et al. Cardiotoxicity associated with tyrosine kinase inhibitor sunitinib. *Lancet.* (2007) 370:2011–9. doi: 10.1016/S0140-6736(07)61865-0
28. McKillop J, Bristow M, Goris M, Billingham M, Bockemuehl K. Sensitivity and specificity of radionuclide ejection fractions in doxorubicin cardiotoxicity. *Am Heart J.* (1983) 106:1048–56. doi: 10.1016/0002-8703(83)90651-8
29. Lipshultz SE, Miller TL, Scully RE, Lipsitz SR, Rifai N, Silverman LB, et al. Changes in cardiac biomarkers during doxorubicin treatment of pediatric patients with high-risk acute lymphoblastic leukemia: associations with long-term echocardiographic outcomes. *J Clin Oncol.* (2012) 30:1042–9. doi: 10.1200/JCO.2010.30.3404
30. de Naurois J, Novitzky-Basso I, Gill MJ, Marti FM, Cullen MH, Roila F, et al. Management of febrile neutropenia: ESMO clinical practice guidelines. *Ann Oncol.* (2010) 21 (Suppl. 5):v252–6. doi: 10.1093/annonc/mdq196
31. Heo J, Jung HJ, Noh OK, Kim L, Park JE. Incidence of influenza among childhood cancer survivors in South Korea: a population-based retrospective analysis. *In Vivo.* (2020) 34:929–33. doi: 10.21873/invivo.11860
32. Ojha RP, Offutt-Powell TN, Gurney JG. Influenza vaccination coverage among adult survivors of pediatric cancer. *Am J Prev Med.* (2014) 46:552–8. doi: 10.1016/j.amepre.2014.01.007
33. Hou YJ, Okuda K, Edwards CE, Martinez DR, Asakura T, Dinnon KH, et al. SARS-CoV-2 reverse genetics reveals a variable infection gradient in the respiratory tract. *Cell.* (2020) 182:429–46.e14. doi: 10.1016/j.cell.2020.05.042
34. Rothan HA, Byrareddy SN. The epidemiology and pathogenesis of coronavirus disease (COVID-19) outbreak. *J Autoimmun.* (2020) 109:102433. doi: 10.1016/j.jaut.2020.102433
35. Wang W, Tang J, Wei F. Updated understanding of the outbreak of 2019 novel coronavirus (2019-nCoV) in Wuhan, China. *J Med Virol.* (2020) 92:441–7. doi: 10.1002/jmv.25689
36. Phan LT, Nguyen TV, Luong QC, Nguyen TV, Nguyen HT, Le HQ, et al. Importation and human-to-human transmission of a novel coronavirus in Vietnam. *N Engl J Med.* (2020) 382:872–4. doi: 10.1056/NEJMc2001272
37. Lei J, Li J, Li X, Qi X. CT imaging of the 2019 novel coronavirus (2019-nCoV) pneumonia. *Radiology.* (2020) 295:18. doi: 10.1148/radiol.2020200236
38. Moccia F, Gerbino A, Lionetti V, Miragoli M, Munaron LM, Pagliaro P, et al. COVID-19-associated cardiovascular morbidity in older adults: a position paper from the Italian Society of Cardiovascular Researches. *Geroscience.* (2020) 42:1021–49. doi: 10.1007/s11357-020-00198-w
39. Penna C, Mercurio V, Tocchetti CG, Pagliaro P. Sex-related differences in COVID-19 lethality. *Br J Pharmacol.* (2020) 177:4375–85. doi: 10.1111/bph.15207
40. Hoffmann M, Kleine-Weber H, Schroeder S, Kruger N, Herrler T, Erichsen S, et al. SARS-CoV-2 cell entry depends on ACE2 and TMPRSS2 and is blocked by a clinically proven protease inhibitor. *Cell.* (2020) 181:271–80.e8. doi: 10.1016/j.cell.2020.02.052
41. Pagliaro P, Penna C. Rethinking the renin-angiotensin system and its role in cardiovascular regulation. *Cardiovasc Drugs Ther.* (2005) 19:77–87. doi: 10.1007/s10557-005-6900-8
42. Pagliaro P, Penna C. ACE/ACE2 ratio: a key also in 2019 coronavirus disease (Covid-19)? *Front Med.* (2020) 7:335. doi: 10.3389/fmed.2020.00335
43. AlGhatrif M, Cingolani O, Lakatta EG. The dilemma of coronavirus disease 2019, aging, and cardiovascular disease: insights from cardiovascular aging science. *JAMA Cardiol.* (2020) 5:747–8. doi: 10.1001/jamacardio.2020.1329
44. Zhou P, Yang XL, Wang XG, Hu B, Zhang L, Zhang W, et al. A pneumonia outbreak associated with a new coronavirus of probable bat origin. *Nature.* (2020) 579:270–3. doi: 10.1038/s41586-020-2951-z
45. Jiang S, Hillyer C, Du L. Neutralizing antibodies against SARS-CoV-2 and other human coronaviruses. *Trends Immunol.* (2020) 41:355–9. doi: 10.1016/j.it.2020.03.007
46. Hartenian E, Nandakumar D, Lari A, Ly M, Tucker JM, Glaunsinger BA. The molecular virology of coronaviruses. *J Biol Chem.* (2020) 295:12910–34. doi: 10.1074/jbc.REV120.013930
47. Kuba K, Imai Y, Rao S, Gao H, Guo F, Guan B, et al. A crucial role of angiotensin converting enzyme 2 (ACE2) in SARS coronavirus-induced lung injury. *Nat Med.* (2005) 11:875–9. doi: 10.1038/nm1267
48. Imai Y, Kuba K, Rao S, Huan Y, Guo F, Guan B, et al. Angiotensin-converting enzyme 2 protects from severe acute lung failure. *Nature.* (2005) 436:112–6. doi: 10.1038/nature03712
49. Crackower MA, Sarao R, Oudit GY, Yagil C, Kozieradzki I, Scanga SE, et al. Angiotensin-converting enzyme 2 is an essential regulator of heart function. *Nature.* (2002) 417:822–8. doi: 10.1038/nature00786
50. Matthay MA, Ware LB, Zimmerman GA. The acute respiratory distress syndrome. *J Clin Invest.* (2012) 122:2731–40. doi: 10.1172/JCI60331
51. Jacob HJ. Physiological genetics: application to hypertension research. *Clin Exp Pharmacol Physiol.* (1999) 26:530–5. doi: 10.1046/j.1440-1681.1999.03078.x
52. Donoghue M, Hsieh F, Baronas E, Godbout K, Gosselin M, Stagliano N, et al. A novel angiotensin-converting enzyme-related carboxypeptidase (ACE2) converts angiotensin I to angiotensin 1-9. *Circ Res.* (2000) 87:E1–9. doi: 10.1161/01.RES.87.5.e1
53. Li G, Fan Y, Lai Y, Han T, Li Z, Zhou P, et al. Coronavirus infections and immune responses. *J Med Virol.* (2020) 92:424–32. doi: 10.1002/jmv.25685
54. Guo YR, Cao QD, Hong ZS, Tan YY, Chen SD, Jin HJ, et al. The origin, transmission and clinical therapies on coronavirus disease 2019 (COVID-19) outbreak - an update on the status. *Mil Med Res.* (2020) 7:11. doi: 10.1186/s40779-020-00240-0
55. Qin C, Zhou L, Hu Z, Zhang S, Yang S, Tao Y, et al. Dysregulation of immune response in patients with coronavirus 2019 (COVID-19) in Wuhan, China. *Clin Infect Dis.* (2020) 71:762–8. doi: 10.1093/cid/ciaa248

56. Crayne CB, Albeituni S, Nichols KE, Cron RQ. The immunology of macrophage activation syndrome. *Front Immunol.* (2019) 10:119. doi: 10.3389/fimmu.2019.00119
57. Zhang Y, Mo P, Ma Z, Song S, Deng L, Xiong Y, et al. Characteristics of peripheral lymphocyte subset alteration in COVID-19 pneumonia. *J Infect Dis.* (2020) 221:1762–9. doi: 10.1093/infdis/jiaa150
58. Tufan A, Avanoglu Guler A, Matucci-Cerinic M. COVID-19, immune system response, hyperinflammation and repurposing antirheumatic drugs. *Turk J Med Sci.* (2020) 50:620–32. doi: 10.3906/sag-2004-168
59. Babapoor-Farrokhran S, Gill D, Walker J, Rasekhi RT, Bozorgnia B, Amanullah A. Myocardial injury and COVID-19: possible mechanisms. *Life Sci.* (2020) 253:117723. doi: 10.1016/j.lfs.2020.117723
60. Madjid M, Safavi-Naeini P, Solomon SD, Vardeny O. Potential effects of coronaviruses on the cardiovascular system: a review. *JAMA Cardiol.* (2020) 5:831–40. doi: 10.1001/jamacardio.2020.1286
61. Inciardi RM, Lupi L, Zaccone G, Italia L, Raffo M, Tomasoni D, et al. Cardiac involvement in a patient with coronavirus disease 2019 (COVID-19). *JAMA Cardiol.* (2020) 5:819–24. doi: 10.1001/jamacardio.2020.1096
62. Wichmann D. Autopsy findings and venous thromboembolism in patients with COVID-19. *Ann Intern Med.* (2020) 173:1030. doi: 10.7326/M20-2003
63. Topol EJ. COVID-19 can affect the heart. *Science.* (2020) 370:408–9. doi: 10.1126/science.abe2813
64. McFadyen JD, Stevens H, Peter K. The emerging threat of (micro)thrombosis in COVID-19 and its therapeutic implications. *Circ Res.* (2020) 127:571–87. doi: 10.1161/CIRCRESAHA.120.317447
65. Libby P, Luscher T. COVID-19 is, in the end, an endothelial disease. *Eur Heart J.* (2020) 41:3038–44. doi: 10.1093/eurheartj/ehaa623
66. Chen L, Li X, Chen M, Feng Y, Xiong C. The ACE2 expression in human heart indicates new potential mechanism of heart injury among patients infected with SARS-CoV-2. *Cardiovasc Res.* (2020) 116:1097–100. doi: 10.1093/cvr/cvaa078
67. Shi S, Qin M, Shen B, Cai Y, Liu T, Yang F, et al. Association of cardiac injury with mortality in hospitalized patients with COVID-19 in Wuhan, China. *JAMA Cardiol.* (2020) 5:802–10. doi: 10.1001/jamacardio.2020.0950
68. Han H, Xie L, Liu R, Yang J, Liu F, Wu K, et al. Analysis of heart injury laboratory parameters in 273 COVID-19 patients in one hospital in Wuhan, China. *J Med Virol.* (2020) 92:819–23. doi: 10.1002/jmv.25809
69. Wang D, Hu B, Hu C, Zhu F, Liu X, Zhang J, et al. Clinical characteristics of 138 hospitalized patients with 2019 novel coronavirus-infected pneumonia in Wuhan, China. *JAMA.* (2020) 323:1061–9. doi: 10.1001/jama.2020.1585
70. Guzik TJ, Mohiddin SA, Dimarco A, Patel V, Savvatis K, Marelli-Berg FM, et al. COVID-19 and the cardiovascular system: implications for risk assessment, diagnosis, and treatment options. *Cardiovasc Res.* (2020) 116:1666–87. doi: 10.1093/cvr/cvaa106
71. Zheng YY, Ma YT, Zhang JY, Xie X. COVID-19 and the cardiovascular system. *Nat Rev Cardiol.* (2020) 17:259–60. doi: 10.1038/s41569-020-0360-5
72. Akhmerov A, Marban E. COVID-19 and the heart. *Circ Res.* (2020) 126:1443–55. doi: 10.1161/CIRCRESAHA.120.317055
73. Zeng JH, Liu YX, Yuan J, Wang FX, Wu WB, Li JX, et al. First case of COVID-19 complicated with fulminant myocarditis: a case report and insights. *Infection.* (2020) 48:773–7. doi: 10.1007/s15010-020-01424-5
74. Hu H, Ma F, Wei X, Fang Y. Coronavirus fulminant myocarditis treated with glucocorticoid and human immunoglobulin. *Eur Heart J.* (2021) 42:206. doi: 10.1093/eurheartj/ehaa190
75. Driggin E, Madhavan MV, Bikdeli B, Chuich T, Laracy J, Biondi-Zoccai G, et al. Cardiovascular considerations for patients, health care workers, and health systems during the COVID-19 pandemic. *J Am Coll Cardiol.* (2020) 75:2352–71. doi: 10.1016/j.jacc.2020.03.031
76. Siripanthong B, Nazarian S, Muser D, Deo R, Santangeli P, Khanji MY, et al. Recognizing COVID-19-related myocarditis: the possible pathophysiology and proposed guideline for diagnosis and management. *Heart Rhythm.* (2020) 17:1463–71. doi: 10.1016/j.hrthm.2020.05.001
77. Liu K, Fang YY, Deng Y, Liu W, Wang MF, Ma JP, et al. Clinical characteristics of novel coronavirus cases in tertiary hospitals in Hubei Province. *Chin Med J.* (2020) 133:1025–31. doi: 10.1097/CM9.0000000000000744
78. Oudkerk M, Buller HR, Kuijpers D, van Es N, Oudkerk SF, McLoud T, et al. Diagnosis, prevention, and treatment of thromboembolic complications in COVID-19: report of the national institute for public health of the Netherlands. *Radiology.* (2020) 297:E216–22. doi: 10.1148/radiol.2020201629
79. Leonard-Lorant I, Delabranche X, Severac F, Helms J, Pauzet C, Collange O, et al. Acute pulmonary embolism in patients with COVID-19 at CT angiography and relationship to d-dimer levels. *Radiology.* (2020) 296:E189–91. doi: 10.1148/radiol.2020201561
80. Al-Shamsi HO, Alhazzani W, Alhuraiji A, Coomes EA, Chemaly RF, Almuhanna M, et al. A practical approach to the management of cancer patients during the novel coronavirus disease 2019 (COVID-19) pandemic: an international collaborative group. *Oncologist.* (2020) 25:e936–45. doi: 10.1634/theoncologist.2020-0213
81. Liang W, Guan W, Chen R, Wang W, Li J, Xu K, et al. Cancer patients in SARS-CoV-2 infection: a nationwide analysis in China. *Lancet Oncol.* (2020) 21:335–7. doi: 10.1016/S1470-2045(20)30096-6
82. Zhang L, Zhu F, Xie L, Wang C, Wang J, Chen R, et al. Clinical characteristics of COVID-19-infected cancer patients: a retrospective case study in three hospitals within Wuhan, China. *Ann Oncol.* (2020) 31:894–901. doi: 10.1016/j.annonc.2020.03.296
83. Zamorano JL, Lancellotti P, Rodriguez Munoz D, Aboyans V, Asteggiano R, Galderisi M, et al. 2016 ESC position paper on cancer treatments and cardiovascular toxicity developed under the auspices of the ESC Committee for Practice Guidelines: the task force for cancer treatments and cardiovascular toxicity of the European Society of Cardiology (ESC). *Eur Heart J.* (2016) 37:2768–801. doi: 10.1093/eurheartj/ehw211
84. Felker GM, Thompson RE, Hare JM, Hruban RH, Clemetson DE, Howard DL, et al. Underlying causes and long-term survival in patients with initially unexplained cardiomyopathy. *N Engl J Med.* (2000) 342:1077–84. doi: 10.1056/NEJM200004133421502
85. Tocchetti CG, Gallucci G, Coppola C, Piscopo G, Cipresso C, Maurea C, et al. The emerging issue of cardiac dysfunction induced by antineoplastic angiogenesis inhibitors. *Eur J Heart Fail.* (2013) 15:482–9. doi: 10.1093/eurjhf/hft008
86. Qi WX, Shen Z, Tang LN, Yao Y. Congestive heart failure risk in cancer patients treated with vascular endothelial growth factor tyrosine kinase inhibitors: a systematic review and meta-analysis of 36 clinical trials. *Br J Clin Pharmacol.* (2014) 78:748–62. doi: 10.1111/bcp.12387
87. Lendvai N, Devlin S, Patel M, Knapp KM, Ekman D, Grundberg I, et al. Biomarkers of cardiotoxicity among multiple myeloma patients subsequently treated with proteasome inhibitor therapy. *Blood.* (2015) 126:4257. doi: 10.1182/blood.V126.23.4257.4257
88. Suter TM, Procter M, van Veldhuisen DJ, Muscholl M, Bergh J, Carlomagno C, et al. Trastuzumab-associated cardiac adverse effects in the herceptin adjuvant trial. *J Clin Oncol.* (2007) 25:3859–65. doi: 10.1200/JCO.2006.09.1611
89. Hu JR, Florido R, Lipson EJ, Naidoo J, Ardehali R, Tocchetti CG, et al. Cardiovascular toxicities associated with immune checkpoint inhibitors. *Cardiovasc Res.* (2019) 115:854–68. doi: 10.1093/cvr/cvz026
90. Foulkes S, Claessen G, Howden EJ, Daly RM, Fraser SF, La Gerche A. The utility of cardiac reserve for the early detection of cancer treatment-related cardiac dysfunction: a comprehensive overview. *Front Cardiovasc Med.* (2020) 7:32. doi: 10.3389/fcvm.2020.00032
91. Farge D, Frere C, Connors JM, Ay C, Khorana AA, Munoz A, et al. 2019 international clinical practice guidelines for the treatment and prophylaxis of venous thromboembolism in patients with cancer. *Lancet Oncol.* (2019) 20:e566–81. doi: 10.1016/S1470-2045(19)30336-5
92. Cuomo A, Pirozzi F, Attanasio U, Franco R, Elia F, De Rosa E, et al. Cancer risk in the heart failure population: epidemiology, mechanisms, and clinical implications. *Curr Oncol Rep.* (2020) 23:7. doi: 10.1007/s11912-020-00990-z
93. Khorana AA, Kuderer NM, Culakova E, Lyman GH, Francis CW. Development and validation of a predictive model for chemotherapy-associated thrombosis. *Blood.* (2008) 111:4902–7. doi: 10.1182/blood-2007-10-116327
94. Sullivan RJ, Johnson DB, Rini BI, Neilan TG, Lovly CM, Moslehi JJ, et al. COVID-19 and immune checkpoint inhibitors: initial considerations. *J Immunother Cancer.* (2020) 8:e000933. doi: 10.1136/jitc-2020-000933
95. Xu Z, Shi L, Wang Y, Zhang J, Huang L, Zhang C, et al. Pathological findings of COVID-19 associated with acute respiratory distress syndrome. *Lancet Respir Med.* (2020) 8:420–2. doi: 10.1016/S2213-2600(20)30076-X

96. Johnson DB, Balko JM, Compton ML, Chalkias S, Gorham J, Xu Y, et al. Fulminant myocarditis with combination immune checkpoint blockade. *N Engl J Med.* (2016) 375:1749–55. doi: 10.1056/NEJMoa1609214
97. Bryant J, Picot J, Levitt G, Sullivan I, Baxter L, Clegg A. Cardioprotection against the toxic effects of anthracyclines given to children with cancer: a systematic review. *Health Technol Assess.* (2007) 11:iii, ix-x:1–84. doi: 10.3310/hta11270
98. Lipshultz SE, Colan SD, Gelber RD, Perez-Atayde AR, Sallan SE, Sanders SP. Late cardiac effects of doxorubicin therapy for acute lymphoblastic leukemia in childhood. *N Engl J Med.* (1991) 324:808–15. doi: 10.1056/NEJM199103213241205
99. Yeh ET, Vejpongsa P. Subclinical cardiotoxicity associated with cancer therapy: early detection and future directions. *J Am Coll Cardiol.* (2015) 65:2523–5. doi: 10.1016/j.jacc.2015.04.012
100. Lipshultz SE, Lipsitz SR, Sallan SE, Dalton VM, Mone SM, Gelber RD, et al. Chronic progressive cardiac dysfunction years after doxorubicin therapy for childhood acute lymphoblastic leukemia. *J Clin Oncol.* (2005) 23:2629–36. doi: 10.1200/JCO.2005.12.121
101. Goldberg JM, Scully RE, Sallan SE, Lipshultz SE. Cardiac failure 30 years after treatment containing anthracycline for childhood acute lymphoblastic leukemia. *J Pediatr Hematol Oncol.* (2012) 34:395–7. doi: 10.1097/MPH.0b013e3182532078
102. Lotrionte M, Biondi-Zoccai G, Abbate A, Lanzetta G, D'Ascenzo F, Malavasi V, et al. Review and meta-analysis of incidence and clinical predictors of anthracycline cardiotoxicity. *Am J Cardiol.* (2013) 112:1980–4. doi: 10.1016/j.amjcard.2013.08.026
103. Mulrooney DA, Yeazel MW, Kawashima T, Mertens AC, Mitby P, Stovall M, et al. Cardiac outcomes in a cohort of adult survivors of childhood and adolescent cancer: retrospective analysis of the childhood cancer survivor study cohort. *BMJ.* (2009) 339:b4606. doi: 10.1136/bmj.b4606
104. Katsumata N, Eguchi K, Fukuda M, Yamamoto N, Ohe Y, Oshita F, et al. Serum levels of cytokines in patients with untreated primary lung cancer. *Clin Cancer Res.* (1996) 2:553–9.
105. Blay JY, Negrier S, Combaret V, Attali S, Goillot E, Merrouche Y, et al. Serum level of interleukin 6 as a prognosis factor in metastatic renal cell carcinoma. *Cancer Res.* (1992) 52:3317–22.
106. Berek JS, Chung C, Kaldi K, Watson JM, Knox RM, Martinez-Maza O. Serum interleukin-6 levels correlate with disease status in patients with epithelial ovarian cancer. *Am J Obstet Gynecol.* (1991) 164:1038–42. Discussion 42–3. doi: 10.1016/0002-9378(91)90582-C
107. Vivarelli S, Falzone L, Grillo CM, Scandurra G, Torino F, Libra M. Cancer management during COVID-19 pandemic: is immune checkpoint inhibitors-based immunotherapy harmful or beneficial? *Cancers.* (2020) 12:2237. doi: 10.3390/cancers12082237

Conflict of Interest: The handling editor is currently organising a Research Topic with one of the authors HM and confirms the absence of any other collaboration.

The authors declare that the research was conducted in the absence of any commercial or financial relationships that could be construed as a potential conflict of interest.

frontiers in Cardiovascular Medicine

MINI REVIEW
published: 27 April 2021
doi: 10.3389/fcvm.2021.624028

Effects of Cardiotoxins on Cardiac Stem and Progenitor Cell Populations

Andrew J. Smith [1,2]*

[1] Faculty of Biological Sciences, School of Biomedical Sciences, University of Leeds, Leeds, United Kingdom, [2] Faculty of Life Sciences and Medicine, Centre for Human and Applied Physiological Sciences, Centre for Stem Cell and Regenerative Medicine, School of Basic and Medical Biosciences, Guy's Campus, King's College London, London, United Kingdom

As research and understanding of the cardiotoxic side-effects of anticancer therapy expands further and the affected patient population grows, notably the long-term survivors of childhood cancers, it is important to consider the full range of myocardial cell types affected. While the direct impacts of these toxins on cardiac myocytes constitute the most immediate damage, over the longer term, the myocardial ability to repair, or adapt to this damage becomes an ever greater component of the disease phenotype. One aspect is the potential for endogenous myocardial repair and renewal and how this may be limited by cardiotoxins depleting the cells that contribute to these processes. Clear evidence exists of new cardiomyocyte formation in adult human myocardium, along with the identification in the myocardium of endogenous stem/progenitor cell populations with pro-regenerative properties. Any effects of cardiotoxins on either of these processes will worsen long-term prognosis. While the role of cardiac stem/progenitor cells in cardiomyocyte renewal appears at best limited (although with stronger evidence of this process in response to diffuse cardiomyocyte loss), there are strong indications of a pro-regenerative function through the support of injured cell survival. A number of recent studies have identified detrimental impacts of anticancer therapies on cardiac stem/progenitor cells, with negative effects seen from both long-established chemotherapy agents such as, doxorubicin and from newer, less overtly cardiotoxic agents such as tyrosine kinase inhibitors. Damaging impacts are seen both directly, on cell numbers and viability, but also on these cells' ability to maintain the myocardium through generation of pro-survival secretome and differentiated cells. We here present a review of the identified impacts of cardiotoxins on cardiac stem and progenitor cells, considered in the context of the likely role played by these cells in the maintenance of myocardial tissue homeostasis.

Keywords: cardiac stem/progenitor cells, cardiotoxicity, heart failure, regeneration, microvasculature

OPEN ACCESS

Edited by:
Jun-ichi Abe,
University of Texas MD Anderson Cancer Center, United States

Reviewed by:
Valentina Sala,
University of Turin, Italy
Yuri D'Alessandra,
Centro Cardiologico Monzino (IRCCS), Italy

***Correspondence:**
Andrew J. Smith
A.J.Smith1@leeds.ac.uk

Specialty section:
This article was submitted to Cardio-Oncology, a section of the journal Frontiers in Cardiovascular Medicine

Received: *02 November 2020*
Accepted: *01 March 2021*
Published: *27 April 2021*

Citation:
Smith AJ (2021) Effects of Cardiotoxins on Cardiac Stem and Progenitor Cell Populations. Front. Cardiovasc. Med. 8:624028. doi: 10.3389/fcvm.2021.624028

INTRODUCTION

Managing anticancer therapy side-effects has been an important component of oncotherapy care since it was first developed, with cardiotoxicity as one of the principal side-effects. As anticancer therapy regimens become more effective and patient long-term survival increases, avoidance of cardiotoxicity, and its long-term management have accordingly become of ever-greater importance. Two developments in healthcare continue to drive this: one positive, the

other negative. The first is improving cancer patient survival: a review of 40 years of cancer care in England and Wales found that patients had 50% survival 1 year after diagnosis in 1971, which rose to 50% survival (predicted) at 10 years after diagnosis in 2011 (1). The second is that cardiovascular disease remains highly prevalent in the wider population, disease to which cancer survivors are no less susceptible. In fact, as the pathophysiology of cardiotoxicity due to many anticancer drugs involves myocardial ischaemia or coronary artery damage (2), along with recognition that cardiotoxicity may manifest in cancer survivors only in the long term (3), the risk is likely notably higher.

Doxorubicin (DOX) and other anthracyclines are long established in anticancer therapy, used for several cancers of childhood (4), but are also well-recognised as cardiotoxic, and DOX has more recently been identified as a cause of cardiotoxic damage manifesting in the long term [for review, see Ref. (3)]. More recent anticancer therapy classes such as tyrosine kinase inhibitors (TKIs) are more precisely targeted, acting to impair tumour cell proliferation (5), migration (6), and tumour angiogenesis (7) *via* focused actions on tyrosine kinases (acting on a few kinases to a broad range, depending on the individual TKI). However, emerging data indicate cardiotoxic side-effects for these drugs, underlining the importance of considering these in patient management, with comparable cardiotoxicity data emerging for the epidermal growth factor receptor-2 inhibitor trastuzumab (8).

Microvascular injury is an early sign of several cardiac disease processes, and the study of its involvement in cardiotoxicity has grown to generate more complete understanding of the underlying pathophysiology, beyond only mechanisms of injury to cardiomyocytes. Application of DOX to human cardiac microvascular vessel specimens *ex vivo* causes significant reduction in flow-mediated dilation responses in both adult and paediatric vessels, although less extensively in paediatric samples, in addition to loss of acetylcholine-induced vessel constriction responses (9). Microvascular damage is also caused by TKIs, with microvascular dysfunction induced by one TKI with clinically identified cardiotoxicity (10).

Although optimising patient care outcomes is the primary concern, healthcare economic considerations are only realistic, particularly as healthcare demands are ever growing and thus economic resources available are ever more hard pressed to meet them. For all of these reasons, optimising understanding of the pathophysiology of cardiotoxicity and identifying means to avert or minimise its impact is of ever-greater importance.

CARDIAC STEM CELLS AND THEIR ROLE IN TISSUE HOMEOSTASIS

From their discovery in 2003 (11), cardiac stem cells (CSCs), also known as cardiac progenitor cells (CPCs), attracted significant research investment and extensive discussion. The natural first course of investigation was assessing CSCs as a potential source of cardiomyocytes, with multiple papers focused on determining this potential (12–15). Although this knowledge expansion was commendably rapid, the advancement to clinical trials of CSC regenerative potential (16, 17) suffered from this rapidity. Major questions arose over the assumptions about CSCs' mode of regeneration in already-started trials (with retraction of underlying laboratory data undermining one trial). These issues caused cessation of some trials and re-appraisal of likely repair mechanisms in others (18, 19).

The fundamental problem was substantially varied rates of cardiomyogenesis across studies, particularly in the myocardial infarction (MI) setting (20), bringing into question the practical utility of CSCs as a source of new myocardium. As this uncertainty developed, more studies focused on CSCs as generators of protective paracrine effects (21, 22), to be exploited as a cardiac disease therapy (23, 24). This mechanism was later held to be a likely cause of many of the benefits seen in clinical trials (19, 22). Notably, however, in the specific context of diffuse injury (as opposed to post-MI), evidence of cardiomyocyte repair and regeneration was more robust (15, 25), although still contested. One notable diffuse cardiac injury model was DOX treatment *in vivo*: this significantly upregulated cardiomyogenic lineage markers in CSCs and increased new cardiomyocyte formation *in situ*, derived from cells bearing the CSC marker c-kit (26).

One factor contributing to variant findings was dissimilarity in genetic lineage tracing approaches. A study directly comparing transgenic and knock-in-based c-kit-tracing models found significantly reduced c-kit expression in knock-in models (thus a limitation of much evidence contesting CSC cardiomyogenesis) but also that c-kit expression was found in already-formed cardiomyocytes and increased post-injury (thus, a limitation to using c-kit to trace *de novo* cardiomyocytes) (27). For an overview of c-kit genetic tracking to quantify CSC cardiomyogenesis, see Ref. (28). Other studies avoided complications by using a dual-recombination model of c-kit tracing (avoiding Cre-related limitations) (29) or a series of CRISPR/Cas9-based tracking models (30): these studies saw respectively little and no identifiable cardiomyocyte formation from non-myocytes post-MI.

Investigation of CSCs coincided with novel research into cardiomyogenesis irrespective of source, demonstrating new cardiomyocyte formation in adult human myocardium, although at a low rate of ∼1% per annum, reduced to ∼0.5% with age (31), compared with ∼15% per annum, and ∼4% per annum in endothelial and mesenchymal cells, respectively, in the human heart (32). This low rate of cardiomyogenesis is consistent with the essentially absent contractile myocardial repair seen in patients post-MI and with progressive ischaemic heart failure, but directly contrasts with claims of high cardiomyogenesis rates in some CSC publications, some of which were later withdrawn (33). Thus, the current overall consensus is that while CSCs may have cardiomyogenic potential in certain contexts, it is very limited and not exploitable clinically, particularly post-MI (34).

While these complex, often-controversial events unfolded over CSC cardiomyogenic potential, relatively little attention was paid to CSC generation of both endothelial cells and vascular smooth muscle cells. These capabilities have been consistently recognised, from their first identification and repeatedly thereafter by multiple independent research groups

(11, 13–15, 20, 29, 30, 35–37). This lesser interest was natural given the well-established ability of vascular cell populations to expand *in situ*, in stark contrast to cardiomyocytes. However, CSC vascular regenerative potential has been shown consistently, including in studies arguing against CSC cardiomyogenesis (20, 29, 37), so is a research avenue separate from the aforementioned controversy.

With the study of CSCs in cardiomyocyte regeneration shifting focus to secretome-based mechanisms, it is worth reviewing the evidence and considering how such paracrine actions may aid cardiac cells beyond cardiomyocytes, in view of evidence about the proportions of cardiac cells that are endothelial (38) and cardiac fibroblast roles in cardiac tissue maintenance (39). The possibility that CSC cell transplant benefits were mediated by paracrine actions was raised quite early in the progress of CSC study (40), with simultaneous articles soon after presenting data and reviewing the understanding to date of paracrine actions of mesenchymal stem cells (MSCs) (41) and CSCs (42), the latter identifying IGF-1 and HGF signalling in CSCs. Increased expression of IGF-1 by CSCs was then shown to increase cardiomyocyte survival *in vitro* (21) and *in vivo* (23, 43).

Increased Notch pathway signalling in a GM mouse model increased CPC expression of TBG-β1 and VEGF, with associated increased myocardial capillary density (44), consistent with the pro-angiogenic actions of those growth factors. Examination of Sca1-positive CSCs found the expression of EGF, TGF-β1, IGF-1, IGF-2, MCP-1, HGF, and IL-6 (45), illustrating that comparable growth factors are expressed in CSCs isolated using different surface markers [the aforementioned studies used c-kit (42, 44)]. This is emphasised by HGF, IGF, and VEGF expression in another class of CSCs, the cardiosphere-derived cells (named for their method of isolation), a type trialled clinically (46).

In summary, while CSC cardiomyogenesis is currently not considered a feasible route for translation, the supportive functions of CSCs—aiding cardiomyocyte survival and microvascular expansion—remain of interest, particularly in diffuse non-infarction cardiac pathologies. Against this background, we consider potential CSC roles in myocardial effects of cancer therapy-related cardiotoxicity.

EFFECTS ON CARDIAC STEM CELLS OF CARDIOTOXIC THERAPIES

With the background of CSC translational potential changing dramatically, the more the niche field of examining CSC roles in the pathogenesis of cardiotoxicity underwent related changes in focus. Initial work presupposed any cardiotoxin impacts to directly impact on cardiomyogenesis potential, whereas later work analysed impacts in view of a broader range of roles. Cardiotoxins examined to date are anthracyclines, trastuzumab, and TKIs, with no studies found examining others in CSCs (**Figure 1**).

The first two studies were published near-simultaneously in 2009–2010 (35, 47), both focusing on DOX effects. The first identified that DOX reduced CSC viability and proliferation both *in vitro* and *in vivo*, but also identified increased markers of CSC differentiation (to both cardiomyocyte and vascular cell lineages) *in vitro* (47). Injection of exogenous CSCs directly into the myocardium reduced DOX-induced myocardial injury, in terms of myocardial fibrosis and wall thickness loss, with associated improved cardiac functional parameters, although the mechanisms were undetermined, so the role(s) of *in situ* CSCs in cardiotoxicity pathogenesis remained uncertain (47). The second study used a model of DOX application in early life, then assessed long-term effects on myocardial homeostasis, to identify damage seen in the long term, perhaps the most likely way that CSCs are involved in cardiotoxicity pathogenesis (35). Notable effects were reduced capillary density and VEGF levels, increased vulnerability to MI in adulthood (infarct sizes in standard MI models were larger post-DOX), and reduced CPC numbers, either infiltrating infarct borders or in uninjured post-DOX hearts (35). A finding contrasting with the prior study (47) was that DOX reduced differentiation, particularly to endothelial cells (35). These findings suggest a role for CSCs in microvasculature formation, a possible way for CSC damage to manifest as long-term cardiotoxicity.

It is notable that DOX cardiotoxicity can develop over a range of time periods, acute (within 2 weeks of treatment completion), early-onset chronic (within 1 year), and late-onset chronic (years or decades later) (48). Loss of CSCs is unlikely to contribute to acute effects, excepting loss of CSC paracrine support for injured cells, but their contribution to angiogenesis could be linked to early- or late-onset chronic effects, respectively. The different rates of cardiotoxicity development in paediatric and adult patients are also notable (49), with cardiomyocyte apoptosis a feasible target for CSC-based protection and CSC protection against this already demonstrated (21).

Another study of DOX in CSCs (albeit those with a phenotype overlapping with MSCs) identified DOX upregulated the stromal cell-derived factor-1/CXC chemokine receptor-4 (SDF1/CXCR4) signal pathway, protecting cells against DOX damage and increasing their migration (50). The SDF1/CXCR4 pathway is upregulated in MI (51) or diffuse myocardial injury (15) and is known to upregulate migration of stem/progenitor cells to injured myocardium (52). Furthermore, blockade of this signalling in CSCs severely reduces their integration into the injured myocardium (15). The pathway also plays a key role in angiogenesis development, *via* a range of different stem/progenitor cells, including endothelial progenitors and MSCs [for review, see (53)].

These combined findings show acute CSC responses to DOX-induced cardiotoxicity, with migration to injured tissue and differentiation (thus, contributing to angiogenesis in damaged tissue), but raises the question on why longer-term depletion of CPCs was seen by Huang et al. (35). There are two possible explanations for this: the first is ongoing mobilisation of the stem cell pool leads to eventual depletion, a phenomenon seen in stem cells that can be induced to generate a prematurely aged phenotype (54). The other explanation is attritional CSC loss from direct DOX toxicity: depleted CSC populations can maintain an acute response, but suffer a critical impairment of their ability to support myocardial homeostasis in the long-term. While SDF application attenuated DOX-induced acute

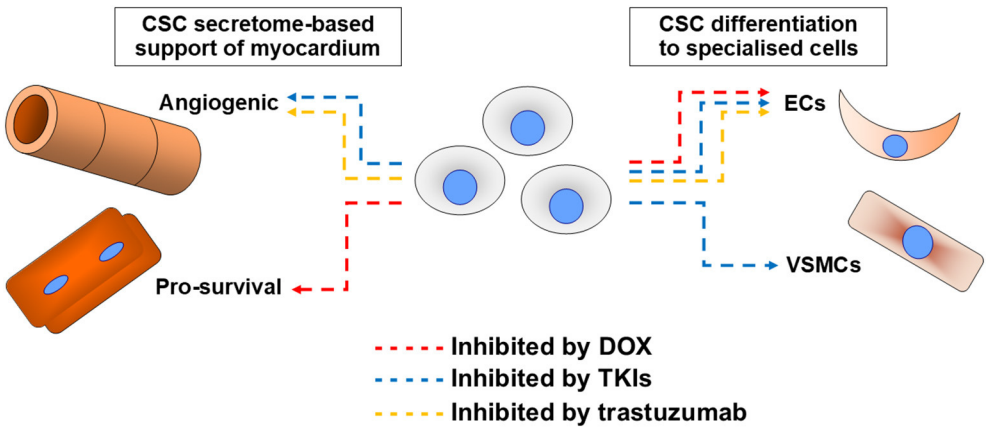

FIGURE 1 | Summary of cardiotoxin effects on cardiac stem cell (CSC) abilities. Impacts of the most examined cardiotoxin doxorubicin (DOX, red), tyrosine kinase inhibitors (TKIs, blue), and trastuzumab (orange) on CSC abilities to support myocardium *via* secretome support of angiogenesis or cell survival (most critically cardiomyocyte survival), or *via* their differentiation into endothelial cells (ECs) or vascular smooth muscle cells (VSMCs).

cardiotoxicity (50), whether this impacted on CSC ability to protect against long-term cardiotoxic effects was not studied.

Examination of the mechanisms of acute DOX toxicity in CPCs identified calcium-linked autophagy signalling as playing an important role (55). This is a DOX toxicity mechanism common to CPCs and cardiomyocytes (55, 56), with the underlying generation of mitochondrial oxidative stress also common to DOX toxicity in both cells (49, 56). Rapamycin application reduced cytosolic calcium accumulation in CPCs, along with indications of reduced mTOR signalling (55). Looking at the complexities of developing cardioprotective treatments that also avoid any interference with the—essential—anti-cancer activity of DOX, this overlap in cell death mechanisms is fortuitous, as treatment (perhaps *via* mTOR manipulation) that provides acute protective benefits to cardiomyocytes could also provide long-term benefits *via* CSC protection.

Further evidence of the value of targeting oxidative stress to prevent DOX toxicity in CSCs was shown by the protection of CSCs *in vitro* by encapsulation in a superoxide dismutase-loaded alginate, which averted DOX-induced metabolic alterations and apoptosis (57). A study into the cardioprotective effects of bergamot citrus extract (with known antioxidant effects) against DOX-induced cardiotoxicity in adult rats examined CSCs isolated after *in vivo* treatment: DOX caused significant intranuclear accumulation of reactive oxygen species and reduced CSC numbers *in situ* (58). Bergamot antioxidant treatment significantly attenuated these effects on CSCs, while also reducing DOX-induced cardiomyocyte apoptosis and prevented the cardiac functional damage of DOX (58). Collectively, these findings support the value of antioxidant treatment of acute DOX-induced cardiotoxicity as a protection for CSCs that will also benefit cardiomyocytes.

Although the initial focus for investigation of cardiotoxins in CSCs was DOX, some recent work examined cardiotoxic impacts of other anticancer therapies, particularly TKIs. Treatment of adult rats with imatinib mesylate, unlike DOX, did not cause fibrosis, or loss of cardiomyocyte tissue volume, although cardiomyocyte apoptosis was increased and densities of myocardial capillaries and arterioles were reduced (59). Imatinib reduced CPC numbers *in situ*, and was shown *ex vivo* to reduce both CPC viability and proliferation, along with repressing CPC ability to differentiate (59). The ability of CPCs to protect cardiomyocytes from apoptosis (21) could give valuable protection to cardiomyocytes from imatinib-induced injury (59). In the longer term, with TKI cardiotoxicity significantly damaging cardiac microvasculature, the CPC contribution to repair and regeneration of these vessel networks is of great value, and its loss would worsen disease prognosis.

Only a very little published research has focused on cardiotoxin impacts on another myocardial cell type, cardiac microvascular pericytes, which also have valuable pro-regenerative pro-angiogenic and paracrine actions (60). One such study examined the effects of the TKI sunitinib, finding that the drug caused cardiac microvascular dysfunction and reduced blood flow, with a loss of pericytes that increased with sunitinib treatment progress (10). Another study reaffirmed the toxicity of sunitinib to pericytes, linking it to the mitochondrial deacetylase sirtuin-3 (61). The more recent introduction (since 2000) of TKIs means that the long-term sequelae of their use are not yet fully apparent (particularly in childhood cancers, for which their use was commenced more recently), although comprehensive assessment should consider the myocardial roles of both pericytes and CSCs, along with the impacts of cardiotoxins on both cell types.

We can turn the tables by moving from cardiotoxins damaging CSCs to considering stem cell paracrine abilities as potential anti-cardiotoxin treatments. One study identified protection by stem cell secretome (human amniotic fluid stem cell secretome) of mouse cardiomyocytes *in vitro* against DOX-induced toxicity (62). Further study of this protection found that one effect increased CPC proliferation, with associated increased angiogenesis: no CPC differentiation was seen, although the

authors suggested their data supported a local paracrine role for CPCs, but this was not definitively shown (63). This group advanced their work by examining the protection given by human CPC secretome (specifically secreted exosomes) against DOX and trastuzumab: intravenous injection of exosomes reduced damage from DOX and trastuzumab therapy to cardiac function (fibrosis and impaired cardiac functional parameters), also lowering reactive oxygen species in isolated cardiomyocytes treated with DOX and trastuzumab (64). Although trastuzumab did not impact on human cardiosphere-derived cell survival or proliferation, it impaired their ability to form microvascular networks or to commence cardiomyogenic differentiation *in vitro* (65). Furthermore, when cells were applied *in vivo* post-MI, trastuzumab co-application reduced their angiogenesis and associated cardiac functional improvement (65).

CSC secretome-based treatments, potentiating angiogenesis and attenuating cardiomyocyte apoptosis, would complement current anti-cardiotoxicity treatments, focused around the use of ACE inhibitors and beta-blockers to control workload in a weakened heart (66). No examination of ACE-inhibitor or beta-blocker effects on CSCs could be identified, the closest being beta-blockade improving the regenerative action of MSCs post-MI (67).

FUTURE DIRECTIONS AND CONCLUSION

Understanding of cardiotoxicity continues to advance, with human cardiomyocytes derived from induced pluripotent stem cells showing great promise [for review, see Ref. (68)]. A striking finding was of cardiac DOX sensitivity at the individual-patient level being reproduced in these cells (69). These developments are very encouraging and rightly reflect a focus on the primacy of cardiomyocytes in cardiotoxicity development. It is, however, important that this progress is complemented by studies considering the other cell types that comprise myocardial tissue and contribute to its maintenance, particularly as cardiomyocyte loss or recovery is partly dependent on these cells.

With ongoing work examining impacts of both older and more novel anticancer therapies on myocardial microvascular cells and tissue (9, 70), indicating that these impacts play key roles in cardiotoxicity development, along with research examining TKI effects on cardiac fibroblasts (71), this essential broader understanding is being built, but much more remains be done.

An important point to stress, the need for this emphasis hopefully illustrated by the brief recap of the CSC-cardiomyogenesis controversy, is what the role played by CSCs in myocardial homeostasis post-cardiotoxicity would likely be. While cardiotoxins destroying or damaging CSCs would indeed diminish the previously assumed function of CSCs as a source of cardiomyogenesis, their support of damaged cardiomyocytes or contribution to new microvasculature formation would be similarly diminished. Therefore, with their recognised potential in these latter areas, determining cardiotoxin impacts on CSCs is a valuable aspect of understanding the long-term pathophysiology of post-cancer treatment cardiotoxicity.

Future developments with the most promise are those harnessing the CSC potential as generators of paracrine protective therapy, either as exogenously generated products applied to injured hearts or as *in situ* mediators. With the *in situ* CSC population sparse (11, 36) and its function declining with age (72), the former route shows more potential as a vector to aid cell survival, microvascular repair or network expansion, with all of these offering clear potential benefits in the drive towards ameliorating the long-term damage wrought by cardiotoxins.

AUTHOR CONTRIBUTIONS

The manuscript was written and edited by AS.

FUNDING

This work was supported by funding from the University of Leeds, with associated research work into TKIs impacts on human CPCs funded by Heart Research UK (Grant Number RG 2641) and the Rosetrees Trust (Grant Number M519).

ACKNOWLEDGMENTS

The author wishes to gratefully acknowledge the advice and guidance of Prof. Georgina Ellison-Hughes, Prof. Bernardo Nadal-Ginard and Prof. Daniele Torella when commencing my research in this field, with further thanks to Prof. Ellison-Hughes for her essential collaborative work with my then newly-founded research group.

REFERENCES

1. Quaresma M, Coleman MP, Rachet B. 40-year trends in an index of survival for all cancers combined and survival adjusted for age and sex for each cancer in England and Wales, 1971-2011: a population-based study. *Lancet*. (2015) 385:1206–18. doi: 10.1016/S0140-6736(14)61396-9
2. Blaes AH, Thavendiranathan P, Moslehi J. Cardiac toxicities in the era of precision medicine: underlying risk factors, targeted therapies, cardiac biomarkers. *Am Soc Clin Oncol Educ Book*. (2018) 38:764–74. doi: 10.1200/EDBK_208509
3. Singal PK, Iliskovic N. Doxorubicin-induced cardiomyopathy. *N Engl J Med*. (1998) 339:900–5. doi: 10.1056/NEJM199809243391307
4. Fulbright JM, Huh W, Anderson P, Chandra J. Can anthracycline therapy for pediatric malignancies be less cardiotoxic? *Curr Oncol Rep*. (2010) 12:411–9. doi: 10.1007/s11912-010-0129-9
5. Pignochino Y, Grignani G, Cavalloni G, Motta M, Tapparo M, Bruno S, et al. Sorafenib blocks tumour growth, angiogenesis and metastatic potential in preclinical models of osteosarcoma through a mechanism potentially involving the inhibition of ERK1/2, MCL-1, and ezrin pathways. *Mol Cancer*. (2009) 8:118. doi: 10.1186/1476-4598-8-118
6. Polena H, Creuzet J, Dufies M, Sidibé A, Khalil-Mgharbel A, Salomon A, et al. The tyrosine-kinase inhibitor sunitinib targets vascular endothelial (VE)-cadherin: a marker of response to antitumoural treatment in metastatic renal cell carcinoma. *Br J Cancer*. (2018) 118:1179–88. doi: 10.1038/s41416-018-0054-5

7. Chinchar E, Makey KL, Gibson J, Chen F, Cole SA, Megason GC, et al. Sunitinib significantly suppresses the proliferation, migration, apoptosis resistance, tumor angiogenesis and growth of triple-negative breast cancers but increases breast cancer stem cells. *Vasc Cell.* (2014) 6:12. doi: 10.1186/2045-824X-6-12
8. Romitan DM, Rădulescu D, Berindan-Neagoe I, Stoicescu L, Grosu A, Rădulescu L, et al. Cardiomyopathies and arrhythmias induced by cancer therapies. *Biomedicines*. (2020) 8:496. doi: 10.3390/biomedicines8110496
9. Hader SN, Zinkevich N, Norwood Toro LE, Kriegel AJ, Kong A, Freed JK, et al. Detrimental effects of chemotherapy on human coronary microvascular function. *Am J Physiol Heart Circ Physiol.* (2019) 317:H705–10. doi: 10.1152/ajpheart.00370.2019
10. Chintalgattu V, Rees ML, Culver JC, Goel A, Jiffar T, Zhang J, et al. Coronary microvascular pericytes are the cellular target of sunitinib malate-induced cardiotoxicity. *Sci Transl Med.* (2013) 5:187–69. doi: 10.1126/scitranslmed.3005066
11. Beltrami AP, Barlucchi L, Torella D, Baker M, Limana F, Chimenti S, et al. Adult cardiac stem cells are multipotent and support myocardial regeneration. *Cell.* (2003) 114:763–76. doi: 10.1016/S0092-8674(03)00687-1
12. Oh H, Bradfute SB, Gallardo TD, Nakamura T, Gaussin V, Mishina Y, et al. Cardiac progenitor cells from adult myocardium: homing, differentiation, and fusion after infarction. *Proc Natl Acad Sci USA*. (2003) 100:12313–8. doi: 10.1073/pnas.2132126100
13. Bearzi C, Rota M, Hosoda T, Tillmanns J, Nascimbene A, De Angelis A, et al. Human cardiac stem cells. *Proc Natl Acad Sci USA*. (2007) 104:14068–73. doi: 10.1073/pnas.0706760104
14. Smith RR, Barile L, Cho HC, Leppo MK, Hare JM, Messina E, et al. Regenerative potential of cardiosphere-derived cells expanded from percutaneous endomyocardial biopsy specimens. *Circulation.* (2007) 115:896–908. doi: 10.1161/CIRCULATIONAHA.106.655209
15. Ellison GM, Vicinanza C, Smith AJ, Aquila I, Leone A, Waring CD, et al. Adult c-kit(pos) cardiac stem cells are necessary and sufficient for functional cardiac regeneration and repair. *Cell.* (2013) 154:827–42. doi: 10.1016/j.cell.2013.07.039
16. Chugh AR, Beache GM, Loughran JH, Mewton N, Elmore JB, Kajstura J, et al. Administration of cardiac stem cells in patients with ischemic cardiomyopathy: the SCIPIO trial: surgical aspects and interim analysis of myocardial function and viability by magnetic resonance. *Circulation.* (2012) 126(Suppl. 1):S54–64. doi: 10.1161/CIRCULATIONAHA.112.092627
17. Malliaras K, Makkar RR, Smith RR, Cheng K, Wu E, Bonow RO, et al. Intracoronary cardiosphere-derived cells after myocardial infarction: evidence of therapeutic regeneration in the final 1-year results of the CADUCEUS trial (CArdiosphere-Derived aUtologous stem CElls to reverse ventricUlar dySfunction). *J Am Coll Cardiol.* (2014) 63:110–22. doi: 10.1016/j.jacc.2013.08.724
18. Bolli R, Chugh AR, D'Amario D, Loughran JH, Stoddard MF, Ikram S, et al. Cardiac stem cells in patients with ischaemic cardiomyopathy (SCIPIO): initial results of a randomised phase 1 trial. *Lancet.* (2011) 378:1847–57. doi: 10.1016/S0140-6736(11)61590-0
19. Ibrahim AG, Cheng K, Marbán E. Exosomes as critical agents of cardiac regeneration triggered by cell therapy. *Stem Cell Rep.* (2014) 2:606–19. doi: 10.1016/j.stemcr.2014.04.006
20. van Berlo JH, Kanisicak O, Maillet M, Vagnozzi RJ, Karch J, Lin SC, et al. c-kit^{+} cells minimally contribute cardiomyocytes to the heart. *Nature.* (2014) 509:337–41. doi: 10.1038/nature13309
21. Kawaguchi N, Smith AJ, Waring CD, Hasan MK, Miyamoto S, Matsuoka R, et al. c-kit^{pos} GATA-4 high rat cardiac stem cells foster adult cardiomyocyte survival through IGF-1 paracrine signalling. *PLoS ONE.* (2010) 5:e14297. doi: 10.1371/journal.pone.0014297
22. Tang XL, Li Q, Rokosh G, Sananalmath SK, Chen N, Ou Q, et al. Long-term outcome of administration of c-kit(POS) cardiac progenitor cells after acute myocardial infarction: transplanted cells do not become cardiomyocytes, but structural and functional improvement and proliferation of endogenous cells persist for at least one year. *Circ Res.* (2016) 118:1091–105. doi: 10.1161/CIRCRESAHA.115.307647
23. Ellison GM, Torella D, Dellegrottaglie S, Perez-Martinez C, Perez de Prado A, Vicinanza C, et al. Endogenous cardiac stem cell activation by insulin-like growth factor-1/hepatocyte growth factor intracoronary injection fosters survival and regeneration of the infarcted pig heart. *J Am Coll Cardiol.* (2011) 58:977–86. doi: 10.1016/j.jacc.2011.05.013
24. Lee HJ, Cho HJ, Kwon YW, Park YB, Kim HS. Phenotypic modulation of human cardiospheres between stemness and paracrine activity, and implications for combined transplantation in cardiovascular regeneration. *Biomaterials.* (2013) 34:9819–29. doi: 10.1016/j.biomaterials.2013.09.013
25. Ellison GM, Torella D, Karakikes I, Purushothaman S, Curcio A, Gasparri C, et al. Acute beta-adrenergic overload produces myocyte damage through calcium leakage from the ryanodine receptor 2 but spares cardiac stem cells. *J Biol Chem.* (2007) 282:11397–409. doi: 10.1074/jbc.M607391200
26. Chen Z, Zhu W, Bender I, Gong W, Kwak IY, Yellamilli A, et al. Pathologic stimulus determines lineage commitment of cardiac C-kit+ cells. *Circulation.* (2017) 136:2359–72. doi: 10.1161/CIRCULATIONAHA.117.030137
27. Gude NA, Firouzi F, Broughton KM, Ilves K, Nguyen KP, Payne CR, et al. Cardiac c-Kit biology revealed by inducible transgenesis. *Circ Res.* (2018) 123:57–72. doi: 10.1161/CIRCRESAHA.117.311828
28. Zhou B, Wu SM. A re-assessment of c-Kit in cardiac cells: a complex interplay between expression, fate, and function. *Circ Res.* (2018) 123:9–11. doi: 10.1161/CIRCRESAHA.118.313215
29. He L, Li Y, Li Y, Pu W, Huang X, Tian X, et al. Enhancing the precision of genetic lineage tracing using dual recombinases. *Nat Med.* (2017) 23:1488–98. doi: 10.1038/nm.4437
30. Li Y, He L, Huang X, Bhaloo SI, Zhao H, Zhang S, et al. Genetic lineage tracing of non-myocyte population by dual recombinases. *Circulation.* (2018) 138:793–805. doi: 10.1161/CIRCULATIONAHA.118.034250LL
31. Bergmann O, Bhardwaj RD, Bernard S, Zdunek S, Barnabé-Heider F, Walsh S, et al. Evidence for cardiomyocyte renewal in humans. *Science.* (2009) 324:98–102. doi: 10.1126/science.1164680
32. Bergmann O, Zdunek S, Felker A, Salehpour M, Alkass K, Bernard S, et al. Dynamics of cell generation and turnover in the human heart. *Cell.* (2015) 161:1566–75. doi: 10.1016/j.cell.2015.05.026
33. Kajstura J, Rota M, Cappetta D, Ogórek B, Arranto C, Bai Y, et al. Cardiomyogenesis in the aging and failing human heart. *Circulation.* (2012) 126:1869–81. doi: 10.1161/CIRCULATIONAHA.112.118380
34. Eschenhagen T, Bolli R, Braun T, Field LJ, Fleischmann BK, Frisén J, et al. Cardiomyocyte regeneration: a consensus statement. *Circulation.* (2017) 136:680–6. doi: 10.1161/CIRCULATIONAHA.117.029343
35. Huang C, Zhang X, Ramil JM, Rikka S, Kim L, Lee Y, et al. Juvenile exposure to anthracyclines impairs cardiac progenitor cell function and vascularization resulting in greater susceptibility to stress-induced myocardial injury in adult mice. *Circulation.* (2010) 121:675–83. doi: 10.1161/CIRCULATIONAHA.109.902221
36. Smith AJ, Lewis FC, Aquila I, Waring CD, Nocera A, Agosti V, et al. Isolation and characterisation of resident endogenous c-kit-positive cardiac stem cells (eCSCs) from the adult mouse and rat heart. *Nat Prot.* (2014) 9:1662–81. doi: 10.1038/nprot.2014.113
37. Sultana N, Zhang L, Yan J, Chen J, Cai W, Razzaque S, et al. Resident c-kit(+) cells in the heart are not cardiac stem cells. *Nat Commun.* (2015) 6:8701. doi: 10.1038/ncomms9701
38. Pinto AR, Ilinykh A, Ivey MJ, Kuwabara JT, D'Antoni ML, Debuque R, et al. Revisiting cardiac cellular composition. *Circ Res.* (2016) 118:400–9. doi: 10.1161/CIRCRESAHA.115.307778
39. Brown RD, Ambler SK, Mitchell MD, Long CS. The cardiac fibroblast: therapeutic target in myocardial remodeling and failure. *Annu Rev Pharmacol Toxicol.* (2005) 45:657–87. doi: 10.1146/annurev.pharmtox.45.120403.095802
40. Wang X, Hu Q, Nakamura Y, Lee J, Zhang G, From AH, et al. The role of the sca-1+/CD31- cardiac progenitor cell population in postinfarction left ventricular remodeling. *Stem Cells.* (2006) 24:1779–88. doi: 10.1634/stemcells.2005-0386
41. Mazhari R, Hare JM. Mechanisms of action of mesenchymal stem cells in cardiac repair: potential influences on the cardiac stem cell niche. *Nat Clin Pract Cardiovasc Med.* (2007) 4(Suppl. 1):S21–6. doi: 10.1038/ncpcardio0770
42. Torella D, Ellison GM, Karakikes I, Nadal-Ginard B. Growth-factor-mediated cardiac stem cell activation in myocardial regeneration. *Nat Clin Pract Cardiovasc Med.* (2007) 4(Suppl. 1):S46–51. doi: 10.1038/ncpcardio0772
43. Jackson R, Tilokee EL, Latham N, Mount S, Rafatian G, Strydhorst J, et al. Paracrine engineering of human cardiac stem cells with insulin-like

growth factor 1 enhances myocardial repair. *J Am Heart Assoc.* (2015) 4:e002104. doi: 10.1161/JAHA.115.002104
44. Gude N, Joyo E, Toko H, Quijada P, Villanueva M, Hariharan N, et al. Notch activation enhances lineage commitment and protective signaling in cardiac progenitor cells. *Basic Res Cardiol.* (2015) 110:29. doi: 10.1007/s00395-015-0488-3
45. Park CY, Choi SC, Kim JH, Choi JH, Joo HJ, Hong SJ, et al. Cardiac stem cell secretome protects cardiomyocytes from hypoxic injury partly *via* monocyte chemotactic protein-1-dependent mechanism. *Int J Mol Sci.* (2016) 17:800. doi: 10.3390/ijms17060800
46. Malliaras K, Li TS, Luthringer D, Terrovitis J, Cheng K, Chakravarty T, et al. Safety and efficacy of allogeneic cell therapy in infarcted rats transplanted with mismatched cardiosphere-derived cells. *Circulation*. (2012). 125:100–12. doi: 10.1161/CIRCULATIONAHA.111.042598
47. De Angelis A, Piegari E, Cappetta D, Marino L, Filippelli A, Berrino L, et al. Anthracycline cardiomyopathy is mediated by depletion of the cardiac stem cell pool and is rescued by restoration of progenitor cell function. *Circulation.* (2010) 121:276–92. doi: 10.1161/CIRCULATIONAHA.109.895771
48. Cardinale D, Colombo A, Bacchiani G, Tedeschi I, Meroni CA, Veglia F, et al. Early detection of anthracycline cardiotoxicity and improvement with heart failure therapy. *Circulation.* (2015) 131:1981–8. doi: 10.1161/CIRCULATIONAHA.114.013777
49. Mancilla TR, Iskra B, Aune GJ. Doxorubicin-induced cardiomyopathy in children. *Compr Physiol.* (2019) 9:905–31. doi: 10.1002/cphy.c180017
50. Beji S, Milano G, Scopece A, Cicchillitti L, Cencioni C, Picozza M, et al. Doxorubicin upregulates CXCR4 *via* miR-200c/ZEB1-dependent mechanism in human cardiac mesenchymal progenitor cells. *Cell Death Dis.* (2017) 8:e3020. doi: 10.1038/cddis.2017.409
51. Kucia M, Dawn B, Hunt G, Guo Y, Wysoczynski M, Majka M, et al. Cells expressing early cardiac markers reside in the bone marrow and are mobilized into the peripheral blood after myocardial infarction. *Circ Res.* (2004) 95:1191–9. doi: 10.1161/01.RES.0000150856.47324.5b
52. Tang J-M, Wang JN, Zhang L, Zheng F, Yang JY, Kong X, et al. VEGF/SDF-1 promotes cardiac stem cell mobilization and myocardial repair in the infarcted heart. *Cardiovasc Res.* (2011) 91:402–11. doi: 10.1093/cvr/cvr053
53. Cencioni C, Capogrossi M, Napolitano M. The SDF-1/CXCR4 axis in stem cell preconditioning. *Cardiovasc Res.* (2012) 94:400–7. doi: 10.1093/cvr/cvs132
54. Vilas JM, Carneiro C, Da Silva-Álvarez S, Ferreirós A, González P, Gómez M, et al. Adult Sox2+ stem cell exhaustion in mice results in cellular senescence and premature aging. *Aging Cell.* (2018) 17:e12834. doi: 10.1111/acel.12834
55. Park JH, Choi SH, Kim H, Ji ST, Jang BW, Kim JH, et al. Doxorubicin regulates autophagy signals *via* accumulation of cytosolic Ca^{2+} in human cardiac progenitor cells. *Int J Mol Sci.* (2016) 17:1680. doi: 10.3390/ijms17101680
56. Abdullah CS, Alam S, Aishwarya, Miriyala S R, Bhuiyan MAN, Panchatcharam M, et al. Doxorubicin-induced cardiomyopathy associated with inhibition of autophagic degradation process and defects in mitochondrial respiration. *Sci Rep.* (2019) 9:2002. doi: 10.1038/s41598-018-37862-3
57. Liu TC, Ismail S, Brennan O, Hastings C, Duffy GP. Encapsulation of cardiac stem cells in superoxide dismutase-loaded alginate prevents doxorubicin-mediated toxicity. *J Tissue Eng Regen Med.* (2013) 7:302–11. doi: 10.1002/term.523
58. Carresi C, Musolino V, Gliozzi M, Maiuolo J, Mollace R, Nucera S, et al. Anti-oxidant effect of bergamot polyphenolic fraction counteracts doxorubicin-induced cardiomyopathy: role of autophagy and c-$kit^{pos}CD45^{neg}CD31^{neg}$ cardiac stem cell activation. *J Mol Cell Cardiol.* (2018) 119:10–8. doi: 10.1016/j.yjmcc.2018.04.007
59. Savi M, Frati C, Cavalli S, Graiani G, Galati S, Buschini A, et al. Imatinib mesylate-induced cardiomyopathy involves resident cardiac progenitors. *Pharmacol Res.* (2018) 127:15–25. doi: 10.1016/j.phrs.2017.09.020
60. Ellison-Hughes GM, Madeddu P. Exploring pericyte and cardiac stem cell secretome unveils new tactics for drug discovery. *Pharmacol Ther.* (2017) 171:1–2. doi: 10.1016/j.pharmthera.2016.11.007
61. Yang Y, Li N, Chen T, Zhang C, Li J, Liu L, et al. Sirt3 promotes sensitivity to sunitinib-induced cardiotoxicity *via* inhibition of GTSP1/JNK/autophagy pathway *in vivo* and *in vitro*. *Arch Toxicol.* (2019) 93:3249–60. doi: 10.1007/s00204-019-02573-9
62. Lazzarini E, Balbi C, Altieri P, Pfeffer U, Gambini E, Canepa M, et al. The human amniotic fluid stem cell secretome effectively counteracts doxorubicin-induced cardiotoxicity. *Sci Rep.* (2016) 6:29994. doi: 10.1038/srep29994
63. Balbi C, Lodder K, Costa A, Moimas S, Moccia F, van Herwaarden T, et al. Reactivating endogenous mechanisms of cardiac regeneration *via* paracrine boosting using the human amniotic fluid stem cell secretome. *Int J Cardiol.* (2019) 287:87–95. doi: 10.1016/j.ijcard.2019.04.011
64. Milano G, Biemmi V, Lazzarini E, Balbi C, Ciullo A, Bolis S, et al. Intravenous administration of cardiac progenitor cell-derived exosomes protects against doxorubicin/trastuzumab-induced cardiac toxicity. *Cardiovasc Res.* (2020) 116:383–92. doi: 10.1093/cvr/cvz108
65. Barth AS, Zhang Y, Li T, Smith RR, Chimenti I, Terrovitis I, et al. Functional impairment of human resident cardiac stem cells by the cardiotoxic antineoplastic agent trastuzumab. *Stem Cells Transl Med.* (2012) 1:289–97. doi: 10.5966/sctm.2011-0016
66. Elghazawy H, Venkatesulu BP, Verma V, Pushparaji B, Monlezun DJ, Marmagkiolis K, et al. The role of cardio-protective agents in cardio-preservation in breast cancer patients receiving anthracyclines ± trastuzumab: a meta-analysis of clinical studies. *Crit Rev Oncol Hematol.* (2020) 153:103006. doi: 10.1016/j.critrevonc.2020.103006
67. Hassan F, Meduru S, Taguchi K, Kuppusamy ML, Mostafa M, Kuppusamy P, et al. Carvedilol enhances mesenchymal stem cell therapy for myocardial infarction *via* inhibition of caspase-3 expression. *J Pharmacol Exp Ther.* (2012) 343:62–71. doi: 10.1124/jpet.112.196915
68. Schwach V, Slaats RH, Passier R. Human pluripotent stem cell-derived cardiomyocytes for assessment of anticancer drug-induced cardiotoxicity. *Front Cardiovasc Med.* (2020) 7:50. doi: 10.3389/fcvm.2020.00050
69. Burridge PW, Li YF, Matsa E, Wu H, Ong SG, Sharma A, et al. Human induced pluripotent stem cell-derived cardiomyocytes recapitulate the predilection of breast cancer patients to doxorubicin-induced cardiotoxicity. *Nat Med.* (2016) 22:547–56. doi: 10.1038/nm.4087
70. Elmadani M, Szabo Z, Raatikainen S, Ruizhu L, Alakoski T, Piuhola J, et al. Sorafenib induces cardiotoxicity *via* damage to cardiac endothelial cells. *Circ Res.* (2019) 125:A731. doi: 10.1161/res.125.suppl_1.731
71. Burke MJ, Walmsley R, Munsey T, Smith AJ. Receptor tyrosine kinase inhibitors cause dysfunction in adult rat cardiac fibroblasts *in vitro*. *Toxicol In Vitro.* (2019) 58:178–86. doi: 10.1016/j.tiv.2019.03.026
72. Lewis-McDougall FC, Ruchaya PJ, Domenjo-Vila E, Shin Teoh T, Prata L, Cottle BJ, et al. Aged-senescent cells contribute to impaired heart regeneration. *Aging Cell.* (2019) 18:e12931. doi: 10.1111/acel.12931

Conflict of Interest: The author declares that the research was conducted in the absence of any commercial or financial relationships that could be construed as a potential conflict of interest.

frontiers in Cardiovascular Medicine

ORIGINAL RESEARCH
published: 16 June 2021
doi: 10.3389/fcvm.2021.639824

Cardiac Safety of Kinase Inhibitors – Improving Understanding and Prediction of Liabilities in Drug Discovery Using Human Stem Cell-Derived Models

*Ricarda Ziegler, Fabian Häusermann, Stephan Kirchner and Liudmila Polonchuk**

Pharmaceutical Sciences, Pharma Research and Early Development, Roche Innovation Center Basel, F. Hoffmann-La Roche Ltd., Basel, Switzerland

Many small molecule kinase inhibitors (SMKIs) used to fight cancer have been associated with cardiotoxicity in the clinic. Therefore, preventing their failure in clinical development is a priority for preclinical discovery. Our study focused on the integration and concurrent measurement of ATP, apoptosis dynamics and functional cardiac indexes in human stem cell-derived cardiomyocytes (hSC-CMs) to provide further insights into molecular determinants of compromised cardiac function. Ten out of the fourteen tested SMKIs resulted in a biologically relevant decrease in either beating rate or base impedance (cell number index), illustrating cardiotoxicity as one of the major safety liabilities of SMKIs, in particular of those involved in the PI3K–AKT pathway. Pearson's correlation analysis indicated a good correlation between the different read-outs of functional importance. Therefore, measurement of ATP concentrations and apoptosis *in vitro* could provide important insight into mechanisms of cardiotoxicity. Detailed investigation of the cellular signals facilitated multi-parameter evaluation allowing integrative assessment of cardiomyocyte behavior. The resulting correlation can be used as a tool to highlight changes in cardiac function and potentially to categorize drugs based on their mechanisms of action.

Keywords: kinase inhibitors, cardiotoxicity, iPS-derived cardiomyocytes, apoptosis, beating rate, cell impedance, CardioExcyte®96

OPEN ACCESS

Edited by:
Susan Currie, University of Strathclyde, United Kingdom

Reviewed by:
Alessandra Ghigo, University of Turin, Italy
Martino Deidda, University of Cagliari, Italy

****Correspondence:***
Liudmila Polonchuk
liudmila.polonchuk@roche.com

Specialty section:
This article was submitted to Cardio-Oncology, a section of the journal Frontiers in Cardiovascular Medicine

Received: *09 December 2020*
Accepted: *31 March 2021*
Published: *16 June 2021*

Citation:
Ziegler R, Häusermann F, Kirchner S and Polonchuk L (2021) Cardiac Safety of Kinase Inhibitors – Improving Understanding and Prediction of Liabilities in Drug Discovery Using Human Stem Cell-Derived Models. Front. Cardiovasc. Med. 8:639824. doi: 10.3389/fcvm.2021.639824

INTRODUCTION

Over the last decade, small molecule kinase inhibitors (SMKIs) development has gained more importance due to the mechanistic role of kinases in various diseases and their ability to control basic functions in normal cells (1). Kinases are involved in a number of essential cellular functions such as mitosis, apoptosis and cell signaling (2). Approximately a dozen were marketed for applications in oncology and several for various other indications (3, 4). Because most SMKIs target the structurally and functionally conserved ATP binding pocket, their inhibitory effect has been associated with toxicities that result from exaggerated pharmacological effect or unselective off-target kinase inhibition. These off-target safety issues remain a major cause for failure in drug development. The unintended inhibition of off-target kinases can lead to undesirable toxicities, which may discourage further drug development (5).

Many small molecule kinase inhibitors have been associated with cardiotoxicity in clinical development and preclinical discovery (6, 7). The cardio-toxicological potential of SMKIs may arise from direct or indirect kinase inhibition, or from the off-target effects. Over 2,000 other nucleotide-dependent enzymes besides kinases exist, including polymerases, chaperones, motor proteins, reductases and methyltransferases, which also have potential binding sites for SMKIs (8). An extensive range of kinase-regulated pathways are involved in essential functions of the heart and could trigger cardiotoxicity when inhibited. For example, cardiovascular energy homeostasis is predominantly regulated by protein kinases that maintains a balance of ongoing energy generation and use essential to avoiding congestive heart failure (CHF) (9). Another important pathway is calcium homeostasis, where calcium/calmodulin-dependent protein kinase II is a key player (10). Any disturbance to calcium regulation can lead to altered cardiac conduction and cardiac hypertrophy (11). The most critical interference in a pathway is with the (PI3K)–AKT pathway which regulates cardiomyocyte survival (12). However, inhibition of specific PI3K–AKT pathway compounds is a common strategy in cancer treatment (13). Moreover, a kinase inhibitor-mediated toxicity mechanism can ablate or suppress the proliferation of protective cell compartment important for heart repair (14). In cancer patients following treatment with SMKIs, adverse cardiac events such as QT prolongation, hypertension, reduced left ventricular ejection fraction (LVEF), congestive heart failure (CHF), acute coronary syndromes (ACS), and myocardial infarction (MI) were often observed (15, 16). In the past, cardiotoxicity could be only addressed with *in vivo* models, missing many earlier toxicological cues leading to cardiovascular safety pharmacology liabilities, which were then identified in late-stage clinical trials or even after product launch (17). With the development of human stem cell-derived cardiomyocytes (hSC-CMS), it became possible to study cardiac function by monitoring synchronous cardiac cell beating and behavior *in vitro* (17). Cellular assays with hSC-CM are proved to be predictive for main functional cardiotoxicity hazards such as arrhythmia, chronotropy, inotropy, and kinase inhibitor induced functional cardiotoxicity, underscoring the importance of cardiotoxicity screening during drug development (18–20). Recently, novel cellular electrophysiology technology enabling simultaneous measurements of cellular impedance and extracellular field potential (EFP) has been implemented to monitor cardiac functional indices *in vitro* (21). CardioExcyte® 96 (Nanion Technologies GmbH, Germany) is a screening platform combining impedance and extracellular field potential (EFP) recordings, which allows label-free simultaneous assessment of electrical activity, beating and electromechanical coupling. Combining standard monitoring cardiomyocyte beating and health with live-cell kinetic imaging and the ATP measurements helps us to gain a valuable, more mechanistic understanding of the compound effect during early stage cardiotoxicity investigations. In this study a selected set of reference SMKIs included low and high selectivity inhibitors targeting various classes of PI3K, GSK-3 and ROCK kinases.

Our study focused on the integration and concurrent measurement of cardiomyocyte beating, health, ATP and apoptosis dynamics in hSC-CMs to gain insights into molecular determinants of compromised cardiac function. The results of this work should help to define optimum end- and time-points for follow up experiments and to design a strategy for compound profiling in early drug development.

MATERIALS AND METHODS

Chemicals and Compounds

Compounds were obtained from commercial suppliers (**Table 1**). Stock solutions (1000x) were prepared in DMSO (cat# D5879, Sigma-Aldrich, St. Louis, Missouri) and the final DMSO concentration was 0.1% v/v. hSC-CM were treated with ascending concentrations of compounds with the highest test concentrations set based on individual compound solubility. 0.1% v/v DMSO was used as a vehicle control.

Cell Culture

Cor.4U® Cardiomyocytes (Ncardia, Netherlands) were cultured in 96-well plates at density of 25,000 – 30,000 cells per well. Cells were maintained at 5% CO_2 and 37 °C for 4 days prior to experiments. The cell culture medium (Cor4U® Complete Culture Medium, cat# Ax-M-HC250E, Axiogenesis AG, Cologne, Germany) was changed every 24 h and was replaced by serum-free BMCC medium (cat# Ax-M-BMCC259, Axiogenesis AG, Cologne, Germany) 12 h prior to drug addition.

CardioExcyte® 96 Experiments

Functional monitoring of cardiomyocytes was done using CardioExcyte® 96 (Nanion technologies GmbH, Germany). Extracellular field potential (EFP) and impedance signals were recorded from hSC-CMs that formed monolayers in the wells of the NSP-96 plate. Beating Rate (BR, per minute) was calculated as the reciprocal of the inter-spike interval (ISI) in EFP signal. Impedance signals from spontaneously beating hSC-CMs were recorded with a sampling rate of 1 ms (1 kHz), and EFP data were collected at 0.1ms (10 kHz). Data acquisition was controlled by CardioExcyte® 96 Control software as previously described (22). The functional parameters recorded in each concentration of test items were compared to the base line values before drug addition (taken as 100%) to define fractional change.

Apoptosis Assay

Determination of apoptosis kinetics was performed with the CellEvent™ Caspase-3/7 Green Detection reagent (cat#1825104, Molecular probes®/Invitrogen™) in BMCC medium over 24 h. The plates were incubated 2 h before compound treatment in the IncuCyte ZOOM (ESSEN BioScience, Ann Arbor, Michigan) to set a baseline before the 24 h compound treatment. Staurosporine (1 μM, cat# 058K4041, Sigma-Aldrich, USA) was used as positive control. Imaging was done using 10x microscope objective of the IncuCyteZOOM with four images per well-taken every 2 h in both phase-contrast and green fluorescence. The fluorescent nuclear signal of the apoptotic cells was separated from background with the integrated object counting algorithm, adjusted to cardiomyocytes, and the calculated total green object area per well (μm^2/well) plotted against time. Data were

TABLE 1 | Test compounds.

Compound	Supplier	CAS-Number	LOT Number
NVP-BEZ235	Cayman Chemical; Ann Arbor, Michigan	915019-65-7	048902-2
LY 294002	Toronto Research Chemicals; North York, Canada	154447-36-6	1-XGI-65-1
GDC-0941	Toronto Research Chemicals; North York, Canada	957054-30-7	1-XGI-79-1
HS-173	Toronto Research Chemicals; North York, Canada	1276110-06-5	2-TIM-79-1
TGX-221	Toronto Research Chemicals; North York, Canada	663619-89-4	1-NAZ-38-1
CZC24832	Fluorochem; Glossop, United Kingdom	1159824-67-5	FCB041717
CAL-101	Cayman Chemical; Ann Arbor, Michigan	870281-82-6	0469747-22
RKI-1447	Lucerna-Chem AG; Luzern, Switzerland	1342278-01-6	10020
GSK-429286	Sigma-Aldrich; St. Louis, Missouri	864082-47-3	012M4614V
Y-27632 (hydrochloride)	Cayman Chemical; Ann Arbor, Michigan	129830-38-2	0499111-18
Fasudil	Alfa Aesar; Ward Hill, Massachusetts	103745-39-7	F23X003
CHIR99021	Sigma-Aldrich; St. Louis, Missouri	252917-06-9	017M4717V
SB 216763	Abcam; Cambridge, United Kingdom	280744-09-4	APN08058-2-3
TWS119	Cayman Chemical; Ann Arbor, Michigan	601514-19-6	0475327-29

normalized to those of the time-matched vehicle control. Data were representative of at least three replicates per concentration.

ATP Assay

The CellTiter-Glo Luminescent Cell Viability Assay (cat# G7572, Promega, USA) was performed for quantification of the cellular ATP concentration according to manufacturer's instructions. Plates were shaken for 2 min in the dark, incubated at ambient temperature for 10 min before measuring luminescence (Integration time 0.1 seconds per well) with Luminescence Counter (Synergy H1, BioTek Instruments, Inc., Winooski, Vermont). The measured ATP concentration values were normalized to the time-matched DMSO controls. Data are representative of at least three replicates per concentration.

Data Analysis

All data were presented as mean ± SEM for each test item concentration and controls. Graphical presentation and statistical analysis of the data by one-way ANOVA with Dunnett multiple comparison or by paired *t*-test were done using Microsoft Excel (USA) and GraphPad Prism v8.4.2 (USA).

RESULTS

Integrative Study Design

In the present study, we used CardioExcyte® 96 for multi-parameter profiling of endogenous responses to 14 SMKIs in hSC-CMs. Cor4U® hSC-derived cardiomyocytes were treated with pan and specific PI3K, ROCK and GSK-3 kinase inhibitors to evaluate short-and long-term effects on impedance and EFP signals after 2 and 24 h, respectively. Complementary to the functional effects on the cellular beating and dynamics in culture, continuous measurement of apoptosis during the compound incubation was performed over 24 h with the Caspase 3/7 assay. Determination of the cells' ATP content was done after 2 and 24 h as visualized in **Figure 1**.

Effects of Kinase Inhibitors on hSC-CMs Characteristics

Apoptosis

Incucyte® live-cell imaging and analysis enabled us to continuously monitor and evaluate apoptotic effects in the hSC-derived myocytes treated with a diverse panel of kinase inhibitors over 24 h. A concentration-dependent increase in apoptosis was detected by caspase-3/7 assay for 10 out of 14 compounds with 5 of them belonging to the group of PI3K inhibitors. An overview of the individual compound results is presented in **Figure 2**, which consists of 4 panels built according to the kinase class and specificity of the inhibitors. Panels A, B, C and D show the results for the PI3K-pan, PI3K isoform-specific, GSK-3 and ROCK kinase inhibitors, respectively. Individual data used to generate graphs are provided in **Data File 1**. 1μM staurosporine used as a positive control induced a strong caspase 3/7 signal that could be monitored over 24 h in hSC-CMs (**Supplementary Figure 1**).

The activation of caspase-3/7 represents a key event and a reliable marker of apoptosis. Activated caspase-3/7 cleaves the caspase-3/7 Green Reagent and releases a DNA-binding dye to identify apoptotic cells by the appearance of fluorescently-labeled nuclei. The accumulation of apoptotic cells was plotted as a function of time to analyze the kinetics of apoptosis in hSC-CMs incubated with the set of kinase inhibitors. This analysis revealed apoptotic profiles specific for the targeted kinase-class.

The pan-PI3K inhibitors NVP-BEZ235, LY 294002, GDC-0941 (**Figure 2A**), PI3K p110α inhibitor HS-173 and PI3K p110δ inhibitor CAL-101(**Figure 2B**) induced apoptosis in hSC-CMs with a fast onset reaching the maximum number of apoptotic cells in the first 12 h, whereas the PI3K p110β and PI3K p110γ-specific compounds (TGX-221 and CZC24832) had no effect (**Figure 2B**). The concentration-dependent caspase-3/7 activation exhibited similar kinetic profiles across all PI3K inhibitors except for the top concentration of pan-PI3K inhibitor LY 294002 which induced a delayed apoptotic response in hSC-CMs.

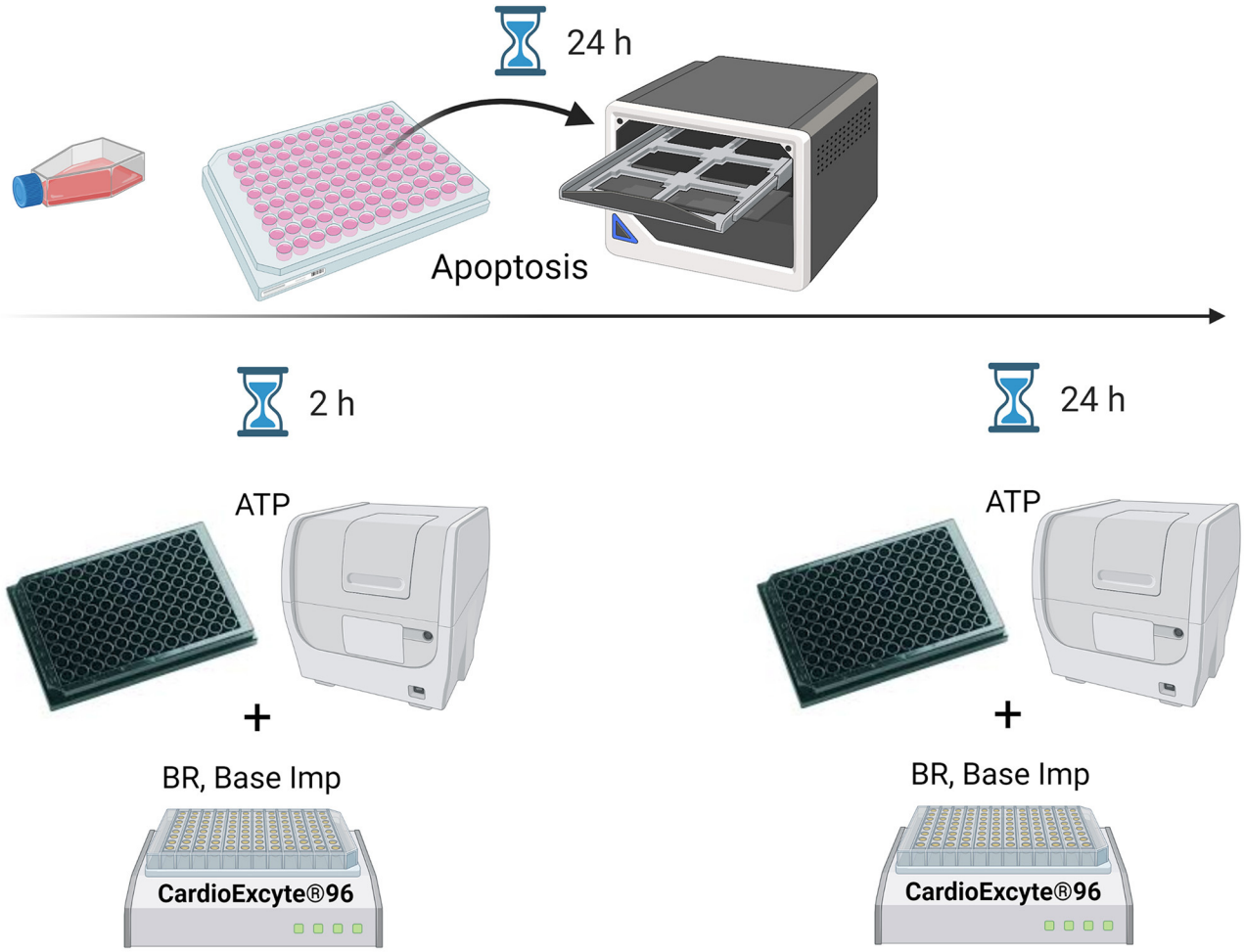

FIGURE 1 | Scheme of assay-specific measurement time points. The ATP and CE96 measurements were conducted 2 and 24 h after the compound treatment whereas apoptosis was continuously monitored over 24 h. BR, beating rate; Base Imp, base impedance.

GSK-3α kinase inhibitor SB 216763 quickly induced a concentration-dependent caspase−3/7 activation in hSC-CMs (**Figure 2C**), which reached a plateau within the first hour and was maintained for the remaining time. The other two GSK-3 kinase inhibitors CHIR99021 (GSK-3α/β) and TWS119 (GSK-3 β) did not have any functionally-relevant effect up to the highest concentrations tested.

Treatment hSC-CMs with ROCK inhibitors Fasudil and Y-27632 (**Figure 2D**) triggered a different apoptotic behavior characterized by a slow initial phase followed by a notable raise in the caspase-3/7 activity after 12–18 h at the highest test concentrations only. In general, hSC-CMs seemed to be more resistant to the apoptosis induced by the ROCK inhibitors, as exemplified by marginal effects observed for RKI-1447 and GSK-429286 at the highest test concentrations only.

Beating Rate and Base Impedance

In this study, monitoring of the hSC-CMs functional activity was done using the CardioExcyte® 96 platform from Nanion technologies GmbH, Germany, which combines impedance and EFP recordings to study pharmacological effects on cardiomyocyte electrophysiology with a sufficient throughput for testing of multiple parallel compounds. Base impedance (or the absolute impedance recorded from each well) was a key parameter for estimation of cell viability. Decrease of this parameter is considered as a surrogate for reduced viability of hSC-CMs. Base impedance and beating rate were recorded in combination to characterize impact of the kinase inhibitors on the cardiac function after 2 and 24 h. Effects of individual compounds are summarized in the corresponding radar plots shown in **Figures 2A–D**. The functional parameters recorded in each concentration of the test items were normalized to the base line values before drug addition to define fractional change. Individual data used to generate radar plots are presented in **Data File 1**.

Treatment with two pan-PI3K inhibitors NVP-BEZ235 and LY 294002, the PI3K p110δ inhibitor CAL-101 and the PI3K p110α inhibitor HS-173 reduced both base impedance and beating rate of hSC-CMs by more than 20% (**Figures 2A,B**), whereas the pan-PI3K inhibitor GDC-0941 only decreased the

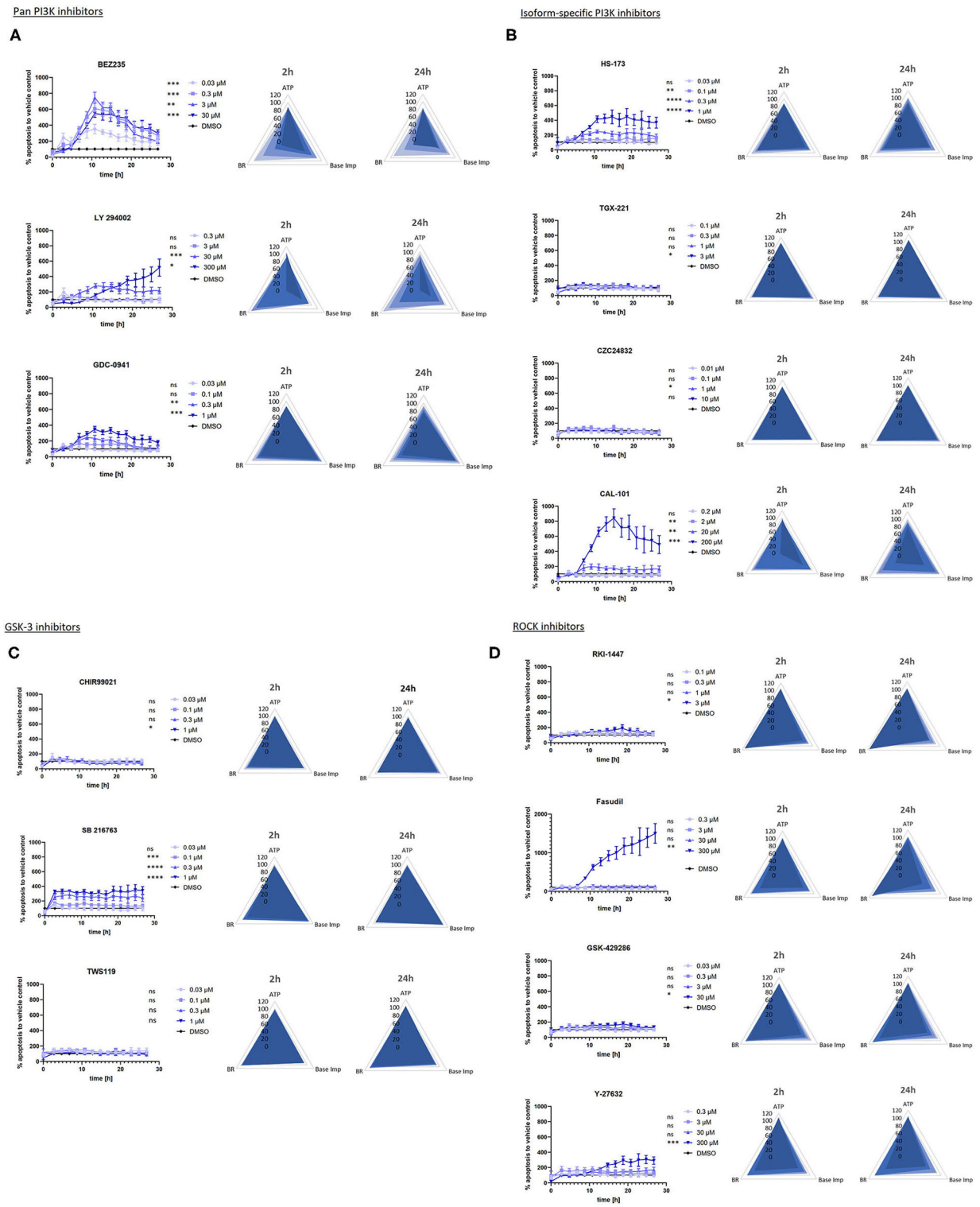

FIGURE 2 | Graphs of apoptosis kinetics and radar plots for beating rate, base impedance and ATP measured in the hSC-CMs treated with SMKI. **(A–D)** show the results for the PI3K-pan, PI3K isoform-specific, GSK-3 and ROCK kinase inhibitors, respectively. The data represent the average of 3–5 repeats for each time point. The apoptosis graphs show mean +/- SEM of kinetic data sampled every 2 h after the addition of compounds. The fractional change from baseline determined for each concentration is compared to that of vehicle control (DMSO). The significance is indicated by asterisk (or ns for p>0.1) next to the specific concentration in the graph legends: *$p < 0.1$, **$p < 0.01$, ***$p < 0.001$, ****$p < 0.0001$. Two-dimensional radar charts present multivariate drug-induced functional profiles in hSC-CMs. They display fractional change from baseline in beating rate, base impedance and ATP content across ascending concentrations of drugs after the short- (2 h) and long-term (24 h) treatment.

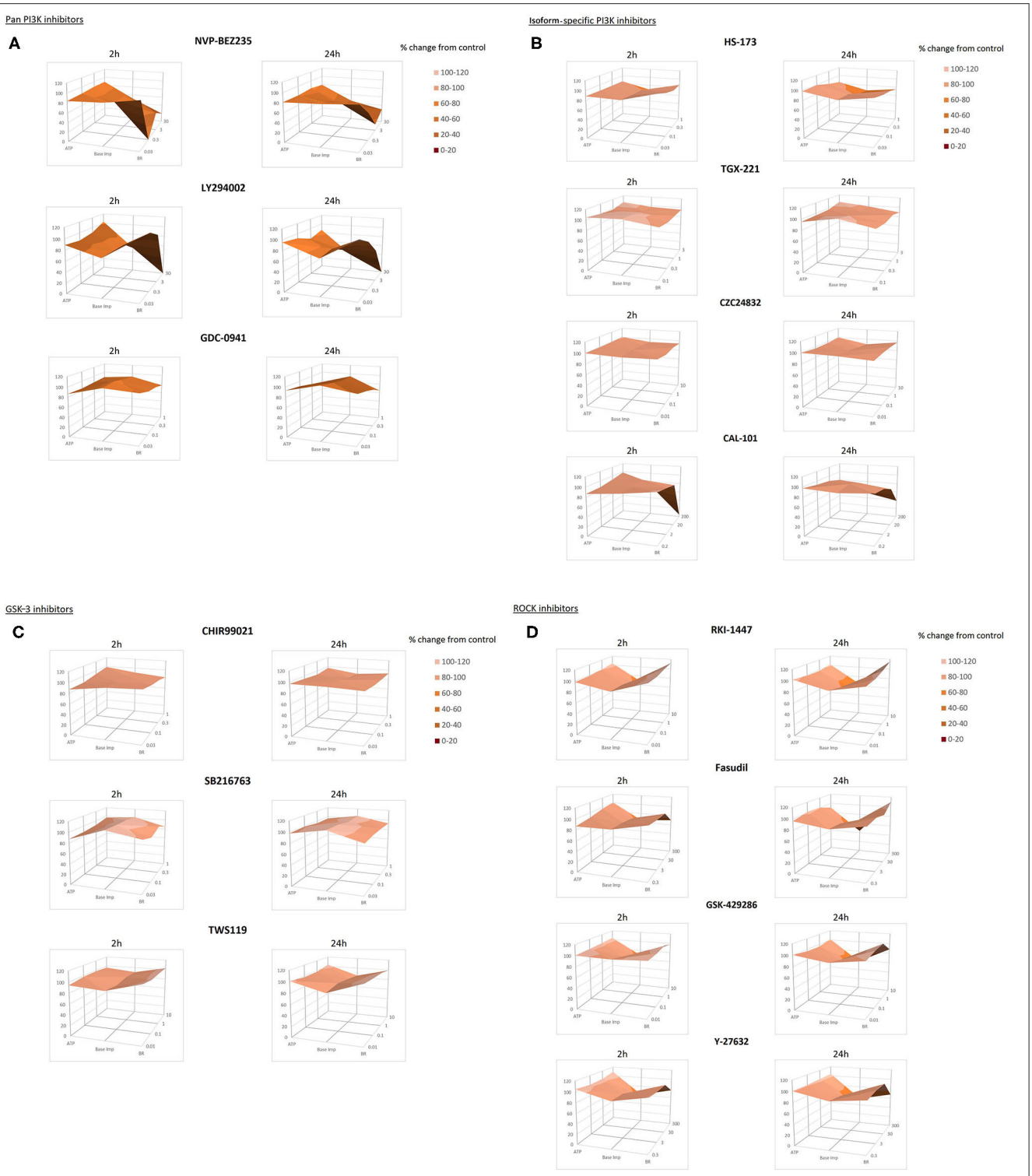

FIGURE 3 | Surface plots for beating rate, base impedance and ATP measured in hSC-CMs after 2 and 24 h of incubation with kinase inhibitors. **(A–D)** show the results for the PI3K-pan, PI3K isoform-specific, GSK-3 and ROCK kinase inhibitors, respectively. Surface plots intend to show compound-specific relationships between individual functional parameters in hSC-CMs: beating rate, base impedance and ATP content. The plots are constructed using the average of 3–5 repeats for each parameter. Similar colors indicate the areas that are in the same range of values specified in the legend.

spontaneous beating rate in a concentration-and time-dependent manner. The PI3K p110β and PI3K p110γ-specific compounds (TGX-221 and CZC24832) did not have any effect on the hSC-CMs function.

The GSK-3 inhibitors CHIR99021, SB 216763 and TWS119 (**Figure 2C**) did not produce functionally relevant changes neither in base impedance nor in beating rate of hSC-CMs.

Incubation of hSC-CMs with ROCK inhibitors RKI-1447, Fasudil, Y-27632 and GSK-429286 (**Figure 2D**) resulted in a concentration-and time-dependent decrease in base impedance. Additionally, the Y-27632 treatment also reduced cardiomyocyte beating at both 2 h and 24 h time points, while Fasudil inhibited the beating rate (by ∼30%) only at the highest test concentration after 2 h of incubation.

ATP Level

Changes in ATP concentrations provoked by treatment of hSC-CMs with the kinase inhibitors are also included in radar plots in **Figures 2A–D**. The measurements were conducted in satellite plates after 2 and 24 h of incubation concomitantly with the readouts for the base impedance and beating rate.

The ATP level in hSC-CMs treated with pan-PI3K inhibitors NVP-BEZ235, LY 294002, GDC-0941, PI3K p110α inhibitor HS-173 and PI3K p110δ inhibitor CAL-101 was decreased by ∼20–25 % only after 24 h of incubation (**Figures 2A,B**). And the PI3K p110β and PI3K p110γ-specific compounds (TGX-221 and CZC24832) did not have any effect on the ATP level in hSC-CMs up to the highest test concentrations.

Similar to the absence of their effect on functional parameters, the GSK-3 inhibitors CHIR99021, SB 216763 and TWS119 did not impact the ATP level in hSC-CMs (**Figure 2C**).

Among ROCK inhibitors RKI-1447, Fasudil, Y-27632 and GSK-429286, only exposure to the Fasudil top concentration produced a slight (9%) reduction in the ATP content (**Figure 2D**).

Correlation Between the hSC-CM Characteristics

Changes in base impedance, beating rate and ATP described above were plotted on a three-dimensional surface to visualize potential interactions and compare short-(2 h) and long-term (24 h) effects of the kinase inhibitors on all three parameters. The resulting surface plots are shown in **Figure 3** sorted according to the kinase class and specificity of the inhibitors: panels A, B, C and D show the results for the PI3K-pan, PI3K isoform-specific, GSK-3 and ROCK kinase inhibitors, respectively. The colors represent values within the same range in 20%-step intervals. The three-dimensional surface is constructed using the average values of parameter changes. In the absence of the effect the surface is perfectly flat, while morphology, smoothness, and topological measures of the surface allow us to visualize the parameter changes. When looking for trends and comparing compound-, target- or time-specific changes in the sets of data, this visualization was especially useful.

Comparison of the surfaces across the set of kinase inhibitors highlighted pronounced effects of the pan-PI3K inhibitors NVP-BEZ235 and LY 294002 and the PI3K p110δ inhibitor CAL-101 on the cardiomyocyte function reflected by the abrupt shape and shading change (**Figures 3A,B**). At the same time the surfaces generated for the pan-PI3K inhibitor GDC-0941, the PI3K p110β inhibitor TGX-221 and the PI3K p110γ-specific inhibitor CZC24832 exhibited only a minor topographical remodeling reflecting physiologically non-relevant change below 20% in the hSC-CMs parameters.

The almost flat 3D surfaces for the GSK-3 inhibitors CHIR99021, SB 216763 and TWS119 (**Figure 3C**) demonstrated minimal functional effect of these compounds in hSC-CMs. And the specific surface deformation for ROCK inhibitors RKI-1447, Fasudil, Y-27632 and GSK-429286 (**Figure 3D**) spotted the concentration-dependent effects of these compounds on the cardiomyocyte base impedance/viability.

In general, these 3D surface plots were helpful for viewing the relationship among variables, while also assisting in the initial qualitative comparisons between the subsets of data. Subsequently, Pearson's coefficient matrix presented in **Table 2** was calculated to quantify the correlation showing the relationship between the parameters measured in the study for 8 compounds that induced apoptosis and notable changes in the hSC-CMs function and the ATP level.

The results showed a good overall correlation among four measured parameters with 91% of the Pearson's coefficient values being between ± 0.50 and ± 1. And some of these quantitative indexes had direct physiological relevance for the cellular process. For instance, correlation between the caspase-3/7 activation and the ATP level was mainly negative indicating an inverse relationship, which most likely reflected the ATP consumption during apoptosis, while impedance and beating rate demonstrated a strong positive correlation indicating the concomitant reduction in cell viability and beating rate.

Interestingly, a time-dependent switch was observed for some parameter pairs. For example, initial caspase-3/7 activation by the kinase inhibitors correlated positively with base impedance and beating rate for almost all compounds after 2 h of incubation. After 24 h the relationship inverted, and the correlation became mainly negative highlighting decline in function with the advance of apoptosis in the cells. The opposite tendency was observed for the correlation between base impedance and the ATP level, which was negative at the early stage and became positive after the prolonged exposure to the compounds. This dynamic highlighted different mechanisms involved in short-vs. long-term effects.

A few compounds such as SB 216763, Fasudil and sometimes HS-173 did not follow these general trends in the parameter correlation. These exceptions may, on one hand, be due to the minimal changes in parameter values and of no physiological importance. On the other hand, they may reflect unknown compound-specific mechanisms of action.

Translation of the *in vitro* Results Into the Clinic

Among the test compounds evaluated in our study, three PI3K inhibitors Dactolisib, Pictilisib and Idelalisib have been used for treatment of malignancies in the clinic. According to the information collated in **Table 3**, the test concentrations used in

TABLE 2 | Pearson's coefficient matrix between sets of parameters in hSC-CMs.

	2h						24h					
Compound	**Caspase: ATP**	**Caspase: Base Imp**	**Caspace: BR**	**BR: ATP**	**BR: Base Imp**	**Base Imp: ATP**	**Caspase: ATP**	**Caspase: Base Imp**	**Caspace: BR**	**BR: ATP**	**BR: Base Imp**	**Base Imp: ATP**
BEZ235	−0.83	0.74	0.93	−0.91	0.93	−0.88	−0.78	−0.51	−0.40	−0.12	0.92	0.18
LY 294002	−0.70	0.80	0.82	−0.97	1.00	−0.96	−0.46	−1.00	−0.99	0.51	0.98	0.44
GDC-0941	−0.39	0.86	0.93	−0.35	0.86	−0.78	−0.93	−0.71	−0.94	1.00	0.91	0.92
HS-173	0.99	0.77	0.99	0.97	0.71	0.85	−0.93	−0.91	−0.98	0.92	0.94	0.98
CAL-101	−0.93	0.67	0.81	−0.94	0.97	−0.84	−0.93	−1.00	−0.99	0.97	0.98	0.90
SB 216763	0.96	−0.96	−0.52	−0.61	0.73	−0.97	−0.82	−0.71	0.42	−0.16	−0.62	0.83
Fasudil	−0.98	0.82	0.78	−0.81	0.99	−0.86	−0.84	−0.95	0.92	−0.75	−0.77	0.73
Y-27632	−0.72	0.71	0.53	−0.88	0.96	−0.85	0.95	−0.94	−0.89	−0.76	0.73	−1.00

Values are formatted using 2-color scale in the range from −1(min) to 1(max). BR, beating rate; Base Imp, base impedance.

the *in vitro* cardiomyocyte study covered the range of compound efficacy in patients. The latter was substantially higher than their IC_{50}-based biological activity determined in the cancer cell-based systems.

A 10-fold and higher safety margin between the clinical exposure and the lowest *in vitro* test concentration with functionally relevant (>20%) reduction in hSC-CMs indices (underlined in **Table 3**) can be estimated for these drugs. Therefore, one could expect cardiac adverse events if the free plasma concentration increases 10-fold above the expected free C_{max} e.g., due to risk factors and/or comorbidities in the clinic.

DISCUSSION

Not only does predicting drug-induced cardio toxicity remain a pharma-industry challenge, it is also one of the major causes of drug withdrawal during clinical development, accounting for up to 33% of drug failure (49). Because regenerative capacity of the heart ceases dramatically after birth and the sources of primary adult cardiomyocytes are limited, commercially available human stem cell-derived cardiomyocytes hold great promise for the study of cardiac biology, pharmacology and safety in drug development.

To make cardiotoxicity testing more biologically relevant, the FDA-sponsored Cardiac Safety Research Consortium and the not-for-profit Health and Environmental Sciences Institute have recommended, as a part of the Comprehensive *in vitro* Proarrhythmia Assay (CiPA) initiative, including hSC-CMs into the nonclinical drug cardiotoxicity assessment with the goal of using them as an integrating model system bridging single receptor-based *in vitro* results and clinical data (50).

While the use of hSC-CMs for prediction of drug-induced arrhythmias has been recently evaluated (51), their application for cardio-oncology is still unexplored. This study attempted to look into utility of hSC-CMs at the pre-clinical stage to predict cardiac adverse effects of SMKIs used for targeted anti-cancer therapy in the clinic.

A set of reference drugs inhibiting individual kinases from the main three classes (PI3Ks, GSK-3s and ROCKs) critical for cardiac function was selected to evaluate the action of their inhibition on hSC-CMs function. In addition to the direct functional readouts of cell viability and beating rate on CardioExcyte® 96, measurements of apoptosis kinetics and ATP were integrated into the experiments enabling mechanistic insight.

An early event in apoptosis is activation of caspases, of which caspase-3 is the most critical apoptotic protease playing an important role in apoptosis of myocardial cells with functional importance (52). Therefore, we monitored the induction of caspase-3/7 to investigate the involvement of SMKIs in apoptosis in hSC-CMs. The kinase-specific caspase-3/7 activation profiles were observed using live-cell imaging analysis for the first time in these cells. They demonstrated the importance of the kinase signaling pathway and selectivity of SMKIs for the apoptosis development in hSC-CMs. Targeting of multiple kinases with the pan-PI3K inhibitors to achieve maximal suppression of

TABLE 3 | Compound biological activity and efficacy information.

Inhibitor	Target IC_{50} (μM)				Test conc. (μM)	C_{max} free (μM)	Reference
PI3KIs	**p110α**	**p110β**	**p110δ**	**p110γ**			
NVP-BEZ235 (Dactolisib)	0.004	0.075	0.007	0.005	0.03 - **0.3** - 3 - 30	**0.02**	IC_{50}: (23–25) C_{max}: (26)
LY 294002	0.5	0.973	0.57		0.3 - 3 - 30 - 300		(27)
GDC-0941 (Pictilisib)	0.003	0.033	0.003	0.075	0.03 - 0.1 - 0.3 - **1**	**0.1**	IC_{50}: (28) C_{max}: (29, 30)
HS-173	0.0008				0.03 - 0.1 - 0.3 - 1		IC_{50}: (31)
TGX-221		0.005			0.1 - 0.3 - 1 - 3		IC_{50}: (32)
CAL-101 (Idelalisib)	0.82	0.056	0.0025	0.089	0.2 - 2 - **20** - 200	**0.7**	IC_{50}: (33) C_{max}: (34)
CZC24832		1.1		0.027	0.01 - 0.1 - 1 - 10		IC_{50}: (35)
ROCKs	**ROCK1**	**ROCK2**					
RKI-1447	0.0145	0.0062			0.1 - 0.3 - 1 - 3		IC_{50}: (36)
Fasudil	0.465	0.509			0.3 - 3 - 30 - 300		IC_{50}: (37, 38)
Y-27632	0.093	0.089			0.3 - 3 - 30 - 300		IC_{50}: (39–43)
GSK-429286	0.014	0.063			0.03 - 0.3 - 3 - 30		IC_{50}: (44, 45)
GSK-3s	**GSK-3α**	**GSK-3β**					
CHIR99021	0.01	0.0067			0.03 - 0.1 - 0.3 - 1		IC_{50}: (46)
SB 216763	0.034				0.03 - 0.1 - 0.3 - 1		IC_{50}: (47)
TWS119		0.03			0.03 - 0.1 - 0.3 - 1		IC_{50}: (48)

The lowest in vitro test concentration with functionally relevant (>20%) reduction in hSC-CMs indices is indicated by the bold format.

activity of that pathway may be a favorable approach in a number of cancers. However, this pathway obviously is also crucial for cardiomyocyte homeostasis and survival, and its inhibition quickly triggers apoptosis resulting in reduced viability and beating of the cardiomyocytes observed for the pan-PI3K inhibitors in this study. Improving the isoform selectivity may help to ameliorate the cardiotoxicity profile of drug candidates as observed in hSC-CMs incubated with the PI3K-β and γ-specific inhibitors. This observation supports the published evidence of cardioprotective effects of the PI3K-α inhibition in heart failure (53) and doxorubicin-induced cardiotoxicity (54). However, this does not apply to all isoforms. The cardiotoxic effects observed in hSC-CMs incubated with HS-173 clearly illustrates a decisive role the PI3K-α signaling inhibition plays in the process of cell death in the heart. In line with our finding, previous studies demonstrated that the use of PI3K-α inhibitors may directly or indirectly compromise cardiac function (55). The PI3K-α pathway inhibition promoted heart atrophy, biventricular remodeling, and increased susceptibility to doxorubicin toxicity in mice (56). Rescue treatment using p38 MAPK inhibitors showed potential as a therapeutic strategy in reversing this chemotherapy-induced cardiotoxicity. Early signal detection in hSC-CMs would be particularly important for risk mitigation and disease modeling since many cardioprotective effects of the PI3K signaling pathways only emerge in heart failure (53, 57, 58) and patients with pre-existing cardiac disease or risk factors, such as hypertension or metabolic syndrome may be at higher risk when given PI3K-α inhibitors. And early clinical studies may not fully appreciate the cardiovascular effects of these agents in the vulnerable population.

Tissue specificity may be another way to avoid potential cardiotoxicity. For instance, PI3Kδ, which is mainly expressed in hemopoietic cells, may be devoid of possible side effects in cardiomyocytes. Conversely to this expectation, the PI3Kδ inhibitor still induced apoptosis, which correlated with the reduced cardiomyocyte viability and beating rate in our hSC-CMs experiments. However, as CAL-101 triggered cardiotoxicity mainly at higher concentrations, it may also be related to the concentration-dependent decrease in selectivity similar to that of the pan-PI3K inhibitors (see **Table 3**).

Shortly after the start of treatment with the GSK-3α inhibitor, a pronounced surge in the caspase activation was detected. However, this surge in activation did not translate into the relevant functional changes in hSC-CMs. This caspase activation pattern may reflect the GSK's regulation by AKT that induces pro-apoptotic factors downstream of PI3Ks. The inhibition of PI3K-α and GSK-3 α is cytotoxic in hSC-CMs. Therefore, compounds that interfere with the PI3K–AKT pathway should be carefully examined, because they can cause cardiotoxicity and cardiovascular effects.

Altogether, our findings in hSC-CMs suggest multiple, critical kinase-regulated pathways that, if inhibited, could aggravate cardiotoxicity. Therefore, an early target assessment including the expression profile in various tissues and tumors and target selectivity (e.g., KinomeScan) profiling of the SMKIs against multiple targets should help eliminating late-stage cardiotoxicity findings. And hSC-CMs-based assays would enable further *in vitro* testing of adverse effects induced by different SMKIs in combination with other cancer therapies and comorbidities.

Development of integrative functional assays for kinase profiling by multiplexing apoptosis measurement with functional readouts and the ATP assessment can enable researchers to better predict cardiotoxicity potential and/or elucidate an underlying mechanism. Implementation of the next generation hybrid biosensor equipment (e.g., Agilent xCELLigence RTCA eSight), which combines the strengths of real-time impedance monitoring with specificity of the live cell imaging, would facilitate integration of the information richness and analytic sensitivity. Correlation between the parameters in hSC-CMs can also assist in characterizing the basic physiology and pharmacology of these cells and their utility for cardiac safety application.

The evaluated cellular endpoints exhibited a good, and physiologically meaningful, correlation. For example, beating rate and impedance demonstrated a strong positive correlation that reflected the slowing of the beating rate following the reduction in cell viability.

Furthermore, the ATP increase which accompanied the caspase-3/7 activation at the early stage (2 h) was reversed with the advance of apoptosis. Beating cardiomyocytes consume vast amounts of ATP. The average ATP concentration determined in the hSC-CM under control conditions was around 5 μM. It is utilized to maintain cellular homeostasis including the necessary gradients of ions driven by the various ion pumps and channels, while also used to generate contractile activity of the sarcomeres. Therefore, disrupting the balance of ongoing energy generation and utilization would result in profound abnormalities in cardiac function. The ATP depletion induced by some SMKIs would activate AMPK, which along with GSK3s inhibits protein synthesis, thereby conserving energy stores. And the negative correlation between the caspase-3/7 activation and the ATP level most likely corresponded to the cellular ATP depletion with the progress of apoptosis after the 24 h of treatment. This kind of time-dependent dynamic observed for the parameter correlation can be integrated with mechanistic models to generate testable predictions in the future. Capturing the peak effect of the test compounds would enable selection of an optimum time-point for follow-up experiments.

As with any experimental model, studies with human stem cell-derived cardiomyocytes are not without limitations. While hSC-CMs have enabled a considerable breakthrough in studying cardiac biology, pharmacology and safety during the last decade, their maturation status poses a serious limitation due to potential differences in signaling pathways from those regulating the main physiological process in adult heart muscle cells. Therefore, benchmarking the target expression profiles to those in the adult human cardiomyocytes is recommended to support translation of the hSC-CM-based preclinical data. The appropriate gene expression profiles for all SMKI targets in this study was confirmed using our internal mRNA gene expression data base (data not shown). It is also important to establish the relationship between cardiotoxicity observed *in vitro* and its predicted clinical manifestation. Studying trastuzumab, sunitinib and other drugs with clinically established cardiotoxic profiles and including them as positive controls should enable setting translational standards for the *in vitro* assays in the future. An example of modeling doxorubicin-induced cardiotoxicity in hSC-CMs has shown that the *in vitro* cellular model recapitulates many of the features of this adverse drug reaction (59). These included dose-dependent increases in apoptotic and necrotic cell death, reactive oxygen species production, mitochondrial dysfunction and slowing cardiomyocyte beating rate which characterize cardiac tissue damage at the cellular level and serve as *in vitro* surrogates of the compromised clinical phenotype. Combining functional cellular monitoring with live imaging allowed us to capture changes in cellular indices for translation of the *in vitro* results into the clinic. It is expected that functionally relevant changes in these parameters at appropriate plasma concentrations would indicate a potential risk. For the clinically tested PI3K inhibitors Dactolisib, Pictilisib and Idelalisib, at least a 10-fold safety margin between the clinical exposure and the lowest *in vitro* test concentration with functionally relevant reduction in cellular indices has been determined in our hSC-CMs assay. Therefore, one would not expect to see cardiotoxicity before the free plasma concentration increases 10-fold above the expected free C_{max}. Clinical trials with these drugs did not report cases of cardiac adverse events. However, the FDA adverse reaction reports from a general population showed that Idelalisib was associated with cases of atrial fibrillation, acute myocardial infarction and congestive heart failure, thus highlighting the need to further assess the cardiovascular risk of Idelalisib in postmarketing surveillance trials (60).

The real risk of cardiotoxicity is not known until the drugs become approved and used in a broader population. New tools such as hSC-CMs derived from patients will allow investigators to directly explore the mechanisms of kinase inhibitor-induced cardiotoxicity and potential mitigation strategies. Recent studies have demonstrated that patient-specific hiPSC-CMs can be utilized to reproduce the cardiotoxic effect of doxorubicin (61) and tyrosine kinase inhibitors *in vitro* (62). Furthermore, lack of significant cardiovascular co-morbidities in patients in early clinical trials (63) makes it difficult to predict true rates of cardiotoxicity for the reverse translation. The predictive value of new hSC-CMs preclinical models can potentially be determined through patient monitoring and the use of the real-world evidence in the future (64).

In summary, the present study evaluates an integrative approach to study the SMKI cardiotoxicity using hSC-CMs and reveals the main challenges of pre-clinical findings that require follow-up investigations and impact drug development programs. We foresee the introduction of new technologies to aid in discovery and to develop early safety methods for regulatory strategies translating biomedical science for novel SMKIs therapeutics into the clinic.

DATA AVAILABILITY STATEMENT

The original contributions presented in the study are included in the article/**Supplementary Material**, further inquiries can be directed to the corresponding author.

AUTHOR CONTRIBUTIONS

SK conceived the study approach and planning. RZ performed and reviewing experiments, data

analysis, and contributed to writing. FH conducted the data analysis. LP did the data evaluation and writing and reviewing of the manuscript. All authors contributed to the article and approved the submitted version.

SUPPLEMENTARY MATERIAL

The Supplementary Material for this article can be found online at: https://www.frontiersin.org/articles/10.3389/fcvm.2021.639824/full#supplementary-material

REFERENCES

1. Vieth M, Sutherland JJ, Robertson DH, Campbell RM. Kinomics: characterizing the therapeutically validated kinase space. *Drug Discovery Today*. (2005) 10:839–46. doi: 10.1016/S1359-6446(05)03477-X
2. Cohen P. The role of protein phosphorylation in human health and disease. *Eur J Bio.* (2001) 268:5001–10. doi: 10.1046/j.0014-2956.2001.02473.x
3. Kremer JM, Bloom BJ, Breedveld FC, Coombs JH, Fletcher MP, Gruben D, et al. The safety and efficacy of a JAK inhibitor in patients with active rheumatoid arthritis: results of a double-blind, placebo-controlled phase IIa trial of three dosage levels of CP-690,550 versus placebo. *Arthritis Rheumatism.* (2009) 60:1895–905. doi: 10.1002/art.24567
4. Skvara H, Dawid M, Kleyn E, Wolff B, Meingassner JG, Knight H, et al. The PKC inhibitor AEB071 may be a therapeutic option for psoriasis. *J Clin Invest.* (2008) 118:3151–9. doi: 10.1172/JCI35636
5. Busse D, Yakes FM, Lenferink AE, Arteaga CL. Tyrosine kinase inhibitors: rationale, mechanisms of action, and implications for drug resistance. *Semin Oncol.* (2001) 28(5 Suppl 16): 47–55. doi: 10.1053/sonc.2001.28550
6. Ho AL, Bendell JC, Cleary JM, Schwartz GK, Burris HA, Oakes P, et al. Phase I, open-label, dose-escalation study of AZD7762 in combination with irinotecan (irino) in patients (pts) with advanced solid tumors. *J Clin Oncol.* (2011) 29(15_suppl):3033. doi: 10.1200/jco.2011.29.15_suppl.3033
7. Lim J, Taoka BM, Lee S, Northrup A, Altman MD, Sloman DL, et al. *Pyrazolo[1,5-a]pyrimidines as mark inhibitors*. Rahway, NJ: Merck Sharp & Dohme Corp (2011).
8. Venter JC, Adams MD, Myers EW, Li PW, Mural RJ, Sutton GG, et al. The sequence of the human genome. *Science.* (2001) 291:1304–51. doi: 10.1126/science.1058040
9. Force T, Kolaja KL. Cardiotoxicity of kinase inhibitors: the prediction and translation of preclinical models to clinical outcomes. *Nat Rev Drug Dis.* (2011) 10:111–26. doi: 10.1038/nrd3252
10. Zhang T, Kohlhaas M, Backs J, Mishra S, Phillips W, Dybkova N, et al. CaMKIIδ isoforms differentially affect calcium handling but similarly regulate HDAC/MEF2 transcriptional responses. *J Biol Chem.* (2007) 282:35078–87. doi: 10.1074/jbc.M707083200
11. Barry SP, Davidson SM, Townsend PA. Molecular regulation of cardiac hypertrophy. *Int J Biochem Cell Biol.* (2008) 40:2023–39. doi: 10.1016/j.biocel.2008.02.020
12. Matsui T, Tao J, del Monte F, Lee K-H, Li L, Picard M, et al. Akt activation preserves cardiac function and prevents injury after transient cardiac ischemia *in vivo*. *Circulation*. (2001) 104:330–35. doi: 10.1161/01.CIR.104.3.330
13. Liu P, Cheng H, Roberts TM, Zhao JJ. Targeting the phosphoinositide 3-kinase pathway in cancer. *Nat Rev Drug Dis.* (2009) 8:627–44. doi: 10.1038/nrd2926
14. Litvinuková M, Talavera-López C, Maatz H, Reichart D, Worth CL, Lindberg EL, et al. Cells of the adult human heart. *Nature*. (2020) 588:466–72. doi: 10.1038/s41586-020-2797-4
15. Force T, Krause DS, Van Etten RA. Molecular mechanisms of cardiotoxicity of tyrosine kinase inhibition. *Nat Rev Cancer.* (2007) 7:332–44. doi: 10.1038/nrc2106
16. Kerkelä R, Grazette L, Yacobi R, Iliescu C, Patten R, Beahm C, et al. Cardiotoxicity of the cancer therapeutic agent imatinib mesylate. *Nat Med.* (2006) 12:908–16. doi: 10.1038/nm1446
17. Peters MF, Lamore SD, Guo L, Scott CW, Kolaja KL. Human stem cell-derived cardiomyocytes in cellular impedance assays: bringing cardiotoxicity screening to the front line. *Cardiov Toxicol.* (2015) 15:127–39. doi: 10.1007/s12012-014-9268-9
18. Guo L, Coyle L, Abrams RMC, Kemper R, Chiao ET, Kolaja KL. Refining the human iPSC-cardiomyocyte arrhythmic risk assessment model. *Toxicol Sci.* (2013) 136:581–94. doi: 10.1093/toxsci/kft205
19. Lamore SD, Kamendi HW, Scott CW, Dragan YP, Peters MF. Cellular impedance assays for predictive preclinical drug screening of kinase inhibitor cardiovascular toxicity. *Toxicol Sci.* (2013) 135:402–13. doi: 10.1093/toxsci/kft167
20. Scott CW, Zhang X, Abi-Gerges N, Lamore SD, Abassi YA, Peters MF. An impedance-based cellular assay using human iPSC-derived cardiomyocytes to quantify modulators of cardiac contractility. *Toxicol Sci.* (2014) 142:331–8. doi: 10.1093/toxsci/kfu186
21. Doerr L, Thomas U, Guinot DR, Bot CT, Stoelzle-Feix S, Beckler M, et al. New easy-to-use hybrid system for extracellular potential and impedance recordings. *J Lab Auto.* (2015) 20:175–88. doi: 10.1177/2211068214562832
22. Bot CT, Juhasz K, Haeusermann F, Polonchuk L, Traebert M, Stoelzle-Feix S. Cross - site comparison of excitation-contraction coupling using impedance and field potential recordings in hiPSC cardiomyocytes. *J Pharmacol Toxicol Meth.* (2018) 93:46–58. doi: 10.1016/j.vascn.2018.06.006
23. Grasso CS, Tang Y, Truffaux N, Berlow NE, Liu L, Debily M-A, et al. Functionally defined therapeutic targets in diffuse intrinsic pontine glioma. *Nat Med.* (2015) 21:555–9. doi: 10.1038/nm.3855
24. Pei Y, Moore CE, Wang J, Tewari AK, Eroshkin A, Cho Y-J, et al. An animal model of MYC-driven medulloblastoma. *Cancer Cell.* (2012) 21:155–67. doi: 10.1016/j.ccr.2011.12.021
25. Wilson TR, Fridlyand J, Yan Y, Penuel E, Burton L, Chan E, et al. Widespread potential for growth-factor-driven resistance to anticancer kinase inhibitors. *Nature.* (2012) 487:505–9. doi: 10.1038/nature11249
26. Rodon J, Pérez-Fidalgo A, Krop IE, Burris H, Guerrero-Zotano A, Britten CD, et al. Phase 1/1b dose escalation and expansion study of BEZ235, a dual PI3K/mTOR inhibitor, in patients with advanced solid tumors including patients with advanced breast cancer. *Cancer Chemother Pharmacol.* (2018) 82:285–98. doi: 10.1007/s00280-018-3610-z
27. Chaussade C, Rewcastle GW, Kendall JD, Denny WA, Cho K, Grønning LM, et al. Evidence for functional redundancy of class IA PI3K isoforms in insulin signalling. *Bio J.* (2007) 404:449–58. doi: 10.1042/BJ20070003
28. Folkes AJ, Ahmadi K, Alderton WK, Alix S, Baker SJ, Box G, et al. The identification of 2-(1 H -Indazol-4-yl)-6-(4-methanesulfonyl-piperazin-1-ylmethyl)-4-morpholin-4-yl-thieno[3,2- d]pyrimidine (GDC-0941) as a potent, selective, orally bioavailable inhibitor of class I PI3 kinase for the treatment of cancer †. *J Med Chem.* (2008) 51:5522–32. doi: 10.1021/jm800295d
29. Salphati L, Pang J, Plise EG, Chou B, Halladay JS, Olivero AG, et al. Preclinical pharmacokinetics of the novel PI3K inhibitor GDC-0941 and prediction of its pharmacokinetics and efficacy in human. *Xenobiotica.* (2011) 41:1088–99. doi: 10.3109/00498254.2011.603386
30. Sarker D, Ang JE, Baird R, Kristeleit R, Shah K, Moreno V, et al. First-in-human phase I study of pictilisib (GDC-0941), a potent pan-class I phosphatidylinositol-3-kinase (PI3K) Inhibitor, in patients with advanced solid tumors. *Clin Cancer Res.* (2015) 21:77–86. doi: 10.1158/1078-0432.CCR-14-0947
31. Kim O, Jeong Y, Lee H, Hong S-S, Hong S. Design and synthesis of imidazopyridine analogues as inhibitors of phosphoinositide 3-kinase signaling and angiogenesis. *J Med Chem.* (2011) 54:2455–66. doi: 10.1021/jm101582z
32. Jackson SP, Schoenwaelder SM, Goncalves I, Nesbitt WS, Yap CL, Wright CE, et al. PI 3-kinase p110β: a new target for antithrombotic therapy. *Nat Med.* (2005) 11:507–14. doi: 10.1038/nm1232

33. Lannutti BJ, Meadows SA, Herman SEM, Kashishian A, Steiner B, Johnson AJ, et al. CAL-101, a p110δ selective phosphatidylinositol-3-kinase inhibitor for the treatment of B-cell malignancies, inhibits PI3K signaling and cellular viability. *Blood.* (2011) 117:591–4. doi: 10.1182/blood-2010-03-275305
34. Wharf C, Kingdom U. *Assessment Report CHMP Sassessment Report*. London, UK: EMA (2011).
35. Bergamini G, Bell K, Shimamura S, Werner T, Cansfield A, Müller K, et al. A selective inhibitor reveals PI3Kγ dependence of TH17 cell differentiation. *Nat Chem Biol.* (2012) 8:576–82. doi: 10.1038/nchembio.957
36. Patel RA, Forinash KD, Pireddu R, Sun Y, Sun N, Martin MP, et al. RKI-1447 is a potent inhibitor of the Rho-associated ROCK kinases with anti-invasive and antitumor activities in breast cancer. *Can Res.* (2012) 72:5025–34. doi: 10.1158/0008-5472.CAN-12-0954
37. Ono-Saito N, Niki I, Hidaka H. H-series protein kinase inhibitors and potential clinical applications. *Pharmacol Ther.* (1999) 82:123–31. doi: 10.1016/S0163-7258(98)00070-9
38. Zhang Y, Kong H, Wu J, Lv T, Wang H, Qi L, et al. *A nitric oxide donor type Fasudil derivative and preparation method and use thereof.* Nanjing: China Pharmaceutical University (2020).
39. Hirose M, Ishizaki T, Watanabe N, Uehata M, Kranenburg O, Moolenaar WH, et al. Molecular dissection of the rho-associated protein kinase (p160ROCK)-regulated neurite remodeling in neuroblastoma N1E-115 cells. *J Cell Biol.* (1998) 141:1625–36. doi: 10.1083/jcb.141.7.1625
40. Ishizaki T, Uehata M, Tamechika I, Keel J, Nonomura K, Maekawa M, et al. Pharmacological properties of Y-27632, a specific inhibitor of rho-associated kinases. *Mol Pharmacol.* (2000) 57:976–83. Available online at: https://molpharm.aspetjournals.org/content/molpharm/57/5/976.full.pdf
41. Nakajima M, Katayama KI, Tamechika I, Hayashi K, Amano Y, Uehata M, et al. Wf-536 inhibits metastatic invasion by enhancing the host cell barrier and inhibiting tumour cell motility. *Clin Exp Pharmacol Physiol.* (2003) 30:457–63. doi: 10.1046/j.1440-1681.2003.03855.x
42. Shaw D, Hollingworth G, Soldermann N, Sprague E, Schuler W, Vangrevelinghe E, et al. Novel ROCK inhibitors for the treatment of pulmonary arterial hypertension. *Bioorg Med Chem Lett.* (2014) 24:4812–7. doi: 10.1016/j.bmcl.2014.09.002
43. Uehata M, Ishizaki T, Satoh H, Ono T, Kawahara T, Morishita T, et al. Calcium sensitization of smooth muscle mediated by a Rho-associated protein kinase in hypertension. *Nature.* (1997) 389:990–4. doi: 10.1038/40187
44. Goodman KB, Cui H, Dowdell SE, Gaitanopoulos DE, Ivy RL, Sehon CA, et al. Development of dihydropyridone indazole amides as selective rho-kinase inhibitors. *J Med Chem.* (2007) 50:6–9. doi: 10.1021/jm0609014
45. Nichols RJ, Dzamko N, Hutt JE, Cantley LC, Deak M, Moran J, et al. Substrate specificity and inhibitors of LRRK2, a protein kinase mutated in Parkinson's disease. *Bio J.* (2009) 424:47–60. doi: 10.1042/BJ20091035
46. Ring DB, Johnson KW, Henriksen EJ, Nuss JM, Goff D, Kinnick TR, et al. Selective glycogen synthase kinase 3 inhibitors potentiate insulin activation of glucose transport and utilization *in vitro* and *in vivo*. *Diabetes.* (2003) 52:588–95. doi: 10.2337/diabetes.52.3.588
47. Coghlan MP, Culbert AA, Cross DAE, Corcoran SL, Yates JW, Pearce NJ, et al. Selective small molecule inhibitors of glycogen synthase kinase-3 modulate glycogen metabolism and gene transcription. *Chem Biol.* (2000) 7:793–803. doi: 10.1016/S1074-5521(00)00025-9
48. Ding S, Wu TYH, Brinker A, Peters EC, Hur W, Gray NS, et al. Synthetic small molecules that control stem cell fate. *Proc Nat Acad Sci USA.* (2003) 100:7632–7. doi: 10.1073/pnas.0732087100
49. MacDonald JS, Robertson RT. Toxicity testing in the 21st Century: a view from the pharmaceutical industry. *Toxicol Sci.* (2009) 110:40–6. doi: 10.1093/toxsci/kfp088
50. Blinova K, Stohlman J, Vicente J, Chan D, Johannesen L, Hortigon-Vinagre MP, et al. Comprehensive translational assessment of human-induced pluripotent stem cell derived cardiomyocytes for evaluating drug-induced arrhythmias. *Toxicol Sci.* (2017) 155:234–47. doi: 10.1093/toxsci/kfw200
51. Gintant G, Kaushik EP, Feaster T, Stoelzle-Feix S, Kanda Y, Osada T, et al. Repolarization studies using human stem cell-derived cardiomyocytes: validation studies and best practice recommendations. *Regulator Toxicol Pharmacol.* (2020) 117:104756. doi: 10.1016/j.yrtph.2020.104756
52. Wang Q, Cui Y, Lin N, Pang S. Correlation of cardiomyocyte apoptosis with duration of hypertension, severity of hypertension and caspase-3 expression in hypertensive rats. *Exp Ther Med.* (2019) 17:2741–2274. doi: 10.3892/etm.2019.7249
53. Perino A, Ghigo A, Ferrero E, Morello F, Santulli G, Baillie GS, et al. Integrating Cardiac PIP3 and cAMP Signaling through a PKA Anchoring Function of p110γ. *Mol Cell.* (2011) 42:84–95. doi: 10.1016/j.molcel.2011.01.030
54. Li M, Sala V, De Santis MC, Cimino J, Cappello P, Pianca N, et al. Phosphoinositide 3-kinase gamma inhibition protects from anthracycline cardiotoxicity and reduces tumor growth. *Circulation.* (2018) 138:696–711. doi: 10.1161/CIRCULATIONAHA.117.030352
55. Sadasivan C, Zhabyeyev P, Labib D, White JA, Paterson DI, Oudit GY. Cardiovascular toxicity of PI3Kα inhibitors. *Clin Sci.* (2020) 134:2595–622. doi: 10.1042/CS20200302
56. McLean BA, Patel VB, Zhabyeyev P, Chen X, Basu R, Wang F, et al. PI3Kα pathway inhibition with doxorubicin treatment results in distinct biventricular atrophy and remodeling with right ventricular dysfunction. *J Am Heart Asso.* (2019) 8:e010961. doi: 10.1161/JAHA.118.010961
57. Damilano F, Franco I, Perrino C, Schaefer K, Azzolino O, Carnevale D, et al. Distinct effects of leukocyte and cardiac phosphoinositide 3-kinase γ activity in pressure overload–induced cardiac failure. *Circulation.* (2011) 123:391–9. doi: 10.1161/CIRCULATIONAHA.110.950543
58. Patel VB, Zhabyeyev P, Chen X, Wang F, Paul M, Fan D, et al. PI3Kα-regulated gelsolin activity is a critical determinant of cardiac cytoskeletal remodeling and heart disease. *Can Res.* (2018) 72:5025–34.
59. Maillet A, Tan K, Chai X, Sadananda SN, Mehta A, Ooi J, et al. Modeling doxorubicin-induced cardiotoxicity in human pluripotent stem cell derived-cardiomyocytes. *Sci Rep.* (2016) 6:25333. doi: 10.1038/srep25333
60. Mahida H, Gharia B, Ugoeke N, Maludum O, Asif A, Calderon D. Evaluation of cardiovascular adverse events associated with ibrutinib, venetoclax and idelalisib used in treatment of chronic lymphocytic leukemia. *Circulation.* (2018) 138. doi: 10.1161/circ.138.suppl_1.11835
61. Burridge PW, Li YF, Matsa E, Wu H, Ong S-G, Sharma A, et al. Human induced pluripotent stem cell–derived cardiomyocytes recapitulate the predilection of breast cancer patients to doxorubicin-induced cardiotoxicity. *Nat Med.* (2016) 22:547–56. doi: 10.1038/nm.4087
62. Sharma A, Burridge PW, McKeithan WL, Serrano R, Shukla P, Sayed N, et al. High-throughput screening of tyrosine kinase inhibitor cardiotoxicity with human induced pluripotent stem cells. *Sci Transl Med.* (2017) 9:eaaf2584. doi: 10.1126/scitranslmed.aaf2584
63. Thavendiranathan P, Abdel-Qadir H, Fischer HD, Camacho X, Amir E, Austin PC, et al. Breast cancer therapy–related cardiac dysfunction in adult women treated in routine clinical practice: a population-based cohort study. *J Clin Oncol.* (2016) 34:2239–46. doi: 10.1200/JCO.2015.65.1505
64. Davies MR, Martinec M, Walls R, Schwarz R, Mirams GR, Wang K, et al. Use of patient health records to quantify drug-related pro-arrhythmic risk. *Cell Rep Med.* (2020) 1:100076. doi: 10.1016/j.xcrm.2020.100076

Conflict of Interest: All authors were employed by F. Hoffmann - La Roche.

frontiers in Cardiovascular Medicine

REVIEW
published: 27 July 2021
doi: 10.3389/fcvm.2021.694711

Updates on Anticancer Therapy-Mediated Vascular Toxicity and New Horizons in Therapeutic Strategies

*Po-Yen Hsu, Aynura Mammadova, Nadia Benkirane-Jessel, Laurent Désaubry and Canan G. Nebigil**

INSERM UMR 1260, Regenerative Nanomedicine, University of Strasbourg, FMTS (Fédération de Médecine Translationnelle de l'Université de Strasbourg), Strasbourg, France

Vascular toxicity is a frequent adverse effect of current anticancer chemotherapies and often results from endothelial dysfunction. Vascular endothelial growth factor inhibitors (VEGFi), anthracyclines, plant alkaloids, alkylating agents, antimetabolites, and radiation therapy evoke vascular toxicity. These anticancer treatments not only affect tumor vascularization in a beneficial manner, they also damage ECs in the heart. Cardiac ECs have a vital role in cardiovascular functions including hemostasis, inflammatory and coagulation responses, vasculogenesis, and angiogenesis. EC damage can be resulted from capturing angiogenic factors, inhibiting EC proliferation, survival and signal transduction, or altering vascular tone. EC dysfunction accounts for the pathogenesis of myocardial infarction, atherothrombosis, microangiopathies, and hypertension. In this review, we provide a comprehensive overview of the effects of chemotherapeutic agents on vascular toxicity leading to hypertension, microvascular rarefaction thrombosis and atherosclerosis, and affecting drug delivery. We also describe the potential therapeutic approaches such as vascular endothelial growth factor (VEGF)-B and prokineticin receptor-1 agonists to maintain endothelial function during or following treatments with chemotherapeutic agents, without affecting anti-tumor effectiveness.

Keywords: vascular toxicity, anti-cancer drugs, cardiotoxicity, hypertension, thrombosis

OPEN ACCESS

Edited by:
Margaret Rose Cunningham, University of Strathclyde, United Kingdom

Reviewed by:
Paola Rizzo, University of Ferrara, Italy
Kerstin Timm, University of Oxford, United Kingdom

****Correspondence:***
Canan G. Nebigil
nebigil@unistra.fr

Specialty section:
This article was submitted to Cardio-Oncology, a section of the journal Frontiers in Cardiovascular Medicine

Received: *13 April 2021*
Accepted: *18 June 2021*
Published: *27 July 2021*

Citation:
Hsu P-Y, Mammadova A, Benkirane-Jessel N, Désaubry L and Nebigil CG (2021) Updates on Anticancer Therapy-Mediated Vascular Toxicity and New Horizons in Therapeutic Strategies. Front. Cardiovasc. Med. 8:694711. doi: 10.3389/fcvm.2021.694711

INTRODUCTION

Anticancer chemotherapies target the vasculature of both tumor and unfortunately other organs. Additionally, mechanism-independent ("off-target") effects of chemotherapies also account for the development of the vascular toxicity. Vascular toxicity occurs during acute chemotherapeutic regimen, and after once treatments have ceased, persists into survival. The susceptibility to develop vascular complications following chemotherapeutics also relates to many factors such as cardiovascular risk and pre-existing vascular diseases, as well as genetic predispositions.

Chemotherapeutics-mediated vascular toxicity often results from loss of endothelial cell (EC) functions (1). ECs sense hemodynamic changes, and accordingly respond to stimuli by the release of vasoactive substances like vasorelaxants such as nitric oxide, (NO), prostacyclin, (PGI_2), vasoconstrictors such as endothelin-1, (ET-1), anti-thrombotic (plasminogen activators), and angiogenic factors such as vascular endothelial growth factor (VEGF) (2) and prokineticins

(3). Disturbance of NO/ET-1 balance is a characteristic of endothelial dysfunction and play an important role in the progression of vascular diseases.

Chemotherapeutics-mediated EC dysfunction in the heart is initially asymptomatic. The long-term consequences of cancer treatments can lead to the onset of cardiovascular disorders such as hypertension, coronary artery disease, and heart failure. Indeed, progressive EC damages make ECs more vulnerable to chronic inflammatory stressors and hyperlipidemia insults (4). EC dysfunction further promotes thrombus formation, and inflammation by releasing plasminogen activator inhibitor 1 (PAI1), platelet-activated factor 4 (PF-4), and interleukins (IL-1 and IL-6) to accelerate atherosclerosis formation. Chemotherapeutics can also have direct pro-coagulant, anti-angiogenesis, and vasoconstriction effects (**Figure 1**).

Vascular damage in the cardiovascular system can be caused not only by anti-angiogenic chemotherapy (inhibitors of vascular endothelial growth factor (VEGFi), but also by anti-tumor antibiotics (bleomycin and anthracyclines) (5, 6). The first line of treatments includes monoclonal antibodies (e.g., bevacizumab), and multiple kinase inhibitors such as sunitinib, a multi-targeted inhibitor, or sorafenib (7). In addition, plant alkaloids (taxanes, vinca alkaloids), alkylating agents (cisplatin, cyclophosphamide), antimetabolites (5-fluorouracil), and radiation therapy also foster vascular damages (8) (**Figure 2**).

Hereafter, we concentrate on these anti-cancer drugs-mediated vascular damages that evoke cardiovascular diseases and impair drug delivery.

Anticancer Therapy-Mediated Oxidative Stress and Vascular Injury

Many chemotherapeutics induce accumulation of the reactive oxygen species (ROS) products (9) that disrupt intracellular homeostasis and damage proteins, lipids, and DNA in the vascular cells. ROS such as superoxide radical anions ($O_{2.}^{-}$), lipid radicals (ROO.$^{-}$), hydroxyl radicals (HO.$^{-}$), and nitric oxide (NO) are formed by all vascular layers, including endothelium, smooth muscle, and adventitia (10). ROS induces VEGF expression in vascular endothelial and smooth muscle cells by upregulating hypoxia-inducible transcription factors (HIF-1). VEGF further stimulates the accumulation of ROS through activation of NADPH oxidase (11). The NO itself has a cardiovascular protective properties (12). However, when NO combines with ROS, it generates peroxynitrite radicals ($ONOO^{\cdot-}$) that promote inflammation, apoptosis, necrosis, and ultimately toxicity (13).

A high production of ROS is also a major promoter for the lipid peroxidation of unsaturated fatty acids, leading to apoptosis, autophagy, and ferroptosis (14). Lipid peroxidation followed by the activation of phospholipase A2 initiates the activation of arachidonic acid (AA) pathway. Thus, lipid peroxidation is not only responsible for the generation of prostaglandins, but also for the induction of inflammation and apoptosis in vascular ECs (14). ROS also promotes peroxidation of a mitochondrion-specific inner membrane phospholipid, cardiolipin to activate intrinsic apoptosis (15). Lipid peroxidation products can bind to specific mitochondrial and autophagy-related proteins driving autophagic cell death (16). Elevated intracellular iron concentration elevates ROS levels that cause lipid peroxidation and consequently to ferroptosis-mediated cell death (17).

Reactive nitrogen species (RNS) are formed by the reaction between ROS and NO that damage mitochondrial DNA. Excessive ROS also induces senescence in endothelial, vascular smooth muscle cell (VSMC), and endothelial progenitor cells (18). Indeed, accumulation of ROS and oxidative stress reduces NO bioavailability and consequently results in development of hypertension (19) (**Figure 2**).

Anticancer Therapy-Mediated Endothelial Dysfunction and Hypertension

Approximately 25% of cancer patients develop hypertension due to adverse effects of VEGFi, TKI, anthracyclines, alkylating agents, and antimetabolites (20). The pathophysiology of hypertension induced by these agents is not fully elucidated. Several mechanisms have been proposed based on the preclinical and clinical studies, including; (1) increased total peripheral resistance induced by endothelial dysfunction due to predominantly the reduced production of vasodilators (NO and PGI2), the increased production of vasoconstrictors (ET-1) and the reduced nitric oxide bioavailability, (2) increase in vascular tone, (3) vascular rarefaction, (4) and renal thrombotic microangiopathy, leading to proteinuria and hypertension, (5) natriuresis and impaired lymphatic function could also contribute to development of hypertension (21).

Inhibitors of VEGF (VEGFi) or Tyrosine Kinase (TKI)

Approximately 80% of patients treated with VEGFi or TKI manifest hypertension (22). VEGF signaling promotes production of NO and the vasodilatory prostanoid prostacyclin (PGI_2) through activation of phospholipase A2 *via* PLCγ/PKC pathways (23). After VEGF binding, VEGF receptor (VEGFR) activates phosphoinositol-3 kinase (PI3K)/serine-threonine protein kinase B (Akt) survival pathway in ECs. Thus, interruption of the VEGF signaling pathway by anticancer drugs leads to development of hypertension. Similarly, the VEGF trap aflibercept promotes hypertension (24), interrupting VEGF-mediated vasodilatory, and survival signaling (25). VEGFi-induced vascular toxicities can also be due to accumulation of ROS and down-regulation of nuclear factor erythroid 2-related factor 2 (Nrf2) that regulates antioxidant genes (26). Prohypertensive effects of VEGFi can also be promoted by microparticles of injured ECs (27).

TKIs stimulate ROS accumulation and reduce NO levels (28). For example, vatalanib or sunitinib increases ROS accumulation in both VSMCs and ECs by inhibiting NO synthase (NOS) thereby reducing NO levels and decreasing endothelium-dependent vasorelaxation (29). Sunitinib-induced hypertension may not depend on endothelium, but may be due to decreased arterioles diameters. Indeed, it inhibits platelet-derived growth factor receptor (PDGFR) that causes coronary microvascular dysfunction due to loss of pericytes, leading to the

FIGURE 1 | Summary of chemotherapy-associated vascular toxicity. Vascular toxicity can be attributed to four main mechanisms (vasomotor alterations, endothelial cell (EC) dysfunction, anti-angiogenesis, pro-thrombosis), which induce hypertension, ischemia and thromboembolism, and damage heart functions. The red arrows highlight direct effects of some of the chemotherapeutics.

mechanical instability of the capillary wall in cardiac and other tissues (30).

Anthracyclines

They cause ≈20% increase in carotid artery stiffness in patients. Anthracyclines also led to a 3-fold increase in vascular stiffness with a 10-year follow-up period in adolescent childhood cancer survivors, indicating that alterations in vascular integrity persist years to decades following anthracycline chemotherapy (31). Anthracycline-induced endothelial toxicity and hypertension can be caused by several mechanisms. The first one is an oxidative stress-mediated process (32). Indeed, doxorubicin binds to endothelial (eNOS) and decreases NO levels, leading to the production of superoxide. Reduced concentration of NO shifts endothelium to a pro-coagulant status and impairs vasodilatation (33). Recently, doxorubicin has been shown to stabilize NRF2 in the cytoplasm thereby reducing detoxification pathway in mice heart (6). Doxorubicin also induces mitochondrial DNA damage in an RNS/ROS-independent manner, along with a possible decrease in B-cell lymphoma (Bcl)-2, that leads to apoptosis of the ECs. The EC death further reduces the availability of NO, ET-1, PGI_2, and neuregulin (NRG)-1 to cardiomyocytes. Indeed, accumulation of ROS and oxidative stress reduces NO bioavailability and consequently results in development of hypertension (34). The second mechanism is apoptosis due to DNA interference (35). Doxorubicin -mediated topoisomerase II-β inhibition and DNA-binding directly induce DNA damage and apoptosis in ECs (36). Doxorubicin also reduces the tight junction protein zona occludens (ZO)-1 in ECs, thereby, increasing microvascular permeability (37). Anthracyclines at the accumulative dosage dysregulate renin-angiotensin-aldosterone

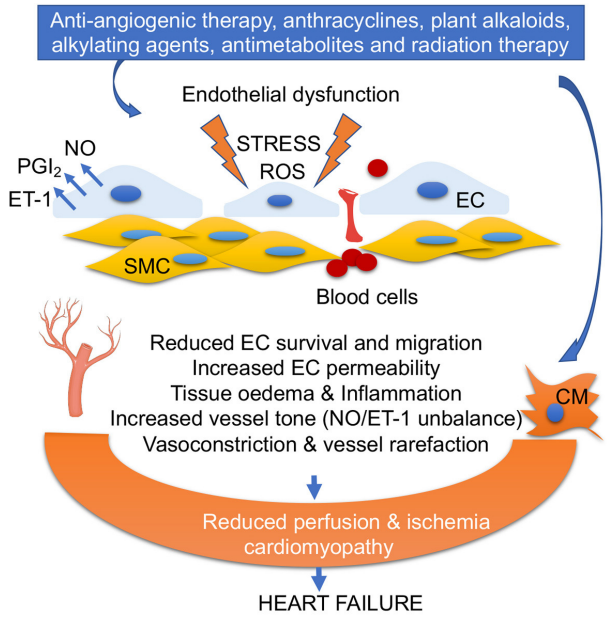

FIGURE 2 | Anticancer drug-mediated endothelial dysfunction. Oxidative stress, ROS accumulation, alteration of PGI_2/ET-1 ratio, and low NO levels in ECs impair EC survival and migration, increase fenestration and blood cell infiltration into vascular smooth muscles (SMC), trigger inflammation, and promote vasoconstriction. EC dysfunction and vascular rarefaction reduce myocardial perfusion, leading ischemia, and cardiomyopathy. Anticancer drug-mediated cardiomyocyte (CM) damage together with EC dysfunction leads to heart failure.

(RAA) system (38), that play significant role in the development of hypertension (39).

Alkylating Agents

Cyclophosphamide or its metabolites reduce vasoactive substance NO, increase ET-1 and inducible (i) NOS (40). They activate the toll-like receptor 4 (TLR-4) and causes subsequent activation of mitogen-activated protein kinase (MAPK) and c-Jun N-terminal kinases (JNK) (41). Once activated, these signaling pathways increase the expression of tissue necrosis factor alpha (TNFα), cyclooxygenase-2 (cox-2), prostaglandins (PGs), and interleukins (ILs). Cyclophosphamide also decreases fatty acid binding protein (H-FABP) and carnitine palmitoyl transferase-I (CPT-1) levels, resulting in the accumulation of free fatty acids and reduction of ATP production (42). Reduced ATP levels lead to the accumulation of intracellular calcium, which activates transforming growth factor beta (TGF-β) and the production of pro-inflammatory cytokines. Cyclophosphamide is associated with development of interstitial pneumonia and pulmonary fibrosis, leading to vascular sclerosis, and pulmonary hypertension (40).

Patients treated with cisplatin-based chemotherapy also develop persistent hypertension due to endothelial cell activation, damage, and subsequent endothelial dysfunction (43). Cisplatin induces release of inflammatory substances such as IL-1 and IL-6 from ECs to produce hydrogen peroxide that provoke oxidative stress, and mitochondrial DNA lesions, orchestrating cell death (44).

Antimetabolites

5-Fluorouracil (5-FU) induces ultrastructural changes in the endothelium of the heart, as well as in various organs by promoting both accumulation of ROS and autophagy process in ECs (45). Its vascular adverse effects include angina with coronary artery spasm and rarely hypertension (46).

In general, anticancer therapies increases blood pressure, therefore, an antihypertensive therapy can be required in case of diastolic blood pressure (DBP) increase >20 mmHg after initiation of anticancer therapy, yet DBP remains within normal limits (47).

Anticancer Therapy-Mediated Microvascular Rarefaction

Anticancer drugs induce capillary rarefaction that is described as a reduction of the density of arterioles and capillaries. One of the causes of microvascular rarefaction is a decrease of survival rate of microvascular EC. The second mechanism involve endothelial dysfunction that participates to thrombosis, leading to a further reduction in vascular perfusion, and micro vessel destruction (48). The molecular mechanisms of capillary rarefaction associated with the loss of pericytes due to inhibition of platelet derived growth factor (PDGF) receptor (PDGFR), and inhibition of angiogenesis by blocking VEGF signaling pathway.

VEGFi and TKIs

Prolonged TKI treatments lead to capillary rarefaction, due to endothelial dysfunction (25). In addition, disruption of both endothelium-dependent and -independent vasodilatation can also promote intense vasoconstriction and microvascular rarefaction. The vascular rarefaction may also be a consequence of VEGFi-associated hypertension (49). Bevacizumab promotes retinal microvascular dysfunction in humans (50). On the other hand, microvascular rarefaction increases peripheral resistance in the microcirculation, thereby, reducing blood flow and further elevating blood pressure.

Anthracyclines

A recent preclinical study has shown that chronic treatment with doxorubicin promotes vessel rarefaction in the heart (6). Moreover, a low dose of doxorubicin inhibits EC motility *in vitro* without causing apoptosis. However, whether doxorubicin provoke hypertension in these mice has not been studied.

Alkylating Agents

Cyclophosphamide causes extravasation of proteins, toxic metabolites, and erythrocytes, which breaks-down ECs, promotes hemorrhage, blocks the small arteries, and induces displacement of vascular ECs that directly damages the blood vessels and cardiac cells (51). Cyclophosphamide may reduce VEGF levels that is associated with microvascular rarefaction.

Cisplatin inhibits EC proliferation and motility *in vitro* and causes apoptosis (52). Cisplatin also inhibits angiogenesis

(53). Thus, both EC dysfunction and anti-angiogenic effects of platinum derivatives promote vascular rarefaction.

Anticancer Therapy-Mediated Hypercoagulation, Thrombosis, and Atherosclerosis

Cancer patients exhibit an increased risk of arterial and venous thrombotic events. Approximately cancer patients develop the risk of arterial (2–5%) and venous (4–20%) thromboembolism during the anti-angiogenic therapies (54). The mechanisms that underline the chemotherapeutic–associated thrombosis is not fully understood. It appears that targeted therapies-mediated thromboembolism is associated with on-target effects. However, conventional chemotherapies-mediated thromboembolism attributed to off-target effects. Based on the preclinical and clinical studies, the proposed mechanisms include; (1) the activation or disruption of the endothelium, (2) decrease in anticoagulants and increase in procoagulants, such as TF (tissue factor), cytokine-controlled defective anticoagulant pathways, and changes in the fibrinolytic pathways, and (3) the activation of platelets (55).

VEGFis and TKIs

They impair the VEGF-mediated tissue-type plasminogen activator (t-PA) release (56), and elevate platelets and coagulation factors to induce thrombosis (57). Additionally, TKIs increase hematocrit and reduce NO- and PGI_2-mediated anti-platelet activity (58). Accordingly, a meta-analysis in patients receiving TKIs demonstrated that the risk of myocardial infarction increased by 3.5-fold, and the development of arterial thrombosis by 1.8-fold, in the treated group (59). VEGFR inhibitors accelerate atherosclerosis and increase the risk of cholesterol embolization syndrome, leading to acute cardiovascular complications (60).

Anthracyclines

Doxorubicin has been shown to a significantly increase a risk of venous thrombosis by 16.0% (47). Several preclinical and clinical studies have showed that doxorubicin-mediated thrombogenic effects are resulted from an elevated prothrombotic state induced by (1) endothelial injury, (2) the down-regulation of the endothelium-based protein C anticoagulant pathway due to the reduced levels of endothelial protein C receptor in ECs, (3) an increased TF procoagulant activity, and (4) activated platelets (61). In patients with breast cancer, doxorubicin increases levels of thrombin-antithrombin complexes, protein C, and activated protein C (62). Its prothrombotic effects are also due to phosphatidylserine-bearing microparticle (MP) generation, promoting intracellular Ca^{2+} increase and ATP depletion in platelets (63). A dysfunction of the NADP-dependent mitochondrial enzyme aldehyde dehydrogenase-2 (ALDH2) in ECs is also involved in the development of doxorubicin-mediated vascular damage and thrombosis (64). Altered levels of endothelium-derived NRG-1, PGI_2, and ET-1 from ECs can also contribute to anti-platelet activity of doxorubicin (65).

Alkylating Agents

Cyclophosphamide and its toxic metabolites stimulate activation and release of platelet factor 4 (PF-4) that initiates the cascade of thrombosis and the binding of oxidized low-density lipoprotein (LDL) to ECs, and aggravates monocyte adhesion to endothelium (41). Cyclophosphamide-induced intrapapillary micro emboli is prominent cause of the ischemic myocardial damage (41). It also fosters acute pericarditis, myocardial hemorrhage, and atrophic and focal necrosis with interstitial edema (66).

Cisplatin facilities endothelial damage, hypercoagulation measured by increased levels of thrombin-antithrombin complexes and D-dimer, and platelet aggregation *via* activation of the arachidonic acid pathway that forms several inflammatory and thrombogenic molecules (67). However, the absolute risk of venous thrombosis associated with this class of agent remains low.

Antimetabolites

5-FU damages ECs and provokes severe vessel leakage and subsequent thrombus formation (68, 69). Patients receiving a cisplatin-based regimen with epirubicin and 5-FU or capecitabine exhibited an incidence of venous thrombosis of 15.1% (70).

In general, anticancer agents have more pronounced effect of the incidence of venous thrombosis than arterial thrombosis. An anticoagulation therapy may be required.

ANTICANCER THERAPY-MEDIATED IMPAIRED VASCULATURE AND DRUG DELIVERY

Anti-angiogenic agents alone or in combination with other chemotherapeutics are widely used to inhibit tumor growth by targeting vascular network (71). Some types of cancers are sensitive to anti-angiogenic therapy, while other types of cancers are completely insensitive. Adaptation to microenvironment, such as metabolic changes (72) or autophagy (73), can determine whether a tumor is sensitive to anti-cancer treatments. Some tumors can initially respond, but then develop acquired resistance during the anti-angiogenic treatment due to activation of alternative pathways, such as vessel co-option and vessel mimicry (74). Development of hypoxia in tumors reduces the activity of the prolyl hydroxylase domain proteins (PHD1–3), and prevents the degradation of HIF-1α and HIF-2α (75). High levels of HIFs in turn increases the transcription of HIF-driven hypoxia-related genes, including the potent angiogenic factors, VEGF to form a neovascular network to further increase tumor growth. Indeed, long-term anti-angiogenic therapy promotes genetic instability in tumor ECs, and causes vascular permeability and metastasis (76). Additionally, tumor-associated macrophages can trans-differentiate into ECs (77). In this case, tumors become highly vascularized and also resistant to chemotherapies. Tumor cells including infiltrated immature myeloid cells (78), fibroblasts (79), and endothelial progenitor cells (80) integrate into vessels or release pro-angiogenic growth factors, such as prokineticin-2

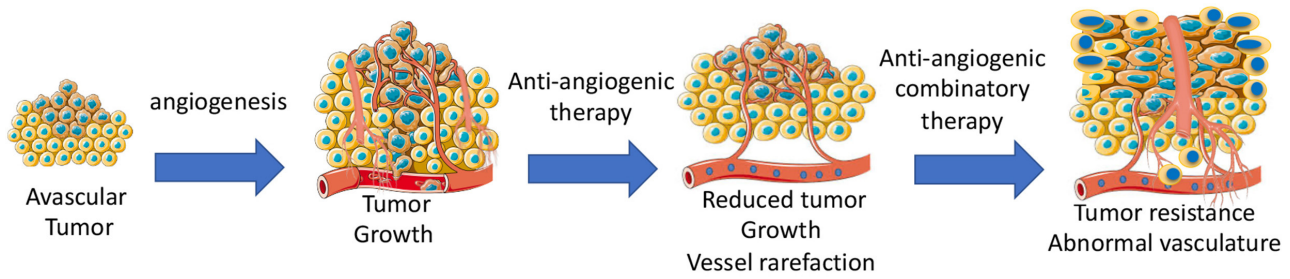

FIGURE 3 | Development of angiogenesis and anti-angiogenic therapy-mediated development of tumor resistance due to abnormal tumor vasculatures.

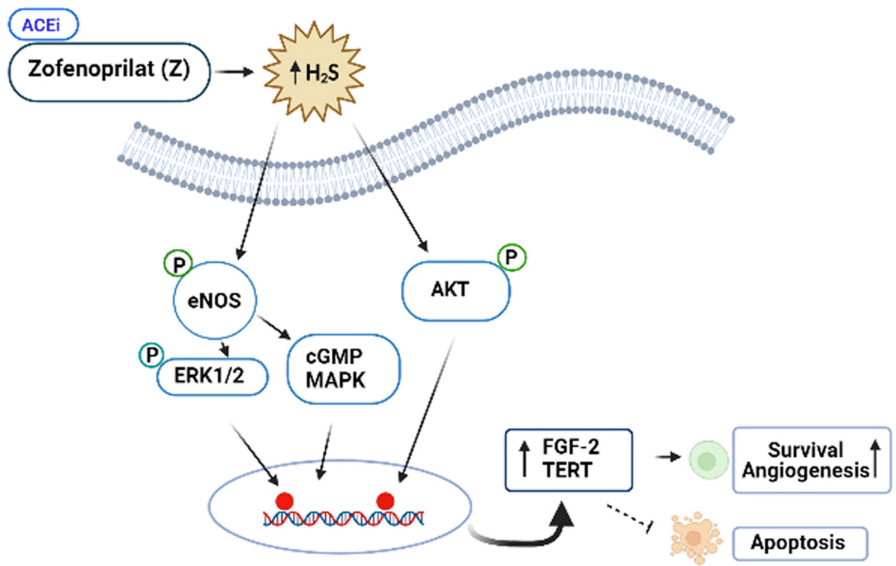

FIGURE 4 | Protective role of the SH-containing ACi, Zofenoprilat, against anticancer-mediated vascular toxicity. Zofenoprilat is the most effective clinically used vascular protectant. It increases survival of ECs and promotes angiogenesis, inhibits apoptosis. The mechanism involves activation of NOS, ERK1/2, cGMP and Akt kinases and increases in the expression levels of fibroblast growth factor (FGF-2) and telomerase reverse transcriptase (TERT). These effects appear to be the off-target effects of zofenoprilat *via* increasing production of H_2S, independent of ACEi properties.

(3) or PDGF-C (79), leading to worse outcomes of drug delivery, invasion, and metastasis (**Figure 3**).

DETECTION OF ENDOTHELIAL DAMAGE AND THROMBOSIS

Endothelial damages alter the expression of adhesion molecules and increase levels of pro-inflammatory cytokines (81). Thus, expression of adhesion molecules such as E-selectin, endothelin-1, and vascular cell adhesion molecule-1 (VCAM-1) are biomarkers of endothelial damage (82). The elevated levels of pro-inflammatory cytokines such as C-reactive protein (CRP) and IL-6 are also indicators of EC damage (83). Because asymmetric dimethylarginine (ADMA) synthesized *via* arginine methylation inhibits eNOS and promotes superoxide generation (84), ADMA is a marker of ROS generation. Indeed, activated ECs initiates procoagulant activity by releasing endothelium-derived glycoproteins such as von Willebrand factor (vWF), NRG-1, soluble thrombomodulin (sTM), and tissue plasminogen factor (t-PA) (85). Thus, increase levels of vWF, NRG-1 sTM, and t-PA are also the indicators of procoagulant activity and thrombosis.

The detection of micro vessel architectural parameters by Magnetic Resonance Imaging (MRI), Vessel Architectural Imaging (VAI), Microvascular Density (MVD), Positron Emission Tomography (PET), 3D ultrasonography, and CT is necessary in the clinic to asses vascular damage and select a proper timing window for tumor vascular normalization by anti-angiogenic therapies (86).

DRUGS PROTECTING ENDOTHELIAL CELL DAMAGE INDUCED BY CHEMOTHERAPEUTIC AGENTS

Angiotensin converting enzyme inhibitors (ACEi), NO donors, antioxidants, and statins have direct effects on ECs, while angiotensin receptor blockers (ARBs), renin

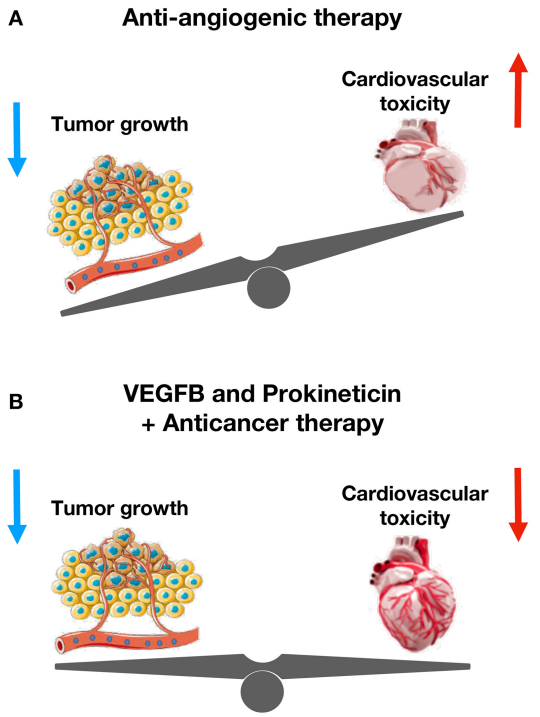

FIGURE 5 | The cardioprotective role of VEGFB and prokineticin against anti-cancer drugs-mediated cardiovascular toxicity. **(A)** Anti-angiogenic therapy reduces tumor size and increases cardiovascular toxicity. **(B)** VEGFB and Prokineticin receptor agonist protects cardiovascular system without altering anti-tumor effect of chemotherapeutics.

inhibitors, beta blockers, and estrogens indirectly affect EC function. Beta blockers, thiazide diuretics, mineralocorticoid receptor antagonists are used as additional antihypertensive agents. Here we focus on the first group of the EC protective drugs.

ACEis

ACEis ameliorates the left ventricular ejection fraction (LVEF) decline, when they are administered together or after anthracyclines. However, the vascular protective effects of ACEi, zofenoprilat, but not other ACEi (i.e., captopril or enalaprilat) are related with activation of survival pathways in cardiac cells, and its antioxidant and ROS scavenger properties. More specifically, zofenoprilat up-regulates the expression of eNOS, FGF-2, and telomerase (TERT) transcripts, thereby, promoting cell survival, rescuing damaged ECs, and inducing physiological angiogenesis without altering vascularization at tumors (87). Thus, zofenoprilat exerts its EC protective effects through off-target mechanisms, and may even maximize cytotoxic drug delivery to tumor cells (8).

Nitric Oxide Donors, Antioxidants, and Statin

Novel NO donor drugs metal-nonoates (88) and the mitochondrial aldehyde dehydrogenase (ALDH2) activator, called Alda-1 may restore eNOS functioning, and FGF-2 production and release, thereby, protecting ECs against anticancer drug-mediated damages (89). ALDH2 plays a central role in the vasodilator actions of nitroglycerin, restores mitochondrial functions, and promotes vascular recovery of ischemic myocardium (90). However, high ALDH2 metabolic activities have been observed in tumor ECs as well. Thus, whether ALDH2 mitigates anti-cancer drug efficacy in tumor should be tested.

Many animal models showed that vitamin E, vitamin C, vitamin A, coenzyme Q, and flavonoids can reduce the anthracycline-mediated cardiovascular toxicity. However, clinical use of antioxidants to protect the heart during anthracycline chemotherapy is paved away due to reduce cytotoxic efficacy toward cancer cells (91).

All FDA-approved statins are effective in lowering serum cholesterol by inhibiting activity of 3-hydroxy-3-methyl-glutaryl-coenzyme A reductase (HMGCR), a rate-limiting enzyme of the mevalonate pathway, in the liver. Therefore, they are integrated into cancer patient care to protect against atherosclerosis development during anticancer therapies. However, epidemiologic studies demonstrated that statin type, dose, and treatment duration, statin sensitivity, and toxicity are all important variables to evaluate statins beneficial effects in adverse effects of anticancer drugs (92).

NEW HORIZONS IN THERAPEUTIC STRATEGIES: PRO-ANGIOGENIC THERAPY TO PREVENT VASCULAR TOXICITY WITHOUT ALTERING ANTI-NEOPLASTIC PROPERTIES OF CHEMOTHERAPEUTICS

VEGF-B-Mediated Endothelial Protection Against Doxorubicin-Mediated Cardiotoxicity

Vascular endothelial growth factor-B (VEGF-B) promotes coronary arteriogenesis, physiological cardiac hypertrophy, and ischemia resistance. It also prevents doxorubicin-induced cardiotoxicity and congestive heart failure. A recent preclinical study has shown that pretreatment of tumor-bearing mice with an adeno-associated viral vector expressing VEGF-B completely inhibits the doxorubicin-induced cardiac atrophy and whole-body wasting (93). VEGF-B also alleviates capillary rarefaction in the heart and improves cardiac function in doxorubicin-treated mice. Indeed, VEGF-B protects EC from apoptosis and restores tube-formation capacity of ECs without altering anti-tumor role of doxorubicin. Importantly, VEGF-B does not affect serum or tissue concentrations of doxorubicin. By inhibiting doxorubicin-induced endothelial damage, VEGF-B could provide a novel therapeutic possibility for the prevention of chemotherapy-associated cardiotoxicity in cancer patients.

TABLE 1 | Vascular damages and diseases induced by the widely prescribed anticancer drugs.

Anti-cancer drugs and their use in type of cancers	Vascular toxicity	Mechanism	Ref.
Anthracyclines (Doxorubicin) Leukemia, lymphoma, melanoma, uterine, breast, and gastric cancers	* Vascular injury * Microvascular rarefaction * Endothelial dysfunction and hypertension * Hypercoagulation, thrombosis, & atherosclerosis	* Oxidative stress-mediated ROS accumulation * Apoptosis due to DNA interference * Disruption of the tight junction protein ZO-1 in ECs * Anti-angiogenesis * Mitochondrial DNA damage * The endothelium-based protein C anticoagulant pathway interruption	(18) (21) (22) (5) (49) (59)
Tyrosine kinase inhibitors (TKI) and VEGF inhibitors (VEGFis) Renal cell cancer, gastro-intestinal stromal tumors, hepatocellular cancer	* Microvascular rarefaction * Hypertension * Anti-platelet activity * Hypercoagulation & thrombosis, & atherosclerosis	* NRF2 downregulation * Anti-VEGF effect, ROS accumulation and disruption of NO levels and PI3K/Akt survival pathway. * Increased vasoconstriction due to disruption of both endothelium-dependent and -independent vasodilatation * Loss of pericytes due to inhibition of PDGF * Increased hematocrit and thrombogenesis activity by reducing NO- and PGI_2-mediated anti-platelet activity * Atherosclerosis and increase in the risk of cholesterol embolization syndrome	(26) (28) (31) (40) (30) (56) (60)
Cyclophosphamide Breast cancer, lymphoid, and pediatric malignancies	* Vascular injury * Microvascular rarefaction * Hypercoagulation, thrombosis, & atherosclerosis	* Increased levels of the expression of tissue necrosis factor * Reduced levels of VEGFs * Activation of platelet factor 4 (PF-4)	(24) (33) (24)
Cisplatin Ovaries, testis cancers, solid tumors of the head and neck	* Vascular injury * Microvascular rarefaction * Endothelial dysfunction and hypertension * Hypercoagulation, thrombosis, & atherosclerosis	* Increased levels of EC- inflammatory substances to produce hydrogen peroxide * Increased platelet aggregation levels *via* the arachidonic acid pathway	(26) (34, 35) (51)
5-Fluorouracil (5-FU) Breast cancer, head and neck cancers, anal, stomach, colon cancers some skin cancers	* Vascular injury * Hypercoagulation, thrombosis, & atherosclerosis	* Ultrastructural changes in the endothelium of the heart * EC damage * Direct prothrombotic effect	(27) (65, 66)
Taxanes Breast, ovarian, lung, bladder, prostate, melanoma, esophageal, other types of solid tumor cancers	* Microvascular rarefaction	* Endothelial damage and impaired angiogenesis	(37)

Prokineticin Receptor-1 Signaling Inhibits Dose- and Time-Dependent Anthracycline-Induced Cardiovascular Toxicity *via* Myocardial and Vascular Protection

Prokineticins (PROK1 and PROK2) are neuropeptides/hormones that are mainly released by macrophages and reproduction organs in the peripheral system (94). They utilize two G-protein–coupled receptors (GPCRs) namely prokineticin receptors (PKR1 and PKR2). Expression of PROK2 and PKR1 levels are altered in patients with abdominal aortic rupture (8), during end-stage cardiac failure (95) after acute myocardial infarction (96), and in adipose tissues from obese patients (97). Interestingly, *PKR1* gene transfer improves survival and heart function in a mouse model of myocardial infarction (95) and promotes coronary arteriogenesis (98). However, *PKR2* overexpression in cardiomyocytes promotes pathological cardiac hypertrophy and causes vascular leakage (99, 100). These receptors have also divergent effects on ECs (101). Thus, a non-peptide agonist specific for PKR1, called IS20, was developed to mimic the cardioprotective effects of PROK2 against heart failure developed by myocardial infarction (102) and anthracyclines (6) in mice.

A recent preclinical study has demonstrated that prolonged exposure to low-dose doxorubicin does not induce apoptosis in ECs, but impairs angiogenesis (6). Importantly, IS20 restores doxorubicin-mediated cardiovascular toxicity by activating Akt or MAPK pathways. Genetic or pharmacological inactivation of PKR1 abolishes these effects of IS20. Mice exposed to chronic doxorubicin treatment exhibit apoptosis in cardiac cells, vascular rarefaction and fibrosis, consequently impaired systolic and diastolic cardiac function, and reduced survival rate. IS20 reverses these detrimental effects of doxorubicin.

IS20 also does not alter the cytotoxicity or antitumor effects of doxorubicin in breast cancer lines or in a mouse model of breast cancer. Altogether, this study provides evidence that PKR-1 is a promising target to combat cardiovascular toxicity of cancer treatments (6).

CONCLUSION AND PERSPECTIVES

Anticancer treatments induce vascular damage, hypertension, and thrombosis, which affect survival and quality of life of the patient (**Table 1**). Therefore, pre-existing hypertension and a thrombosis risk assessment should be conducted before starting any type of chemotherapies (103). A continued characterization of changes of microvessel network patterns and blood pressure by anticancer drugs is necessary to prevent development of hypertension and organ damages, especially during the 1st cycle of therapy when the patients experience a secondary elevation in blood pressure.

Several mechanisms for anticancer drug-mediated vascular toxicity have been identified (104), however, there are still many unknown molecular processes that need to be unraveled to better understand exactly how anticancer treatments provoke vascular damages. Endothelial metabolism and new signaling pathways could be novel targets of the vascular protectant.

Identification of underlying pathological mechanisms of development of vascular toxicity is a key element to optimize benefits in tumor development and drug delivery of chemotherapies.

The improvement in cancer therapy of the past two decades is due to the development of numerous novel targeted therapies. These drugs are also used in combination with other new anti-cancer drugs including inhibitors of immune check points, poly (ADP-ribose) polymerase (PARP), and histone deacetylase (HDAC). However, most of these treatments also induce vascular toxicity, leading to hypertension, thromboembolism, vasculitis, development of atherosclerotic plaques, and fibrotic heart disease. More clinical trials of cancer therapies are needed to be better document the vascular complications of the chemotherapeutics.

Some of the new cardiovascular protectants including GPCR-targeted compounds are potential drug candidates to improve management and prevention of the cardio vascular toxicity of anti-cancer therapy (105). Whether, these potential vascular protective agents minimize thrombotic risk associated with chemotherapies should also be examined. Further, studies are also necessary to examine their effects on the efficacy of anti-tumor drugs.

AUTHOR CONTRIBUTIONS

AM, P-YH, and CGN: create the figure and contribute to the writing. LD, NB-J, and CGN: conribute writing. CGN: conribution to editing, designing, and orginization of the idea. All authors contributed to the article and approved the submitted version.

FUNDING

This work was supported in part by grants from the ANR-16-ECVD-000, ERA-CVD (JTC 2016) Transnational Research Projects on Cardiovascular Diseases and Fondation de France (R20085MM).

ACKNOWLEDGMENTS

The authors thank Prof. Pascal Dollé (IGBMC, Illkirch) for his kind editing and discussions. The *drawings* in Graphical (**Figures 1–5**) were produced and adapted, *using Servier Medical Art* illustration resources (www.servier.com) and Biorender (www.Biorender.com) (**Figure 4**).

REFERENCES

1. Gao Y, Galis ZS. Exploring the role of endothelial cell resilience in cardiovascular health and disease. *Arterioscler Thromb Vasc Biol.* (2021) 41:179–85. doi: 10.1161/ATVBAHA.120.314346
2. Kruger-Genge A, Blocki A, Franke RP, Jung F. Vascular endothelial cell biology: an update. *Int J Mol Sci.* (2019) 20:4411. doi: 10.3390/ijms20184411
3. Shojaei F, Wu X, Zhong C, Yu L, Liang XH, Yao J, et al. Bv8 regulates myeloid-cell-dependent tumour angiogenesis. *Nature.* (2007) 450:825–31. doi: 10.1038/nature06348
4. Cameron AC, Touyz RM, Lang NN. Vascular complications of cancer chemotherapy. *Can J Cardiol.* (2016) 32:852–62. doi: 10.1016/j.cjca.2015.12.023
5. Lv H, Tan R, Liao J, Hao Z, Yang X, Liu Y, et al. Doxorubicin contributes to thrombus formation and vascular injury by interfering with platelet function. *Am J Physiol Heart Circ Physiol.* (2020) 319:H133–43. doi: 10.1152/ajpheart.00456.2019
6. Gasser A, Chen Y-W, Audebrand A, Daglayan A, Charavin M, Escoubet B, et al. Prokineticin receptor-1 signaling inhibits dose- and time-dependent anthracycline-induced cardiovascular toxicity *via* myocardial and vascular protection. *JACC Cardiooncol.* (2019) 1:84–102. doi: 10.1016/j.jaccao.2019.06.003
7. Versmissen J, Mirabito Colafella KM, Koolen SLW, Danser AHJ. Vascular cardio-oncology: vascular endothelial growth factor inhibitors and hypertension. *Cardiovasc Res.* (2019) 115:904–14. doi: 10.1093/cvr/cvz022
8. Morbidelli L, Donnini S, Ziche M. Targeting endothelial cell metabolism for cardio-protection from the toxicity of antitumor agents. *Cardiooncology.* (2016) 2:3. doi: 10.1186/s40959-016-0010-6
9. Varricchi G, Ameri P, Cadeddu C, Ghigo A, Madonna R, Marone G, et al. Antineoplastic drug-induced cardiotoxicity: a redox perspective. *Front Physiol.* (2018) 9:167. doi: 10.3389/fphys.2018.00167
10. Ray PD, Huang BW, Tsuji Y. Reactive oxygen species (ROS) homeostasis and redox regulation in cellular signaling. *Cell Signal.* (2012) 24:981–90. doi: 10.1016/j.cellsig.2012.01.008
11. Moris D, Spartalis M, Spartalis E, Karachaliou GS, Karaolanis GI, Tsourouflis G, et al. The role of reactive oxygen species in the pathophysiology of cardiovascular diseases and the clinical significance of myocardial redox. *Ann Transl Med.* (2017) 5:326. doi: 10.21037/atm.2017.06.27
12. Forstermann U, Li H. Therapeutic effect of enhancing endothelial nitric oxide synthase (eNOS) expression and preventing eNOS uncoupling. *Br J Pharmacol.* (2011) 164:213–23. doi: 10.1111/j.1476-5381.2010.01196.x
13. Lim W, Kim JH, Gook E, Kim J, Ko Y, Kim I, et al. Inhibition of mitochondria-dependent apoptosis by 635-nm irradiation in sodium

nitroprusside-treated SH-SY5Y cells. *Free Radic Biol Med.* (2009) 47:850–7. doi: 10.1016/j.freeradbiomed.2009.06.023
14. Su LJ, Zhang JH, Gomez H, Murugan R, Hong X, Xu D, et al. Reactive oxygen species-induced lipid peroxidation in apoptosis, autophagy, and ferroptosis. *Oxid Med Cell Longev.* (2019) 2019:5080843. doi: 10.1155/2019/5080843
15. Zhong H, Xiao M, Zarkovic K, Zhu M, Sa R, Lu J, et al. Mitochondrial control of apoptosis through modulation of cardiolipin oxidation in hepatocellular carcinoma: a novel link between oxidative stress and cancer. *Free Radic Biol Med.* (2017) 102:67–76. doi: 10.1016/j.freeradbiomed.2016.10.494
16. Xie Y, Li J, Kang R, Tang D. Interplay between lipid metabolism and autophagy. *Front Cell Dev Biol.* (2020) 8:431. doi: 10.3389/fcell.2020.00431
17. Feng H, Stockwell BR. Unsolved mysteries: how does lipid peroxidation cause ferroptosis? *PLoS Biol.* (2018) 16:e2006203. doi: 10.1371/journal.pbio.2006203
18. Liang Y, Li J, Lin Q, Huang P, Zhang L, Wu W, et al. Research progress on signaling pathway-associated oxidative stress in endothelial cells. *Oxid Med Cell Longev.* (2017) 2017:7156941. doi: 10.1155/2017/7156941
19. Schulz E, Jansen T, Wenzel P, Daiber A, Munzel T. Nitric oxide, tetrahydrobiopterin, oxidative stress, and endothelial dysfunction in hypertension. *Antioxid Redox Signal.* (2008) 10:1115–26. doi: 10.1089/ars.2007.1989
20. Zhu X, Wu S, Dahut WL, Parikh CR. Risks of proteinuria and hypertension with bevacizumab, an antibody against vascular endothelial growth factor: systematic review and meta-analysis. *Am J Kidney Dis.* (2007) 49:186–93. doi: 10.1053/j.ajkd.2006.11.039
21. Narayan V, Ky B. Common cardiovascular complications of cancer therapy: epidemiology, risk prediction, and prevention. *Annu Rev Med.* (2018) 69:97–111. doi: 10.1146/annurev-med-041316-090622
22. Small HY, Montezano AC, Rios FJ, Savoia C, Touyz RM. Hypertension due to antiangiogenic cancer therapy with vascular endothelial growth factor inhibitors: understanding and managing a new syndrome. *Can J Cardiol.* (2014) 30:534–43. doi: 10.1016/j.cjca.2014.02.011
23. Olsson AK, Dimberg A, Kreuger J, Claesson-Welsh L. VEGF receptor signalling - in control of vascular function. *Nat Rev Mol Cell Biol.* (2006) 7:359–71. doi: 10.1038/nrm1911
24. Sinicrope FA, Williamson EE, Borgeson DD. Aflibercept and its role in the treatment of colorectal cancer–letter. *Clin Cancer Res.* (2013) 19:6057. doi: 10.1158/1078-0432.CCR-13-2056
25. Mourad JJ, des Guetz G, Debbabi H, Levy BI. Blood pressure rise following angiogenesis inhibition by bevacizumab. A crucial role for microcirculation. *Ann Oncol.* (2008) 19:927–34. doi: 10.1093/annonc/mdm550
26. Neves KB, Rios FJ, van der Mey L, Alves-Lopes R, Cameron AC, Volpe M, et al. VEGFR (Vascular Endothelial Growth Factor Receptor) inhibition induces cardiovascular damage *via* redox-sensitive processes. *Hypertension.* (2018) 71:638–47. doi: 10.1161/HYPERTENSIONAHA.117.10490
27. Neves KB, Rios FJ, Jones R, Evans TRJ, Montezano AC, Touyz RM. Microparticles from vascular endothelial growth factor pathway inhibitor-treated cancer patients mediate endothelial cell injury. *Cardiovasc Res.* (2019) 115:978–88. doi: 10.1093/cvr/cvz021
28. Teppo HR, Soini Y, Karihtala P. Reactive oxygen species-mediated mechanisms of action of targeted cancer therapy. *Oxid Med Cell Longev.* (2017) 2017:1485283. doi: 10.1155/2017/1485283
29. Thijs AM, van Herpen CM, Verweij V, Pertijs J, van den Broek PH, van der Graaf WT, et al. Impaired endothelium-dependent vasodilation does not initiate the development of sunitinib-associated hypertension. *J Hypertens.* (2015) 33:2075–82. doi: 10.1097/HJH.0000000000000662
30. Chintalgattu V, Rees ML, Culver JC, Goel A, Jiffar T, Zhang J, et al. Coronary microvascular pericytes are the cellular target of sunitinib malate-induced cardiotoxicity. *Sci Transl Med.* (2013) 5:187ra69. doi: 10.1126/scitranslmed.3005066
31. Parr SK, Liang J, Schadler KL, Gilchrist SC, Steele CC, Ade CJ. Anticancer therapy-related increases in arterial stiffness: a systematic review and meta-analysis. *J Am Heart Assoc.* (2020) 9:e015598. doi: 10.1161/JAHA.119.015598
32. Wolf M, Baynes J. The anti-cancer drug, doxorubicin, causes oxidant stress-induced endothelial dysfunction. *Biochim Biophys Acta.* (2006) 1760:267–71. doi: 10.1016/j.bbagen.2005.10.012
33. He H, Wang L, Qiao Y, Zhou Q, Li H, Chen S, et al. Doxorubicin induces endotheliotoxicity and mitochondrial dysfunction *via* ROS/eNOS/NO pathway. *Front Pharmacol.* (2019) 10:1531. doi: 10.3389/fphar.2019.01531
34. Vaitiekus D, Muckiene G, Vaitiekiene A, Maciuliene D, Vaiciuliene D, Ambrazeviciute G, et al. Impact of arterial hypertension on doxorubicin-based chemotherapy-induced subclinical cardiac damage in breast cancer patients. *Cardiovasc Toxicol.* (2020) 20:321–7. doi: 10.1007/s12012-019-09556-3
35. Zhang S, Liu X, Bawa-Khalfe T, Lu LS, Lyu YL, Liu LF, et al. Identification of the molecular basis of doxorubicin-induced cardiotoxicity. *Nat Med.* (2012) 18:1639–42. doi: 10.1038/nm.2919
36. Wojcik T, Buczek E, Majzner K, Kolodziejczyk A, Miszczyk J, Kaczara P, et al. Comparative endothelial profiling of doxorubicin and daunorubicin in cultured endothelial cells. *Toxicol In Vitro.* (2015) 29:512–21. doi: 10.1016/j.tiv.2014.12.009
37. Wilkinson EL, Sidaway JE, Cross MJ. Cardiotoxic drugs herceptin and doxorubicin inhibit cardiac microvascular endothelial cell barrier formation resulting in increased drug permeability. *Biol Open.* (2016) 5:1362–70. doi: 10.1242/bio.020362
38. Sobczuk P, Czerwinska M, Kleibert M, Cudnoch-Jedrzejewska A. Anthracycline-induced cardiotoxicity and renin-angiotensin-aldosterone system-from molecular mechanisms to therapeutic applications. *Heart Fail Rev.* (2020) 1–25. doi: 10.1007/s10741-020-09977-1
39. Kuriakose RK, Kukreja RC, Xi L. Potential therapeutic strategies for hypertension-exacerbated cardiotoxicity of anticancer drugs. *Oxid Med Cell Longev.* (2016) 2016:8139861. doi: 10.1155/2016/8139861
40. Soultati A, Mountzios G, Avgerinou C, Papaxoinis G, Pectasides D, Dimopoulos MA, et al. Endothelial vascular toxicity from chemotherapeutic agents: preclinical evidence and clinical implications. *Cancer Treat Rev.* (2012) 38:473–83. doi: 10.1016/j.ctrv.2011.09.002
41. Iqubal A, Iqubal MK, Sharma S, Ansari MA, Najmi AK, Ali SM, et al. Molecular mechanism involved in cyclophosphamide-induced cardiotoxicity: old drug with a new vision. *Life Sci.* (2019) 218:112–31. doi: 10.1016/j.lfs.2018.12.018
42. Kurauchi K, Nishikawa T, Miyahara E, Okamoto Y, Kawano Y. Role of metabolites of cyclophosphamide in cardiotoxicity. *BMC Res Notes.* (2017) 10:406. doi: 10.1186/s13104-017-2726-2
43. de Vos FY, Nuver J, Willemse PH, van der Zee AG, Messerschmidt J, Burgerhof JG, et al. Long-term survivors of ovarian malignancies after cisplatin-based chemotherapy cardiovascular risk factors and signs of vascular damage. *Eur J Cancer.* (2004) 40:696–700. doi: 10.1016/j.ejca.2003.11.026
44. Herradon E, Gonzalez C, Uranga JA, Abalo R, Martin MI, Lopez-Miranda V. Characterization of cardiovascular alterations induced by different chronic cisplatin treatments. *Front Pharmacol.* (2017) 8:196. doi: 10.3389/fphar.2017.00196
45. Sudhoff T, Enderle MD, Pahlke M, Petz C, Teschendorf C, Graeven U, et al. 5-Fluorouracil induces arterial vasocontractions. *Ann Oncol.* (2004) 15:661–4. doi: 10.1093/annonc/mdh150
46. Shiga T, Hiraide M. Cardiotoxicities of 5-fluorouracil and other fluoropyrimidines. *Curr Treat Options Oncol.* (2020) 21:27. doi: 10.1007/s11864-020-0719-1
47. Zangari M, Siegel E, Barlogie B, Anaissie E, Saghafifar F, Fassas A, et al. Thrombogenic activity of doxorubicin in myeloma patients receiving thalidomide: implications for therapy. *Blood.* (2002) 100:1168–71. doi: 10.1182/blood-2002-01-0335
48. Chen N, Ren M, Li R, Deng X, Li Y, Yan K, et al. Bevacizumab promotes venous thromboembolism through the induction of PAI-1 in a mouse xenograft model of human lung carcinoma. *Mol Cancer.* (2015) 14:140. doi: 10.1186/s12943-015-0418-x
49. Steeghs N, Gelderblom H, Roodt JO, Christensen O, Rajagopalan P, Hovens M, et al. Hypertension and rarefaction during treatment with telatinib, a small molecule angiogenesis inhibitor. *Clin Cancer Res.* (2008) 14:3470–6. doi: 10.1158/1078-0432.CCR-07-5050
50. Reimann M, Folprecht G, Haase R, Trautmann K, Ehninger G, Reichmann H, et al. Anti-Vascular endothelial growth factor therapy impairs endothelial function of retinal microcirculation in colon

cancer patients - an observational study. *Exp Transl Stroke Med.* (2013) 5:7. doi: 10.1186/2040-7378-5-7
51. Dhesi S, Chu MP, Blevins G, Paterson I, Larratt L, Oudit GY, et al. Cyclophosphamide-induced cardiomyopathy: a case report, review, and recommendations for management. *J Investig Med High Impact Case Rep.* (2013) 1:80346. doi: 10.1177/2324709613480346
52. Ramer R, Schmied T, Wagner C, Haustein M, Hinz B. The antiangiogenic action of cisplatin on endothelial cells is mediated through the release of tissue inhibitor of matrix metalloproteinases-1 from lung cancer cells. *Oncotarget.* (2018) 9:34038–55. doi: 10.18632/oncotarget.25954
53. Muscella A, Vetrugno C, Biagioni F, Calabriso N, Calierno MT, Fornai F, et al. Antitumour and antiangiogenic activities of [Pt(O,O'-acac)(gamma-acac)(DMS)] in a xenograft model of human renal cell carcinoma. *Br J Pharmacol.* (2016) 173:2633–44. doi: 10.1111/bph.13543
54. Grover SP, Hisada YM, Kasthuri RS, Reeves BN, Mackman N. Cancer therapy-associated thrombosis. *Arterioscler Thromb Vasc Biol.* (2021) 41:1291–305. doi: 10.1161/ATVBAHA.120.314378
55. Levi M, Sivapalaratnam S. An overview of thrombotic complications of old and new anticancer drugs. *Thromb Res.* (2020) 191(Suppl. 1):S17–21. doi: 10.1016/S0049-3848(20)30391-1
56. Oliver JJ, Webb DJ, Newby DE. Stimulated tissue plasminogen activator release as a marker of endothelial function in humans. *Arterioscler Thromb Vasc Biol.* (2005) 25:2470–9. doi: 10.1161/01.ATV.0000189309.05924.88
57. Elice F, Rodeghiero F, Falanga A, Rickles FR. Thrombosis associated with angiogenesis inhibitors. *Best Pract Res Clin Haematol.* (2009) 22:115–28. doi: 10.1016/j.beha.2009.01.001
58. Eremina V, Quaggin SE. Biology of anti-angiogenic therapy-induced thrombotic microangiopathy. *Semin Nephrol.* (2010) 30:582–90. doi: 10.1016/j.semnephrol.2010.09.006
59. Faruque LI, Lin M, Battistella M, Wiebe N, Reiman T, Hemmelgarn B, et al. Systematic review of the risk of adverse outcomes associated with vascular endothelial growth factor inhibitors for the treatment of cancer. *PLoS ONE.* (2014) 9:e101145. doi: 10.1371/journal.pone.0101145
60. Mir O, Mouthon L, Alexandre J, Mallion JM, Deray G, Guillevin L, et al. Bevacizumab-induced cardiovascular events: a consequence of cholesterol emboli syndrome? *J Natl Cancer Inst.* (2007) 99:85–6. doi: 10.1093/jnci/djk011
61. Woodley-Cook J, Shin LY, Swystun L, Caruso S, Beaudin S, Liaw PC. Effects of the chemotherapeutic agent doxorubicin on the protein C anticoagulant pathway. *Mol Cancer Ther.* (2006) 5:3303–11. doi: 10.1158/1535-7163.MCT-06-0154
62. Mukherjee SD, Swystun LL, Mackman N, Wang JG, Pond G, Levine MN, et al. Impact of chemotherapy on thrombin generation and on the protein C pathway in breast cancer patients. *Pathophysiol Haemost Thromb.* (2010) 37:88–97. doi: 10.1159/000324166
63. Kim SH, Lim KM, Noh JY, Kim K, Kang S, Chang YK, et al. Doxorubicin-induced platelet procoagulant activities: an important clue for chemotherapy-associated thrombosis. *Toxicol Sci.* (2011) 124:215–24. doi: 10.1093/toxsci/kfr222
64. Ge W, Yuan M, Ceylan AF, Wang X, Ren J. Mitochondrial aldehyde dehydrogenase protects against doxorubicin cardiotoxicity through a transient receptor potential channel vanilloid 1-mediated mechanism. *Biochim Biophys Acta.* (2016) 1862:622–34. doi: 10.1016/j.bbadis.2015.12.014
65. Luu AZ, Chowdhury B, Al-Omran M, Teoh H, Hess DA, Verma S. Role of endothelium in doxorubicin-induced cardiomyopathy. *JACC Basic Transl Sci.* (2018) 3:861–70. doi: 10.1016/j.jacbts.2018.06.005
66. Moschella F, Torelli GF, Valentini M, Urbani F, Buccione C, Petrucci MT, et al. Cyclophosphamide induces a type I interferon-associated sterile inflammatory response signature in cancer patients' blood cells: implications for cancer chemoimmunotherapy. *Clin Cancer Res.* (2013) 19:4249–61. doi: 10.1158/1078-0432.CCR-12-3666
67. Oppelt P, Betbadal A, Nayak L. Approach to chemotherapy-associated thrombosis. *Vasc Med.* (2015) 20:153–61. doi: 10.1177/1358863X14568705
68. Sara JD, Kaur J, Khodadadi R, Rehman M, Lobo R, Chakrabarti S, et al. 5-fluorouracil and cardiotoxicity: a review. *Ther Adv Med Oncol.* (2018) 10:80140. doi: 10.1177/17588359187 80140
69. Sorrentino MF, Kim J, Foderaro AE, Truesdell AG. 5-fluorouracil induced cardiotoxicity: review of the literature. *Cardiol J.* (2012) 19:453–8. doi: 10.5603/CJ.2012.0084
70. Cunningham D, Sirohi B, Pluzanska A, Utracka-Hutka B, Zaluski J, Glynne-Jones R, et al. Two different first-line 5-fluorouracil regimens with or without oxaliplatin in patients with metastatic colorectal cancer. *Ann Oncol.* (2009) 20:244–50. doi: 10.1093/annonc/mdn638
71. Lugano R, Ramachandran M, Dimberg A. Tumor angiogenesis: causes, consequences, challenges and opportunities. *Cell Mol Life Sci.* (2020) 77:1745–70. doi: 10.1007/s00018-019-03351-7
72. De Palma M, Biziato D, Petrova TV. Microenvironmental regulation of tumour angiogenesis. *Nat Rev Cancer.* (2017) 17:457–74. doi: 10.1038/nrc.2017.51
73. Chandra A, Rick J, Yagnik G, Aghi MK. Autophagy as a mechanism for anti-angiogenic therapy resistance. *Semin Cancer Biol.* (2020) 66:75–88. doi: 10.1016/j.semcancer.2019.08.031
74. Lupo G, Caporarello N, Olivieri M, Cristaldi M, Motta C, Bramanti V, et al. Anti-angiogenic therapy in cancer: downsides and new pivots for precision medicine. *Front Pharmacol.* (2016) 7:519. doi: 10.3389/fphar.2016.00519
75. Macklin PS, McAuliffe J, Pugh CW, Yamamoto A. Hypoxia and HIF pathway in cancer and the placenta. *Placenta.* (2017) 56:8–13. doi: 10.1016/j.placenta.2017.03.010
76. Itatani Y, Kawada K, Yamamoto T, Sakai Y. Resistance to anti-angiogenic therapy in cancer-alterations to anti-VEGF pathway. *Int J Mol Sci.* (2018) 19:1232. doi: 10.3390/ijms19041232
77. Riabov V, Gudima A, Wang N, Mickley A, Orekhov A, Kzhyshkowska J. Role of tumor associated macrophages in tumor angiogenesis and lymphangiogenesis. *Front Physiol.* (2014) 5:75. doi: 10.3389/fphys.2014.00075
78. Chung AS, Wu X, Zhuang G, Ngu H, Kasman I, Zhang J, et al. An interleukin-17-mediated paracrine network promotes tumor resistance to anti-angiogenic therapy. *Nat Med.* (2013) 19:1114–23. doi: 10.1038/nm.3291
79. Crawford Y, Kasman I, Yu L, Zhong C, Wu X, Modrusan Z, et al. PDGF-C mediates the angiogenic and tumorigenic properties of fibroblasts associated with tumors refractory to anti-VEGF treatment. *Cancer Cell.* (2009) 15:21–34. doi: 10.1016/j.ccr.2008.12.004
80. Shaked Y, Ciarrocchi A, Franco M, Lee CR, Man S, Cheung AM, et al. Therapy-induced acute recruitment of circulating endothelial progenitor cells to tumors. *Science.* (2006) 313:1785–7. doi: 10.1126/science.1127592
81. Deanfield JE, Halcox JP, Rabelink TJ. Endothelial function and dysfunction: testing and clinical relevance. *Circulation.* (2007) 115:1285–95. doi: 10.1161/CIRCULATIONAHA.106.652859
82. Daiber A, Steven S, Weber A, Shuvaev VV, Muzykantov VR, Laher I, et al. Targeting vascular (endothelial) dysfunction. *Br J Pharmacol.* (2017) 174:1591–619. doi: 10.1111/bph.13517
83. Meroni PL, Borghi MO, Raschi E, Ventura D, Sarzi Puttini PC, Atzeni F, et al. Inflammatory response and the endothelium. *Thromb Res.* (2004) 114:329–34. doi: 10.1016/j.thromres.2004.06.045
84. Landim MB, Casella Filho A, Chagas AC. Asymmetric dimethylarginine (ADMA) and endothelial dysfunction: implications for atherogenesis. *Clinics.* (2009) 64:471–8. doi: 10.1590/S1807-59322009000500015
85. Goncharov NV, Nadeev AD, Jenkins RO, Avdonin PV. Markers and biomarkers of endothelium: when something is rotten in the state. *Oxid Med Cell Longev.* (2017) 2017:9759735. doi: 10.1155/2017/9759735
86. Sandoo A, Kitas GD. A methodological approach to non-invasive assessments of vascular function and morphology. *J Vis Exp.* (2015) 45:267–73. doi: 10.3791/52339
87. Donnini S, Terzuoli E, Ziche M, Morbidelli L. Sulfhydryl angiotensin-converting enzyme inhibitor promotes endothelial cell survival through nitric-oxide synthase, fibroblast growth factor-2, and telomerase cross-talk. *J Pharmacol Exp Ther.* (2010) 332:776–84. doi: 10.1124/jpet.109.159178
88. Monti M, Solito R, Puccetti L, Pasotti L, Roggeri R, Monzani E, et al. Protective effects of novel metal-nonoates on the cellular components of the vascular system. *J Pharmacol Exp Ther.* (2014) 351:500–9. doi: 10.1124/jpet.114.218404
89. Solito R, Corti F, Chen CH, Mochly-Rosen D, Giachetti A, Ziche M, et al. Mitochondrial aldehyde dehydrogenase-2 activation prevents

beta-amyloid-induced endothelial cell dysfunction and restores angiogenesis. *J Cell Sci.* (2013) 126:1952–61. doi: 10.1242/jcs.117184
90. Putman DM, Liu KY, Broughton HC, Bell GI, Hess DA. Umbilical cord blood-derived aldehyde dehydrogenase-expressing progenitor cells promote recovery from acute ischemic injury. *Stem Cells.* (2012) 30:2248–60. doi: 10.1002/stem.1206
91. Vincent DT, Ibrahim YF, Espey MG, Suzuki YJ. The role of antioxidants in the era of cardiooncology. *Cancer Chemother Pharmacol.* (2013) 72:1157–68. doi: 10.1007/s00280-013-2260-4
92. Longo J, van Leeuwen JE, Elbaz M, Branchard E, Penn LZ. Statins as anticancer agents in the era of precision medicine. *Clin Cancer Res.* (2020) 26:5791–800. doi: 10.1158/1078-0432.CCR-20-1967
93. Rasanen M, Degerman J, Nissinen TA, Miinalainen I, Kerkela R, Siltanen A, et al. VEGF-B gene therapy inhibits doxorubicin-induced cardiotoxicity by endothelial protection. *Proc Natl Acad Sci U S A.* (2016) 113:13144–49. doi: 10.1073/pnas.1616168113
94. Nebigil CG. Prokineticin receptors in cardiovascular function: foe or friend? *Trends Cardiovasc Med.* (2009) 19:55–60. doi: 10.1016/j.tcm.2009.04.007
95. Urayama K, Guilini C, Messaddeq N, Hu K, Steenman M, Kurose H, et al. The prokineticin receptor-1 (GPR73) promotes cardiomyocyte survival and angiogenesis. *FASEB J.* (2007) 21:2980–93. doi: 10.1096/fj.07-8116com
96. Nguyen TL, Gasser A, Nebigil CG. Role of Prokineticin Receptor-1 in Epicardial Progenitor Cells. *J Dev Biol.* (2020) 8:32. doi: 10.3390/jdb8040032
97. Szatkowski C, Vallet J, Dormishian M, Messaddeq N, Valet P, Boulberdaa M, et al. Prokineticin receptor 1 as a novel suppressor of preadipocyte proliferation and differentiation to control obesity. *PLoS ONE.* (2013) 8:e81175. doi: 10.1371/journal.pone.0081175
98. Arora H, Boulberdaa M, Qureshi R, Bitirim V, Gasser A, Messaddeq N, et al. Prokineticin receptor-1 signaling promotes epicardial to mesenchymal transition during heart development. *Sci Rep.* (2016) 6:25541. doi: 10.1038/srep25541
99. Urayama K, Dedeoglu DB, Guilini C, Frantz S, Ertl G, Messaddeq N, et al. Transgenic myocardial overexpression of prokineticin receptor-2 (GPR73b) induces hypertrophy and capillary vessel leakage. *Cardiovasc Res.* (2009) 81:28–37. doi: 10.1093/cvr/cvn251
100. Demir F, Urayama K, Audebrand A, Toprak-Semiz A, Steenman M, Kurose H, et al. Pressure overload-mediated sustained PKR2 (Prokineticin-2 Receptor) signaling in cardiomyocytes contributes to cardiac hypertrophy and endotheliopathies. *Hypertension.* (2021) 77:1559–70. doi: 10.1161/HYPERTENSIONAHA.120.16808
101. Guilini C, Urayama K, Turkeri G, Dedeoglu DB, Kurose H, Messaddeq N, et al. Divergent roles of prokineticin receptors in the endothelial cells: angiogenesis and fenestration. *Am J Physiol Heart Circ Physiol.* (2010) 298:H844–52. doi: 10.1152/ajpheart.00898.2009
102. Gasser A, Brogi S, Urayama K, Nishi T, Kurose H, Tafi A, et al. Discovery and cardioprotective effects of the first non-Peptide agonists of the G protein-coupled prokineticin receptor-1. *PLoS ONE.* (2015) 10:e0121027. doi: 10.1371/journal.pone.0121027
103. Abdol Razak NB, Jones G, Bhandari M, Berndt MC, Metharom P. Cancer-associated thrombosis: an overview of mechanisms, risk factors, and treatment. *Cancers.* (2018) 10:380. doi: 10.3390/cancers10100380
104. Hahn VS, Lenihan DJ, Ky B. Cancer therapy-induced cardiotoxicity: basic mechanisms and potential cardioprotective therapies. *J Am Heart Assoc.* (2014) 3:e000665. doi: 10.1161/JAHA.113.000665
105. Audebrand A, Desaubry L, Nebigil CG. Targeting GPCRs against cardiotoxicity induced by anticancer treatments. *Front Cardiovasc Med.* (2019) 6:194. doi: 10.3389/fcvm.2019.00194

Conflict of Interest: The authors declare that the research was conducted in the absence of any commercial or financial relationships that could be construed as a potential conflict of interest.

Publisher's Note: All claims expressed in this article are solely those of the authors and do not necessarily represent those of their affiliated organizations, or those of the publisher, the editors and the reviewers. Any product that may be evaluated in this article, or claim that may be made by its manufacturer, is not guaranteed or endorsed by the publisher.

frontiers in Cardiovascular Medicine

ORIGINAL RESEARCH
published: 29 October 2021
doi: 10.3389/fcvm.2021.721080

Clinical Profile and Prognosis of a Real-World Cohort of Patients With Moderate or Severe Cancer Therapy-Induced Cardiac Dysfunction

Alberto Esteban-Fernández[1], Juan Fernando Carvajal Estupiñan[2], Juan José Gavira-Gómez[3], Sonia Pernas[4], Pedro Moliner[5], Alberto Garay[5], Álvaro Sánchez-González[6], Inmaculada Fernández-Rozas[1] and José González-Costello[5]*

[1] Cardiology Service, Hospital Universitario Severo Ochoa, Leganés, Spain, [2] Cardiology Service, Instituto del Corazón de Bucaramanga, Bucaramanga, Colombia, [3] Cardiology Department, Clínica Universidad de Navarra, Pamplona, Spain, [4] Oncology Department, Hospital Duran i Reynals, Institut Català d'Oncologia, L'Institut d'Investigació Biomèdica de Bellvitge (IDIBELL), L'Hospitalet de Llobregat, Barcelona, Spain, [5] Cardiology Department, Hospital Universitari de Bellvitge, IDIBELL, L'Hospitalet de Llobregat, Barcelona, Spain, [6] Bladder, Functional and Oncological Pathology Unit, Urology Department, Hospital Universitario Ramón y Cajal, Instituto Ramón y Cajal de Investigación Sanitaria (IRYCIS), University of Alcalá, Madrid, Spain

OPEN ACCESS

Edited by:
Susan Currie,
University of Strathclyde,
United Kingdom

Reviewed by:
Christian Cadeddu Dessalvi,
University of Cagliari, Italy
Jan Danser,
Erasmus Medical Center, Netherlands

***Correspondence:**
Alberto Esteban-Fernández
athalbertus@gmail.com

Specialty section:
This article was submitted to Cardio-Oncology, a section of the journal Frontiers in Cardiovascular Medicine

Received: 05 June 2021
Accepted: 29 September 2021
Published: 29 October 2021

Citation:
Esteban-Fernández A, Carvajal Estupiñan JF, Gavira-Gómez JJ, Pernas S, Moliner P, Garay A, Sánchez-González Á, Fernández-Rozas I and González-Costello J (2021) Clinical Profile and Prognosis of a Real-World Cohort of Patients With Moderate or Severe Cancer Therapy-Induced Cardiac Dysfunction. Front. Cardiovasc. Med. 8:721080. doi: 10.3389/fcvm.2021.721080

Introduction and Objectives: Cancer therapy-related cardiac dysfunction (CTRCD) is a common cause of cancer treatment withdrawal, related to the poor outcomes. The cardiac-specific treatment could recover the left ventricular ejection fraction (LVEF). We analyzed the clinical profile and prognosis of patients with CTRCD in a real-world scenario.

Methods: A retrospective study that include all the cancer patients diagnosed with CTRCD, defined as LVEF $< 50\%$. We analyzed the cardiac and oncologic treatments, the predictors of mortality and LVEF recovery, hospital admission, and the causes of mortality (cardiovascular (CV), non-CV, and cancer-related).

Results: We included 113 patients (82.3% women, age 49.2 $\pm$ 12.1 years). Breast cancer (72.6%) and anthracyclines (72.6%) were the most frequent cancer and treatment. Meantime to CTRCD was 8 months, with mean LVEF of 39.4 $\pm$ 9.2%. At diagnosis, 27.4% of the patients were asymptomatic. Cardiac-specific treatment was started in 66.4% of patients, with LVEF recovery-rate of 54.8%. Higher LVEF at the time of CTRCD, shorter time from cancer treatment to diagnosis of CTRCD, and younger age were the predictors of LVEF recovery. The hospitalization rate was 20.4% (8.8% linked to heart failure). Treatment with trastuzumab and lower LVEF at diagnosis of CTRCD were the predictors of mortality. Thirty point nine percent of patients died during the 26 months follow-up. The non-CV causes and cancer-related were more frequent than CV ones.

Conclusions: Cardiac-specific treatment achieves LVEF recovery in more than half of the patients. LVEF at the diagnosis of CTRCD, age, and time from the cancer treatment initiation to CTRCD were the predictors of LVEF recovery. The CV-related deaths were less frequent than the non-CV ones. Trastuzumab treatment and LVEF at the time of CTRCD were the predictors of mortality.

Keywords: cardio-oncology, cancer therapy-related cardiac dysfunction, cardiotoxicity, left ventricular systolic dysfunction (LVSD), cancer therapies

KEY POINTS

What is known about the topic?

In the patients with CTRCD, the cardiac-specific treatment can lead to LVEF recovery, although there is a lack of evidence about the clinical profile and the best strategy to manage these patients. Moreover, cardiotoxicity leads to the cancer treatment withdrawal, which impacts prognosis.

What does it bring back?

Cardio-oncology units can provide an early diagnosis and treatment of cardiotoxicity. The multidisciplinary teams can also allow continuing the cancer treatments, improving prognosis in the patients with CTRCD, emphasizing that most deaths are due to non-CV ones, such as cancer.

INTRODUCTION

A cancer therapy-related cardiac dysfunction (CTRCD) is a structural or functional myocardial injury secondary to cancer treatment. The cardiac damage depends on the type, dosage, and schedule of cancer therapies and other factors, such as the pre-existing cardiovascular (CV) risk factors and cardiac disease, age, or prior exposure to cardiotoxic therapy. In addition, cancer itself has been related to the increased cardiac peptides, associating higher mortality from any cause (1).

The incidence of CTRCD varies according to the definition and series. In a recently published multicenter registry, the incidence of cardiotoxicity, defined as a decrease in left ventricular ejection fraction (LVEF) below 50%, elevated cardiac biomarkers, or presence of other abnormal echo parameters, such as a significant decrease in the global longitudinal strain (GLS), reached 37.5%. The advanced stages of CTRCD imply left ventricular systolic dysfunction (LVSD), with different ranges of ejection fraction impairment (2). However, there is a lack of clinical trial-based evidence on the specific management of patients with LVSD secondary to the cancer treatment, and they are treated similarly to the rest of patients with LVSD (3). Recently, sacubitril-valsartan showed a potential benefit in cardiac remodeling in oncological patients (4, 5).

The prognosis of the patients with CTRCD seems to be worse than in other cardiomyopathies (6), and in the patients with heart failure (HF), non-CV causes of death, especially cancer, were more prevalent than HF progression or sudden death (7). Additionally, the cardiotoxic effects are a critical treatment-limiting adverse effect of some chemotherapies and targeted therapies, affecting the prognosis (8). It is essential to implement the multidisciplinary cardio-oncology units to diagnose and treat LVSD early (3).

Although the possibility of cardiotoxicity due to the cancer treatment is well-known, there is a lack of studies describing the clinical profile, LVEF dynamics, and the prognosis of patients with CTRCD in a real-world setting. Our study aimed to analyze the clinical profile, management, and prognosis of a cohort of oncological patients with moderate or severe cardiotoxicity in a real-world clinical practice.

Abbreviations: CTRCD, cancer therapy-related cardiac dysfunction; CV, cardiovascular; ESC, European Society of Cardiology; HF, heart failure; LVSD, left ventricular systolic dysfunction; NYHA, New York Heart Association.

MATERIALS AND METHODS

Study Population and Ethics

We retrospectively included all the consecutive patients diagnosed with CTRCD in the two tertiary hospitals in Spain: Clínica Universidad de Navarra between 2000 and 2011 and Hospital Universitari de Bellvitge between 2010 and 2016. The patients with cancer were referred to the cardiology units by the oncologists or hematologists to evaluate and treat cardiotoxicity before implementing the cardio-oncology units in these centers. The LVSD was defined as LVEF $<$ 50%, with a previously normal value, after cancer treatment administration, such as chemotherapy and targeted therapies, such as immunotherapy. The patients with baseline cardiac function not available or those with a previous history of LVSD were excluded. The study complied with the Declaration of Helsinki, and all the patients gave consent for using their data for research purposes.

Baseline Assessment and Follow-Up

The baseline characteristics, cardiovascular risk factors, type of cancer, and treatment received were recorded. The baseline cardiac function was analyzed by either echocardiogram or single photon emission computed tomography (SPECT) before the treatment and monitored periodically during follow-up to detect CTRCD. Both the methods have been validated to assess the myocardial function in the patients with cancer (9, 10). We analyzed the cardiac-specific treatment prescribed after the LVSD diagnosis according to medical criteria and recommendations of the European Society for Medical Oncology (ESMO) (11) and European Society of Cardiology (ESC) HF guidelines (2),

TABLE 1 | The baseline characteristics of patients with cancer therapy-related cardiac dysfunction (CTRCD).

Baseline characteristics	All patients (*n* = 113)	LVEF recovery (*n* = 63)	Non-LVEF recovery (*n* = 21)	Unknown LVEF recovery (*n* = 29)	*p*-value*
Sex (female)-*n* (%)	93 (82.3)	54 (85.7)	17 (81.0)	7 (24.1)	0.508
Age (years old)	49.2 (12.1)	49.6 (11.4)	51.1 (13.3)	47.0 (12.9)	0.620
Tobacco history-*n* (%)					0.756
Never smoker	85 (75.2)	49 (77.7)	15 (71.4)	21 (72.4)	
Past smoker	15 (13.3)	6 (9.5)	4 (19.0)	5 (17.2)	
Current smoker	13 (11.5)	8 (12.7)	2 (9.5)	3 (10.3)	
Arterial hypertension-*n* (%)	21 (18.6)	15 (23.8)	6 (28.6)	0 (0)	0.011
Diabetes-*n* (%)	6 (5.3)	4 (6.4)	2 (9.5)	0 (0)	0.325
Dyslipidemia-*n* (%)	15 (13.3)	9 (14.3)	4 (19.0)	2 (6.9)	0.519
BMI (kg/m^2)	25.4 (3.8)	25.4 (4.1)	24.9 (3.5)	26.6 (1.3)	0.777
Previous cancer-*n* (%)	15 (13.3)	9 (14.3)	2 (9.5)	4 (13.8)	0.868
Chronic kidney disease-*n* (%)	0 (0)				
Previous cardiopathy-*n* (%)	3 (2.7)	2 (3.2)	1 (4.8)	0 (0)	0.594
Baseline LVEF (%)	57.7 (5.5)	58.4 (5.8)	56.7 (4.5)	56.9 (5.6)	0.210
Previous HF-*n* (%)	0 (0)				
SBP (mmHg)	119.1 (14.2)	117.6 (13.3)	124.2 (16.6)	124.7 (21.4)	0.292
Previous AF-*n* (%)	2 (1.8)	2 (3.2)	0 (0)	0 (0)	0.833
HR (bpm)	84.0 (9.6)	84.2 (9.7)	82.3 (7.7)	85.7 (15.3)	0.667
Prior medical treatment-*n* (%)					0.186
Beta-blockers	1 (0.9)	0 (0)	1 (4.8)	(0)	
ACE-I/ARB	11 (9.7)	9 (14.3)	2 (9.5)	(0)	
Digoxin	1 (0.9)	1 (1.6)	0 (0)	(0)	
Diuretics	6 (5.3)	5 (7.9)	1 (4.8)	(0)	
Statins	6 (5.3)	3 (4.8)	1 (4.8)	2 (6.9)	
Type of cancer-n (%)					0.880
Breast cancer	82 (72.6)	49 (77.8)	15 (71.4)	18 (62.1)	
Hematological diseases	18 (15.9)	9 (14.3)	3 (14.3)	6 (20.7)	
Bone cancer	4 (3.5)	2 (3.2)	1 (4.8)	1 (3.5)	
Gynecologic non-breast cancer	3 (2.7)	1 (1.6)	1 (4.8)	1 (3.5)	
Other	6 (5.3)	2 (3.2)	1 (4.8)	3 (10.3)	
Chemotherapy agent-*n* (%)					
Trastuzumab	38 (33.6)	32 (50.8)	3 (14.3)	3 (10.3)	0.004
Anthracycline	82 (72.6)	46 (73.0)	16 (76.2)	20 (69.0)	0.750
Cyclophosphamide	54 (47.8)	33 (52.4)	8 (38.1)	11 (37.9)	0.236
Docetaxel	36 (31.9)	23 (36.5)	4 (19.0)	9 (31.0)	0.130
Cisplatin/Carboplatin	24 (21.2)	17 (27.0)	3 (14.3)	4 (13.8)	0.560
Gemcitabine	10 (8.8)	2 (3.2)	4 (19.0)	4 (13.8)	0.015
Fluorouracil	35 (31.0)	19 (30.2)	5 (23.8)	11 (37.9)	0.556
Paclitaxel	25 (2.1)	14 (22.2)	6 (28.6)	5 (17.2)	0.584
Thoracic radiotherapy-*n* (%)	60 (53.1)	37 (58.7)	8 (38.1)	15 (51.7)	0.396
Time from chemotherapy to CTRCD (months)					
Median time	8 (4, 19)	9 (4, 17)	5 (2.5; 12)	5 (2.5; 12)	0.221
Mean time	30.2 (57.8)	27.8 (54.3)	65.4 (86.2)	9.8 (12.8)	0.07
Start cardiac- specific treatment-*n* (%)	75 (66.4)	54 (85.7)	17 (81)	4 (13.8)	0.127
Death patients-*n* (%)	35 (30.9)	20 (31.7)	7 (33.3)	8 (27.6)	0.297
CV causes	8 (7.1)	3 (4.8)	4 (19.1)	1 (3.5)	0.06
Non-CV causes	12 (10.6)	8 (12.7)	1 (4.8)	3 (10.3)	0.552
Cancer	15 (13.3)	9 (14.3)	2 (9.5)	4 (13.8)	0.804

ACE-I, angiotensin-converting-enzyme inhibitor; AF, atrial fibrillation; ARB, angiotensin II receptor blockers; BMI, body mass index; BPM, beats per minute; CTRCD, cancer therapy-related cardiac dysfunction; CV, cardiovascular; HF, heart failure; HR, heart rate; LVEF, left ventricular ejection fraction; MRA, mineralocorticoid receptor antagonist; SBP, systolic blood pressure. Cardiac-specific treatment meant to receive at least ACE-I/ARB after CTRCD diagnosis.

**p-value is calculated to compare LVEF recovery and non-LVEF recovery patients.*

defined as starting treatment with at least an angiotensin-converting enzyme inhibitors (ACE-I) or an angiotensin receptor blockers (ARB). The follow-up was performed during the routine clinic visits by reviewing the electronic medical records. We recorded different events: the New York Heart Association (NYHA) functional class, hospital admission, medical treatment changes, LVEF recovery, the need for heart transplantation, and death (CV, cancer, and non-CV). The heart transplantation was considered a CV death in the survival analysis. The LVEF recovery was defined as LVEF $\geq$ 50% at any time during the follow-up.

Statistical Analysis

The quantitative variables are expressed as mean and SD or median and interquartile range (IQR) when data did not fit a normal distribution and the qualitative variables as number and percentage. The continuous quantitative variables were compared using the Student's *t*-test or the sum of Wilcoxon's ranges for non-normally distributed variables. The categorical variables were compared with the chi-square test and Fisher's exact test when appropriate. A significance level of $\leq$ 0.05 (bilateral) was established for all the statistical tests.

The survival distribution related to time to an event was evaluated using the Kaplan–Meier method, in the whole population, and according to LVEF recovery. The log-rank test was employed to compare the survival curves.

A multivariate binary logistic regression analysis was performed to evaluate the LVEF recovery predictors, using the sequential inclusion and exclusion method, with inclusion threshold $p < 0.05$ and exclusion higher than 0.2 in the univariate analysis. A multivariate Cox proportional hazards regression model was conducted to calculate the adjusted hazard ratios (HR) and to determine the effect of several variables on survival function. A univariate analysis was performed to select the variables for both the multivariate analyses, with inclusion threshold $p < 0.05$ and exclusion >0.2. In the multivariate analysis, a $p < 0.05$ was considered statistically significant. Age was selected for the multivariate analysis due to its clinical relevance. A statistical analysis was performed with SPSS 23.0 (IBM, NY, USA).

RESULTS

We included 113 patients whose baseline characteristics are summarized in **Table 1**. The most frequent diagnoses were breast cancer (72.6%) and hematological malignancies (15.9%). In total, 72% of the patients underwent surgery, and 53.1% thoracic radiotherapy. The most used chemotherapy treatments were: anthracyclines (72.6%), cyclophosphamide (47.8%), and trastuzumab (33.6%).

TABLE 3 | Treatment initiated in the patients with cancer therapy-related cardiomyopathy.

Drug	Total (*n* = 75)	Patients with LVEF recovery (*n* = 54)	Patients with LSVD persistence (*n* = 17)	*p*-value
Beta-blocker-*n* (%)	56 (74.7)	38 (70.4)	14 (82.4)	0.888
Carvedilol	45 (60.0)	33 (61.1)	9 (52.9)	0.029
Bisoprolol	10 (13.3)	5 (9.3)	5 (29.4)	
Nevibolol	1 (1.3)	1 (1.9)	0 (0)	
ACE-I-*n* (%)	62 (82.7)	44 (81.5)	14 (82.4)	0.174
Enalapril	52 (69.3)	37 (68.5)	11 (64.7)	0.545
Ramipril	7 (9.3)	5 (9.3)	2 (11.8)	
Otros	2 (2.7)	1 (1.9)	1 (5.9)	
ARB-*n* (%)	11 (14.6)	8 (14.8)	3 (17.6)	0.770
Losartan	5 (6.6)	5 (9.3)	0 (0)	0.048
Valsartan	4 (5.3)	3 (5.6)	1 (5.9)	
Candesartan	2 (2.7)	0 (0)	2 (11.8)	
MRA-*n* (%)	15 (20.0)	10 (18.5)	3 (17.6)	0.663
Spironolacton	12 (16.0)	9 (16.7)	2 (11.8)	0.242
Eplerenone	3 (4.0)	1 (1.9)	1 (5.9)	
Digoxin-*n* (%)	8 (10.7)	5 (9.3)	3 (17.6)	0.816
Diuretics-*n* (%)	44 (58.7)	27 (50.0)	14 (82.4)	0.209

ACE-I, angiotensin-converting-enzyme inhibitor; ARB, angiotensin II receptor blockers; LVEF, left ventricular ejection fraction; LVSD, left ventricular systolic dysfunction; MRA, mineralocorticoid receptor antagonists.
We excluded four patients from the sub-analysis due to lost data regarding LVEF recovery.

TABLE 2 | Evolution of left ventricular ejection fraction (LVEF) during follow-up of patients with cancer therapy-related to cardiomyopathy.

Parameter	Baseline	Diagnosis of CTRCD	Last Follow-up	*p*-value
LVEDD (mm)	49.5 (4.4)	54.7 (5.2)	49.1 (5.5)	0.0001
LVESD (mm)	35.7 (4.1)	42.7 (6.1)	34.3 (5.8)	0.0001
LVEDV (mL)	118.8 (22.1)	140.5 (34.6)	107.3 (33.0)	0.002
LVESV (mL)	55.3 (12.9)	83.7 (25.8)	46.1 (19.5)	0.0001
LVEF (%)	58.2 (5.5)	38.8 (8.5)	54.1 (9.2)	0.0001
LVEF in recovered patients (%)	58.3 (5.8)	39.6 (8.3)	56.8 (5.6)	0.0001
LVEF in patients with persistence of LVSD (%)	57.7 (2.9)	34.1 (8.9)	38.3 (9.9)	0.0001

LVEDD, end-diastolic diameter of the left ventricle; LVEDV, end-diastolic volume of the left ventricle; LVESD, end-systolic diameter of the left ventricle; LVESV, end-systolic volume of the left ventricle; LVEF, left ventricular ejection fraction; LVSD, left ventricular systolic dysfunction.
The baseline values are those before starting the cancer treatment. LVEDD, LVEDV, LVESD, and LVESV are only presented when we had echocardiographic studies (n = 68).

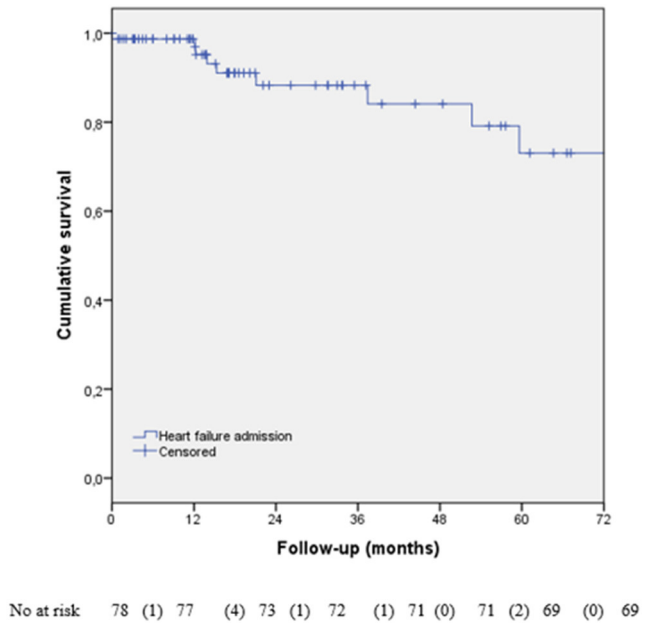

FIGURE 1 | Kaplan–Meier analysis of heart failure (HF) hospital admission during follow-up. We have lost data about HF admission in the 35 patients.

TABLE 4 | Maintenance of cardiac treatment in the patients with LVEF recovery after cancer therapy-related cardiomyopathy.

Drug	Patients ($n = 37$)	*p*-value	Time (months)
Beta-blockers-*n* (%)	37 (100)		12 [IQR: 7 to 33]
Carvedilol	31 (83.8)	0.039	
Bisoprolol	6 (16.2)		
ACE-I-*n* (%)	35 (94.6)		13 [IQR: 6.8 to 34.5]
Enalapril	33 (89.2)	0.24	
Ramipril	2 (5.4)		
ARB-*n* (%)	9 (24.3)		24 [IQR: 24 to 24]
Valsartan	4 (10.8)	0.13	
Losartán	5 (13.5)		
ARM-*n* (%)	13 (35.1)		
Spironolacton	12 (32.4)	0.009	
Eplerenone	1 (2.7)		
Digoxin-*n* (%)	4 (10.8)		14.5 [IQR: 8.8 to 21.8]
Diuretics-*n* (%)	16 (43.2)		
Statins-*n* (%)	16 (43.2)		

ACE-I, angiotensin-converting-enzyme inhibitor; ARB, angiotensin II receptor blockers; ARM, mineralocorticoid receptor antagonist.
Time refers to the median time that the cardiac-specific treatment was maintained after LVEF recovery.

Cancer therapy-related cardiac dysfunction was diagnosed by echocardiography in 68 patients (60.2%) and SPECT in 45 (39.8%). The mean LVEF was 39.4 ± 9.2% at the time of diagnosis of CTRCD (**Table 2**). The median time from starting chemotherapy to the diagnosis of cardiotoxicity was 8 months [IQR: 4–19]. At the time of diagnosis, 31 patients (27.4%) were asymptomatic, 41 were in NYHA II (36.3%), 13 in NYHA III (11.5%), and 5 in NYHA IV (4.4%). Of the symptomatic ones, 25 (21.2%) had been admitted for HF. In 43 patients (38.1%), the diagnosis of CTRCD implied a change in the chemotherapy dose-schedule or withdrawal of cancer therapy.

The cardiac-specific treatment was started in 75 patients (66.4%), as shown in **Table 3**. After a median follow-up of 26.2 months [IQR:12.2–94.5], most of the patients were in NYHA I (39.5%) or II (48.1%). Twenty-three patients were admitted to the hospital (one for a CV event, 10 for HF (**Figure 1**), and 12 for non-CV causes, excluding cancer routine admissions).

Left ventricular ejection fraction was recovered in 62 patients (54.8%), 54 of them (87.1%) receiving cardiac-specific treatment. LVSD persisted in 21 patients (18.6%). LVEF determination during the follow-up was lost in 30 patients (26.5%), but there were data about survival status in all the patients included. After LVEF recovery, 37 patients (58.7%) continued cardiac-specific treatment, as is shown in **Table 4**. Among the patients who continued treatment, eight patients presented recurrent LVEF dysfunction, five of them due to the new chemotherapy treatment.

In the binary logistic regression analysis (**Table 5**), higher LVEF at the time of CTRCD [*OR* 1.13; *CI* 95% 1.03–1.25; $p = 0.008$], shorter time from starting chemotherapy to the diagnosis of CTRCD [*OR* 0.99; *CI* 95% 0.98–1.00; $p = 0.023$], and younger age [*OR* 0.94; *CI* 95% 0.88–0.99; $p = 0.03$] were identified as the predictors of LVEF recovery, independently of trastuzumab treatment, HF admission at diagnosis of CTRCD, and Carvedilol treatment after dysfunction. For each 5% of LVEF increase at the time of diagnosis of CTRCD, the probability of recovery of LVEF increased by 1.75.

In addition, we identified the treatment with trastuzumab [*HR* 1.25; *CI* 95% 1.02–4.96; $p = 0.045$] and lower LVEF at the time of diagnosis of CTRCD [*HR* 0.94; *CI* 95% 0.91–0.97; $p = 0.0001$] as the predictors of mortality independent of age, dyslipidemia, anthracyclines treatment, and LVEF recovery during the follow-up (**Table 6**).

As it is shown in **Figure 2**, 78 (69.1%) patients were alive, and 35 (30.9 %) had died at the end of follow-up (six of CV causes and two were transplanted, 15 of cancer and 12 of non-CV causes) (**Table 1**). There were no differences in the mortality according to the presence of LVEF recovery, but there was a trend to earlier mortality from the CV causes in those with the absence of LVEF recovery (**Figure 3**).

DISCUSSION

This is one of the largest real-world cohorts reported in the literature of patients with moderate to severe CTRCD and long-term follow-up to the best of our knowledge. The main findings of our study were: (1) with appropriate cardiac treatment in 66% of all patients, up to 55% of patients achieve LVEF recovery; (2) early CTRCD diagnosis is associated with improved LVEF recovery after initiation of cardiac-specific treatment; (3) less advanced LVSD at the time of CTRCD diagnosis is associated with the

TABLE 5 | Binary logistic regression analysis to identify the predictors of LVEF recovery in the patients with cancer therapy-related cardiomyopathy.

	Predictors of LVEF recovery					
	Univariate			**Multivariate**		
	OR	**CI 95%**	***p*-value**	**OR**	**CI 95%**	***p*-value**
Age (1 year)	0.99	0.95–1.03	**0.63**	0.94	0.88–0.99	**0.03**
Female sex	1.39	0.38–5.08	0.62			
No smoking history	0.93	0.18–4.98	0.94			
Arterial hypertension	0.80	0.26–2.42	0.79			
Dyslipidemia	0.72	0.20–2.64	0.62			
Diabetes	0.66	0.11–3.86	0.64			
BMI (1 kg/m^2)	1.03	0.85–1.24	0.77			
Baseline LVEF (1%)	1.07	0.97–1.17	0.20			
LVEF at the time of diagnosis of CTRCD (1%)	1.10	1.03–1.2	**0.002**	1.13	1.03–1.25	**0.008**
Trastuzumab treatment	6.00	1.60–22.46	**0.008**	3.15	0.44–22.8	0.26
Anthracyclines treatment	0.83	0.26–2.61	0.75			
Thoracic radiotherapy	2.1	0.75–6.03	0.16			
HF admission at CTRCD diagnosis	0.35	0.10–1.28	0.11			
Cardiac specific treatment	1.56	0.42–5.80	0.51			
Beta-blocker treatment	0.80	0.28–2.29	0.68			
Carvedilol treatment	4.58	1.02–20.69	**0.048**	1.78	0.27–11.6	0.55
ACE-I treatment	1.19	0.41–3.45	0.74			
ARB treatment	0.91	0.22–3.78	0.89			
MRA treatment	1.04	0.25–4.26	0.96			
Time from starting chemotherapy to dysfunction (1 month)	0.99	0.98–1.00	**0.035**	0.99	0.98–1.00	**0.023**

ACE-I, angiotensin-converting-enzyme inhibitor; ARB, angiotensin II receptor blockers; BMI, body mass index; CI, confidence interval; CTRCD, cancer therapy-related cardiac dysfunction; CV, cardiovascular; HF, heart failure; LVEF, left ventricular ejection fraction; MRA, mineralocorticoid receptor antagonist; OR, odds ratio.
Cardiac-specific treatment meant to receive at least ACE-I/ARB after CTRCD diagnosis. Bold means statistically significant ($p < 0.05$).

improved LVEF recovery and increased overall survival, and (4) all-cause mortality in the patients with CTRCD was ∼40% at 5 years of follow-up. There was a trend to earlier mortality from the CV causes in those that did not achieve LV recovery. Our findings emphasize the need to develop multidisciplinary cardio-oncology units to make an early diagnosis of CTRCD and start the cardiac-specific treatment as soon as possible to improve the prognosis.

Some factors associated with CTRCD are CV risk factors, older age, or ischemic disease. However, in our real-life cohort, most of them were young women with breast cancer and low incidence of CV risk factors. In other registers, breast cancer and hematological diseases were the most frequent ones (12). The criteria for CTRCD diagnosis varied in different studies, and we established a cut-off of LVEF <50% according to the ESC guidelines and other similar studies (2, 7). All the patients in our cohort had reduced to mid-range ejection fraction (LVEF 39.4 ± 9.2%).

Depending on the type of cancer, treatment schedule, and individual characteristics, some studies reported that the cardiotoxicity usually appeared during the first year after starting chemotherapy (13–15), similar to our cohort (8 months). Most importantly, LVEF at the moment of diagnosis of CTRCD was linked to LVEF recovery and mortality in our study, emphasizing the need to perform early diagnosis of CTRCD and initiate the treatment before LVEF deteriorates further that include new parameters, such as GLS. This is important as 27.4% of our patients were asymptomatic at the time of diagnosis. Thus, the development of protocols with the periodic cardiac function assessment is necessary to detect CTRCD, as the time to dysfunction after starting the cancer drug treatment was one of the most relevant parameters for LVEF recovery in our study.

Early medical treatment has been demonstrated to improve LVEF (13), and the ESC guidelines recommended the cardiac-specific treatment in the symptomatic patients with LVSD (2). In the patients with CTRCD, the evidence with ACE-I and beta-blockers in the asymptomatic patients was limited to the SAVE trial in ischemic patients (16) and SAFEHEART to prevent the development of symptoms (17). When our study was performed, the international guidelines recommended that the patients who developed CTRCD during or following treatment with Type II agents (i.e., trastuzumab) in the absence of anthracyclines could be observed if they remained asymptomatic and LVEF remained ≥40% (11). This explains why 34% of patients in our series did not receive cardiac-specific treatment, as many of our patients had mid-range LVEF and were asymptomatic. In these cases, trastuzumab was interrupted, and LVEF was reassessed 1 month later without cardiac-specific treatment initiation. This could have led to slower or less LVEF recovery and more interruptions of treatment with trastuzumab, which could have influenced the fact that trastuzumab was associated with increased mortality in our series. Also, it may be possible that

TABLE 6 | The Cox regression analysis to identify the predictors of mortality in the patients with cancer therapy-related cardiomyopathy.

	Predictors of mortality					
	Univariate			Multivariate		
	HR	CI 95%	*p*-value	HR	CI 95%	*p*-value
Age (1 year)	1.01	0.98–1.03	**0.69**	1.01	0.98–1.05	0.482
Female sex	1.24	0.54–2.84	0.62			
No smoking history	1.03	0.42–0.25	0.96			
Arterial hypertension	1.00	0.35–2.88	0.99			
Dyslipidemia	5.58	0.76–40.78	**0.09**	5.73	0.78–42.0	0.09
Diabetes	1.12	0.15–8.32	0.92			
BMI (1 kg/m^2)	0.88	0.63–1.22	0.44			
Baseline LVEF (1%)	0.97	0.90–1.03	0.31			
LVEF at the time of diagnosis of CTRCD (1%)	0.94	0.91–0.97	**0.001**	0.94	0.91–0.97	**0.0001**
Trastuzumab treatment	1.83	0.84–3.98	**0.14**	2.25	1.02–4.96	**0.045**
Anthracyclines treatment	1.88	0.95–3.70	**0.07**	1.56	0.78–3.12	0.212
Thoracic radiotherapy	1.37	0.70–2.67	0.35			
HF admission at diagnosis	1.64	0.77–3.51	0.20			
Cardiac specific treatment	0.75	0.29–1.99	0.56			
Beta-blocker treatment	0.79	0.38–1.63	0.52			
Carvedilol treatment	0.43	0.05–3.49	0.43			
ACE-I treatment	1.58	0.70–3.60	0.27			
ARB treatment	0.21	0.03–1.55	0.13			
MRA treatment	1.95	0.83–4.59	0.13			
Time from starting chemotherapy to dysfunction (1 month)	1.00	0.99–1.01	0.72			
LVEF recovery during follow-up	1.33	0.54–1.33	0.53			
HF admission during follow-up	1.09	0.32–3.73	0.89			

ACE-I, angiotensin-converting-enzyme inhibitor; ARB, angiotensin II receptor blockers; BMI, body mass index; CI, confidence interval; CTRCD, cancer therapy-related cardiac dysfunction; CV, cardiovascular; HF, heart failure; HR, hazard ratio; LVEF, left ventricular ejection fraction; MRA, mineralocorticoid receptor antagonist.
Cardiac-specific treatment meant to receive at least ACE-I/ARB after CTRCD diagnosis. Bold means statistically significant ($p < 0.05$).

the increase of mortality with trastuzumab happened in more advanced oncological patients.

In our study, 87.1% of patients who recovered LVEF received the cardiac-specific treatment, emphasizing the need for cardio-oncology units to start the cardiac treatment as early as possible in all the patients with CTRCD to improve the outcomes. The most employed drugs were ACE-I and beta-blockers, specially Carvedilol and Enalapril, similar to other studies (18). Martin-Garcia et al. recently demonstrated in a small 67 patients study that sacubitril-valsartan improved the remodeling and functional status in the patients with CTRCD (5), so future studies should focus on this possibility.

Left ventricular ejection fraction recovery rate varied according to the definition in different studies. Cardinale et al. distinguished between the partial recovery (LVEF increase >5 total points and >50%) and full recovery (LVEF recovery to baseline) (13). Lupon et al., in a study with 1,057 patients with HF and LVSD, considered recovered a LVEF $\geq$ 45% after a previous one of <45% (19). In the study of Pareek et al., with 535 patients with CTRCD, they reported a recovery rate of 94% with the treatment, but they considered a LVEF change from 45 to 53% (20). In our study, we established a cut-off of 50% to consider LVEF recovery. In total, 55% of our cohort recovered LVEF, similar to other studies [Cardinale et al. [42%] (18), Hamirani et al. [44%] (15), or Ohtani et al. [67.3%] (21)].

The presence of severe CTRCD (18) and the use of drugs, such as anthracyclines (22) have been related to non-reversible myocardial damage. However, although most of the patients received anthracyclines in our cohort, more than half of them recovered LVEF, probably because of the cardiac-specific treatment and a short time to CTRCD diagnosis.

The mean follow-up of our cohort was similar to CARDIOTOX (12), but some of our patients, especially with LVSD persistence, had long-term follow-up (26 months, IQR 12.2–94.5). Hospital admission during CTRCD has been poorly studied. Yoon et al. reported 9% of HF admission and 11% of symptomatic patients during the follow-up (23). In another study, only 10% of patients were in NYHA III-IV during follow-up, similar to our cohort (12.4%) (20). The hospital admission rate of our cohort was 20.4%, mainly due to non-CV causes (excluding cancer routine admission), with only 8.8% because of HF, similar to Yoon et al. study (23).

The long-term maintenance of cardiac-specific treatment after recovery was supported by treatment for heart failure in patients with recovered dilated cardiomyopathy (TRED-HF) trial (24). In our study, 58.7% of the patients maintained long-term cardiac treatment after recovery. In the study by Pareek et al., 88% of the

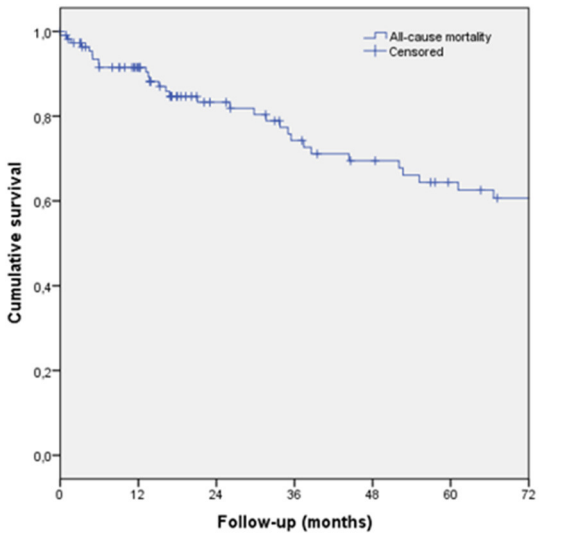

No at risk	113	(3)	110	(6)	104	(0)	104	(5)	99	(1)	98	(4)	94	(6)	88

FIGURE 2 | Kaplan–Meier survival analysis according to all-cause of death.

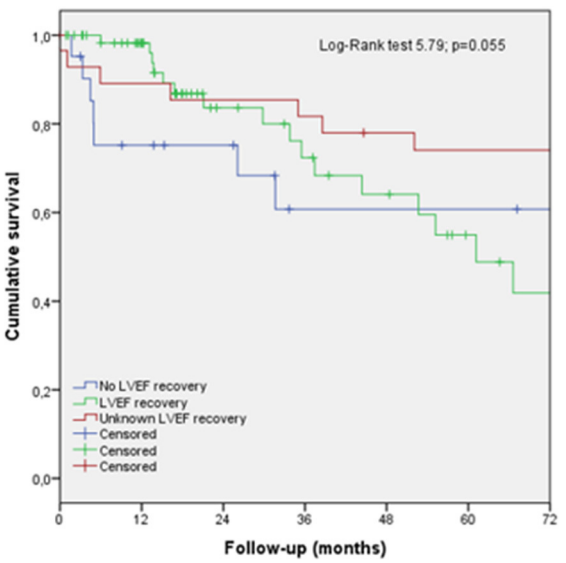

No at risk															
No LVEFr	21	(5)	16	(2)	14	(0)	14	(0)	14	(0)	14	(0)	14	(0)	14
LVEFr	63	(1)	62	(5)	57	(2)	55	(3)	52	(1)	51	(2)	49	(1)	48
Unknown	29	(3)	26	(1)	25	(0)	25	(2)	23	(0)	23	(1)	22	(0)	22

FIGURE 3 | Kaplan–Meier survival analysis according to left ventricular ejection fraction (LVEF) recovery. LVEF, left ventricular ejection fraction; LVEFr, left ventricular ejection fraction recovery. Unknown refers to the patients with lost data about LVEF recovery. Heart transplantation was included as cardiovascular (CV) death.

patients continued cancer treatment after cardiac optimization and close follow-up in a cardio-oncology unit (20), slightly above what was achieved in our cohort (62%). If the patients needed to continue the cancer treatments, we should avoid cardiotoxic ones to reduce the risk of further new dysfunction, as 12.9% of our patients with LVEF recovery had recurrent LVSD in our study. Some studies demonstrated that LVEF recovery improved the morbidity and mortality (19), but it remained controversial in the patients with CTRCD. Yoon et al., in a study with 243 patients, reported the worst outcomes in the non-recovered group (symptomatic HF, HF hospitalization, and death), but they did not analyze the mortality separately (23). Our study did not see the statistical differences in mortality in the patients with LVEF recovery, but those that did not achieve the LVEF recovery had a trend to earlier CV-specific mortality.

In CARDIOTOX, severe cardiotoxicity meant a 10-fold increase in the total mortality compared with mild or no CTRCD. Abdel-Qadir et al. published a study in which women with early-stage breast cancer died mostly of cancer, but those above 66 years with at least 5 years of survival had more mortality for CV causes than cancer (25). In our study, 30.9% of patients died, with only 22.8% of deaths related to the CV causes. In the patients with CTRCD, the most critical issue for the prognosis seemed not to be the cardiac problem, but also non-CV causes and cancer. Thus, the establishment of multidisciplinary cardio-oncology units can help avoid discontinuing the cancer treatment, as the prognosis is linked mostly to their cancer.

Cancer therapy-related cardiac dysfunction diagnosis is the most common indication for chemotherapy interruption (up to 38.1% in our cohort) (26). For instance, the patients with HER2-breast cancer with early trastuzumab interruption had higher rates of cancer recurrence and death than the patients receiving uninterrupted treatment (8). This fact could explain that trastuzumab was identified as a predictor of mortality in our cohort, emphasizing the negative impact of chemotherapy withdrawal on the prognosis.

Our study has some limitations. First, there were some missing visits or incomplete data collection during the follow-up related to the research nature of a retrospective registry. Second, all the CTRCD and LVEF recovery diagnoses were based only on LVEF, and we did not use other parameters, such as GLS (3). Also, we cannot have biomarkers (i.e., natriuretic peptides or Troponin) in most of the patients. Third, all the patients did not start cardiac-specific treatment due to the changing recommendations during the inclusion period. Finally, there was no specific follow-up protocol, and this meant that it was performed according to the usual clinical practice.

CONCLUSIONS

In a real-world scenario, we have shown that up to 55% of the patients with CTRCD achieve LVEF recovery. Cardiac-specific treatment was given to 66% of the patients. The predictors of LVEF recovery were LVEF at CTRCD diagnosis, age, and time from starting the chemotherapy to cardiac dysfunction. Conversely, the predictors of mortality were

trastuzumab treatment and LVEF at the time of CTRCD. Of note, only 23% of our patients died of CV causes. Our findings emphasize the need to develop cardio-oncology units to make an early diagnosis of CTRCD and initiate the cardiac treatment to improve the prognosis of the patients with cancer.

DATA AVAILABILITY STATEMENT

The raw data supporting the conclusions of this article will be made available by the authors, without undue reservation.

ETHICS STATEMENT

The studies involving human participants were reviewed and approved by Clinica Universidad de Navarra, Pamplona, Spain. The Ethics Committee waived the requirement of written informed consent for participation.

AUTHOR CONTRIBUTIONS

AE-F and JG-C: conception and design or analysis, interpretation of data, drafting of the manuscript, revising it critically for important intellectual content, and final approval of the manuscript submitted. JC and JG-G: conception and design or analysis and final approval of the manuscript submitted. SP, AG, ÁS-G, and IF-R: drafting the manuscript or revising it critically for important intellectual content and final approval of the manuscript submitted. PM: interpretation of data and final approval of the manuscript submitted. All authors contributed to the article and approved the submitted version.

FUNDING

Fundación para la Investigación Biomédica del hospital Universitario Puerta de Hierro supports authors with fees to open access.

REFERENCES

1. Pavo N, Raderer M, Hülsmann M, Neuhold S, Adlbrecht C, Strunk G, et al. Cardiovascular biomarkers in patients with cancer and their association with all-cause mortality. *Heart.* (2015) 101:1874–80. doi: 10.1136/heartjnl-2015-307848
2. Ponikowski P, Voors AA, Anker SD, Bueno H, Cleland JGF, Coats AJS, et al. (2016). ESC Guidelines for the diagnosis and treatment of acute and chronic heart failure. *Eur Heart J.* (2016) 37:2129–200. doi: 10.1093/eurheartj/ehw128
3. Zamorano JL, Lancellotti P, Rodriguez Muñoz D, Aboyans V, Asteggiano R, Galderisi M, et al. 2016 ESC Position Paper on cancer treatments and cardiovascular toxicity developed under the auspices of the ESC Committee for Practice Guidelines. *Eur Heart J.* (2016) 37:2768–801. doi: 10.1093/eurheartj/ehw211
4. Martín-García A, Díaz-Peláez E, Martín-García AC, Sánchez-González J, Ibáñez B, Sánchez PL. Myocardial function and structure improvement with sacubitril/valsartan in cancer therapy-induced cardiomyopathy. *Rev Esp Cardiol.* (2020) 73:268–9. doi: 10.1016/j.rec.2019.07.006
5. Martín-Garcia A, López-Fernández T, Mitroi C, Chaparro-Muñoz M, Moliner P, Martin-Garcia AC, et al. Effectiveness of sacubitril–valsartan in cancer patients with heart failure. *ESC Hear Fail.* (2020) 7:763–7. doi: 10.1002/ehf2.12627
6. Felker GM, Thompson RE, Hare JM, Hruban RH, Clemetson DE, Howard DL, et al. Underlying causes and long-term survival in patients with initially unexplained cardiomyopathy. *N Engl J Med.* (2000) 342:1077–84. doi: 10.1056/NEJM200004133421502
7. Moliner P, Lupón J, de Antonio M, omingo M, Santiago-Vacas E, Zamora E, et al. Trends in modes of death in heart failure over the last two decades: less sudden death but cancer deaths on the rise. *Eur J Heart Fail.* (2019) 21:1259–66. doi: 10.1002/ejhf.1569
8. Copeland-Halperin RS, Al-Sadawi M, Patil S, Liu JE, Steingart RM, Dang CT, et al. Early trastuzumab interruption and recurrence-free survival in ERBB2 -positive breast cancer. *JAMA Oncol.* (2020) 6:1971–2. doi: 10.1001/jamaoncol.2020.4749
9. Russell RR, Alexander J, Jain D, Poornima IG, Srivastava A V, Storozynsky E, et al. The role and clinical effectiveness of multimodality imaging in the management of cardiac complications of cancer and cancer therapy. *J Nucl Cardiol.* (2016) 23:856–84. doi: 10.1007/s12350-016-0538-8
10. Carlos Plana J, Galderisi M, Barac A, Ewer MS, Ky B, Scherrer-Crosbie M, et al. Expert consensus for multimodality imaging evaluation of adult patients during and after cancer therapy: a report from the american society of echocardiography and the European Association of Cardiovascular Imaging from the Cleveland Clinic. *J Am Soc Echocardiogr.* (2014) 27:911–39. doi: 10.1016/j.echo.2014.07.012
11. Curigliano G, Cardinale D, Suter T, Plataniotis G, De azambuja E, Sandri MT, et al. Cardiovascular toxicity induced by chemotherapy, targeted agents and radiotherapy: ESMO clinical practice guidelines. *Ann Oncol.* (2012) 23:vii155–66. doi: 10.1093/annonc/mds293
12. López-Sendón J, Ávarez-Ortega C, Zamora Auñon P, Buño Soto A, Lyon AR, Farmakis D, et al. Classification, prevalence, and outcomes of anticancer therapy-induced cardiotoxicity: the CARDIOTOX registry. *Eur Heart J.* (2020) 41:1720–9. doi: 10.1093/eurheartj/ehaa006
13. Cardinale D, Colombo A, Bacchiani G, Tedeschi I, Meroni CA, Veglia F, et al. Early detection of anthracycline cardiotoxicity and improvement with heart failure therapy. *Circulation.* (2015) 131:1981–8. doi: 10.1161/CIRCULATIONAHA.114.013777
14. Khan AA, Ashraf A, Singh R, Rahim A, Rostom W, Hussain M, et al. Incidence, time of occurrence and response to heart failure therapy in patients with anthracycline cardiotoxicity. *Intern Med J.* (2017) 47:104–9. doi: 10.1111/imj.13305
15. Hamirani Y, Fanous I, Kramer CM, Wong A, Salerno M, Dillon P. Anthracycline- and trastuzumab-induced cardiotoxicity: a retrospective study. *Med Oncol.* (2016) 33:82. doi: 10.1007/s12032-016-0797-x
16. Vantrimpont P, Rouleau JL, Wun CC, Ciampi A, Klein M, Sussex B, et al. Additive beneficial effects of beta-blockers to angiotensin-converting enzyme inhibitors in the Survival and Ventricular Enlargement (SAVE) study. *J Am Coll Cardiol.* (1997) 29:229–36. doi: 10.1016/S0735-1097(96)00489-5
17. Lynce F, Barac A, Geng X, Dang C, Yu AF, Smith KL, et al. Prospective evaluation of the cardiac safety of HER2-targeted therapies in patients with HER2-positive breast cancer and compromised heart function: the SAFE-HEaRt study. *Breast Cancer Res Treat.* (2019) 175:595–603. doi: 10.1007/s10549-019-05191-2
18. Cardinale D, Colombo A, Lamantia G, Colombo N, Civelli M, De Giacomi G, et al. Anthracycline-induced cardiomyopathy. Clinical relevance and response to pharmacologic therapy. *J Am Coll Cardiol.* (2010) 55:213–20. doi: 10.1016/j.jacc.2009.03.095
19. Lupón J, Díez-López C, de Antonio M, Domingo M, Zamora E, Moliner P, et al. Recovered heart failure with reduced ejection fraction and outcomes: a prospective study. *Eur J Heart Fail.* (2017) 19:1615–23. doi: 10.1002/ejhf.824
20. Pareek N, Cevallos J, Moliner P, Shah M, Tan LL, Chambers V, et al. Activity and outcomes of a cardio-oncology service in the United Kingdom—a five-year experience. *Eur J Heart Fail.* (2018) 20:1721–31. doi: 10.1002/ejhf.1292
21. Ohtani K, Fujino T, Ide T, Funakoshi K, Sakamoto I, Hiasa K-I, et al. Recovery from left ventricular dysfunction was associated with the early introduction of heart failure medical treatment in cancer patients with

anthracycline-induced cardiotoxicity. *Clin Res Cardiol.* (2019) 108:600–11. doi: 10.1007/s00392-018-1386-0
22. Ameri P, Canepa M, Anker MS, Belenkov Y, Bergler-Klein J, Cohen-Solal A, et al. Cancer diagnosis in patients with heart failure: epidemiology, clinical implications and gaps in knowledge. *Eur J Heart Fail.* (2018) 20:879–87. doi: 10.1002/ejhf.1165
23. Yoon HJ, Kim KH, Kim HY, Park H, Cho JY, Hong YJ, et al. Impacts of non-recovery of trastuzumab-induced cardiomyopathy on clinical outcomes in patients with breast cancer. *Clin Res Cardiol.* (2019) 108:892–900. doi: 10.1007/s00392-019-01417-x
24. Halliday BP, Wassall R, Lota AS, Khalique Z, Gregson J, Newsome S, et al. Withdrawal of pharmacological treatment for heart failure in patients with recovered dilated cardiomyopathy (TRED-HF): an open-label, pilot, randomised trial. *Lancet.* (2019) 393:61–73. doi: 10.1016/S0140-6736(18)32484-X
25. Abdel-Qadir H, Austin PC, Lee DS, Amir E, Tu J V, Thavendiranathan P, et al. A population-based study of cardiovascular mortality following early-stage breast cancer. *JAMA Cardiol.* (2017) 2:88–93. doi: 10.1001/jamacardio.2016.3841
26. Yu AF, Yadav NU, Lung BY, Eaton AA, Thaler HT, Hudis CA, et al. Trastuzumab interruption and treatment-induced cardiotoxicity in early HER2-positive breast cancer. *Breast Cancer Res Treat.* (2015) 149:489–95. doi: 10.1007/s10549-014-3253-7

Conflict of Interest: SP has received a travel and accommodation grant from Novartis and advisor/consultant role for AstraZeneca, Daiichi-Sankyo, Polyphor, Roche, and Seattle Genetics.

The remaining authors declare that the research was conducted in the absence of any commercial or financial relationships that could be construed as a potential conflict of interest.

Publisher's Note: All claims expressed in this article are solely those of the authors and do not necessarily represent those of their affiliated organizations, or those of the publisher, the editors and the reviewers. Any product that may be evaluated in this article, or claim that may be made by its manufacturer, is not guaranteed or endorsed by the publisher.

frontiers in Cardiovascular Medicine

ORIGINAL RESEARCH
published: 19 November 2021
doi: 10.3389/fcvm.2021.732554

Periplocymarin Alleviates Doxorubicin-Induced Heart Failure and Excessive Accumulation of Ceramides

*Weijing Yun†, Lei Qian†, Ruqiang Yuan† and Hu Xu**

Advanced Institute for Medical Sciences, Dalian Medical University, Dalian, China

OPEN ACCESS

Edited by:
Susan Currie,
University of Strathclyde,
United Kingdom

Reviewed by:
Satoru Kobayashi,
New York Institute of Technology,
United States
Arturo Cesaro,
University of Campania Luigi
Vanvitelli, Italy

***Correspondence:**
Hu Xu
xuhu1024@126.com

†These authors have contributed equally to this work

Specialty section:
This article was submitted to Cardiovascular Therapeutics, a section of the journal Frontiers in Cardiovascular Medicine

Received: *29 June 2021*
Accepted: *25 October 2021*
Published: *19 November 2021*

Citation:
Yun W, Qian L, Yuan R and Xu H (2021) Periplocymarin Alleviates Doxorubicin-Induced Heart Failure and Excessive Accumulation of Ceramides. Front. Cardiovasc. Med. 8:732554. doi: 10.3389/fcvm.2021.732554

Doxorubicin-driven cardiotoxicity could result in dilated cardiomyopathy and heart failure (HF). Previously, we showed that periplocymarin exerted a cardiotonic role by promoting calcium influx and attenuating myocardial fibrosis induced by isoproterenol (ISO) by improving the metabolism of cardiomyocytes. However, the impact of periplocymarin on doxorubicin (DOX)-triggered cardiomyopathy has not been investigated. In the current study, C57BL/6 mice were randomly divided into three groups, namely, the control, DOX, and DOX+periplocymarin groups. The cardiac function and apoptosis were measured. Our results revealed that periplocymarin administration greatly improved the DOX-induced cardiac dysfunction manifested by the ejection fraction (EF%), fractional shortening (FS%), left ventricular posterior wall thickness (LVPW), left ventricular anterior wall thickness (LVAW), left ventricular (LV) mass, and attenuated DOX-induced cardiomyocyte apoptosis assessed by hematoxylin and eosin (H&E) staining, terminal deoxynucleotidyl transferase dUTP nick end labeling (TUNEL) staining, and western blotting. Further study using H9c2 cells revealed that the pretreatment of periplocymarin suppressed DOX-induced apoptosis evidenced by annexin V staining. Moreover, liquid chromatography with tandem mass spectrometry (LC-MS/MS) analysis demonstrated that DOX lead to an accumulation in serum ceramide, and the pre-treatment of periplocymarin could reverse this phenomenon. Network pharmacology also demonstrated that ceramide metabolism was involved in the process. Consistently, real-time PCR showed that periplocymarin significantly abolished the induction of the genes involved in the *de novo* synthesis of ceramide, i.e., *CerS2*, *CerS4*, *CerS5*, and *CerS6*, and the induction was attributed to the treatment of DOX. Collectively, these results suggested that periplocymarin reduced cardiomyocyte apoptosis to protect hearts from DOX-induced cardiotoxicity and the *de novo* synthesis of ceramides was involved in this process.

Keywords: periplocymarin, doxorubicin, heart failure, metabolomics, ceramide, apoptosis

INTRODUCTION

Doxorubicin (DOX) has been approved for the treatment of diverse cancers involving leukemia, neuroblastoma, and breast cancer (1). Unfortunately, despite the effective antineoplastic feature of DOX, it also exhibits side effects. It has been reported that the dose-dependent cardiotoxicity of DOX often results in cardiac systolic dysfunction and ultimately leads to heart failure (HF). This potential risk greatly restricted the clinical application of DOX. Therefore, identifying novel therapeutic drugs to block or reverse DOX-induced cardiotoxicity are urgently needed to be developed (1–3).

Accumulating evidence has elucidated the underlying mechanism involved in the pathogenesis of DOX-induced cardiotoxicity (4). After birth, cardiomyocytes no longer enter the cell cycle and eventually differentiate into a mature state, hence their survival is crucial. Besides, increasing cardiomyocyte apoptosis will contribute to contractile tissue loss, decompensated hypertrophy, irreversible fibrosis, and eventually leading to HF (5). Accordingly, developing effective therapeutic drugs or targets that are capable of combatting cardiomyocytes apoptosis triggered by DOX is greatly warranted.

With the development of modern pharmacology, emerging evidence proved that Chinese medicine could enhance cardiac function (6), including Ginsenoside Rg1 (7), Astragaloside IV (8), and Tanshinone IIA (9). In addition, many traditional Chinese materia medica preparations, such as Qiliqiangxin capsules and Qishenyiqi dripping pills, can also enhance myocardial contractility and improve cardiac dysfunction, which have been widely applied in clinics (10, 11). Periplocymarin is a pharmacodynamic substance in Qiliqiangxin capsules, which is extracted from Periplocae Cortex (12). Periplocymarin shares the basic molecular structure of cardiac glucoside. Studies have demonstrated that periplocymarin has a strong anticancer activity characterized by the inhibition of tumor cell proliferation and the promotion of cell apoptosis (13, 14). We previously reported that periplocymarin improves cardiac function by elevating the cardiomyocyte calcium ion (Ca^{2+}) concentration (15). Additionally, periplocymarin prevents isoproterenol (ISO)-induced cardiac fibrosis *via* improving the cardiomyocyte metabolism by targeting endothelial nitric oxide synthase (eNOS) and cyclooxygenase-2 (COX-2) (16). However, the role of periplocymarin on DOX-induced HF is largely unknown.

Ceramides are bioactive membrane lipids regulating signal transduction pathways that contain a basic skeleton of sphingosine which links to fatty acyl chains of different lengths (17). Ceramide accumulation is strongly associated with the pathogenesis of many diseases, such as diabetes, cardiomyopathy, and atherosclerosis (18). Serum ceramide levels have been shown to be accurate biomarkers of undesirable cardiovascular events in humans (19, 20). The study showed associations of higher plasma levels of N-palmitoyl-sphingosine (Cer16:0) and N-palmitoyl-sphingosyl-phosphorylcholine (SM16:0) with increased risk of HF and higher levels of N-behenoyl-sphingosine (Cer22:0), N-arachidoyl-sphingosyl-phosphorylcholine (SM20:0), N-behenoyl-sphingosyl-phosphorylcholine (SM22:0), and N-lignoceroyl-sphingosyl-phosphorylcholine (SM24:0) with decreased risk of HF (21). Previous investigations revealed that ceramides participate in the regulation of cardiac contractility and the process of cardiomyocyte apoptosis (22–24).

In the present study, we demonstrated that the administration of periplocymarin improved DOX-induced HF in mice, and we uncovered that periplocymarin ameliorated cardiomyocytes apoptosis and suppressed ceramides production induced by DOX both *in vivo* and *in vitro*.

MATERIALS AND METHODS

Chemicals and Drugs

Periplocymarin was purchased from Sigma-Aldrich (St. Louis, Missouri, United States). Doxorubicin was purchased from MedChemExpress (New Jersey, United States). The purities of compounds were more than 98% determined by HPLC. Bcl-2, caspase-3, and cleaved caspase-3 antibodies were purchased from Cell Signaling Technology (Danvers, Massachusetts, United States). eIF5 antibody was purchased from Santa Cruz.

Animals and Animal Models With HF

Adult (8–10 weeks) male C57BL/6 mice were used in the study. The mice were bred at the Animal Center of Dalian Medical University with a temperature of 23°C and 12-h light/dark cycles. The animals reached a fresh diet and sterile water freely. The animal protocol was approved by the Animal Care and Use Review Committee of Dalian Medical University and the procedure was in accordance with the Guide for the Care and Use of Laboratory Animals (National Institutes of Health). The mice were randomly divided into three groups, i.e., the control group ($n = 5$), DOX group ($n = 7$), and DOX plus periplocymarin group ($n = 6$). Firstly, the DOX plus periplocymarin group was injected with periplocymarin at a dose of 5 mg/kg for 3 days. Then, the DOX plus periplocymarin and DOX groups were abdominally injected with DOX (20 mg/kg) once to build the mouse model of HF (25). After that, the DOX plus periplocymarin group was injected with periplocymarin for 3 days. The control and DOX groups were injected with saline for 3 days.

Cell Culture

Isolation and Culture of Cardiomyocyte

Cardiomyocytes were isolated and cultured from neonatal Sprague-Dawley (SD) rats as described previously (26). In brief, neonatal SD rat pups (within 2 days) were euthanized and the hearts were digested with 0.1% collagenase I. The cardiomyocytes were obtained by differential adhesion method: the digested cells were plated on 10 cm dishes for 3–4 h; the unattached cells were cardiomyocytes and they were moved to a new dish. The cardiomyocytes were cultured for 48 h in a Dulbecco's Modified Eagle Medium (DMEM) medium containing 10% fasting blood sugar (FBS). Then the cardiomyocytes were pretreated with 0.1 μM of periplocymarin for 24 h and then treated with 5 μM of DOX for 12 h in DMEM containing 1% FBS.

H9c2 Cell Line Culture

H9c2 cell line (rat embryonic ventricular myocyte) was purchased from the Shanghai Institute of Biochemistry and Cell Biology (China). The H9c2 cells were cultured in a DMEM medium containing 10% FBS at the condition of 37°C and 5% calcium dioxide (CO_2) and the cells were passaged at 70–80% confluence (27). For the experiment, the H9c2 cells were pretreated with 0.1 μM of periplocymarin for 24 h and then treated with 5 μM of DOX for 12 h in DMEM containing 1% FBS.

Flow Cytometry Analysis

Cell apoptosis was detected using an Annexin V-FITC apoptosis kit and following the provided procedure (Beyotime, Shanghai, China). After pretreatment with periplocymarin for 24 h, the cells were treated with 5 μM of DOX for 12 h. Then they were harvested using 0.25% trypsin and washed twice with cold phosphate-buffered saline (PBS). The harvested cells were centrifuged at 2,000 rpm/min for 5 min and the cells were resuspended with 1 × binding buffer to a density of 1×10^5 cells/ml. Afterward, 100 μl of each sample was stained with an Annexin V-FITC staining solution in a 1.5 ml Eppendorf tube at room temperature and avoided light for 15 min. Then, 400 μl of 1 × binding buffer was added into the tubes. The apoptotic cell population was then quantified using a flow cytometer (BD FACSVerse, Becton, Dickinson and Company, United States) and Cell Quest Research Software (FlowJo_V10, Becton, Dickinson and Company, United States).

Echocardiography

Echocardiography was performed using the Vevo 3,100 high-resolution imaging system (Fujifilm Visual Sonics Inc., Minato City, Tokyo, Japan) to analyze the cardiac function of the animals. The mice were anesthetized using isoflurane (1%) and the heart rate was controlled at 500 ± 30 b.p.m. The percentage of ejection fraction (EF%), fractional shortening (FS%), left ventricular posterior diastolic wall thickness (LVPW; d), left ventricular posterior systolic wall thickness (LVPW; s), left ventricular anterior diastolic wall thickness (LVAW; d), and left ventricular anterior systolic wall thickness (LVAW; s) were measured or calculated as previously described (15).

Hematoxylin and Eosin (H&E) and Terminal Deoxynucleotidyl Transferase dUTP Nick end Labeling (TUNEL) Staining

The mice were euthanized with overdose CO_2 inhalation and perfused with PBS through the heart, then the heart tissues were removed into 4% formalin. The hearts were embedded in paraffin and cut into 5 μm sections. Hematoxylin and eosin staining and TUNEL assay were performed according to the standard procedures.

Real-Time PCR

The cells or heart tissues were lysed in TRIZOL reagent (Invitrogen, United States) and the total RNA was extracted. Then the RNA samples were quantified by NanoDrop 2000 (Thermo Fisher Scientific, United States) and were reverse transcribed to complementary DNA (cDNA). Real-time PCR primers were designed on the National Center for Biotechnology Information (NCBI) website using known sequences, and the primer pairs were listed in **Supplementary Table 1**. The internal standard control used was 18S. A mix of nucleoside triphosphates (NTP) and SYBR Green was used and the real-time PCR was performed on the LightCyler96 Sequence Detection System (Roche, Basel, Switzerland). The reaction condition was 94°C for 5 min, followed by 35 cycles of 94°C for 30 s, 60°C for 30 s, 72°C for 30 s, then extension at 72°C for 5 min (28).

Western Blot

For western blot, the method was followed as previously reported (28). Briefly, the heart tissues or cells were lysed in a radioimmunoprecipitation assay (RIPA) buffer containing the protease and phosphatase inhibitor cocktail. After centrifugation at 12,000 g for 15 min at 4°C, the supernatant containing the total protein was quantified by a bicinchoninic acid (BCA) Assay Kit, the lysates were mixed with 5 × sodium dodecyl sulfate (SDS) loading buffer. After fractionated with 10% sodium dodecyl sulfate-polyacrylamide gel electrophoresis (SDS-PAGE), the proteins were transferred onto a nitrocellulose filter membrane. The primary antibodies were incubated overnight at 4°C and followed by incubation with an horseradish peroxidase (HRP)-labeled secondary antibody for 1 h at room temperature. The bands on the membranes were visualized after enhanced chemiluminescence (ECL) incubation using a Chemiluminescent Imaging System (Tanon 5200, China). Image J software (NIH) was used to analyze the intensities of the bands.

Metabolomics Analysis

Metabolites Extraction

Serum samples (100 μl) were mixed with 300 μl of cooled methanol, vortexed for 60 s, then 600 μl of chloroform was added, and the solution was vortexed for 2 min and incubated for about 1 h at room temperature. The mix solution was centrifuged at 2,600 g for 10 min, and that chloroform phase was removed and dried under vacuum. Before analysis, the extracted sample was dissolved in 100 μl of chloroform/methanol (2:1, V/V) and then diluted two-fold with methanol.

Afterward, 300 μl cold MeOH was added to the cell samples, then, the cells were sucked out by a pipette. Two volumes of chloroform were added to each sample, and the solution was vortexed for 2 min and incubated for about 1 h at room temperature. After that, the process was the same as serum.

All samples of equal quantity were pooled together to generate quality control samples (QC) and inserted into the analysis batch every six samples to ensure consistent system performance and good metabolic profile quality.

Liquid Chromatography With Tandem Mass Spectrometry (LC-MS/MS) Analysis of Ceramides

All the experiments were performed on a Qtrap 5,500 mass spectrometer (SCIEX, United States) with electrospray ionization. Multiple reaction monitoring detection was used for the detection of metabolites. An acquity ultra performance liquid chromatography ethylene bridged hybrid (UPLC BEH) Amide Column (2.1 × 100 mm, 1.7 m) was employed for metabolites

separation at 40°C. Mobile phase A was 10 mM ammonium acetate in water with 0.1% formic acid, and mobile phase B was 0.1% formic acid in acetonitrile. The gradient was from 95 to 80% B over 5 min, 80 to 60% B over 9 min, held for 3 min, then the column was returned to its starting condition. The flow rate was 0.2 ml/min and the injection volume was 2 μl. The collection was carried out in positive ion mode (**Supplementary Table 2** for 31 metabolites).

Data Processing and Pathway Analysis

The retention time (RT), peak area, peak width, peak width at 50% height, and signal to noise ratio (S/N) were generated in MultiQuant 3.0 (SCIEX, United States). The software (Version 14.1, Umetrics, Umea, Sweden) was used to perform pattern recognition analysis on all peaks detected in each data file, including partial least squares discriminant analysis (PLS-DA) and orthogonal partial least squares discriminate analysis (OPLS-DA). In the OPLS-DA model, metabolites with variable importance in projection (VIP) > 1 were used as potential biomarkers. The database of MetaboAnalyst 4.0 (http://www.metaboanalyst.ca/) was used to predict the relevant pathway of potential biomarkers.

Network Pharmacology Study and Gene Expression Omnibus (GEO) Database Validation

The potential targets of periplocymarin were gathered from the database Bioinformatics Analysis Tool for Molecular mechANism of Traditional Chinese Medicine (BATMAM-TCM) (http://bionet.ncpsb.org.cn/batman-tcm/). The HF-related genes were derived from the GeneCard database (https://www.GeneCards.org/). Then through jvenn (http://jvenn.toulouse.inra.fr/app/example.html), the intersections with periplocymarin and HF were analyzed. Potential periplocymarin targets and HF-related genes were imported into Cytoscape software (National Institute of General Medical Sciences (NIGMS), United States) to construct the network. The protein-protein interaction (PPI) networks of 246 intersecting genes were created by using the Search Tool for the Retrieval of Interacting Genes/Proteins (STRING) database (https://string-db.Org/) with a medium confidence level (interaction score > 0.40) and the Cytoscape software. The Gene Ontology (GO) and Kyoto Encyclopedia of Genes and Genomes (KEGG) pathway enrichment analyses of the intersecting genes were carried out using the database Metascape (https://metascape.org/gp/index.html#/main/step1). The RNA-sequencing data (GSE157282) was obtained from the GEO database and the gene expression (FPKM) of the control and DOX treated group was analyzed.

Statistics

The experimental data were analyzed and plotted using GraphPad Prism 8.3.0 software (GraphPad Software Inc., San Diego, California, United States). The results are presented as the mean ± SEM. Student's *t*-test was used for two-group comparison, and ANOVA was used for multi-group comparison. $p < 0.05$ was considered significant.

RESULTS

Periplocymarin Prevented the HF Induced by DOX

To investigate the effect of periplocymarin on DOX-induced heart failure, we initially performed echocardiography to evaluate the cardiac function in three groups of mice (**Figure 1A**). As expected, both EF% and FS% in the DOX group were reduced compared with the vehicle. Intriguingly, periplocymarin treatment successfully rescued the decrease in EF% and FS% triggered by DOX (**Figures 1B,C**). Further analysis revealed that DOX treatment led to the thinning of the left ventricular wall characterized by reduced LVAW and LVPW in both the diastole and systole. To our surprise, the levels of LVAW and LVPW were markedly reversed by periplocymarin (**Figures 1D–G**). Correspondingly, the LV mass was significantly decreased in the DOX group, while this decrease was largely prevented by periplocymarin (**Figure 1H**). Moreover, the mice hearts were harvested, and the heart-to-body weight (HW/BW) ratio and heart weight-to-tibia length (HW/TL) ratio were also assessed. Consistent with the echocardiography results, the ratios of HW/BW and HW/TL were reduced after the DOX treatment, which were obviously reversed by the periplocymarin treatment (**Figures 1I–K**). Altogether, these data indicated that periplocymarin exerted an efficaciously protective effect on DOX-induced HF in mice.

Periplocymarin Mitigated DOX-Induced Cardiomyocyte Apoptosis

To further investigate the cardiac protective effect of periplocymarin, H&E staining was performed and deranged cellular structures, edematous cardiomyocytes, and dissolved myofibers were observed in DOX-treated hearts. However, these abnormalities were notably ameliorated by periplocymarin (**Figure 2A**). To provide sufficient evidence to exhibit the damage and repair of cardiomyocytes, TUNEL staining was applied to examine the DOX-induced cytotoxicity and display the protective effect of periplocymarin on cardiomyocyte apoptosis. Indeed, TUNEL positive cardiomyocytes were markedly increased in the DOX-treated hearts, suggesting massive apoptosis after the DOX treatment. Oppositely, when co-treated with periplocymarin, this undesirable phenomenon was obviously rescued (**Figures 2B,C**). Further analysis of apoptotic proteins using western blot showed that the expression of Bcl-2 was significantly decreased in the DOX group, at the same time, the expression of cleaved caspase 3 was significantly upregulated in the DOX group, this phenomenon was reversed by the administration of periplocymarin (**Figures 2D,E**). Furthermore, *in vitro* study using H9c2 cells was performed to evaluate the cytotoxicity of periplocymarin and to confirm the antiapoptotic role of periplocymarin in DOX-treated cardiomyocytes. The Cell Counting Kit-8 (CCK-8) assay exhibited that periplocymarin had no cytotoxicity when the concentration was lower than 1 μM, and the IC_{50} was 84.74 μM (**Supplementary Figure 1**). According to the annexin V staining, periplocymarin treatment alone did not affect cell apoptosis.

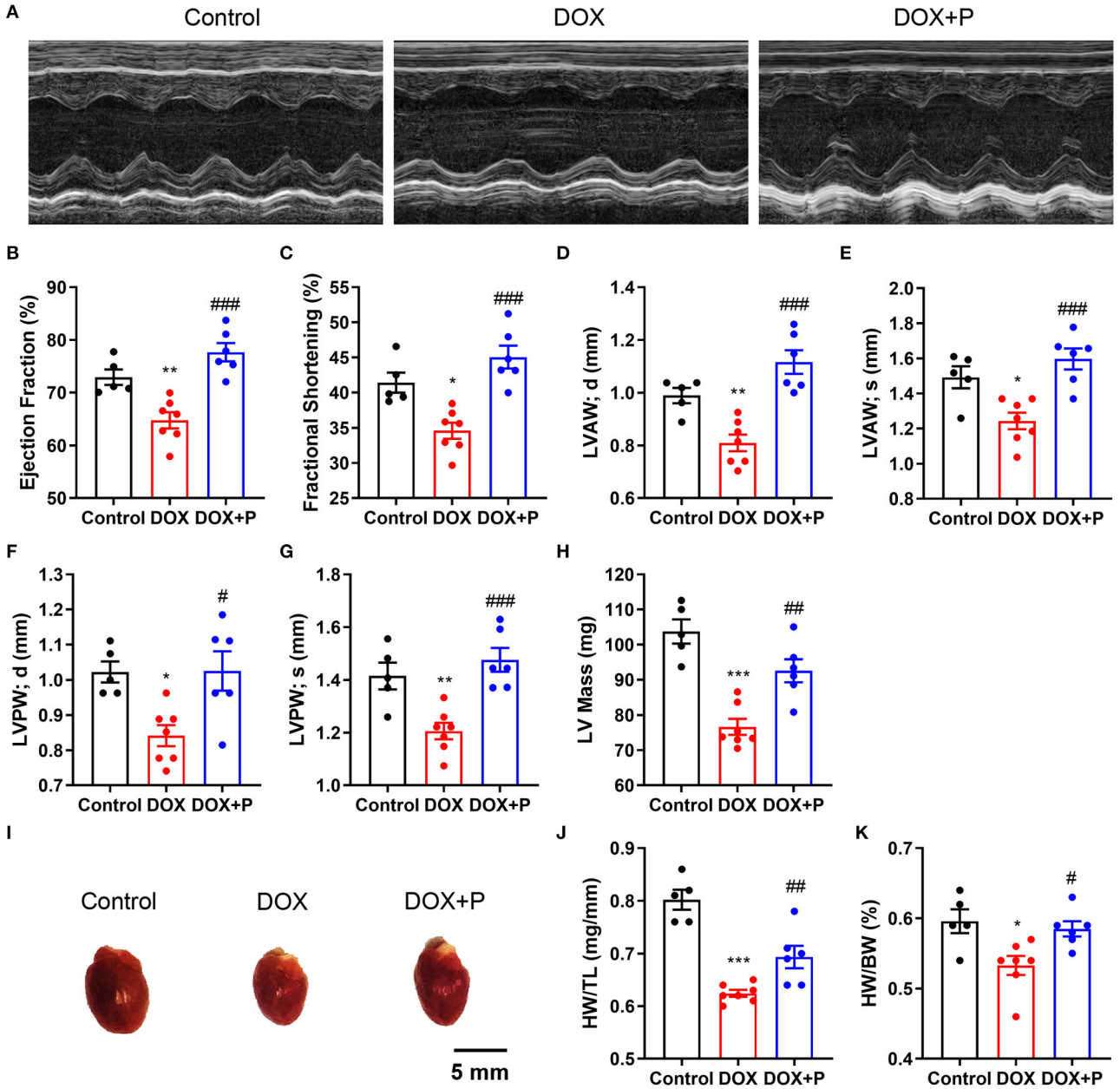

FIGURE 1 | Effects of periplocymarin on cardiac function and heart weight after 3-day doxorubicin (DOX) treatment in mice. The cardiac function of the mice was determined by the echocardiography in M-mode on the aspect of the short axis. **(A)** Representative images of echocardiography. **(B–H)** The ejection fraction (EF%) **(B)**, fractional shortening (FS%) **(C)**, left ventricular anterior diastolic wall thickness (LVAW; d) **(D)**, left ventricular anterior systolic wall thickness (LVAW; s) **(E)**, left ventricular posterior diastolic wall thickness (LVPW; d) **(F)**, left ventricular posterior systolic wall thickness (LVPW; s) **(G)** and left ventricular mass **(H)** were calculated according to the M-mode echocardiography. Data are presented as mean ± SEM; $n = 5$–7, $^{*}p < 0.05$, $^{**}p < 0.01$, $^{***}p < 0.001$ vs. control; $^{\#}p < 0.05$, $^{\#\#}p < 0.01$, $^{\#\#\#}p < 0.001$ vs. DOX. **(I)** The mice were euthanized and the representative images of the hearts were shown. Scale bar, 5 mm. **(J)** The ratios of heart weights to tibia length were calculated. Data are presented as mean ± SEM; $n = 5$–7. $^{***}p < 0.001$ vs. control, $^{\#\#}p < 0.01$ vs. DOX. **(K)** The ratios of heart weights to body weights were calculated. Data are presented as mean ± SEM; $n = 5$-7. $^{*}p < 0.05$ vs. control, $^{\#}p < 0.05$ vs. DOX.

Doxorubicin alone caused the significant apoptosis of H9c2 by ∼50% in comparison to the control. Importantly, treatment of the cells with periplocymarin dramatically counteracted the DOX-mediated apoptosis (**Figures 2F–H**). However, periplocymarin had an optimal antiapoptotic effect at the concentration of 0.1 μM (**Supplementary Figure 2**). Besides, DOX induced a massive accumulation of reactive oxygen species (ROS) in H9c2 cells, while periplocymarin significantly

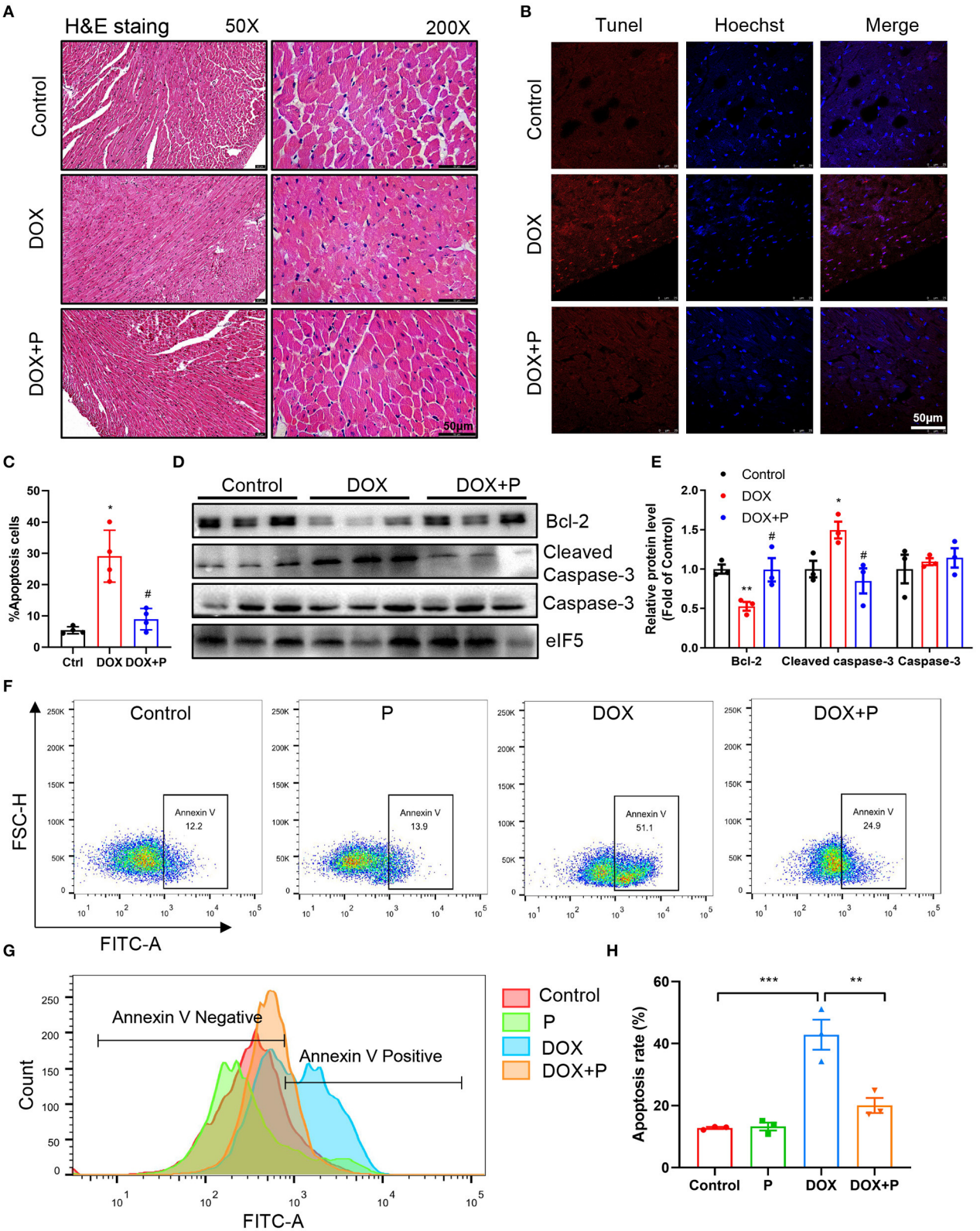

FIGURE 2 | Periplocymarin improved cardiomyocyte apoptosis induced by DOX. **(A)** Representative micrographs of hematoxylin and eosin (H&E) staining. The left panel is 50X (Scale bar, 50 μm), the right panel is 200X (Scale bar, 50 μm). **(B,C)** Representative fluorescent images of terminal deoxynucleotidyl transferase dUTP

(Continued)

FIGURE 2 | nick end labeling (TUNEL) staining of the hearts **(B)**. Scale bar, 50 μm. Quantitative analysis of TUNEL staining in different groups **(C)**. Data are presented as mean ± SEM; $n = 4$, $^{*}p < 0.05$ vs. control, $\#p < 0.05$ vs. DOX. **(D)** Western blot analysis of Bcl-2, cleaved caspase-3, and caspase-3 protein levels in heart tissues. **(E)** Quantitative analysis of Bcl-2, cleaved caspase-3, and caspase-3 expression in **D**. Data are presented as mean ± SEM; $n = 3$, $^{*}p < 0.05$ vs. control, $^{**}p < 0.001$ vs. control, $\#p < 0.05$ vs. DOX. **(F)** Flow cytometric scatterplot of Annexin-V-FLTC staining of H9c2 cell apoptosis. **(G)** Flow cytometric histogram of Annexin-V-FLTC staining of H9c2 cell apoptosis. **(H)** Quantitative analysis of apoptotic H9c2 cells in different groups using bar graphs. Data are presented as mean ± SEM; $n = 3$. $^{**}p < 0.01$, $^{***}p < 0.001$.

suppressed ROS production (**Supplementary Figure 3**). Overall, co-treatment with periplocymarin improved DOX-induced cardiac injury, especially cardiomyocytes apoptosis.

Periplocymarin Regulated Ceramides Metabolism Disorder Induced by DOX

Recently, the role of ceramides in HF has been extensively investigated. Serum ceramides contents have been shown to be strongly associated with adverse cardiovascular disease outcomes (20). Accordingly, we tested serum ceramide levels in three groups of mice. Liquid chromatography-MS/MS was used to detect the serum ceramide content in the control, DOX, and DOX plus periplocymarin group. The relative standard deviation (RSD) of the peak areas of ceramides was 4.66–13.48% (**Supplementary Table 3**), which indicated that the method had qualified stability and repeatability.

The heatmap analysis was applied to visualize these potential biomarkers, with changes in color from deep red to navy blue indicating high to low relative levels of metabolites (**Figures 3A,E**). The PLS-DA method was used to analyze data. As shown in **Figure 3B**, a distinct aggregation state was observed among QC samples in PLS-DA, indicating that the experimental conditions were in a stable state. In addition, the sample points of different groups showed obvious separation. The results showed that there were significant differences among the three groups.

The OPLS-DA method was used to find identification ions which were helpful for the classification between groups. The score map of OPLS-DA showed significant separation between the control group and the DOX treated group (**Figure 3C**). The data (**Supplementary Table 4**) showed performance statistics of $R^2X = 0.898$, $R^2Y = 0.902$, and predictive parameter $Q^2Y = 0.836$, suggesting that the models were valid and highly predictive. Metabolites with a VIP >1 in the OPLS-DA model could be selected as potential biomarkers. According to that, six metabolites were differentially expressed between the control and DOX group (**Supplementary Table 5**). A new OPLS-DA model was created to find the distinguishing metabolites between the DOX and the DOX+P group (**Figure 3D**). The prediction and sufficient reliability in this model were enough (**Supplementary Table 4**). According to the VIP values, 15 potential biomarkers were selected from the DOX group and DOX+P group (**Supplementary Table 6**).

To investigate whether periplocymarin can regulate ceramide metabolism *in vitro*, H9c2 cells were employed to assess the regulation of periplocymarin on ceramides metabolism. The stability and repeatability of the method were qualified with the RSD of the relative peak areas of ceramides were 3.37–13.07% (**Supplementary Table 7**).

Firstly, the PLS-DA method was used to analyze differences between the four groups. As shown in **Figure 3F**, the QC samples showed an aggregation state in PLS-DA, indicating that the experimental conditions were in a stable state. More importantly, the dots with different colors showed obvious separation, suggesting that there were significant differences between the four groups.

Then the OPLS-DA was used to analyze the metabolites and relationships among the different groups. As shown in **Figure 3G**, there was a distinct separation between the control and DOX groups. Another OPLS-DA model showed that metabolites in the DOX group and DOX+P group also had obvious differences (**Figure 3H**). According to the VIP-values (**Supplementary Table 9**), six potential biomarkers were selected from the control and DOX groups, and five potential biomarkers were selected from the DOX group and DOX+P group (**Supplementary Table 10**). In addition, the OPLS-DA model parameter is shown in **Supplementary Table 8**.

Periplocymarin Attenuated the Increase of Ceramide-Induced by DOX *in vivo* and *in vitro*

Based on the above analysis, we obtained three key metabolites that appeared in four analyses (**Supplementary Tables 5**, **6**, **9**, **10**). To further verify the regulation of the periplocymarin on these three metabolites, we analyzed the relative peak areas of these three metabolites *in vivo* and *in vitro*. Certain ceramide species, such as Cer16:0 (N-palmitoyl-sphingosine), Cer18:0 (N-stearoylsphingosine), Cer24:1 (N-nervonoyl-sphingosine), and Cer24:0 (N-lignoceroyl-sphingosine), were significantly increased in response to DOX, the administration of periplocymarin notably decreased the levels of these three key metabolites (**Figures 4A–D**). Consistent with the observations of *in vivo* study, treatment with periplocymarin suppressed the DOX triggered elevation of Cer16:0, Cer18:0, Cer24:1, and Cer24:0 in H9c2 cells. However, periplocymarin alone did not decrease these ceramides compared with the control group (**Figures 4H–K**).

Clinical studies have shown that the ratios of Cer16:0, Cer18:0, Cer24:1, and Cer24:0 are strongly associated with the occurrence and development of cardiovascular disease, and positively correlated with the risk of cardiovascular disease. In our *in vivo* study, these ratios were significantly increased after DOX treatment, and they were reversed by the administration of periplocymarin (**Figures 4E–G**). And the *in vitro* experiments using H9c2 cells exhibited similar results (**Figures 4L–N**). Together with the foregoing observations, these data suggested

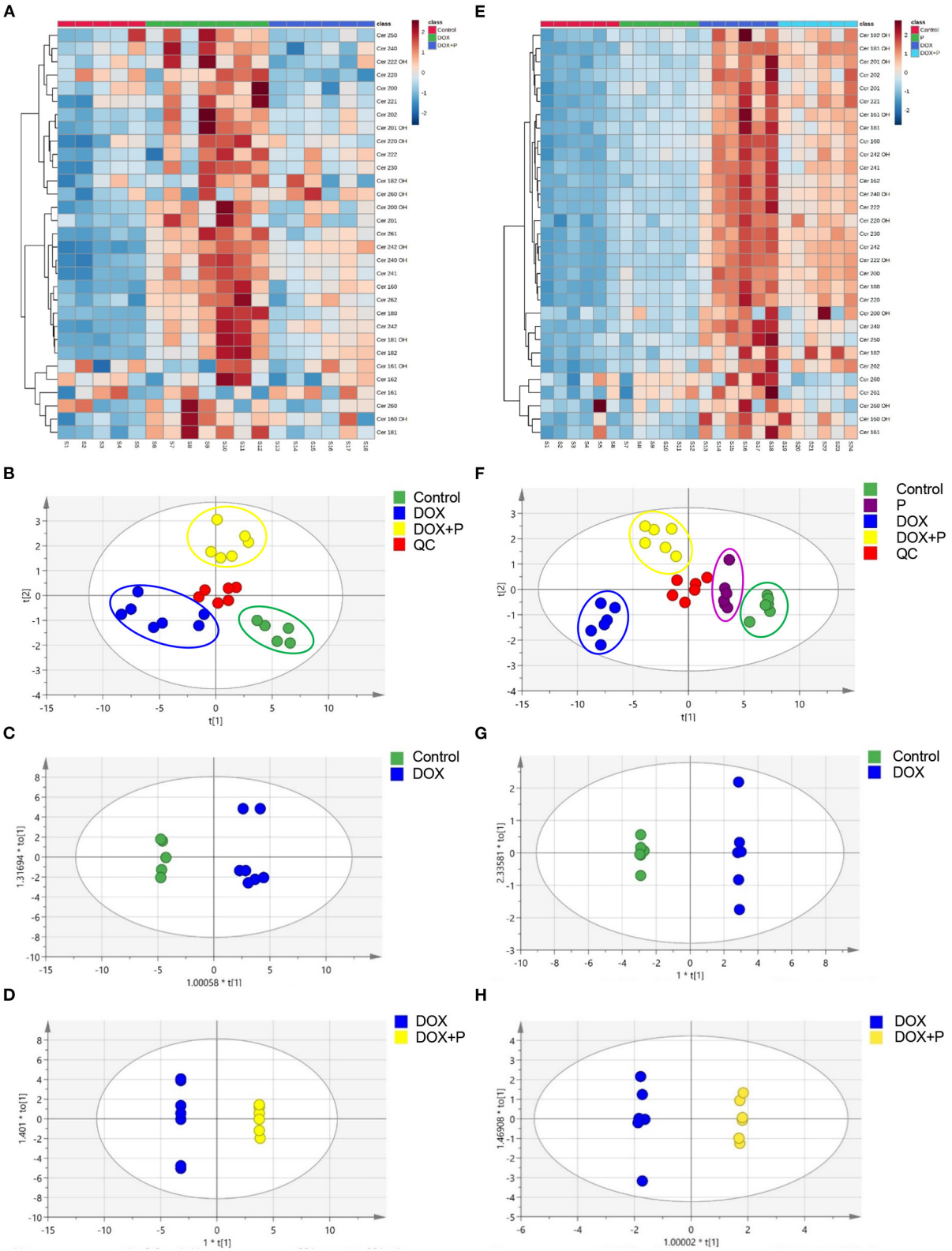

FIGURE 3 | Periplocymarin regulated metabolic disorders induced by DOX. **(A–D)**. The ceramides in mice serum were measured by liquid chromatography with tandem mass spectrometry (LC-MS/MS). The cluster heatmap of ceramides was presented **(A)**. The score scatter plots of the quality control (QC) and the mice serum

(Continued)

FIGURE 3 | partial least squares discriminant analysis (PLS-DA) data were presented **(B)**. Paired comparison of orthogonal partial least squares discriminate analysis (OPLS-DA) score scatter plots between the control group and DOX group **(C)**. Paired comparisons of OPLS-DA score scatter plots between the DOX group and DOX + periplocymarin group **(D)**. **(E–H)** Ceramides in H9c2 cells were measured by LC-MS/MS. The cluster heatmap of ceramides in H9c2 cell **(E)**. The score scatter plots of the quality control (QC) and the H9c2 cells PLS-DA data were displayed **(F)**. Paired comparisons of OPLS-DA score scatter plots between the control and DOX groups **(G)**. Paired comparisons of OPLS-DA score scatter plots between the DOX and DOX + periplocymarin groups **(H)**. The dots of different colors represented different groups, the green dots represented control samples, the purple dots represented the periplocymarin group, the blue dots represented the six samples come from the DOX group, the yellow dots represented the six samples of DOX + periplocymarin group and the red dots represented QC samples.

that ceramide metabolic disturbance accounts for the beneficial effect of periplocymarin in DOX-induced HF.

Target Network Analysis of Periplocymarin and HF

To further elucidate the underlying mechanism of how periplocymarin attenuates the DOX-induced HF, network pharmacology was performed. A total of 300 periplocymarin-related targets (**Supplementary Table 11**) were obtained through BATMAN-TCM prediction, and 8,776 HF-related targets (**Supplementary Table 12**) were obtained through the disease databases. Upon uploading targets of periplocymarin and HF to jvenn, 246 overlapping targets were found as shown in **Figure 5A**. The detailed information of these targets was shown in **Figure 5B**. These might be the targets of periplocymarin in the treatment of HF.

The STRING database was used to construct the PPI network of 246 shared targets by drugs and disease as shown in **Figure 5C**. The information derived from the STRING database was imported into Cytoscape3.7.2 software for further analysis, and a visualized PPI network was constructed, with the dot size and color reflecting the degree of freedom. The greater degree of freedom indicates that more biological functions were involved. The KEGG pathway and GO were analyzed by Metascape to clarify the mechanisms of how periplocymarin improved HF. The top 20 pathways were screened out according to the KEGG analysis (**Supplementary Table 13**). The results showed that the sphingolipid signaling pathway might be the related pathway for periplocymarin to treat HF, in which several key enzymes in ceramide biosynthesis were included (**Figure 5D**). The biological process enrichment analysis suggested that periplocymarin may improve HF by the regulation of membrane potential, system process, and inorganic ion homeostasis (**Figure 5E**). Besides, cellular component enrichment indicated that periplocymarin may regulate the transmembrane transporter complex, synaptic membrane, intrinsic component of the synaptic membrane, and postsynaptic specialization (**Figure 5F**). Molecular function enrichment suggested that periplocymarin may act on neurotransmitter receptor activity, gated channel activity, organic acid-binding, and structural constituent of the cytoskeleton (**Figure 5G**). The relationship between KEGG pathways and pathway-related genes was shown in **Figure 5H**. Squares represent the targets; inverted triangles represent the pathways. The area of the node represents its degree, and the larger the area, the more important the node. Ceramide biosynthesis enzymes, including CerS1, CerS2, CerS3, CerS4, and CerS5, were related to the ceramide biosynthesis pathway (has04071) (**Figure 5H**). These results further suggested that periplocymarin may improve HF by regulating the sphingolipid signaling and ceramide biosynthesis pathway.

Periplocymarin Regulated the Expression of Enzymes Involved in the Production of Ceramide

We next aimed to determine the effect of periplocymarin on ceramide biosynthesis (**Supplementary Figure 4**). The analysis of several key enzymes in the ceramide biosynthesis pathway by real-time PCR revealed that the expression of *CerS1-6*, responsible for the ceramide synthesis. The expression of *CerS1*, *CerS2*, and *CerS4-6* in the messenger RNA (mRNA) level were increased in response to the DOX treatment *in vivo*, and administration of periplocymarin successfully decreased the level of *CerS1*, *CerS2,* and *CerS4-6* (**Figure 6A**). Similarly, *in vitro* study using primary cardiomyocytes revealed that except *CerS1*, the expression of *CerS2-6* were increased after DOX treatment, while pre-treatment with periplocymarin downregulated the mRNA levels of *CerS1-6* compared with the DOX group (**Figure 6B**). However, we also found that the expression of *Asah1* also increased after the treatment of DOX, and returned to normal after the treatment of periplocymarin (**Supplementary Figure 5**). *Asah1* encoded acid ceramidase, which was responsible for the metabolism of ceramide into sphingosine. The regulation of *Asah1* expression may be attributable to the fact that the body itself had a regulatory effect on the metabolism of ceramide. The expression of other genes related to ceramide syntheses, such as *Spt1*(encoding serin palmitoyl transferase), *Cerk*, and *ASMase*, showed no significant difference among the three groups (**Supplementary Figure 5**). In addition, we further validated our results using the published RNA-sequencing data from the GEO database (GSE157282). As shown in **Figure 6C**; **Supplementary Figure 6**, *CerS2*, *CerS4*, *CerS5*, and *Asah1* were relatively high-expressed, while *CerS1*, *CerS3*, and *CerS6* were relatively low-expressed in human induced pluripotent stem cell (hiPS)-derived cardiomyocytes. Strikingly, similar to our results, DOX treatment upregulated the expression of *CerS1*, *CerS2*, *CerS3*, *CerS5*, *CerS6*, and *Cerk*, except *CerS4* and *Asah1*. However, *Spt1* and *ASMase* were not detected in the RNA-sequencing data. Altogether, our findings implied that treatment with periplocymarin mainly regulated the expression *CerSs*, the enzymes related to ceramide synthesis, and thus amazingly rescuing DOX-induced ceramide accumulation.

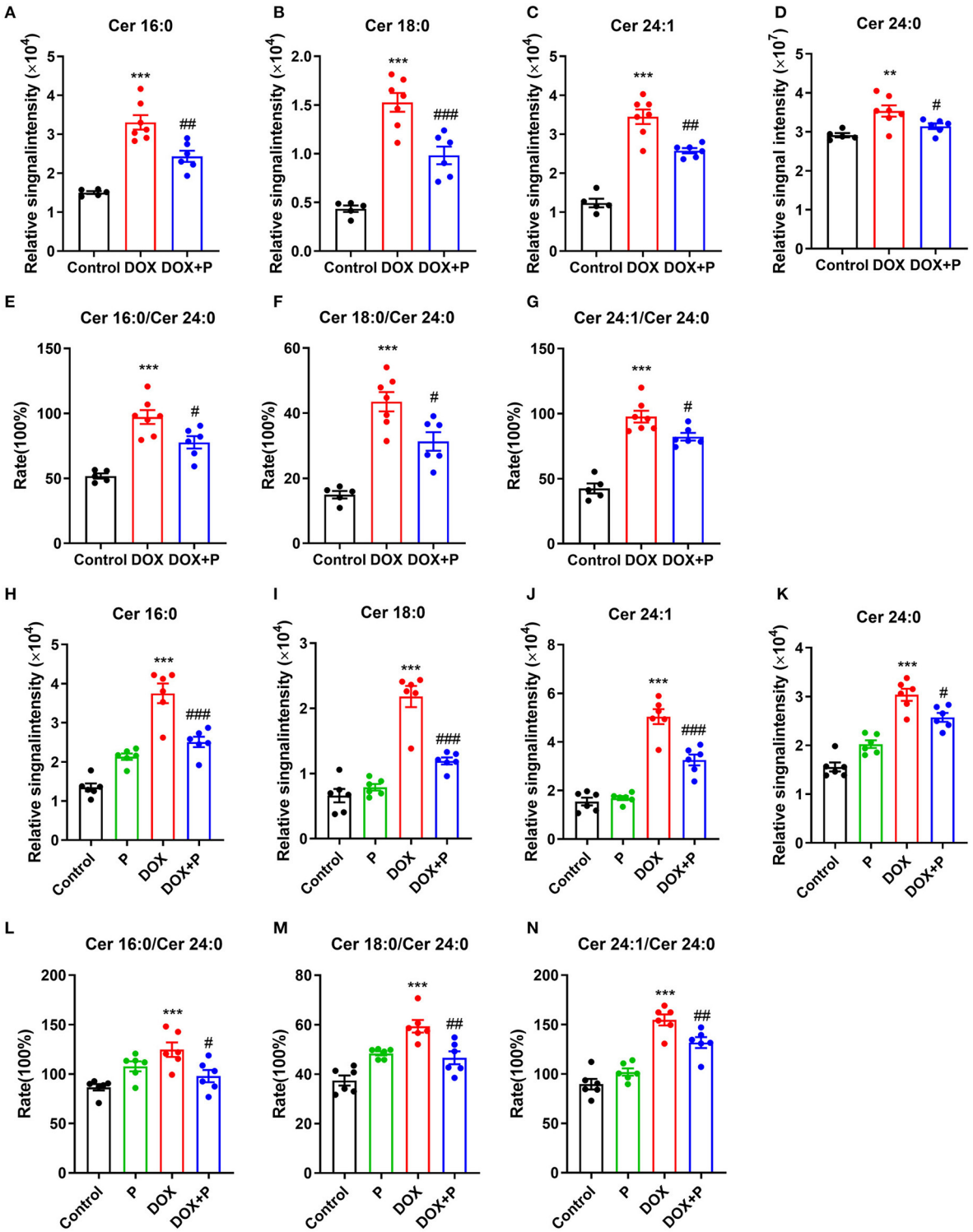

FIGURE 4 | Periplocymarin regulated ceramides metabolism disorder induced by DOX. **(A–D)** Relative abundance of Cer16:0 **(A)**, Cer18:0 **(B)**, Cer24:1 **(C)**, and Cer24:0 **(D)** ceramides in mice serum. **(E–G)** The ratios of Cer16:0 to Cer24:0 **(E)**, Cer18:0 to Cer24:0 **(F)**, and Cer24:1 to Cer24:0 **(G)** in mice serum. Data are presented as mean ± SEM; $n = 6$, $^{**}p < 0.01$, $^{***}p < 0.001$ vs. control; $^{\#}p < 0.05$, $^{\#\#}p < 0.01$, $^{\#\#\#}p < 0.001$ vs. DOX. **(H–K)** Relative abundance of Cer16:0 **(H)**, Cer18:0 **(I)**, Cer24:1 **(J)**, and Cer24:0 **(K)** ceramides in H9c2 cells. **(L–N)** The ratios of Cer16:0 to Cer24:0 **(L)**, Cer18:0 to Cer24:0 **(M)** and Cer24:1 to Cer24:0 **(N)** in H9c2 cells. Data are presented as mean ± SEM; $n = 6$, $^{***}p < 0.001$ vs. control; $^{\#}p < 0.05$, $^{\#\#}p < 0.01$, $^{\#\#\#}p < 0.001$ vs. DOX.

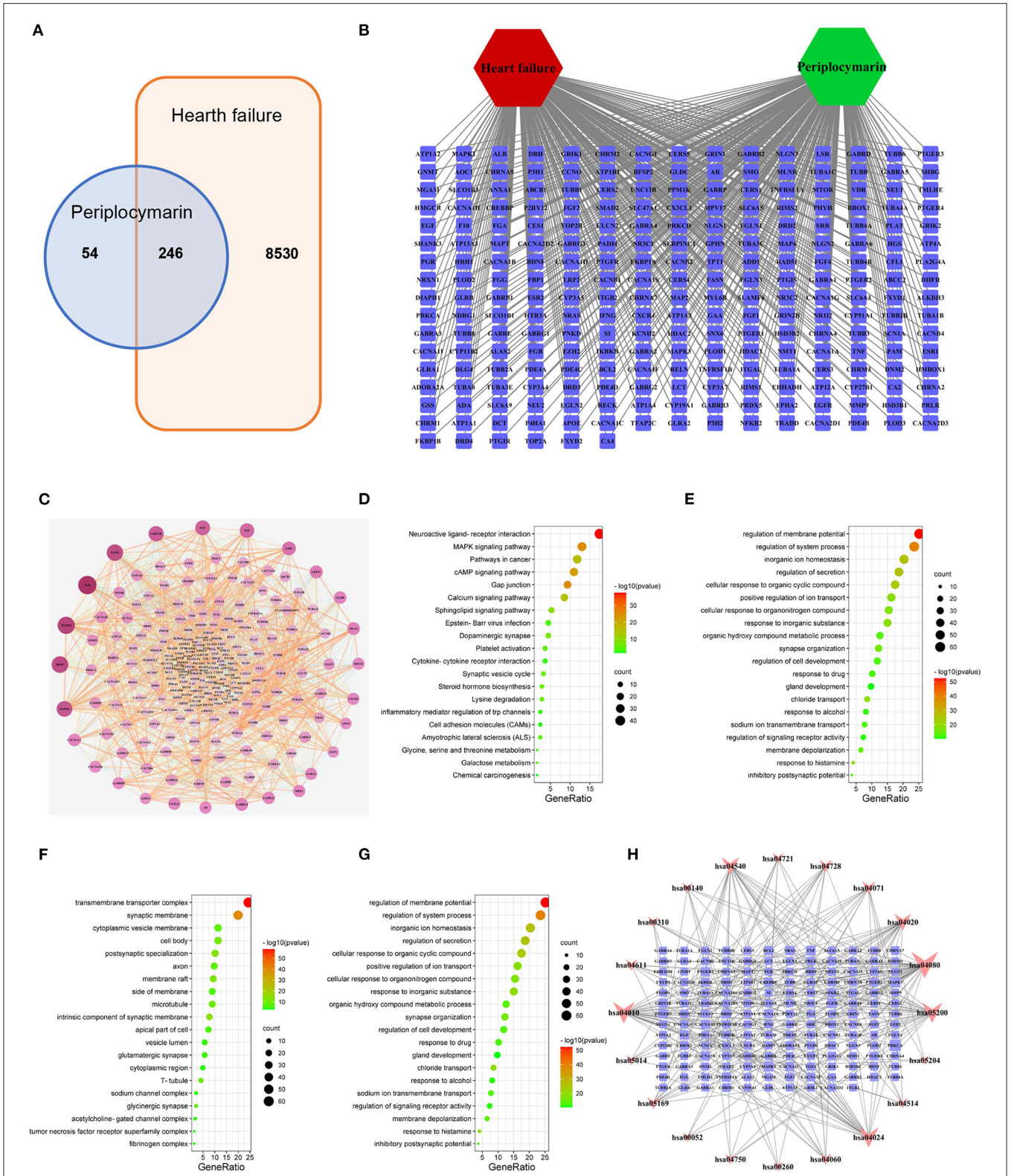

FIGURE 5 | Network pharmacology to explore the mechanism of periplocymarin in the treatment of heart failure. **(A)** Intersection targets of periplocymarin and heart failure. Periplocymarin:300 targets; heart failure:8,770 targets. **(B)** The network of heart failure-targets-periplocymarin. Green hexagon represent compound, red

(Continued)

FIGURE 5 | hexagon represents disease, squares represent targets. **(C)** Protein-protein interaction network of 246 intersecting targets. The darkness of colors and sizes of circles represent the degree of freedom. **(D–G)** Bubble plot of Gene Ontology (GO) enrichment analysis of shared targets by periplocymarin and heart failure. Bubble plot: letters on the left are GO names, numbers on the bottom are the proportions of genes, sizes of the circles indicate the numbers of enriched genes, and colors reflect *p* values. The redder the colors are, the more enriched the genes are, and the smaller the *p* values are. The Kyoto Encyclopedia of Genes and Genomes (KEGG) pathway analyses **(D)**, biological process (BP) enrichment **(E)**, cellular components (CC) enrichment **(F)**, and molecular function (MF) enrichment **(G)** of the 246 intersecting genes. **(H)** Network of KEGG pathway and the 166 related targets. Squares represent the targets, inverted triangles represent the pathways; The area of nodes represents their degree, and the larger the area, the more important the node.

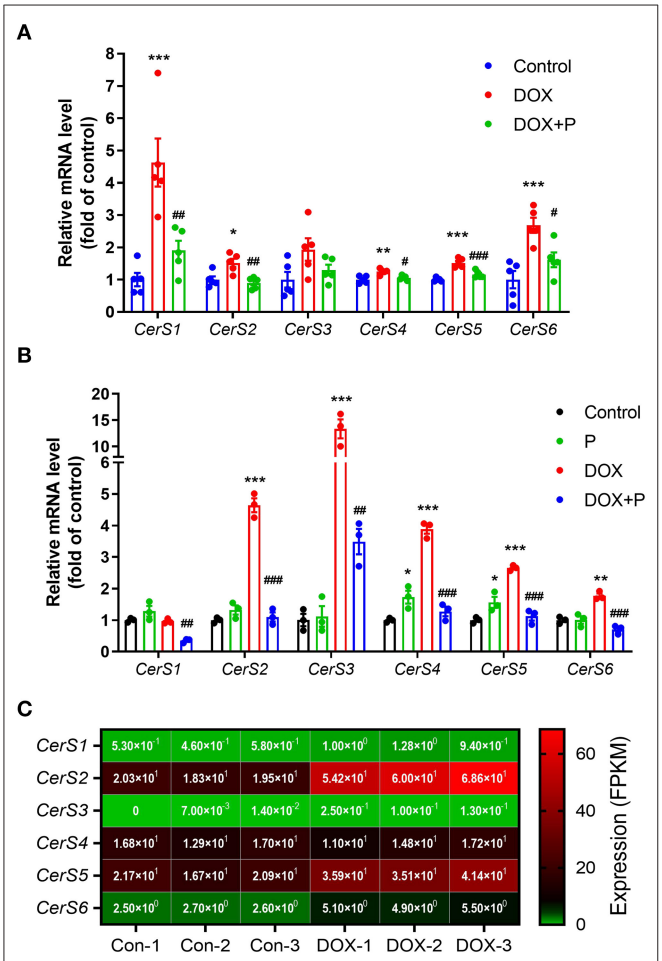

FIGURE 6 | Periplocymarin regulated the expression of enzymes involved in ceramides metabolism. **(A)** *CerS1-6* messenger RNA (mRNA) expression in the heart tissues was measured by real-time PCR. Data are presented as mean ± SEM; $n = 5$, $^{*}p < 0.05$, $^{**}p < 0.01$, $^{***}p < 0.001$ vs. control; $^{\#}p < 0.05$, $^{\#\#}p<0.01$, $^{\#\#\#}p<0.001$ vs. DOX. **(B)** *CerS1-6* mRNA expression in the primary cardiomyocytes was measured by real-time PCR. Data are presented as mean ± SEM; $n = 3$, $^{*}p < 0.05$, $^{**}p < 0.01$, $^{***}p < 0.001$ vs. control; $^{\#\#}p < 0.01$, $^{\#\#\#}p < 0.001$ vs. DOX. **(C)** The expression of *CerS1-6* in the RNA sequencing data (GSE157282).

DISCUSSION AND CONCLUSION

The anthracycline antibiotic drug DOX, also known as Adriamycin, is widely used to treat malignant tumors, but its clinical application is greatly restricted by acute, sub-acute, or chronic side-effects (1). Doxorubicin exhibits a high affinity for cardiomyocytes, so DOX is very easy to lead to cardiotoxicity, causing arrhythmia, cardiomyopathy, and chronic heart failure (2, 3). Therefore, precise and effective therapy or drugs are urgently needed to counteract the cardiotoxicity of DOX. It is a common method to establish models of heart failure by abdominally injected DOX (29, 30). Periplocae Cortex is a traditional Chinese medicine applied in the cardiotonic formula of traditional Chinese medicine, which is widely used. Our group previously reported that periplocymarin is a bio-effective component of the Periplocae cortex with a strong cardiotonic effect (15). The present study demonstrated that the pre-treatment of periplocymarin significantly alleviates DOX-induced cardiomyopathy both *in vivo* and *in vitro*. The metabolomics analysis further revealed that periplocymarin treatment restored the metabolic disorders of ceramides induced by DOX. Periplocymarin may become a novel promising therapeutic agent to ameliorate cardiotoxicity and improve cardiac function in patients with DOX chemotherapy.

Ceramides were recognized as an important lipid second messenger, which mediates downstream events including cell proliferation, cell differentiation, cell cycle arrest, and cell apoptosis (31). Previous studies have demonstrated that ceramides are accumulated and ceramide biosynthesis enzymes are upregulated in the falling myocardium both in humans and in mice with HF (32). Besides, multiple investigations suggested that ceramides contribute to cardiomyocytes apoptosis. For instance, ceramide analogs are sufficient to trigger the apoptosis of cardiomyocytes (23) and palmitate-induced endogenous ceramides also initiate apoptosis of cardiomyocytes (20). Additionally, the overexpression of ceramide synthesis key enzymes, such as *CerS2*, promoted mitochondrial dysfunction and apoptosis in cardiomyocytes (33). More importantly, DOX exposure could induce ceramide generation in cultured adult rat ventricular myocytes and then lead to myocyte apoptosis (34). Based on these previous works, we firstly detected and found that DOX elevated the contents of Cer16:0, Cer18:0, and Cer24:1 *in vivo* and *in vitro*. More importantly, periplocymarin treatment obviously decreased the level of the ceramides. These results suggested that periplocymarin efficaciously inhibit DOX-induced ceramides metabolic disorders.

In recent years, the role of ceramides in cardiovascular disease has received more and more attention. In patients with or without coronary artery disease, it was found that elevated plasma ceramides concentrations are independently related to adverse cardiovascular events (35). Clinical studies have shown that risk prediction models based on plasma ceramides levels can effectively identify people at high risk of adverse cardiovascular

events in the future, predict the recurrence of coronary events, and then optimize the secondary prevention strategy, especially for those who have reached the target of blood lipids. Some studies have demonstrated that a high ratio of Cer16:0/Cer24:0 is tightly associated with potentially adverse subclinical cardiac structure and function changes (36). Another study pointed that the ratio of Cer24:0/Cer16:0 may become a helpful biomarker for the risk of coronary heart disease, HF, and all-cause mortality in the community (37). The concentrations of Cer16:0, Cer22:0, Cer24:0, and Cer24:1 ceramides were found to be independent risk factors for the occurrence of primary end events of cardiovascular disease (38). By conducting a long-term follow-up on 495 patients with coronary angiography, Meeusen et al. found that Cer16:0, Cer18:0, and Cer24:1 ceramide levels and the ratios of Cer16:0/Cer24:0, Cer18:0/Cer24:0, and Cer24:1/Cer24:0 ceramides could predict the occurrence of major adverse cardiovascular events during the 4-year follow-up (35). In our study, we found the contents of Cer16:0, Cer18:0, and Cer24:1 were significantly increased after the treatment of DOX, periplocymarin decreased the levels of these metabolites, and the same trend was observed *in vivo* and *in vitro*. Cer16:0/Cer24:0, Cer18:0 /Cer24:0, and Cer24:1/Cer24:0 ceramide ratios were elevated in the DOX group, periplocymarin pre-treatment reversed this phenomenon. Combined with the echocardiography result, we confirmed that periplocymarin could improve metabolic disorders of ceramides and then improve HF.

Ceramides can be synthesized through the *de novo* pathway in the ER or the salvage pathway in lysosomes (39). The *de novo* pathway for ceramides synthesis with the condensation of serine and palmitate to form 3-keto-dihydroshingosine is catalyzed by the enzyme serine palmitoyltransferase (SPT) (39, 40). 3-Ketosphinganine reductase catalyzed 3-ketosphinganine converted to sphinganine. Sphinganine is then converted to ceramide by ceramide synthase (CerS) (40, 41). Six distinct CerS have been identified in mammalian cells that can be distinguished by their high specificity for different fatty acyl chain substrates (41). The next step of the pathway is the transition of dihydroceramide to ceramide, a reaction that is catalyzed by dihydroceramide desaturase (41). Ceramide can be resolved into sphingosine by acidic ceramidase (ASAH), at the same time, sphingosine can return to ceramide by CerS (41). The salvage pathway in the lysosomes consists of the degradation of sphingomyelin to ceramides by acid sphingomyelinase (ASMase) and ceramides to sphingosine by ceramidases (39, 42). Cells possess several isoforms of SMase, they have been classified into acid, neutral, and alkaline SMase according to their features. Acid sphingomyelinase and NSMase are mainly involved in signal transduction processes. Besides, sphinganine can be converted to ceramide-1-phosphate by Cerk. In our study, the expression of *Spt1*, *Cerk*, *Asah1*, *ASMase*, and *CerS1-6* were detected by Real-time PCR. No obvious difference was found in the expression of *Spt1*, *ASMase*, and *Cerk* among the three groups. However, the mRNA levels of *CerS2-6* were obviously elevated in response to DOX *in vivo* and *in vitro*. This elevation was significantly ameliorated after periplocymarin treatment. Mass-spectrometry analyses have shown that ceramides levels were increased in the DOX group, which was reversed by periplocymarin. Altogether, these results suggested that the treatment of DOX resulted in ceramide accumulation by up-regulating the expression of *CerS2-6*, which are responsible for encoding key enzymes in ceramide synthesis. The administration of periplocymarin successfully prevented this phenomenon. However, the acidic ceramidase (*Asah1*) expression was higher in the DOX group, and periplocymarin treatment reversed its levels to a normal level that was consistent with the literature (43). That may be a self-protection mechanism of the body because the Asah1 overexpression could reduce the concentrations of ceramides in the cells, thus limiting the harmful accumulation of ceramides in the liver (43).

Given that periplocymarin is a promising anti-cancer drug (13, 14), the use of periplocymarin in clinical patients receiving DOX chemotherapy may have advantages: firstly, it synergistically promotes the anti-cancer effect of DOX; secondly, it reduces the dose of DOX; last but not least, it improves DOX-induced cardiac dysfunction. However, whether and how periplocymarin can cooperate with DOX still needs further experimental verification.

In conclusion, our study provided first-hand evidence that periplocymarin ameliorated DOX-induced HF. Through combined metabolomic analysis study and experimental validation, we confirmed that periplocymarin regulated ceramide synthases gene expression to improve ceramides metabolism disorder, and ameliorated DOX-induced cardiomyocytes apoptosis and HF. Periplocymarin is promising to be a potent therapeutic agent for HF, especially DOX-induced HF.

DATA AVAILABILITY STATEMENT

The datasets presented in this study can be found in online repositories. The names of the repository/repositories and accession number(s) can be found in the article/**Supplementary Material**.

ETHICS STATEMENT

The animal study was reviewed and approved by Animal Care and Use Review Committee of Dalian Medical University.

AUTHOR CONTRIBUTIONS

WY: conceptualization, methodology, data curation, formal analysis, funding acquisition, writing—original draft, and writing—review and editing. LQ: investigation, project administration, and resources. RY: methodology, investigation, software, and validation. HX: funding acquisition, supervision, and visualization. All authors contributed to the article and approved the submitted version.

FUNDING

This work was supported by the National Natural Science Foundation of China Grants (81900267), Doctoral Scientific Research Initiation Fund of Liaoning Province (2019-BS-078), Dalian Youth Science and Technology Star Project (2019RQ103), and Scientific Research Fund Project of Liaoning Provincial Department of Education (LZ2019014, LZ2020053, LJKZ0840, and LJKZ0847).

SUPPLEMENTARY MATERIAL

The Supplementary Material for this article can be found online at: https://www.frontiersin.org/articles/10.3389/fcvm.2021.732554/full#supplementary-material

REFERENCES

1. Kalyanaraman B. Teaching the basics of the mechanism of doxorubicin-induced cardiotoxicity: have we been barking up the wrong tree? *Redox Biol.* (2020) 29:101394. doi: 10.1016/j.redox.2019.101394
2. Kankeu C, Clarke K, Passante E, Huber HJ. Doxorubicin-induced chronic dilated cardiomyopathy-the apoptosis hypothesis revisited. *J Mol Med.* (2017) 95:239–48. doi: 10.1007/s00109-016-1494-0
3. An J, Li P, Li J, Dietz R, Donath S. ARC is a critical cardiomyocyte survival switch in doxorubicin cardiotoxicity. *J Mol Med.* (2009) 87:401–10. doi: 10.1007/s00109-008-0434-z
4. Mitry MA, Edwards JG. Doxorubicin induced heart failure: phenotype and molecular mechanisms. *Int J Cardiol Heart Vasc.* (2016) 10:17–24. doi: 10.1016/j.ijcha.2015.11.004
5. Pu J, Yuan A, Shan P, Gao E, Wang X, Wang Y, et al. Cardiomyocyte-expressed farnesoid-X-receptor is a novel apoptosis mediator and contributes to myocardial ischaemia/reperfusion injury. *Eur Heart J.* (2013) 34:1834–45. doi: 10.1093/eurheartj/ehs011
6. Wang Y, Wang Q, Li C, Lu L, Zhang Q, Zhu R, et al. A review of chinese herbal medicine for the treatment of chronic heart failure. *Curr Pharmaceutic Design.* (2017) 23:5115–24. doi: 10.2174/1381612823666170925163427
7. Xu ZM, Li CB, Liu QL, Li P, Yang H. Ginsenoside rg1 prevents doxorubicin-induced cardiotoxicity through the inhibition of autophagy and endoplasmic reticulum stress in mice. *Int J Mol Sci.* (2018) 19:58. doi: 10.3390/ijms19113658
8. Dong Z, Zhao P, Xu M, Zhang C, Guo W, Chen H, et al. Astragaloside IV alleviates heart failure via activating PPARα to switch glycolysis to fatty acid β-oxidation. *Scien Rep.* (2017) 7:2691. doi: 10.1038/s41598-017-02360-5
9. Zhang X, Wang Q, Wang X, Chen X, Shao M, Zhang Q, et al. Tanshinone IIA protects against heart failure post-myocardial infarction via AMPKs/mTOR-dependent autophagy pathway. *Biomed Pharmacotherap.* (2019) 112:108599. doi: 10.1016/j.biopha.2019.108599
10. Wang L, Wang L, Zhou X, Ruan G, Yang G. Qishen yiqi dropping pills ameliorates doxorubicin-induced cardiotoxicity in mice via enhancement of cardiac angiogenesis. *Med Sci Monit.* (2019) 25:2435–2444. doi: 10.12659/MSM.915194
11. He L, Liu Y, Yang K, Zou Z, Fan C, Yao Z, et al. The discovery of Q-markers of Qiliqiangxin Capsule, a traditional Chinese medicine prescription in the treatment of chronic heart failure, based on a novel strategy of multi-dimensional "radar chart" mode evaluation. *Phytomedicine.* (2021) 82:153443. doi: 10.1016/j.phymed.2020.153443
12. Yun WJ, Yao ZH, Fan CL, Qin ZF, Tang XY, Gao MX, et al. Systematic screening and characterization of Qi-Li-Qiang-Xin capsule-related xenobiotics in rats by ultra-performance liquid chromatography coupled with quadrupole time-of-flight tandem mass spectrometry. *J Chromatogr B Analyt Technol Biomed Life Sci.* (2018) 1090:56–64. doi: 10.1016/j.jchromb.2018.05.014
13. Bloise E, Braca A, De Tommasi N, Belisario MA. Pro-apoptotic and cytostatic activity of naturally occurring cardenolides. *Cancer Chemother Pharmacol.* (2009) 64:793–802. doi: 10.1007/s00280-009-0929-5
14. Martey ON, He X, Xing H, Deng F, Feng S, Li C, et al. Periplocymarin is a potential natural compound for drug development: highly permeable with absence of P-glycoprotein efflux and cytochrome P450 inhibitions. *Biopharm Drug Dispos.* (2014) 35:195–206. doi: 10.1002/bdd.1884
15. Yun W, Qian L, Cheng Y, Tao W, Yuan R, Xu H. Periplocymarin plays an efficacious cardiotonic role via promoting calcium influx. *Frontiers in pharmacology.* (2020) 11:1292. doi: 10.3389/fphar.2020.01292
16. Yun W, Qian L, Yuan R, Xu H. Periplocymarin protects against myocardial fibrosis induced by β-adrenergic activation in mice. *Biomed Pharmacotherapy.* (2021) 139:111562. doi: 10.1016/j.biopha.2021.111562
17. Akolkar G, da Silva Dias D, Ayyappan P, Bagchi AK, Jassal DS, Salemi VMC, Irigoyen MC, De Angelis K, Singal PK. Vitamin C mitigates oxidative/nitrosative stress and inflammation in doxorubicin-induced cardiomyopathy. *Heart Circulat Physiol.* (2017) 313:H795–809. doi: 10.1152/ajpheart.00253.2017
18. Holland WL, Summers SA. Sphingolipids, insulin resistance, and metabolic disease: new insights from in vivo manipulation of sphingolipid metabolism. *Endocrine Rev.* (2008) 29:381–402. doi: 10.1210/er.2007-0025
19. de Carvalho LP, Tan SH, Ow GS, Tang Z, Ching J, Kovalik JP, et al. Plasma ceramides as prognostic biomarkers and their arterial and myocardial tissue correlates in acute myocardial infarction. *JACC.* (2018) 3:163–75. doi: 10.1016/j.jacbts.2017.12.005
20. Choi RH, Tatum SM, Symons JD, Summers SA, Holland WL. Ceramides and other sphingolipids as drivers of cardiovascular disease. *Nat Rev Cardiol.* (2021) 36:1. doi: 10.1038/s41569-021-00536-1
21. Lemaitre RN, Jensen PN, Hoofnagle A, McKnight B, Fretts AM, King IB, et al. Plasma ceramides and sphingomyelins in relation to heart failure risk. *Circul.* (2019) 12:e005708. doi: 10.1161/CIRCHEARTFAILURE.118.005708
22. Li H, Junk P, Huwiler A, Burkhardt C, Wallerath T, Pfeilschifter J, et al. Dual effect of ceramide on human endothelial cells: induction of oxidative stress and transcriptional upregulation of endothelial nitric oxide synthase. *Circul.* (2002) 106:2250–6. doi: 10.1161/01.CIR.0000035650.05921.50
23. Bielawska AE, Shapiro JP, Jiang L, Melkonyan HS, Piot C, Wolfe CL, et al. Ceramide is involved in triggering of cardiomyocyte apoptosis induced by ischemia and reperfusion. *Am J Pathol.* (1997) 151:1257–63.
24. Krown KA, Page MT, Nguyen C, Zechner D, Gutierrez V, Comstock KL, et al. Tumor necrosis factor alpha-induced apoptosis in cardiac myocytes. involvement of the sphingolipid signaling cascade in cardiac cell death. *J Clinic Investigat.* (1996) 98:2854–65. doi: 10.1172/JCI119114
25. Antoniak S, Tatsumi K, Schmedes CM, Grover SP, Pawlinski R, Mackman N. Protease-activated receptor 1 activation enhances doxorubicin-induced cardiotoxicity. *J Mol Cell Cardiol.* (2018) 122:80–7. doi: 10.1016/j.yjmcc.2018.08.008
26. Nuamnaichati N, Sato VH, Moongkarndi P, Parichatikanond W, Mangmool S. Sustained β-AR stimulation induces synthesis and secretion of growth factors in cardiac myocytes that affect on cardiac fibroblast activation. *Life Sci.* (2018) 193:257–69. doi: 10.1016/j.lfs.2017.10.034
27. Wen J, Zhang L, Liu H, Wang J, Li J, Yang Y, et al. Salsolinol attenuates doxorubicin-induced chronic heart failure in rats and improves mitochondrial function in h9c2 cardiomyocytes. *Front Pharmacol.* (2019) 10:1135. doi: 10.3389/fphar.2019.01135
28. Xu H, Fang B, Du S, Wang S, Li Q, Jia X, et al. Endothelial cell prostaglandin E2 receptor EP4 is essential for blood pressure homeostasis. *JCI insight.* (2020) 5:e138505. doi: 10.1172/jci.insight.138505
29. Zhang S, Liu X, Bawa-Khalfe T, Lu LS, Lyu YL, Liu LF, et al. Identification of the molecular basis of doxorubicin-induced cardiotoxicity. *Nat Med.* (2012) 18:1639–42. doi: 10.1038/nm.2919
30. Fang X, Wang H, Han D, Xie E, Yang X, Wei J, et al. Ferroptosis as a target for protection against cardiomyopathy. *Proceed Nat Acad Sci USA.* (2019) 116:2672–80. doi: 10.1073/pnas.1821022116

31. Parra V, Eisner V, Chiong M, Criollo A, Moraga F, Garcia A, et al. Changes in mitochondrial dynamics during ceramide-induced cardiomyocyte early apoptosis. *Cardiovascul Res.* (2008) 77:387–97. doi: 10.1093/cvr/cvm029
32. Ji R, Akashi H, Drosatos K, Liao X, Jiang H, Kennel PJ, et al. Increased *de novo* ceramide synthesis and accumulation in failing myocardium. *JCI Insight.* (2017) 2:922. doi: 10.1172/jci.insight.82922
33. Law BA, Liao X, Moore KS, Southard A, Roddy P, Ji R, et al. Lipotoxic very-long-chain ceramides cause mitochondrial dysfunction, oxidative stress, and cell death in cardiomyocytes. *FASEB J.* (2018) 32:1403–16. doi: 10.1096/fj.201700300R
34. Delpy E, Hatem SN, Andrieu N, de Vaumas C, Henaff M, Rucker-Martin C, et al. Doxorubicin induces slow ceramide accumulation and late apoptosis in cultured adult rat ventricular myocytes. *Cardiovascul Res.* (1999) 43:398–407. doi: 10.1016/S0008-6363(99)00142-X
35. Meeusen JW, Donato LJ, Bryant SC, Baudhuin LM, Berger PB, Jaffe AS. Plasma ceramides. *Arterioscler Thromb Vascul Biol.* (2018) 38:1933–9. doi: 10.1161/ATVBAHA.118.311199
36. Nwabuo CC, Duncan M, Xanthakis V, Peterson LR, Mitchell GF, McManus D, et al. Association of circulating ceramides with cardiac structure and function in the community: the framingham heart study. *J Am Heart Assoc.* (2019) 8:e013050. doi: 10.1161/JAHA.119.013050
37. Peterson LR, Xanthakis V, Duncan MS, Gross S, Friedrich N, Völzke H, et al. Ceramide remodeling and risk of cardiovascular events and mortality. *J Am Heart Assoc.* (2018) 7: doi: 10.1161/JAHA.117.007931
38. Wang DD, Toledo E, Hruby A, Rosner BA, Willett WC, Sun Q, et al. Plasma ceramides, mediterranean diet, and incident cardiovascular disease in the predimed trial (prevención con dieta mediterránea). *Circulation.* (2017) 135:2028–2040. doi: 10.1161/CIRCULATIONAHA.116.024261
39. Kurz J, Parnham MJ, Geisslinger G, Schiffmann S. Ceramides as novel disease biomarkers. *Trends Mol Med.* (2019) 25:20–32. doi: 10.1016/j.molmed.2018.10.009
40. Baranowski M, Blachnio A, Zabielski P, Gorski J. Pioglitazone induces *de novo* ceramide synthesis in the rat heart. *Prostaglandins Other Lipid Mediat.* (2007) 83:99–111. doi: 10.1016/j.prostaglandins.2006.10.004
41. Presa N, Gomez-Larrauri A, Dominguez-Herrera A, Trueba M, Gomez-Muñoz A. Novel signaling aspects of ceramide 1-phosphate. *Biochimica et biophysica acta.* (2020) 1865:158630. doi: 10.1016/j.bbalip.2020.158630
42. Castro BM, Prieto M, Silva LC. Ceramide: a simple sphingolipid with unique biophysical properties. *Progress Lipid Res.* (2014) 54:53–67. doi: 10.1016/j.plipres.2014.01.004
43. Presa N, Clugston RD, Lingrell S, Kelly SE, Merrill AH, et al. Vitamin E alleviates non-alcoholic fatty liver disease in phosphatidylethanolamine N-methyltransferase deficient mice. *Biochimica et biophysica acta.* (2019) 1865:14–25. doi: 10.1016/j.bbadis.2018.10.010

Conflict of Interest: The authors declare that the research was conducted in the absence of any commercial or financial relationships that could be construed as a potential conflict of interest.

Publisher's Note: All claims expressed in this article are solely those of the authors and do not necessarily represent those of their affiliated organizations, or those of the publisher, the editors and the reviewers. Any product that may be evaluated in this article, or claim that may be made by its manufacturer, is not guaranteed or endorsed by the publisher.

frontiers in Cardiovascular Medicine

CASE REPORT
published: 06 December 2021
doi: 10.3389/fcvm.2021.727445

Case Report: Cardiac Toxicity Associated With Immune Checkpoint Inhibitors

Ru Chen[1,2], *Ling Peng*[3], *Zhihua Qiu*[2], *Yan Wang*[1,2], *Fen Wei*[1], *Min Zhou*[4,5]* and *Feng Zhu*[1,2]*

[1] Department of Cardiology, Union Hospital, Tongji Medical College, Huazhong University of Science and Technology, Wuhan, China, [2] Clinic Center of Human Gene Research, Union Hospital, Tongji Medical College, Huazhong University of Science and Technology, Wuhan, China, [3] Cancer Center, Union Hospital, Tongji Medical College, Huazhong University of Science and Technology, Wuhan, China, [4] Department of Pulmonary and Critical Care Medicine, Tongji Hospital, Tongji Medical College, Huazhong University of Science and Technology, Wuhan, China, [5] Key Laboratory of Respiratory Diseases, National Ministry of Health of the People's Republic of China and National Clinical Research Center for Respiratory Disease, Wuhan, China

Immune checkpoint inhibitors (ICIs) have now emerged as a mainstay of treatment for various cancer. Along with the development of ICIs, immune-related adverse effects (irAEs) have been the subject of wide attention. The cardiac irAE, a rare but potentially fatal and fulminant effect, have been reported recently. This article retrospectively reviewed 10 cases from our hospital with cardiac irAEs, with severity ranging from asymptomatic troponin-I elevations to cardiac conduction abnormalities and even fulminant myocarditis. In our series, all the cases were solid tumors and lung cancer was the most frequent cancer type (4,40%). In total, three (30.0%) patients experienced more than one type of life-threatening complication. A systemic corticosteroid was given to nine patients (90.0%). The majority of cases (7, 70%) were performed at an initial dose of 1–2 mg/kg/day. Two (20.0%) patients were admitted to ICU, three (30.0%) patients were put on mechanical ventilation, two (20.0%) patients received the plasma exchange therapy, and one patient was implanted with a pacemaker. Two (20.0%) of the patients succumbed and died, with a median duration of 7.5 days (IQR5.0–10.0) from diagnosis of cardiac irAE to death. Based on these results, we recommend that clinicians be alert to cardiac irAEs, including performing cardiovascular examinations before ICI treatment to accurately diagnose suspected myocarditis, enabling immediate initiation of immunosuppressive therapy to improve prognosis.

Keywords: immune checkpoint inhibitors, cancer, myocardial injury, immune-related adverse events, myocarditis

OPEN ACCESS

Edited by:
Xiaofeng Yang,
Temple University, United States

Reviewed by:
Arturo Cesaro,
University of Campania Luigi Vanvitelli, Italy
Zhenzhong Zheng,
The First Affiliated Hospital of Nanchang University, China

***Correspondence:**
Min Zhou
minzhou@tjh.tjmu.edu.cn
Feng Zhu
zhufeng@hust.edu.cn

Specialty section:
This article was submitted to Cardiovascular Therapeutics, a section of the journal Frontiers in Cardiovascular Medicine

Received: *18 June 2021*
Accepted: *08 November 2021*
Published: *06 December 2021*

Citation:
Chen R, Peng L, Qiu Z, Wang Y, Wei F, Zhou M and Zhu F (2021) Case Report: Cardiac Toxicity Associated With Immune Checkpoint Inhibitors. Front. Cardiovasc. Med. 8:727445. doi: 10.3389/fcvm.2021.727445

INTRODUCTION

Immune checkpoints are involved in the key negative regulatory pathways of immune surveillance, aiding tumor cells to avoid immune detection and destruction. Immune checkpoint inhibitors (ICIs) are monoclonal antibodies targeting blocked immune checkpoint proteins such as cytotoxic T lymphocyte-associated antigen 4 (CTLA-4), programmed cell death 1 (PD-1), and PD-1 ligand (PD-L1) (1). ICIs increase T cell activation as well as T-cell mediated anti-tumor effect, and have become a revolutionary treatment that prolongs the survival of various malignancies previously endowed with poor prognosis over the last decade (2). Along with the prosperity of ICIs,

system-wide immune-related adverse events (irAEs) have emerged and drawn increasing attention. Dermatologic, hepatic, gastrointestinal, and endocrine toxicities are among the most common irAEs reported in patients treated with monotherapy or combined ICIs therapy (3).

Cardiotoxicity, one of the rare irAEs, used to be underestimated and has roused clinicians' attention in recent years. The incidence of ICIs related myocarditis varies from 0.1 to 1% (4, 5). However, the mortality rate of ICI-related myocarditis ranges from 35 to 50% (6, 7). Over the past few years, several cases of myocarditis associated with ICIs have been reported, and most of the patients presented unspecific manifestations, along with atypical laboratory abnormalities and imaging features (8). Despite treatment with high doses of steroids, the poor outcome was fatal in some cases. Because it is rare but potentially fatal with a fulminant effect, it is important to characterize cardiac irAEs in an early stage. This study presents a series of 10 cases that developed ICI related cardiac irAEs, as well as subsequent treatment and outcomes.

MATERIALS AND METHODS

A retrospective case study was performed on patients who presented with ICI related myocardial injury at Union Hospital in the Tongji Medical College of Huazhong University of Science and Technology, Wuhan (China) from January 1, 2018, to August 30, 2021. ICI related myocarditis was defined according to the criteria proposed by Marc P. Bonaca et al. (9) and classified as definite myocarditis, probable myocarditis, and possible myocarditis.

The study was approved by the Ethics committee of the Tongji Medical College of Huazhong University of Science and Technology (China). Data were retrieved from electronic medical records including demographic features, clinical features, laboratory findings, and images. Two physicians (Zhihua Qiu and Fen Wei) independently reviewed the data.

RESULTS

Demographic and Clinical Characteristics of Enrolled Cases With Cardiac irAE

This study enrolled 10 patients with ICI-related cardiac cardiotoxicity who were admitted to the hospital between January 1, 2018, and August 30, 2021. The detailed descriptions of each case are provided in the **Supplementary Materials**, and the characteristics are displayed in **Supplementary Table 1**.

As shown in **Table 1**, the median age of patients was 62.5 (55.0–73.0) years old. Half of the cases were male. Four (40%) patients were diagnosed with lung cancer and 2 patients were diagnosed with thymoma. Other cancer types included cervical cancer, pyriform sinus squamous cell carcinoma, gallbladder carcinoma, and hepatocellular carcinoma. Furthermore, one patient diagnosed with cervical cancer had a previous history of breast cancer, and one patient with lung adenocarcinoma was once diagnosed with papillary thyroid carcinoma. Before ICI treatment, 70% of the patients were treated with surgeries, and 80% had received chemotherapy. Radiotherapy was performed on 60% of the patients, and two (20%) patients also received angiogenesis inhibitors. Only two patients were found to

TABLE 1 | Demographic and base line clinical characteristics of the patients with cardiac irAE.

Characteristic	Patients (*n*=), Median (IQR), No. (%)
Median age (IQR), year	62.5 (55.0–73.0)
Male sex	5 (50.0)
Tumor diagnosis	
Lung cancer	4 (40.0)
Thymoma	2 (20.0)
Cervical cancer	1 (10.0)
Pyriformsinus squamous cell carcinoma	1 (10.0)
Gallbladder carcinoma	1 (10.0)
Hepatocellular carcinoma	1 (10.0)
History of prior treatment	
Operation	7 (70.0)
Chemotherapy	8 (80.0)
Radiotherapy	6 (60.0)
Angiogenesis inhibitors	2 (20.0)
Interventional therapy	2 (20.0)
Co-morbidities	
Hypertension	1 (10.0)
Coronary heart disease	1 (10.0)
Types of ICI	
Anti-PD-1 antibody	
Sintilimab	3 (30.0)
Tislelizumab	1 (10.0)
Camrelizumab	3 (30.0)
Pembrolizumab	2 (20.0)
Anti-PD-L1 antibody	
ZKAB001	1 (10.0)
Days from first dose of ICI to onset	28.5 (17.8–63.5)
Symptoms and signs on admission	
Fever	1 (10.0)
Palpitation	3 (30.0)
Chest tightness	5 (50.0)
Dyspnea	2 (20.0)
Fatigue	3 (30.0)
Neuromuscular symptom	
Blepharoptosis	4 (40.0)
Diplopia	1 (10.0)
Conscious disturbance	1 (10.0)
Types of cardiac irAE	
Definite myocarditis	2 (20.0)
Probable myocarditis	0 (0.0)
Possible myocarditis	2 (20.0)
other myocardial injury	6 (60.0)
Grade of cardiac irAE	
G1-2	6 (60.0)
G3-4	2 (20.0)
G5	2 (20.0)

IQR, interquartile range; CHD, coronary heart disease; ICI, immune checkpoint inhibitor; irAE, immune-related adverse event.

TABLE 2 | Laboratory tests and echocardiogram findings of the patients with cardiac irAE.

Last lab test indexes before Steroids (*U*; normal range), change	**Median (IQR), No. (%)**
Leucocytes ($\times 10^9$ per L; 3.5–9.5), Increased	7.4 (5.6–9.2), 3 (30.0)
Lymphocytes ($\times 10^9$ per L; 1.1–3.2), Decreased	1.0 (0.7–1.1), 7 (70.0)
Neutrophils ($\times 10^9$ per L; 1.8–6.3), Increased	5.8 (3.7–7.1), 5 (50.0)
Lab test indexes at peak (*U*; normal range)	
ALT (U/L; 9.0–50.0), Increased	135.0 (32.5–212.3), 6 (60.0)
AST (U/L; 15.0–40.0), Increased	168.0 (49.8–544.8), 9 (90.0)
LDH (U/L; 120.0–250.0), Increased	765.0 (414.5–1223.8), 9 (90.0)
Hs-TnI (ng/L; <26.2), Increased	1,252.1 (213.7–20058.5), 9 (90.0)
CK-MB (ng/mL; <6.6), Increased	75.0 (10.9–417.7), 9 (90.0)
CK (U/L; 38–174), Increased	3,573.0 (662.3–9,900.0), 9 (90.0)
BNP (pg/ml, <100), Increased	178.9 (25.3–369.8), 4 (50.0), $N = 8$
C-reactive protein (mg/L; 0.0–10.0), Increased	42.7 (9.8–82.4), 4 (80.0), $N = 5$
Positive autoantibodies against β1-AR	2 (100.0), $N = 2$
Positive autoantibodies against L-type calcium channel	2 (100.0), $N = 2$
Positive autoantibodies against MHC	2 (100.0), $N = 2$
Positive autoantibodies against ANT	2 (100.0), $N = 2$
Electrocardiogram findings	**No. (%)**
Sinus tachycardia	8 (80.0)
Atrial extrasystole	2 (20.0)
Ventricular extrasystole	0 (0.0)
Atrioventricular block	4 (40.0)
Bundle branch block	3 (30.0)
ST segment elevation	2 (20.0)
Others[a]	4 (40.0)
Echocardiogram findings	**No. (%)**
Reduced ejection fraction	3 (30.0)
Cardiac dilatation	2 (20.0)
Wall motion abnormality	3 (30.0)

ALT, Alanine aminotransferase; AST, Aspartate aminotransferase; LDH, Lactate dehydrogenase; Hs-TnI, high-sensitivity troponin I; CK-MB, creatine kinase-muscle and brain; CK, creatine kinase; BNP, type B natriuretic peptide.
[a]*Indicates unspecific ST-T change and Q wave.*

have previous cardiovascular disease, one was diagnosed with hypertension and the other was diagnosed with coronary heart disease.

The most frequent ICIs treatment for the cases were sintilimab (30%) and camrelizumab (30%). Nine patients were treated with anti-PD-1 therapy, while the remaining one received anti-PD-L1 therapy. Median time from the use of the first dose of ICI to onset was 28.5 (17.8–63.5) days and symptoms at onset varied markedly. The most common symptoms presented in our cases were chest tightness, which occurred in 50% of the patients. Palpitations and fatigue were presented in 30% of the patients. Neuromuscular symptoms also occurred in ICI-related cardiac irAE. Forty percentage of the patients presented with blepharoptosis, one patient showed diplopia and one patient developed conscious disturbance during the disease.

Based on the diagnosing criteria proposed by Marc P. Bonaca et al. (9), only two patients were classified as having definite myocarditis. Six cases were classified as other myocardial injury and two patients were regarded as having possible myocarditis, mainly due to the lack of confirmed examinations such as coronary angiography to rule out acute coronary syndrome. Sixty percentage of the patients were mild cases classified as G1-2.

Laboratory, Electrocardiogram, and Echocardiogram Findings of Enrolled Cases With Cardiac irAE

Laboratory, electrocardiogram, and echocardiogram findings for the patients with cardiac irAE were shown in **Table 2**. Lymphopenia was frequently found in the cardiac irAE (7, 70%). The elevated level of serum alanine aminotransferase (ALT) and aspartate aminotransferase (AST) was observed in six (60%) and nine (90%) patients, respectively. Markedly evaluated levels of creatinine kinase (CK), creatinine kinase-muscle and brain type (CK-MB), and troponin I (TnI) were found in nine (90%) patients. B-type natriuretic peptide (BNP) tests were available in eight patients, and levels were significantly elevated in four (50%) of them. The serum levels of C-reactive protein (CRP), an important biomarker in systemic inflammation, were available in five patients, and CRP levels were elevated in four (80%). Four heart-specific autoantibodies were measured in two patients

(Case 1 and 4, see **Supplementary Material 1**) by enzyme-linked immunosorbent assay, and both of their serum samples were positive.

12-lead ECG and transthoracic echocardiography were performed in all cases. Cardiac conduction disorders including atrioventricular block (AVB) and bundle branch block were found in seven (70%) patients. One patient presented I-II°AVB, which eventually progressed to complete AVB (case 1, **Supplementary Material 1**). Systolic function was preserved in seven (70%) patients, and only three (30%) patients developed systolic dysfunction with left ventricular hypokinesia.

Treatment and Clinical Outcome of the Patients With Cardiac irAE

As shown in **Table 3**, systemic corticosteroid was given to nine patients (90.0%). Methylprednisolone was initiated on the 9th day (IQR 7.0–15.0) after symptom onset or detection of increased serum markers. The majority of cases (6, 60%) were treated at an initial high dose of 1–2 mg/kg/day. Two cases (case 3 and 4) initiated 500–1,000 mg daily methylprednisolone because of multiple life-threatening complications, and another case (case 9) was prescribed initial methylprednisolone at 0.5 mg/kg/day due to no symptom and mild elevation of CK-MB. The median duration of corticosteroids in our series was 5.0 weeks (IQR 5.0–6.0). Moreover, intravenous immunoglobin was prescribed to two patients (10%). Therapy for heart disease included ACEI (1, 10%), β-blocker (5, 50%), trimetazidine (6, 60%), and coenzyme Q10 (4, 40%).

As the disease progressed, four (40.0%) patients had life-threatening complications. Three patients experienced more than one type of complication, and one case experienced five types of complication including CCD with unstable hemodynamics, heart failure, respiratory failure, cardiac arrest, and myasthenia.

During the course two (20.0%) patients were admitted to ICU, three (30.0%) patients were put on mechanical ventilation, two (20.0%) patients received plasma exchange therapy, and one patient was implanted with a pacemaker. None of the cases received extracorporeal membrane oxygenation (ECMO) in our series.

Eight (80.0%) patients had been discharged with a median hospital stay of 10.5 days (IQR 5.75–23.0). However, two (20.0%) of the patients succumbed and died with a median time from diagnosis of cardiac irAE to death 7.5 days (IQR5.0–10.0). Only one patient was advised to rechallenge ICI therapy in the follow-up period.

TABLE 3 | Treatment and clinical outcome of the patients with cardiac irAE.

Treatment	No. (%), median (IQR)
Medicine therapy	
Systemic Steroids	9 (90.0)
Immunoglobin	2 (20.0)
AECI/ARB/ARNI	1 (10.0)
β blockers	5 (50.0)
Trimetazidine	6 (60.0)
Coenzyme Q10	4 (40.0)
Advanced therapy	
Mechanical ventilation	3 (30.0)
Plasma exchange	2 (20.0)
Pacemaker	1 (10.0)
ECMO	0 (0.0)
Admission to ICU	2 (20.0)
Complications	5 (50.0)
Single type (myasthenia)	1
Multiple types (CCD, heart failure, respiratory failure, cardiac arrest, and myasthenia)	
2[a] types	2 (20.0)
4[b] types	1 (10.0)
5[c] types	1 (10.0)
Clinical symptoms evaluation	
Improvement	8 (80.0)
Worse	2 (20.0)
Clinical outcomes	
Discharge from hospital	8 (80.0)
Death	2 (20.0)
Hospital stay (Pts. discharge), days	10.5 (5.75–23.0)
Time from diagnosis of cardiac irAE to death, days	7.5 (5.0–10.0), $N = 2$
Rechallenge ICIs	
Yes	1 (10.0)
No	7 (70.0)

IQR, interquartile range; AECI/ARB/ARNI, angiotensin II converting enzyme inhibitors/angiotensin receptor blocker/Angiotensin receptor neprilysin inhibitor; ECMO, extracorporeal membrane oxygenation; ICU, intensive care unit; CCD, cardiac conduction defect; ICIs, immune checkpoint inhibitors.

[a] *1 case with heart failure and myasthenia, the other case with respiratory failure, and myasthenia.*

[b] *1 case complicated with CCD, heart failure, respiratory failure, and cardiac arrest.*

[c] *1 case complicated with CCD, heart failure, respiratory failure, cardiac arrest, and myasthenia.*

DISCUSSION

The main cardiotoxicity associated with ICIs is myocarditis (10). The presentation of ICI related myocarditis encompasses a wide spectrum of symptoms including chest pain, chest distress, heart failure, and palpitations, etc. An elevation of cardiac biomarkers (troponin, CK, CK isoforms, and even BNP) was found in most patients (9). ECG changes were broad, including arrhythmia (atrial tachyarrhythmia, premature ventricular contractions, and ventricular tachycardia, ST-T wave abnormalities, PR segment changes, cardiac conduction defects, and so on) (11). Patients with ICI related myocarditis may present changes including left ventricular dysfunction and segmental wall motion abnormality in echocardiography however it is non-sensitive and unspecific (12). Cardiac magnetic resonance imaging (CMR) is preferred to echocardiography when diagnosing myocarditis. The presence of late gadolinium

enhancement (LGE) was 48% in patients and the presence of elevated T2-weighted short tau inversion recovery (STIR) was 28% (13). Endomyocardial biopsy typically demonstrates infiltration of CD8+ T-cells, CD68+ macrophages, and signs of myocardial fibrosis (14).

By integrating all the related clinical characteristics, the uniform diagnostic criteria for ICI related myocarditis were proposed in 2019 (9). According to the principle, only two of our cases were definite myocarditis. Based on current criteria, evidence from cardiac biopsy, CMR and ultrasound are vital in diagnosing definite myocarditis. However, cardiac biopsy is hard to perform not only due to its technical difficulty but also the poor health condition of most cancer patients. CMR and ultrasound are easier to access, but in our cases, patients who underwent CMR showed no instructional abnormality and most echocardiograms showed no change compared to the previous results. Therefore, it is sometimes confusing in clinical work to give a definite diagnosis when confronted with myocardial injury after ICI treatment, especially when some rule out the need for potentially harmful examinations such as coronary CTA or angiography. Apart from myocarditis, another cardiotoxicity related to ICI has been reported. B.P. Geisler et al. reported a case of takotsubo-like syndrome in a melanoma patient treated with ipilimumab (15). ICI-induced hypertension, symptomatic sinus tachycardia, and angina pectoris have also been reported (16). In our cases, one patient developed I°AVB without elevation of hsTnI. Thus, a comprehensive understanding of ICI related cardiotoxicity and specific biomarkers for each cardiac irAEs are needed.

While T cell-mediated cardiac impairment is considered the overarching mechanism for ICI-related myocardial injuries, the PD-1 deficiency animal models suggest a potential role of heart-specific autoantibodies involved in myocardial injuries. Genetic deletion of PD-1 led to spontaneous dilated cardiomyopathy caused by autoantibodies targeting cardiac troponin I in BALB/c mice (17, 18). PD-1 deficiency in autoimmune Murphy Roths Large mice led to the development of fatal myocarditis with T cell and macrophage infiltration and generation of high-titer autoantibodies against cardiac myosin (19). There has also been an increasing number of reports regarding irAEs with the autoantibody profiles traditionally associated with autoimmune diseases, such as myositis (20), hypothyroidism (21), dermatitis (22, 23), and nephritis (24). However, to date, antibody-antigen deposits were not found in biopsy specimens from ICI-associated myocarditis in humans (8). Interestingly, we found two cases that were positive for circulating heart-specific autoantibodies related to heart failure. These autoantibodies can influence cardiac function by negative chronotropic and/or negative inotropic effects. Removing or neutralizing circulating autoantibodies by immunoadsorption or intravenous immunoglobulins may improve cardiac function and reduce morbidity in patients with heart failure (25). Further studies are warranted to elucidate the generation of circulating autoantibodies against heart and autoantibody-mediated damage on cardiac function in ICI-related myocardial injuries.

High dose steroids are currently regarded as the first-line treatment for rescuing the unspecific hyperactive immune response caused by ICI therapy. It was recommended that initiated 1–2 mg/kg/d of methylprednisolone followed by an oral steroid tapered slowly could be effective (26). However, it might be insufficient to deal with severe ICI-related cardiotoxicity by steroids alone. The other immunosuppressive therapies including plasmapheresis, intravenous immunoglobulins, mycophenolate, tacrolimus, and infliximab also should be considered if the patients get worse after steroid treatment for 24 h (27). Patients should also be treated with conventional therapy for each cardiovascular manifestation such as heart failure. In our cases, most patients responded well to steroid therapy, and traditional therapy for myocarditis including large doses of vitamin C, trimetazidine, and coenzyme Q10, might also help.

Compared with chemotherapy or radiotherapy, ICIs significantly improve the durable response rate and prolongs long-term survival with relatively limited adverse effects in both monotherapy and combination therapy for advanced cancers. In the last 3 years, ∼11 kinds of ICIs have been approved for clinical application in various advanced cancers worldwide, as well as in China. More interdisciplinary physicians have also performed ICIs due to their accessibility and relatively low economic burden, especially for domestic ICIs drugs. In our study, we found that the systemic steroids were initiated 9 days (IQR 7.0–15.0) after symptom onset or detection of increased serum marker, which is not a relative early initiation time (6). This indicated relatively insufficient familiarity with adverse reactions for interdisciplinary physicians. The management of adverse events implicated assessment significantly, including cardiac baseline assessment, subsequent monitoring, multidisciplinary consultation, high clinical suspicion, and early diagnosis. Especially for ICI related myocarditis, which is a rare but potentially fatal and fulminant side effect, it is imperative to transfer patients in which this is suspected to a cardiology department or ICU for early improvement. Furthermore, currently, there is no treatment regime for different clinical types of ICI related myocardial injury that has been tested by randomized clinical trials. Perspective cohorts and randomized clinical trials are required to gain further information and standardize the management of ICI induced cardiac irAEs.

There are several limitations to our study. First, because four of our cases were asymptomatic and three of our cases were fulminant, it was challenging to perform confirmation tests (such as myocardial biopsy, CMR and coronary tests) in every case. Therefore, several cases could only be classified as unspecific myocardial injuries (9). Second, cases were collected from different sub-specialty departments and were of different severity, which restricted our overall analysis. Third, we collected cases mainly from 2018 to 2019, when guidelines were lacking for the diagnosis and treatment of ICI related myocardial injury.

To sum up, ICIs are currently increasingly utilized for a wide variety of malignancies. Along with the prosperity of ICIs, clinicians need to be aware of irAEs especially cardiac toxicities because of the potentially high risk for mortality in the short term.

DATA AVAILABILITY STATEMENT

The original contributions presented in the study are included in the article/**Supplementary Material**, further inquiries can be directed to the corresponding author/s.

ETHICS STATEMENT

Written informed consent was obtained from the individual(s) for the publication of any potentially identifiable images or data included in this article.

AUTHOR CONTRIBUTIONS

RC and LP collected all the clinical data. ZQ and FW independently reviewed the data. RC and YW prepared the manuscript. MZ and FZ proposed the idea for this work. All authors contributed to the article and approved the submitted version.

FUNDING

This work was supported by grants from the National Natural Science Foundation of China (No. 81570348).

ACKNOWLEDGMENTS

We thank the patients for their participation in this study.

SUPPLEMENTARY MATERIAL

The Supplementary Material for this article can be found online at: https://www.frontiersin.org/articles/10.3389/fcvm.2021.727445/full#supplementary-material

Supplementary Figure 1 | Clinical characteristics of case 1. **(A)** Typical electrocardiograms **(ECG)** of case 1: ECG on the left indicated II° atrioventricular block; ECG on the right side indicated III° atrioventricular block. **(B)** SPECT of case 1 showed extensive myocardial perfusion reduction. **(C)** Serum level of hsTnI and CK-MB. **(D)** Endomyocardial biopsy of the patient showed cardiomyocyte degeneration and mild effusion.

Supplementary Figure 2 | Clinical characteristics of case 2. **(A)** Serum level of hsTnI and CK-MB. **(B)** Typical ECGs of case 2 showed sinus tachycardia on the left side and III°AVB and elevation of ST segment in I and aVL on the right side.

Supplementary Figure 3 | Clinical characteristics of case 3. **(A)** Typical electrocardiogram of case 3 showed elevated ST segment in II, III, aVF and V1-6 leads and complete right bundle branch block. **(B)** Serum level of hsTnI and CK-MB. **(C)** Typical electrocardiogram of case 3 showed complete right bundle branch block.

REFERENCES

1. Hargadon KM, Johnson CE, Williams CJ. Immune checkpoint blockade therapy for cancer: an overview of FDA-approved immune checkpoint inhibitors. *Int Immunopharmacol.* (2018) 62:29–39. doi: 10.1016/j.intimp.2018.06.001
2. Diesendruck Y, Benhar I. Novel immune check point inhibiting antibodies in cancer therapy-opportunities and challenges. *Drug Resist Updat.* (2017) 30:39–47. doi: 10.1016/j.drup.2017.02.001
3. Postow MA, Sidlow R, Hellmann MD. Immune-related adverse events associated with immune checkpoint blockade. *N Engl J Med.* (2018) 378:158–68. doi: 10.1056/NEJMra1703481
4. Johnson DB, Balko JM, Compton ML, Chalkias S, Gorham J, Xu Y, et al. Fulminant myocarditis with combination immune checkpoint blockade. *N Engl J Med.* (2016) 375:1749–55. doi: 10.1056/NEJMoa1609214
5. Nghiem PT, Bhatia S, Lipson EJ, Kudchadkar RR, Miller NJ, Annamalai L, et al. PD-1 Blockade with pembrolizumab in advanced merkel-cell carcinoma. *N Engl J Med.* (2016) 374:2542–52. doi: 10.1056/NEJMoa1603702
6. Mahmood SS, Fradley MG, Cohen JV, Nohria A, Reynolds KL, Heinzerling LM, et al. Myocarditis in patients treated with immune checkpoint inhibitors. *J Am Coll Cardiol.* (2018) 71:1755–64. doi: 10.1016/j.jacc.2018.02.037
7. Neilan TG, Rothenberg ML, Amiri-Kordestani L, Sullivan RJ, Steingart RM, Gregory W, et al. Myocarditis associated with immune checkpoint inhibitors: an expert consensus on data gaps and a call to action. *Oncologist.* (2018) 23:874–8. doi: 10.1634/theoncologist.2018-0157
8. Hu JR, Florido R, Lipson EJ, Naidoo J, Ardehali R, Tocchetti CG, et al. Cardiovascular toxicities associated with immune checkpoint inhibitors. *Cardiovasc Res.* (2019) 115:854–68. doi: 10.1093/cvr/cvz026
9. Bonaca MP, Olenchock BA, Salem JE, Wiviott SD, Ederhy S, Cohen A, et al. Myocarditis in the setting of cancer therapeutics: proposed case definitions for emerging clinical syndromes in cardio-oncology. *Circulation.* (2019) 140:80–91. doi: 10.1161/CIRCULATIONAHA.118.034497
10. Herrmann J. Adverse cardiac effects of cancer therapies: cardiotoxicity and arrhythmia. *Nat Rev Cardiol.* (2020) 17:474–502. doi: 10.1038/s41569-020-0348-1
11. Palaskas N, Lopez-Mattei J, Durand JB, Iliescu C, Deswal A. Immune checkpoint inhibitor myocarditis: pathophysiological characteristics, diagnosis, and treatment. *J Am Heart Assoc.* (2020) 9:e013757. doi: 10.1161/JAHA.119.013757
12. Løgstrup BB, Nielsen JM, Kim WY, Poulsen SH. Myocardial oedema in acute myocarditis detected by echocardiographic 2D myocardial deformation analysis. *Eur Heart J Cardiovasc Imaging.* (2016) 17:1018–26. doi: 10.1093/ehjci/jev302
13. Zhang L, Awadalla M, Mahmood SS, Nohria A, Hassan MZO, Thuny F, et al. Cardiovascular magnetic resonance in immune checkpoint inhibitor-associated myocarditis. *Eur Heart J.* (2020) 41:1733–43. doi: 10.1093/eurheartj/ehaa051
14. Laubli H, Balmelli C, Bossard M, Pfister O, Glatz K, Zippelius A. Acute heart failure due to autoimmune myocarditis under pembrolizumab treatment for metastatic melanoma. *J Immunother Cancer.* (2015) 3:11. doi: 10.1186/s40425-015-0057-1
15. Geisler BP, Raad RA, Esaian D, Sharon E, Schwartz DR. Apical ballooning and cardiomyopathy in a melanoma patient treated with ipilimumab: a case of takotsubo-like syndrome. *J Immunother Cancer.* (2015) 3:4. doi: 10.1186/s40425-015-0048-2
16. Zimmer L, Goldinger SM, Hofmann L, Loquai C, Ugurel S, Thomas I, et al. Neurological, respiratory, musculoskeletal, cardiac and ocular side-effects of anti-PD-1 therapy. *Eur J Cancer.* (2016) 60:210–25. doi: 10.1016/j.ejca.2016.02.024
17. Nishimura H, Okazaki T, Tanaka Y, Nakatani K, Hara M, Matsumori A, et al. Autoimmune dilated cardiomyopathy in PD-1 receptor-deficient mice. *Science.* (2001) 291:319–22. doi: 10.1126/science.291.5502.319
18. Okazaki T, Tanaka Y, Nishio R, Mitsuiye T, Mizoguchi A, Wang J, et al. Autoantibodies against cardiac troponin I are responsible for dilated cardiomyopathy in PD-1-deficient mice. *Nat Med.* (2003) 9:1477–83. doi: 10.1038/nm955
19. Wang J, Okazaki IM, Yoshida T, Chikuma S, Kato Y, Nakaki F, et al. PD-1 deficiency results in the development of fatal myocarditis in MRL mice. *Int Immunol.* (2010) 22:443–52. doi: 10.1093/intimm/dxq026
20. Seki M, Uruha A, Ohnuki Y, Kamada S, Noda T, Onda A, et al. Inflammatory myopathy associated with PD-1 inhibitors.

J Autoimmun. (2019) 100:105–13. doi: 10.1016/j.jaut.2019.03.005
21. Osorio JC, Ni A, Chaft JE, Pollina R, Kasler MK, Stephens D, et al. Antibody-mediated thyroid dysfunction during T-cell checkpoint blockade in patients with non-small-cell lung cancer. *Ann Oncol.* (2017) 28:583–9. doi: 10.1093/annonc/mdw640
22. Brunet-Possenti F, Mignot S, Deschamps L, Descamps V. Antiepidermis autoantibodies induced by anti-PD-1 therapy in metastatic melanoma. *Melanoma Res.* (2016) 26:540–3. doi: 10.1097/CMR.0000000000000287
23. Naidoo J, Schindler K, Querfeld C, Busam K, Cunningham J, Page DB, et al. Autoimmune bullous skin disorders with immune checkpoint inhibitors targeting PD-1 and PD-L1. *Cancer Immunol Res.* (2016) 4:383–9. doi: 10.1158/2326-6066.CIR-15-0123
24. Kishi S, Minato M, Saijo A, Murakami N, Tamaki M, Matsuura M, et al. IgA nephropathy after nivolumab therapy for postoperative recurrence of lung squamous cell carcinoma. *Intern Med.* (2018) 57:1259–63. doi: 10.2169/internalmedicine.9814-17
25. Kaya Z, Leib C, Katus HA. Autoantibodies in heart failure and cardiac dysfunction. *Circ Res.* (2012) 110:145–58. doi: 10.1161/CIRCRESAHA.111.243360
26. Zhou YW, Zhu YJ, Wang MN, Xie Y, Chen CY, Zhang T, et al. Immune checkpoint inhibitor-associated cardiotoxicity: current understanding on its mechanism, diagnosis and management. *Front Pharmacol.* (2019) 10:1350. doi: 10.3389/fphar.2019.01350
27. Ball S, Ghosh RK, Wongsaengsak S, Bandyopadhyay D, Ghosh GC, Aronow WS, et al. Cardiovascular toxicities of immune checkpoint inhibitors: JACC review topic of the week. *J Am Coll Cardiol.* (2019) 74:1714–27. doi: 10.1016/j.jacc.2019.07.079

Conflict of Interest: The authors declare that the research was conducted in the absence of any commercial or financial relationships that could be construed as a potential conflict of interest.

Publisher's Note: All claims expressed in this article are solely those of the authors and do not necessarily represent those of their affiliated organizations, or those of the publisher, the editors and the reviewers. Any product that may be evaluated in this article, or claim that may be made by its manufacturer, is not guaranteed or endorsed by the publisher.

frontiers | Frontiers in Cardiovascular Medicine

ORIGINAL RESEARCH
published: 15 April 2022
doi: 10.3389/fcvm.2022.739044

Anti-cancer Drugs Associated Atrial Fibrillation—An Analysis of Real-World Pharmacovigilance Data

Javaria Ahmad[1], Aswani Thurlapati[1†], Sahith Thotamgari[1†], Udhayvir Singh Grewal[1], Aakash Rajendra Sheth[1], Dipti Gupta[2], Kavitha Beedupalli[3] and Paari Dominic[4]*

[1] Department of Medicine, Louisiana State University Health Sciences Center-Shreveport, Shreveport, LA, United States, [2] Department of Medicine, Cardiology Service, Memorial Sloan Kettering Cancer Center, New York City, NY, United States, [3] Department of Hematology and Oncology and Feist Weiller Cancer Center, Louisiana State University Health Sciences Center-Shreveport, Shreveport, LA, United States, [4] Center of Excellence for Cardiovascular Diseases and Sciences, Louisiana State University Health Sciences Center-Shreveport, Shreveport, LA, United States

OPEN ACCESS

Edited by:
Michael Cross,
University of Liverpool,
United Kingdom

Reviewed by:
Aaron L. Sverdlov,
University of Newcastle, Australia
Rohit Moudgil,
Cleveland Clinic, United States
Irma Bisceglia,
San Camillo-Forlanini Hospital, Italy
Zaza Iakobishvili,
Clalit Health Services, Israel

***Correspondence:**
Paari Dominic
paari.dominic@lsuhs.edu

[†] These authors have contributed equally to this work

Specialty section:
This article was submitted to Cardio-Oncology, a section of the journal Frontiers in Cardiovascular Medicine

Received: 09 July 2021
Accepted: 15 March 2022
Published: 15 April 2022

Citation:
Ahmad J, Thurlapati A, Thotamgari S, Grewal US, Sheth AR, Gupta D, Beedupalli K and Dominic P (2022) Anti-cancer Drugs Associated Atrial Fibrillation—An Analysis of Real-World Pharmacovigilance Data. Front. Cardiovasc. Med. 9:739044. doi: 10.3389/fcvm.2022.739044

Background: Several anti-cancer drugs have been linked to new onset atrial fibrillation (AF) but the true association of these drugs with AF is unknown. The FDA Adverse Event Reporting System (FAERS), a publicly available pharmacovigilance mechanism provided by the FDA, collects adverse event reports from the United States and other countries, thus providing real-world data.

Objectives: To identify anti-cancer drugs associated with AF using the FAERS database.

Methods: The FAERS database was searched for all drugs reporting AF as an adverse event (AE). The top 30 anti-cancer drugs reporting AF cases were shortlisted and analyzed. Proportional reporting ratio (PRR) was used to measure disproportionality in reporting of adverse events for these drugs.

Results: When analyzed for AF as a percentage of all reported AE for a particular drug, Ibrutinib had the highest percentage (5.3%) followed distantly by venetoclax (1.6%), bortezomib (1.6%), carfilzomib (1.5%), and nilotinib (1.4%). The percentage of cardiac AE attributable to AF was also highest for ibrutinib (41.5%), followed by venetoclax (28.4%), pomalidomide (23.9%), bortezomib (18.2%), and lenalidomide (18.2%). Drugs with the highest PRR for AF included ibrutinib (5.96, 95% CI= 5.70–6.23), bortezomib (1.65, 95% CI = 1.52–1.79), venetoclax (1.65, 95% CI = 1.46–1.85), carfilzomib (1.53, 95% CI = 1.33–1.77), and nilotinib (1.46, 95% CI = 1.31–1.63).

Conclusions: While newer anti-cancer drugs have improved the prognosis in cancer patients, it is important to identify any arrhythmias they may cause early on to prevent increased morbidity and mortality. Prospective studies are needed to better understand the true incidence of new onset AF associated with anti-cancer drugs.

Keywords: chemotherapy, atrial fibrillation, cardiotoxicity, cardiac adverse events, FAERS

INTRODUCTION

The introduction of novel anti-cancer agents has significantly increased the survival in many malignancies, but none of these drugs is free of adverse effects. Rigorous identification of the toxicity profile of these drugs is crucial, given the better prognosis for patients treated with the newer agents. Cardiovascular toxicity is well established as a side effect of cancer therapy and is likely to be one of the most morbid of all adverse reactions. Although frequently reported as a part of the cardiovascular toxicity of anti-cancer drugs, cardiac arrhythmias, particularly atrial fibrillation (AF), have not been studied in a controlled manner (1).

AF is the most common cardiac arrhythmia, with an overall prevalence of 1–2% in the United States. The risk of AF increases with age, which is also a known risk factor for cancer (2). Management of AF in cancer patients can pose a unique challenge, particularly in hematological malignancies, where the risk of thrombogenesis has to be weighed against the risk of increased bleeding. Various anti-cancer agents have also been reported to cause new onset AF, but the true incidence is ambiguous. Although there is some emerging literature describing cancer treatment-induced arrhythmias, there is a dearth of real-world data exploring the association of AF with specific anti-cancer drugs (1). Ibrutinib is the only anti-cancer agent that has been relatively well studied with respect to the development of AF, with a reported incidence of 4–16% (3, 4) from clinical trials.

The importance of post-marketing surveillance of drugs cannot be emphasized enough as the real-world use of drugs and their adverse events (AE) differs from their use (and AE) in controlled clinical trials that are short-term and usually exclude vulnerable populations. FAERS is a publicly accessible international database containing AE reports submitted to the FDA by healthcare professionals, consumers, and manufacturers. We used the FAERS database to study anti-cancer drugs reported to have caused AF, to better understand the association of AF with these drugs.

METHODS

Study Design and Data Source

A retrospective, observational, pharmacovigilance study was done on a de-identified publicly available FAERS dataset, which did not require IRB approval. FAERS complies with the international safety reporting guidance issued by the International Conference on Harmonization (ICH E2B). It collects AER submitted by healthcare professionals, consumers, and manufacturers around the world.

The database was searched using the reaction term "Atrial Fibrillation." All the reported cases of AF for each drug (queried by generic names) were collected from inception to February 10, 2021, and a shortlist created of the top 30 anti-cancer drugs based on reported AF cases. The selected drugs were then individually searched using the generic names and the reported AE were collected individually for each drug. Data were further narrowed down by applying various filters such as age, received year, sex, and outcomes (**Figure 1**).

Statistical Methods and Analysis

First, a descriptive analysis of the data was performed. Then, a comparative analysis was done among the drugs in the group. The proportional reporting ratio (PRR) (5) was calculated for various parameters to determine the disproportionality in reporting. Data on patient characteristics and outcomes were collected and analyzed.

Descriptive Analysis

For each drug, AF cases were represented as a percentage of all AE as well as cardiac adverse events (CAE). In addition, AF cases by sex and by age were calculated as percentage of the total AF cases for the drug. The proportion of deaths among reported AF cases for each drug of interest was calculated. This proportion was then divided by the proportion of deaths among reported AF cases for all drugs that are reported to FAERS for AF to arrive at comparative mortality ratio (CMR).

Disproportionality Approach

PRR is a statistical tool used for quantitative signal detection in surveillance databases (6). PRR compares the frequency of reporting of an AE of a certain drug to the frequency of reporting of the same AE for other drugs in the reference group. A PRR >1 for a drug indicates that an AE is reported more frequently for the drug of interest relative to the drugs in the comparison group. Similarly, a PRR of 2 will suggest that the AE was reported twice as frequently for that drug compared to other drugs in the analysis and a PRR of 2 or more is generally considered significant disproportionality in AE reporting. We calculated the PRR of each drug for CAE, total AF cases, AF cases by sex, and total deaths in reported AF cases.

RESULTS

A total of 72,488 cases of AF were reported to FAERS. The top 30 anti-cancer drugs accounted for 17,098 of these cases (23.5% of total AF reports in FAERS). These drugs are listed in **Table 1**.

Anti-cancer Drugs and Cardiac Adverse Events (CAE)

Nilotinib had the highest proportion of CAE, which accounted for 15.6% of the total reported AE of the drug, followed by trastuzumab (14.5%), ibrutinib (12.8%), carfilzomib (12.5%), and doxorubicin (11%). Nilotinib had the highest PRR for CAE (2.05, 95% CI = 1.99–2.11), followed by trastuzumab (1.92, 95% CI = 1.87–1.97), ibrutinib (1.68, 95% CI = 1.64–1.73) and carfilzomib (1.63, 95% CI = 1.56–1.71) (**Figure 2**).

Anti-cancer Drugs and AF

When analyzed for AF as a percentage of all reported AE for a particular drug, Ibrutinib had the highest percentage (5.3%) followed distantly by venetoclax (1.6%), bortezomib (1.6%), carfilzomib (1.5%), and nilotinib (1.4%). Similarly, the percentage of CAE attributable to AF was also highest for ibrutinib

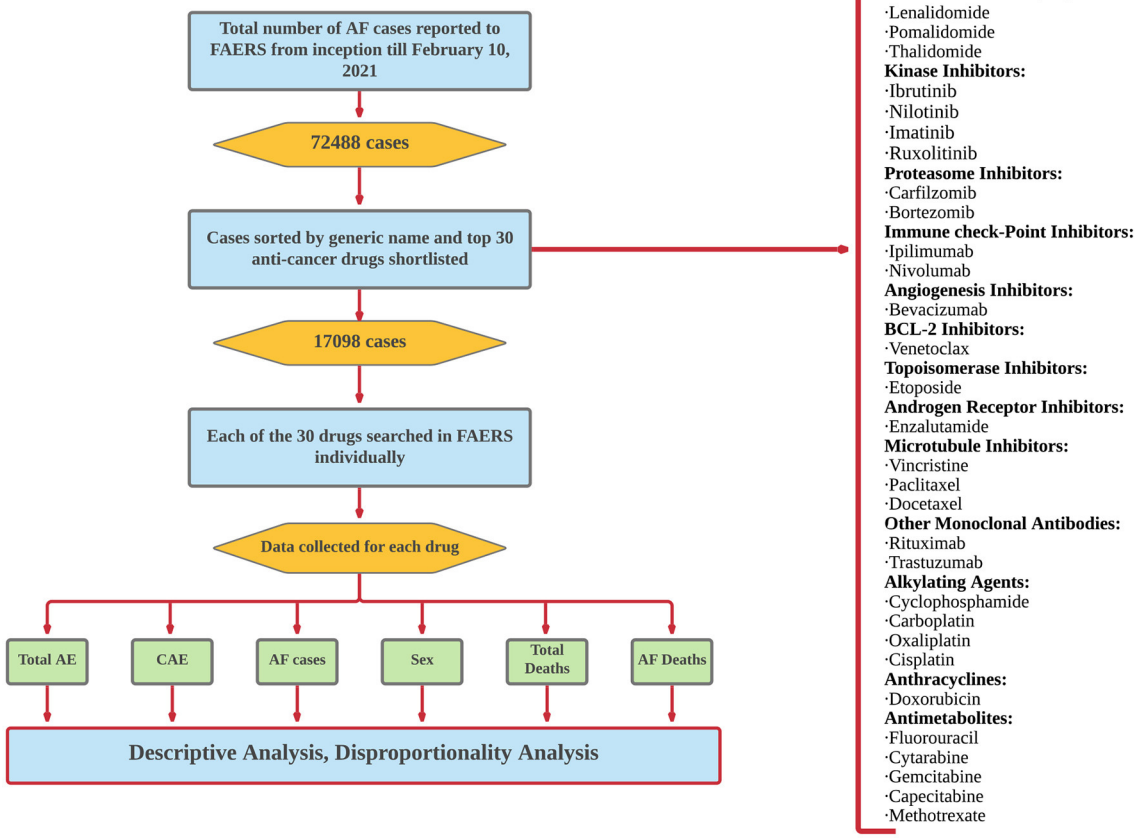

FIGURE 1 | Algorithm of FAERS search and selection of anti-cancer drugs reported for AF.

(41.5%), followed by venetoclax (28.4%), pomalidomide (23.9%), bortezomib (18.2%), and lenalidomide (18.2%). Drugs with the highest PRR for AF included ibrutinib (5.96, 95% CI = 5.70–6.23), bortezomib (1.65, 95% CI = 1.52–1.79), venetoclax (1.65, 95% CI = 1.46–1.86), carfilzomib (1.53, 95% CI = 1.33–1.77), and nilotinib (1.46, 95% CI = 1.31–1.63) (**Figure 3**).

The PRR for AF in men was highest for ibrutinib (6.95, 95% CI = 6.55–7.37), followed by venetoclax (2.17, 95% CI = 1.87–2.51), carfilzomib (1.81, 95% CI = 1.50–2.17), nilotinib (1.70, 95% CI = 1.47–1.96), and bortezomib (1.65, 95% CI = 1.47–1.84) (**Supplementary Figure 1**). Similarly, PRR for AF in women was also highest for ibrutinib (4.12, 95% CI = 3.78–4.49), followed by trastuzumab (1.66, 95% CI = 1.45–1.91), paclitaxel (1.59, 95% CI = 1.44–1.76), nilotinib (1.37, 95% CI = 1.13 −1.65), and bortezomib (1.32, 95% CI = 1.14–1.53) (**Supplementary Figure 2**).

Deaths in Patients Reported to Have AF During Anti-cancer Therapy

The percentage of reported AF cases in patients who died, of the total number of deaths reported for a drug, was highest for cytarabine (35.9%), followed by capecitabine (30.2%), etoposide (26.9%), gemcitabine (26.5%) and cisplatin (25.9%). Paralleling this, the comparative mortality ratio (CMR) was highest for cytarabine (2.7), followed by capecitabine (2.2), etoposide (2.03), gemcitabine (2) and cisplatin (1.9). However, when assessed using disproportional reporting measures, the PRR for deaths in reported AF cases was highest for ibrutinib (4.62, 95% CI = 4.07–5.24), followed by carfilzomib (2.06, 95% CI = 1.51–2.82), bortezomib (1.72, 95% CI = 1.44–2.06), cisplatin (1.44, 95% CI = 1.22–1.70), and cytarabine (1.44, 95% CI = 1.21–1.71) (**Figure 4**).

DISCUSSION

Key Results

Our comparison of anti-cancer drugs using the PRR to assess the signal-to-noise ratio of public reporting to FAERS of cardiac-related AE showed that nilotinib, ibrutinib, trastuzumab, and carfilzomib had the most CAE reported, while ibrutinib, venetoclax, bortezomib, carfilzomib, and nilotinib had the highest AF cases reported when compared to other drugs in the analysis (**Figure 5**). The drugs with highest reported deaths among AF cases were ibrutinib, bortezomib, carfilzomib, cisplatin, and cytarabine.

Atrial fibrillation in cancer patients has been shown to be associated with poor outcomes (7). The incidence of

TABLE 1 | The proportion of cases of AF, CAE, deaths, and PRR for all variables for all 30 drugs included in the analysis.

	Drug	Total AEs reported	Total CAEs reported	Total AF cases	CAE as % of Total AE	PRR of CAE	AF as % of all AE of the drug	PRR of AF	AF as % of CAE of the drug	PRR of AF as % of CAE	PRR of AF in men	PRR of AF in women	Comparative mortality ratio	PRR of AF deaths
1	Lenalidomide	231,623	12,954	2,363	5.59	0.695	1.02	1.027	18.24	1.479	1.115	1.127	1.154	1.012
2	Ibrutinib	40,151	5,149	2,138	12.82	1.688	5.32	5.961	41.52	3.532	6.953	4.126	0.887	4.625
3	Rituximab	109,507	9,130	1,225	8.33	1.086	1.12	1.131	13.42	1.042	0.82	1.255	1.27	1.222
4	Cyclophosphamide	104,111	9,110	959	8.75	1.143	0.92	0.919	10.53	0.804	0.722	1.07	1.796	1.015
5	Paclitaxel	71,106	6,934	762	9.75	1.278	1.07	1.078	10.99	0.844	0.823	1.594	1.636	1.409
6	Doxorubicin	73,947	8,183	749	11.06	1.462	1.01	1.017	9.15	0.695	0.752	1.289	1.765	1.216
7	Bortezomib	37,496	3,337	609	8.89	1.157	1.62	1.652	18.25	1.428	1.653	1.326	1.526	1.728
8	Carboplatin	58,634	4,999	599	8.52	1.108	1.02	1.026	11.98	0.925	0.989	1.166	1.702	1.347
9	Pomalidomide	49,099	2,421	579	4.93	0.632	1.18	1.189	23.92	1.882	1.362	1.274	1.005	0.941
10	Methotrexate	12,9001	7,000	578	5.42	0.686	0.45	0.43	8.26	0.627	0.255	0.738	1.372	0.886
11	Cisplatin	52,205	4,522	574	8.66	1.126	1.1	1.106	12.69	0.982	1.463	0.707	1.961	1.445
12	Bevacizumab	72,696	4,998	558	6.87	0.886	0.77	0.762	11.16	0.86	0.687	0.864	1.218	0.496
13	Fluorouracil	57,638	5,459	521	9.47	1.237	0.9	0.904	9.54	0.731	0.989	0.872	1.174	0.948
14	Docetaxel	68,681	4,045	410	5.88	0.755	0.6	0.589	10.14	0.78	0.625	0.651	1.732	1.219
15	Oxaliplatin	42,595	3,960	388	9.29	1.21	0.91	0.912	9.8	0.753	1.062	0.749	1.616	1.348
16	Cytarabine	38,000	3,609	376	9.49	1.237	0.99	0.992	10.42	0.802	1.098	0.67	2.712	1.442
17	Nivolumab	47,764	3,174	362	6.64	0.857	0.76	0.755	11.41	0.881	1.023	0.535	1.836	0.639
18	Thalidomide	37,592	3,163	353	8.41	1.092	0.94	0.941	11.16	0.861	0.983	0.961	1.798	0.538
19	Etoposide	41,950	3,569	342	8.50	1.105	0.82	0.814	9.58	0.737	0.983	0.502	2.032	0.891
20	Nilotinib	22,347	3,496	325	15.64	2.054	1.45	1.468	9.3	0.714	1.705	1.371	0.906	1.028
21	Capecitabine	59,896	3,890	291	6.49	0.836	0.49	0.478	7.48	0.572	0.488	0.505	2.284	0.522
22	Venetoclax	16,683	958	273	5.74	0.742	1.64	1.652	28.5	2.226	2.171	1.216	1.024	0.709
23	Imatinib	49,904	3,241	260	6.49	0.837	0.52	0.515	8.02	0.615	0.535	0.582	1.395	0.259
24	Ruxolitinib	38,969	1,917	241	4.91	0.632	0.62	0.615	12.57	0.973	0.255	0.279	1.661	0.797
25	Trastuzumab	33,628	4,904	240	14.58	1.923	0.71	0.712	4.89	0.37	0.057	1.666	1.668	1.135
26	Vincristine	30,753	2,129	225	6.92	0.895	0.73	0.73	10.57	0.816	0.584	0.725	1.679	0.769
27	Enzalutamide	44,071	1,776	214	4.02	0.515	0.49	0.481	12.05	0.932	0.912	0	1.377	0.421
28	Ipilimumab	23,455	1,313	206	5.59	0.722	0.88	0.879	15.69	1.217	1.274	0.537	1.76	1.029
29	Carfilzomib	12,437	1,565	190	12.58	1.637	1.53	1.538	12.14	0.939	1.81	0.802	1.551	2.066
30	Gemcitabine	18,915	1,488	188	7.86	1.019	0.99	0.997	12.63	0.978	1.029	0.883	2.009	1.315

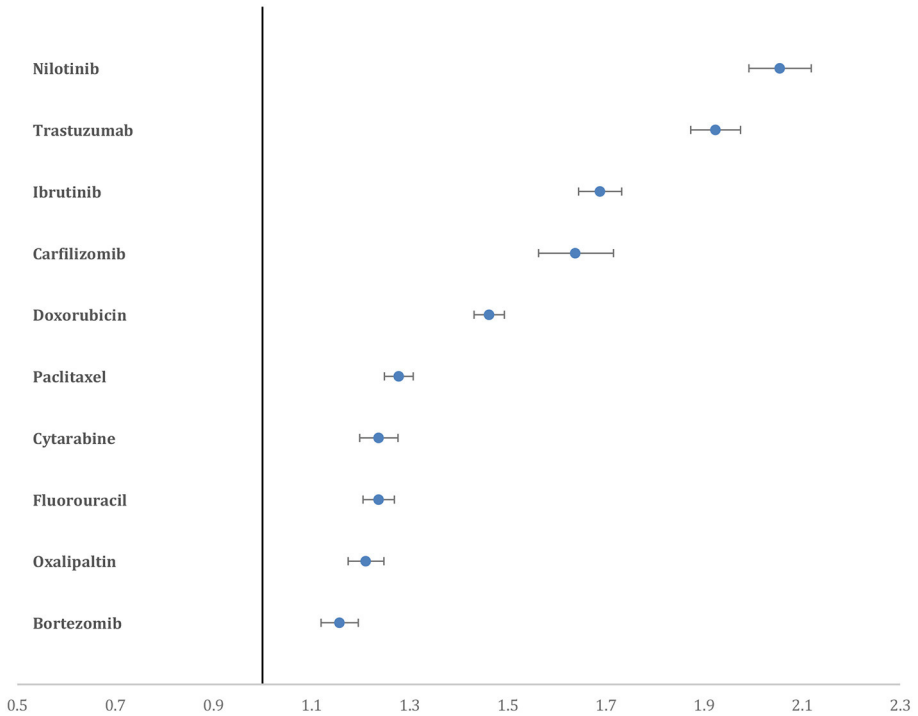

FIGURE 2 | Forest plot showing the PRR of CAE for the top 10 drugs. Nilotinib and trastuzumab have higher PRR compared to all other drugs.

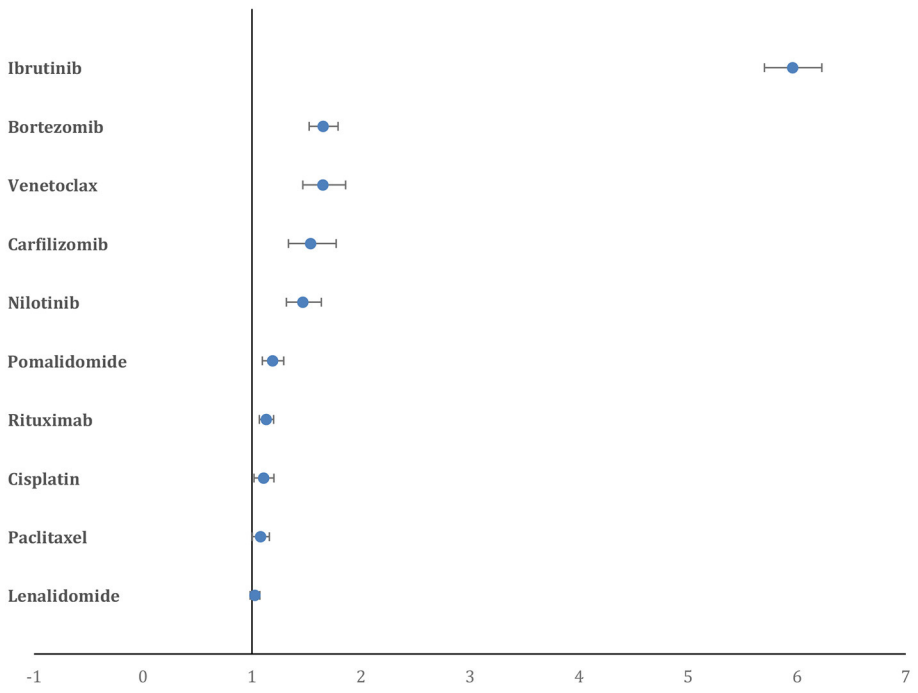

FIGURE 3 | Forest plot showing the PRR of AF for the top 10 drugs. Ibrutinib has a significantly higher PRR compared to all other drugs.

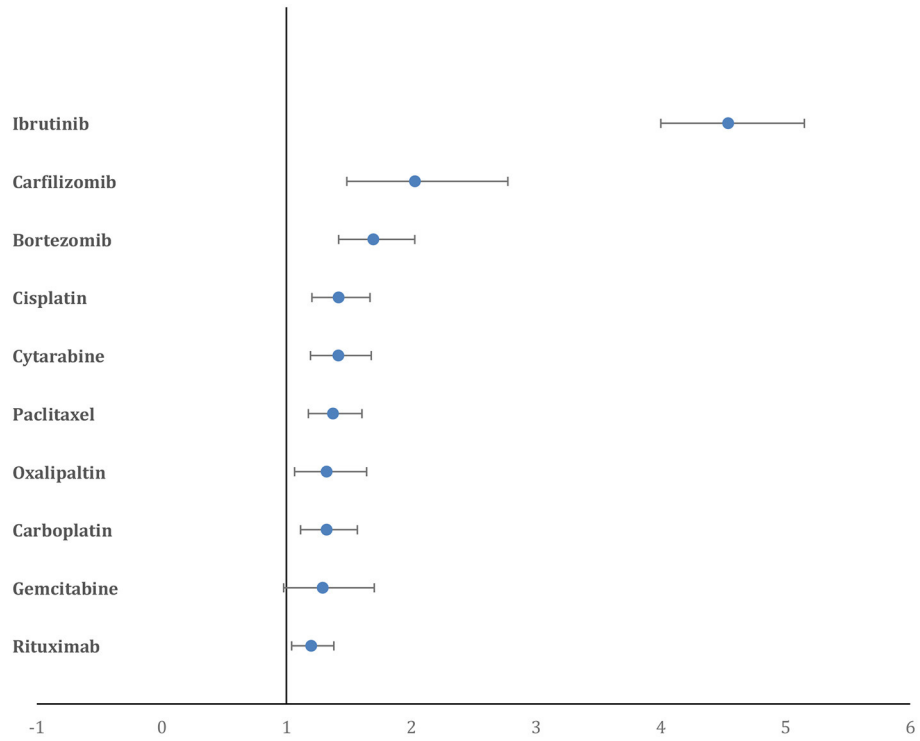

FIGURE 4 | Forest plot showing the PRR of deaths in AF cases for the top 10 drugs. Ibrutinib has a significantly higher PRR compared to all other drugs.

thromboembolism in cancer patients with new onset AF increases two-fold (8). In addition, various anti-cancer drugs increase the risk of thrombogenesis (9). Finally, the risk of bleeding in cancer patients on anticoagulants is higher than that in patients who do not have cancer (10). All these factors make the management of AF in cancer patients a unique challenge, underscoring the relevance of our findings identifying newer anti-cancer drugs that are disproportionately reported to FAERS for AF as an AE.

Anti-cancer Therapy and AF

A variety of modalities of cancer treatment, including chemotherapy, immunotherapy, hormone and radiation therapy, and surgical resection, have each been separately associated with AF. Various anti-cancer drugs, including ibrutinib, doxorubicin, and cisplatin, amongst others, have been associated with AF (11). We have previously established that radiation therapy may be an independent risk factor for AF development (12). Postoperative AF has been associated with surgical resection of lung, colorectal, and esophageal tumors (13–15). Patients with cancer often receive multiple treatment modalities and multiple chemotherapeutic agents. The amalgamation of conventional risk factors, cancer itself, and cancer treatment creates a unique scenario in which the assessment of the specific AF risk with a certain drug can be challenging. Below, we briefly discuss some of the drugs from our analysis that had significantly disproportional reporting for AF and what is known in terms of their association with AF.

Ibrutinib and Nilotinib

Ibrutinib is an irreversible Bruton's tyrosine kinase inhibitor that prevents downstream activation of B-cells. It is currently used in the treatment of chronic lymphocytic leukemia (CLL), mantle cell lymphoma, marginal zone lymphoma, small lymphocytic lymphoma, and the plasma cell disorder Waldenstrom's macroglobulinemia. An AF incidence of 6% was noted for ibrutinib in the landmark RESONATE and RESONATE-2 trials that led to the FDA approval of the drug (16). A meta-analysis by Yun et al. (17) of AF in patients treated with ibrutinib vs. other chemo-immunotherapeutic agents for B-cell malignancies showed an approximately nine-fold increased risk of AF following treatment with ibrutinib. Our results showing the highest AF PRR for ibrutinib (5.96, 95% CI = 5.70–6.23) are in line with the known evidence for AF and the drug. Based on a risk prediction model, the risk of AF in patients treated with ibrutinib may be modified by co-existent conditions, including age >65 years, male sex, valvular heart disease, cardiomyopathy, thyroid abnormality, chronic lung disease, diabetes mellitus, and grade-3 infections (18). The precise mechanism behind the pathogenesis of AF in connection with ibrutinib treatment is unknown.

Nilotinib is another member of the TKI family used in the treatment of CML (19), that is known to be highly vasculotoxic and cardiotoxic. No prior evidence of an association between AF and nilotinib exists in the literature. In a Phase II trial in which 73 patients treated with nilotinib were followed for 6 years, only 1 developed AF. Similarly, another study reported that AF occurred in 1 of 81 patients treated with nilotinib (20). Another

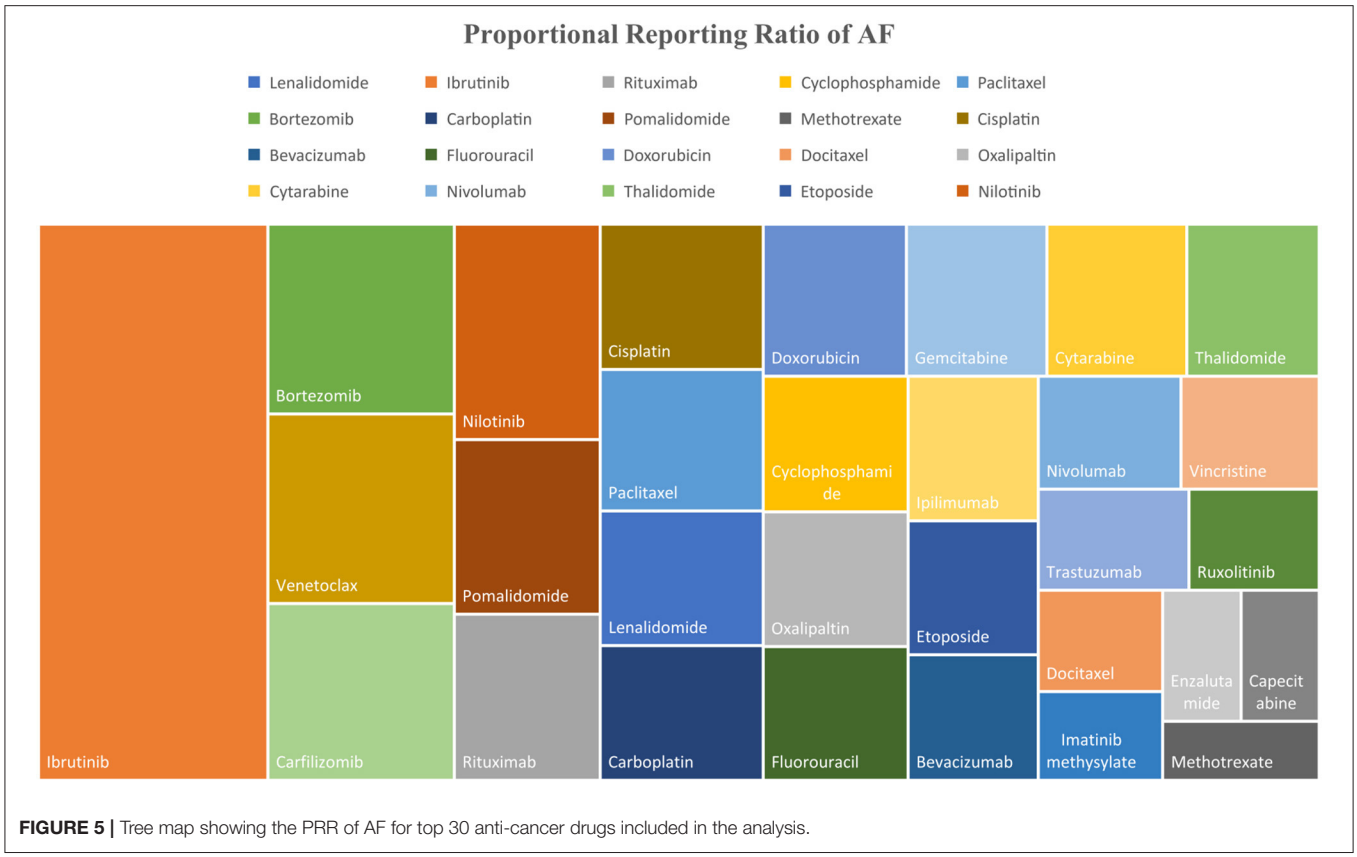

FIGURE 5 | Tree map showing the PRR of AF for top 30 anti-cancer drugs included in the analysis.

study of the cardiotoxicity of TKI in the FAERS database reported a significantly increased adjusted Reporting Odds Ratio (aROR) for cardiac arrhythmias following treatment with nilotinib (2.7), but did not specify the type of arrhythmia (21). While our study highlights a potential novel association, further prospective studies are warranted to confirm the association and determine the causation.

Bortezomib and Carfilzomib

Bortezomib and carfilzomib are both proteasome inhibitors (PI) that act by inhibiting the NF-κB pathway on multiple myeloma (MM) cells leading to cell death. The available data on the incidence of AF in connection with these drugs are scarce and inconsistent. A study of four Phase II clinical trials of carfilzomib showed that cardiac arrhythmias developed in 13.3% of the patients ($n = 526$); however, 73.6% of the patients enrolled had a prior history of cardiovascular events (22). Another meta-analysis of cardiovascular adverse events related to treatment with carfilzomib reported cardiac arrhythmias in 2.4% of patients from a total of 13 studies (23). A smaller prospective study ($n = 95$) compared the CAE that resulted from treatment with carfilzomib to those of bortezomib. Results showed that the CAE were significantly higher in patients treated with carfilzomib than in those treated with bortezomib (51% vs. 17% respectively), consistent with our results (PRR for CAE: carfilzomib, 1.63 (95% CI = 1.56–1.71) vs. bortezomib, 1.15 (95% CI = 1.11–1.19). The incidence of AF was comparable for the two drugs, with 2 of 65 patients treated with carfilzomib and 1 of 30 patients treated with bortezomib developing AF (24). Similar to these results, we found a comparable increase in the reporting of AF for both bortezomib and carfilzomib [1.65 (95% CI = 1.52–1.79) and 1.53 (95% CI = 1.33–1.77), respectively].

One difficulty in differentiating between these two drugs and their association with AF is that carfilzomib is mostly reserved for relapsed or refractory MM and most of the patients receiving carfilzomib had already been treated with bortezomib (25). Bortezomib is one of the newer anti-cancer drugs identified for its association with AF by Alexandre et al. in their pharmacovigilance study based on the World Health Organization's Vigibase AE dataset; however, any association of AF with carfilzomib was not reported (26). Even though our study highlights a potential association between proteasome inhibitors and AF, the results should be looked upon with caution. Due to lack of comorbidity data and temporal association, causation and definitive conclusions cannot be drawn. An important confounding factor in these drugs is the high prevalence of cardiac disease in MM patients due to increased age, hyper-viscosity, arteriovenous shunts, anemia, and amyloidosis (27). It cannot be determined whether the AF was caused by the drugs alone, or by the combination of all other factors, but the over-reporting in studies from two different databases merits further investigation.

Venetoclax and Pomalidomide

Venetoclax is a B-cell lymphoma (BCL-2) homology domain-3 (BH-3) mimetic, selective B-cell lymphoma (BCL-2) inhibitor used in the treatment of lymphomas and leukemias (28). We found increased reporting of AF with venetoclax (PRR 1.65, 95% CI = 1.46–1.85). It is difficult to positively identify the association of venetoclax with AF, because it is used either as first line for the treatment of CLL or used subsequently after progression on ibrutinib, that is known for its association with AF. A Phase II RCT investigating the combination of ibrutinib and venetoclax used to treat high-risk elderly CLL patients showed an incidence of AF in 15% of the patients (29) that is nearly the same as that reported for ibrutinib (30), providing strong evidence for ibrutinib as the cause of AF rather than venetoclax (29). No studies have reported on the incidence of AF during treatment with venetoclax alone.

Pomalidomide is a novel immunomodulatory agent used in the treatment of MM. Prior to our study, pharmacovigilance analysis of the Vigibase dataset showed that AF was reported to occur following treatment with pomalidomide (26). It should be noted that this drug is approved for use in treating MM that is refractory to at least two prior therapies, including lenalidomide and bortezomib, both of which have been reported to be associated with AF. It is important to note that patients with MM are at increased risk of AF in the first place due to age and high cardiovascular disease burden. While there is increased reporting of AF with the above-mentioned drugs, the results should be interpreted with caution as the association does not imply causation.

Mortality Associated With Reported AF Cases

AF increases the risk of heart failure, bleeding complications, myocardial infarction, and all-cause mortality (7, 31). Although a large number of AF patients reported to be on treatment with cytarabine (35.9%), etoposide (26.9%), and gemcitabine (26.5%) died compared to AF patients being treated with other chemotherapeutic agents, this could reflect the severity of the cancer being treated with these drugs rather than an association with the AF reported for the drug. These traditional chemotherapeutic drugs are commonly used to treat cancers with unfavorable survival rates such as AML, pancreatic cancer, bladder cancer, metastatic lung cancer, and ovarian cancer. Therefore, to refine the signal-to-noise ratio, we calculated the PRR for deaths in patients with reported AF. Ibrutinib had a significantly higher PRR for deaths in patients with reported AF, almost three-fold higher than the PRR for the next highest anti-cancer drug, carfilzomib. This suggests that the adverse events related to AF with Ibrutinib could be associated with increased mortality and merits further prospective studies.

Evidence Concerning AF and Anti-cancer Drugs: Vigibase vs. FAERS

Recently, a pharmacovigilance study by Alexandre et al. (26) based on the Vigibase dataset identified 19 anti-cancer drugs associated with AF. Of the 19 drugs identified, new associations with AF were reported for nine drugs including lenalidomide, pomalidomide, nilotinib, ponatinib, midostaurin, azacytidine, clofarabine, docetaxel, and obinutuzumab. Our results confirm the over-reporting of AF with lenalidomide, pomalidomide, and nilotinib, but our PRR for docetaxel was <1. In addition, ponatinib, midostaurin, azacytidine, clofarabine, and obinutuzumab were not included in our analysis due to the small number of cases reported to FAERS. For example, midostaurin has had no AF cases reported to FAERS, and the study by Alexandre et al. had only 20 AF cases. On the other hand, we found significant over-reporting of cases for AF following use of carfilzomib and venetoclax.

In general, FAERS had a higher number of total AF cases reported for most of the chemotherapeutic drugs compared to reports in Vigibase, which is a global database. In addition, we used a different quantitative signal detection tool than Alexandre et al. used; in their study, the Reporting Odds Ratio (ROR) was used as a measure of disproportionality analysis, but on the other hand we used PRR. While PRR and ROR are two different measures and have their own advantages and drawbacks, both are authentic qualitative signal detection tools (5). Another difference is that Alexandre et al. adjusted the ROR for age, sex, geographical region, and comorbidities, whereas inconsistent reporting in FAERS prevented us from performing such adjustments.

LIMITATIONS

Our study had limitations inherent to pharmacovigilance design. First, since there was no reported temporal relationship between the incidence of AF or the outcomes and the specified drug, causation could not be established. To overcome this, we calculated the PRR to detect the disproportionality in reporting and to aid in quantitative signal detection. Second, it is possible that both under-reporting and over-reporting occurred due to missing and duplicate reports. Reported adverse event data cannot be used to calculate the incidence of AF in the population; instead, it should be used to identify the potential hazards of the drug. Third, we did not have data on co-morbidities of the patients to calculate the adjusted reporting ratio. Finally, we shortlisted the drugs by the number of AF cases reported to FAERS. Therefore, comparatively newer drugs, or infrequently used drugs, which might have been associated with AF but had inadequate cases reported to FAERS, could have been missed in our analysis.

CONCLUSION

Atrial fibrillation associated with cancer therapy has lately attracted the attention of the cardio-oncology community, but there is no real data available to help guide the detection, monitoring, and treatment of AF in these patients. Our analysis of the reported cases to FAERS has uncovered anti-cancer drugs that were previously less known for their association with AF. Focused prospective studies should be conducted to gain a better

understanding of the true incidence of AF associated with these anti-cancer agents.

DATA AVAILABILITY STATEMENT

Publicly available datasets were analyzed in this study. This data can be found here: https://www.fda.gov/drugs/questions-and-answers-fdas-adverse-event-reporting-system-faers/fda-adverse-event-reporting-system-faers-public-dashboard.

AUTHOR CONTRIBUTIONS

PD and JA: study conception and design. JA and AT: data collection. ST: statistical analysis. JA with input from all authors: draft preparation. UG, AS, KB, DG, and PD: critical revision. All authors: interpretation of results. All authors reviewed and approved the final version of manuscript.

FUNDING

This publication was supported by an Institutional Development Award from the National Institutes of General Medical Sciences of the National Institutes of Health (NIH) under Grant Number P20GM121307 to C.G. Kevil.

ACKNOWLEDGMENTS

We thank Georgia Morgan for her assistance editing this manuscript.

SUPPLEMENTARY MATERIAL

The Supplementary Material for this article can be found online at: https://www.frontiersin.org/articles/10.3389/fcvm.2022.739044/full#supplementary-material

REFERENCES

1. Guglin M, Aljayeh M, Saiyad S, Ali R, Curtis AB. Introducing a new entity: chemotherapy-induced arrhythmia. *Europace.* (2009) 11:1579–86. doi: 10.1093/europace/eup300
2. Go AS, Hylek EM, Phillips KA, Chang Y, Henault LE, Selby JV, et al. Prevalence of diagnosed atrial fibrillation in adults: national implications for rhythm management and stroke prevention: the AnTicoagulation and Risk Factors in Atrial Fibrillation (ATRIA) Study. *JAMA.* (2001) 285:2370–5. doi: 10.1001/jama.285.18.2370
3. Wiczer TE, Levine LB, Brumbaugh J, Coggins J, Zhao Q, Ruppert AS, et al. Cumulative incidence, risk factors, and management of atrial fibrillation in patients receiving ibrutinib. *Blood Adv.* (2017) 1:1739–48. doi: 10.1182/bloodadvances.2017009720
4. Ganatra S, Sharma A, Shah S, Chaudhry GM, Martin DT, Neilan TG, et al. Ibrutinib-Associated Atrial Fibrillation. *JACC Clin Electrophysiol.* (2018) 4:1491–500. doi: 10.1016/j.jacep.2018.06.004
5. van Puijenbroek EP, Bate A, Leufkens HGM, Lindquist M, Orre R, Egberts ACG, et al. comparison of measures of disproportionality for signal detection in spontaneous reporting systems for adverse drug reactions. *Pharmacoepidemiol Drug Saf.* (2002) 11:3–10. doi: 10.1002/pds.668
6. Evans SJ, Waller PC, Davis S. Use of proportional reporting ratios (PRRs) for signal generation from spontaneous adverse drug reaction reports. *Pharmacoepidemiol Drug Saf.* (2001) 10:483–6. doi: 10.1002/pds.677
7. Melloni C, Shrader P, Carver J, Piccini JP, Thomas L, Fonarow GC, et al. Management and outcomes of patients with atrial fibrillation and a history of cancer: the ORBIT-AF registry. *Eur Heart J Qual Care Clin Outcomes.* (2017) 3:192–7. doi: 10.1093/ehjqcco/qcx004
8. Hu Y, Liu C, Chang PM, Tsao H, Lin Y, Chang S, et al. Incident thromboembolism and heart failure associated with new-onset atrial fibrillation in cancer patients. *Int J Cardiol.* (2013) 165:355–7. doi: 10.1016/j.ijcard.2012.08.036
9. Nadir Y, Hoffman R, Brenner B. Drug-related thrombosis in hematologic malignancies. *Rev Clin Exp Hematol.* (2004) 8:E4.
10. Angelini DE, Radivoyevitch T, McCrae KR, Khorana AA. Bleeding incidence and risk factors among cancer patients treated with anticoagulation. *Am J Hematol.* (2019) 94:780–5. doi: 10.1002/ajh.25494
11. Yang X, Li X, Yuan M, Tian C, Yang Y, Wang X, et al. Anticancer Therapy-Induced Atrial Fibrillation: Electrophysiology and Related Mechanisms. *Front Pharmacol.* (2018) 9:1058. doi: 10.3389/fphar.2018.01058
12. Apte N, Dherange P, Mustafa U. Ya'qoub L, Dawson D, Higginbotham K, et al. Cancer radiation therapy may be associated with atrial fibrillation. *Front Cardiovasc Med.* (2021) 8:610915. doi: 10.3389/fcvm.2021.610915
13. Bhave PD, Goldman LE, Vittinghoff E, Maselli J, Auerbach A. Incidence, predictors, and outcomes associated with postoperative atrial fibrillation after major noncardiac surgery. *Am Heart J.* (2012) 164:918–24. doi: 10.1016/j.ahj.2012.09.004
14. Siu C-W, Tung H-M, Chu K-W, Jim M-H, Lau C-P, Tse H-F. Prevalence and predictors of new-onset atrial fibrillation after elective surgery for colorectal cancer. *Pacing Clin Electrophysiol.* (2005) 28:S120–3. doi: 10.1111/j.1540-8159.2005.00024.x
15. Beck-Nielsen J, Sorensen HR, Alstrup P. Atrial fibrillation following thoracotomy for non-cardiac diseases, in particular cancer of the lung. *Acta Med Scand.* (1973) 193:425–9. doi: 10.1111/j.0954-6820.1973.tb10604.x
16. Burger JA, Tedeschi A, Barr PM, Robak T, Owen C, Ghia P, et al. Ibrutinib as initial therapy for patients with chronic lymphocytic leukemia. *N Engl J Med.* (2015) 373:2425–37. doi: 10.1056/NEJMoa1509388
17. Yun S, Vincelette ND, Acharya U, Abraham I. Risk of atrial fibrillation and bleeding diathesis associated with ibrutinib treatment: a systematic review and pooled analysis of four randomized controlled trials. *Clin Lymphoma Myeloma Leuk.* (2017) 17:31–7.e13. doi: 10.1016/j.clml.2016.09.010
18. Visentin A, Deodato M, Mauro FR, Autore F, Reda G, Vitale C, et al. A scoring system to predict the risk of atrial fibrillation in chronic lymphocytic leukemia and its validation in a cohort of ibrutinib-treated patients. *Blood.* (2018) 132:3118. doi: 10.1182/blood-2018-99-114899
19. Gresse M, Kim TD. le Coutre P. Nilotinib Recent Results. *Cancer Res.* (2018) 212:69–85. doi: 10.1007/978-3-319-91439-8_3
20. Kim TD. le Coutre P, Schwarz M, Grille P, Levitin M, Fateh-Moghadam S, et al. Clinical cardiac safety profile of nilotinib. *Haematologica.* (2012) 97:883–9. doi: 10.3324/haematol.2011.058776
21. Cirmi S, El Abd A, Letinier L, Navarra M, Salvo F. Cardiovascular toxicity of tyrosine kinase inhibitors used in chronic myeloid leukemia: an analysis of the FDA Adverse Event Reporting System Database (FAERS). *Cancers (Basel).* (2020) 12:826. doi: 10.3390/cancers12040826
22. Siegel D, Martin T, Nooka A, Harvey RD, Vij R, Niesvizky R, et al. Integrated safety profile of single-agent carfilzomib: experience from 526 patients enrolled in 4 phase II clinical studies. *Haematologica.* (2013) 98:1753–61. doi: 10.3324/haematol.2013.089334
23. Waxman AJ, Clasen S, Hwang W-T, Garfall A, Vogl DT, Carver J, et al. Carfilzomib-associated cardiovascular adverse events: a systematic review and meta-analysis. *JAMA Oncol.* (2018) 4:e174519. doi: 10.1001/jamaoncol.2017.4519
24. Cornell RF, Ky B, Weiss BM, Dahm CN, Gupta DK, Du L, et al. Prospective study of cardiac events during proteasome inhibitor therapy for relapsed multiple myeloma. *J Clin Oncol.* (2019) 37:1946–55. doi: 10.1200/JCO.19.00231

25. Groen K, van de Donk N, Stege C, Zweegman S, Nijhof I. Carfilzomib for relapsed and refractory multiple myeloma. *Cancer Manag Res.* (2019) 11:2663–75. doi: 10.2147/CMAR.S150653
26. Alexandre J, Salem J-E, Moslehi J, Sassier M, Ropert C, Cautela J, et al. Identification of anticancer drugs associated with atrial fibrillation—analysis of the WHO pharmacovigilance database. *Eur Heart J Cardiovasc Pharmacother*. (2020) 7:312–20. doi: 10.1093/ehjcvp/pvaa037
27. Kyle RA, Gertz MA, Witzig TE, Lust JA, Lacy MQ, Dispenzieri A, et al. Review of 1027 patients with newly diagnosed multiple myeloma. *Mayo Clin Proc.* (2003) 78:21–33. doi: 10.4065/78.1.21
28. Roberts AW. Therapeutic development and current uses of BCL-2 inhibition. *Hematology Am Soc Hematol Educ Program.* (2020) 2020:1–9. doi: 10.1182/hematology.2020000154
29. Jain N, Keating M, Thompson P, Ferrajoli A, Burger J, Borthakur G, et al. Ibrutinib and venetoclax for first-line treatment of CLL. *N Engl J Med.* (2019) 380:2095–103. doi: 10.1056/NEJMoa1900574
30. Brown JR, Moslehi J, O'Brien S, Ghia P, Hillmen P, Cymbalista F, et al. Characterization of atrial fibrillation adverse events reported in ibrutinib randomized controlled registration trials. *Haematologica.* (2017) 102:1796–805. doi: 10.3324/haematol.2017.171041
31. Ruddox V, Sandven I, Munkhaugen J, Skattebu J, Edvardsen T, Otterstad JE. Atrial fibrillation and the risk for myocardial infarction, all-cause mortality and heart failure: a systematic review and meta-analysis. *Eur J Prev Cardiol.* (2017) 24:1555–66. doi: 10.1177/2047487317715769

Conflict of Interest: The authors declare that the research was conducted in the absence of any commercial or financial relationships that could be construed as a potential conflict of interest.

Publisher's Note: All claims expressed in this article are solely those of the authors and do not necessarily represent those of their affiliated organizations, or those of the publisher, the editors and the reviewers. Any product that may be evaluated in this article, or claim that may be made by its manufacturer, is not guaranteed or endorsed by the publisher.

Advantages of publishing in Frontiers

OPEN ACCESS
Articles are free to read for greatest visibility and readership

FAST PUBLICATION
Around 90 days from submission to decision

HIGH QUALITY PEER-REVIEW
Rigorous, collaborative, and constructive peer-review

TRANSPARENT PEER-REVIEW
Editors and reviewers acknowledged by name on published articles

Frontiers
Avenue du Tribunal-Fédéral 34
1005 Lausanne | Switzerland

Visit us: www.frontiersin.org
Contact us: frontiersin.org/about/contact

REPRODUCIBILITY OF RESEARCH
Support open data and methods to enhance research reproducibility

DIGITAL PUBLISHING
Articles designed for optimal readership across devices

FOLLOW US
@frontiersin

IMPACT METRICS
Advanced article metrics track visibility across digital media

EXTENSIVE PROMOTION
Marketing and promotion of impactful research

LOOP RESEARCH NETWORK
Our network increases your article's readership